LUMINESCENT N^2-MODIFIED GUANOSINES: SYNTHESIS, SELF-ASSEMBLY AND METAL ION INTERACTIONS

by

Sanela Martić

A thesis submitted to the Department of Chemistry

in conformity with the requirements

for the degree of Doctor of Philosophy

Queen's University

Kingston, Ontario, Canada

September, 2009

Abstract

The objective of this thesis was to synthesize N^2-modified guanosines (**N^2G**) in order to introduce fluorescent and chelating ligands, such as diphenylamino, 2,2'-dipridylamino, 2-(2'-pyridyl)benzimidazolyl and *p*-pyrenylphenyl functionalities. Their photophysical properties were examined in order to gain further knowledge about the effect of guanine modification on its electronic structure.

The impact of N^2-modification was first studied in terms of self-assembly of the luminescent guanosines in solution and gas phase. Extensive NMR and ESI-MS studies provided evidence that these N^2-modified guanosines self-assemble exclusively into octamers with high-fidelity, in the presence of Group 1 and Group 2 metal ions. In addition, the first example of "empty" G-octamer (free of metal cations) was identified by ESI MS. Experimental results suggested that N^2-substituents provide additional electronic and steric effects which drive the diastereoselectivity of self-assembly and provide additional stability.

Hydrogen bonding of **N^2Gs** with cytidine was monitored using fluorescence and NMR. In addition to GC base pair formation, the G-quartet-to-GC base pair structural transformation was studied using CD, fluorescence, and NMR spectroscopy.

Due to the luminescent and chelating nature of some of the **N^2G** derivatives, their interactions with a number of metal ions, such as Zn^{2+}, Cd^{2+}, Hg^{2+}, La^{3+}, Tb^{3+} and Eu^{3+} ions, were probed by using various spectroscopic methods. The overall optical response in the presence of metal ions was highly dependent on the nature of N^2-substituent, and it varied from "turn-on" to "turn-off" response, clearly indicating that the modification at the N^2-site of guanosine can be used to finely tune the optical response of these

nucleosides. Finally, synthesis of a phosphorescent N^2-arylguanosine containing the Ru^{2+} metal center was achieved and its photophysical and electrochemical properties were examined.

Acknowledgements

Voljela bih da počnem sa zahvaljivanjem mojoj porodici, roditeljima i sestri što su čekali sa nestrpljenjem moje finalno diplomiranje. Školski dani su gotovi! Dragi roditelji hvala vam na vašoj konstantnoj ljubavi i podršci koje nikad ne slabe nego koje radije snaga ispunjava iz dana u dan. Nadam se da sa ovim činom naš život će da započne novu lagodniju egzistenciju. With this I would like to thank my fiancé (finally) John for hanging in there with me and for patiently waiting for our life together to start.

The successful Ph.D. work and scientific development would not have been possible without my supervisor Dr. Suning Wang who was extremely helpful and supportive throughout my studies. She is an excellent supervisor and a wonderful scientist. Additional thanks are in order to my co-supervisor Dr. Gang Wu, who provided scientific contributions that make this thesis complete. I am thankful to my supervisory committee members Dr. Donal H. Macartney and Dr. Anne Petitjean who provided me with wonderful comments and suggestions which made this thesis better. Thanks to Dr. Yi-min She, Dr. Rui-Yao Wang and Dr. Francoise Sauriol for their help with instrumentation and running the experiments.

I had a wonderful time at Queen's, thanks to the past and present Wang and Wu group members. They made the graduate studies fun and they also provided me with valuable help and suggestions. I wish you all the best!

Statement of Originality

I hereby certify that all of the work presented in this thesis is the original work of the author carried out under the supervision of Prof. Suning Wang and Prof. Gang Wu with the following exceptions. Dr. Xiangyang Liu synthesized and characterized the N^2-(4-*n*-butylphenyl)-*2',3',5'*-*O*-triacetylguanosine (**nBuGTAG**) described in Chapter 3 and 4. Any published (or unpublished) ideas and/or methods from the work of other in Wang and Wu group are fully acknowledged in accordance with the standard referencing practices. The work presented in this Thesis has been published or submitted for publication as described bellow:

1) Martić, S.; Gang, Wu; Wang, S. *Inorg. Chem.* **2008**, *47*, 8315.

2) Martić, S.; Liu, X. Y.; Gang, Wu; Wang, S. *Chem. Eur. J.* **2008**, *14*, 1196.

3) Martić, S.; Gang, Wu; Wang, S. *Org. Biomol. Chem.* Submitted.

4) Martić, S.; Wang, S.; Gang, Wu. *Chem. Commun.* Submitted.

(Sanela Martić)

(September, 2009)

Table of Contents

List of Tables

List of Figures

List of Symbols and Abbreviations

Å	angstrom(s)
B3LYP	Becke-3-Parameter Exchange, Lee and Parr
BINAP	2,2’-bis(diphenylphosphino)-1,1’-binaphthyl
bpy	2,2’-bipyridine
°C	degree Celsius
CD	circular dichroism
COSY	correlation spectroscopy
CV	cyclic voltametry
d	doublet
dd	doublet of doublets
DFT	density functional theory
dG	deoxyguanosine
DMAP	dimethylaminopyridine
DMF	dimethylformamide
DMSO	dimethylsulfoxide
DNA	deoxyribonucleic acid
DOSY	diffusion ordered spectroscopy
ds	double strand
dt	doublet of triplets
D_t	diffusion coefficient
ESI	electrospray ionization
ET	electron(energy) transport

eV	electron volt
FDCD	fluorescence detected circular dichroism
FRET	fluorescence energy transfer
g	gram
G	guanosine
$[G]_2$	guanosine dimer
$[G]_4$	guanosine tetramer
$[G]_8$	guanosine octamer
$[G]_{12}$	guanosine dodecamer
$[G]_{16}$	guanosine hexadecamer
GC	guanine-cytosine base pair
5'-GMP	guanosine-5'-monophosphate
3'-GMP	guanosine-4'-monophosphate
G-q	quadruplex
G-quartet	guanine quartet
G-nucleoside	(deoxy)guanosine
h	hour
hh	head-to-head
ht	head-to-tail
Hz	hertz
HOMO	highest occupied molecular orbital
HRMS	high resolution mass spectrometry
ISC	inter-system crossing
J	coupling constant

K	Kelvin
kJ	kilojoule
l	path length
L	liter
LC	ligand centered
LLCT	ligand to ligand charge transfer
LMCT	ligand to metal charge transfer
m	meter, multiplet
M	molar
mg	milligram
MHz	megahertz
mL	milliliter
MLCT	metal to ligand charge transfer
mmol	millimole
MO	molecular orbital
mol	mole
m. p.	melting point
MS	mass spectrometry
nm	nanometers
nBuGTAG	N^2-(4-*n*-butylphenyl)-*2',3',5'*-*O*-triacetylguanosine
N^2G	N^2-modified guanosine
NMR	nuclear magnetic resonance
NOESY	nuclear overhauser effect spectroscopy
OAc	acetate

PET	photo-induced electron transfer
picrate	2,4,6-trinitrophenolate
ppm	part(s) per million
RNA	ribonucleic acid
ROESY	rotating frame Overhauser effect spectrocopy
s	second
ss	single strand
S_0	singlet ground state
S_1	singlet excited state
t	triplet
T_1	triplet excited state
TAG	*2',3',5'-O*-triacetylguanosine
TBAF	tetrabutylammonium fluoride
TD-DFT	time-dependent density functional theory
tfa	trifluoroacetate
th	tail-to-head
THF	tetrahydrofuran
UV	ultraviolet
UV-Vis	ultraviolet-visible
δ	chemical shift
μ	micro
λ	wavelength
λ_{ex}	excitation wavelength
λ_{em}	emission wavelength

φ	quantum yield
τ	lifetime
θ	millidegrees
Λ	lambda
Δ	delta
°	degree
ε	extinction coefficient

Chapter 1
Introduction

Molecular self-assembly using non-covalent interactions represents a useful method towards developing nanostructures and biomimetic architecture.[1] Among electrostatic interactions, hydrogen bonding (H-bonding) has directionality, specificity and biological relevance, making it the ideal intermolecular force in molecular self-assembly.[2] The orientation of H-bond acceptor and H-bond donor groups is crucial in molecular recognition and self-assembly processes. For example, selective recognition between base pairs, via H-bonding, in DNA and RNA chemistry plays an important role in storage of genetic information and regulation. The propensity of nucleobases to form high-order structures can be used to build supramolecular networks. Hence, a nucleobase is a natural choice as a supramolecular building unit when the aim is to develop functional supramolecular materials with high fidelity. Among nucleobases, guanine has the greatest propensity and versatility for H-bonding, so is an excellent candidate for functional supramolecular design. The most famous H-bonding motif of guanine involves the use of the Watson-Crick face[3] in the interaction with its complementary base cytosine, to form a guanine-cytosine (GC) base pair as seen in DNA or RNA double helices (Figure 1.1).

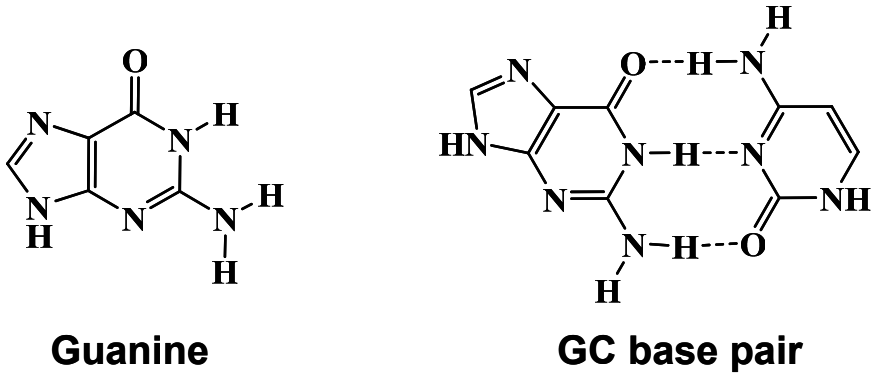

Figure 1.1 Structural representation of guanine and guanine-cytosine (GC) base pair.

In addition to the H-bonding patterns formed in duplexes, guanosine in RNA and deoxyguanosine (dG) in DNA are prone to self-assembly in the presence of metal ions, leading to the formation of the G-quartet ($[\mathbf{G}]_4$) motif. G-quartets may be formed from the DNA sequences found at the end of linear chromosomes called telomeres.[4] The guanine-rich strand folds, in the presence of metal ions, into G-quadruplex[5] (G-q) structures, such as that shown in Figure 1.2, which consists of stacked G-quartets. These G-qs are believed to play an important role in the regulation of cell growth and telomerase inhibition.[6] This is because the guanine-rich region of telomere is a prime substrate for telomerase activity, which is highly active in cancer cells. Unlike a single-stranded (ss) guanine-rich sequence, a folded G-q is not a substrate for telomerase. Hence development of therapeutics capable of stabilizing the G-q structure has been a target of anticancer research.[7]

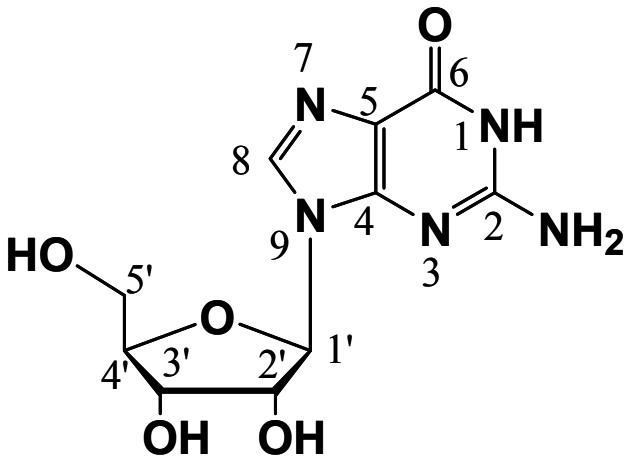

Guanosine

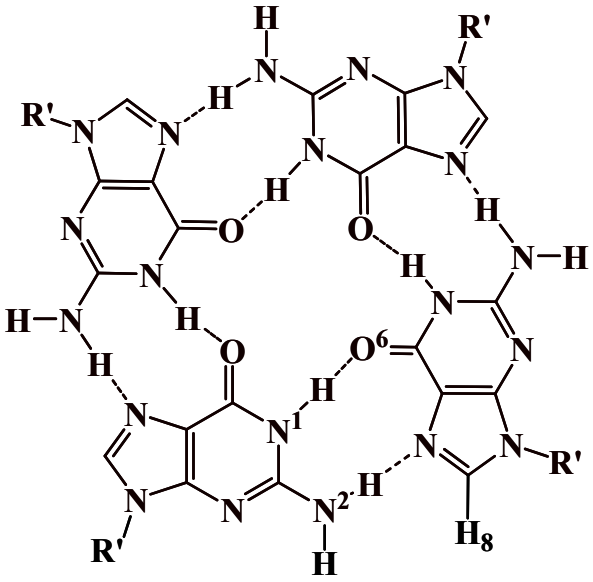

G-quartet

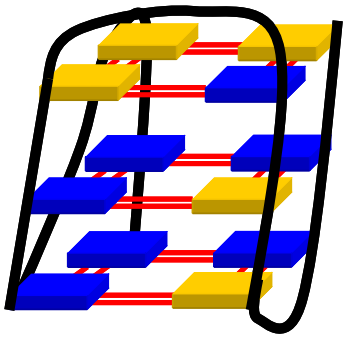

G quadruplex

Figure 1.2 Structural representation of guanosine, G-quartet and G-quadruplex.

The G-quartet motif has found applications not only in biological and medicinal chemistry (anticancer research), but also in nanotechnology.[8] The most important functions of G-quartet based assemblies are ion transporters[9], and ion or chiral separators.[10] Some of the pertinent examples are briefly mentioned below. For example, a calix[4]arene-guanosine conjugate was recently shown to self-assemble into G-quartets,[11] which was found useful in metal cation extractions. G-quartet ionophores have been used for the extraction and separation of radioactive pollutants such as $^{226}Ra^{2+}$ ions,[12] in chiral separation of anions and as the stationary phase in chromatography.[13] In addition, the G-quartet motif has been used as a building block for directing assembly of sophisticated structures. The so called "synaptic domains", or repeating G-G units, dimerize in the presence of metal cations to give rise to variable nanostructures.[14] DNA nanostructures such as "G-wires" have been reported since the mid-1990s, and are useful as molecular electronics due to the electronic communication between stacked G-quartets.[15]

Investigation on developing functional guan(os)ines,[16] with new photophysical and electrochemical properties has been rather limited due to synthetic challenges associated with guanine modification, despite the potential of luminescent guan(os)ines and their self-assembled supramolecular entities in diagnostic and sensing applications. The focus of this introduction is on the self-assembly, chemical modification and potential sensing applications of (deoxy)guanosine nucleosides (G-nucleosides).

1.1 Guanosine as a Supramolecular Building Block

1.1.1 Guanosine conformers

The ribose conformation is instrumental in determining the extent and the type of G-nucleoside self-assembly. Naturally occurring G-nucleosides exist sometimes in an equilibrium between two major conformers known as C2'-*endo* (South (S)) and C3'-*endo* (North (N)), both of which are shown in Figure 1.3. While C3'-*endo* is predominant in RNA and A-form DNA, B-form of DNA is restricted to C2'-*endo*.[5] Chemical modification of a G-nucleoside can be used to push the equilibrium one way or another.

In addition to the conformational flexibility of ribose, the base can also take different orientations with respect to the ribose due to rotation about the $C_{1'}$-N_9 bond. In general, a G-nucleoside adopts either a *syn* or *anti* conformation (Figure 1.4). The conformation refers to the dihedral angle χ (glycosidic torsion angle) defined as $O_{4'}$-$C_{1'}$-N_9-C_4, with the *anti* isomer between $-120 < \chi < 180^{o}$ and the *syn* isomer in $0 < \chi < 90^{o}$ range.[5] This structural feature can be controlled by chemical modification of either ribose or guanine.

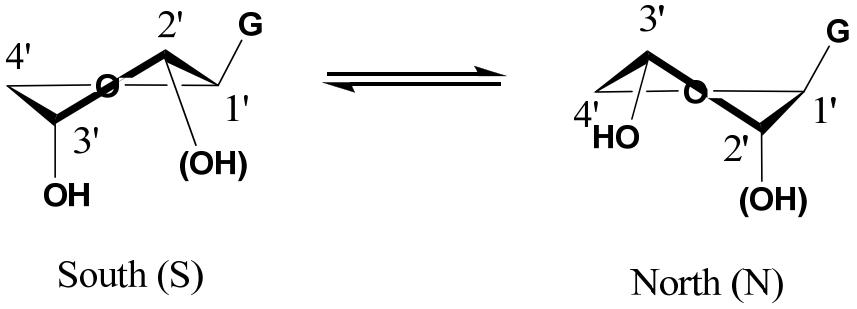

Figure 1.3 Structural representation of the South (S) and North (N) ribose puckering.

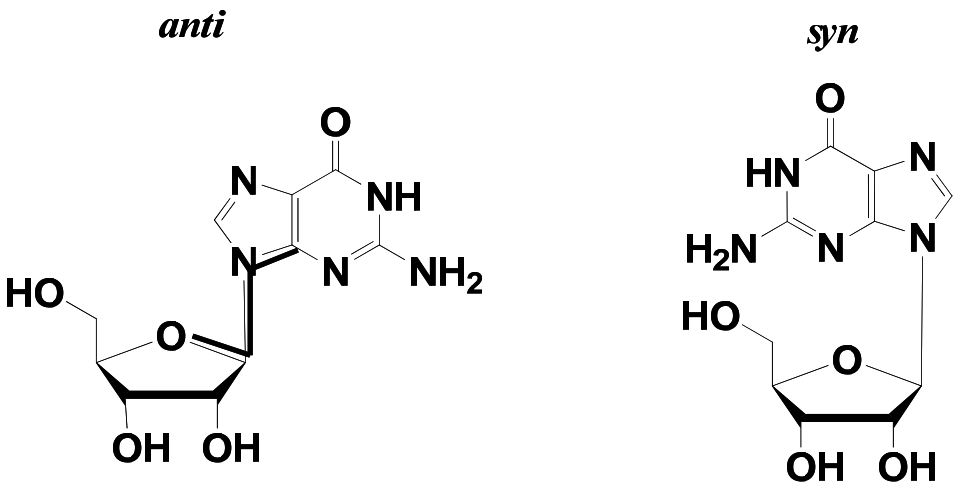

Figure 1.4 Structural representation of guanosine in *syn* and *anti* conformation (the solid line maps out a dihedral angle).

1.1.2 H-bonding motifs of guanine

The G-nucleoside has a great propensity for H-bonding either with a complementary base, unnatural receptors or with itself due to the presence of a number of H-bond donor and acceptor sites as illustrated in Figure 1.5. By using a G-nucleoside as a building block, a variety of structures can be generated such as dimers, trimers, ribbons and G-quartets, depending on the directionality of H-bonds (Figure 1.6). The G-quartet will be described in more detail in section 1.2.

Formations of dimers ($[\mathbf{G}]_2$) and trimers ($[\mathbf{G}]_3$) have not been well studied so far due to their small association constants. A notable exception is that $[\mathbf{G}]_2$ has been recently identified for guanosines-5'-monophosphate (5'-GMP) in the complex mixture of G-quartet aggregates and monomers.[17]

Free G-nucleoside molecules can self-assemble into linear structures such as ribbons in both aqueous and organic media.[18] Two different types of ribbons are known,

ribbon A and ribbon B, depending on the H-bonding (Figure 1.6). Ribbon formation is governed by a number of factors such as solvent, ribose conformation, and total concentration. For example, if G-nucleoside is in the *syn* conformation, one of the faces on the guanine subunit is blocked so that N^3, a H-bond acceptor, and an N_2H hydrogen bond donor would be unable to form H-bonds, which in turn prevents the formation of the ribbon B structure.[19] In addition, inter-tape H-bonds between neighboring ribbons can lead to the formation of a 2D-sheet.[20]

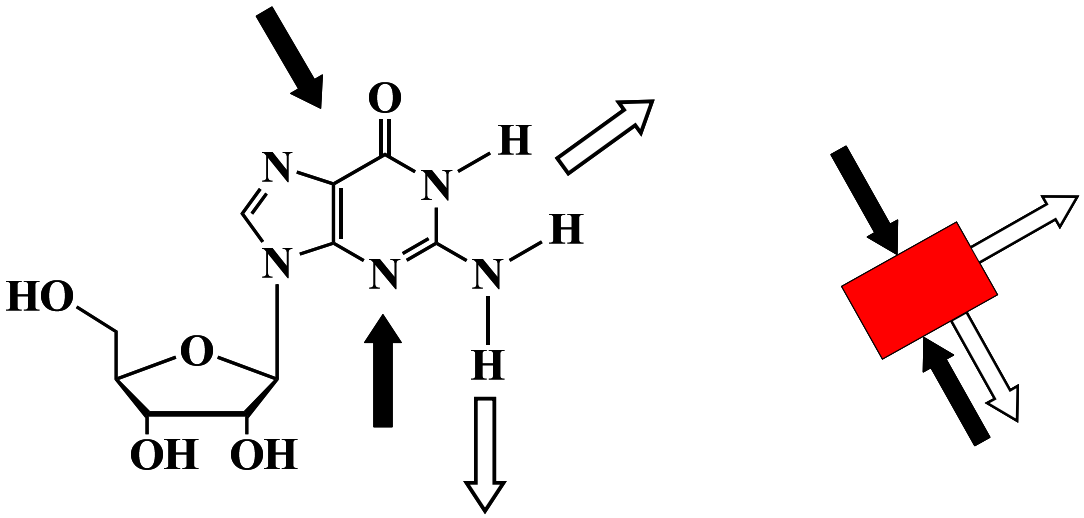

Figure 1.5 H-bond donor (hollow arrow) and H-bond acceptor (solid arrow) sites in guanine.

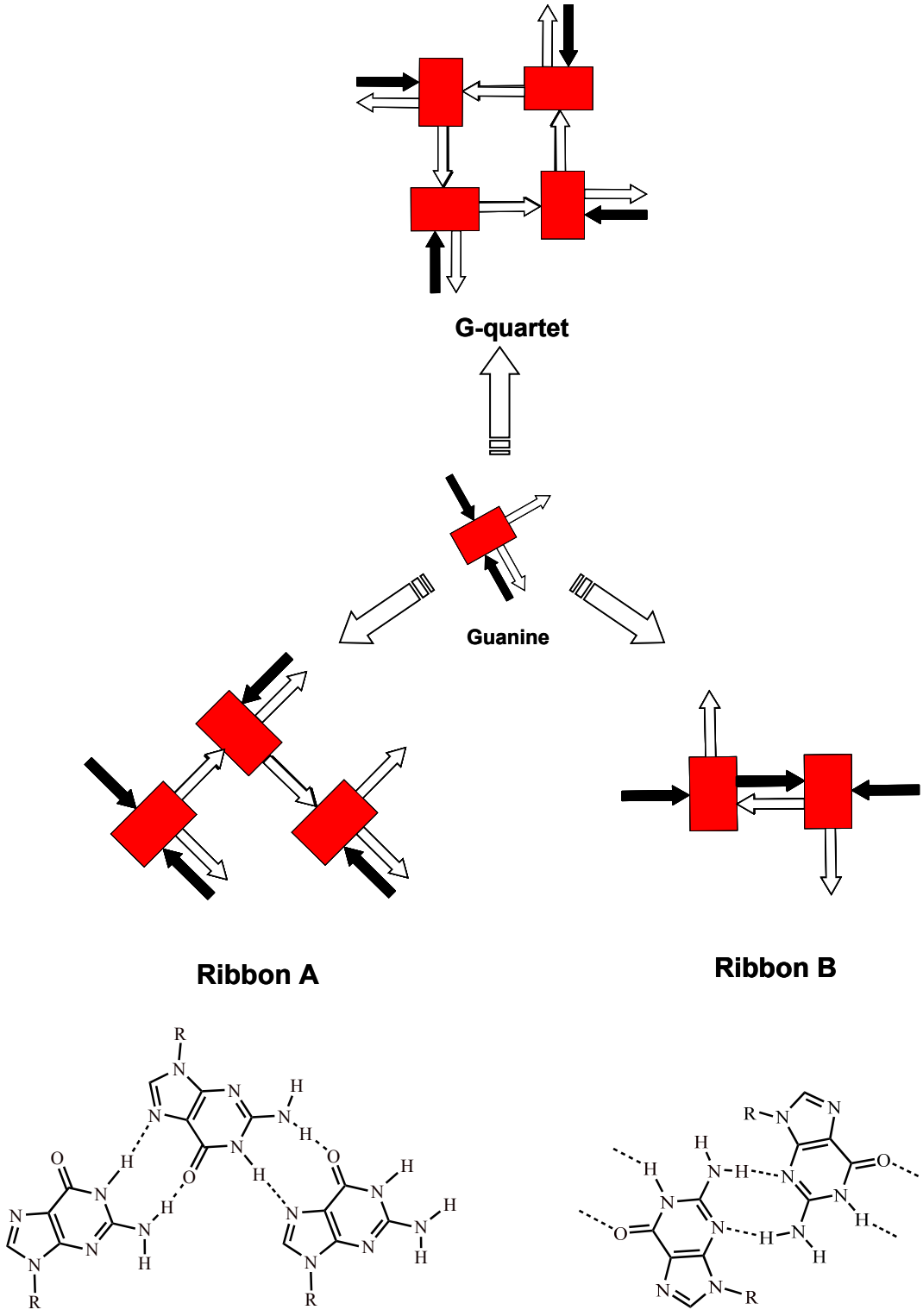

Figure 1.6 Structural representation of H-bond directionality and its effects on the self-assembly of G-nucleoside.

1.2 G-Quartet

1.2.1 General introduction on G-quartet structures

The H-bond donor and H-bond acceptor faces of guanine are 90° to each other which is a perfect orientation for a planar G-quartet formation. The planar G-quartet is held together by eight H-bonds such as N_1H---O^6 and N_2H---N^7 between neighboring bases, using both the Watson-Crick and Hoogsteen faces. Additional stabilization comes from metal cations binding to the carbonyl oxygen atoms. Theoretical studies have shown that the partial negative charge on the carbonyl oxygen atoms is partially neutralized by the presence of metal cations.[21] The oxygen–metal ion interaction provides greater stabilization energy than either H-bonding or π - π stacking.[21]

Because each ribose within the G-quartet can be in either *syn* or *anti* conformation, four conformational arrangements are possible, i.e., all *syn*, all *anti*, alternating structure (*syn-anti-syn-anti*) and adjacent structure (*syn-syn-anti-anti*) as illustrated in Figure 1.7. G-quartet stacking energies of various arrangements of ribose units have been investigated by Straham et al., who reported that two adjacent *syn* G-quartets are more stable than an *anti-syn* stack.[22] Since the first reported case of an all *syn* octamer of oligonucleotides, many other examples have been demonstrated to posses all *syn* stacked G-quartets over other possible ribose arrangements.[23]

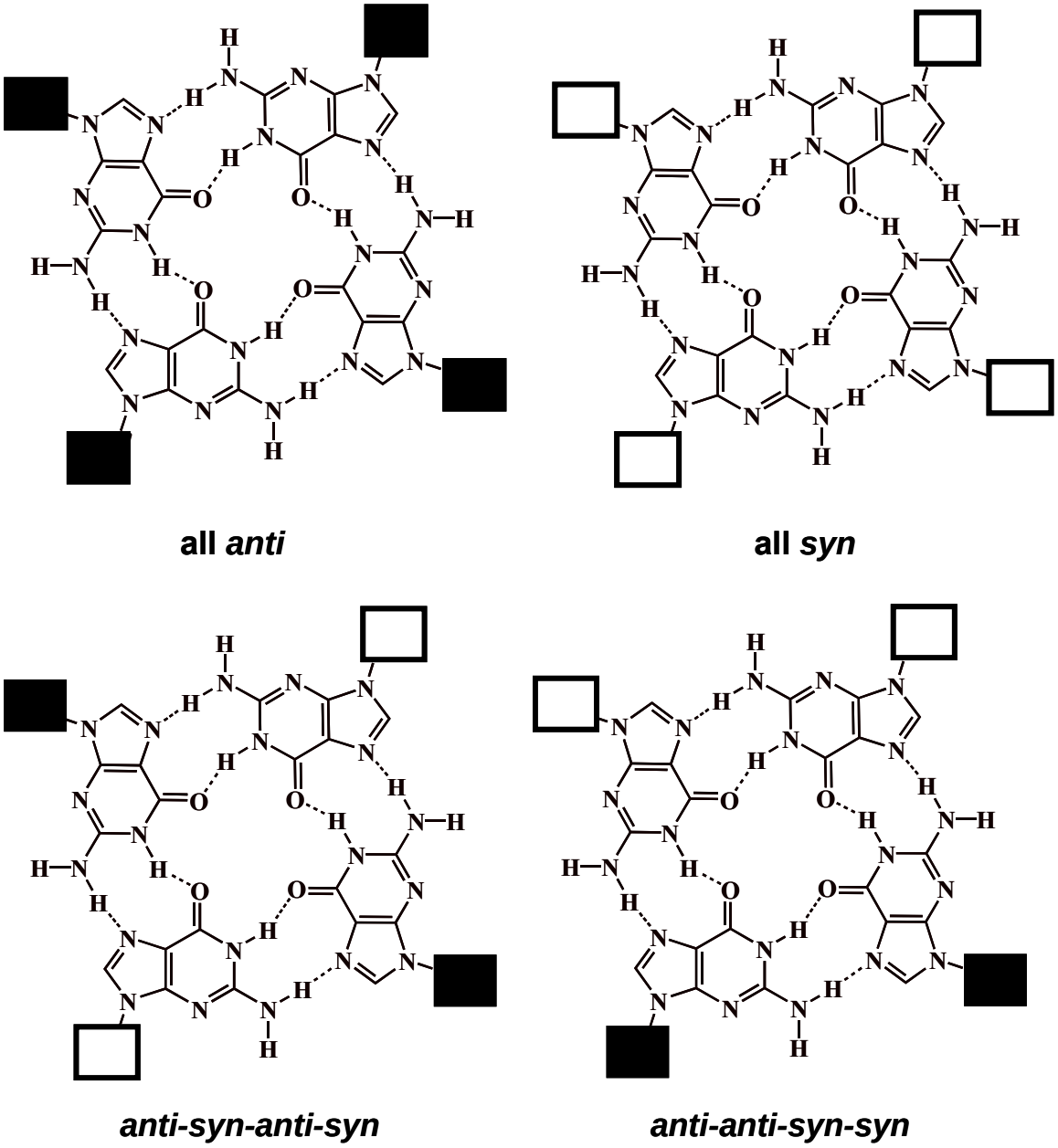

Figure 1.7 Guanine arrangements with possible *anti* (black square) and *syn* (empty square) combinations.

Based on the direction of H-bonds within each G-quartet, a G-quartet has two diastereotopic faces: a "head" (*h*) and a "tail" (*t*) as defined in Figure 1.8. The face is defined by applying the right hand-rule to the arrow pointing from the H-bond donor to H-bond acceptor with the thumb pointing towards the "head" face.[24] This structural element becomes relevant when two G-quartets stack together to give rise to four possible relative orientations: *ht*, *hh*, *tt* and *th*. The stacked G-quartets are typically arranged with a twist angle of 30 - 45^{o} and an interquartet distance of ~ 3.3 Å, to maximize the base π - π overlap and minimize the repulsion between carbonyl oxygens.

G-quartets can further assemble in the presence of metal ions into cylinder type systems such as octamers ($[\mathbf{G}]_8$), dodecamers ($[\mathbf{G}]_{12}$) and hexadecamers ($[\mathbf{G}]_{16}$), which are potential precursors towards high-order supramolecular structures, such as columnar aggregates (Figure 1.9).[25] The extent of G-quartet stacking depends on the nature of the building unit and experimental conditions which will be described in more detail in the following sections.

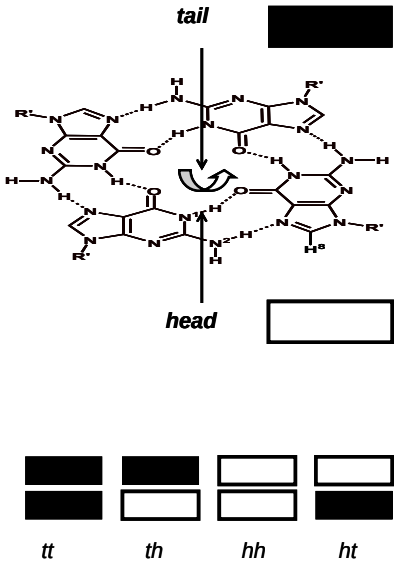

Figure 1.8 G-quartet arrangements with four possible head and tail combinations.

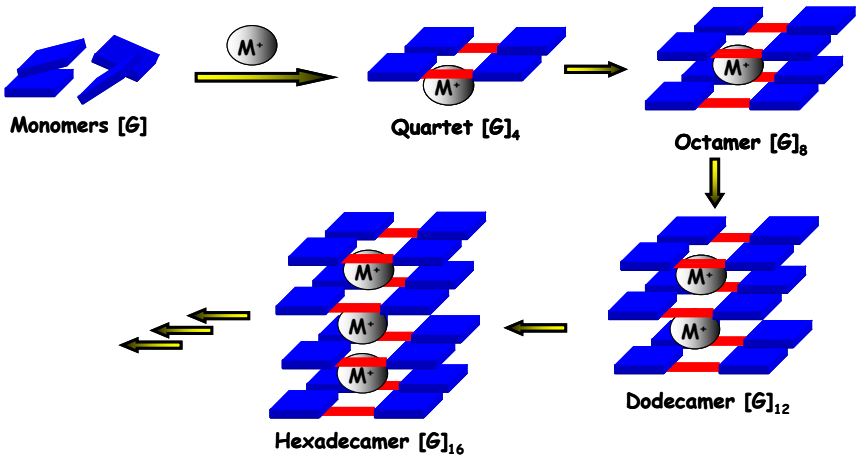

Figure 1.9 Potential G-quartet structures in the presence of metal cations.

1.2.2 Solvent effects on the self-assembly of G-nucleosides

Solvent polarity has been known to have a critical impact on G-nucleoside structures. Solvents with high dielectric constants and potential H-binding sites disrupt H-bonds, while low polarity solvents allow for H-bonding between guanine units to take place. For example, CH_3OH, DMSO, and acetone possess H-bonding sites and can successfully compete with guanine units for H-bonding and in turn impede G-quartet formation. Chlorinated organic solvents are excellent media for studying H-bonding interactions because of their lower polarity; however, they do require the use of lipophilic G-nucleosides derivatives.

The most recent systematic study on the solvent effect was performed by Rodriguez et al.[26], who found that lipophilic guanosine derivatives form $[\mathbf{G}]_8$ in THF-d_8, $[\mathbf{G}]_{12}$ in acetone-d_6, and $[\mathbf{G}]_{16}$ in CD_3CN. The trend was attributed to the solvent dielectric constants, wherein larger assemblies were favoured by more polar solvents, due

to the greater solvation efficiency of the anions. Solvent-induced switching of G-nucleoside self-assembly is a newly discovered phenomenon. Rivera et al.[27] successfully demonstrated a switch from $[\mathbf{G}]_{16}$ to $[\mathbf{G}]_8$ by changing the solvent from CD_3CN to $CDCl_3$.

1.2.3 Metal cation effects on the self-assembly of G-nucleosides

1.2.3.1 Role of monovalent metal ions in the self-assembly

Initially, G-quartet formation was attributed to the presence of alkali metal cations, such as Na^+ and K^+, which may adopt two different binding modes, either in-plane or sandwich-type, as shown in Figure 1.10, depending on the nature of cation. A cation such as Na^+ is capable of residing in-plane, as in several G-q[28] structures; however, it may also exhibit the sandwich-type binding between two G-quartets in extended structures.[29] By contrast, K^+ prefers the sandwich-type binding due to its larger ionic radius (1.3 Å for K^+ versus 0.9 Å for Na^+). An 8-coordinate cation, such as K^+, is surrounded by two G-quartets and forms cation-dipole interactions with O^6 atoms of eight guanosines to give $[\mathbf{G}]_8$. Selectivity for the channel site follows the order: $K^+ > Na^+ \sim Rb^+$, which has been attributed to the ionic radii and the hydration energies of the metal cations.[30] A preference for K^+ over Na^+, for the G-q cavity, is due to a more favourable dehydration energy associated with K^+.

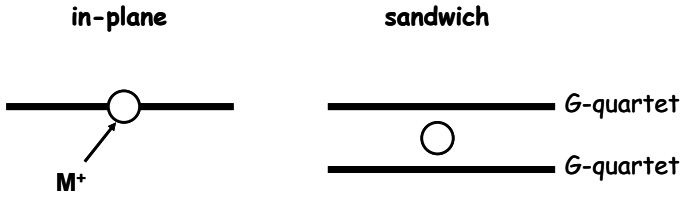

Figure 1.10 Schematic representation of metal cation binding sites.

1.2.3.2 Role of divalent metal ions in the self-assembly

Recently, divalent cations such as Ba^{2+} and Sr^{2+} were shown to promote G-quartet formation as well. In a lipophilic hexadecamer, $[\mathbf{G}]_{16}\bullet 2Ba^{2+}$, each of the divalent cations is sandwiched within individual octamers as depicted in Figure 1.11.[31] In this complex, the charge-charge repulsion between the cations is reduced because the two M^{2+} ions are separated by ~ 6.8 Å. The stability of the aggregate is enhanced by the greater charge density of divalent cations over monovalent ones. In this case, the stronger ion-dipole interactions are at work. The structures based on divalent cations are more stable than those with monovalent ions such as K^+. In addition to Group 2 metal cations, Davis et al.[32] also provided evidence for formation of similar $[\mathbf{G}]_{16}$ based on the complexation with Pb^{2+}.

In addition, divalent cations were also shown to promote stereoselectivity within supramolecular structures. For example, in the presence of Ba^{2+} a homochiral $[\mathbf{G}]_{16}$ is formed from the mixture of D- and L-G-nucleoside as in Figure 1.12, while such chiral sorting was not observed with K^+.[31] A second example involves the use of Ba^{2+} with the mixture of isoguanosine (isoG) and guanosine, to drive self-sorting into specific aggregates.[33]

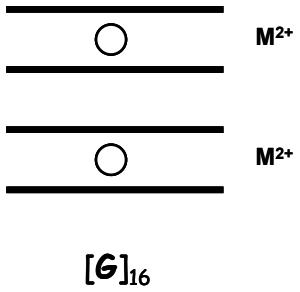

Figure 1.11 Schematic representation of $[\mathbf{G}]_{16}$ with two divalent cations.

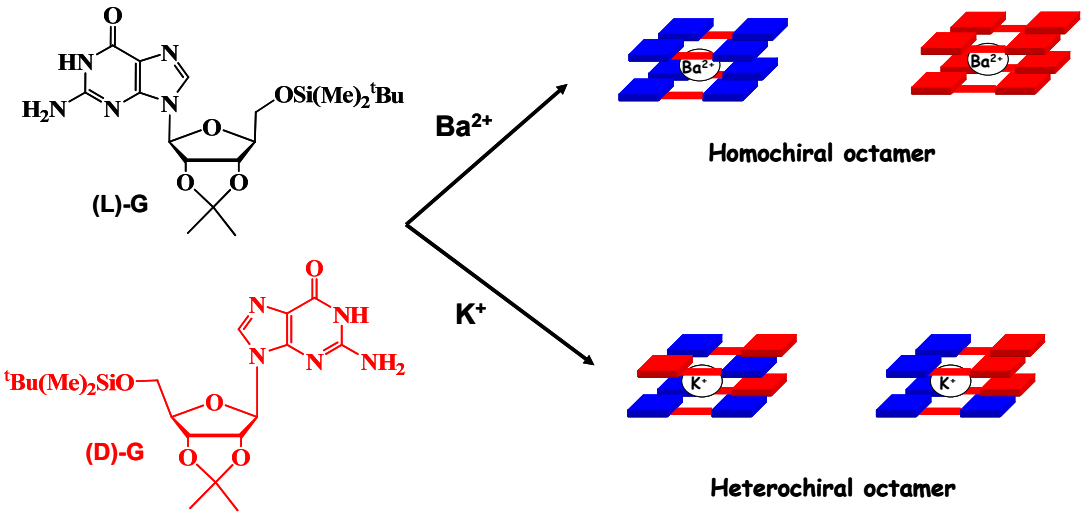

Figure 1.12 Illustration of chiral self-recognition driven by metal ions.[31]

1.2.3.3 Role of trivalent metal ions in the self-assembly

Examples of G-quartet formation in the presence of lanthanides (Ln^{3+}) are rare. One of the first NMR and ESI-MS studies with evidence that Ln^{3+} promotes G-quartet formation was presented by Kwan et al.[34] In this example, $[\mathbf{G}]_{12}$ was formed by *2',3',5'-O*-triacetylguanosine, **TAG**, in the presence of Eu^{3+} and La^{3+} ions, while a mixture of $[\mathbf{G}]_8$ and $[\mathbf{G}]_{12}$ was observed for other cations such as Tb^{3+} and Dy^{3+}. The aggregate size difference in these complexes was ascribed to the ionic radii.

1.2.4 Anion effects on the self-assembly of G-nucleosides

In addition to metal cations, anions may also affect the self-assembly of lipophilic G-nucleosides.[35] Upon G-quartet formation, a cation is usually pulled inside the G-q cavity while an anion is left outside at the periphery of the complex. As a result, the self-association is controlled by the ease of the ion pair separation. The energy required for this process depends on the extent of Coulomb interactions, i.e., the cation-anion distance,

and on the solvation of the dissociated anion. A recent systematic study on the ion-pair effect on the self-assembly of lipophilic G-nucleosides suggests that the solubilization of anion by the solvent guides the formation of extended structures.[36]

H-bonded assemblies can be further stabilized by using a component that interacts with the functional groups on the assembly's exterior. For example, nitro-derivatives of the phenolate anion were found to form bifurcated H-bonds with the N_2H of the inner G-quartets, within $[\mathbf{G}]_{16}$. As shown in Figure 1.13, four [picrate]$^-$ (picrate = 2,4,6-trinitrophenolate) anions (only one is shown for clarity) stabilize the $[\mathbf{G}]_{16}$ structure *via* H-bonds by clipping to the inner G-quartets.[37] Inspired by this secondary interaction, a dipicrate ion was used to promote the self-assembly between hexadecamers.[38] It was found that the extended structures are formed *via* bridging dianions. This example shows that anions can also play an important role in self-assembly of G-nucleosides.[39]

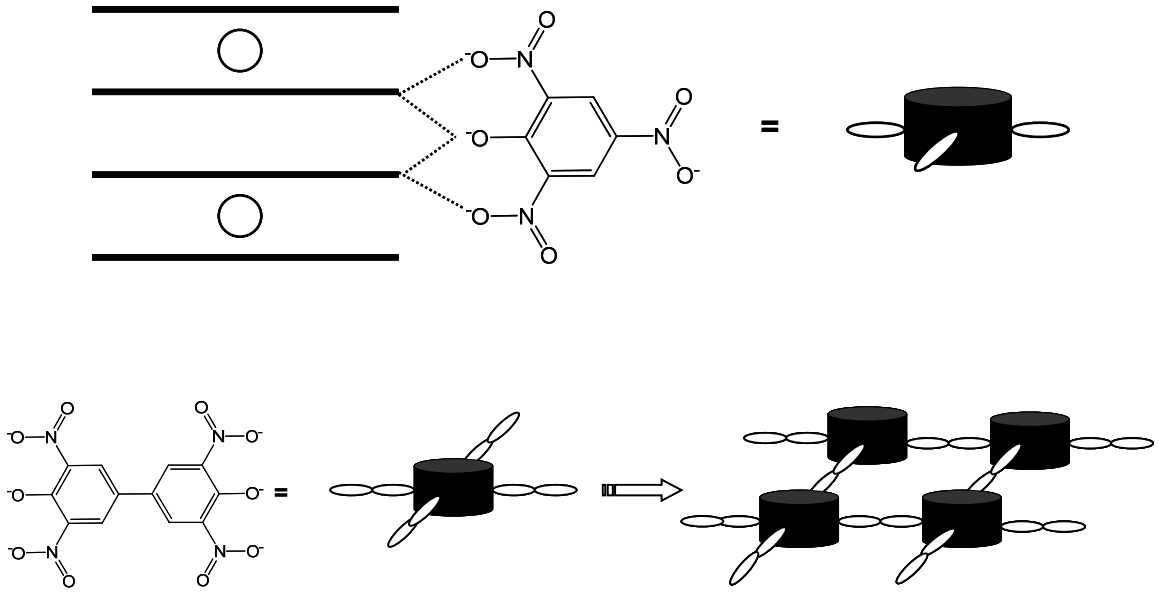

Figure 1.13 Anion binding in $[\mathbf{G}]_{16}$ and extended nano-sheet structures formed by dianion bridges.[38]

1.2.5 Effects of chemical modification on the self assembly of G-nucleosides

Unlike the extrinsic factors discussed above, the effects of chemical modification on self-assembly of G-nucleosides are not clearly understood. Since a G-nucleoside consists of two important functional groups: guanine and (deoxy)ribose moiety, the impact of their chemical modification on the self-assembly will be discussed separately, as they pertain to the G-quartet structure. More detailed discussion on the chemical modification of guanine unit geared towards functionalization of G-nucleosides will be provided in section 1.3.

1.2.5.1 Role of ribose modification in the self-assembly

Even though a general study of the effects of ribose substitution on G-nucleosides self-assembly has not been reported previously, several isolated studies have indicated that the ribose group has two effects on the self-assembly: steric and electronic. Recently, efforts have been made on using chemical modification of ribose towards development of new structures.[40] For example, olefin metathesis reaction was used to cross-link the hexadecamer subunits together generating a unimolecular G-q as shown in Figure 1.14.[41] Due to its stability, this system was successfully used as a transmembrane cation transporter. Template-assembled synthetic G-quartets (TASQs)[42] depicted in Figure 1.15 were developed by taking advantage of the ease of modification at the ribose ring by introducing cavitand scaffolds, and such pre-organized guanine units were shown to form G-quartet structures.

While earlier investigations on G-nucleoside self-assembly focused on lipophilic analogues, information on H-bonding of hydrophilic G-nucleosides has been rather scarce.[43] Recently, Wu et al.[44] studied the self-assembly of 5'-GMP, in D_2O/H_2O in the

presence of excess Na^+, and found that low fidelity self-assembly gives rise to a mixture of columnar aggregates of indefinite length stacked monomers and dimers. Lehn et al.[45] used a 5'-hydrazide guanosine analogue in reversible G-quartet gel formation for controlled bioactive molecule release. Typically, high total concentrations of ligand and metal ions are required for the self-assembly to take place in a competitive polar solvent, such as D_2O.

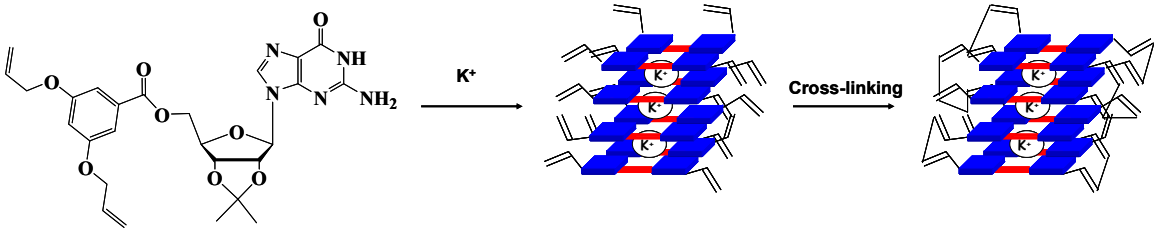

Figure 1.14 The formation and synthesis of covalent G-q.[41]

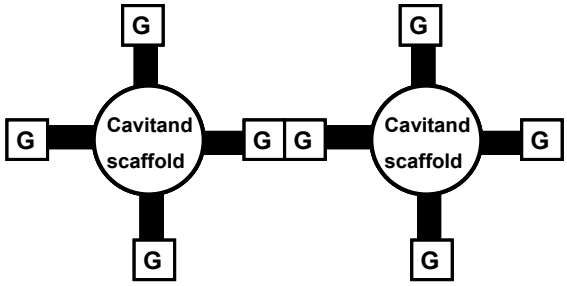

Figure 1.15 Structural representation of TASQs.[42]

1.2.5.2 Role of guanine modification in the self-assembly

Although G-quartet formation from lipophilic G-nucleosides has been extensively investigated, details concerning the impact of guanine modification on self-assembly are less known. Most reports in the literature are concerned with self-assembly of a C^8- or N^2-modified G-nucleoside, or a combination thereof.

Amongst these, C^8-modified G-nucleosides were investigated in greater detail some of which are shown in Figure 1.16. An earlier work by Sessler et al.[46] demonstrated that the C^8-modified G-nucleoside (**1.1**) forms exclusively G-quartets even in the absence of metal ions. This was the first example of the "empty" G-quartet identified by X-ray crystallography and NMR. The term "empty" refers to the formation of G-quartet in the absence of metal ions. They attributed the exclusive "empty" G-quartet formation and stability to the conformationally constrained monomer, wherein the C^8-substituent forces the ribose unit into the *syn* position, further blocking the N^3 site and preventing ribbon formation.

Rivera et al.[47] performed a systematic study of the effects of C^8-substituents on the self-assembly with the focus on the electronic and steric factors. Regardless of the substituent, modification at this site does not impede G-quartet formation, but it does greatly affect the extent of G-quartet stacking. The heterocyclic groups at the C^8-site, as in **1.2,** promote $[\mathbf{G}]_{12}$ formation while arene substituents (**1.3**) promote $[\mathbf{G}]_8$ formation, exclusively. The exact explanation for this observation was not provided by the authors. It can be postulated that the extensive intraquartet interactions between ribose units and C^8-substituent provide steric factors that drive stacking selectivity. Moreover, interquartet π - π stacking interactions between C^8-aryl groups could also contribute to the diastereoselectivity. During their study, they noticed that changing acetyl groups on the ribose unit to glycol ethers induces the switch from $[\mathbf{G}]_8$ to $[\mathbf{G}]_{16}$ for G-nucleosides with identical C^8-groups. The exact reason for such selectivity is still unclear and cannot be attributed solely to interquartet steric interactions. The work on C^8-modified G-nucleosides was recently expanded by Spada et al.[48] who developed radical nitroxyl

guanosine (**1.4**) which was found to display electron spin-spin exchange interactions when self-assembled into a [**G**]$_8$ structure.

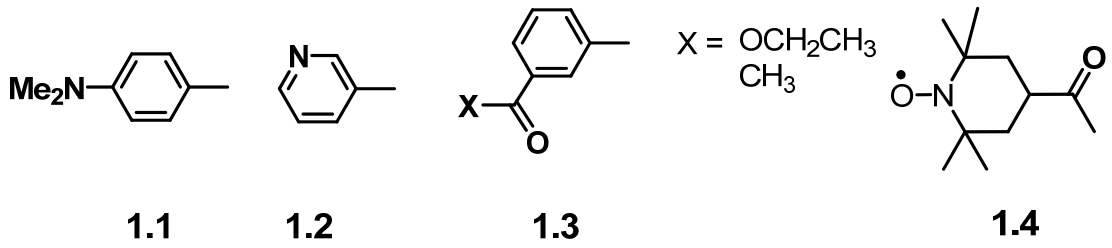

1.1 **1.2** **1.3** **1.4**

Figure 1.16 Structures of C^8-substituents in G-nucleosides.

There are only a few examples in the literature where self-assembly of N^2-modified G-nucleosides is studied. An earlier work on N^2-methyl-dG, incorporated into oligonucleotides, was used to probe the effects of chemical modification on the stability of G-q, and it was discovered that such a simple modification greatly stabilizes G-q structure.[49] Recently, self-assembly of N^2-modified guanosine (**N^{2}G)** containing a 4-n-butylphenyl group, (**nBuGTAG**), depicted in Figure 1.17, was investigated in $CDCl_3$ and CD_2Cl_2 in the presence of metal ions. A detailed NMR study revealed that **nBuGTAG** forms discrete [**G**]$_8$ in solution in the presence of $KClO_4$ and K^+[picrate]$^-$.[50] This octamer was characterized by *th* stacking with all *syn* orientation about the glycosidic bond. A diastereoselectivity observed in this system was ascribed to the presence of a N^2-substituent, however the exact reasons for this effect were unclear. Additional information concerning the self-assembly of this **N^{2}G** molecule in solution, solid-state, or the gas phase is unavailable. However, this study indicated that modification at the N^2-site of guanine does not affect its H-bonding ability; rather it induces stereoselectivity into the self-assembly process. For this reason, it would be interesting to develop

functionalized G-nucleosides, by N^2-modification of guanine, that are capable of self-assembling into discrete structures and at the same time exhibit interesting photophysical and electrochemical properties.

Another interesting example is provided by Davis et al.,[51] who used a combination of C^8- and N^2-modifications of guanine to develop a disubstituted compound **1.5** illustrated in Figure 1.18. This bifunctional molecule forms discrete $[\mathbf{G}]_8$ in solution and the gas phase in the presence of Ba^{2+}. Several other studies describe the effects of C^8- and N^2-substitution on the G-q structure and indicate that the substitution at both sites may have a stabilizing effect on the overall structure.[52] Given the scarcity of the information on the **N^2G** systems, more work needs to be done in order to understand the effect of such guanine modification on its structure and function.

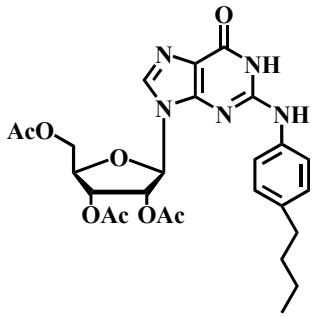

nBuGTAG

Figure 1.17 Structure of **nBuGTAG**.[50]

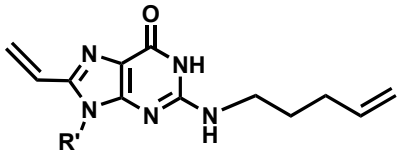

1.5

Figure 1.18 Structure of disubstituted G-nucleoside.[51]

1.3 Synthetic Approaches for G-Nucleoside Modification

Functionalization of G-nucleosides is challenging due to the presence of multiple reaction sites on ribose and guanine. In order to develop functional G-nucleosides with interesting photophysical and electrochemical properties, chemical modification at the guanine ring is desirable. In keeping with the H-bonding requirement for G-quartet and GC base pair formation, direct modification at the C^8- and/or N^2-sites of guanine is required and will be discussed in detail in this section. Despite the synthetic challenges associated with preparation of functionalized G-nucleosides, several synthetic strategies have been developed in the literature. In the following section, these known strategies will be reviewed.

1.3.1 C^8-modification of G-nucleosides

1.3.1.1 C^8-alkynylation

A Sonagashira-Hagihara[53] cross-coupling Pd-Cu catalyzed reaction is used for the coupling of arylhalides with terminal acetylenes. By using a direct alkynylation of unprotected 8-bromoguanosine,[54] syntheses of several fluorescent nucleosides were achieved (Figure 1.19 and Figure 1.20). These C^8-alkynylated G-nucleosides were characterized by the linear π-conjugation which can be finely tuned by altering the electron-donating characteristics of the *para*-substituent on the phenyl ring, and in turn affect the through-bond energy transfer. For example, several C^8-alkynylated guanosines are blue-emitters in the 450 - 510 nm range, stemming from the through-bond energy transfer from the phenyl to the guanine moiety. Sessler et al. used the alkynylation

reaction to introduce porphyrin[55] and zinc-porphyrin[56] groups at the C^8-site of G-nucleosides, to be used in the electron transfer studies via H-bonding (Figure 1.20). In these systems, the electronic communication between the C^8-substituent and the guanine unit has been used to monitor H-bonding at the guanine site. Several other examples where C^8-alkynylated G-nucleosides were used to study of H-bonding in DNA will be discussed in section 1.4. To date, metal ion interactions with fluorescent G-nucleosides have not been investigated.

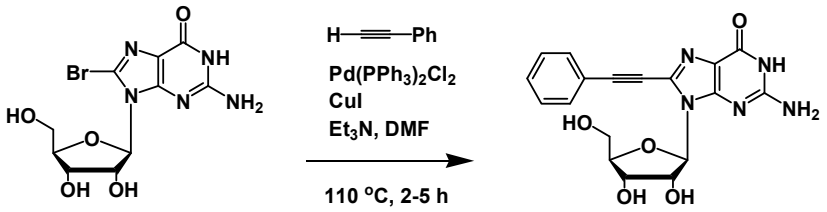

Figure 1.19 C^8-alkynylation of 8-bromoguanosine with terminal acetylene via a Sonagashira-Hagihara coupling reactions.[54]

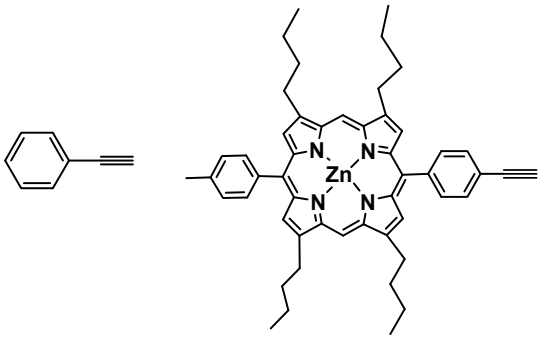

Figure 1.20 Structures of C^8-alkynyl substituents in G-nucleosides introduced via a Sonagashira-Hagihara coupling reaction.

1.3.1.2 C^8-arylation via C-C cross-coupling reactions

In general, the Pd-catalyzed C-C cross-coupling reaction is an important strategy towards synthesis of poly heterocyclic aryls. Suzuki-Miyaura[57] and Stille[58] coupling reactions are widely used for this purpose and they differ only in the intermediate used.

The Suzuki-Miyaura coupling reaction is characterized by the use of organoboronic acid while the Stille reaction involves the use of organotin intermediates. Several examples on the use of such C-C cross coupling strategies for the synthesis of C^8-arylated G-nucleosides exist. A few representative examples of such reactions are presented here.

Perhaps the most impressive work on a direct C-C coupling of G-nucleosides was performed by Shaughnessy et al. who successfully used Suzuki-Miyaura cross-coupling reactions in the synthesis of several C^8-modified G-nucleosides.[59] Here, the standard reactions using 8-halopurine and arylboronic acid were performed with a water-soluble Pd-catalyst and phosphine ligands in a homogeneous reaction as shown in Figure 1.21. The modification of the G-nucleoside is specifically achieved by the use of Suzuki-Miyaura coupling of unprotected 8-bromo(deoxy)guanosine with various phenylboronic acids in aqueous solution. The authors noted, however, that this methodology has limitations especially when the substrate is (deoxy)guanosine. The poor reactivity of 8-bromo(deoxy)guanosine was attributed to the competitive coordination of palladium to guanine via N^7- site under basic conditions. Another drawback of this methodology is that the aqueous-phase Suzuki-Miyaura coupling reaction cannot tolerate aqueous-base labile functional groups.

A second synthetic approach towards C-C cross coupling is Stille coupling reaction between protected halo(deoxy)guanosines and arylstannanes (Figure 1.22).[60] This method is not a direct cross-coupling reaction since the protection of ribose is necessary prior to synthesis. Despite this drawback, it has been successfully used for chemical modification of G-nucleosides and several representative examples are shown in Figure 1.23.

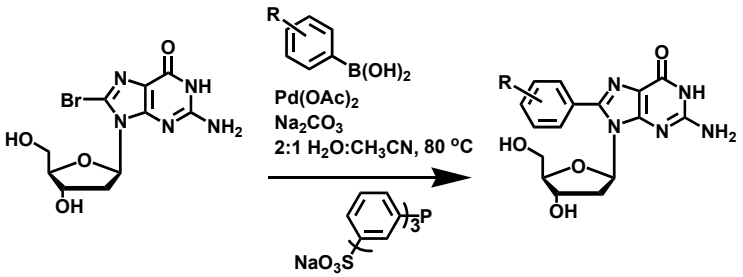

Figure 1.21 C^8-arylation of 8-bromodeoxyguanosine via a Suzuki-Miyaura coupling reaction.[59]

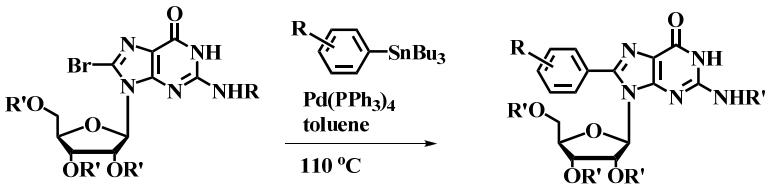

Figure 1.22 C^8-arylation of protected 8-bromoguanosines via a Stille cross-coupling reaction.[60]

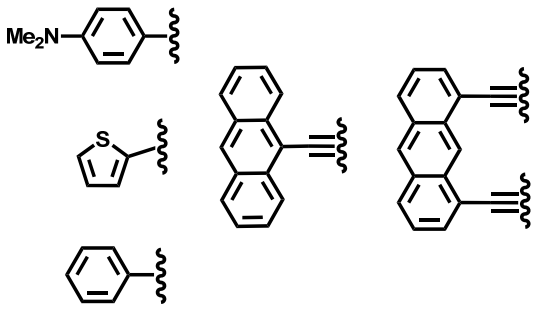

Figure 1.23 Structures of C^8-substituents in G-nucleosides introduced via a Stille cross-coupling reactions.

1.3.1.3 C^8-arylation via C-N cross-coupling reactions

A common C-N cross-coupling methodology is the Pd-catalyzed Buchwald-Hartwig[61] cross-coupling reaction between arylhalides and amines. This synthetic approach provides easy access to a number of desired N-arylated G-nucleosides in high yields, and it has been widely employed in synthesis of C^8-arylamino G-nucleosides. Two common reactions for the C^8-arylamination of G-nucleosides exist. The first synthetic

method involves the use of protected 8-bromo-dG and arylamine in the presence of $Pd_2(dba)_3$ (dba = dibenzylideneacetone) and 2,2'-bis(diphenylphosphino)-1,1'-binaphthyl (BINAP), as shown in Figure 1.24.[62] The second commonly used strategy towards C^8-arylamines is by reacting 8-amino(deoxy)guanosine with arylbromides (Figure 1.25).[63] The latter method requires additional protection at N^2-site in addition to protection of ribose unit and O^6-site. It is noteworthy that the C^8-arylamino G-nucleoside is highly susceptible to hydrolysis under acidic and weakly basic conditions leading to depurination.[64] Hence it is less desirable as a target molecule. Several examples are provided in Figure 1.26.

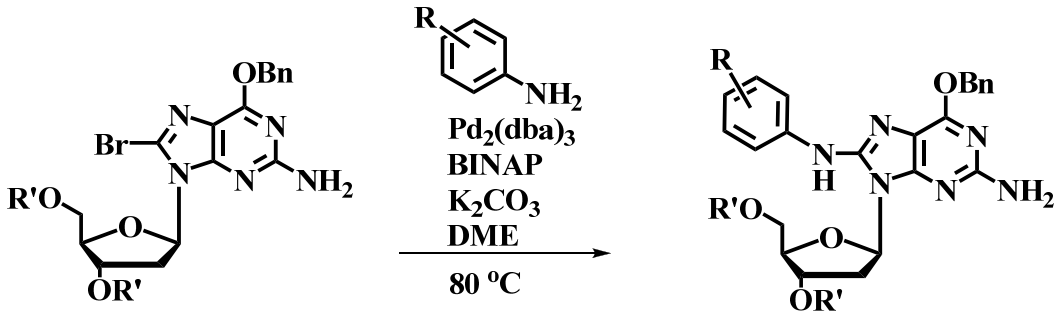

Figure 1.24 C^8-N cross-coupling reaction of protected 8-bromodeoxyguanosine via a Buchwald-Hartwig cross-coupling reactions.[62]

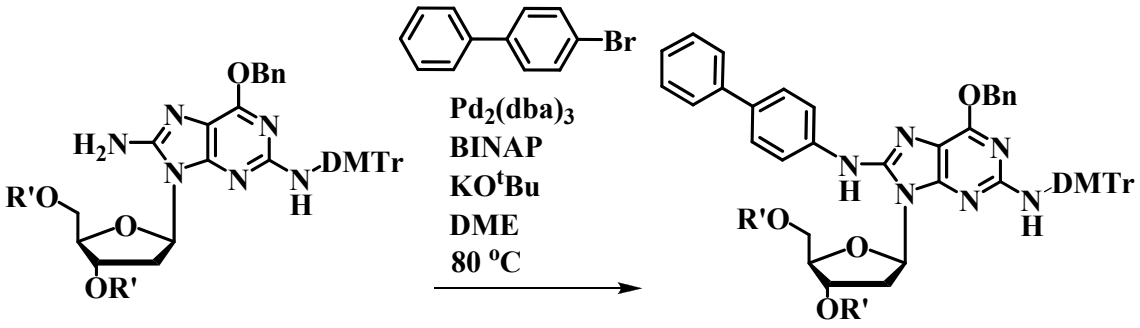

Figure 1.25 C^8-N cross-coupling reaction of protected 8-aminodeoxyguanosine via a Buchwald-Hartwig cross-coupling reactions.[62]

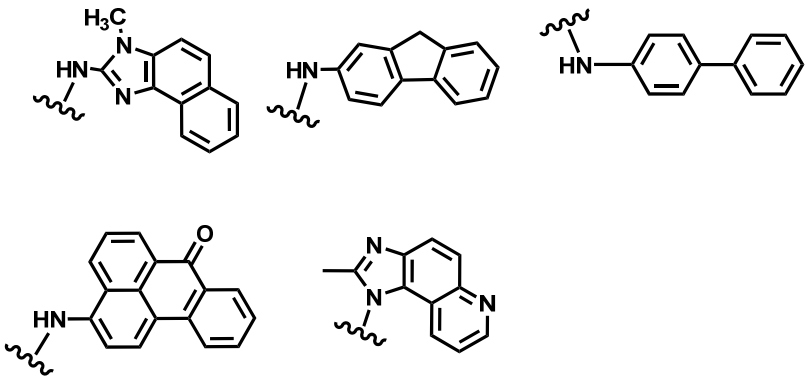

Figure 1.26 Structures of C^8-substituents introduced via Buchwald-Hartwig cross-coupling reactions.

1.3.2 N^2-Arylation of G-nucleosides

Despite the difficulties in synthesis of N^2-modified G-nucleosides, several reports exist in the literature. The C-N cross-coupling via Buchwald-Hartwig Pd-catalyzed N-arylation chemistry has also found great success toward functionalization at the N^2-site of G-nucleosides. The synthesis employs a standard coupling reaction between protected G-nucleoside and arylhalides as in Figure 1.27.[65] While this synthesis gives excellent yields, the reaction requires protection of the (deoxy)ribose group and the O^6-site.[66] The protection of the O^6-site is necessary since the N_1H is acidic (pKa ~ 9) and could potentially interfere with arylation. This strategy was also used to synthesize a diguanosine cross-linked adduct shown in Figure 1.28 and several other interesting molecules illustrated in Figure 1.29.[67] The use of arylhalides with protected G-nucleoside gives high yields when the aryl moieties are electron-deficient.

This methodology quickly triggered more efforts toward direct C-N cross-coupling of G-nucleosides. Syntheses of various N^2-arylated G-guanosine compounds via direct cross-coupling are known to be very challenging. By modifying Buchwald-Hartwig

methodology, a direct N^2-arylation of dG was achieved by Wakabayashi et al. who used $Pd_2(dba)_3$, BINAP or 4,5-bis(diphenylphosphino)-9,9-dimethylxanthene (xantphos) ligand, in the presence of a base for the reaction between aryliodide and unprotected dG in DMSO.[68] This method depends on the type of phosphine ligand used, making a direct N^2-modification more challenging. Interestingly, the Cu-catalyzed Ullmann condensation cross-coupling reaction, which is typically performed with arylhalides and arylamines, has found little use in N^2-modification. One recent example on use of Ullmann condensation for N^2-modification of G-nucleosides was demonstrated with O^6-benzyl-dG compound;[69] however O^6-protection was still required for the coupling to take place.

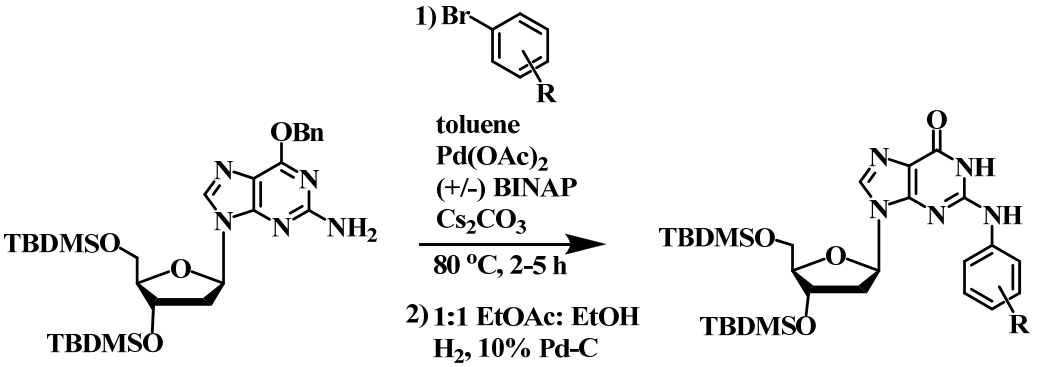

Figure 1.27 C-N cross-coupling of protected G-nucleoside via a Buchwald-Hartwig cross-coupling reaction.

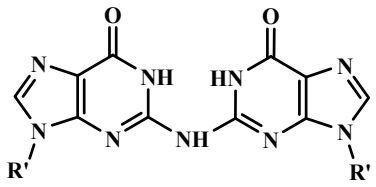

Figure 1.28 Structural representation of the diguanosine adduct formed via a Buchwald-Hartwig cross-coupling reaction.

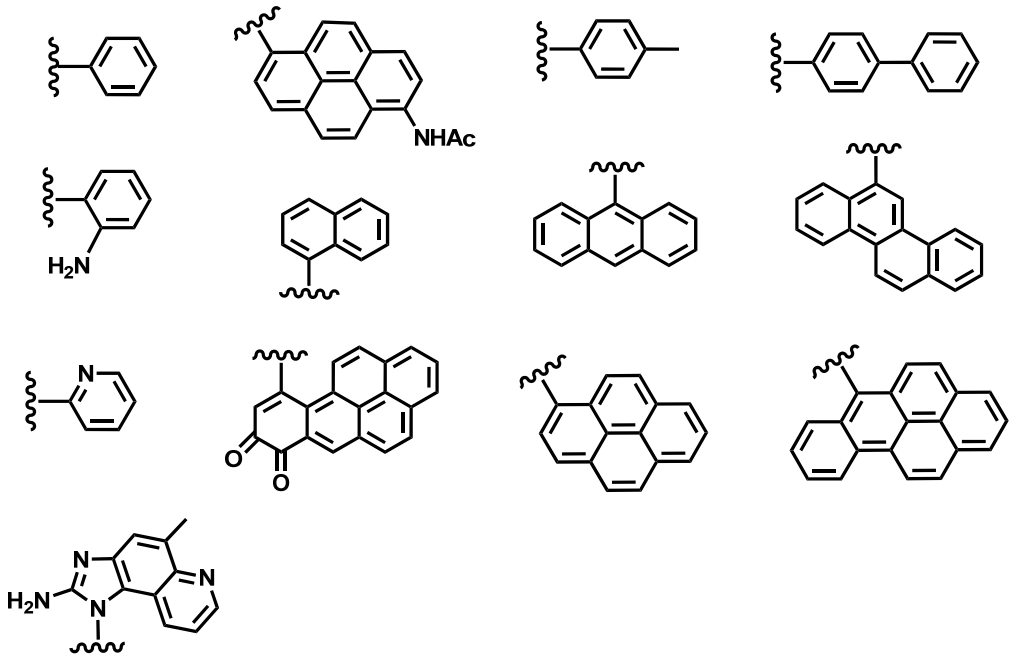

Figure 1.29 Structural representation of N^2-substituents in G-nucleosides introduced via Buchwald-Hartwig cross-coupling reactions.

1.4 Characterization Methods in G-Quartet Structure Determination

1.4.1 X-ray crystallography

X-ray crystallography is an ideal tool for structure determination in the solid-state. By using fiber X-ray diffraction, the G-quartet motif formed by 5'-GMP and 3'-GMP was first identified several decades ago.[70] More recently, single crystal X-ray crystallography was used for structural elucidation of G-q.[71] This method was also applied in the study of lipophilic G-nucleosides. Davis et al.[72] solved a number of crystal structures of G-quartet aggregates, such as $[\mathbf{G}]_{16}$, formed by *5'-O*-silyl-*2'3'-O*-isopropylideneguanosines in the presence of K^+[picrate]$^-$. Crystallographic analysis provides valuable insight into the location of metal ions, ribose conformation and overall structure.

1.4.2 NMR spectroscopy

Nuclear magnetic resonance (NMR) spectroscopy[73] is a useful technique for both structural elucidation and study of the dynamic properties of G-nucleoside supramolecular architectures. A combination of 1D NMR (for example ^{1}H, ^{13}C, ^{15}N and ^{31}P) with 2D NMR methods can be a powerful tool for studing self-assembly of G-nucleosides.

Correlation spectroscopy (COSY) NMR is a 2D NMR method that provides correlations between protons through scalar spin-spin couplings in order to establish connectivities within the molecule. It provides a way of mapping out the specific species within a complex spectrum.

Nuclear Overhauser effect spectroscopy (NOESY) is a technique that provides information on internuclear distances, which in turn can be used to establish molecular conformation. It is based on the dipolar interactions between protons, and the extent of the through-space interaction is inversely proportional to the 6^{th} power of the internuclear distance between the nuclei of interest. For example, NOESY experiments can provide the proof of G-quartet structure, if the NOE interaction between H_8 of one guanine and N_2H of neighboring guanine within the G-quartet can be observed. Moreover, the ribose conformation and ribose puckering can also be identified by using NOE interactions.

Rotating frame Overhauser effect spectroscopy (ROESY) monitors the through space interactions between nuclei and provides information in terms of NOE interactions and detects chemical and conformational exchange. Hence, it is useful for the study of dynamic systems.

Diffusion-ordered spectroscopy (DOSY) is a technique which associates the diffusion constant (D_t) values with the molecular size and hence it can be effectively used to differentiate between the species present in the solution. Because DOSY provides direct information about the molecular size it has been widely used to determine the size of G-nucleoside aggregates.[74] The technique involves monitoring the decay of the NMR signals as a function of gradient pulse, which occurs at the rate proportional to the diffusion coefficient of the given molecule. According to the Stokes-Einstein equation (k = Boltzmann constant, T = temperature, R = hydrodynamic radius and η = solvent viscosity), a sphere's diffusion coefficient is inversely proportional to its hydrodynamic radius (R) (eq 1.1).

$$D_t = \frac{kT}{6\pi\eta R} \qquad (1.1)$$

In addition to solution NMR studies, solid-state NMR is a useful method for the study of metal ions to gain more insights into the formation and stabilization of G-quartet structures. The Wu group has demonstrated the usefulness of this methodology for the direct detection of surface and channel metal ions in G-q and 5'-GMP.[75]

1.4.3 Circular dichroism (CD) spectroscopy

1.4.3.1 Basic principles of CD spectroscopy and representative examples

Circular dichroism (CD) is an analytical method for the study of conformational and configurational analysis of chiral molecules.[76] The principle of CD uses interaction of the sample with left and right circularly polarized light beams for determination of the degree of the difference in absorptivity between the two (eq 1.2):[77]

$$CD = A^l - A^r \qquad (1.2)$$

While CD is typically expressed in mdeg (θ), the concentration effect can be used through the Lambert and Beer Law in order to define molar ellipticity, [θ], where c is the concentration and b is the path length, as in eq 1.3:

$$\Delta\varepsilon = \varepsilon^{l} - \varepsilon^{r} = CD/cb \qquad (1.3)$$

In supramolecular chemistry, the induced CD (ICD) can be produced by formation of a host-guest complex by several scenarii: a) a chiral guest and an achiral host, b) an achiral chromophore binding to a biopolymer, c) the coupling between several guests bound to a macromolecular host, and d) a non-chromophoric ligand coordinating to a metal-ion promoting *d*- or *f*-type transitions.

Examples of CD use for sensing purposes include bis-porphyrin tweezers for detecting chiral amines and alcohols.[78] In these systems, the induced bisignate CD band is due to porphyrin-porphyrin exciton coupling, upon complexation with chiral guest molecule, and the overall sign is directly related to the stereochemistry of the guest.

Another useful example of CD applications is in the study of cyclodextrins. Cyclodextrins are chiral but CD-silent above 200 nm. Inclusion of a chromophoric achiral guest results in the amplification of the CD signal related to the absorbance of the guest molecule.[79] The overall sign of the bisignate CD curve is related to the location of the guest within the host cavity, such that when the electric transition dipole of the guest is parallel to cyclodextrin symmetry axis, a positive sign is obtained when guest is inside the cavity. The opposite is true for the electric transition dipole of the guest being perpendicular to the host axis.

Unlike these supramolecular hosts, simple metal complexes have been used to a much lesser extent as reporters of chirality. CD-silent electronic transitions, due to low absorptivity, can be amplified upon coordination of chiral guest molecules, such as diols, diamines and carboxylic acids.[80]

An alternative to CD is the fluorescence detected circular dichroism (FDCD) method, which takes advantage of the fluorescence and chirality of the molecules.[81] This recently developed technique measures differential emission of light from the sample excited with left circularly polarized and right circularly polarized radiation. The working assumption is that the amount of light emitted depends exclusively on the amount absorbed. This methodology has not been previously applied to the study of luminescent G-nucleosides or luminescent G-quartet structures.

1.4.3.2 CD study of G-quartet formation

In terms of G-quartet structure determination, CD spectroscopy is extremely useful since it can be used to establish G-quartet stacking and handedness of the supramolecular structure.[82] The ribose moieties are chiral and during the self-assembly their chirality is transferred to the supramolecular organization of the G-quartets. The CD signature curve corresponds to the long-axis polarized transition of the guanine chromophores between the stacked G-quartets,[19a] which is described in more detail below.

When two identical chromophores, with non-vanishing electric dipoles, such as guanines are in close proximity, the so-called exciton coupling takes place. The coupling between two equal chromophores leads to splitting of excited states producing the bisignate CD couplet around λ_0 in the absorption spectrum. The sign of the exciton is

related to the absolute sense of the twist of the electric transition moments. Hence, it can be evaluated by looking through the center of the two dipoles of the chromophores. A negative sign is defined when an anticlockwise rotation is used to bring the dipole in the front onto that in the back. That is, the chirality is defined as negative as depicted in Figure 1.30.

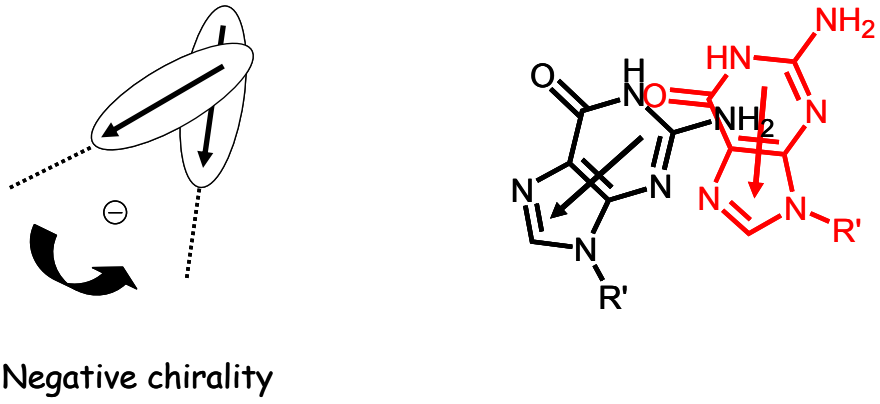

Figure 1.30 Exciton couplet representation of negative chirality between two chirally twisted guanines (solid arrow represents a transition dipole).

1.4.4 Electrospray ionization mass spectrometry (ESI MS)

For the determination of aggregate size and overall stability of supramolecular entities, electrospray ionization mass spectrometry (ESI MS) is typically used. ESI MS is a relatively gentle method to study non-covalent interactions.[83] This technique has been used in the identification of the G-nucleoside complexes and in the probing of their stability.[84]

1.4.5 Basic principles of luminescence

Luminescence spectroscopy is a method to study luminescent molecules which, upon photon absorption, emit light. The excited states are generated in a variety of ways,

including absorption of light energy (photoluminescence) and electrical energy (electroluminescence). Photoexcitation produces a singlet excited state (S_1) which can relax back to the ground state (S_0) in several manners: a) non-radiative decay or b) radiative decay *via* fluorescent emission as illustrated in Figure 1.31. In the event of inter-system crossing (ISC) between a singlet-state S_1 and a triplet-state T_1, the energy can be released either as phosphorescence or non-radiative decay.

Organic aromatic molecules can exhibit both fluorescent and phosphorescent emissions. The latter emission is typically weak due to various quenching processes during the long decay lifetimes (~ seconds); quenching can be greatly enhanced in the presence of a heavy atom. By contrast, several metal complexes exhibit strong phosphorescence due to the heavy atom effect *via* spin-orbit coupling, which effectively causes the mixing of S_1 and T_1 states and promotes a more efficient ISC.[85] In general, the phosphorescent emission from a metal complex depends on the relative energy level of the *d* orbitals of the metal center and the ligands. In the event that the HOMO level is dominated by the contributions from the metal center but the LUMO is localized on the ligands, the phosphorescence can be described as metal-to-ligand charge transfer (MLCT).[86] The opposite arrangement of the HOMO and LUMO levels produces ligand-to-metal charge transfer (LMCT).[87] In addition, when both the HOMO and LUMO are centered on the ligands, the transition is termed a ligand-centered (LC) transition.

The emissions associated with lanthanides are a unique case of phosphorescent emissions. Because of the weak absorption coefficients associated with Ln^{3+}, the phosphorescence is weak and it typically requires the use of an organic chromophore for activation of its emission. In the presence of a strongly absorbing organic chromophore,

energy transfer from T_1 excited state of the ligand is used for the excitation of Ln^{3+} from its ground state to the excited states; subsequently, the relaxation from the excited states of lanthanide (*f**) leads to the emissive decay between two spin-forbidden states and results in Ln^{3+} phosphorescent emission.[88]

Several examples exist in the literature where luminescent and phosphorescent model systems are used to study DNA, RNA, and G-q structure and function. For example, fluorescence resonance energy transfer (FRET) between a donor and acceptor fluorophores, which are covalently attached to the 5' and 3' ends of G-rich strand, is often used to probe G-q structure.[89]

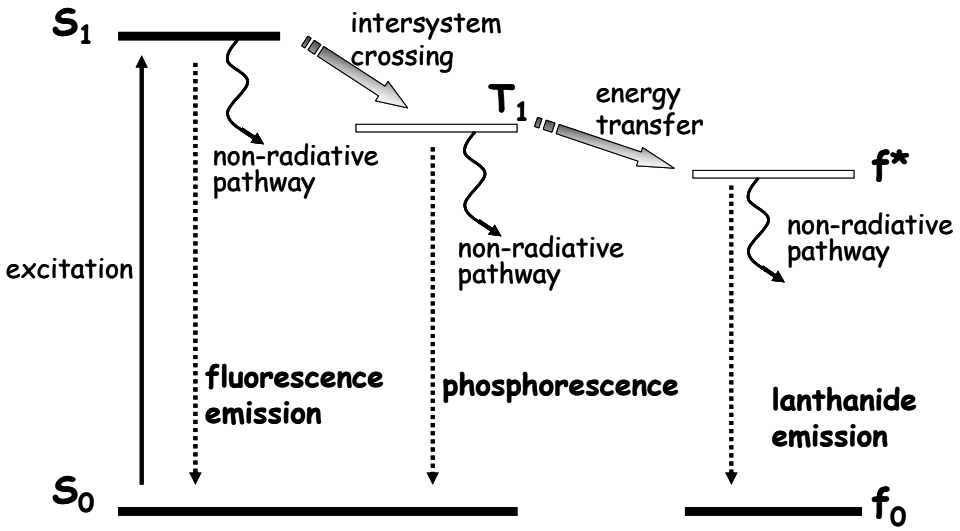

Figure 1.31 Simplified energy diagram of luminescence process.

1.5 Monitoring H-bonding of G-Nucleosides by CD and Fluorescence Spectroscopy

1.5.1 Base pairing

Recently, considerable efforts have been made on the development of functional G-nucleosides for sensing applications. Several elegant examples have been reported for using fluorescent probes in the study of DNA and RNA structure[90] and DNA hybridization.[91] For example, Sonagashira et al. successfully used solvatochromic PRODAN-C^8-alkylated deoxyguanosine (PRODAN = 6-propionyl-2-dimethylaminonaphthalene) (**1.6**) shown in Figure 1.32 to probe the solvent polarity changes upon DNA hybridization.[92] Amongst fluorescent G-nucleosides, 8-azaguanosine (**1.7**)[93] has been commonly used in RNA studies. The major challenge associated with the development of fluorescent G-nucleosides is that luminescence is often compromised upon oligonucleotide incorporation. Hence, fluorescent G-nucleosides with high fluorescent quantum yields are highly desirable for such applications.

Direct monitoring of H-bonding with fluorescent mono-G-nucleosides has only been recently investigated.[94] An interesting approach was demonstrated by Houlton et al. who studied the H-bonding interaction between Os^{2+}-labeled cytosine and Ru^{2+}-labeled guanine as presented in Figure 1.33.[95] The formation of this GC base pair causes phosphorescent quenching of the Ru^{2+} emission but only with low sensitivity due to the use of alkyl linkers. This example demonstrates that phosphorescent G-nucleoside complexes are potentially useful as sensing probes of H-bonding interactions. Highly

sensitive phosphorescent probes could be developed by using conjugated linkers in order to promote efficient communication between guanine and the Ru^{2+} metal center.

In addition to using phosphorescence, fluorescence can also be used to monitor H-bonding interactions. This approach has been extensively explored by Sessler et al.[96] for monitoring GC base pair formation. C^8-Modified guanines and C^5-modified cytosines containing variety of substituents such as zinc-porphyrin, porphyrin, quinine, and fullerene, and a combinations thereof, were used.[97] A representative example developed by Sessler is shown in Figure 1.34. The photo-induced electron transfer (PET) observed in these systems was associated with the quenching of the donor excited state by a given acceptor. The luminescent lifetimes and transient absorption profiles revealed that the triplet-triplet energy-transfer from the guanine base to cytosine was facilitated through H-bonds.

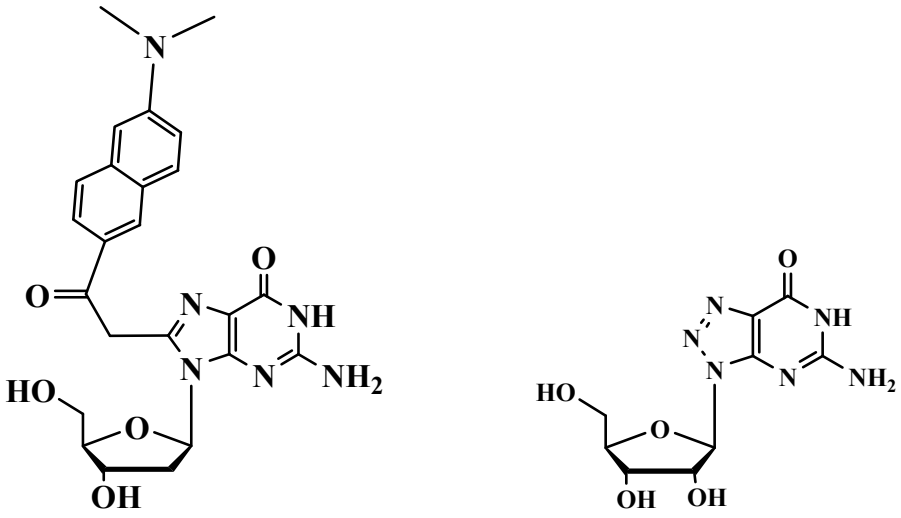

1.6 **1.7**

Figure 1.32 Structures of luminescent G-nucleosides incorporated into oligonucleotides.

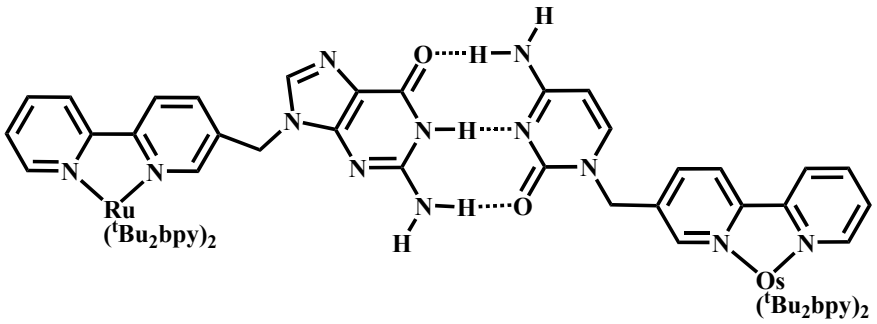

Figure 1.33 Structure of GC base pair prepared by Houlton et al.[95]

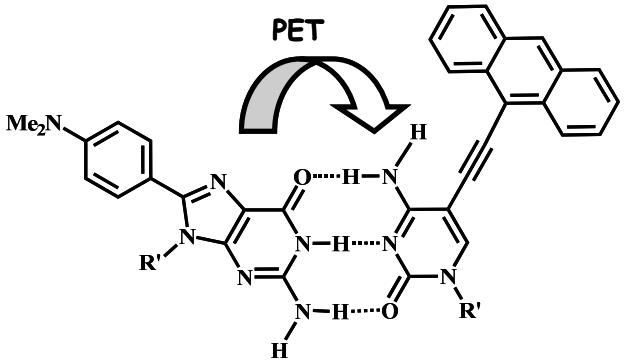

Figure 1.34 Photo-induced electron transfer in the GC base pair developed by Sessler et al.[96]

The PET model systems based on GC ensembles are useful if both nucleosides are properly modified. Addition of an unmodified cytidine to Sessler's systems, results in a fluorescent intensity increase, but only due to the de-aggregation of porphyrin rings rather than due to the energy transfer *via* H-bonding. Another example of studying unmodified cytidine involves the use of N^9-alkylpyrenyl guanine.[98] The addition of cytidine to this fluorescent guanine causes a fluorescent emission quenching with a small association constant. The exact nature of the fluorescent-quenching mechanism in this system remains unclear. To this end, fluorescent G-nucleosides could potentially be used to monitor the GC base pair formation with unmodified cytidine.

1.5.2 Monitoring G-quartet formation

CD has been routinely used to determine G-q conformation. For example, a four-stranded parallel quadruplex forms a right-handed helix with a four-fold symmetry, with all guanosines having an *anti* conformation as shown in Figure 1.35. Hence the CD spectrum of this structure exhibits a positive band at ~ 260 nm and a negative band at ~240 nm.[99] The G-quartets all have the same polarity i.e., *ht* stacking. In contrast, the structure of an antiparallel quadruplex formed by two folded-back strands produce a right-handed helix with alternating *syn* and *anti* ribose conformation. Hence the CD spectrum exhibits a positive band at ~ 295 nm and a negative band at ~ 260 nm. This antiparallel G-q exhibits *ht* and *hh* arrangements of the G-quartets. Davis et al.[72] and Spada et al.[18] have used CD to monitor the self-assembly of lipophilic G-nucleosides. Typically, a negative to positive sequence of the CD band was associated with a counterclockwise rotation around the C_4 symmetry axis from one G-quartet to the next to produce the left-handed stacks. The CD spectrum of G-quartets is characterized by the bisignate doublet originating from the exciton interactions between stacked quartets, such that a negative skew angle between the quartets produces left-handed *th* structure with the negative exciton CD curve centered at ~ 250 nm as presented in Figure 1.36.

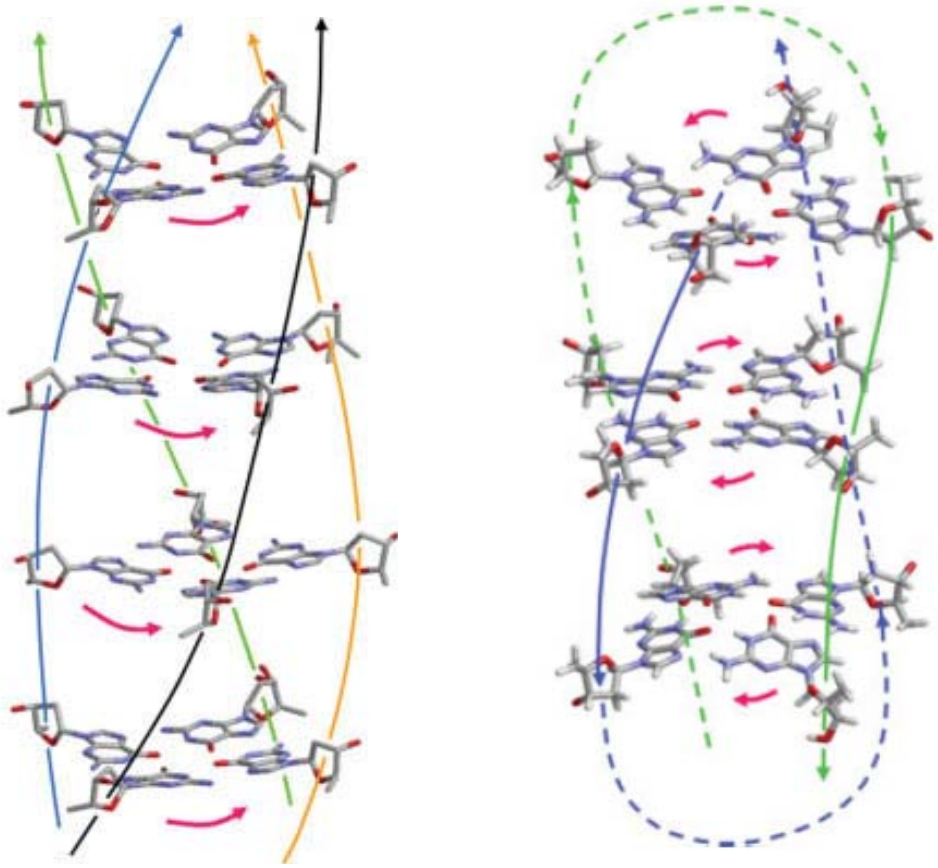

Figure 1.35 Arrangement of the stacked G-quartets between four parallel paired strands (left) and antiparallel strands (right).[99]

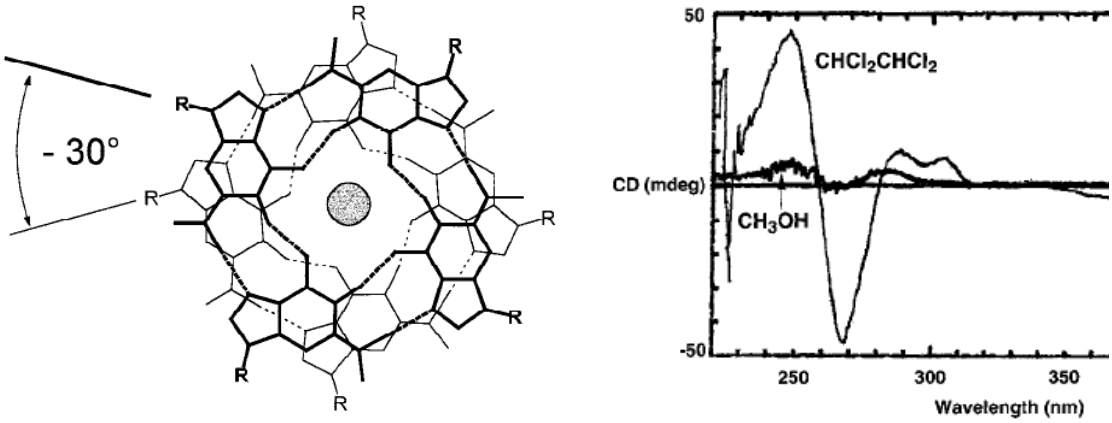

Figure 1.36 Representation of the *ht* left-handed $[\mathbf{G}]_8$ and its typical CD spectrum.[14]

G-q formation has been very well studied by using fluorescent oligonucleotides at the ribose ends in the FRET process.[100] In contrast, an oligonucleotide containing fluorescent G-nucleosides is rare.[101] One example was presented by Okamoto et al., who incorporated C^8-pyrenyl-dG into oligonucleotides in order to monitor structural changes between the three key states: a single-strand, a duplex and a G-q (Figure 1.37).[102] This wonderful example shows that luminescent G-nucleosides have a great potential in biosensing applications. The structural transformation of this sort has not been previously attempted by using discrete structures formed by the lipophilic G-nucleosides. The model systems based on small luminescent G-nucleoside aggregates, such as $[\mathbf{G}]_8$ or $[\mathbf{G}]_{16}$, can render themselves useful in the study of G-quartet-to-GC base pair transformation as will be demonstrated later in this thesis.

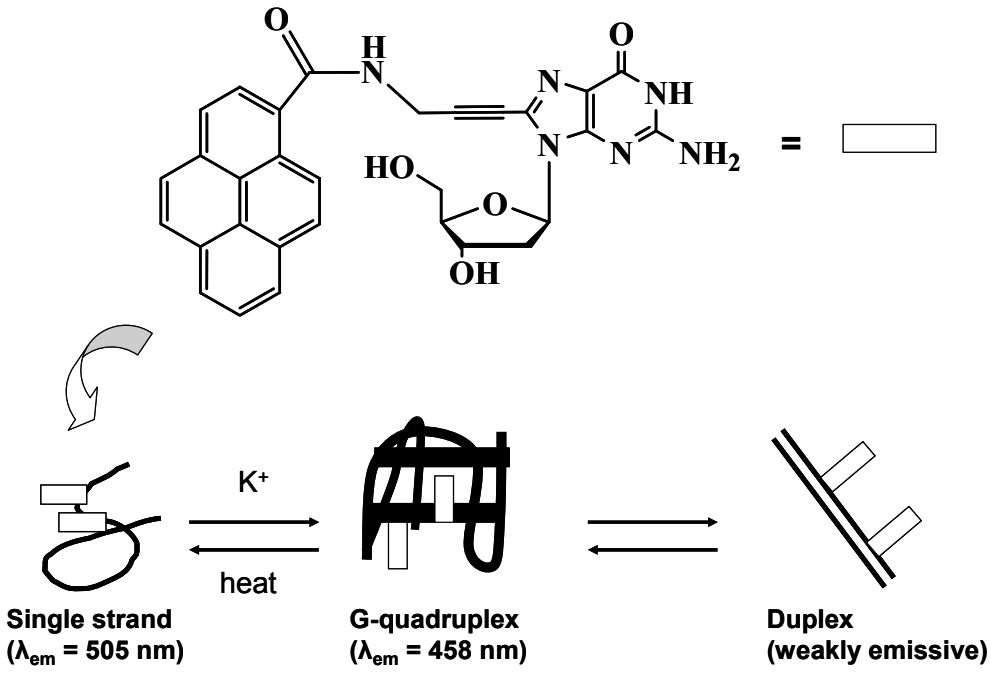

Figure 1.37 Structural representation of fluorescent dG and its use in monitoring ss-to-G-q-to-duplex structural change.[102]

1.6 Metal Ion Interactions with G-Nucleosides

Interactions between metal ions and G-nucleosides play important roles in DNA/RNA chemistry and in their applications.[103] Lippert et al. [104] have done excellent work on the metal ions/guanine interactions with the focus on platinum and palladium chemistry.[105] Other metal complexes containing (di)nucleotide,[106] guanine,[107] and (deoxy)guanosine[108] analogues have been developed as well. Some transition metal complexes are of biological and medical interest and act as anti-cancer[109] and anti-viral[110] agents. Consequently, monitoring or sensing the activity of metal ions using fluorescent G-nucleosides is of current interest. For these reasons, development of DNA-based biosensors for metal ions[111] is a targeted research area. For the purpose of studying metal ion interactions with G-nucleosides, two general approaches have been used. The first involves the use of metal complexes to probe the structure and function of G-nucleosides. Some of the more general examples include the use of Ln^{3+} and polypyridyl Ru^{2+} complexes as efficient DNA and RNA probes. Investigation of their interactions with G-nucleosides and derivatives will be presented in this section. The second approach towards understanding metal ion-G-nucleoside interactions involves the use of luminescent G-nucleosides. The latter approach has an important advantage, the direct monitoring of the structural and functional changes by using guanine unit as the receptor. However, despite their potential applications, fluorescent G-nucleosides have rarely been used for the study of metal ion interactions.

1.6.1 Metal complexes as sensing probes

1.6.1.1 Interactions of Ln^{3+} with G-nucleosides and derivatives

Several Ln^{3+} complexes have been well investigated as sensing probes for DNA[112] and RNA.[113] The efficient sensitization process in DNA and RNA systems was attributed to energy transfer primarily from the guanine base. Because of the site specific activation of Ln^{3+} complexes by guanine, investigation was extended to G-q. The earliest work on interactions of G-q with Tb^{3+} ions proposed that the primary binding sites are the charged phosphate groups and guanine, rather than the quadruplex cavity.[112a] Later on, Galezowska et al.[114] showed by using competitive fluorescence experiments that two types of Tb^{3+} binding events were evident for G-q, i.e., the loop binding and the cavity binding *via* O^6-sites and that only the latter leads to the sensitized emission of Ln^{3+} ions.

Studies of Ln^{3+} with non-functionalized G-nucleosides exist. For example, the Wu group[115] has demonstrated that **TAG** interacts with Ln^{3+} ions by forming G-quartets. The sandwich-type structures $[\mathbf{G}]_{12}$, identified by ESI-MS, are thought to be held together *via* ion-dipole interactions, similar to those observed for Group 1 and 2 metal ions. The signature G-quartet cross peaks were also identified in NOESY NMR spectra of the complexes containing La^{3+} ions. However, very poor Tb^{3+} fluorescence activation was observed in this system. This is not surprising since unmodified G-nucleosides are known to be poor Ln^{3+} activators.[116] Some more recent studies suggest that 5'-GMP and 3'-GMP are effective sensitizers, an ability which was ascribed to the presence of the phosphate group.[117] The most important finding, however, was on the effects of chemical modification of 5'-GMP on Tb^{3+} sensitization. A chemical modification at the N^7-, N^1-, N^2- or C^8-sites of guanine ring has a detrimental effect on Ln^{3+} activation. This is the first

demonstration that the electronic character of guanine and availability of binding sites affect the sensitization of Ln^{3+} emissions. Because of these new findings, it might be advantageous to functionalize G-nucleosides in order to develop metal-ion probes which can act as potential sensitizers of Ln^{3+} emission.

1.6.1.2 Interactions of Ru^{2+} complexes with DNA and RNA

Interactions between octahedral Ru^{2+} complexes with ssDNA or double-stranded (ds) DNA have been investigated extensively. Several Ru^{2+} complexes act as efficient intercalators *via* π - π stacking interactions with the nucleobases and interactions with the grooves.[118] Electrostatic interactions between negatively charged phosphate groups and cationic metal ions or organic ligands are considered to be important. A major or minor groove binding takes place between functional groups in metal complexes or organic ligands with the edge of the base pairs. To increase the binding affinity of Ru^{2+} complexes to DNA, new ligands have been developed with extended planarity or with pendant organic chromophores which are also capable of π - π stacking with nucleobases, thus providing secondary interactions for further stabilization.[119] In some Ru^{2+} complexes, ligand binding to polynucleotides causes an increase in phosphorescent emission and prolongs the excited state lifetimes of the complexes, due to the rigidity of the DNA microenvironment and protection from solvent quenching. This trend, however, is not general since it highly depends on the nature of the ligands in Ru^{2+} complexes.

Octahedral Ru^{2+} complexes may exist in two enantiomeric forms, as shown in Figure 1.38 for $[Ru(bpy)_3]^{2+}$ (bpy = 2,2'-bipyridine) complex.[120] Enantiomeric Ru^{2+} complexes capable of intercalation are interesting DNA probes, since they may become useful in the sequence specific recognition as well as in conformational studies. Barton et

al.[121] found that enantiomers of $[Ru(phen)_3]^{2+}$ (phen = 1,10 phenanthroline) interact with left- and right-handed DNA duplexes differently, exhibiting chiral recognition. This property of Ru^{2+} complexes should be further explored.

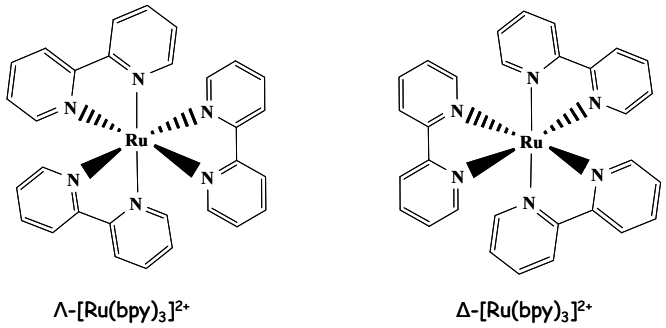

Figure 1.38 Structural representation of $[Ru(bpy)_3]^{2+}$ enantiomers.

1.6.2 Potential sensing probes based on G-nucleosides

More recently, considerable research efforts have been directed to functionalization of G-nucleosides and investigation of their potential in sensing applications. These probes have an advantage because they can form both H-bonds and coordination bonds which can lead to the formation of interesting macromolecules. Luminescent multinuclear transition metal complexes of G-nucleosides are potentially useful as well. For example, phosphorescent Ru^{2+} complexes of G-nucleosides can act as the redox or luminescent reporters towards anions, cations or nucleosides. In addition, Ru^{2+} complexes directly attached to a guanine can promote sequence specific binding and provide greater sensitivity and selectivity. Due to the chiral recognition observed for some Ru^{2+} complexes with DNA, designing optically pure G-nucleoside complexes is of interest for conformational and sequence specific binding studies.

Several examples of Ru^{2+} complexes containing G-nucleosides exist in the literature. Earlier examples include an alkylated guanine complex containing a Ru^{2+} (**1.8**) as depicted in Figure 1.39.[95a] Its poor performance, however, was attributed to the presence of the flexible linker. The recently developed Ru^{2+} complex **1.9**[122] was found to be more useful as a sensing probe for quantitative detection of Ru^{2+} incorporation into oligonucleotides, even in the presence of other fluorescent nucleotides. The properties of Ru^{2+} complexes with G-nucleosides depend on several factors, including the position of the conjugate linkage on nucleoside, the nature of the spacer, and the location of the linker on the supporting bpy ligand.

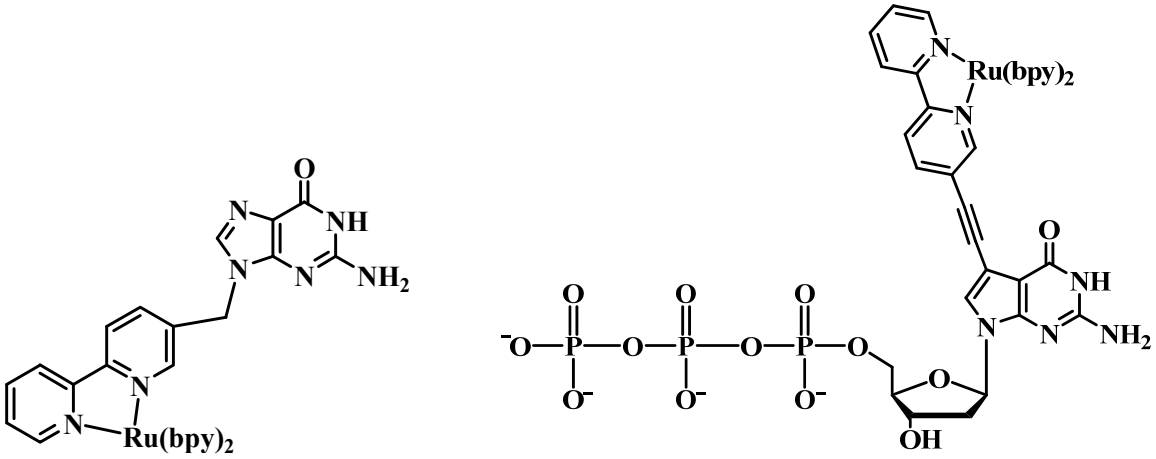

1.8 **1.9**

Figure 1.39 Structures of Ru^{2+} complexes of G-nucleosides.[95a, 122]

1.7 Scope of the Thesis

Because guanosine is an ideal building block in supramolecular chemistry, functionalized guanosines may offer a handle towards high fidelity self-assembly with desirable photophysical and electrochemical responses. This thesis is inspired by the possibilities surrounding functionalized guanosines and their sensing applications. The aim of the thesis is to synthesize new guanosine derivatives that are multifaceted and exhibit stereoselective self-assembly, luminescence, and a chelating ability for metal ion binding.

The rest of the thesis is organized as follows. Chapter 2 reports on synthesis of new luminescent **N^{2}Gs**, containing fluorescent chelating and non-chelating ligands, and their photophysical properties. Self-assembly of these new fluorescent **N^{2}Gs**, in solution and the gas phase, is presented in Chapters 3 and 4, respectively. The kinetics and thermodynamics for the monomer-to-octamer dynamic process of **N^{2}Gs** are investigated. A fluorescence and NMR study of Watson-Crick base pairing involving **N^{2}Gs** is described in Chapter 5. G-octamer-to-GC base pair structural transformation has also been studied by these methods. The interactions of chelating **N^{2}Gs** with Group 12 metal ions are explored in Chapter 6 with the focus on Zn^{2+} ion sensing. Fluorescence, CD and NMR spectroscopies were used in the investigation of the metal-ion interactions with functionalized guanosines. Chapter 7 presents our study on the interactions of Ln^{3+} ions with new **N^{2}Gs** and the development of phosphorescent Ru^{2+} complexes of **N^{2}G**. The conclusions and proposed future work are provided in Chapter 8.

1.8 References

[1] Lehn, J.M. *Chem. Soc. Rev.* **2007**, *36*, 151.

[2] (a) Jeffrey, G. A.; Seanger, W. *Hydrogen Bonding in Biological Structures*; Springer: Berlin, 1991. (b) Mingos, D. M. P. *Supramolecular Assembly via Hydrogen Bonds*; Springer: New York, 2004.

[3] Watson, J. D.; Crick, F. H. *Nature* **1953**, *171*, 737.

[4] (a) Luu, N. K.; Phan, A. T.; Kuryavyi, V.; Lacroix, L.; Patel, D. J. *J. Am. Chem. Soc.* **2006**, *128*, 9963. (b) Blackburn, E. H. *Cell* **1994**, *77*, 621. (c) Zakian, V. A. *Science* **1995**, *270*, 1601.

[5] (a) Neidle, S.; Balasubramanian, S. *Quadruplex Nucleic Acids*; RCS Publishing: Cambridge, 2006. (b) Xu, Y.; Suzuki, Y.; Komiyama, M. *Angew. Chem. Int. Ed.* **2009**, *48*, 3281. (c) Balasubramanian, S.; Neidle, S. *Curr. Opin. Chem. Biol.* **2009**, *13*, 345.

[6] (a) Guschlbauer, W.; Chantot, J. F.; Thiele, D. J. *Biomol. Struct.* **1990**, *8*, 491. (b) Gilbert, D. E.; Feigon, J. *Curr. Opin. Struc. Biol.* **1999**, *9*, 305. (c) Arthanari, H.; Bolton, P. H. *Chem. Biol.* **2001**, *8*, 221.

[7] Shin, Y. K.; Wierzba, K.; Matsuo, K.I.; Ohtani, T.; Yamada, Y.; Furihata, K.; Hayakawa, Y.; Seto, H. *J. Am. Chem. Soc.* **2001**, *123*, 1262.

[8] (a) Gavathios, E.; Heald, R. A.; Stevens, M. F. G.; Searle, M. S. *Angew. Chem. Int. Ed.* **2001**, *113*, 4885. (b) Guo, Q.; Lu, M.; Marky, L. A.; Kallenbach, N. R. *Biochemistry* **1992**, *31*, 2451. (c) Sun, D. Y.; Thompson, B.; Cathers, B. E.; Salzar, M.; Kerwin, S. M.; Trent, J. O.; Jenkins, T. C.; Neidle, S.; Hurley. L. H. *J. Med. Chem.* **1997**, *40*, 2113. (d) Clark, G. R.; Pytel, P. D.; Squire, C. J.; Neidle, S. *J. Am. Chem. Soc.* **2003**, *125*, 4066. (e)

Shin, Y. K.; Wierzba, K.; Matsuo, K.; Ohtani, T.; Yamada, Y.; Furihata, K.; Hayakawa, Y.; Seto, H. *J. Am. Chem. Soc.* **2001**, *124*, 2098. (f) Andrisano, V.; Gottarelli, G.; Masiero, S.; Heijne, E. H.; Pieraccini, S.; Spada, G. P. *Angew. Chem. Int. Ed.* **1999**, *38*, 2386. (g) Calzolari, A.; Di Felice, R; Molinari, E.; Garbesi, A. *J. Phys. Chem. B* **2004**, *108*, 2509. (h) Kotlyar, A. B.; Borovok, N.; Molotsky, T.; Cohen, H.; Shapir, E.; Porath, D. *Adv. Mater.* **2005,** *17*, 1901. (i) Keniry, M. A. *Biopolymers* **2001**, *56*, 123.

[9] Ma, L.; Harrell, A. W.; Davis, J. T. *Org. Lett.* **2009**, *11*, 2599.

[10] (a) Kostrikis, L. G.; Tyagi. S.; Mhlanga, M. M.; Ho, D. D.; Kramer, F. R. *Science* **1998,** *279*, 1228. (b) Sakamoto, K.; Gouzu, H.; Komiya, K.; Kiga, D.; Yokoyama, S.; Yokomori, T.; Hagiya, M. *Science* **2000**, *288*, 1223. (c) Smith, E. A.; Kyo, M.; Kumasawa, H.; Nakatani, K.; Saito, I.; Corn, R. M. *J. Am. Chem. Soc.* **2002**, *124*, 6810. (d) Davis, J. T.; Spada, G. P. *Chem. Soc. Rev.* **2007**, *36*, 296.

[11] (a) Sidorov, V.; Kotch, F. W.; El-Kouedi, M.; Davis, J. T. *Chem. Commun.* **2000**, 2369. (b) Van Leeuwen, F. W. B.; Davis, J. T.; Verboom, W.; Reinhoudt, D. N. *Inorg. Chim. Acta* **2006**, *359*, 1779.

[12] Van Leeuwan, F. W. B.; Verboom, W.; Shi, X.; Davis, J. T.; Reinhoudt, D. N. *J. Am. Chem. Soc*. **2004**, *126*, 16575.

[13] (a) Kotia, R. B.; Li, J. L.; McGowan, L. B. *Anal. Chem.* **2000**, *72*, 827. (b) Ueyama, J. L.; Takagi, M.; Takenaka, S. *J. Am. Chem. Soc.* **2002**, *124*, 14286.

[14] (a) Fahlman, R. P.; Sen, D. *J. Mol. Biol.* **1998,** *280*, 237. (b) Alberti, P.; Bourdoncle, A.; Sacca, B.; Lacroix, L.; Mergny, J. L. *Org. Biomol. Chem.* **2006**, *4*, 3383.

[15] (a) Felice, R. D.; Calzolari, A.; Molinari, E.; Garbesi, A. *Phys. Rev. B* **2001**, *65*, 1. (b) Marsh, T. C.; Henderson, E. *Biochemistry* **1994**, *33*, 10718.

[16] Song, H.; Kraatz, H. B. *Inorg. Chim. Acta* **2009**, *362*, 1365.

[17] Wu, G.; Kwan, I. C. M. *J. Am. Chem. Soc.* **2009**, *131*, 3180.

[18] (a) Gottarelli, G.; Spada, G. P. *Chem. Rec*. **2004**, *4*, 39. (b) Sivakova, S.; Rowan, S. J. *Chem. Soc. Rev*. **2005**, *34*, 9. (c) Gottarelli, G.; Masiero, S.; Mezzina, E.; Pieraccini, S.; Rabe, J. P.; Samori, P.; Spada, G. P. *Chem. Eur. J*. **2000**, *6*, 3242. (d) Pieraccini, S.; Masiero, S.; Pandoli, O.; Samori, P.; Spada, G. P. *Org. Lett.* **2006**, *8*, 3125.

[19] (a) Gottarelli, G.; Masiero, S.; Mezzina, E.; Spada, G. P.; Mariani, P.; Racanatini, M. *Helv. Chim. Acta.* **1998**, *81*, 2078. (b) Kato, T. *Science* **2002,** *295*, 2414. (c) Pieraccini, S.; Gottarelli, G.; Mariani, P.; Masiero, S.; Saturini, L.; Spada, G. P. *Chirality* **2001**, *13*, 7. (d) Rinaldi, R.; Maruccio, G.; Biasco, A.; Arima, V.; Cingolani, R.; Giorgi, T.; Masiero, S.; Spada, P. G.; Gottarelli, G. *Nanotechnology* **2002**, *13*, 398. (e) Maruccio, G.; Visconti, P.; Arima, V.; D'Amico, S.; Blasco, A.; D'Amone, E.; Cingolani, R.; Rinaldi, R.; Masiero, S.; Giorgi, T.; Gottarelli, G. *Nano Lett.* **2003**, *3*, 479. (f) Rinaldi, R.; Branca, E.; Cingolani, R.; Masiero, S.; Spada, P. G.; Gottarelli, G. *Appl. Phys. Lett.* **2001**, *78*, 3541. (g) Neogi, A.; Li, J.; Noegi, P. B.; Sarkar, A.; Moroc, H. *Elec. Lett.* **2004**, *40*, 1.

[20] (a) Sato, T.; Seko, M.; Takasawa, R.; Yoshikawa, I.; Araki, K. *J. Mater Chem*. **2001**, *11*, 3018. (a) Lena, S.; Masiero, S.; Pieraccini, S.; Spada, G. P. *Chem. Eur. J.* **2009**, *15*, 7792.

[21] Meyer, M.; Steinke, T.; Brandl, M.; Suhnel, J. *J. Comp. Chem.* **2001**, *22*, 109.

[22] Straham, G. D.; Shafer, R. H.; Keniry, M. A. *Biophys. J.* **1998**, *75*, 968.

[23] Straham, G. D.; Shafer, R. H.; Keniry, M. A. *Nucleic Acids Res.* **1994**, *22*, 5447.

[24] Smith, F. W.; Lau, F. W.; Feigon, J. *Biochemistry* **1994**, *91*, 10556.

[25] (a) Marlow, A. L.; Mezzina, E.; Spada, G. P.; Masiero, S.; Davis, J. T.; Gottarelli, G. *J. Org. Chem.* **1999**, *64*, 5116. (b) Davis, J. T. *Angew. Chem. Int. Ed*. **2004**, *43*, 668. (c) Gubala, V.; Betancourt, J. E.; Rivera, J. M.; *Org. Lett*. **2004**, *6*, 4735. (d) Mezzina, E.; Mariani, P; Itri, R.; Masiero, S.; Pieraccini, S.; Spada, G. P.; Spinozzi, F.; Davis, J. T.; Gottarelli, G. *Chem. Eur. J.* **2001**, *7*, 388. (e) Ross, W. S; Hardin, C. C. *J. Am. Chem. Soc.* **1994**, *116*, 6070. (f) Lehn, J. M. *Chem. Eur. J.* **1999**, *5*, 2455. (g) Cousins, G. R. L.; Poulsen, S. A.; Sanders, J. K. *Curr. Opin. Chem. Biol.* **2000**, *4*, 270.

[26] Rodriguez, G. D.; van Dongen, J. L. J.; Lutz, M.; Spek, A. L.; Schenning, A. P. H. J.; Meijer, E. W. *Nature Chem.* **2009**, *1*, 151.

[27] Betancourt, J. E.; Hidalgo, M. M.; Gubala, V.; Rivera, J. M. *J. Am. Chem. Soc.* **2009**, *131*, 3186.

[28] Laughlan, G.; Murchie, A. I. H.; Norman, D. G.; Moore, M. H.; Moody, P. C. E.; Lilley, D. M. J.; Luisi, B. *Science* **1994**, *265*, 520.

[29] Wu, G.; Wong, A. *Biochem. Biophys. Res. Commun.* **2004**, *323*, 1139.

[30] Hud, N. V.; Smith, F. W.; Anet, F. A. L.; Feigon, J. *Biochemistry* **1996**, *35*, 15383.

[31] Shi, X.; Fettinger, J. C.; Davis, J. T. *J. Am. Chem. Soc.* **2001**, *123*, 6738.

[32] Kotch, F. W.; Fettinger, J. C.; Davis, J. T. *Org. Lett.* **2000**, *2*, 3277.

[33] Cai, M.; Shi, X.; Sidorov, V.; Fabris, D.; Lam, Y. F.; Davis, J. T. *Tetrahedron* **2002**, *58*, 661.

[34] Kwan, I. C. M.; She, Y. M.; Wu, G. *Chem. Commun.* **2007**, 4286.

[35] Shi, X.; Mullaugh, K. M.; Fettinger, J. C.; Jiang, Y.; Hofstadler, S. A.; Davis, J. T. *J. Am. Chem. Soc.* **2003**, *125*, 10830.

[36] Rodriguez, G. D.; van Dongen, J. L. J.; Lutz, M.; Spek, A. L.; Schenning, A. P. H. J.; Meijer, E. W. *Nature Chem.* **2009**, *1*, 151.

[37] (a) Shi, X.; Fettinger, J. C.; Davis, J. T. *Angew. Chem. Int. Ed.* **2001**, *113*, 2909. (b) Shi, X.; Fettinger, J. C.; Davis, J. T. *Angew. Chem. Int. Ed.* **2001**, *40*, 2827.

[38] Zhong, C.; Wang, J. L.; Wu, N.; Wu, G.; Zavalij, P.Y.; Shi, X. *Chem. Commun.* **2007**, 3148.

[39] Salem, E. T.; Frish, L.; Van Leeuwen, F. W. B.; Reinhoudt, D. N.; Verboom, W.; Kaucher, M. S.; Davis, J. T.; Cohen, Y. *Chem. Eur. J.* **2007**, *13*, 1969.

[40] Likhitsup, A.; Yu, S.; Hg, Y. H.; Chai, C. L. L.; Tam, E. K. W. *Chem. Commun.* **2009**, 4070.

[41] Kaucher, M. S.; Harrell, W. H.; Davis, J. T. *J. Am. Chem. Soc.* **2006**, *128*, 38.

[42] (a) Nikan, M.; Sherman, J. C. *Angew. Chem. Int. Ed.* **2008**, *120*, 4978. (b) Nikan, M.; Sherman, J. C. *J. Org. Chem.* **2009**, *74*, 5211.

[43] Mariani, P.; Spinozzi, F.; Federiconi, F.; Amenitsch, H.; Spindler, L.; Olenik, D. I. *J. Phys. Chem. B* **2009**, *113*, 7934.

[44] Wu, G.; Kwan, I. C. M. *J. Am. Chem. Soc.* **2009**, *131*, 3180.

[45] (a) Screenivasachary, N.; Lehn, J. M. *Chem. Asian J.* **2008**, *3*, 134. (b) Screenivasachary, N.; Lehn, J. M. *Proc. Natl. Acad. Sci.* **2005**, *102*, 5938. (c) Buhler, E.; Sreenivasachary, N.; Candau, S. J.; Lehn, J. M. *J. Am. Chem. Soc.* **2007**, *129*, 10058.

[46] Sessler, J. L.; Sathiosatham, M.; Doerr, K.; Lynch, V.; Abboud, K. A. *Angew. Chem. Int. Ed.* **2000**, *39*, 1300.

[47] Sanchez, M. C. R.; De SAnctis, I. A.; Arriage, M. G.; Gubala, V.; Hobley, G.; Rivera, J. M. *J. Am. Chem. Soc.* **2009**, *131*, 10403.

[48] (a) Graziano, C.; Masiero, S.; Pieraccini, S.; Lucarini, M.; Spada, G. P. *Org. Lett.* **2008**, *10*, 1739. (b) Neviani, P.; Mileo, E.; Masiero, S.; Pieraccini, S.; Lucarini, M.; Spada, G. P. *Org. Lett.* **2009**, *11*, 3004.

[49] Koizumi, M.; Akahori, K.; Ohmine, T.; Tsutsumi, S.; Junko, S.; Kosaka, T.; Kaneko, M.; Kimura, S.; Shimada, K. *Bioorg. Med. Chem. Lett.* **2000**, *10*, 2213.

[50] Liu, X.; Kwan, I. C. M.; Wang, S.; Wu, G. *Org. Lett.* **2006**, *8*, 3685.

[51] Kaucher, M. S.; Davis, J. T. *Tetrahedron Lett.* **2006**, 6381.

[52] He, G. X.; Krawczyk, S. H.; Swaminathan, S.; Shea, R. G.; Dougherty, J. P.; Terhorst, T.; Law, V. S.; Griffin, L. C.; Coutre, S.; Bischofberger, N. *J. Med. Chem.* **1998**, *41*, 2243.

[53] Sonagashira, K. *J. Organomet. Chem.* **2002**, *653*, 46.

[54] Firth, A. G.; Fairlamb, I. J. S.; Darley, K.; Baumann, C. G. *Tetrahedron Lett.* **2006**, *47*, 3529.

[55] Berman, A.; Izraeli, E. S.; Levanon, H.; Wang, B.; Sessler, J. L. *J. Am. Chem. Soc.* **1995**, *117*, 8252.

[56] (a) Sessler, J. L.; Wang, B.; Harriman, A. *J. Am. Chem. Soc.* **1995**, *117*, 704. (b) Sessler, J. L.; Wang, B.; Harriman, A. *J. Am. Chem. Soc.* **1993**, *115*, 10418.

[57] Suzuki, A. *Pure Appl. Chem.* **1991**, *63*, 419.

[58] Milstein, D.; Stille, J. K. *J. Am. Chem. Soc.* **1978**, *100*, 3636.

[59] (a) Western, E. C.; Daft, J. R.; Johnson, E. M.; Gannett, P. M.; Shaughnessy, K. H. *J. Org. Chem.* **2003**, *68*, 6767. (b) Western, E. C.; Shaughnessy, K. H. *J. Org. Chem.* **2005**, *70*, 6378.

[60] (a) Sessler, J. L.; Sathiosatham, M.; Brown, C. T.; Rhodes, T. A.; Wiederrecht, G. *J. Am. Chem. Soc.* **2001**, *123*, 3655 (b) Arsenyan, P.; Ikaunieks, M.; Belyakov, S. *Tetrahedron Lett.* **2007**, *48*, 961.

[61] Wolfe, J. P.; Buchwald, S. L. *Org. Synth.* **2004**, *10*, 423.

[62] (a) Boge, N.; Grasl, S.; Meier, C. *J. Org. Chem.* **2006**, *71*, 9728. (b) Gillet, L. C. J.; Scharer, O. D. *Org. Lett.* **2002**, *4*, 4205. (c) Collier, A.; Wagner, G. *Org. Biomol. Chem.* **2006**, *4*, 4526. (d) Elmquist, C. E.; Stover, J. S.; Wang, Z.; Rizzo, C. J. *J. Am. Chem. Soc.* **2004**, *126*, 11189.

[63] Takamura, E. T.; Ishikawa, S.; Mochizuki, M.; Wakabayashi, K. *Tetrahedron Lett.* **2003**, *44*, 5969.

[64] Novak, M.; Ruenz, M.; Kazerani, S.; Toth, K.; Nguyen, T. M.; Heinrich, B. *J. Org. Chem.* **2002**, *67*, 2303.

[65] (a) De Riccardis, F.; Bonala, R. R.; Johnson, F. *J. Am. Chem. Soc.* **1999**, *121*, 1453. (b) Stover, J. S.; Rizzo, C. J. *Org. Lett.* **2004**, *6*, 4988.

[66] (a) Srivastava, P. C.; Robins, R. K.; Meyer, R. B.; Townsend, L. B. *Chemistry of Nucleosides and Nucleotides;* Plenum Press: New York, 1988. (b) Trivedi, B. K.; *Nucleos. Nucleot.* **1988**, *7*, 393. (c) Trivedi, B. K.; Bruns, R. F. *J. Med. Chem.* **1989**, *32*, 1667. (d) Steinbrecher, T.; Wameling, C.; Oesch, F.; Seidel, A. *Angew. Chem. Int. Ed.* **1993**, *32*, 404. (e) Harwood, E. A.; Sigurdsson, S. T.; Edfeldt, N. B. F.; Reid, B. R.; Hopkins, P. B. *J. Am. Chem. Soc.* **1999**, *121*, 5081. (f) De Riccardis, F.; Johnson, F. *Org. Lett.* **2000**, *2*, 293. (g) Chakraborti, D.; Colis, L.; Schneider, R.; Basu, A. K. *Org. Lett.* **2003**, *5*, 2861. (h) Lakshman, M. K.; Ngassa, F. N.; Bae, S.; Buchanan, D. G.; Hahn, H.

G.; Mah, H. *J. Org. Chem.* **2003**, *68*, 6020. (k) Dai, Q.; Ran, C.; Harvey, R. G. *Org. Lett.* **2005**, *7*, 999.

[67] (a) Qian, M.; Glaser, R. *J. Am. Chem. Soc.* **2005**, *127*, 880. (b) Kirchner, J. J.; Sigurdsson, S. T.; Hopkins, P. B. *J. Am. Chem. Soc.* **1992**, *114*, 4021. (c) Harwood, E. A.; Hopkins, P. B.; Sigurdsson, S. T. *J. Org. Chem.* **2000**, *65*, 2959.

[68] Takamura, E. T.; Enomoto, S.; Wakabayashi, K. *J. Org. Chem.* **2006**, *71*, 5599.

[69] Ran, C.; Dai, Q.; Harvey, R. G. *J. Org. Chem.* **2005**, *70*, 3724.

[70] Gellert, M.; Lipsett, M. N.; Davies, D. R. *Proc. Natl. Acad. Sci. USA* **1962**, *48,* 2013.

[71] (a) Parkinson, G. N.; Lee, M. P.; Neidle, S. *Nature* **2002**, *417*, 876. (b) Haider, S.; Parkinson, G. N.; Neidle, S. *J. Mol. Biol.* **2002**, *320*, 189. (c) Hazel, P.; Parkinson, G. N.; Neidle, S. *J. Am. Chem. Soc.* **2006**, *128*, 5480. (d) Kang, C.; Zhang, X.; Ratliff, R.; Moyzis, R.; Rich, A. *Nature* **1992**, *356*, 126.

[72] Forman, S. L.; Fettinger, J. C.; Pieraccini, S.; Gottarelli, G.; Davis, J. T. *J. Am. Chem. Soc.* **2000**, *122*, 4060.

[73] Wuthrich, K. *NMR of Proteins and Nucleic Acids*; Wiley: New York, 1986.

[74] (a) Kaucher, M. S.; Lam, Y. F.; Pieraccini, S.; Gottarelli, G.; Davis, J. T. *Chem. Eur. J.* **2005**, *11*, 164. (b) Wong, A.; Ida, R.; Spindler, L.; Wu, G.; *J. Am. Chem. Soc.* **2005**, *127*, 6990.

[75] (a) Wu, G.; Wong, A. *Chem. Commun.* **2001**, 2658. (b) Wu, G.; Wong, A.; Gan, A.; Davis, J. T. *J. Am. Chem. Soc.* **2003**, *125*, 7182. (c) Wong, A.; Wu, G.; *J. Am. Chem. Soc.* **2003**, *125*, 13895. (d) Ida, R.; Wu, G. *J. Am. Chem. Soc.* **2008**, *130*, 3590. (e) Ida, R.; Kwan, I. C. M.; Wu, G. *Chem. Commun.* **2007**, 795.

[76] Fischbeck, A.; Bartke, N.; Humpf, H. U. *Monatsh. Chem.* **2005**, *136*, 397.

[77] Berova, N.; Bari, L. D.; Pescitelli, G. *Chem. Soc. Rev.* **2007**, *36*, 914.

[78] (a) Kurtan, T.; Nesnas, N.; Li, Y. Q.; Huang, K.; Nakanishi, K.; Berova, N. *J. Am. Chem. Soc.* **2001**, *123*, 5962. (b) Yang, Q.; Olmsted, C.; Borhan, B. *Org. Lett.* **2002**, *4*, 3423.

[79] Allenmark, S. *Chirality* **2003**, *15*, 409.

[80] Frelek, J.; Geiger, M.; Voelter, W. *Curr. Org. Chem.* **1999**, *3*, 117.

[81] Tanaka, K.; Pescitelli, G.; Nakanishi, K.; Berova, N. *Monatsh. Chem.* **2005**, *136*, 367.

[82] (a) Gottarelli, G.; Lena, S.; Masiero, S.; Pieraccini, S.; Spada, G. P. *Chirality* **2008**, *20*, 471. (b) Arnal-Herault, C.; Banu, A.; Barboiu, M.; Michau, M.; van der Lee, A. *Angew. Chem. Int. Ed.* **2007**, *46*, 4268.

[83] Shalley, G. A.; Castellano, R. K.; Brody, M. S.; Rudkevich, D. M.; Siazdak, G.; Rebek, J. *J. Am. Chem. Soc.* **1999**, *121*, 4568.

[84] (a) Manet, I.; Francini, L.; Masiero, S.; Pieraccini, S.; Spada, G. P.; Gottarelli, G. *Helv. Chim. Acta* **2001**, *84*, 2096. (b) Salem, T. E.; Frish, L.; van Leeuwen, F. W. B.; Reinhoudt, D. H.; Verboom, W.; Kaucher, M. S.; Davis, J. T.; Cohen, Y. *Chem. Eur. J.* **2007**, *13*, 1969. (c) Vairamani, M.; Gross, M. *J. Am. Chem. Soc.* **2003**, *125*, 42.

[85] Lees, A. J. *Chem. Rev.* **1987**, *87*, 711.

[86] Nazeeruddin, M. K.; Humphry-Baker, R.; Berner, D.; Rivier, S.; Zuppiroli, L.; Graetzel, M. *J. Am. Chem. Soc.* **2003**, *125*, 8790.

[87] Lee, Y. A.; McGarrah, J. E.; Lachicotte, R. J.; Eisenberg, R. *J. Am. Chem. Soc.* **2002**, *124*, 10662.

[88] Bunzli, J. C.; Piguet, C. *Chem. Rev.* **2002**, *102*, 1897.

[89] (a) Simonsson, T.; Sjoback, R. *J. Biol. Chem.* **1999**, *274*, 17379. (b) Juskowiak, B. *Anal. Chim. Acta* **2006**, *568*, 171. (c) Mergny, J. T.; Lacroix, L.; Fichou, M. P.; Hounsou, C.; Guittat, L.; Hoarau, M.; Arimondo, P. B.; Vigneron, J. P.; Lehn, J. M.; Riou, J. F.; Garestier, T.; Helene, C. *Proc. Natl. Acad. Sci. USA* **2007**, *98*, 3062.

[90] Kim, H. Y. H.; Cooper, M.; Nechev, L. V.; Harris, C. M.; Harris, T. M. *Chem. Res. Toxicol.* **2001**, *14*, 1306.

[91] Lakowicz, J. R. *Topics in Fluorescence Spectroscopy: DNA Technology*; Plenum Publishers: New York, 2003.

[92] Tainaka, K.; Tanaka, K.; Ikeda, S.; Nishiza, K. I.; Unzai, T.; Fujiwara, Y.; Saito, I.; Okamoto, A. *J. Am. Chem. Soc.* **2007**, *129*, 4776.

[93] (a) Da Costa, C. P.; Fedor, M. J.; Scott, L. G. *J. Am. Chem. Soc.* **2007**, *129*, 3426. (b) Seela, F.; Xiong, H.; Leonard, P.; Budow, S. *Org. Biomol. Chem.* **2009**, *7*, 1374.

[94] Park, T.; Zimmerman, S. C.; Nakashima, S. *J. Am. Chem. Soc.* **2005**, *127*, 6520.

[95] (a) Encinas, S.; Simpson, N. R.; Andrews, P.; Ward, M. D.; White, C. M.; Armaroli, N.; Barigelletti, F.; Houlton, A. *New J. Chem.* **2000**, *24*, 987. (b) Armaroli, N.; Barigelletti, F.; Calogero, G.; Flamigni, L.; White, C. M.; Ward, M. D. *Chem. Commun.* **1997**, 2181.

[96] (a) Sessler, J. L.; Sathiosatham, M.; Brown, C. T.; Rhodes, T. A.; Wiederrecht, G. *J. Am. Chem. Soc.* **2001**, *123,* 3655. (b) Harriman, A.; Magda, D. J.; Sessler, J. L. *J. Phys. Chem.***1991**, *95*, 1530.

[97] (a) Harriman, A.; Magda, D. J.; Sessler, J. L. *J. Chem. Soc., Chem. Commun.* **1991**, 345. (b) Sessler, J. L.; Jayawickramarajah, J.; Gouloumis, A.; Pantos, G. D.; Torres, T.; Guldi, D. M. *Tetrahedron* **2006**, *62*, 2123.

[98] Kawai, T.; Ikegami, M.; Kawai, K.; Majima, T.; Nishimura, Y.; Arai, T. *Chem. Phys. Lett.* **2005**, *407*, 58.

[99] (a) Gray, D. M.; Wen, J. D.; Gray, C. W.; Repges, R.; Repges, C.; Raabe, G.; Fleischhauer, J. *Chirality* **2008**, *20*, 431. (b) Proni, G.; Gottarelli, G.; Mariani, P.; Spada, G. P. *Chem. Eur. J.* **2000**, *6*, 3249.

[100] He, F.; Tang, Y.; Wang, S.; Li, Y.; Zhu, D. *J. Am. Chem. Soc.* **2005**, *127*, 12343.

[101] (a) He, F.; Tang, Y.; Yu, M.; Feng, F.; An, L.; Sun, H.; Wang, S.; Li, Y.; Zhu, D.; Bazan, G. C. *J. Am. Chem. Soc.* **2006**, *128*, 6764. (b) Bourdoncle, A.; Torres, A. E.; Gosse, C.; Lacroix, L.; Vekhoff, P.; Le Saux, T.; Jullien, L.; Mergny, J. L. *J. Am. Chem. Soc.* **2006**, *128*, 11094. (c) Kumar, N.; Maiti, S. *Biochem. Biophys. Res. Commun.* **2004**, *319*, 759. d) Kumar, N.; Maiti, S. *Nucleic Acids Res.* **2005**, *33*, 6723.

[102] Okamoto, A.; Kanatani, K.; Ochi, Y.; Saito, Y.; Saito, I. *Tetrahedron Lett.* **2004**, *45*, 6059.

[103] (a) Pyle, A. M. *J. Biol. Inorg. Chem.* **2002**, *7*, 679. (b) Kraatz, H. B.; Nolte, N. M. *Concepts and Models in Bioinorganic Chemistry*; Wiley: Weinheim, 2006. (c) Jaouen, G. *Bioorganometallics*; Wiley: Weinheim, 2006.

[104] Lippert, B. *Coord. Chem. Rev.* **2000**, *200-202*, 487.

[105] (a) Siegel, R. K. O.; Lippert, B. *Chem. Commun.* **1999**, 2167. (b) Freisinger, E.; Meier, S.; Lippert, B. *J. Chem. Soc., Dalton Trans.* **2000**, 3274. (c) Jamieson, E. R.; Lippard, S. J. *Chem. Rev.* **1999**, *99*, 2467.

[106] (a) Zimmer, C.; Luck, G.; Holy, A. *Nucleic Acids Res.* **1976**, *3*, 2757. (b) Sigel, H.; Massoud, S. S.; Corfu, N. A. *J. Am. Chem Soc.* **1994**, *116*, 2958.

[107] (a) Shipman, M. A.; Price, C.; Gibson, A. E.; Elsegood, M. R. J.; Clegg, W.; Houlton, A. *Chem. Eur. J.* **2000**, *6*, 4371. (b) Muthiah, P. T.; Mazumdar, S. K.; Chaudhuri, S. *J. Inorg. Biochem.* **1983**, *19*, 237. (c) Taylor, M. R. *Acta Crystallogr.* **1973**, *B29*, 884. (d) Taylor, M. R.; Vilkins, L. M.; McCall, M. J. *Acta Crystallogr.* **1989**, *C45*, 1625. (e) Maixner, J.; Zachova, J. *Acta Crystallogr.* **1993**, *C49*, 927. (f) Amo, O. P.; Miguel, P. J. S.; Castillo, O.; Sabat, M.; Lippert, B.; Zamora, F. *J. Biol. Inorg. Chem.* **2007**, *12*, 543.

[108] (a) Purohit, C. S.; Mishra, A. K.; Verma, S. *Inorg. Chem.* **2007**, *46*, 8493. (b) Sigel, H.; Massoud, S. S.; Corfu, N. A. *J. Am. Chem. Soc.* **1994**, *116*, 2958. (c) Anorbe, M. G.; Welzel, T.; Lippert, B. *Inorg. Chem.* **2007**, *46*, 8222. (d) Melchart, M.; Habtemariam, A.; Novakova, O.; Moggach, S. A.; Fabbiani, F. P. A.; Parson, S.; Brabec, V.; Sadler, P. J. *Inorg. Chem.* **2007**, *46*, 8950. (e) Vrabel, M.; Pohl, R.; Klepetarova, B.; Votruba, I.; Hocek, M. *Org. Biomol. Chem.* **2007**, *5*, 2849. (f) Song, H.; Li, X.; Long, Y.; Schatte, G.; Kraatz, H. B. *Dalton Trans.* **2006**, 4696. (g) Ochoa, A. P.; Catillo, O.; alexandre, S. S.; Welte, L.; de Pablo, P. J.; Tapiador, M. R.; Herrero, J. G.; Zamora, F. *Inorg. Chem.***2009**, *48*, 7931.

[109] (a) Shaw, C. F. *Chem. Rev.* **1999**, *99*, 2589. (b) Wong, E.; Giandomenico, C. M. *Chem. Rev.* **1999**, *99*, 2451. (c) Jiang, P.; Guo, Z. *Coord. Chem. Rev.* **2004**, *248*, 205. (d) Breaker, R. R.; Joyce, G. F. *Chem. Biol.* **1995**, *2*, 655. (e) Monchaud, D.; Fichou, M. P. T. *Org. Biomol. Chem.* **2008**, *6*, 627.

[110] (a) Thompson, K. H.; Orvig, C. *Coord. Chem. Rev.* **2001**, *219*, 1033. (b) Sun, R. W. Y.; Ma, D. L.; Wong, E. L. M.; Che, C. M. *Dalton Trans.* **2007**, 4884.

[111] Clever, G. H.; Kaul, C.; Carell, T. *Angew. Chem. Int. Ed.* **2007**, *46*, 6226.

[112] (a) Nagesh, N.; Bhargava, P.; Chatterji, D. *Biopolymers* **1992**, *32*, 1421. (b) Ringer, D. P.; Etheredge, J. L.; Kizer, D. E. *J. Inorg. Biochem.* **1985**, *24*, 137.

[113] (a) Sigel, R. K.; Pyle, A. M. *Met. Ions Biol. Syst.* **2003**, *40*, 477. (b) Matsmura, K.; Komiyama, M. *J. Biochem.* **1997**, *122*, 387. (c) Hargittai, M. R.; Musier, F. K. *RNA* **2000**, *6*, 1672. (d) Schaferling, M.; Wolfbeis, O. S. *Chem. Eur. J.* **2007**, *13*, 4342.

[114] Galezowska, E.; Gluszynska, A.; Juskowiak, B. *J. Inorg. Chem.* **2007**, *101*, 678.

[115] Kwan, I.C.M.; She, Y.M.; Wu, G. *Chem. Commun.* **2007**, 4286.

[116] (a) Formoso, C. *Biochem. Biophys. Res. Commun.* **1973**, *53*, 1084. (b) Fu, P. K. L.; Turro, C. *J. Am .Chem. Soc.* **1999**, *121*, 1.

[117] Ringer, D. P.; Burchett, S.; Kizer, D. E. *Biochemistry* **1978**, *17*, 4118.

[118] Moucheron, C.; Mesmaeker, A. K. D.; Kelly, J. M. *J. Photochem. Photobio. B: Bio.* **1997**, *40*, 91.

[119] Gao, F.; Chen, X.; Wang, J. Q.; Chen, Y.; Chao, H.; Ji, L. N. *Inorg. Chem.* **2009**, *48*, 5599.

[120] Papakyriakou, A.; Malandrinos, G.; Garoufis, A. *J. Inorg. Biochem.* **2006**, *100*, 1842.

[121] Barton, J. K.; Danishefsky, A. T.; Goldberg, J. M. *J. Am. Chem. Soc.* **1984**, *206*, 2172.

[122] Vrabel, M.; Horakova, P.; Pivonkova, H.; Kalachora, L.; Cernocaka, H.; Cahova, H.; Pohl, R.; Sebest, P.; Havran, L.; Hocek, M.; Fojta, M. *Chem. Eur. J.* **2009**, *15*, 1144.

Chapter 2
Chemical Modification of Guanosine

2.1 Introduction

In recent years, extensive research has been focused on molecular self-assembly of non-fluorescent G-nucleosides in both solution and solid state.[1] Much less is known about the effects of chemical modification of guanine on its H-bonding ability.[2] In addition to molecular recognition and self-organization, understanding the electronic properties of G-nucleosides and their architectures is an important research area. Chemical modification at the guanine ring could dramatically alter its electronic structure and allow for fine tuning of its photophysical properties. This kind of luminescent G-nucleosides is an attractive probe for monitoring metal ion binding and H-bonding.[3] The usefulness of luminescent the G-nucleosides stems from several important aspects, such as the structural similarity to natural purines, base-pairing and stacking participation and potential for monitoring subtle interactions in DNA or RNA structures. For these reasons, syntheses of fluorescent G-nucleosides, modified at C^8-site[4] or N^2-sites,[5] have been previously reported by employing Pd-catalyzed C-C or C-N cross-coupling reactions. However, direct functionalization of G-nucleosides is much less common. Furthermore, little effort has been made towards using fluorescent G-nucleosides for sensing applications.

We have been particularly interested in functionalizing the G-nucleosides with fluorescent chromophores since they may allow easy detection/monitoring by

fluorescence spectroscopy. In order to retain the biological activity of guanosines, the H-bonding sites and the ribose unit must remain intact, which is a key concern in G-nucleoside functionalization. For this reason, our targets are model **N^2G** compounds that can self-assemble in addition to being fluorescent. We have also considered the chelating ability of the functional groups in our design of **N^2Gs**. Our earlier investigation has shown that diarylamines such as 2,2'-dipyridylamino and heterocyclic groups such as 2-(2'-pyridyl)benzimidazolyl are highly emissive when attached to an aryl group,[6] and are able to chelate to a variety of metal ions, readily producing fluorescent or phosphorescent metal complexes.[7] Based on these considerations, we decided to incorporate several fluorescent chelating emitters at the N^2-site of guanosine to produce new luminescent nucleosides, **2.1a** – **2.4a** as shown in Figure 2.1. The non-fluorescent guanosine (**2.5a**) was made as an intermediate for the use in cross-coupling reactions. The fluorescent but non-chelating diaminobiphenyl group was introduced at the N^2-site, **2.1a**, in order to probe the binding affinity of guanine. A pyrenyl moiety in **2.4a** was introduced for several reasons. First, pyrene has large fluorescence quantum yield and it is one of the bright emitters. Second, pyrene can form excimers, induced by interaction between two pyrene rings, in a sterically constrained environment.[8] This phenomenon could become useful in the study of self-assembly, such as G-quartet formation and stacking. These compounds also possess H-bonding sites necessary for the extended self-assembly and Watson-Crick base pairing. Hence, the lipophilic **N^2Gs**, **2.1b**, **2.2b** and **2.4b** presented in Figure 2.2 were developed for the study of H-bonding. In this chapter, the syntheses and the study of photophysical properties of **N^2Gs** are presented.

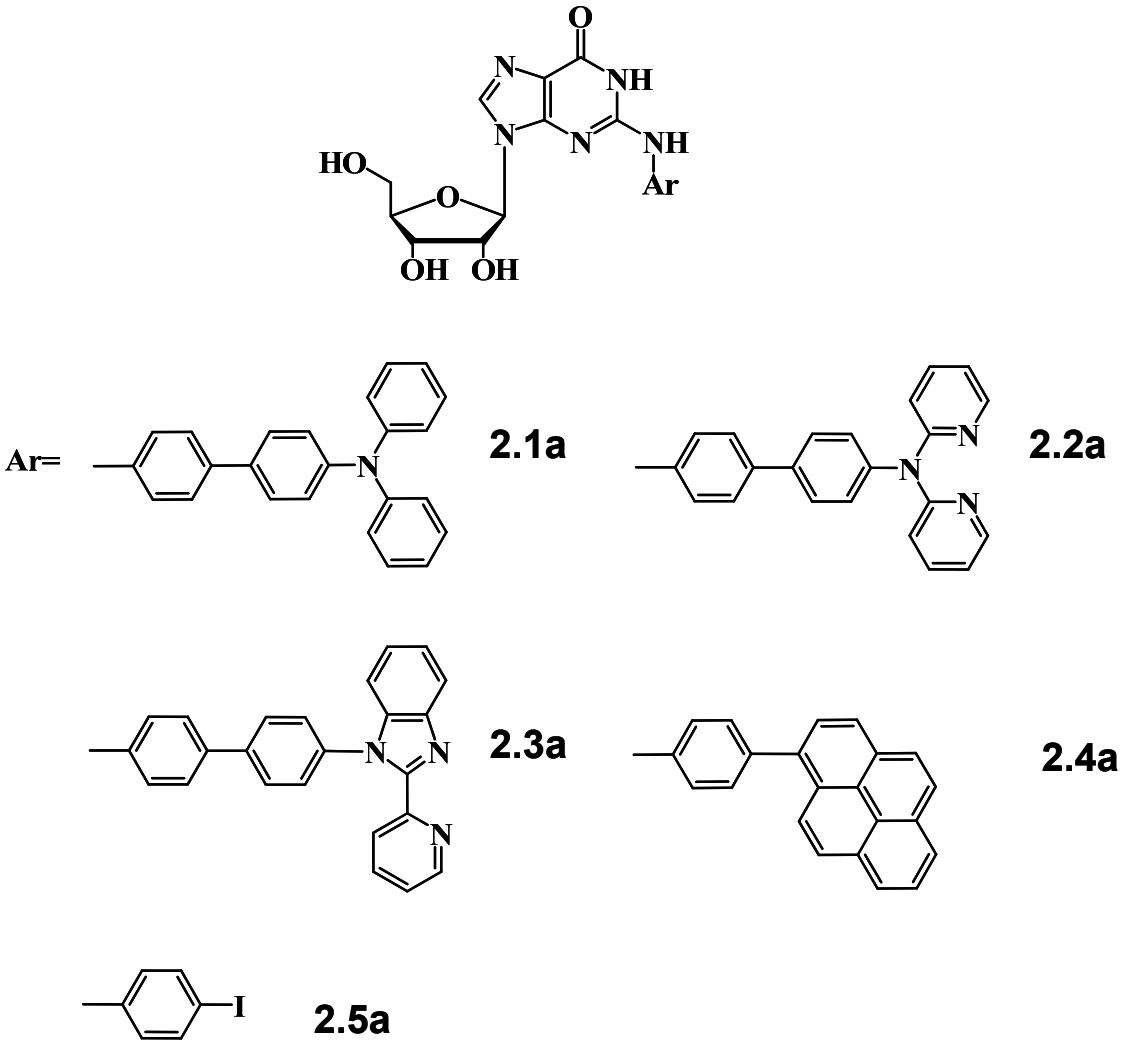

Figure 2.1 Structural representation of fluorescent hydrophilic N^2-modified guanosines, **2.1a** – **2.5a**, synthesized and studied.

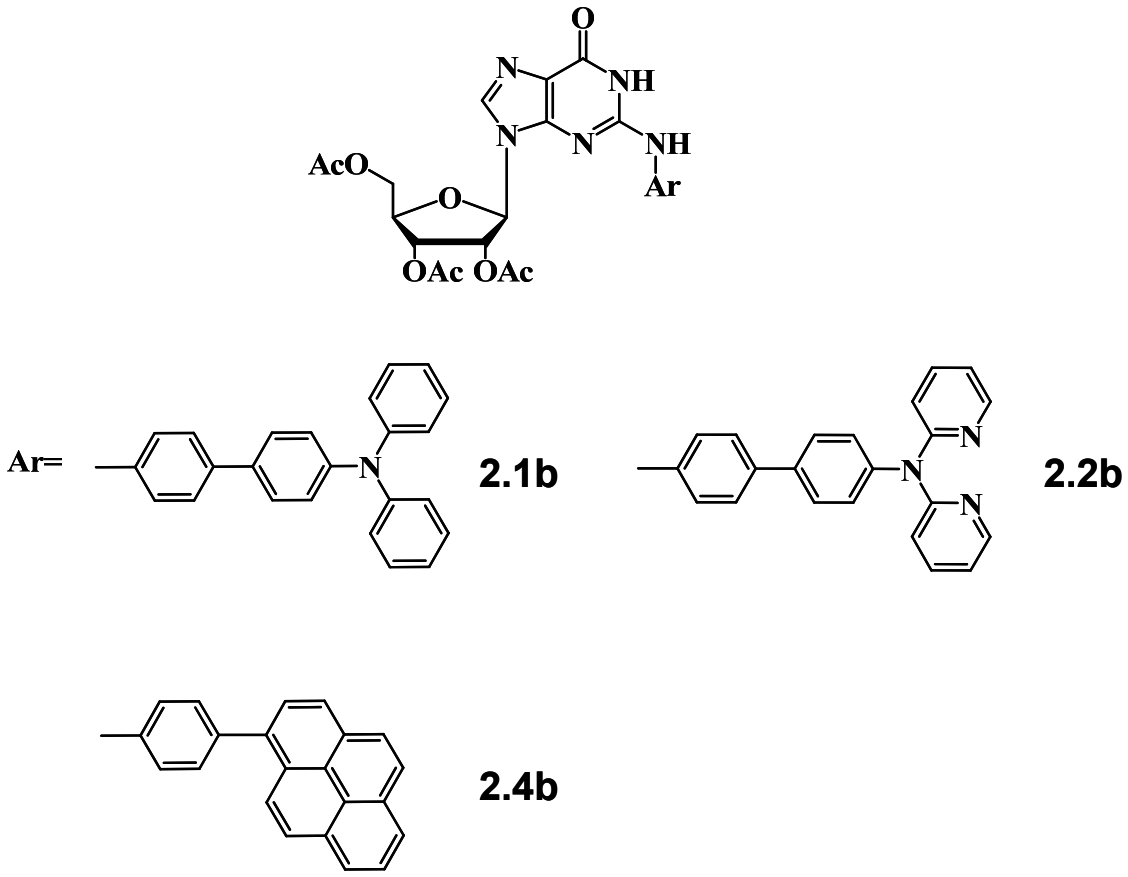

Figure 2.2 Structural representation of fluorescent lipophilic N^2-modified guanosines, **2.1b**, **2.1b** and **2.4b**, synthesized and studied.

2.2 Experimental Procedure

2.2.1 General considerations

All reagents were purchased from Aldrich Chemical Co. and used without further purification unless stated otherwise. Typical coupling reactions were carried under a nitrogen atmosphere while the coupling reaction involving guanosine was performed in a sealed tube. Thin-layer chromatography was carried out by using silica gel 60 plates, and the column chromatography was performed by using silica gel of particle size 60 – 200

μm and C-18 silica gel for reversed-phase chromatography, all of which were purchased from Silicycle. All 1D and 2D NMR experiments (COSY and HMQC) were recorded on Bruker Avance 400 MHz or 500 MHz spectrometers at 298 K, unless otherwise specified, with the solvent peaks used as the reference. Low resolution and high-resolution mass spectrometry experiments were performed using the electrospray ionization mode on QSTAR XL MS/MS Systems using the Analyst QS Method. Excitation and emission spectra were recorded on a Photon Technologies International QuantaMaster Model C-60 spectrometer. All UV-Vis spectra were collected by using an Ocean Optics Inc. spectrometer and Spectra Suite software. Circular dichroism (CD) spectra were recorded on a Jasco 715 spectrometer with a 1 cm path length cell at 298 K and 5 scans on average.

2.2.2 Synthesis of *p*-2,2'-diphenylaminoiodobiphenyl (2.1)

2,2'-Diphenylamine (4.91 g, 29.1 mmol), 4,4'-diiodobiphenyl (18.9 g, 58.9 mmol), cesium carbonate (11.3 g, 34.8 mmol), 1,10-phenanthroline (1.04 g, 5.81 mmol) and copper iodide (0.55 g, 2.12 mmol) were placed in a 250 mL round bottom flask. To the solid mixture, DMF (10 mL) was added and the reaction flask was heated to 160 ^{o}C for 18 h. The reaction was monitored by TLC. After the reaction mixture was cooled, water (50 mL) and dichloromethane (150 mL) were used to dissolve solids. After extraction, the organic fractions were dried over anhydrous $MgSO_4$ and the product was isolated by using a chromatographic column with hexane: ethyl acetate (2:1 %vv) (R_f = 0.7) as the eluent to give **2.1** as white crystals (3.26 g, 25% yield). mp. 141-143 ^{o}C. ^{1}H NMR (400 MHz, CD_2Cl_2, 298 K) δ 7.79 (d, *J* = 8.3 Hz, 2H), 7.50 (d, *J* = 7.5 Hz, 2H), 7.38 (d, *J* = 8.3 Hz, 2H), 7.32 (t, *J* = 7.5 Hz, 4H), 7.15 (m, *J* = 4.2, 8.7 Hz, 6H), 7.11 (t, *J* = 7.5 Hz, 2H) ppm. ^{13}C NMR (400 MHz, CD_2Cl_2, 298 K) δ 148.1, 147.9 (2C), 140.5,

138.2 (2C), 133.9, 129.7 (4C), 128.8 (2C), 127.8 (2C), 124.9 (4C), 123.9 (2C), 123.5 (2C), 92.5 (C-I) ppm. MS-EI *m/z* 447.0417 [$M^{+\cdot}$]. HRMS EI^+ *m/z* calcd for $C_{24}H_{18}NI^+$ 447.0484, found 447.0473.

2.2.3 Synthesis of N^2-(*p*-4,4'-biphenyldiphenylamino)guanosine (2.1a)

To a mixture of *p*-2,2'-diphenylaminiodobiphenyl (**2.1**) (2.68 g, 5.6 mmol), guanosine (2.38 g, 8.4 mmol), cesium carbonate (2.18 g, 6.7 mmol) and copper iodide (0.16 g, 0.84 mmol, 15%), DMSO was added (8 mL). The solution was degassed with nitrogen for 10 minutes. A preheated oil bath was used and the reaction was carried out in a sealed tube at 140 ^oC for 17 h. To the reaction mixture water (10 mL) was added, and the solution was neutralized to pH ~ 7 using aqueous HCl (0.1 M). Further addition of water (30 mL) led to precipitation of the product as a beige solid. The solid was washed further with water (20 mL) to remove unreacted guanosine. The crude solid was further purified using a C-18 reverse phase silica gel column with CH_2Cl_2, followed by CH_2Cl_2:CH_3OH (95:5 % vv to 60:40 %vv) as eluents to give **2.1a** as a white solid (1.14 g, 35% yield). m.p. >299 ^oC. ^1H NMR (400 MHz, DMSO-d_6, 298 K) δ 11.8 (broad, s, 1H, N_1H), 10.1 (broad, s, 1H, N_2H), 8.04 (s, 1H, H_8), 7.8 (d, *J* = 7.4 Hz, 2H), 7.61 (q, *J* = 2.8, 8.4 Hz, 4H), 7.32 (t, *J* = 7.7 Hz, 4H), 7.03 (m, 8H), 5.80 (d, *J* = 5.5 Hz, 1H, $H_{1'}$), 5.47 (d, *J* = 5.8 Hz, 1H, C_2-OH), 5.17 (d, *J* = 4.3 Hz, 1H, C_3-OH), 5.00 (t, *J* = 5.2 Hz, 1H, C_5-OH), 4.55 (d, *J* = 5.0 Hz, 1H, $H_{2'}$), 4.11 (d, *J* = 3.6 Hz, 1H, $H_{3'}$), 3.89 (d, *J* = 3.9 Hz, 1H, $H_{4'}$), 3.63 (m, *J* = 4.5, 7.3 Hz, 1H, $H_{5'}$), 3.52 (m, *J* = 4.9, 7.4 Hz, 1H, $H_{5''}$) ppm. ^{13}C NMR (400 MHz, DMSO-d_6, 298 K) δ 151.1, 147.9, 146.8, 139.8, 137.3, 134.9, 133.7, 130.3 (4C), 127.8 (2C), 127.2 (2C), 125.1, 124.7 (4C), 124.5 (2C), 123.8 (2C), 120.1 (2C), 119.2, 115.9, 114.7, 87.8 (C_1), 85.9 (C_4), 74.4 (C_2), 71.1 (C_3), 62.2 (C_5) ppm. ESI-MS *m/z*

603.1907 $[M+H]^+$. HRMS ESI^+ *m/z* calcd for $C_{34}H_{30}N_6O_5 \cdot H^+$ 603.23559, found 603.23565.

2.2.4 Synthesis of *2',3',5'-O*-triacetyl-N^2-(*p*-4,4'-biphenyldiphenylamino)guanosine (2.1b)

To a suspension of compound **2.1a** (0.34 g, 0.57 mmol) and dimethylaminopyridine (DMAP) (0.005 g, 0.04 mmol) in dry CH_3CN (10 mL), freshly distilled triethylamine (0.30 mL, 2.21 mmol) was added. After stirring for 5 minutes, freshly distilled acetic anhydride (0.19 mL, 2.00 mmol) was added dropwise over 5 minutes, and the mixture was stirred for 2 hour at room temperature. The reaction mixture was quenched with methanol (5 mL), and the organic solvents were removed to dryness. The residue was treated using a chromatographic column with CH_2Cl_2 and CH_2Cl_2/CH_3OH (95:5%vv) as eluents to give **2.1b** as white solid (0.17 g, 43% yield). mp. > 300 ^oC. ^1H NMR (400 MHz, DMSO-d_6, 298 K) δ 10.82 (broad, N_1H, 1H), 8.96 (broad, N_2H, 1H), 8.00 (s, 1H), 7.61-7.58 (m, *J* = 5.8, 8.6 Hz, 6H), 7.32 (t, *J* = 7.9 Hz, 4H), 7.05 (m, *J* = 7.8, 8.5 Hz, 8H), 6.02 (d, *J* = 5.0 Hz, 1H, $H_{1'}$), 6.00 (t, *J* = 5.8 Hz, 1H, $H_{2'}$), 5.37 (t, *J* = 5.7 Hz, 1H, $H_{3'}$), 4.28 (dd, *J* = 4.4, 5.3 Hz, 1H, $H_{4'}$), 4.20 (m, *J* = 4.1, 12.1 Hz, 1H, $H_{5'}$), 4.13 (m, *J* = 4.1, 12.4 Hz, 1H, $H_{5''}$), 2.07 (s, CH_3, 3H), 2.05 (s, CH_3, 3H), 1.84 (s, CH_3, 3H) ppm. ^{13}C NMR (500 MHz, CD_3OD, 298 K) δ 171.2, 170.1, 169.9, 148.1, 138.1, 134.3, 129.6 (6C), 127.6 (2C), 127.1 (2C), 124.6 (6C), 124.1 (2C), 123.3 (2C), 122.3 (2C), 121.1, 115.6, 96.8 (2C), 87.5 (C_1), 80.1 (C_4), 72.6 (C_2), 70.9 (C_3), 63.1 (C_5), 19.6 (CH_3), 19.5 (CH_3), 19.4 (CH_3) ppm. ESI-MS^+ *m/z* 729.2465 $[M+H]^+$. HRMS EI^+ *m/z* calcd for $C_{40}H_{36}N_6O_8$ 728.2594, found 728.2538.

2.2.5 Synthesis of *p*-2,2'-dipyridylaminoiodobiphenyl (2.2).

2,2'-Dipyridylamine (5.68 g, 33.1 mmol), 4,4'-diiodobiphenyl (27.0 g, 66.2 mmol), cesium carbonate (12.9 g, 39.2 mmol), 1,10-phenanthroline (1.18 g, 6.62 mmol) and copper iodide (0.63 g, 3.34 mmol) were placed in a 250 mL round bottom flask. To the solid mixture DMF (10 mL) was added and the reaction flask was heated to 160 ^{o}C for 18 h. The reaction was monitored by TLC. After the reaction mixture was cooled, water (50 mL) and dichloromethane (100 mL) were used to dissolve solids. After the extraction, the organic fractions were dried over anhydrous $MgSO_4$ and the product was isolated by using a chromatographic column with hexane:ethyl acetate (2:1 %vv) (R_f = 0.8) as the eluent to obtain compound **2.2** as a white crystalline solid (9.12 g, 67% yield). mp. 166-167 ^{o}C. ^{1}H NMR (400 MHz, CD_2Cl_2, 298 K) δ 8.32 (q, *J* = 9.8, 5.5 Hz, 2H), 7.82 (d, *J* = 8.4 Hz, 2H), 7.62 (m, *J* = 6.6, 8.5 Hz, 4H), 7.42 (d, *J* = 8.4 Hz, 2H), 7.24 (d, *J* = 8.4 Hz, 2H), 7.08 (d, *J* = 8.3 Hz, 2H), 7.00 (m, *J* = 7.6, 6.3 Hz, 2H) ppm. ^{13}C NMR (400 MHz, CD_2Cl_2, 298 K) δ 158.3 (2C), 148.7 (2C), 145.3, 140.3, 138.2 (2C), 137.7 (2C), 136.9, 129.1 (2C), 128.1 (2C), 127.7 (2C), 118.6 (2C), 117.4 (2C), 92.9 (C-I) ppm. MS-EI$^+$ *m/z* 448.0913 $[M-H]^+$. HRMS EI$^+$ *m/z* calcd for $C_{22}H_{15}N_3I^+$ $[M-H]^+$ 448.0311, found 448.0320.

2.2.6 Synthesis of N^2-(*p*-4,4'-biphenyl-2,2'-dipyridylamino)guanosine (2.2a).

To a mixture of *p*-2,2'-dipyridylaminoiodobiphenyl (**2.2**) (2.98 g, 6.63 mmol), guanosine (2.21 g, 7.81 mmol), cesium carbonate (2.61 g, 8.02 mmol) and copper iodide (0.19 g, 1.00 mmol, 15%), DMSO was added (8 mL). The solution was degassed with nitrogen for 10 minutes. A preheated oil bath was used and the reaction was carried out in the sealed tube at 140 ^{o}C for 17 h. To the reaction mixture water (10 mL) was added, and

the solution was neutralized to pH ~ 7 using aqueous HCl (0.1 M). Further addition of water (30 mL) led to precipitation of the product as a beige solid. The solid was washed further with water (20 mL) to remove unreacted guanosine. The crude solid was further purified using a C-18 reverse phase silica gel column with CH_2Cl_2, followed by CH_2Cl_2:CH_3OH (95:5 % vv to 60:40 %vv) as eluents to provide compound **2.2a** as a white solid (1.16 g, 29% yield). m.p. 226-228 ^oC. ^1H NMR (400 MHz, DMSO-d_6, 298 K) δ 10.64 (s, 1H, N_1H), 8.96 (s, 1H, N_2H), 8.23 (d, J = 3.8 Hz, 2H), 8.07 (s, 1H, H_8), 7.67 (m, J = 8.3 Hz, 8H), 7.14 (d, J = 8.4 Hz, 2H), 7.03 (m, J = 5.1, 7.2, 8.4 Hz, 4H), 5.78 (d, J = 5.6 Hz, 1H, $H_{1'}$), 5.46 (d, J = 6.0 Hz, 1H, C_2-OH), 5.17 (d, J = 4.9 Hz, 1H, C_3-OH), 4.98 (m, J = 5.2 Hz, 1H, C_5-OH), 4.50 (q, J = 5.5 Hz, 1H, $H_{2'}$), 4.11 (d, J = 4.2 Hz, 1H, $H_{3'}$), 3.89 (d, J = 3.8 Hz, 1H, $H_{4'}$), 3.65 (m, J = 4.2, 13.3 Hz, 1H, $H_{5'}$), 3.52 (m, J = 4.5, 13.6 Hz, 1H, $H_{5''}$) ppm. ^{13}C NMR (400 MHz, DMSO-d_6, 298 K) δ 158.4, 158.3 (2C), 157.3, 150.6, 150.3, 149.9, 148.9 (2C), 146.3, 147.8, 144.5, 138.7 (2C), 137.2, 134.5, 128.1 (2C), 128.0 (2C), 127.7 (2C), 120.3, 119.2 (2C), 117.6 (2C), 88.1 (C_1), 86.1 (C_4), 74.6 (C_2), 71.0 (C_3), 62.1 (C_5) ppm. ESI-MS *m/z* 605.2189 $[M+H]^+$. HRMS ESI^+ *m/z* calcd for $C_{32}H_{28}N_8O_5{\cdot}H^+$ 605.2255, found 605.2212.

2.2.7 Synthesis of *2',3',5'-O*-triacetyl-N^2-(*p*-4,4'-biphenyldipyridylamino)guanosine (2.2b)

To a suspension of compound **2.2a** (0.23 g, 0.38 mmol) and 4-dimethylaminopyridine (0.004 g, 0.03 mmol) in dry CH_3CN (6 mL), freshly distilled triethylamine (0.21 mL, 1.46 mmol) was added. After stirring for 5 minutes, freshly distilled acetic anhydride (0.13 mL, 1.36 mmol) was added dropwise over 5 minutes, and the mixture was stirred for 4 hours at room temperature. The reaction mixture was

quenched with methanol (6 mL), and the organic solvents were removed to dryness. The residue was treated using a chromatographic column with CH_2Cl_2 and CH_2Cl_2/CH_3OH (95:5%vv) as eluents to give **2.2b** as a white solid (0.11 g, 40% yield). mp. 241-250 ^oC. ^1H NMR (400 MHz, DMSO-d_6, 298 K) δ 10.83 (broad, N_1H, 1H), 8.97 (broad, N_2H, 1H), 8.25 (d, J = 3.7 Hz, 2H), 8.02 (s, 1H, H_8), 7.72-7.65 (m, J = 7.8, 8.4 Hz, 8H), 7.16 (d, J = 8.4 Hz, 2H), 7.04 (d, J = 5.3 Hz, 2H), 6.99 (d, J = 8.8 Hz, 2H), 6.08 (d, J = 5.3 Hz, 1H, $H_{1'}$), 6.01 (t, J = 5.8 Hz, 1H, $H_{2'}$), 5.39 (t, J = 5.7 Hz, 1H, $H_{3'}$), 4.28 (m, J = 4.3, 9.6 Hz, 1H, $H_{4'}$), 4.22 (m, J = 3.9, 12.4 Hz, 1H, $H_{5'}$), 4.19 (m, J = 3.9, 12.3 Hz, 1H, $H_{5''}$), 2.09 (s, CH_3, 3H), 2.06 (s, CH_3, 3H), 1.85 (s, CH_3, 3H) ppm. ^{13}C NMR (500 MHz, CD_3OD, 298 K) δ 170.9, 170.2, 170.1, 158.2, 150.4, 147.9 (3C), 144.1, 138.8 (3C), 138.4, 138.1, 137.6, 136.4, 127.9 (3C), 127.3 (2C), 127.2 (3C), 122.5 (2C), 119.0 (2C), 117.9 (2C), 87.6 (C_1), 80.0 (C_4), 72.5 (C_2), 70.8 (C_3), 62.8 (C_5), 19.3 (CH_3), 19.2 (CH_3), 19.1 (CH_3) ppm. MS-ESI$^+$ *m/z* 731.8851 $[M+H]^+$. HRMS ESI$^+$ *m/z* calcd for $C_{38}H_{34}N_8O_8$+H 731.2572, found 731.2578.

2.2.8 Synthesis of *2',3',5'-O*-triacetyl-N^2-acetyl- N^2-(*p*-4,4'-biphenyldipyridylamino)guanosine (2.2c)

To a suspension of **2.2a** (0.23 g, 0.38 mmol) and 4-dimethylaminopyridine (0.004 g, 0.03 mmol) in dry CH_3CN (6 mL), freshly distilled triethylamine (0.21 mL, 1.46 mmol) was added. After stirring for 5 minutes, freshly distilled acetic anhydride (0.13 mL, 1.36 mmol) was added dropwise over 5 minutes, and the mixture was stirred for 4 hours at room temperature. The reaction mixture was quenched with methanol (6 mL), and the organic solvents were removed to dryness. The residue was treated using a chromatographic column with CH_2Cl_2 and CH_2Cl_2/CH_3OH (95:5%vv) as eluents to give **2.2c** as a white solid (0.04 g, 18% yield). mp. 156-164 ^oC. ^1H NMR (400 MHz, CD_3CN,

298 K) δ 12.98 (broad, N_1H, 1H), 8.24 (d, J = 4.5 Hz, 2H), 7.82 (d, J = 8.4 Hz, 2H), 7.73 (s, 1H, H_8), 7.72 (d, J = 6.5 Hz, 2H), 7.65 (dt, J = 1.8, 9.1 Hz, 2H), 7.48 (d, J = 8.4 Hz, 2H), 7.21 (d, J = 8.5 Hz, 2H), 7.02 (m, 4H), 5.75 (d, J = 4.6 Hz, 1H, $H_{1'}$), 5.57 (t, J = 4.9 Hz, 1H, $H_{2'}$), 4.41 (t, J = 6.0 Hz, 1H, $H_{3'}$), 4.05 (m, J = 5.1, 11.5 Hz, 1H, $H_{4'}$), 3.71 (m, 2H, $H_{5'}$, $H_{5''}$), 2.03 (s, CH_3, 3H), 1.94 (s, CH_3, 3H), 1.88 (s, CH_3, 3H), 1.86 (s, CH_3, 3H) ppm. ^{13}C NMR (400 MHz, CD_3CN, 298 K) δ 175.7, 170.2, 169.4, 169.3, 158.1 (2C), 155.3, 150.5, 148.3, 147.5 (2C), 145.4, 140.7, 139.4, 138.0 (2C), 137.7 (2C), 135.9, 129.7 (2C), 128.4 (2C), 127.9 (2C), 127.3 (2C), 121.9, 118.6 (2C), 117.3, 87.9 (C_1), 79.4 (C_4), 71.9 (C_2), 70.7 (C_3), 63.8 (C_5), 25.8 (CH_3), 19.8 (CH_3), 19.6 (CH_3), 19.5 (CH_3) ppm. HRMS ESI^+ *m/z* calcd for $C_{40}H_{36}N_8O_9H^+$ 773.2678, found 773.2666.

2.2.9 Synthesis of *p*-2-(2'-pyridyl)benzimidazolyliodobiphenyl (2.3)

2-(2'-Pyridyl)benzimidazole (5.18 g, 26.1 mmol), 4,4'-diiodobiphenyl (16.4 g, 41.2 mmol), cesium carbonate (10.1 g, 31.2 mmol), 1,10-phenanthroline (0.93 g, 5.22 mmol) and copper iodide (0.49 g, 2.63 mmol) were placed in a 250 mL round bottom flask. To the solid mixture DMF (10 mL) was added and the reaction flask was heated to 160 ^oC for 18 h. The reaction was monitored by TLC. After the reaction mixture was cooled, water (50 mL) and dichloromethane (100 mL) were used to dissolve solids. After extraction, the organic fractions were dried over anhydrous $MgSO_4$ and the product was isolated by using a chromatographic column with hexane:ethylacetate (2:1 %vv) (R_f = 0.5) as the eluent to provide compound **2.3** as a white solid (8.03 g, 66% yield). mp. 170-173 ^oC. ^1H NMR (500 MHz, $CDCl_3$, 298 K) δ 8.42 (d, J = 3.5 Hz, 1H), 8.26 (d, J = 5.6 Hz, 1H), 7.99 (td, J = 7.3 Hz, 1H), 7.82 (m, J = 7.6, 8.5 Hz, 3H), 7.68 (d, J = 7.6 Hz, 2H),

7.41 (m, J = 7.1 Hz, 5H), 7.36 (m, J = 6.1, 6.9, 8.5 Hz, 2H), 7.28 (d, J = 7.5 Hz, 1H) ppm. ^{13}C NMR (500 MHz, $CDCl_3$, 298 K) δ 150.4, 149.5, 140.4, 139.9, 138.4 (2C), 137.6, 137.3, 137.1, 131.9, 129.3 (2C), 129.2, 128.2 (2C), 128.1 (2C), 125.4, 124.8, 124.5, 124.2, 120.3, 111.5, 94.1 (C-I) ppm. EI-MS *m/z* 473.0233 [$M^{+\cdot}$]. HRMS EI^+ *m/z* calcd for $C_{24}H_{16}N_3I^+$ 473.0346, found 473.0337.

2.2.10 Synthesis of N^2-(*p*-4,4'-biphenyl-2-(2'-pyridyl)benzimidazolyl)guanosine (2.3a).

To a mixture of 2-(2'-pyridyl)benzimidazolyliodobiphenyl (**2.3**) (3.51 g, 7.39 mmol), guanosine (1.90 g, 6.72 mmol), cesium carbonate (2.67 g, 8.86 mmol) and copper iodide (0.037 g, 2.21 mmol, 15%), DMSO was added (8 mL). The solution was degassed with nitrogen for 10 minutes. A preheated oil bath was used and the reaction was carried out in a sealed tube at 140 ^{o}C for 17 h. To the reaction mixture water (10 mL) was added, and the solution was neutralized to pH ~ 7 using aqueous HCl (0.1 M). Further addition of water (30 mL) led to precipitation of the product as beige solid. The solid was washed further with water (30 mL) to remove unreacted guanosine. The crude solid was further purified using a C-18 reverse phase silica gel column with CH_2Cl_2, followed by CH_2Cl_2:CH_3OH (95:5 % vv to 60:40 %vv) as the eluent to obtain the compound **2.3a** as a beige solid (0.53 g, 11% yield). m.p. 253-256 ^{o}C. ^{1}H NMR (500 MHz, DMSO-d_6, 298 K) δ 10.68 (s, 1H, N_1H), 9.01 (s, 1H, N_2H), 8.39 (d, J = 4.2 Hz, 1H, H_{py}), 8.21 (d, J = 7.88 Hz, 1H, H_{Bn}), 8.09 (s, 1H, H_8), 7.97 (t, J = 7.6 Hz, 1H, H_{Bn}), 7.84 (d, J = 7.4 Hz, 2H), 7.73 (m, 4H), 7.46 (d, J = 8.3 Hz, 2H), 7.37 (m, J = 1.0, 6.5, 7.7 Hz, 5H), 5.81 (d, J = 5.5 Hz, 1H, $H_{1'}$), 5.46 (d, J = 6.0 Hz, 1H, C_2-OH), 5.18 (d, J = 4.8 Hz, 1H, C_3-OH), 4.99 (d, J = 5.3 Hz, 1H, C_5-OH), 4.54 (d, J = 5.4 Hz, 1H, $H_{2'}$), 4.14 (d, J = 4.3 Hz, 1H, $H_{3'}$), 3.93 (d,

J = 3.8 Hz, 1H, $H_{4'}$), 3.66 (m, *J* = 6.8, 11.8 Hz, 1H, $H_{5'}$), 3.64 (m, *J* = 6.8, 11.8 Hz, 1H, $H_{5''}$) ppm. ^{13}C NMR (500 MHz, DMSO-d_6, 298 K) δ 151.3, 150.7, 149.9, 149.6, 143.2, 139.9, 137.9 (2C), 137.8, 137.7, 128.5, 128.4 (2C), 128.0 (2C), 127.9 (2C), 127.7 (2C), 125.5, 125.1 (2C), 124.8, 123.8, 120.8, 120.4 (2C), 119.4, 111.8, 88.1 (C_1), 86.2 (C_4), 74.7 (C_2), 71.1 (C_3), 62.3 (C_5) ppm. ESI-MS *m/z* 629.2216 $[M+H]^+$. HRMS ESI^+ *m/z* calcd for $C_{34}H_{28}N_8O_5 \cdot H^+$ 629.2260, found 629.2263.

2.2.11 Synthesis of *p*-pyrenyliodophenyl (2.4).

To a round bottom flask in THF (100 mL) containing bromopyrene (0.71 g, 2.54 mmol), a hexane solution of n-BuLi (1.75 ml, 2.79 mmol, 1.6 M) at -78 ^{o}C was added. After being stirred for 1h at this temperature, $ZnCl_2$ (0.41 g, 3.04 mmol) was added and stirring was continued for 0.5 hrs at 0 ^{o}C. Diiodobenzene (1.81 g, 5.4 mmol) and tetrakis(triphenylphosphine)palladium (0) ($Pd(PPh_3)_4$) (0.22 g, 9 mol%) were added to the above mixture and the reaction was allowed to warm up to room temperature and stirred over night under N_2. The solution was partitioned using ethylacetate (100 mL) and water (100 mL). The aqueous layer was further extracted with dichloromethane (3 × 40 mL) and the combined organic fractions were dried over anhydrous $MgSO_4$ and reduced under vacuum. The product, **2.4**, was isolated, using column chromatography with hexane: ethyl acetate (5:1 %vv) (R_f = 0.6), as a white solid (0.61 g, 60% yield). m.p. 169-171 ^{o}C. ^{1}H NMR (400 MHz, $CDCl_3$, 298 K) δ 8.24-7.94 (m, *J* = 3.6, 7.8, 9.2 Hz, 9H), 7.91 (d, *J* = 8.3 Hz, 2H, H_o), 7.39 (d, *J* = 8.3 Hz, 2H, H_m) ppm. ^{13}C NMR (400 MHz, $CDCl_3$, 298 K) δ 140.7, 137.5, 136.4, 132.5, 131.5, 131.2, 130.9, 130.8, 128.3, 128.1, 127.7, 127.6, 127.4, 127.3, 126.1, 125.8, 125.3, 125.0, 124.9, 124.8, 124.6, 93.1 (C-I) ppm. HRMS EI^+ *m/z* calcd for $C_{22}H_{13}I$ 404.0062, found 404.0046.

2.2.12 Synthesis of N^2-(4-pyrenylphenyl)guanosine (2.4a).

To a mixture of *p*-pyrenyliodophenyl (**2.4**) (0.20 g, 0.49 mmol), guanosine (0.21 g, 0.73 mmol), cesium carbonate (0.19 g, 0.59 mmol) and copper iodide (0.014 g, 0.07 mmol, 15 mol%) in a small sealed vial (25 mL), DMSO was added (5 mL). The solution was degassed with nitrogen for 10 minutes. A preheated oil bath was used and the reaction was carried out at 140 ^{o}C for 24 h. To the reaction mixture water was added (10 mL), and the solution was neutralized to pH ~ 7 using aqueous HCl (0.1 M). Further addition of water (30 mL) led to precipitation of the product as a beige solid. The solid was washed further with water (20 mL) to remove unreacted guanosine. The obtained solid was further purified using a C-18 reversed phase silica with CH_2Cl_2, followed by CH_2Cl_2:CH_3OH (95:5 % vv to 60:40 %vv), to obtain **2.4a** as a beige solid (0.06 g, 22% yield). m.p. 220-225 ^{o}C. ^{1}H NMR (400 MHz, DMSO-d_6, 298 K) δ 10.76 (broad, s, 1H, N_1H), 9.14 (broad, s, 1H, N_2H), 8.4-8.26 (m, 3H), 8.21 (d, J =9.17 Hz, 4H), 8.11 (s, 1H, H_8), 8.06 (t, J = 8.0 Hz, 2H), 7.86 (d, J = 8.3 Hz, 2H, H_o), 7.64 (d, J = 8.2 Hz, 2H, H_m), 5.83 (d, J = 5.5 Hz, 1H, $H_{1'}$), 5.53 (d, J = 5.9 Hz, C_2-OH), 5.21 (d, J = 5.1 Hz, C_3-OH), 5.02 (t, J = 5.2, 5.3 Hz, C_5-OH), 4.55 (q, J = 5.3, 5.9 Hz, 1H, $H_{2'}$), 4.13 (d, J = 4.3 Hz, 1H, $H_{3'}$), 3.9 (d, J = 3.5 Hz, 1H, $H_{4'}$), 3.55 (m, J = 4.0, 10.7 Hz, 2H, $H_{5'}$, $H_{5''}$) ppm. ^{13}C NMR (400 MHz, DMSO-d_6, 298 K) δ 157.7, 150.9, 150.5, 138.9, 137.9, 132.1 (2C), 131.9 (2C), 131.5, 131.1, 128.8 (2C), 128.7 (2C), 128.5 (2C), 127.6, 126.4, 126.1 (2C), 125.4, 125.3, 125.2, 123.8, 121.4 (2C), 120.2, 86.9 (C_1), 79.5 (C_4), 72.3 (C_2), 70.4 (C_3), 63.3 (C_5) ppm. HRMS ESI$^+$ *m/z* calcd for $C_{32}H_{25}N_5O_5 \cdot H^+$ 560.1934, found 560.1943.

2.2.13 Synthesis *of 2′,3′,5′-O*-triacetyl-N^2-(4-pyrenylphenyl)guanosine (2.4b).

To a suspension of compound **2.4a** (0.041 g, 0.07 mmol) and 4-dimethylaminopyridine (0.003 g, 0.02 mmol) in a mixture of CH_3CN (6 mL) and triethylamine (0.151 mL, 1.08 mmol), was added acetic anhydride (0.094 mL, 0.98 mmol) at room temperature. After stirring for 1 hour when all of the starting material had dissolved, methanol (5 mL) was added to the mixture and stirring was continued for an additional 5 minutes. The solution was then evaporated to dryness and the resulting oil was precipitated with *iso*-propanol (^{i}PrOH) (5 mL). The solid was isolated by centrifugation and washed with ether. The solid was dissolved in THF and preparatory TLC plates were used for further purification. The solvent system used was CH_3OH:CH_2Cl_2 (10:90%vv) and CH_3OH:ethyl acetate (10:90%vv). After extensive purification a white product, **2.4b**, was recovered (15 mg, 32 % yield). ^{1}H NMR (400 MHz, DMSO-d_6, 298 K) δ 10.93 (broad, s, 1H, N_1H), 9.17 (broad, s, 1H, N_2H), 8.39-8.03 (m, J = 3.1, 4.2, 8.3 Hz, 10H, 9H pyrene, H_8), 7.78 (d, J = 8.4 Hz, 2H, H_o), 7.63 (d, J = 8.4 Hz, 2H, H_m), 6.13 (d, J = 5.1 Hz, 1H, $H_{2'}$), 6.08 (t, J = 5.8 Hz, 1H, $H_{1'}$), 5.45 (t, J = 5.4 Hz, 1H, $H_{3'}$), 4.31 (m, J = 3.4, 4.0 Hz, 1H, $H_{4'}$), 4.28 (m, J = 4.6, 6.1, 10.1 Hz, 1H, $H_{5''}$), 4.15 (m, J = 4.8, 6.1, 10.2 Hz, 1H, $H_{5'}$), 2.06 (s, 3H, CH_3), 2.02 (s, 3H, CH_3), 1.86 (s, 3H, CH_3) ppm. ^{13}C NMR (400 MHz, DMSO-d_6, 298 K) δ 171.7, 170.2, 170.1, 157.3, 150.5, 150.2, 138.8, 137.6, 135.7, 131.8, 131.6 (2C), 131.2, 130.7, 128.4 (2C), 128.3 (2C), 128.2 (2C), 127.2, 126.1, 125.8, 125.7 (2C), 125.4, 125.0, 124.9, 121.1 (2C), 87.3 (C_1), 79.9 (C_4), 72.6 (C_2), 70.8 (C_3), 63.6 (C_5), 21.3 (CH_3), 21.0 (CH_3), 20.8 (CH_3) ppm. HRMS ESI$^+$ *m/z* calcd for $C_{38}H_{31}N_5O_8{\cdot}H^+$ 686.2251, found 686.2276.

2.2.14 Synthesis of N^2-(4-iodophenyl)guanosine (2.5a).

To a mixture of *p*-diiodobenzene (10.1 g, 30.1 mmol), guanosine (4.25 g, 15.2 mmol), cesium carbonate (5.85 g, 18.1 mmol) and copper iodide (0.88 g, 4.51 mmol, 15%) in a small sealed vial (25 mL), DMSO was added (5 mL). The solution was degassed with nitrogen for 10 minutes. Preheated oil bath was used and reaction was carried out at 140 ^{o}C for 40 h. To the reaction mixture water was added (10 mL), and the solution was neutralized to pH ~ 7 using aqueous HCl (0.1 M). Further addition of water (30 mL) led to precipitation of the product as beige solid. The solid was washed further with water (20 mL) to remove unreacted guanosine. The obtained solid was further purified using a C-18 reversed phase silica with CH_2Cl_2 followed by CH_2Cl_2:CH_3OH (95:5 % vv to 60:40 %vv) to obtain compound **2.5a** as a beige solid (0.65 g, 9 % yield). m.p. > 300 ^{o}C. ^{1}H NMR (400 MHz, DMSO-d_6, 298 K) δ 11.02 (broad, s, 1H, N_1H), 9.49 (broad, s, 1H, N_2H), 8.08 (s, 1H, H_8), 7.67 (d, J = 7.9 Hz, 2H, H_o), 7.51 (d, J = 6.5 Hz, 2H, H_m), 5.76 (d, J = 5.1 Hz, 1H, $H_{1'}$), 5.48 (d, J = 5.3 Hz, 1H, C_2-OH), 5.21 (d, J = 4.8 Hz, 1H, C_3-OH), 5.01 (t, J = 5.2 Hz, 1H, C_5-OH), 4.48 (q, J = 5.2, 9.2 Hz, 1H, $H_{2'}$), 4.10 (q, J = 4.6, 7.7 Hz, 1H, $H_{3'}$), 3.90 (d, J = 3.8, 7.6 Hz, 1H, $H_{4'}$), 3.63 (m, J = 4.2, 9.1 Hz, 1H, $H_{5'}$), 3.53 (m, J = 4.8, 10.1 Hz, 1H, $H_{5''}$) ppm. ^{13}C NMR (400 MHz, DMSO-d_6, 298 K) δ 149.5, 149.3, 138.9, 138.2, 137.4 (2C), 121.4 (2C), 118.6, 87.3 (C_1), 85.5 (C-I), 85.2 (C_4), 73.8 (C_2), 70.1 (C_3), 61.3 ($C_{5'}$) ppm. MS-ESI$^+$ *m/z* 486.0311 $[M+H]^+$. HRMS ESI$^+$ *m/z* calcd $C_{16}H_{16}N_5O_5I \cdot H^+$ 486.0268, found 486.0268.

2.2.15 Molecular orbital calculations

The *ab initio* molecular orbital calculations were performed in the ground and excited states for molecules **2.1a - 2.4a** using the restricted density functional theory at

the B3LYP level of theory with 6-311++G** as the basis set. The Gaussian 03 program suite[9] was used for all molecular-geometry optimization and molecular-orbital calculations. Time-dependent density functional theory (TD-DFT) calculations were performed on the optimized ground-state structures.

2.2.16 Fluorescence quantum yield measurements

The fluorescence emission quantum yields were determined relative to anthracene as a reference in DMSO, THF and CH_3OH at 298 K (Φ = 0.36). The absorbance of all samples and the standard at the excitation wavelength were ~ 0.097 – 0.102. The quantum yields were calculated by previously reported procedure.[10]

2.3 Results and Discussion

2.3.1 Syntheses

2.3.1.1 Synthesis of intermediates ***2.1 – 2.4***

The starting materials, aromatic iodides were obtained in moderate yields by the reaction of *p*-diiodobiphenyl with diphenylamine, 2,2'-dipyridylamine and 2-(2'-pyridyl)benzimidazole, respectively, using Ullmann condensation procedure,[11] in 25 - 67 % yields as shown in Figure 2.3.[12] Compound **2.4** was synthesized using a Negishi[13] coupling reaction between bromopyrene and diiodobenzene, due to the availability of the starting materials, in ~ 60 % yield (Figure 2.4).

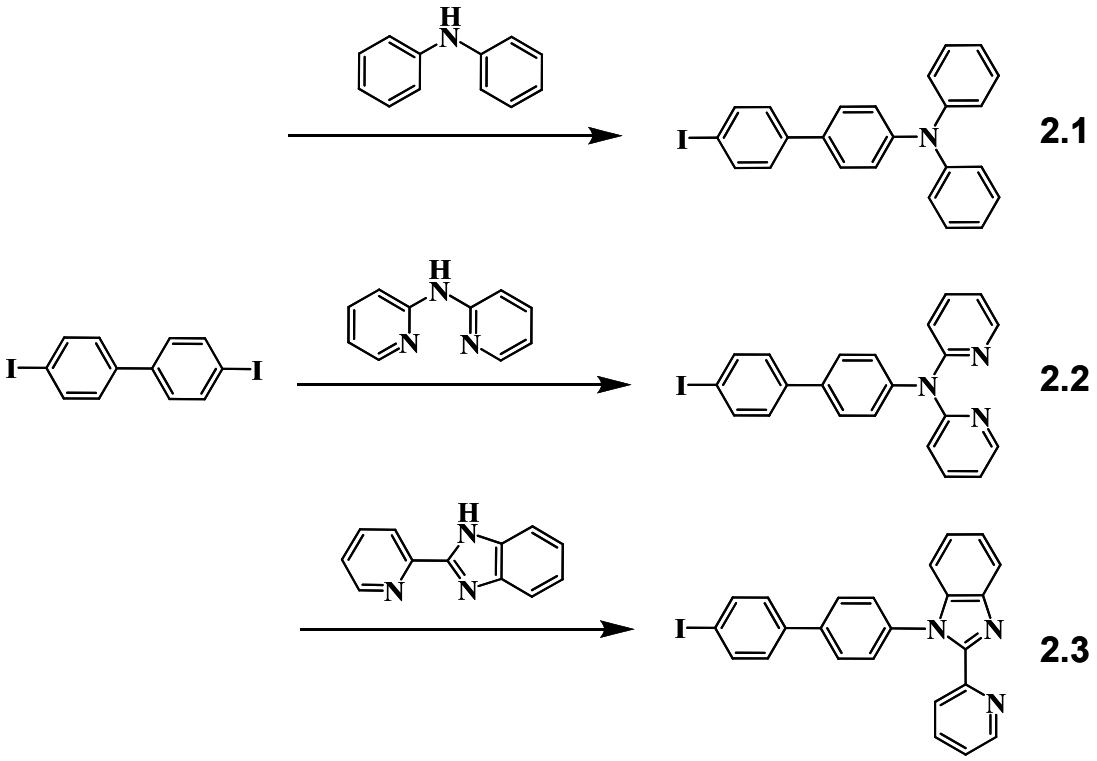

Figure 2.3 Reaction scheme showing the synthesis of aryliodide intermediates **2.1** - **2.3** (CuI, Cs_2CO_3, 1,10-phenanthroline, DMF, 160 ^oC).

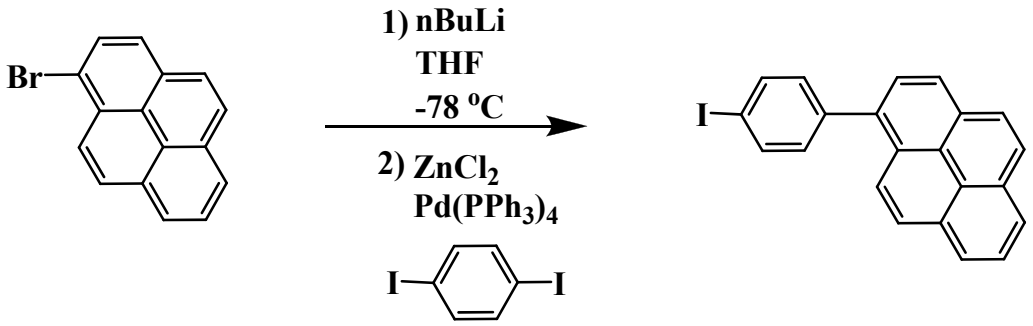

Figure 2.4 Reaction scheme showing the synthesis of aryliodide intermediate **2.4**.

2.3.1.2 Synthesis of N^2-modified guanosines

The guanine core is perhaps the most difficult to modify by functional groups, among nucleobases, due to the presence of multiple reactive sites. In order to avoid the protection/deprotection steps, a direct modification of guanosine is desirable. Recently, N^6-arylation of deoxyadenosine was achieved *via* copper-catalyzed C-N coupling reactions with aryl halides.[14] This methodology failed when deoxyguanosine was used possibly due to weaker nucleophilicity of the N^2-amino group.

The Ullmann condensation reaction,[15] used for the coupling arylhalides with arylamines, is high yielding and requires a reaction temperature of > 180 °C and long reaction times (8 - 12 h). Controlling the reaction temperature is the key in order to avoid the nucleoside depurination and the formation of side products. The temperatures above 150 °C over a long period of time produced a dark black solution which indicates a partial decomposition and depurination of the nucleoside. The choice of appropriate solvent and catalyst is an important parameter in N^2-arylation reactions. The use of DMF as a solvent was undesirable due to the issues related to the isolation and purification of the final products. Excess CuI catalyst loading (> 30 %) gave a trace amounts of product, possibly due to coordination of Cu^{1+} ion to the guanine ring. In addition, $CuSO_4$, as a catalyst, failed to work. The use of arylbromides under Ullmann condensation conditions was not fruitful, due to their lower reactivity over aryliodides, as expected.

Fluorescent N^2-modified guanosines: N^2-(*p*-4,4'-biphenyl-diphenylamino)guanosine (**2.1a**), N^2-(*p*-4,4'-biphenyl-dipyridylamino)guanosine (**2.2a**), N^2-(*p*-4,4'-biphenyl-2-(2'-pyridyl)benzimidazolyl)guanosine (**2.3a**) and N^2-(*p*-4,4'-phenylpyrenyl)guanosine (**2.4a**) were successfully synthesized using Ullmann

condensation reactions as shown in Figure 2.5 and Figure 2.6. A non-fluorescent N^2-(4-iodophenyl)guanosine (**2.5a**), was synthesized for comparison purpose in terms of fluorescence and has not been studied in great detail, rather it has been synthesized as a precursor for additional cross-coupling reactions.

We have found that the optimal conditions for the synthesis of **2.1a – 2.5a** is to carry out the reaction in DMSO at 140 °C in the presence of CuI and Cs_2CO_3. Using this simple procedure, the selective arylation at the exocyclic amine without the N^1, N^3 and/or N^7-arylated side products was achieved, as determined by ^{1}H NMR. The purification of the final compounds was achieved using reverse-phase column chromatography under the following conditions: CH_2Cl_2 as eluent for removal of unreacted aryliodides followed by the treatment with CH_2Cl_2/CH_3OH solvent gradient from 95:5 %vv to 60:40 %vv. Using this methodology, compounds **2.1a – 2.5a** were isolated in moderate yields (9 – 35 %) and were fully characterized using high-resolution mass spectrometry, ^{1}H, ^{13}C, COSY and HMQC NMR spectroscopy. The relatively low yields may be attributed to the necessary use of suboptimal reaction temperatures.

The lipophilic guanosines, **2.1b**, **2.2b, 2.2c** and **2.4b** were synthesized by using freshly distilled Et_3N and acetic anhydride in the presence of DMAP in CH_3CN (Figure 2.7). The overall success and yield of the acetylation reaction was dependent on the quality and purity of the starting materials. The best yields were obtained when freshly distilled and recrystallized starting materials were used.

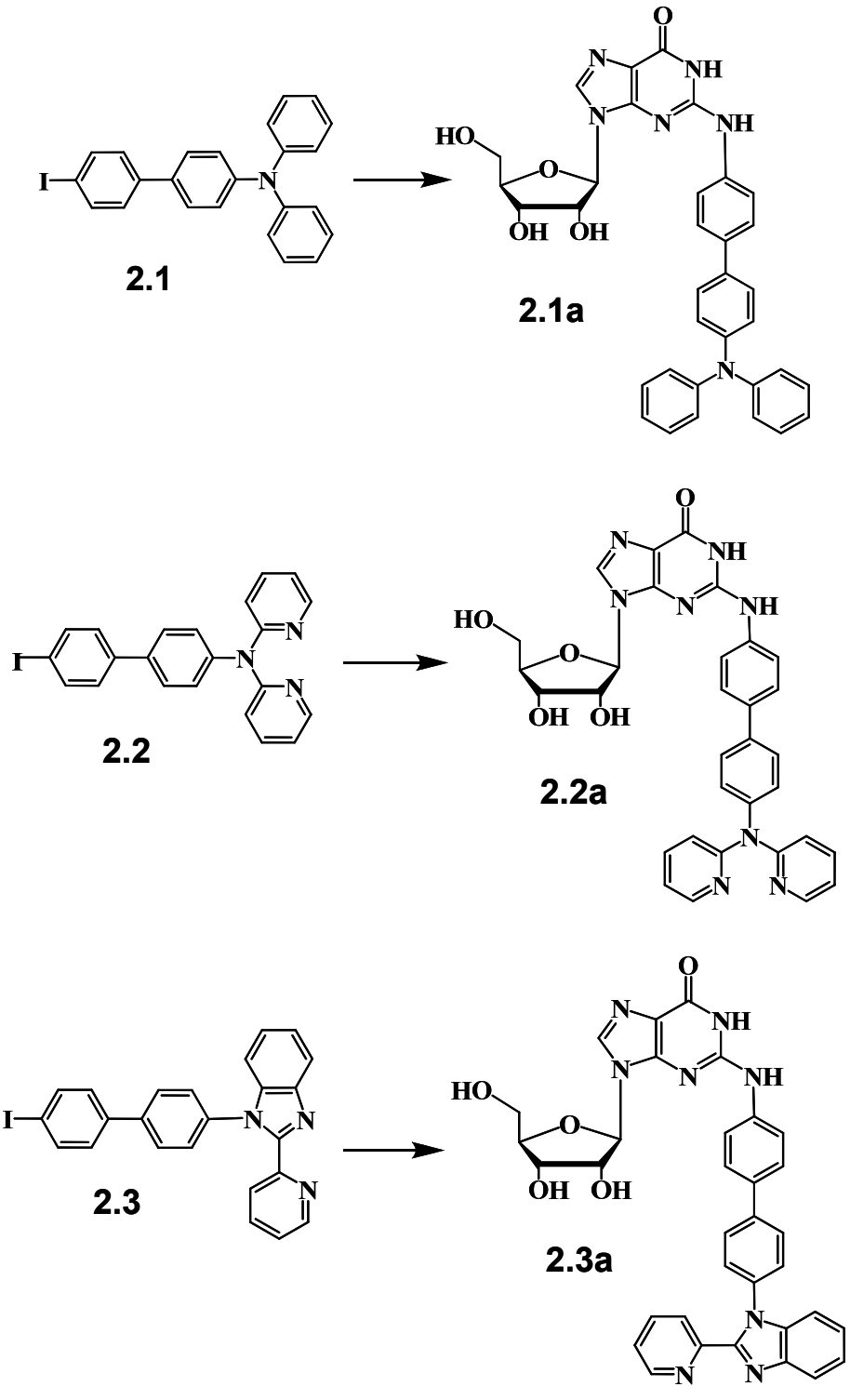

Figure 2.5 Reaction scheme for the synthesis of compounds **2.1a - 2.3a** (CuI, Cs_2CO_3, DMSO, 140 ^{o}C).

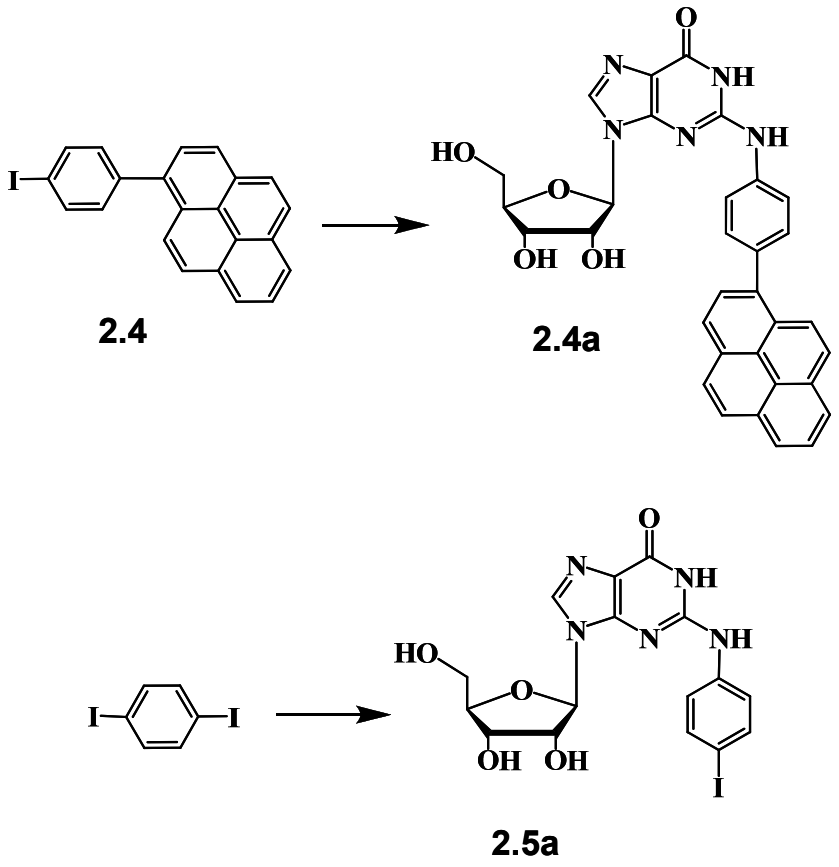

Figure 2.6 Reaction scheme for the synthesis of compounds **2.4a** - **2.5a** (CuI, Cs_2CO_3, DMSO, 140 ^oC).

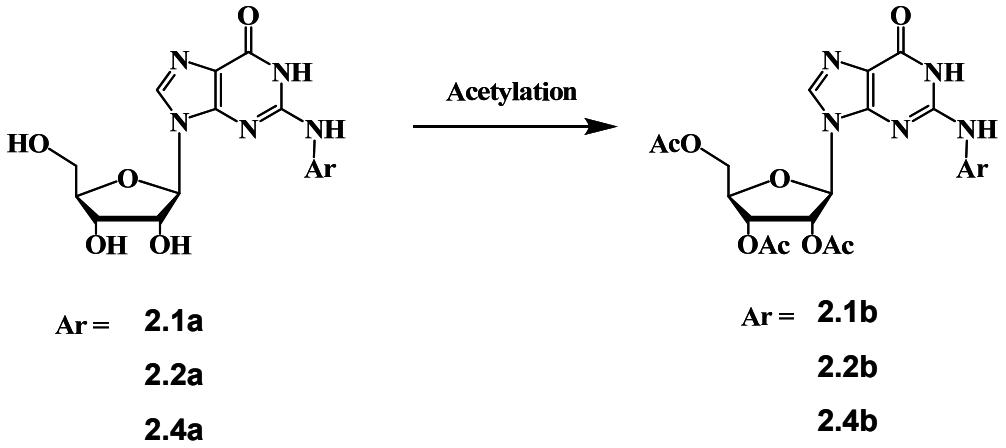

Figure 2.7 Reaction scheme for the synthesis of acetylated N^2-arylguanosines **2.1b**, **2.2b** and **2.4b** (DMAP, CH_3CN, Et_3N and acetic anhydride).

2.3.1.3 Attempted synthesis of N^2-arylguanosines by using other synthetic methodologies

It should be pointed out that the synthesis of **N^2G** was not limited to the use of Ullmann condensation reaction. Buchwald-Hartwig Pd-catalyzed C-N methodology was tested with the aim of lowering the operating temperatures, so that the additional functionalities could be introduced at the N^2-site. Pd-catalyzed direct N-arylation of nucleosides was successfully performed by Enya et al.[16] between guanosine and aryliodides in the presence of $Pd(dba)_2$, xantphos or BINAP and tetraethylammonium fluoride (TEAF) in DMSO or dioxane. A number of phosphine ligands were screened, however only a few proved to be efficient.

Inspired by Enya, we performed a similar reaction between guanosine and diiodobenzene in the presence of $Pd(dba)_2$, BINAP and Cs_2CO_3 in DMSO at 100 °C for 18 h as described in Figure 2.8. Essentially no conversion was observed as evidenced by ^{1}H NMR. Similar conditions were employed but in the presence of $Pd(OAc)_2$, as a catalyst, no reaction was observed either.

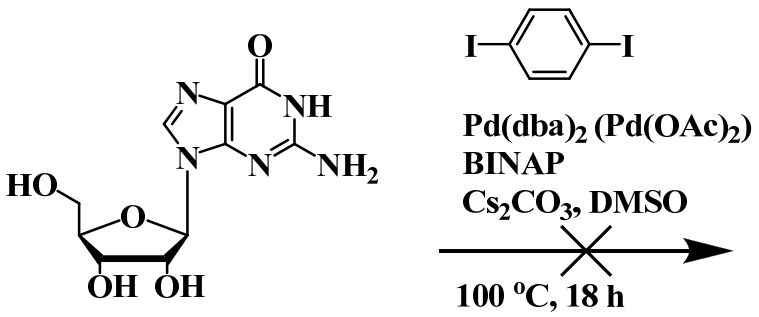

Figure 2.8 Proposed scheme for the synthesis of N^2-arylguanosine.

2.3.1.4 Attempted synthesis of boron-containing guanosines

In addition to synthesizing donor type **N^2Gs**, containing arylamine groups, we also attempted to synthesize **N^2G** containing the electron accepting groups, such as dimesitylboron. The incorporation of a triarylboron moiety into guanosine is based on the following considerations. First, the luminescent triarylboron compounds were shown to act as efficient chemical sensors for fluoride or cyanide anions.[17] Second, intra- or intermolecular charge transfer between nitrogen donor groups and the three-coordinate boron acceptor has been demonstrated previously. It can be proposed that a similar intramolecular charge transfer could take place between two guanosines containing the arylamino and triarylboron groups. Moreover, intermolecular charge transfer can be envisioned between a stacked all-nitrogen G-quartet on top of an all-boron G-quartet.

However, due to the thermal instability of dimesitylboron functionality lower reaction temperatures had to be applied, which excluded the use of the Ullmann condensation reaction as the synthetic route. Hence, we turned to other methodologies, such as the Suzuki cross-coupling reaction which has been successfully used by Western et al. in the synthesis of arylated unprotected halonucleosides by employing the water-soluble Pd-catalysts and phosphine ligands.[18] Inspired by this, a Suzuki cross-coupling reaction was attempted using **2.5a** and the previously synthesized *p*-dimesitylboronbiphenylboronic acid[19] using the degassed solvent mixture $CH_3CN/H_2O/CH_3OH$ (2:1:1) in the presence of palladium(II) acetate ($Pd(OAc)_2$) (2.5 mol %) and tris(3-sulfonatophenyl)phosphine (TPPTS) (5 mol %) for 20 h (Figure 2.9). No products were, however, identified. The failure of the reaction can be attributed to the low solubility of the **2.5a** under the given reaction conditions or to the poor ability of the

phosphine ligand to activate the Pd-catalyst. Western et al. established earlier that phosphine ligands bulkier than TPPTS are more effective in the arylation of 8-bromoguanosine. The researchers were intrigued by the unexpected ligand dependence on the catalyst activity and the reaction yields with G-nucleoside substrates. The success of their methodology was highly dependent on several factors, such as the ligand, catalyst, solvent and substrates under investigation. Dramatic differences in the activity of halonucleosides were observed especially for guanosine-based substrates. Since the ideal solvent mixture could not be determined for the C-C coupling reaction involving **2.5a**, this methodology was abandoned and the Ullmann condensation reaction was primarily used to synthesize all of the new **N^2Gs**.

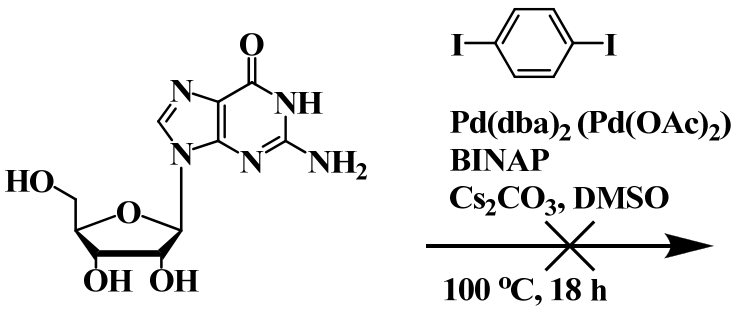

Figure 2.9 Proposed scheme for the synthesis of boron-containing guanosine.

2.3.2 UV-Vis study of 2.1a- 2.4a

Compounds **2.1a** – **2.4a** were studied in solution (THF, CH_3OH and DMSO) at 298 K and their photophysical properties are presented in Table 1. **2.1a** – **2.4a** display an intense absorption band in the UV region with an absorption maxima below 270 nm, typical of the guanine base, and absorption bands in the 270 - 370 nm region which can be assigned to the π - π^* electronic transitions associated with the N^2-aryl substituents as

shown in Figure 2.10 and Figure 2.11. Solvent polarity has little influence on the absorption maxima of the **N^2Gs**. Quantum yields of all three compounds are significantly lower in CH_3OH than in other solvents, due to the hydrogen bonding ability of the medium.

Table 2.1 Absorption and luminescence data for **2.1a – 2.4a** (in solution at 298 K).[a]

Compound	Solvent	Absorption λ_{max} [nm]	e_{max} [$M^{-1}cm^{-1}$]	λ_{ex} [nm]	λ_{em} [nm]	Q.Y. (%)
2.1a (N^2Ph_2)	THF	238 339	9600 28000	358	395	13
	CH_3OH	250 295 334	15000 25000 30000	358	406	6.3
	DMSO	261 308 343	13000 22300 29000	320	407	28
2.2a (N^2Py_2)	THF	220 253 317	24000 17000 37000	346	370 385	7
	CH_3OH	221 278 313	24000 20000 38000	350	406	0.4
	DMSO	262 278 322	15000 18000 37000	353	387	11
2.3a (N^2PyBn)	THF	224 258 315	23000 20000 39000	343	410	10
	CH_3OH	211 258 311	32000 23000 39000	344	401	1.3
	DMSO	265 311	24000 39000	352	423	3.1
2.4a (N^2Pyr)	THF	243 269 345	16000 11000 8600	357	418	26
	CH_3OH	210 240 278 341	13000 19000 15000 10000	347	413	16
	DMSO	282 349	16000 10000	364	443	27

[a] All spectra were recorded by using a solution of 6.9×10^{-5} M for **2.1a – 2.3a** and 1.1×10^{-5} M for **2.4a**.

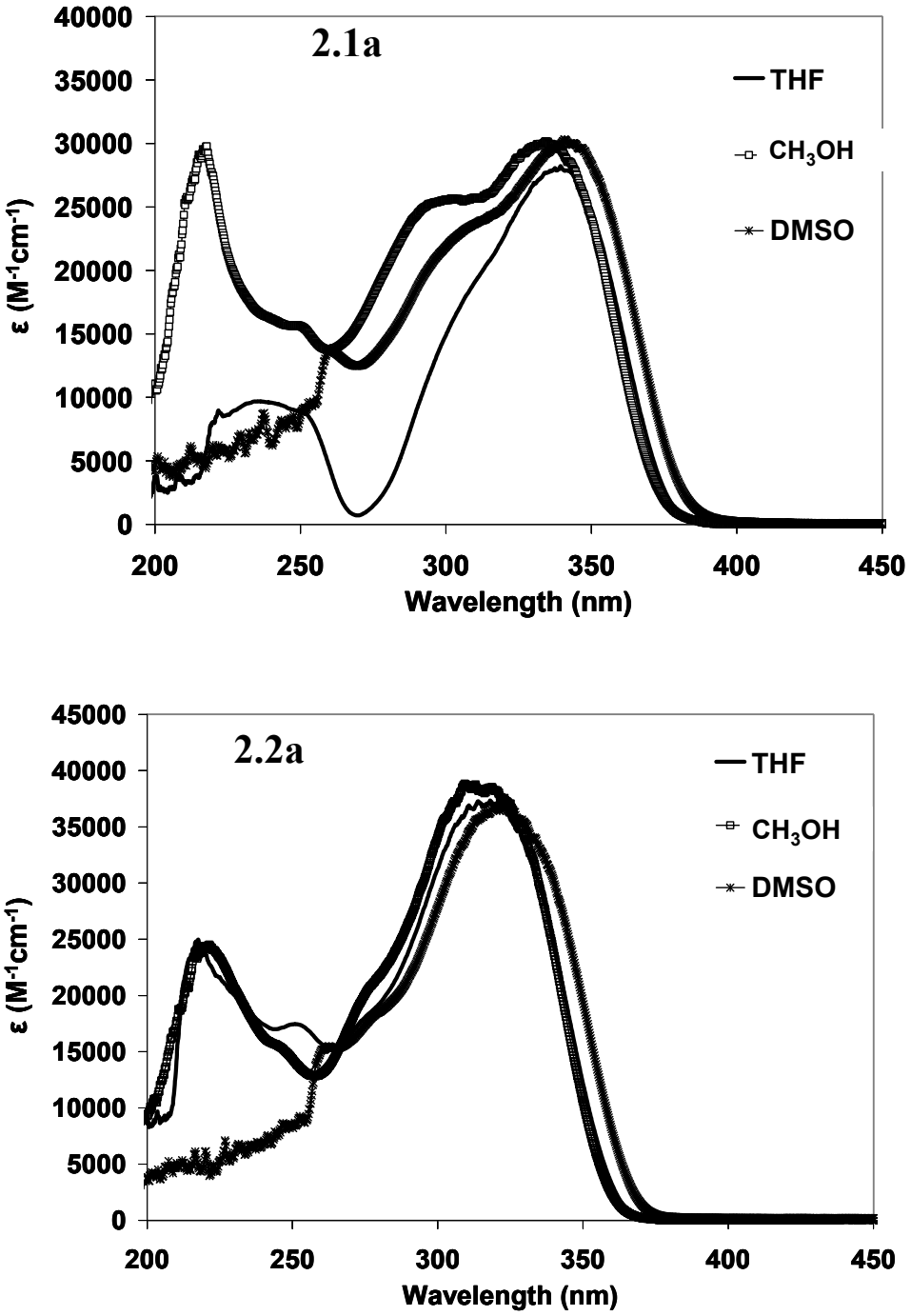

Figure 2.10 UV-Vis spectra of **2.1a** and **2.2a** in various solvents (7 x 10^{-5} M).

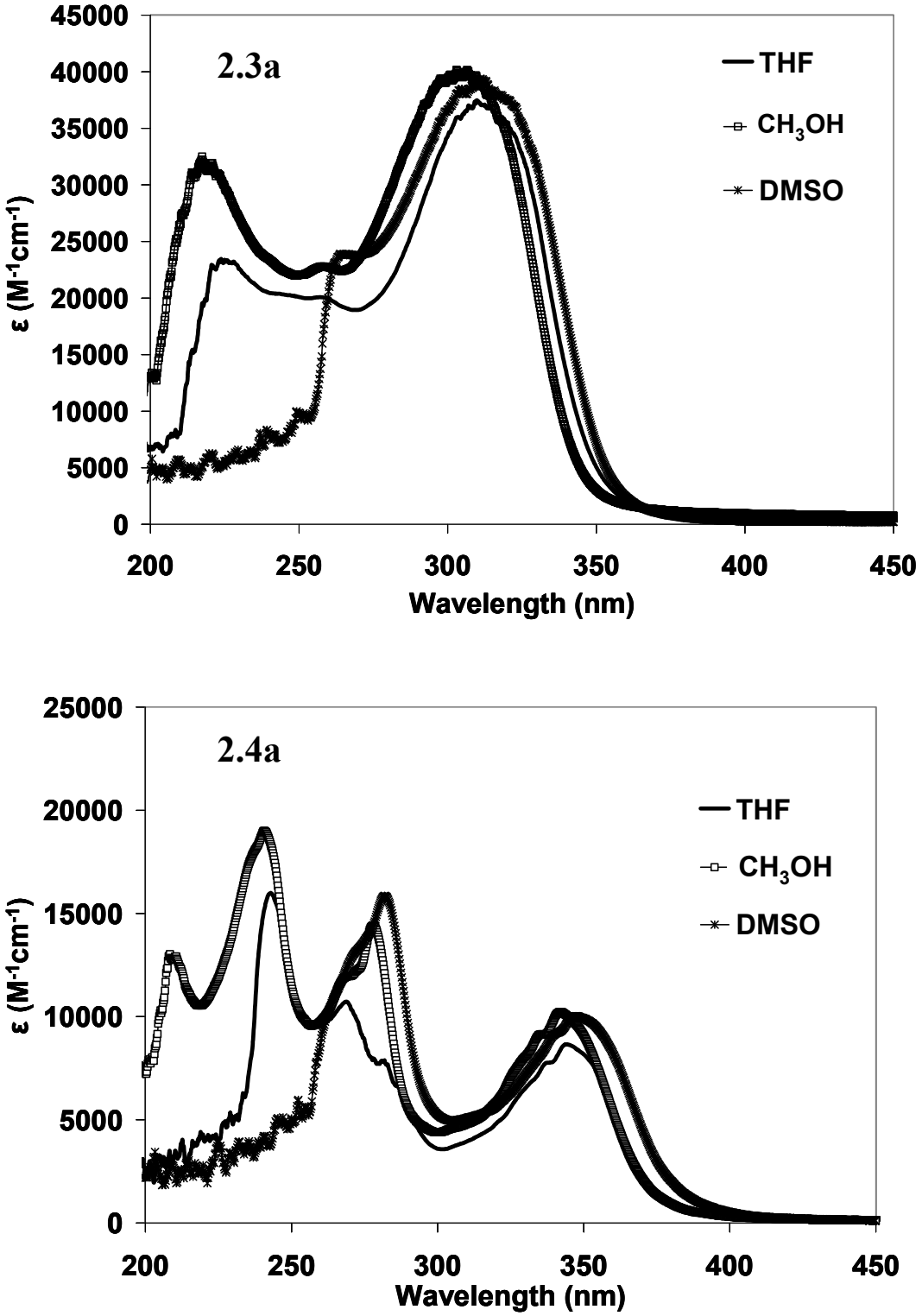

Figure 2.11 UV-Vis spectra of **2.3a** and **2.4a** in various solvents ([**2.3a**] = 7 x 10^{-5} M, [**2.4a**] = 1 x 10^{-5} M).

2.3.3 Luminescent properties of 2.1a – 2.4a

Compounds **2.1a – 2.4a** emit a bright blue color in solution, when irradiated by UV light, at λ_{em} = 395 nm, 370 nm, 418 nm and 418 nm, with a quantum efficiency (Φ) = 13, 7, 10 and 26 % in THF, respectively (Table 2.1). Notably, compound **2.4a** is characterized by the greatest quantum yields in all three solvents, which is expected given the presence of the pyrenyl moiety. Because the non-functionalized guanosine has no detectable emission bands in the same region, the blue emission of **2.1a** – **2.4a** is a direct consequence of the attachment of the (bi)phenyl-diaryl amino or pyrenyl moiety at the N^2 site. In fact, the emission spectral profile of **2.1a** and **2.4a** closely resembles that of parent fluorophores: aryl-diphenylamine, aryl-dipyridylamine, aryl-2-(2'-pyridyl)benzimidazole and aryl-pyrenyl, an indication that the emission is most likely from these chromophores. Consistent with this is the fact that the non-functionalized N^2-iodophenyl guanosine (**2.5a**) is only weakly fluorescent with a quantum efficiency of 0.28 %. Therefore, the N-$aryl_2$ functional group is important in achieving the luminescent guanosine derivatives. It should be noted that none of the compounds exhibits a concentration dependent emission, which suggests that a minimal amount of aggregation takes place in solution.

Compounds **2.1a** and **2.2a** exhibit an emission with a small solvent dependence (~ 40 nm) (Figure 2.12 and Figure 2.13). The emission spectra of **2.3a** and **2.4a** display a red shift with increasing solvent polarity, by ~ 60 nm (Figure 2.14 and Figure 2.15). The emission of **2.4a** in CH_2Cl_2 is at 405 nm and it is shifted to 445 nm in DMSO, which suggests the presence of polarized electronic transition. However, the trend is not followed by other solvents, hence additional factors must influence the emission energy of **2.4a**. The emission of **2.3a** in CH_2Cl_2 is at 375 nm, which shifts to 425 nm in DMSO.

Interestingly, however, in THF, which is a slightly less polar solvent than CH_2Cl_2, the emission band also shifts to 418 nm. Hence, the solvent polarity is not the only reason for the shift in the emission energy of **2.3a**. In addition, compound **2.3a** exhibits a very broad emission band that does not resemble that of the corresponding parent ligand **2.3**, indicative of the presence of possible multiple emission pathways. Based on these observations, the emission of **2.3a** is most likely a combination of electronic transitions that involve the π - π^* orbitals and intramolecular charge transfer.

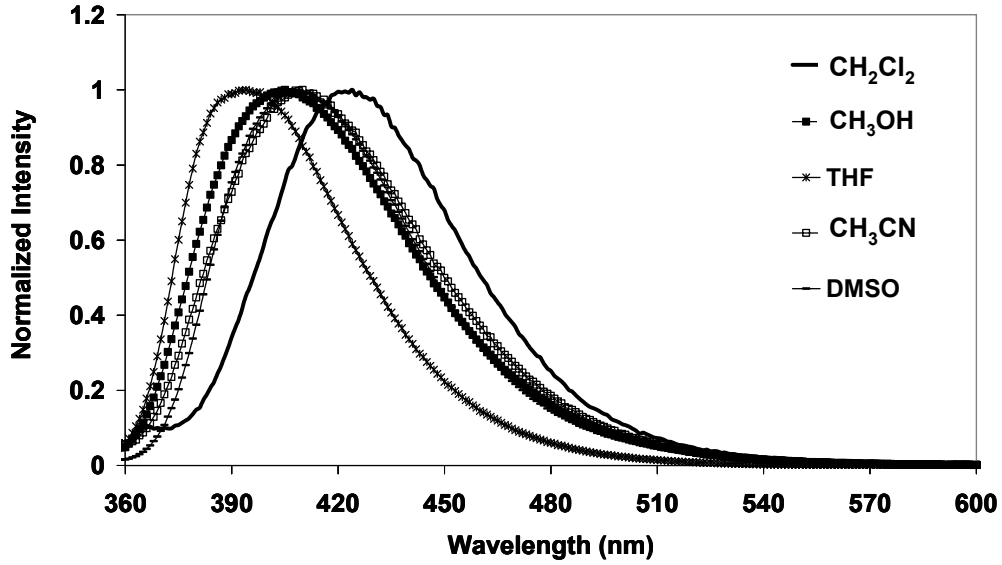

Figure 2.12 Emission spectra of compound **2.1a** in various solvents (7 x 10^{-5} M).

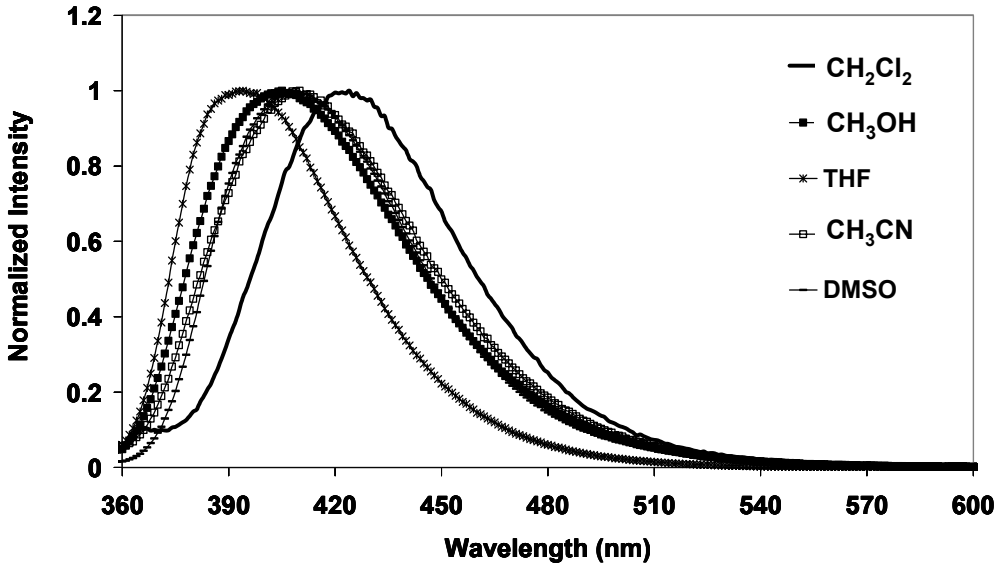

Figure 2.13 Emission spectra of compound **2.2a** in various solvents (7 x 10^{-5} M).

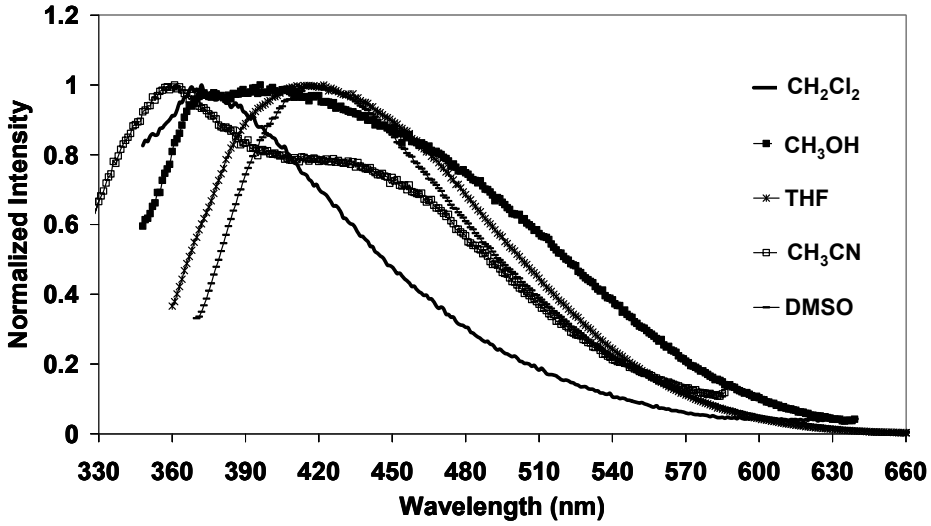

Figure 2.14 Emission spectra of compound **2.3a** in various solvents (7 x 10^{-5} M).

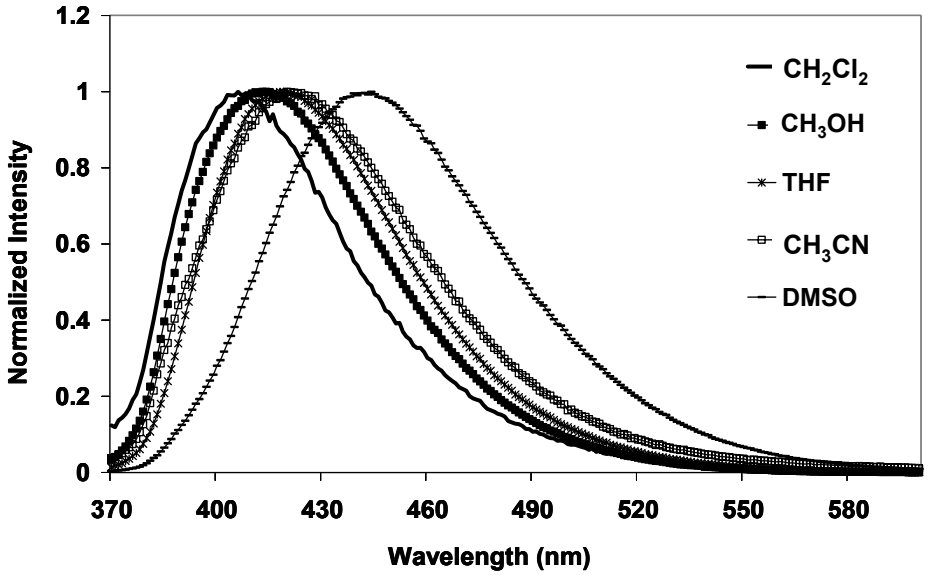

Figure 2.15 Emission spectra of compound **2.4a** in various solvents (1 x 10^{-5} M).

Compound **2.3a** displays excitation-dependent emission in DMSO. When excited at 286 nm (near guanine absorption), the fluorescent emission maxima are observed at 370 and 460 nm. Increasing the excitation wavelength to 349 nm (absorption of N^2-ligand) leads to a single emission band at ~ 420 nm as shown in Figure 2.16. From the excitation profiles at 370, 422 and 460 nm in Figure 2.17, it can be seen that the red shifted emission over 400 nm is related to the excitation at the N^2-aryl chromophore. The emission at the shorter wavelength, at ~ 370 nm, stems from the excitation at the N^2-ligand in addition to the large contribution from the guanine chromophore. The excitation-dependent behaviour indicates that emission originates from two different excited states, and suggests two different relaxation decay mechanisms. In order to gain further information about the nature of electronic transitions the molecular orbital calculations were employed.

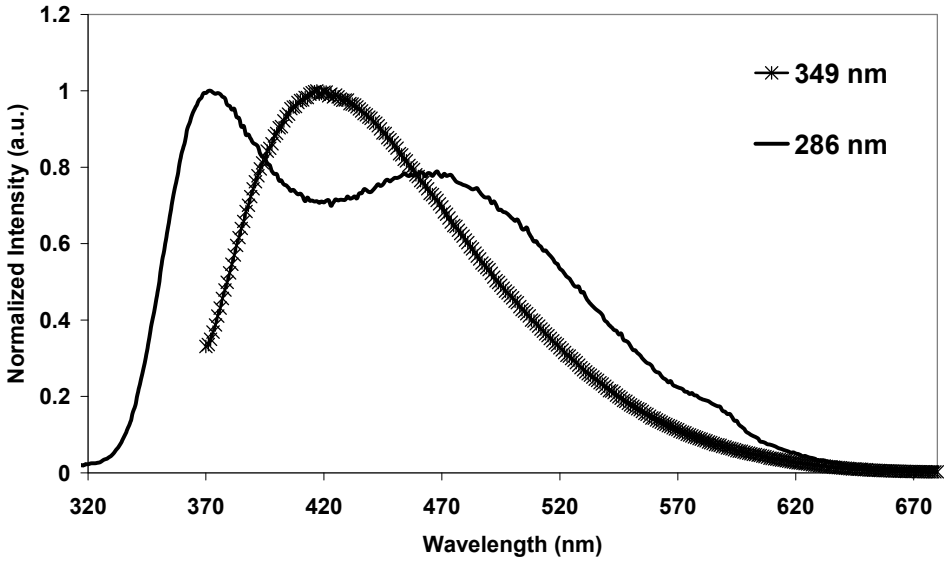

Figure 2.16 Excitation dependent emission spectra of **2.3a** at λ_{ex} = 286 and 349 nm (DMSO).

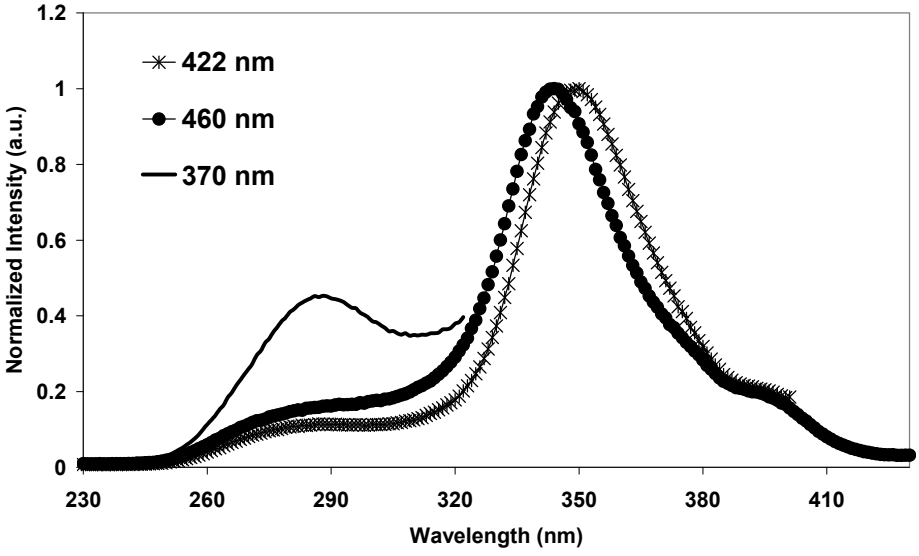

Figure 2.17 Excitation spectra of **2.3a** (at λ_{em} = 370, 422 and 460 nm, DMSO).

2.3.4 Molecular orbital calculations for N^2-arylguanosines 2.1a – 2.4a.

To understand the electronic and luminescent properties of compounds **2.1a – 2.4a** we performed molecular orbital calculations. The ground-state structures of all compounds were fully geometry optimized by density-functional theory (DFT) at a B3-LYP/6-311G** level of theory using the Gaussian 03 suite.[9] The optimized structures along with the diagrams of HOMO and LUMO energy levels for all four compounds are shown below, and the computed and experimental HOMO and LUMO energy gaps are given in Table 2.2. The experimental optical energy gap was determined from the edges of their respective UV-Vis absorption spectra. The HOMO and LUMO orbital diagrams generated for **2.1a** and **2.2a** are dominated by π and π* orbitals localized on the biphenyl-$NAryl_2$ group and guanine as depicted in Figure 2.18 and Figure 2.19. The MO calculation results indicate that there is little difference between **2.1a** and **2.2a** in terms of their electronic transitions, which is consistent with their similar luminescent properties. However, **2.2a** has a slightly larger energy gap which is due to the presence of pyridyl groups. By contrast, the HOMO level of **2.3a** has contributions from the π orbital of the N^2-biphenyl and guanine moiety, while the LUMO level consists of contributions exclusively from the π* orbitals of the 2-(2'-pyridyl)benzimidazolyl group (Figure 2.20). DFT calculations show that there is no conjugation between the 2-(2'-pyridyl)benzimidazolyl group and the guanine-biphenyl portion, and as a result, the lowest electronic transition in **2.3a** may be assigned to intramolecular charge transfer between the two parts of the molecule. In fact, these two groups are nearly orthogonal to each other, which is consistent with the previously reported crystallographic data for aryl-2-(2'-pyridyl)benzimidazole molecules and it is attributable to the non-bonding interactions between the *ortho*-hydrogen atoms of the 2-(2-pyridyl)benzimidazolyl and

the phenyl ring. This lack of conjugation between the chelate chromophore and the guanine-biphenyl unit is clearly responsible for the unique photophysical properties of **2.3a**. The HOMO of compound **2.4a** is localized on the N^2-phenylpyrenyl and the guanine π orbitals, while the LUMO predominantly stems from the N^2-phenylpyrenyl π* orbitals, with a small contribution from the guanine ring as depicted in Figure 2.21. This lowest electronic transition in **2.4a** is similar to those observed in **2.1a** and **2.2a**.

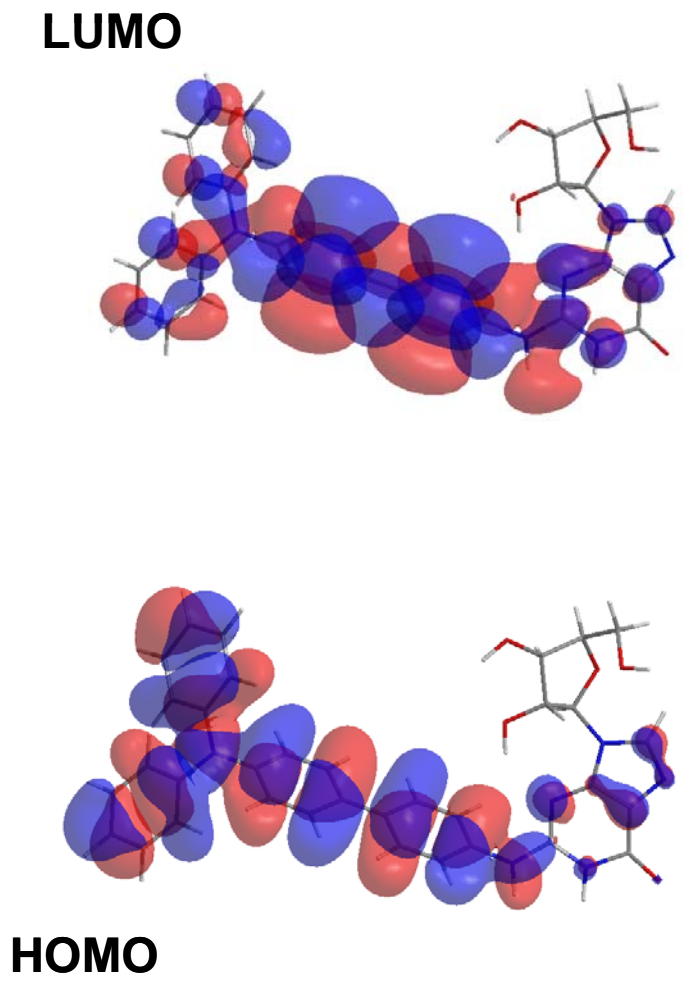

Figure 2.18 HOMO and LUMO diagrams of **2.1a**.

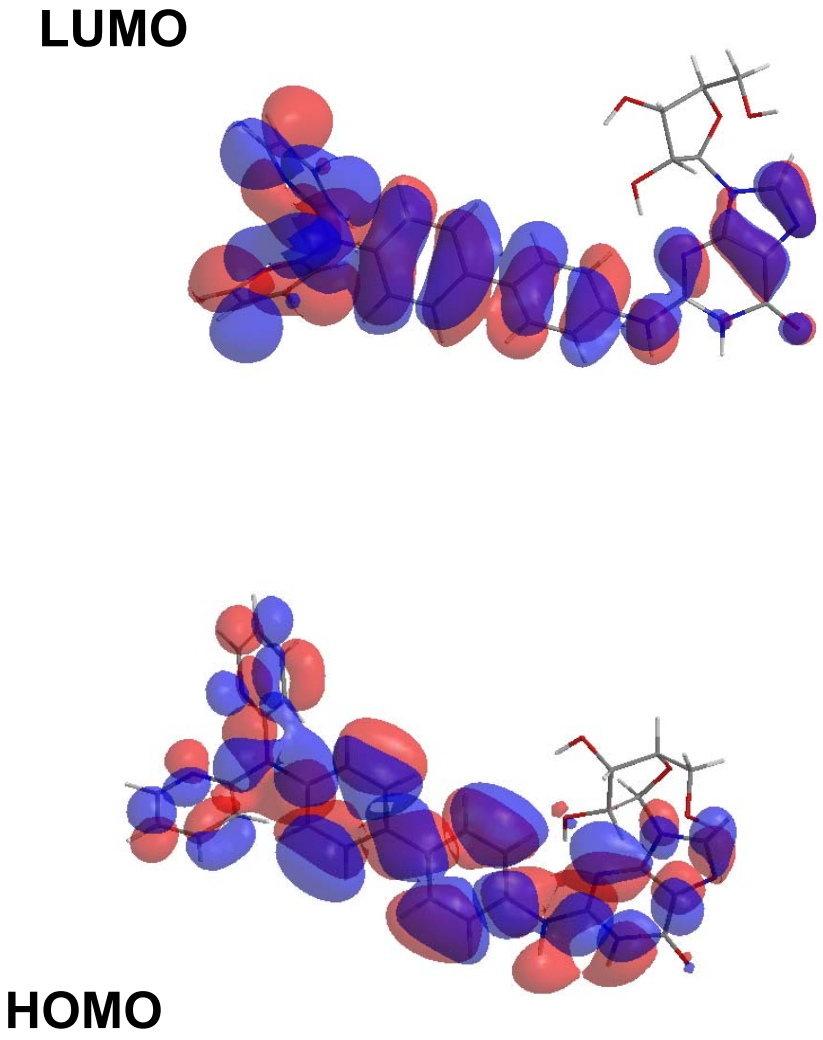

Figure 2.19 HOMO and LUMO diagrams of **2.2a**.

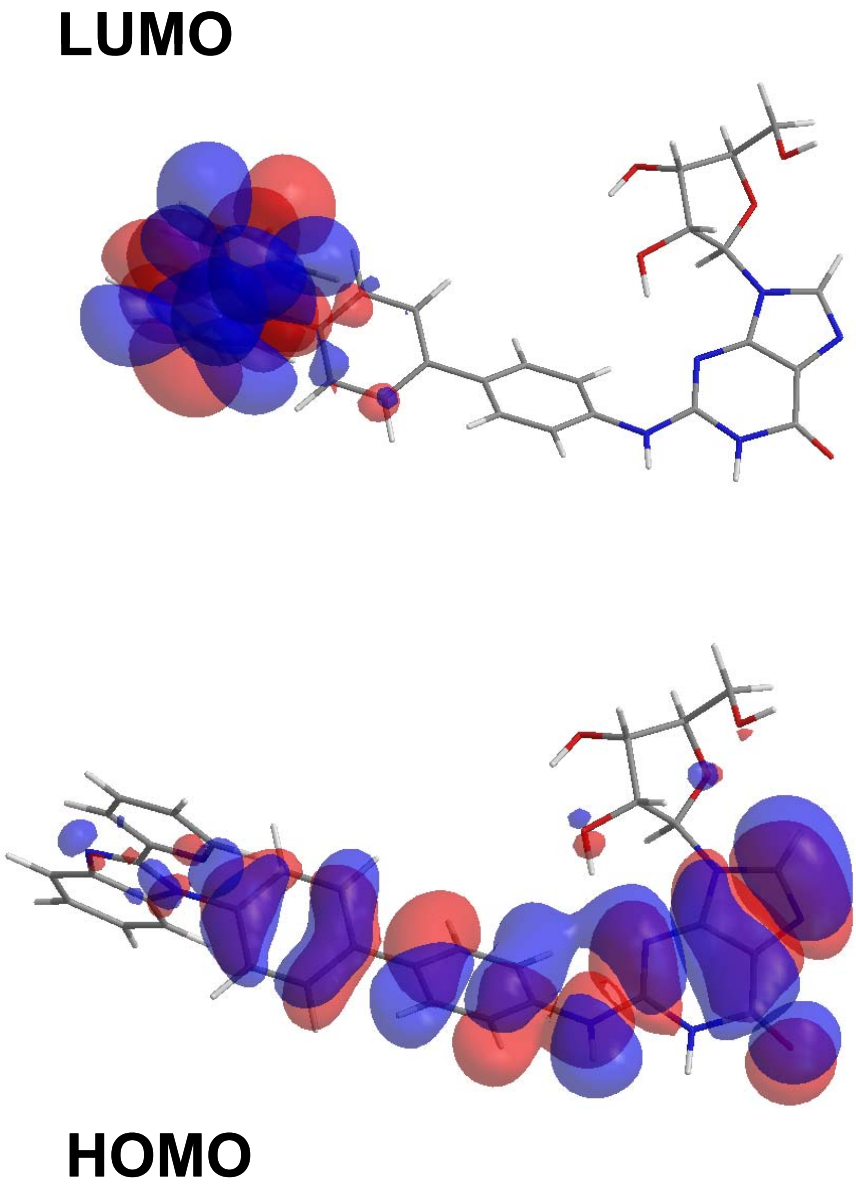

Figure 2.20 HOMO and LUMO diagrams of **2.3a**.

LUMO

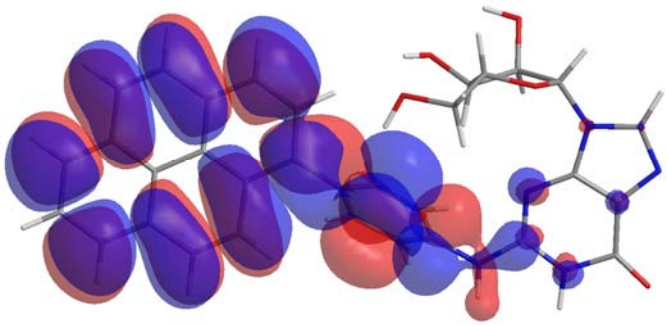

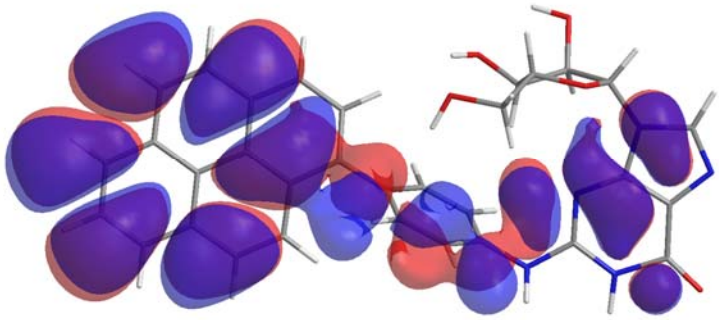

HOMO

Figure 2.21 HOMO and LUMO diagrams of **2.4a**.

Table 2.2 HOMO and LUMO energy levels of **2.1a – 2.4a**.

Compound	LUMO (eV)	HOMO (eV)	Calculated HOMO-LUMO Gap (eV)	Optical Energy Gap (eV)[a]
2.1a	-1.36	-5.25	3.89	3.19
2.2a	-1.46	-5.49	4.02	3.33
2.3a	-1.65	-5.87	4.22	3.11
2.4a	-2.12	-5.74	3.62	3.01

[a] calculated from UV-Vis spectra in THF.

To further understand the nature of electronic transitions in **2.1a** – **2.4a**, we carried out time-dependent density functional theory (TD-DFT) calculations on optimized structures. TD-DFT is a useful tool in calculating electronic excitations and it has been previously used to investigate the effect of H-bonding[20] and stacking interactions[21] between nucleosides on their electronic structures. In the TD-DFT, the first 50 singlet states were calculated to determine the electronic transitions and their oscillator strengths. The computed $S_0 \rightarrow S_1$ electronic transition data for isolated nucleosides **2.1a – 2.4a** are given in Table 2.3. For **2.1a** and **2.2a**, the transition from the $S_0 \rightarrow S_1$ state involves mainly the HOMO (π) and LUMO (π^*) orbitals, as expected. In contrast, the $S_0 \rightarrow S_1$ transition in **2.3a** is a combination of several transitions as shown in Figure 2.22, among which the lowest electronic transition involves a HOMO (π of guanine-biphenyl) to LUMO+1 (π^* of guanine-biphenyl) transition (64%) and a HOMO (π of guanine-biphenyl) to LUMO (π^* of 2-(2'-pyridyl)benzimidazolyl) transition (19%). The 2nd

lowest electronic transition in **2.3a** is HOMO-1 (π of 2-(2'-pyridyl)benzimidazolyl) to LUMO (π* of 2-(2'-pyridyl)benzimidazolyl) (63%) transition, which is ~ 0.2 eV higher in energy than the HOMO-LUMO or HOMO-LUMO+1 transitions. These data supports the fact that the $S_0 \rightarrow S_1$ transitions in **2.3a** have mixed contributions from both π - π* transition, centered on either the guanine-biphenyl portion or the 2-(2'-pyridyl)benzimidazolyl portion, and the charge transfer between the guanine-biphenyl moiety and the 2-(2'-pyridyl)benzimidazolyl group. This finding is consistent with the broad emission band of **2.3a**, and its solvent- and excitation-dependent emissions. The lowest electronic transition in **2.4a** is dominated by the HOMO to LUMO transitions, however small contributions from other electronic transitions exist.

Optical spectra obtained by TD-DFT calculations for **2.1a** - **2.4a** match well with the experimental ones in terms of the UV-Vis absorptions, as can be seen in Figure 2.23, Figure 2.24, Figure 2.25 and Figure 2.26, respectively, which confirms that most of the transitions with high oscillator strengths are dominated by the guanine-N^2-aryl contributions.

Table 2.3 The $S_0 \rightarrow S_1$ transition data of **2.1a** – **2.4a** (TD-DFT, B3-LYP/6-311G**).

Compound	Oscillator strength (*f*)	Transition	Energy (nm/eV)
2.1a	0.81	HOMO→LUMO (67%)	361/3.43
2.2a	0.88	HOMO→LUMO (67%)	351/3.53
2.3a	0.60	HOMO→LUMO+1 (64%) HOMO→LUMO (19%)	317/3.91
	0.57	HOMO-1→LUMO (63%)	304/4.08
2.4a	0.57	HOMO→LUMO (61%) HOMO-1→LUMO (21%) HOMO-2→LUMO+1 (11%)	367/3.37

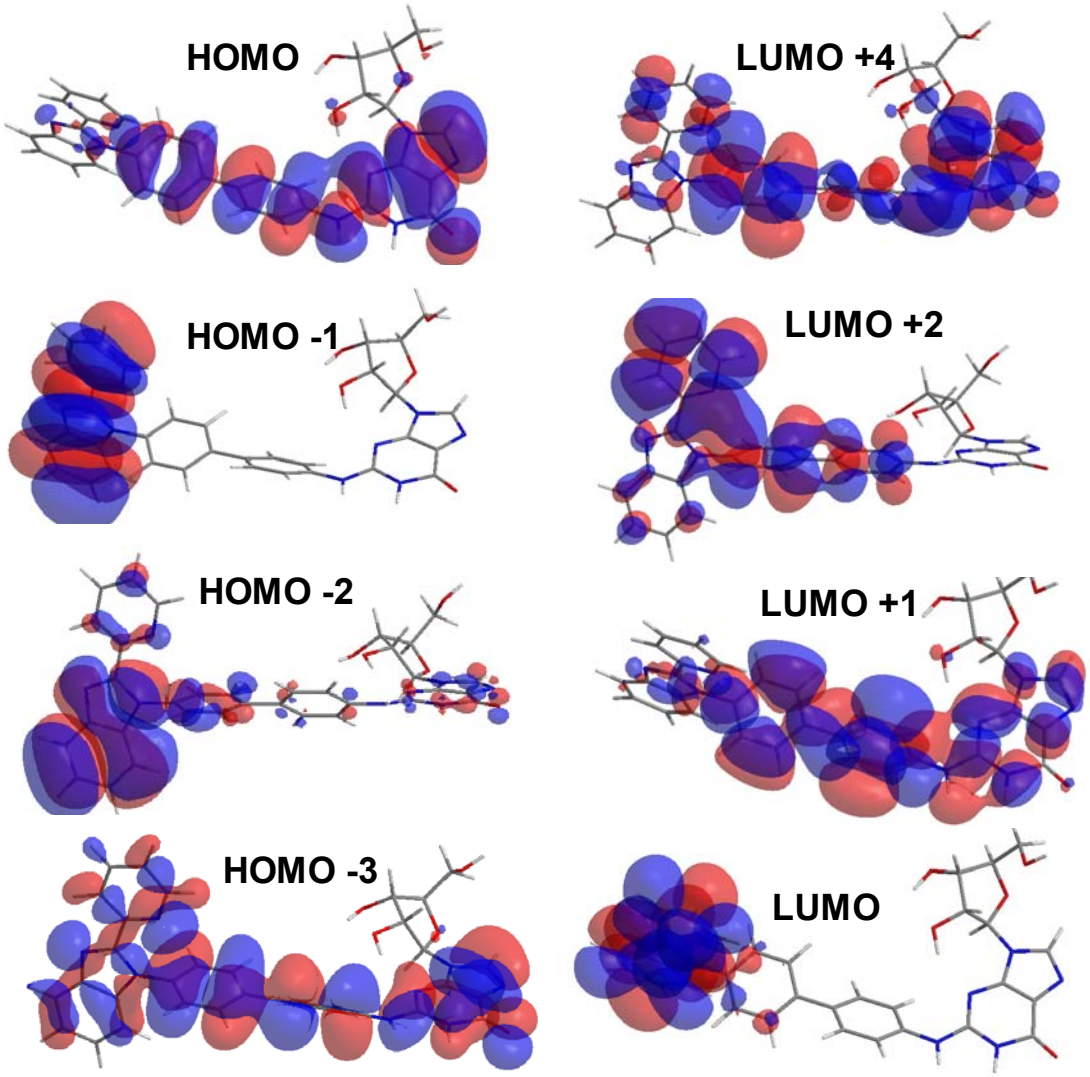

Figure 2.22 Frontier orbitals for compound **2.3a**.

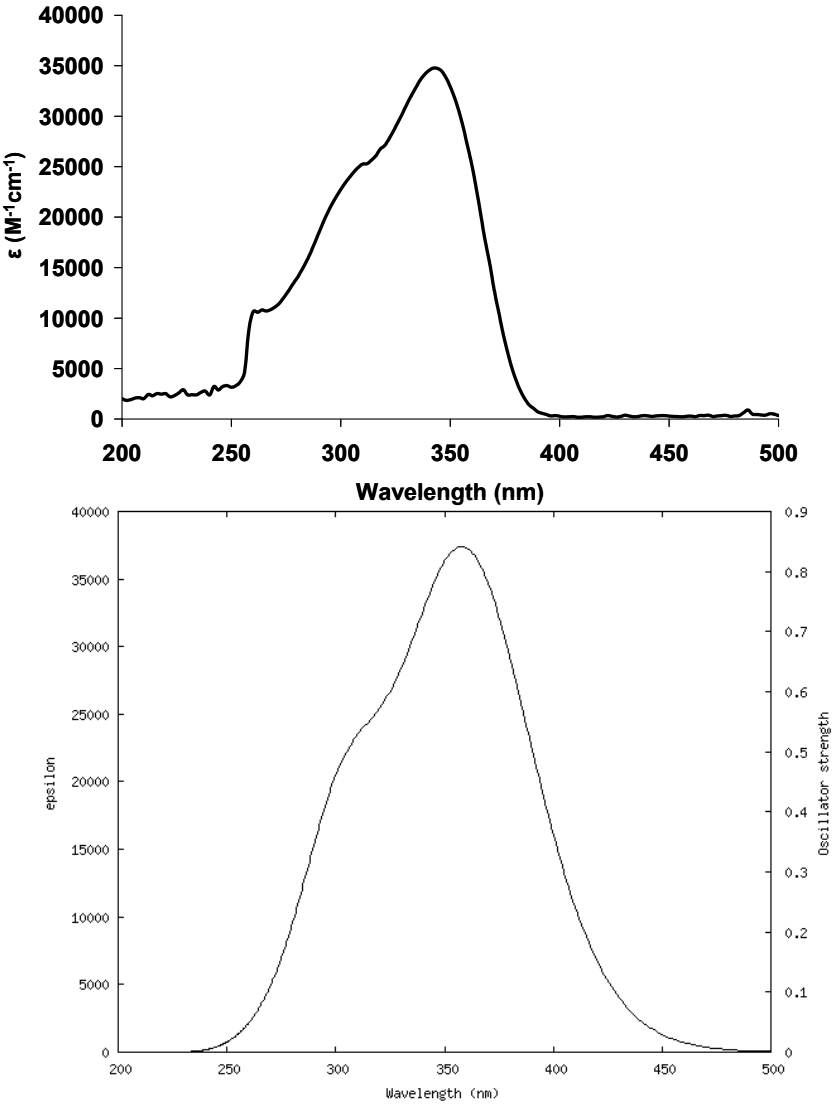

Figure 2.23 Experimental (top) and theoretical (bottom) UV-Vis absorption spectra of **2.1a**.

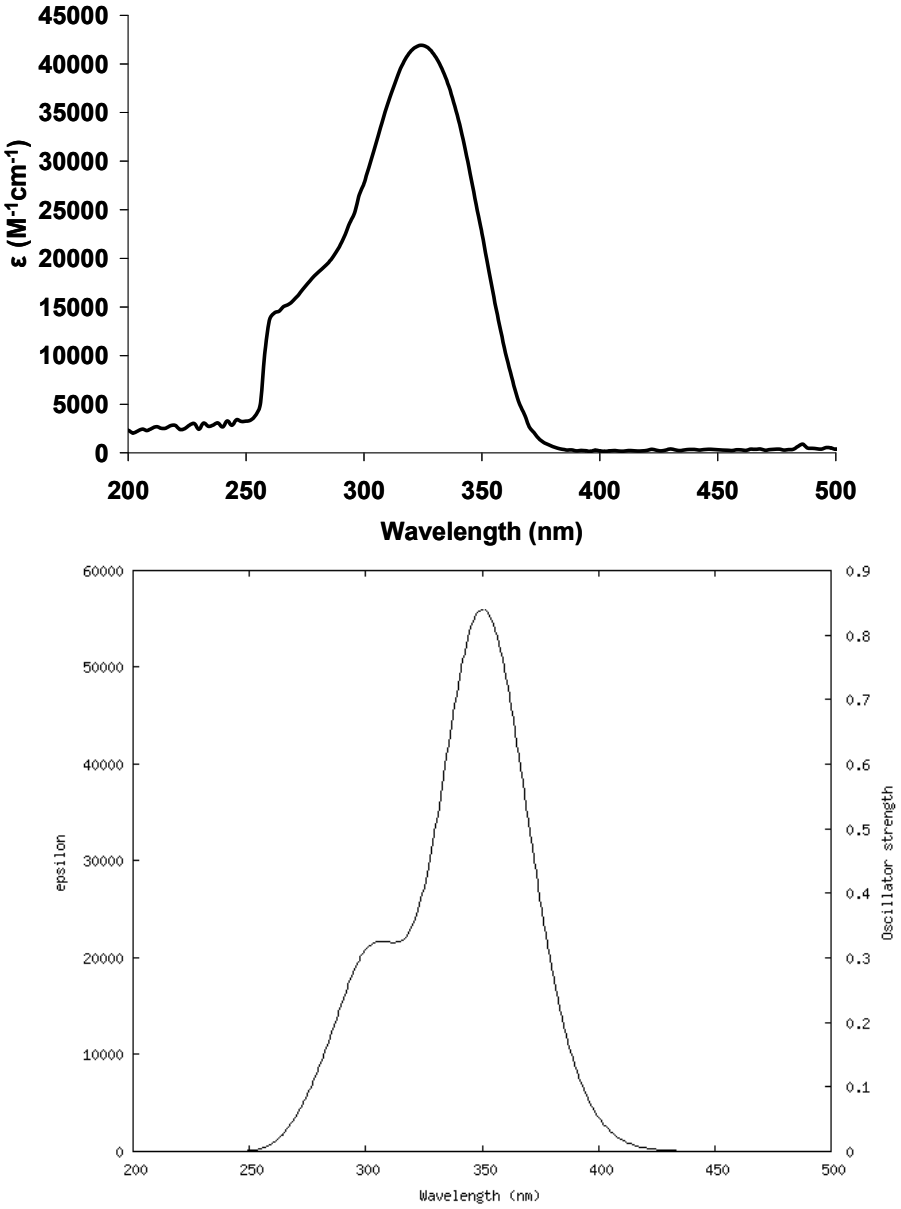

Figure 2.24 Experimental (top) and theoretical (bottom) UV-Vis absorption spectra of **2.2a**.

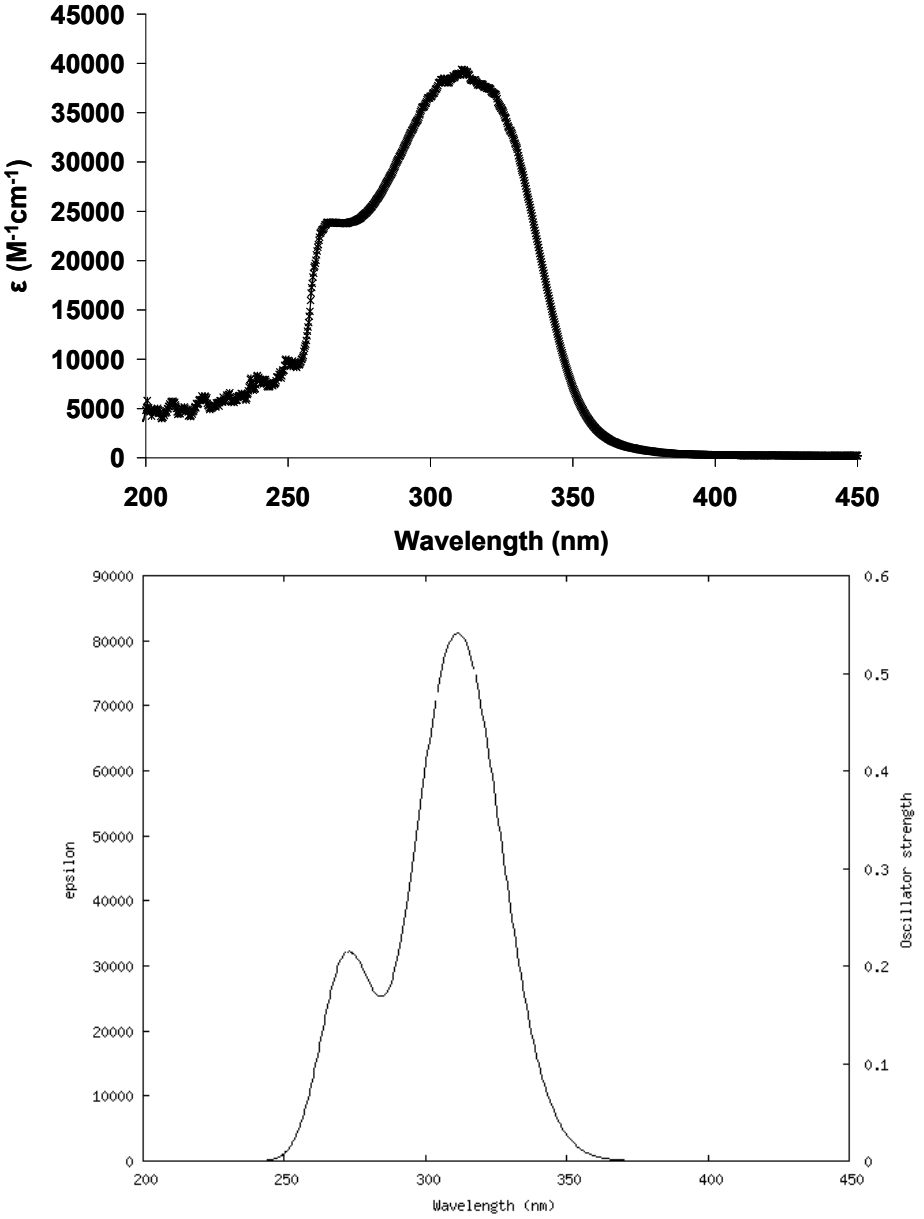

Figure 2.25 Experimental (top) and theoretical (bottom) UV-Vis absorption spectra of **2.3a**.

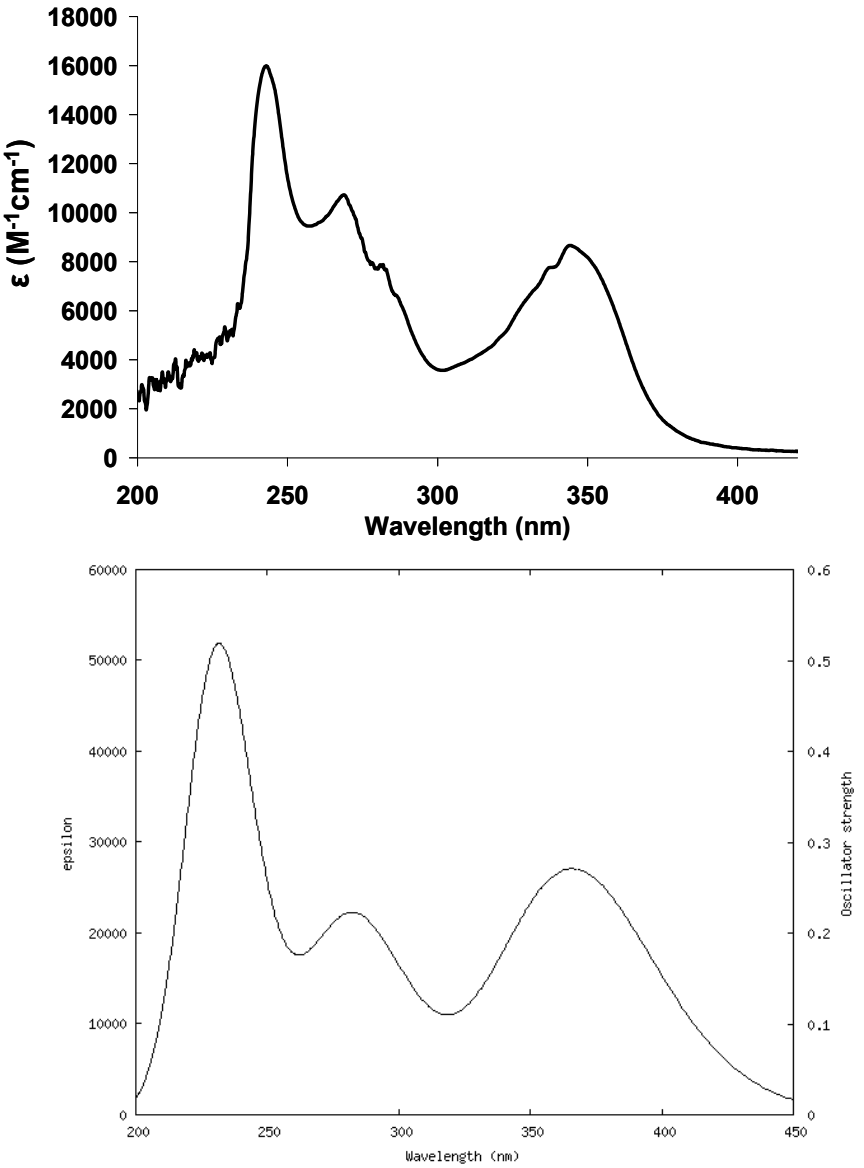

Figure 2.26 Experimental (top) and theoretical (bottom) UV-Vis absorption spectra of **2.4a**.

2.3.5 Circular dichroism (CD) study of 2.1a – 2.4a

The circular dichroism spectra of **2.1a** – **2.4a** are presented in Figure 2.27, along with the unmodified guanosine, **TAG**, in order to ascertain the impact of the chromophore at the N^2-site on the overall chirality. The unmodified guanosine, **TAG**, exhibits a weak negative band in the 200 – 280 nm range, characteristic of the long-axis

polarized transition of guanine. For **N^{2}G**, the CD curve consists of positive band in the 270 – 380 nm range that is associated with the absorption of a N^2-chromophore, in addition to the negative band in the 220 – 270 nm range that is related to the guanine absorption. Compound **2.4a** clearly exhibits much lower CD absorption, and this behaviour could be attributed to the lower concentration. A comparison between unmodified and modified guanosines reveals two important points: a) the overall CD signal intensity is improved in the presence of chromophores at the N^2-site and b) new CD bands in the 270 – 400 nm range can become useful in sensing applications. Theoretical (derived from TD-DFT MO calculations) and experimental CD spectra are a poor match due to the solvent effects and the limitation of DFT calculations to the gas phase calculations and with poorly defined excited states (Figure 2.28, Figure 2.29, Figure 2.30 and Figure 2.31).

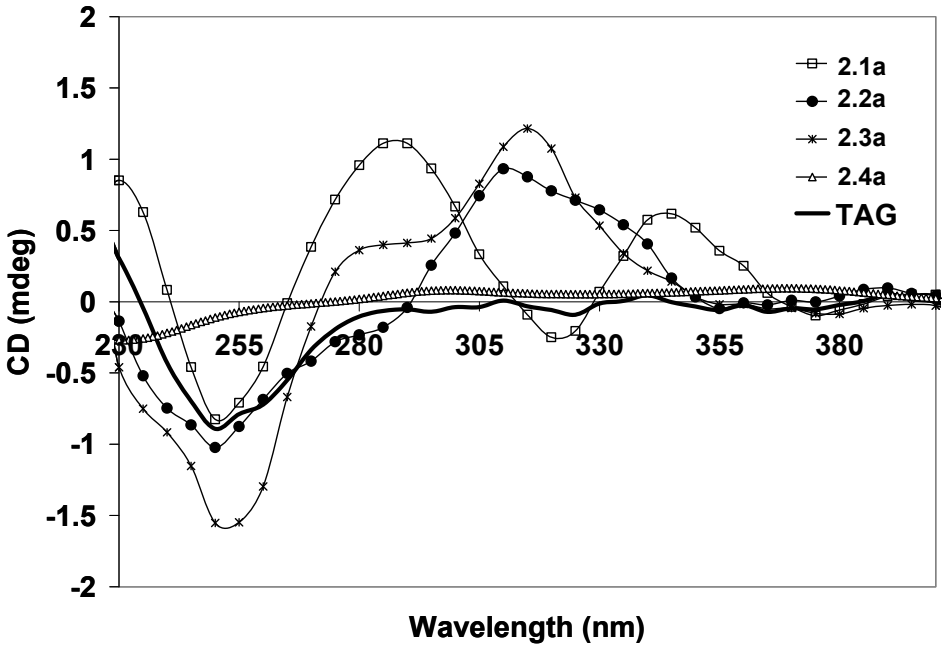

Figure 2.27 CD spectra of **2.1a - 2.4a** and **TAG** (THF, [**2.1a**] = 3 x 10^{-5} M, [**2.2a**] = 3 x 10^{-5} M, [**2.3a**] = 3 x 10^{-5} M, [**2.4a**] = 1 x 10^{-5} M and [**TAG**] = 3 x 10^{-5} M).

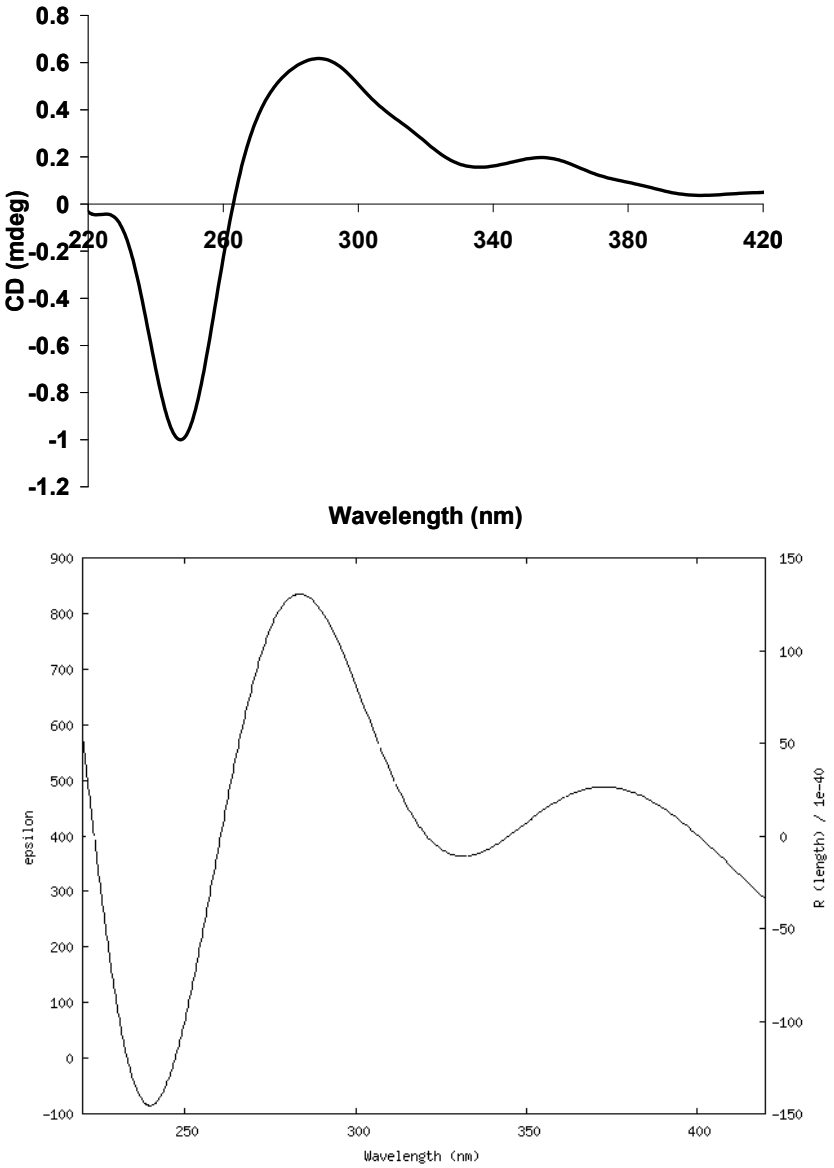

Figure 2.28 Experimental (top) and theoretical (bottom) CD spectra of **2.1a**.

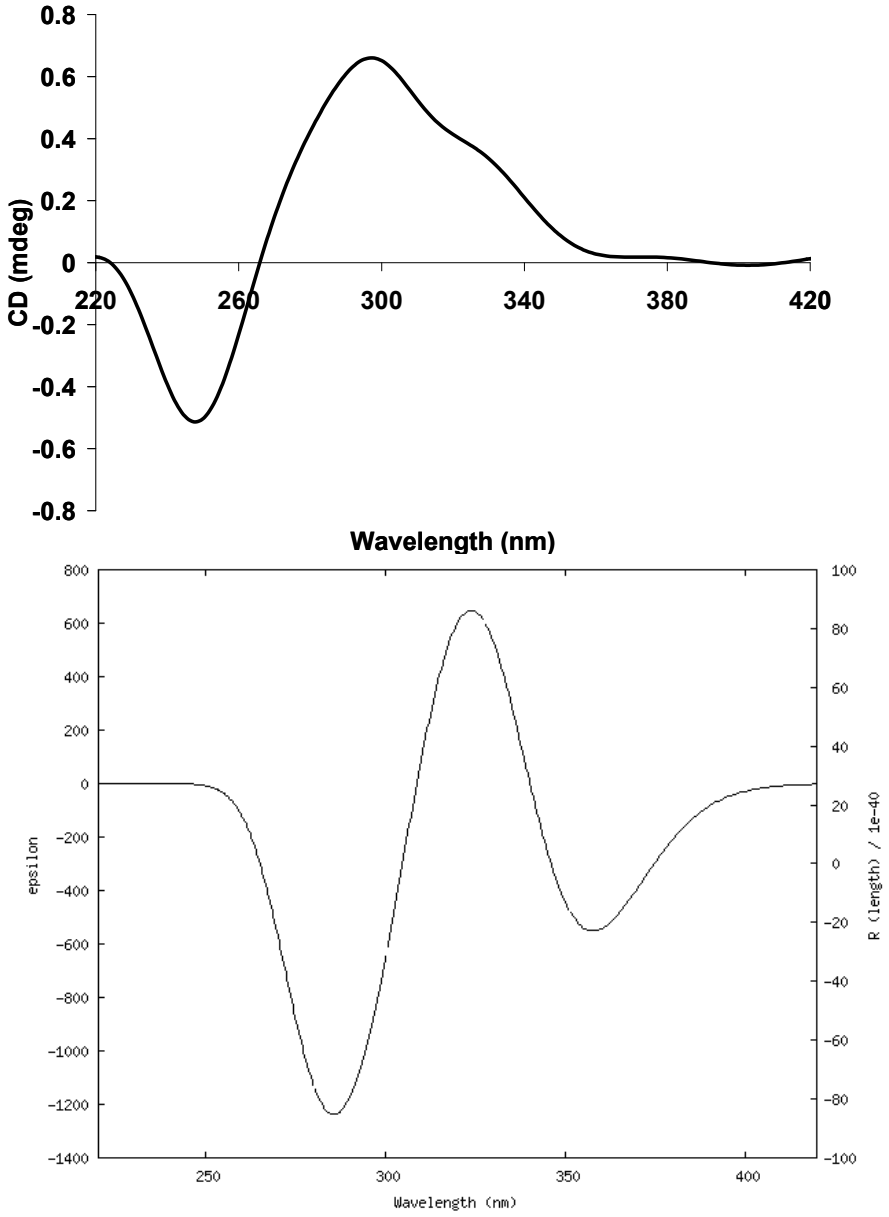

Figure 2.29 Experimental (top) and theoretical (bottom) CD spectra of **2.2a**.

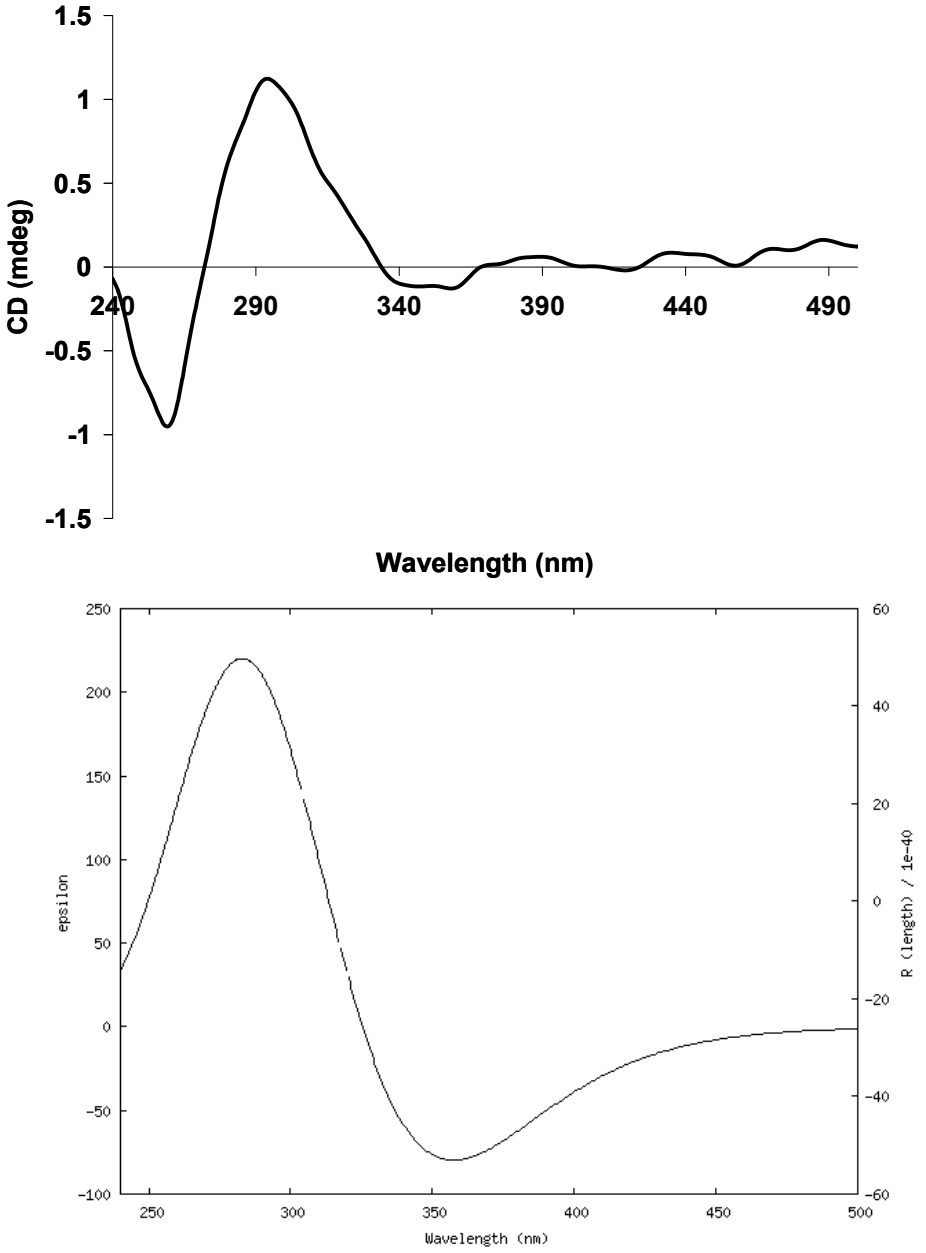

Figure 2.30 Experimental (top) and theoretical (bottom) CD spectra of **2.3a**.

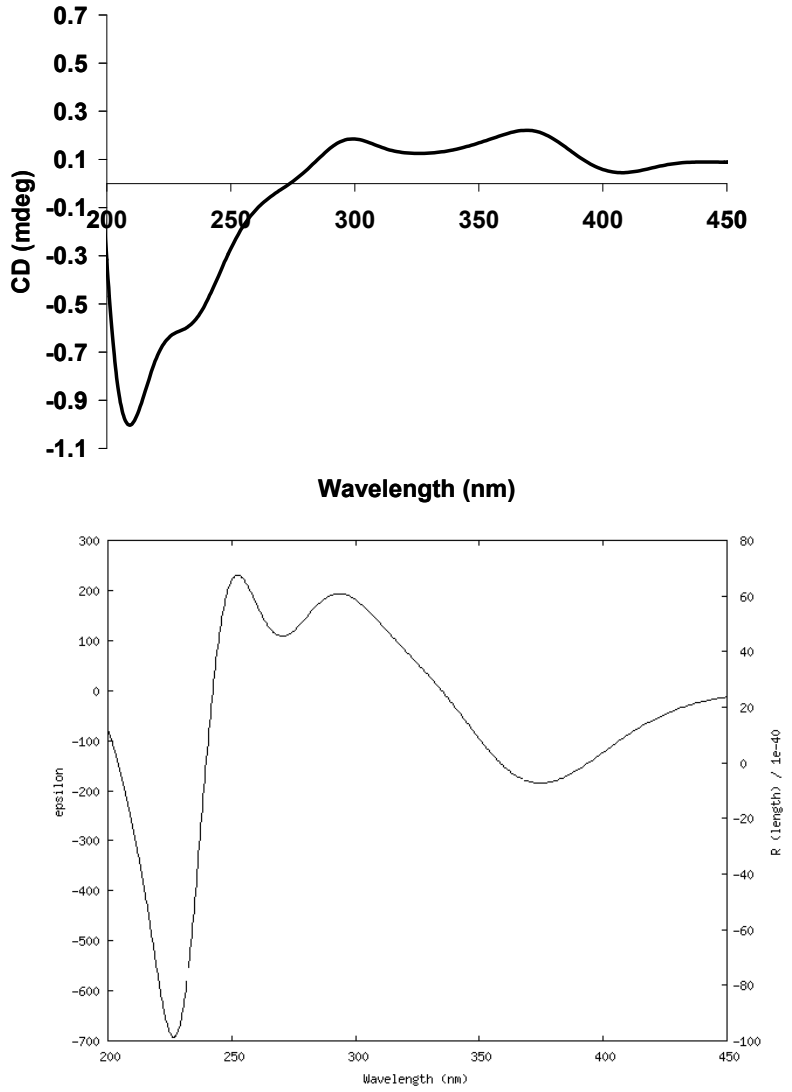

Figure 2.31 Experimental (top) and theoretical (bottom) CD spectra of **2.4a**.

2.4 Conclusions

In this chapter, the synthesis of four new fluorescent **N^{2}Gs** containing both chelating and non-chelating fluorophores was presented. The Ullmann cross-coupling reaction was successfully used, for the first time, in the synthesis of **N^{2}Gs**. Photophysical properties of these compounds were further investigated using UV-Vis, fluorescence and CD measurements. Molecular orbital calculations for the compounds containing a

diarylamino group clearly identify the lowest electronic transitions between HOMO and LUMO levels localized on the N^2-biphenyl-diarylamino guanine moiety. However, changing the substituent from a simple diarylamino group to 2-(2'-pyridyl)benzimidazolyl has a large impact on the electronic structure of the target molecule. The electronic transition of compound **2.3a** is a combination of interactions involving a typical ligand-centered and charge transfer $\pi - \pi^*$ transitions, which is characterized by a broad solvent- and excitation-dependent emissions. One of the important aspects presented in this chapter is the feasibility of fine tuning the electronic structure *via* direct modification at the N^2-site of guanosine.

2.5 References

[1] Gottarelli, G.; Spada, G. P. *Chem. Rec*. **2004**, *4*, 39.

[2] (a) Betancourt, J. E.; Hidalgo, M. M.; Gubala, V.; Rivera, J. M. *J. Am. Chem. Soc.* **2009**, *131*, 3186. (b) Rodriguez, G. D.; van Dongen, J. L. J.; Lutz, M.; Spek, A. L.; Schenning, A. P. H. J.; Meijer, E. W. *Nature Chem.* **2009**, *1*, 151.

[3] (a) Okamoto, A.; Kanatani, K.; Ochi, Y.; Saito, Y.; Saito, I. *Tetrahedron Lett.* **2004**, *45*, 6059. (b) Prober, J. M.; Trainor, G. L.; Dam, R. J.; Hobbs, F. G.; Robertson, C. W.; Zagursky, R. J.; Cocuzza, A. J.; Jensen, M. A.; Baumeister, K. *Science* **1987**, *238*, 336.

[4] (a) Firth, A. G.; Fairlamb, I. J. S.; Darley, K.; Baumann, C. G. *Tetrahedron Lett.* **2006**, *47*, 3529. (b) Berman, A.; Izraeli, E. S.; Levanon, H.; Wang, B.; Sessler, J. L. *J. Am. Chem. Soc.* **1995**, *117*, 8252. (c) Sessler, J. L.; Wang, B.; Harriman, A. *J. Am. Chem. Soc.* **1995**, *117*, 704. (d) Sessler, J. L.; Wang, B.; Harriman, A. *J. Am. Chem. Soc.* **1993**, *115*, 10418.

[5] (a) Srivastava, P. C.; Robins, R. K.; Meyer, R. B.; Townsend, L. B. *Chemistry of Nucleosides and Nucleotides;* Plenum Press: New York, 1988. (b) Trivedi, B. K.; *Nucleosides Nucleotides* **1988**, *7*, 393. (c) Trivedi, B. K.; Bruns, R. F. *J. Med. Chem.* **1989**, *32*, 1667. (d) Steinbrecher, T.; Wameling, C.; Oesch, F.; Seidel, A. *Angew. Chem. Int. Ed.* **1993**, *32*, 404. (e) Harwood, E. A.; Sigurdsson, S. T.; Edfeldt, N. B. F.; Reid, B. R.; Hopkins, P. B. *J. Am. Chem. Soc.* **1999**, *121*, 5081. (f) De Riccardis, F.; Johnson, F. *Org. Lett.* **2000**, *2*, 293. (g) Chakraborti, D.; Colis, L.; Schneider, R.; Basu, A. K. *Org. Lett.* **2003**, *5*, 2861. (h) Lakshman, M. K.; Ngassa, F. N.; Bae, S.; Buchanan, D. G.; Hahn,

H. G.; Mah, H. *J. Org. Chem.* **2003**, *68*, 6020. (k) Dai, Q.; Ran, C.; Harvey, R. G. *Org. Lett.* **2005**, *7*, 999.

[6] (a) Wang, S. *Coord. Chem. Rev.* **2001**, *215*, 79. (b) Pang, J.; Marcotte, E. P. J.; Seward, C.; Brown, R. S.; Wang, S. *Angew. Chem. Int. Ed.* **2001**, *40*, 4042. (c) Seward, C.; Pang, J.; Wang, S. *Eur. J. Inorg. Chem.* **2002**, 1390. (d) Kang, Y.; Wang, S. *Tetrahedron Lett.* **2002**, *43*, 3711.

[7] (a) Jia, W. L.; McCormick, T.; Tao, Y.; Lu, J. P.; Wang, S. *Inorg. Chem.* **2005**, *44*, 5706. (b) Jia, W. L.; Hu, Y. F.; Gao, J.; Wang, S. *Dalton Trans.* **2006**, 1721. (c) Durantaye, L. D. L.; McCormick, T.; Liu, X. Y.; Wang, S. *Dalton Trans.* **2006**, 5675. (d) Kang, Y.; Seward, C.; Song, D.; Wang, S. *Inorg. Chem.* **2003**, *42*, 2789.

[8] Lodeiro, C.; Lima, J. C.; Parola, A. J.; Seixas de Melo, J. S.; Capelo, J. L.; Covelo, B.; Tamayo, A.; Pedera, B. *Sensors and Actuators B* **2006**, *115*, 276.

[9] Gaussian 03, Revision C.02, Fisch, M. J.; Trucks, G. W.; Schlegel, H. B.; Scuseria, G. E.; Robb, M. A.; Cheesman, J. R.; Montgamery, Jr. J. A.; Vreven, T.; Kudin, K. N.; Burant, J. C.; Millam, J. M.; Iyengar, S. S.; Tomasi, J.; Barone, V.; Mennucci, B.; Cossi, M.; Scalmani, G.; Rega, N.; Petersson, G. A.; Nakatsuji, H.; Hada, M.; Ehra, M.; Toyota, K.; Fukuda, R.; Hasegawa, J.; Ishida, M.; Nakajima, T.; Honda, Y.; Kitao, O.; Nakai, H.; Klene, M.; Li, X.; Knox, J. E.; Hratchian, H. P.; Cross, J. B.; Bakken, V.; Adamo, C.; Jarmillo, J.; Gomperts, R.; Stratmann, R. E.; Yazyev, O.; Austin, A. J.; Cammi, R.; Pomelli, C.; Ochterski, J. W.; Ayala, P. Y.; Morokuma, K.; Voth, G. A.; Salvador, P.; Dannenberg, J. J.; Zakrzewski, V. G.; Dapprich, S.; Daniels, A. D.; Strain, M. C.; Farkas, O.; Malick, D. K.; Rabuck, A. D.; Raghavachari, K.; Foresman, J. B.; Ortiz, J. V.; Cui, Q.; Baboul, A. G.; Clifford, S.; Cioslowski, J.; Stefanov, B. B.; Liu, G.; Liashenko, A.;

Piskorz, P.; Komaromi, I.; Martin, R. L.; Fox, D. J.; Keith, T.; Al-Laham, M. A.; Peng, C. Y.; Nanayakkara, A.; Challacombe, M.; Gill, P. M. W.; Johnson, B.; Chen, W.; Wong, M. W.; Bonzales, C.; Pople, J. A.; Gaussian, Inc., Wallingford CT, 2004.

[10] (a) Demas, N. J.; Crosby, G. A.; *J. Am. Chem. Soc.* **1970**, *29*, 7262. (b) Berlman, I. B. *Handbook of Fluorescence Spectra of Aromatic Molecules*; Academic Press: New York, 1971.

[11] Liu, Q. D.; Jia, W. L.; Wang, S. *Inorg. Chem.* **2005,** *44*, 1332.

[12] Liu, Q.; Jia, W.; Wu, G.; Wang, S. *Organometallics* **2003**, *22*, 3781.

[13] King, A. O.; Okukado, N.; Negishi, E. I. *J. Chem. Soc. Chem. Commun.* **1977**, 683.

[14] Ran, C.; Dai, Q.; Harvey, R. G. *J. Org. Chem.* **2005**, *70*, 3724.

[15] Beletskaya, I. P.; Cheprakov, A.V. *Coord. Chem. Rev.* **2004**, *248*, 2337.

[16] Enya, T. T.; Enomoto, S.; Wakabayashi, K. *J. Org. Chem.* **2006**, *71*, 5599.

[17] (a) Yamaguchi, S.; Shirasaka, T.; Akiyama, S.; Tamao, K. *J. Am. Chem. Soc.* **2002**, *124*, 8816. (b) Sole, G.; Gabbai, F. P. *Chem. Commun.* **2004**, 1284. (c) Liu, X. Y.; Bai, D. R.; Wang. S. *Angew. Chem. Int. Ed.* **2006**, *45*, 5475.

[18] Western, E. C.; Daft, J. R.; Johnson, E. M.; Gannett, P. M.; Shaughnessy, K. H. *J. Org. Chem.* **2003**, *68*, 6767.

[19] Jia, W. L.; Bai, D. R.; McCormick, T.; Liu, Q. D.; Motala, M.; Wang, R. Y.; Seward, C.; Tao, Ye.; Wang, S. *Chem. Eur. J.* **2004**, *10*, 994.

[20] (a) Shukla, M. K.; Leszczynski, J. *J. Phys. Chem. A* **2002**, *106*, 1011. (b) Shukla, M. K.; Leszczynski, J. *J. Phys. Chem. A* **2002**, *106*, 4709.

[21] Versano, D.; Di Felice, R.; Marques, M. A. L.; Rubio, A. *J. Phys. Chem. B* **2006**, *110*, 7129.

Chapter 3
Self-Assembly of N^2-Modified Guanosines in Solution

3.1 Introduction

The self-assembly of guanine unmodified lipophilic G-nucleosides[1] has been extensively explored, however modified lipophilic analogues have been less studied. Earlier investigations focused mainly on C^8-modified guanosines.[2] A recent study by Liu et al. has demonstrated for the first time that an N^2-modified guanosine **nBuGTAG** self-assembles into $[\mathbf{G}]_8$ in the presence of K^+ ions.[3] Extensive NMR data and the observation of a $[\mathbf{G}]_8 \bullet K^+$ molecular ion in the ESI-MS spectra supported this conclusion. This study indicates that modification at the N^2-site plays a key role in stabilizing the $[\mathbf{G}]_8$ structure and promotes diastereoselective self-assembly. To build on this preliminary result for a non-fluorescent $\mathbf{N^2G}$, fluorescent $\mathbf{N^2Gs}$ are potentially useful as building blocks for the development of functional supramolecular architectures. H-bonding of G-nucleosides is a dynamic process and fluorescent $\mathbf{N^2Gs}$ might become useful probes for this phenomenon. Although extensive data exist on the thermodynamics of G-q,[4] much less is known about the self-assembly of mono G-nucleosides and G-nucleotides. It is noteworthy that Davis et al.[5] reported previously on the [iso**G**]-to-$[\text{iso}\mathbf{G}]_{10}$ and [iso**G**]-to-$[\text{iso}\mathbf{G}]_4$ exchange.[6] Information on [**G**]-to-$[\mathbf{G}]_8$ transformation of guanosine is unavailable.

We have described the synthesis of fluorescent blue $\mathbf{N^2Gs}$ in Chapter 2. Now we turn our focus to the self-assembly aspect of these compounds in solution. In particular, the self-assembly of lipophilic N^2-arylguanosines **2.1b**, **2.2.b** and **2.4b**, in the presence of

$K^+[picrate]^-$ and $Ba^{2+}[picrate]^-_2$, was investigated using NMR spectroscopy. The H-bonding ability of hydrophilic N^2-guanosines, **2.1a – 2.3a**, is also explored in this chapter.

This chapter is organized as follows. First, NMR and CD evidence is presented for G-quartet and $[\mathbf{G}]_8$ formation from $\mathbf{N^2Gs}$. Second, molecular modeling is used to generate a $[\mathbf{G}]_8$ model in accordance with experimental evidence. Third, a complete thermodynamic and kinetic study of the [**G**]-to-$[\mathbf{G}]_8$ transformation is described.

3.2 Experimental Procedure

3.2.1 General considerations

All reagents were purchased from the Aldrich Chemical Co. and used without further purification unless stated otherwise. For the study of self-assembly the following salts were used: in-house picrate salts (ie. $K^+[picrate]^-$ and $Ba^{2+}[picrate]^-_2$ or $KClO_4$. The self-assembly was promoted either by liquid-liquid extraction or simple salt addition depending on the solvent used. All 1D and 2D NMR experiments (COSY, NOESY and DOSY) were recorded on Bruker Avance 400 MHz or 600 MHz spectrometers at 298 K, unless otherwise specified, with the solvent peaks used as the reference. Excitation and emission spectra were recorded on a Photon Technologies International QuantaMaster Model C-60 spectrometer.

3.2.2 Ligand-cation complexation *via* liquid-liquid extraction

To a solution of a given $\mathbf{N^2G}$ suspended in CH_2Cl_2 in a vial (~ 5 mg in 3 mL), an aqueous solution of picrate salt in excess (~ 20 mg in 3 mL) was added and the biphasic mixture was stirred overnight in order to ensure complete association. The aqueous layer was removed and the yellow organic layer was air dried.

3.2.3 NMR experiments

Diffusion experiments were carried out on a Bruker Avance-600 MHz spectrometer using the pulse sequence of longitudinal–eddy-current delay (LED) with bipolar-gradient pulses. The ^{1}H 90^{o} and 180^{o} pulse widths were 10 and 20 μs, respectively. The pulse filed gradient duration was varied from 4 - 15 ms, and the variable gradient (G) was changed from 6 to 350 mT/m. The diffusion period was varied from 50 to 90 ms. A total of 16 transients were collected for each of the 32 increment steps with 12 s recyling delay. The eddy-current delay was set to 5 μs. Diffusion coefficients were obtained by integration of the desired peaks to a single exponential decay curve using "Simfit Bruker XWINNMR" software. Calibration of the field gradient strength was achieved by measuring the value of the translational diffusion coefficient (D) for the residual ^{1}H signal in D_2O (99.99%, ^{2}H atom), for which $D = 1.91 \times 10^{-9}$ m^2/s.

All NOESY spectra at 298 K were acquired using a mixing time of 0.3 or 0.4 s and a total of 64 transients with the recycling delay of 10 s. NOESY experiment at 218 K was acquired using a mixing time of 0.1 s and the recycling delay of 2 s and the total of 64 transients.

Selective saturation transfer experiments were performed for **nBuGTAG** in CD_3CN between 283 and 313 K. The experiments were conducted using a selective saturation pulse on the peak of interest. An irradiation at H_8 of the monomer or octamer was used at 283 and 313 K, while irradiation at $H_{1'}$ of the monomer or octamer was performed at 298 K. The spectra were collected by varying the mixing time from 0 to 14 s for a total of 24 data points. Each ^{1}H NMR spectrum was acquired using 32 scans.

3.2.4 CD experiments

Standard CD spectra were recorded on a Jasco 715 circular dichroism spectrometer in a 1 cm path length cell. The wavelength was varied from 190 - 600 nm at a scan rate of 200 nm per minute with 5 overall scans. A monomer-to-octamer exchange study was performed using a 0.1 cm path length cuvette. The wavelength was varied from 190 to 800 nm at 1000 nm per minute with 10 overall scans. The equilibrium CD curves were obtained in the 285 – 325 K range and a suitable time (10 min) was used to achieve the equilibrium before recording the CD spectrum.

3.3 Results and Discussion

3.3.1 NMR study of self-assembly of N^2Gs

In general, self-assembly of **N^2Gs** can be induced by liquid-liquid extraction using picrate salts or by solid-liquid extraction. The picrate anion is a desirable counterion since its singlet proton peak can be used as an internal NMR reference, which can provide further clues about the stoichiometry of the formed G-aggregates. Hence, we have investigated the self-assembly of **2.1b, 2.2b** and **2.4b** in the presence of K^+ ions and **2.1b – 2.2b** in the presence of Ba^{2+} ions. A more detailed description on the self-assembly of these **N^2Gs** follows.

The ^{1}H NMR spectrum of the non-chelating analogue **2.1b** in the absence of metal ions in CD_2Cl_2, shown in Figure 3.1, exhibits some signals in the 10 – 13 ppm range, indicative of the weak H-bonding in the presence of residual metal ions introduced during the synthesis and purification of the ligand. In the presence of added metal ions, **2.1b** self-assembles into specific structures characterized by one set of proton peaks. The downfield chemical shifts of the exchangeable imino and amino protons are caused by H-bonding

and are found to depend on the valence of the metal ion. The specific stoichiometry was established using the picrate signal located at δ = 8.7 ppm. The overall ratio of N_1H or N_2H peaks to picrate from the NMR integrations was used to derive the final ligand-to-metal cation (L:M) ratios. The final L:M ratio was found to be 8:1 for the [**2.1b-G**]$_8$•K^+ and [**2.1b-G**]$_8$•Ba^{2+} complexes suggesting that there is only one metal ion per octamer that is sandwiched between two G-quartets. The G-quartet structure formed from **N^{2}G** is depicted in Figure 3.2 for reference. To further verify the proposed [**2.1b-G**]$_8$ structure, NOESY and COSY NMR experiments were used. In the [**2.1b-G**]$_8$•K^+ complex, the NOE cross peak between N_2H and H_8 protons indicates the formation of a G-quartet motif (Figure 3.3). In addition, the strong NOE correlation between H_8 and $H_{1'}$ suggests an all *syn* ribose conformation. In the [**2.1b-G**]$_8$•Ba^{2+} complex, the strong interaction observed between the H_8 and H_a resonances in Figure 3.4 indirectly supports the G-quartet formation. Perhaps the broadness of the H_8 resonance is responsible for the absence of NOE cross peak with N_2H. In Figure 3.5, the NOE correlation between H_8 and $H_{1'}$ is representative of all *syn* ribose orientation. Notably, the cross peak between H_8/H_a protons is absent in the corresponding COSY spectrum (Figure 3.6), indicating that only through space interactions exist between them. In conclusion, **2.1b** forms G-quartet motifs in the presence of K^+[picrate]$^-$ and Ba^{2+}[picrate]$^-_2$ with an all *syn* ribose orientation.

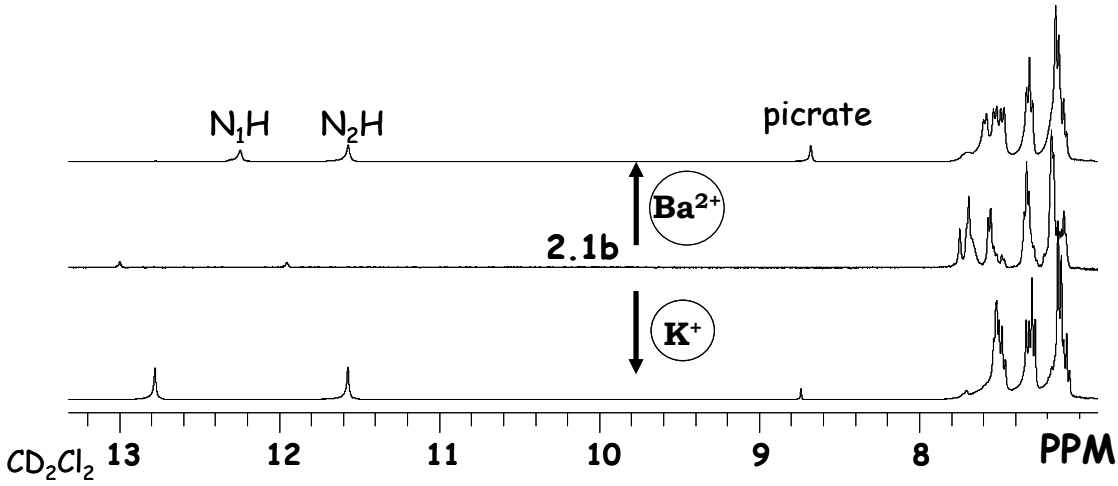

Figure 3.1 Partial NMR spectra of **2.1b** in the presence of $K^+[picrate]^-$ and $Ba^{2+}[picrate]^-_2$ in CD_2Cl_2 at 298 K.

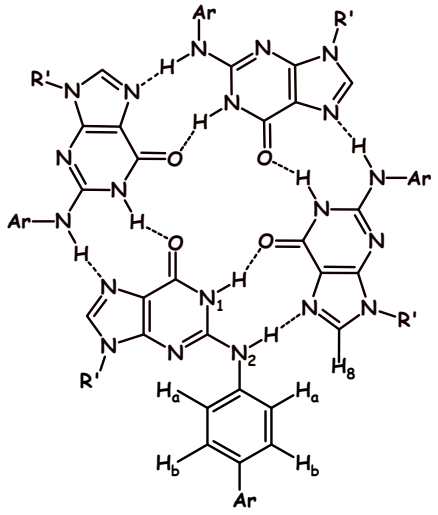

Figure 3.2 Structure of G-quartet from **N^{2}G** showing all pertinent protons.

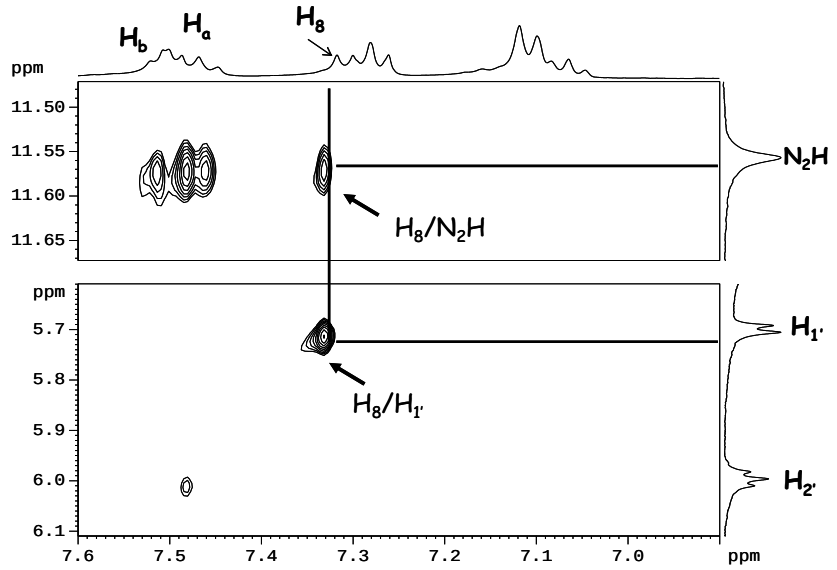

Figure 3.3 A portion of the 2D NOESY NMR spectrum of the [**2.1b-G**]$_8$•K^+ complex (CD_2Cl_2 at 298 K).

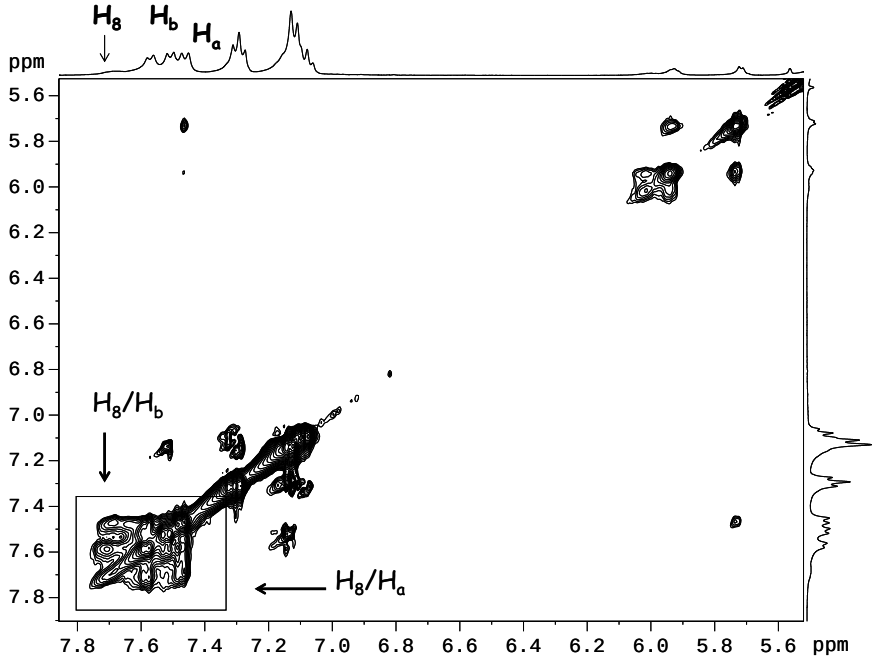

Figure 3.4 A portion of the 2D NOESY NMR spectrum of the [**2.1b-G**]$_8$•Ba^{2+} complex (CD_2Cl_2 at 298 K).

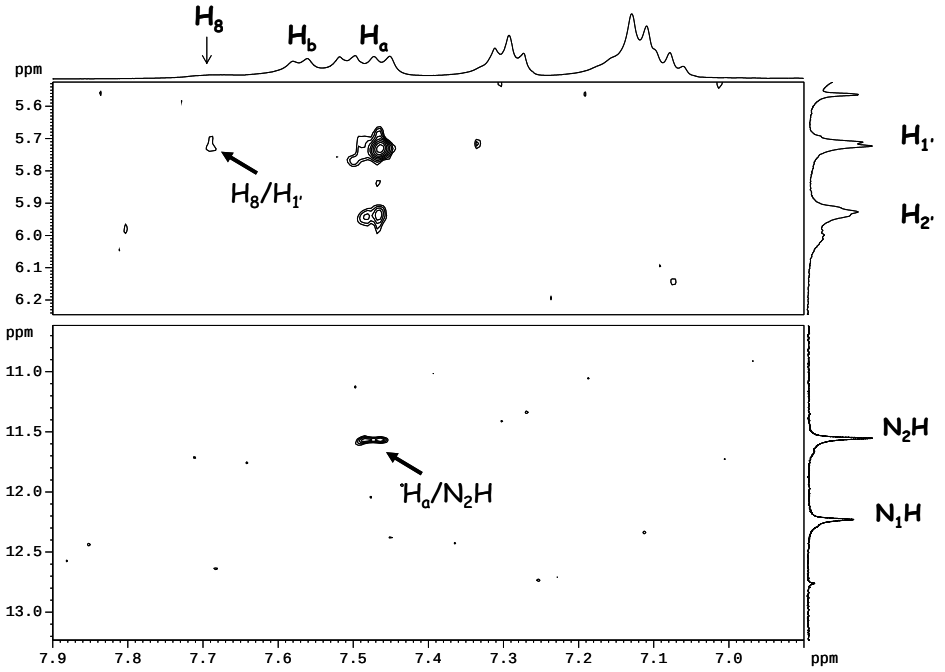

Figure 3.5 A portion of the 2D NOESY NMR spectrum of the [**2.1b-G**]$_8$•Ba^{2+} complex (CD_2Cl_2 at 298 K).

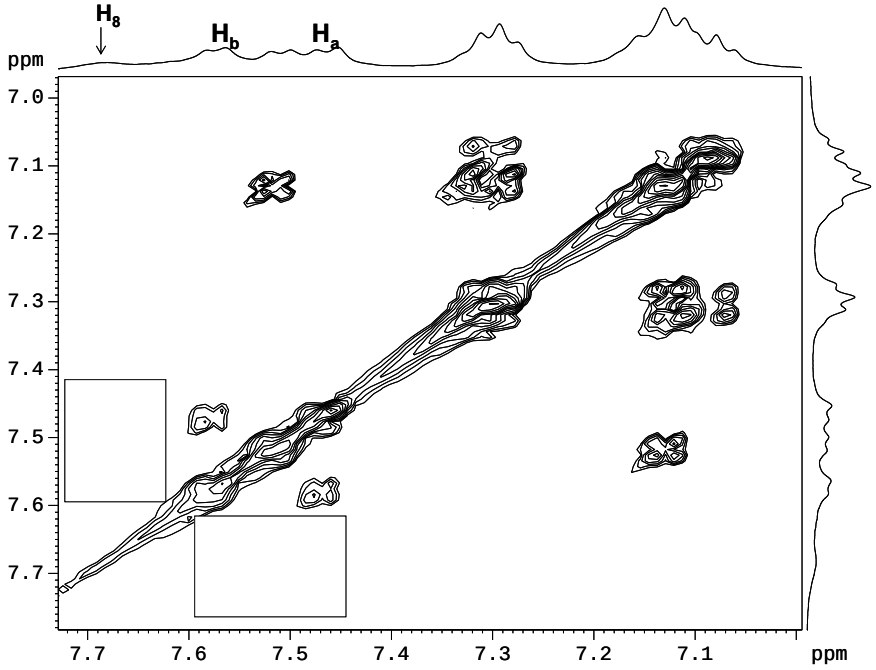

Figure 3.6 A portion of the 2D COSY NMR spectrum of the [**2.1b-G**]$_8$•Ba^{2+} complex (CD_2Cl_2 at 298 K).

The solution ^{1}H NMR spectrum of **2.2b**, in Figure 3.7, in the presence of metal cations, exhibits the spectral features similar to those observed for complexes of **2.1b**. The initial NMR integration for the imino, amino and picrate protons revealed that the final stoichiometry was 8:1 (L:M) for the filled octamer. The downfield shifts of the imino and amino protons and the strong NOE interaction observed in Figure 3.8 between H_8 and N_2H resonances confirms the G-tetramer formation in the presence of K^+[picrate]$^-$. The strong NOE between H_8 and $H_{1'}$ suggests *syn* orientation. In the [**2.1b-G**]$_8$•Ba^{2+} complex similar NOE correlations are observed for H_8/N_2H and $H_8/H_{1'}$ proton pairs (Figure 3.9).

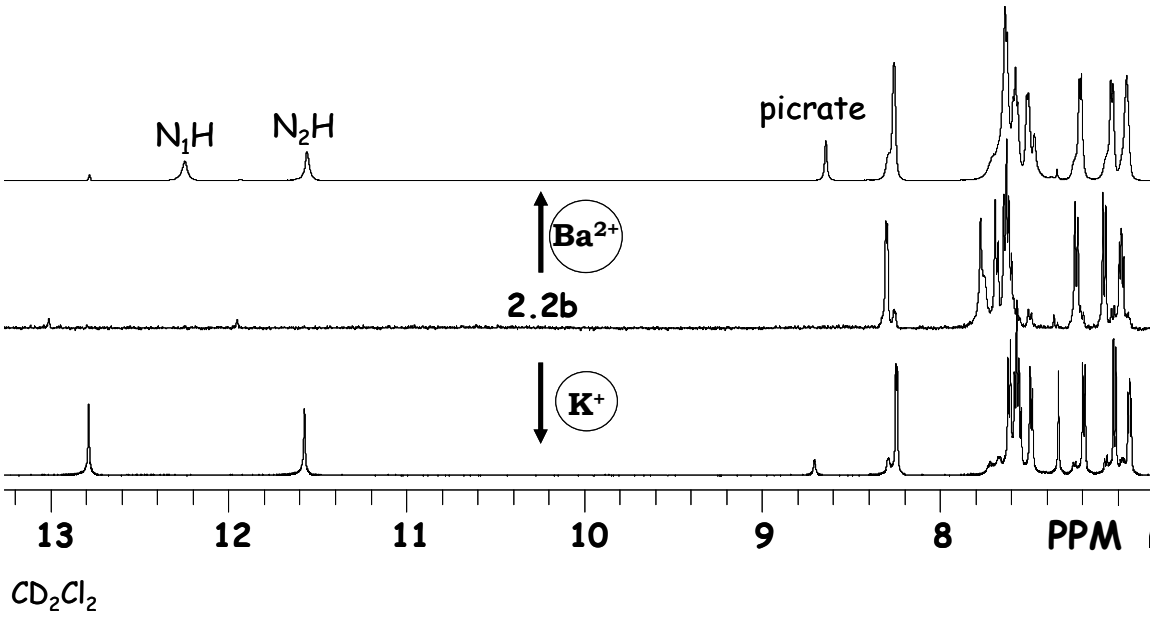

Figure 3.7 Partial NMR spectra of **2.2b** in the presence of K^+[picrate]$^-$ and Ba^{2+}[picrate]$^-_2$ (CD_2Cl_2 at 298 K).

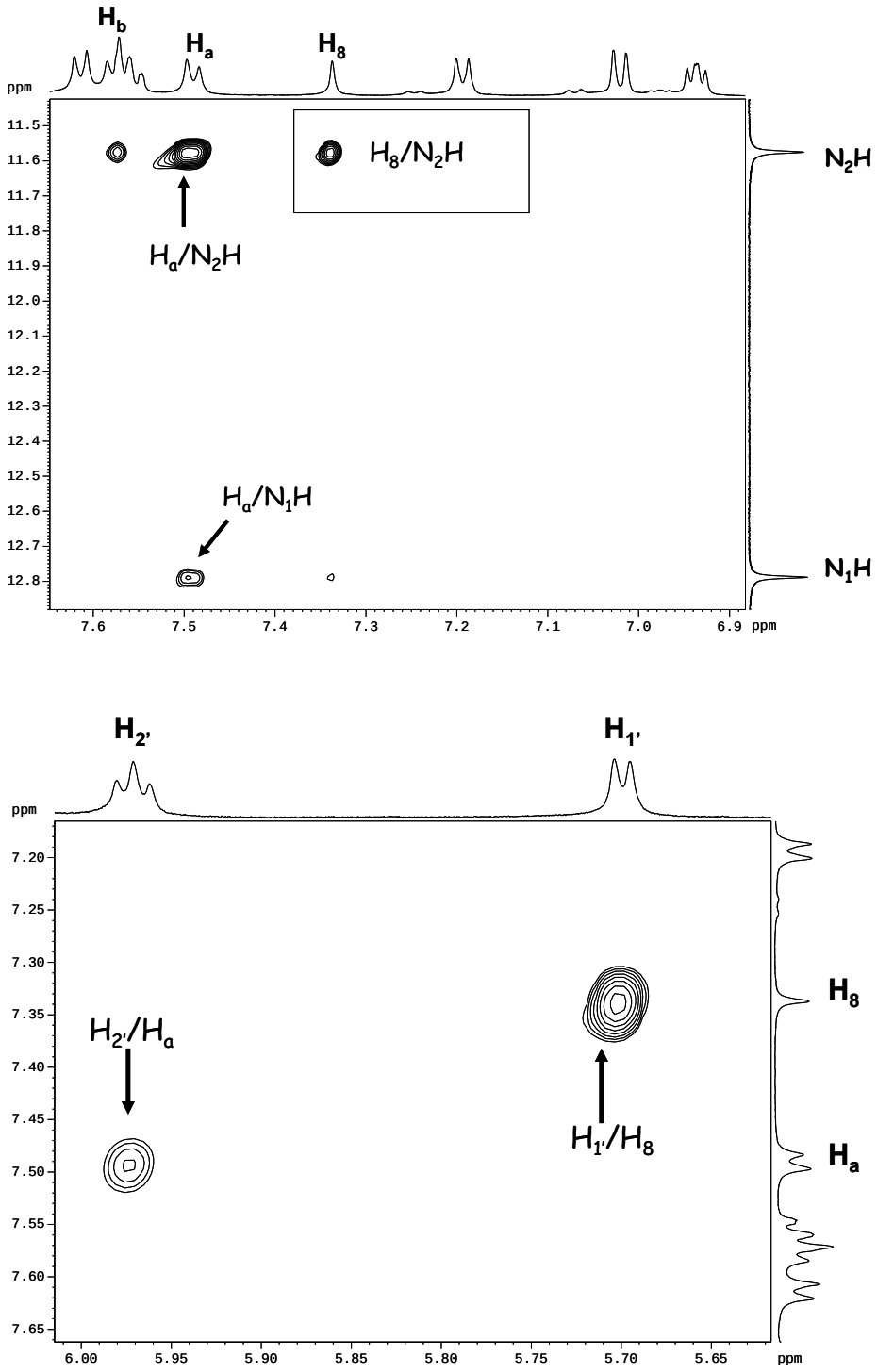

Figure 3.8 A portion of the 2D NOESY NMR spectrum of the [**2.2b-G**]$_8$•K^+ complex (CD_2Cl_2 at 298 K).

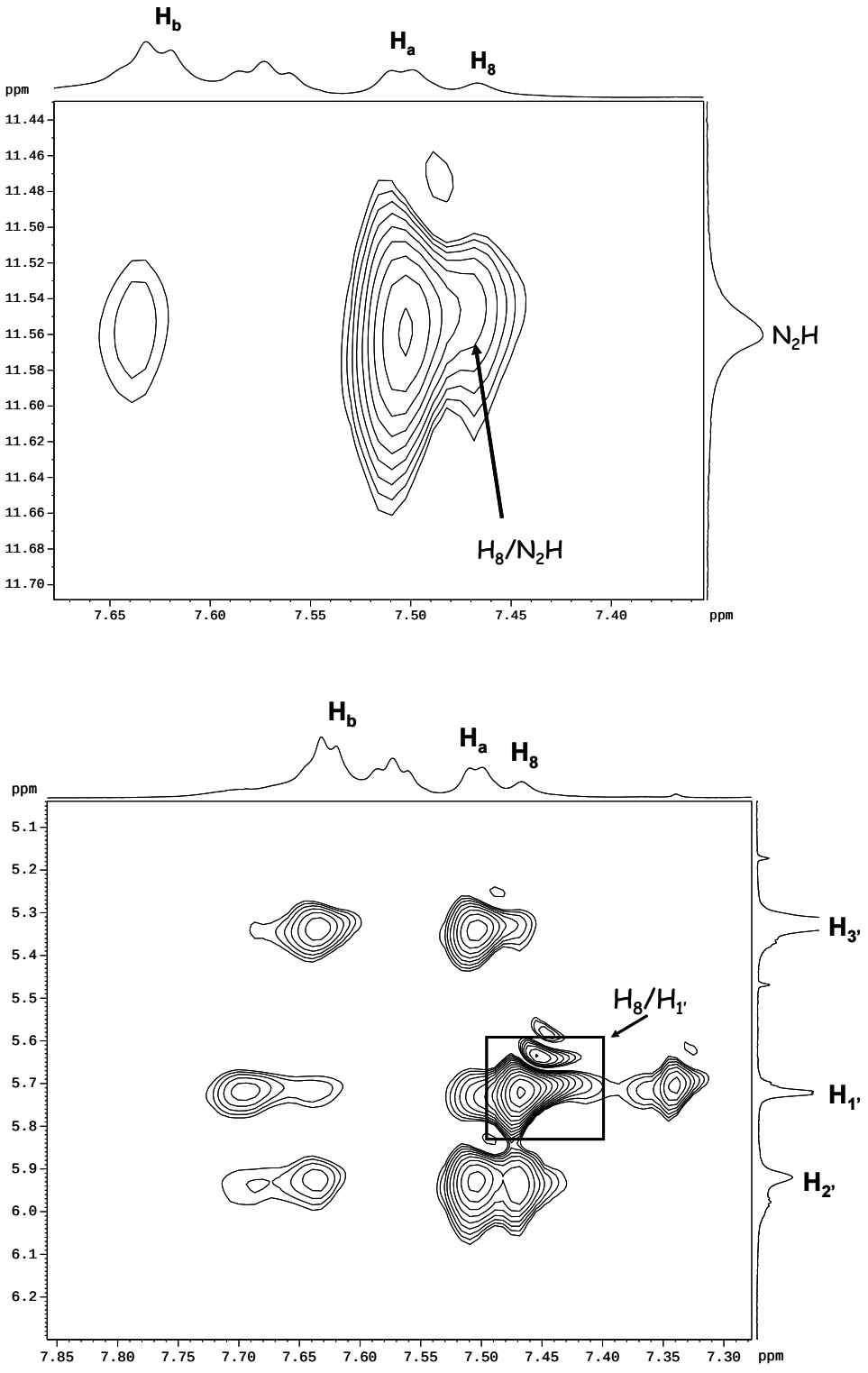

Figure 3.9 A portion of the 2D NOESY NMR spectrum of the [**2.2b-G**]$_8$•Ba^{2+} complex (CD_2Cl_2 at 298 K).

We find an analogous type of behaviour for **2.4b**, in the presence of $KClO_4$, as it exhibits the sharp resonances above 11 ppm associated with imino and amino protons that are participating in H-bonding (Figure 3.10). In Figure 3.11, the observed inter-base NOE cross peaks between the H_8 and N_2H protons is the characteristic spectral signatures of G-quartet formation. Due to the limited amount of isolated **2.4b** we have only performed complexation studies with K^+ ions, but given the above findings, a reasonable assumption would be that octamers would form even in the presence of Ba^{2+} ions. Similar to **2.1b** and **2.2b**, the N^2-pyrenyl guanosine compound also assumes an all *syn* ribose orientation with respect to the guanine ring judging by the strong NOE cross peak between $H_{1'}$ and H_8 protons.

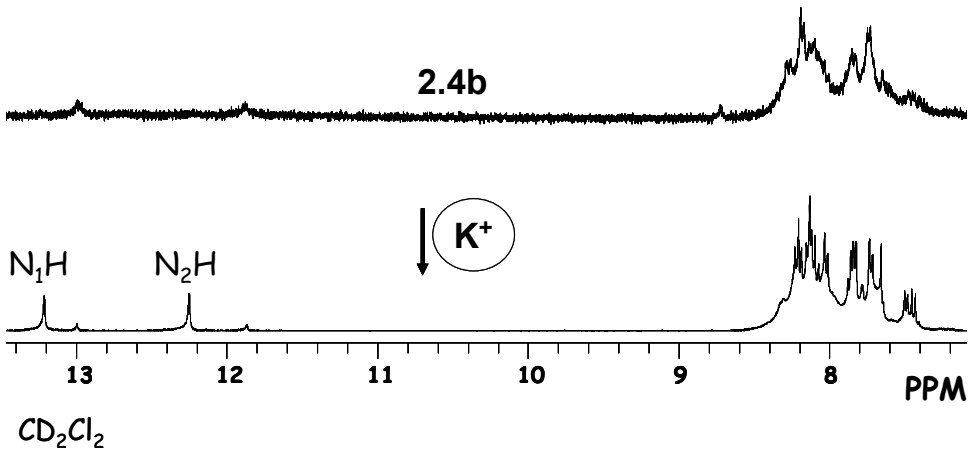

Figure 3.10 Partial NMR spectra of **2.4b** in the presence of $KClO_4$ (CD_2Cl_2 at 298 K).

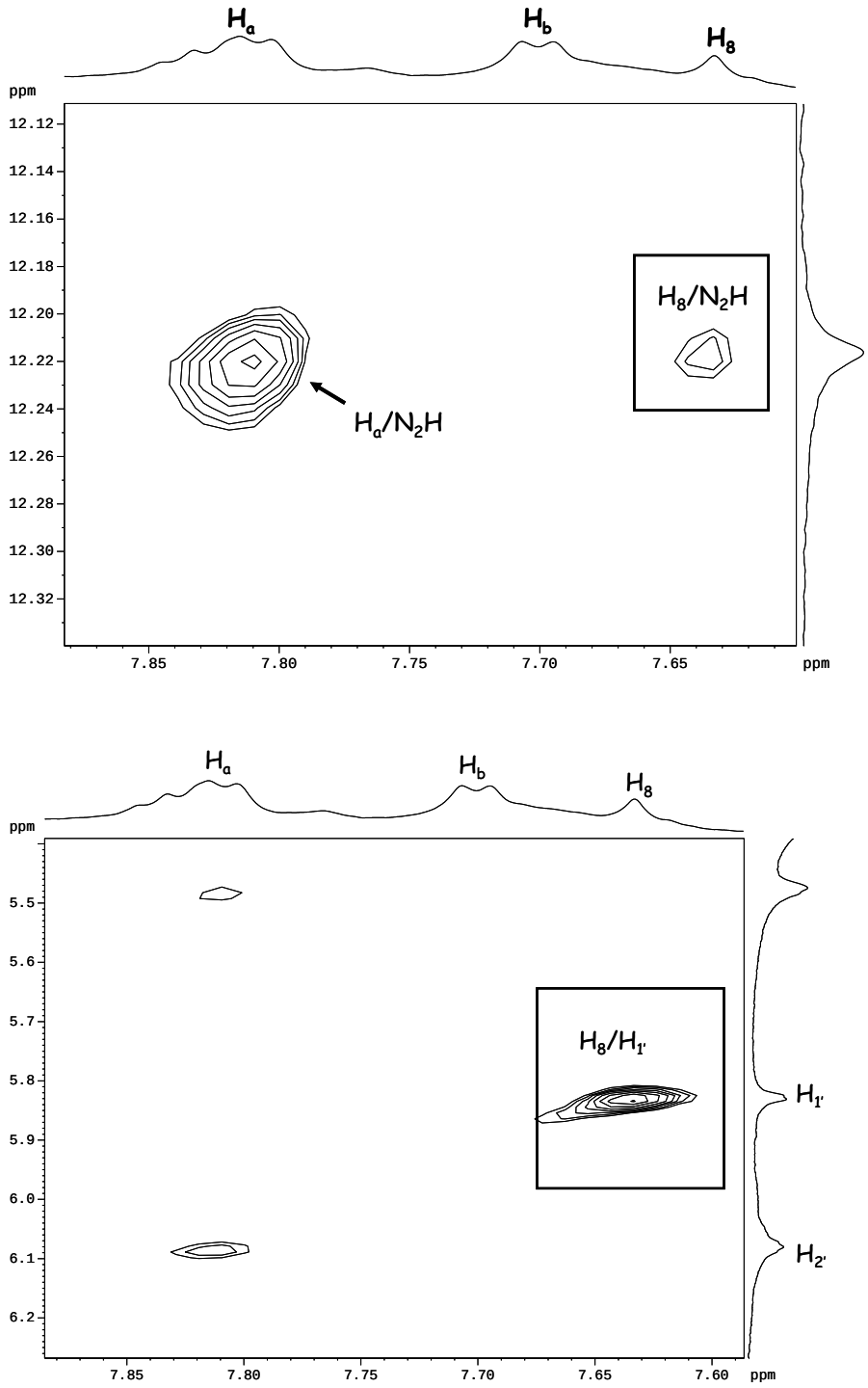

Figure 3.11 A portion of the 2D NOESY NMR spectrum of the [**2.4b-G**]$_8$•K^+ complex (CD_2Cl_2 at 298 K).

In conclusion, similar to **TAG** and **nBuGTAG**, **N^2Gs** self-assemble into high-order structures. Both monovalent and divalent cations were found to promote G-quartet formation of these nucleosides. All three compounds self-assemble in solution into discrete $[\mathbf{G}]_8$ with metal ions situated in the middle of the channel. The fact that a single set of ^{1}H NMR signals for each octamer is observed suggests that the N^2-guanosine octamers are D_4-symmetric. Such a symmetric constriction makes the two G-quartets identical which is only possible if the *hh* or *tt* stacking is present. The nature of metal ions does not affect the type of structure formed, unlike in the case of **TAG**. It should be reiterated that **N^2Gs** provide a degree of stereoselectivity in self-association which has not been observed for **TAG**. Moreover, **TAG**-based aggregates are composed of a mixture of *syn* and *anti* conformers which further complicates the spectrum. Our observations fall into the general trend that N^2- or C^8- modified guanosine derivatives usually prefer to adopt a *syn* conformation. The preference for a *syn* conformer is typically observed for the C^8-modified guanosines due to the steric hindrance. The strong COSY cross peaks between $H_{1'}$ and $H_{2'}$, stemming from the large ^3J coupling constant, indicate that C2'-*endo* puckering of the ribose ring persists in all **N^2G** octamers.

To examine the extent of G-quartet stacking the DOSY NMR technique was used with **TAG** as an internal reference. Even though the self-assembly of **nBuGTAG** has been analyzed, the actual D_t values have never been reported. The diffusion coefficients of the **2.1b, 2.2b, 2.4b** and **nBuGTAG** monomers and octamers are given in Table 3.1. Smaller D_t values were observed for the complexes than for their respective monomers which supports the formation of larger G-aggregates. The values of D_t for **N^2Gs** are much smaller than that for **TAG** indicating that the N^2 modification plays a role in the overall

shape of the molecule, compared with that of the unmodified guanosine. On average, the ratio of the diffusion coefficient for the monomer (D_m) and the octamer (D_8) of a given compound is ~ 0.55 in the presence of K^+ ions. However, slightly larger D_8/D_m ratios (~ 0.65) were observed for the aggregates in the presence of Ba^{2+}. If the error margin for the DOSY experiment is ~ 10 %, we can conclude that $[\mathbf{G}]_8$ is the only aggregate present in solution for all **N^{2}Gs**. Similar octamer/monomer ratios were observed by Davis et al.[74] for $[\mathbf{G}]_8$ formed from *5'-O*-acetyl-*2',3'-O*-isopropylideneguanosine in $CDCl_3$ in the presence of Na^+ ions. In terms of the approximate octamer size, it was previously established that the monomer and G-quartet diameters are ~ 10 and ~ 26 Å, respectively.[7] Provided that the interquartet distance is ~ 3.4 Å, the length of the $[\mathbf{G}]_8$ can be then estimated to be < 8 Å. The preferential formation of the exclusive diastereomer is attributable to and driven by the steric effects induced by the N^2-substituent and ribose group in addition to the hydrophobic interactions between aromatic moieties. The self-association of **N^{2}Gs** is independent of metal ion concentration, which cannot be said for lipophilic unmodified G-nucleosides.[8]

Table 3.1 Average translational diffusion coefficients determined for **TAG**, **2.1b, 2.2b** and **2.4b** and **nBuGTAG** in the presence of K^+ (Ba^{2+}) metal ions. All NMR diffusion measurements were performed at 298 K.

Compound	$\langle D_t \rangle$ (10^{-10} m^{2}s^{-1}) Monomer [G]	$\langle D_t \rangle$ (10^{-10} m^{2}s^{-1}) Octamer $[G]_8$	D_8/D_m *Ratio*
2.1b	7.83	4.35 (5.40)	0.56 (0.68)
2.2b	5.74	3.14 (4.41)	0.54 (0.75)
2.4b	8.14	4.18	0.51
nBuGTAG	6.06	3.09	0.51
TAG	8.42	(5.02[a])	(0.61)

[a] Taken with permission from M.Sc. thesis (Irene C.M. Kwan)

3.3.2 Study of the self-assembly by CD

In order to gain information regarding the chirality of **N^{2}Gs** and their aggregates, CD spectroscopy was employed. The shape and location of the CD couplet can vary depending on the structure of the building unit, the type of facing between the G-quartets, and the ribose orientation.

Absence of the CD bands above 370 nm, in **N^{2}G** system, suggests that an achiral picrate anion does not interact with the chiral G-aggregate. In monomers, very weak π – π^* transitions of the guanine chromophore in the ~ 260 – 350 nm region give rise to the very weak monosignate band. Upon complexation with metal ions, a strong negative exciton bisignate CD curve is obtained, due to the interactions between the guanines in the stacked G-quartets. Most of the aggregates from **N^{2}Gs** are characterized by a red-shifted CD couplet at ~ 300 nm as shown in Figure 3.12 and Figure 3.13, due to the extended conjugation provided by the chromophores attached at the N^2 site. An intense negative CD coupling observed in the 300 – 390 nm range is a diagnostic feature of chirally rotated stacked G-quartets.

Judging by the sign of the CD couplet and the likelihood of the *hh* or *tt* stacking, it can be concluded that the $[\mathbf{G}]_8$ belongs to D_4-symmetry. Similar findings were reported by Spada et al. for the D_4-symmetric $[\mathbf{G}]_8 \bullet K^+$ structure from unmodified lipophilic G-nucleoside.[9]

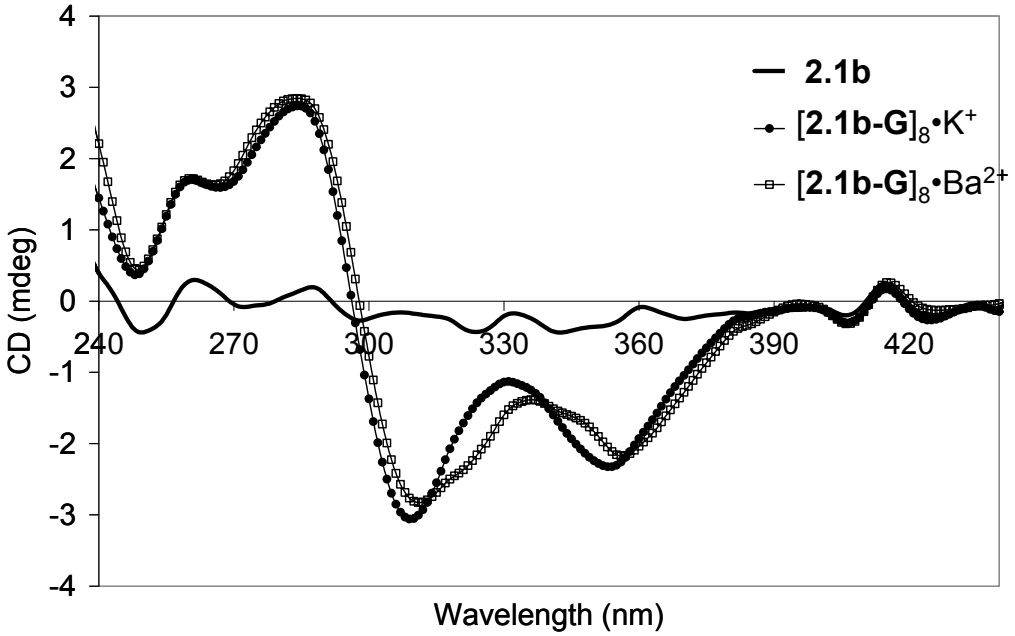

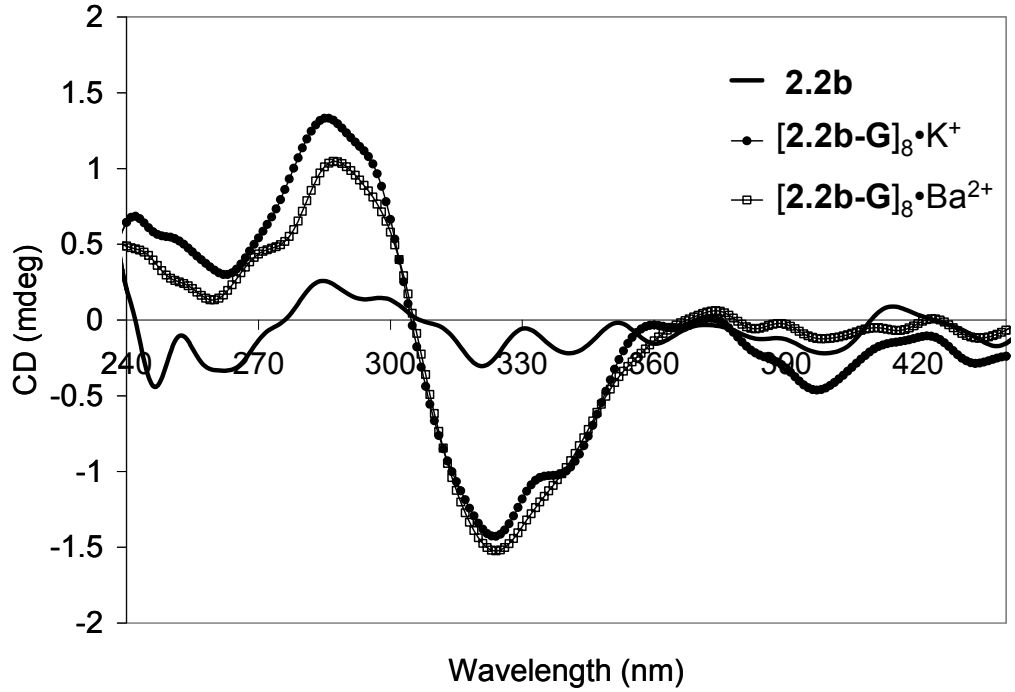

Figure 3.12 CD spectra of monomers **2.1b** and **2.2b** and their octamers (~ 1 x 10^{-5} M, CH_2Cl_2).

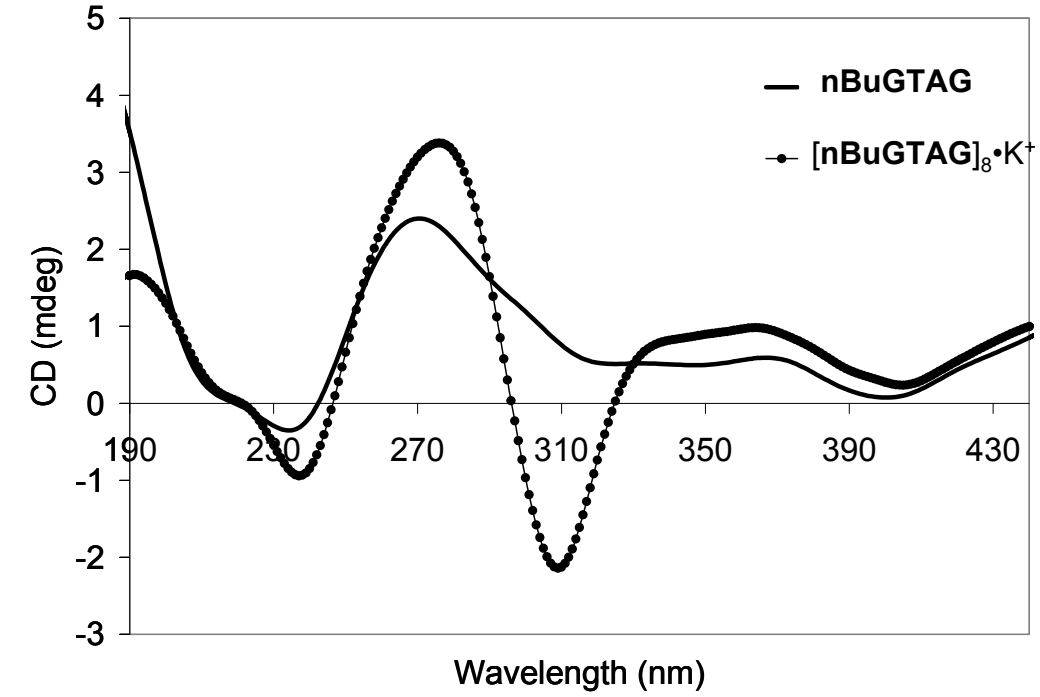

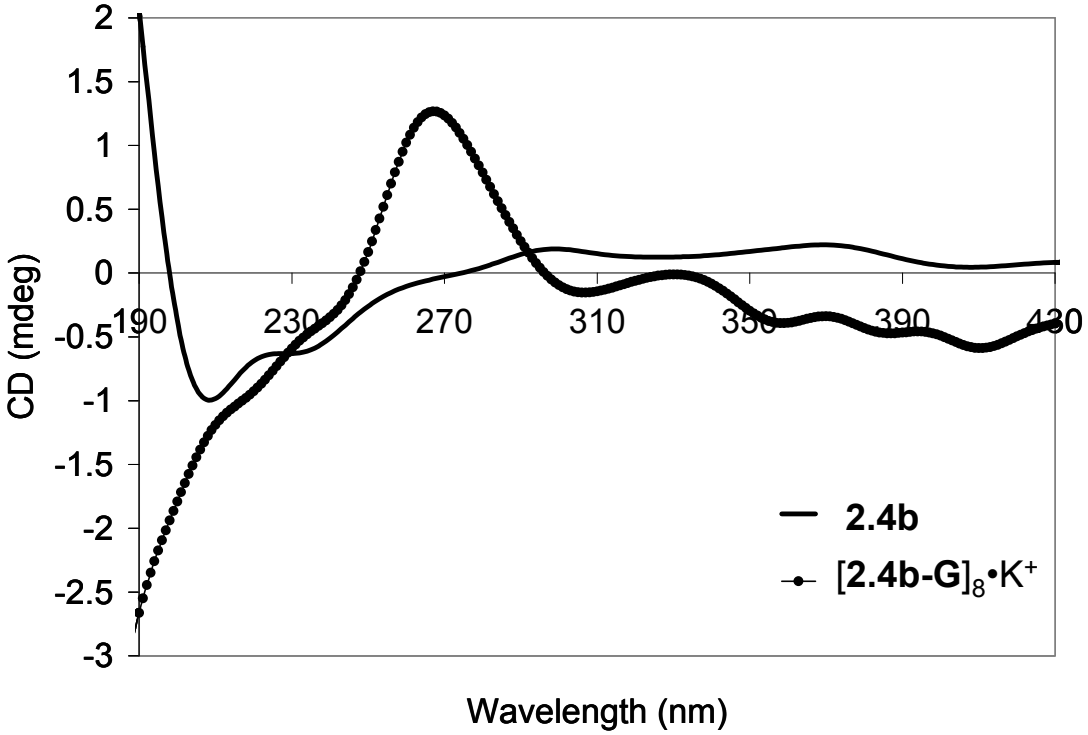

Figure 3.13 CD spectra of monomers **nBuGTAG** (2.5 x 10^{-4} M, CH_3CN) and **2.4b** (~ 1 x 10^{-5} M, CH_2Cl_2) and their octamers.

3.3.3 Molecular modeling of N^2G octamer

In this section, the molecular structure of **N^2G** octamer is discussed in more detail. Because crystallization of [**G**]$_8$ was unsuccessful, the model building in this section is based primarily on the NMR and CD evidence.

As mentioned earlier, the ^{1}H NMR data suggest that all the compounds form D_4-symmetric octamers, each of which contains two all *syn* G-quartets. Hence, the monomer-to-octamer transformation takes place with the retention of the overall *syn* orientation about glycosyl $C_{1'}$-N_9 bond. The strong COSY cross peaks observed between $H_{1'}$ and $H_{2'}$ for all **N^2Gs** monomers and octamers immediately suggest that the preferred sugar conformation is C2'-*endo* in both systems. The interquartet π - π stacking interactions between the N^2-substituent arms is likely involved in the *hh* or *tt* structures. Indeed, the observed ^{1}H chemical shifts for the phenyl protons (H_a and H_b) for the **2.1b, 2.2b** and **nBuGTAG** octamers are considerably more shielded than those in their respective monomers. For example in $CDCl_3$ or CD_2Cl_2, such changes amount to $\Delta\delta$ = 0.25 – 0.34 and 0.18 ppm for H_a and H_b, respectively, for compounds **2.1b, 2.2b** and **nBuGTAG** as can be seen from Figure 3.14. The NMR data suggest that the N^2-phenyl rings in the respective G-quartets are π – π stacked, which further stabilizes [**G**]$_8$.

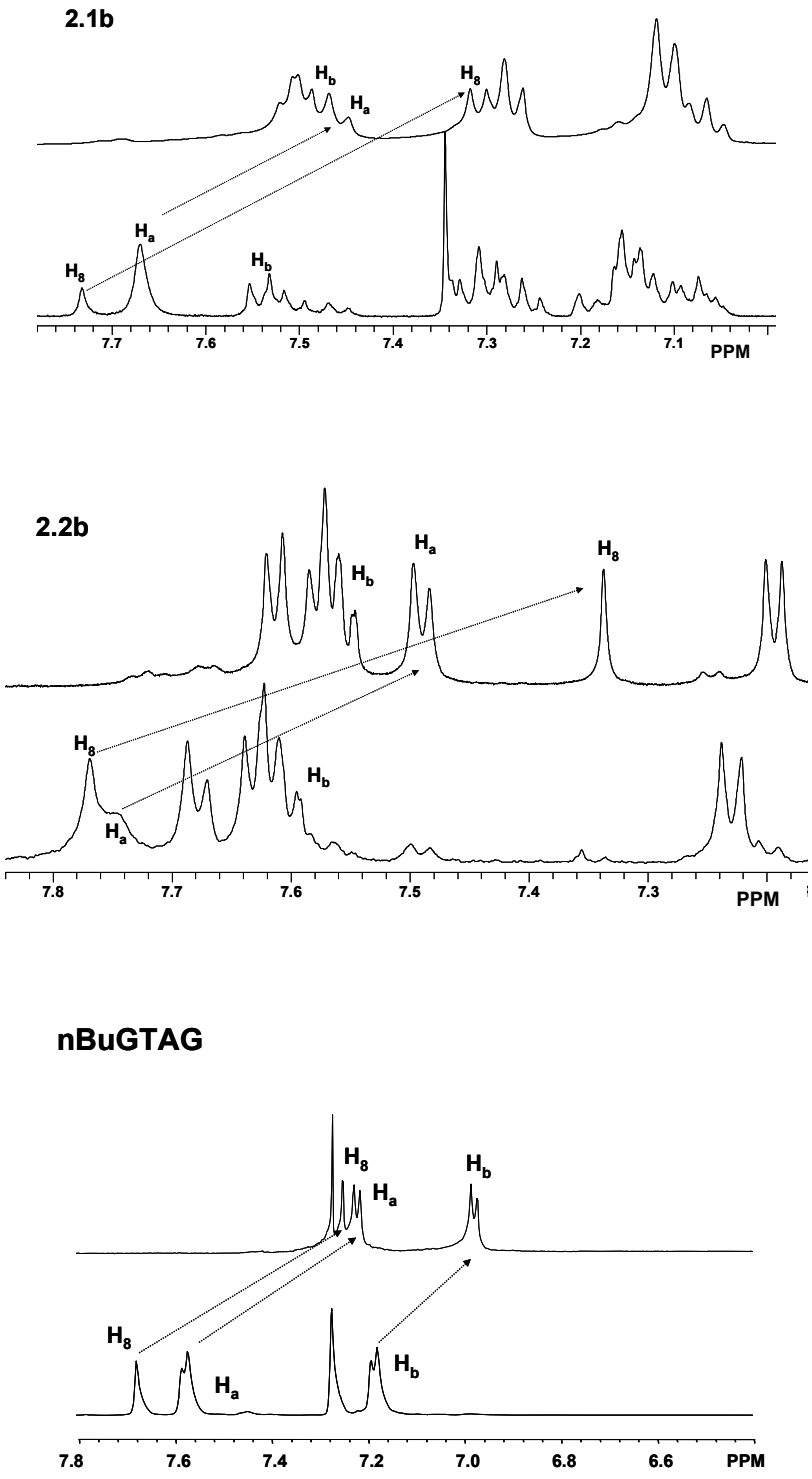

Figure 3.14 Partial ^{1}H NMR spectra of **2.1b**, **2.2b** (CD_2Cl_2) and **nBuGTAG** ($CDCl_3$) monomers (bottom) and $[\mathbf{G}]_8$ (top).

Based on these findings, the $[\mathbf{G}]_8$ model was built assuming the given glycosyl torsion angle, sugar conformation and extensive π - π stacking between the substituent arms. Because each G-quartet has two faces, head and tail, there are still two possible ways to form a D_4-symmetric octamer, i.e., either *hh* or *tt*. Our model suggests that the *tt* stacking is most likely to occur because of the arrangement of the three acetyl groups. In particular the *2′* and *3′-O*-acetyl groups are on the head side of the G-quartet and *5′-O*-acetyl group is on the tail side. As a result, the head face is more crowded than the tail side as depicted in Figure 3.15.

Furthermore, because of the additional $-CH_2-$ group linked to the 5′-*O*-acetyl group, it is more flexible than the *2′* and *3′-O*-acetyl groups that are directly attached to the ribose ring. A modified G-nucleoside with a *syn* orientation is expected to form smaller aggregates, due to the repulsion between additional G-quartets because of the folded structure between the guanine and the ribose. A *tt* octamer formation can also provide an explanation for the fact that further stacking between octamers has not been observed for any of $\mathbf{N^2Gs}$. The proposed structure of the $[\mathbf{G}]_8 \bullet M^+$ is shown in Figure 3.16.

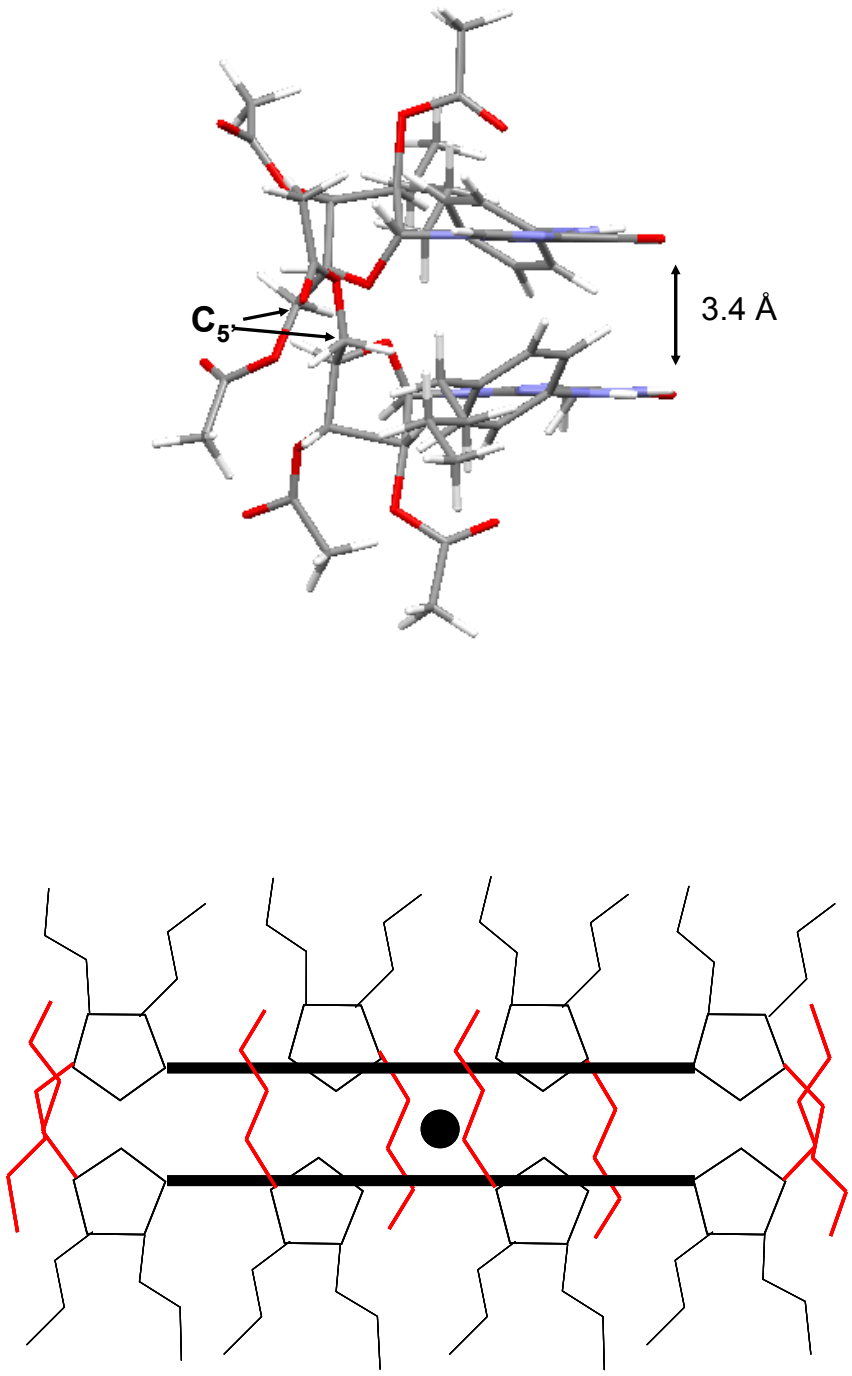

Figure 3.15 A part of an octamer showing $C_{2'}$ and $C_{3'}$ acetyl groups on the periphery and $C_{5'}$ acetyl chains (in red) pointing inwards (top) and $[\mathbf{G}]_8 \bullet M^+$ representation of the same (bottom).

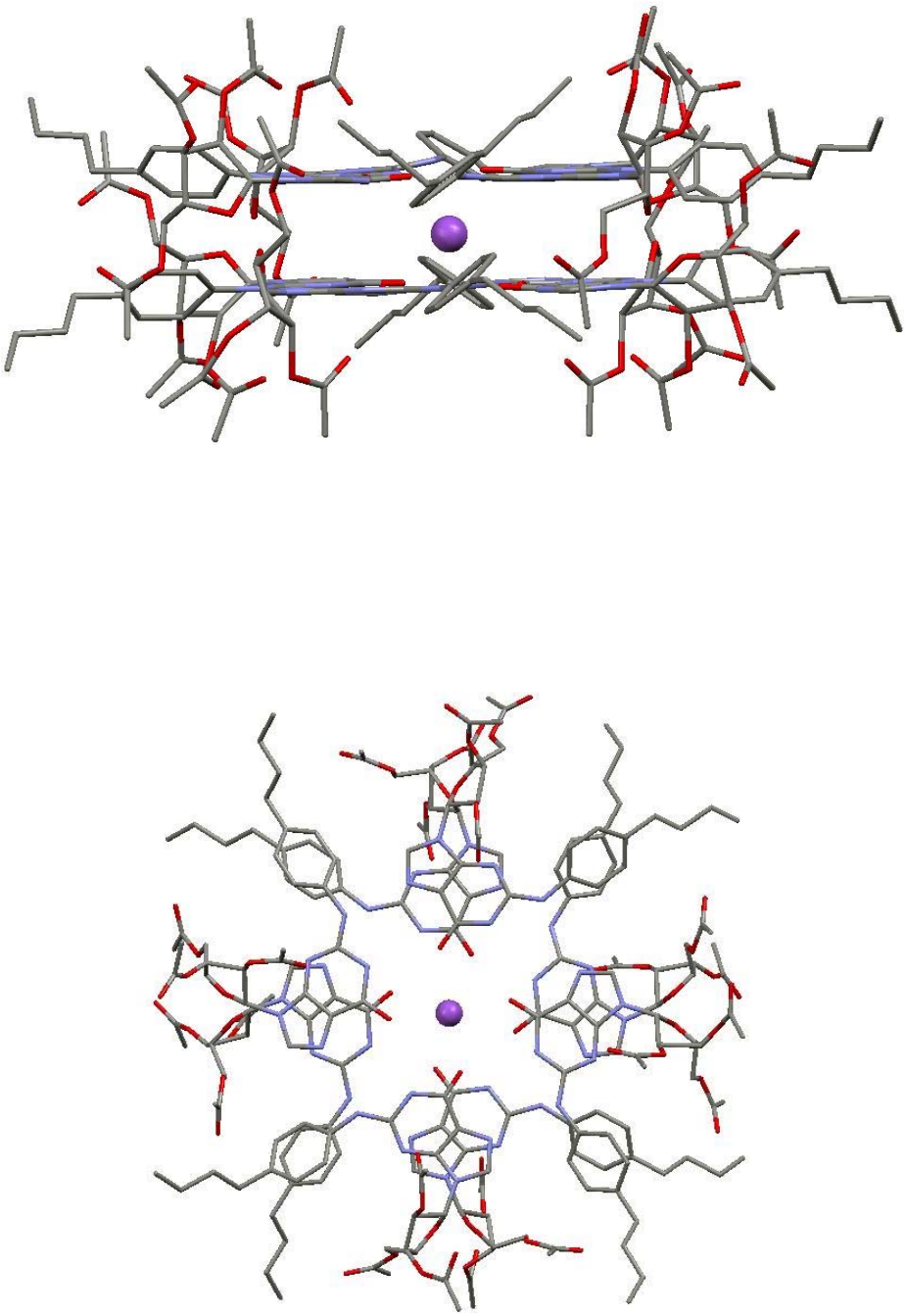

Figure 3.16 Molecular model depicting [**nBuGTAG**]$_8$•M^+: side view and top view.

On the contrary, for **2.4b** significant ^{1}H chemical shift changes (ca. $\Delta\delta \approx 0.5$ ppm) were observed for H_7 and H_2 of the pyrenyl group (Figure 3.17), while the H_a and H_b protons remained unchanged. These chemical shift changes are comparable to those observed for the H_8 protons ($\Delta\delta = 0.45$ ppm), which are due to the π - π stacking between the guanine bases. Other protons of the pyrenyl group, even in the absence of a complete assignment, also show small chemical shift changes. All of these observations are consistent with the formation of π - π stacking. Interestingly, the phenyl protons in the **2.4b** octamer exhibit little chemical shift change compared to those in the monomer. This finding suggests that the type of stacking between the substituents of **2.4b** is very different from that seen above.

Inspection of the molecular model in Figure 3.18 reveals that in the $[\mathbf{G}]_8$ of **2.4b** the phenyl rings are more perpendicular to the guanine base plane than those in the $[\mathbf{G}]_8$ of **nBuGTAG**. In particular, the C_2–N_2–C_{ipso}–C_{ortho} torsion angle in the **2.4b** octamer is 78° whereas it is only 41° in the **nBuGTAG** octamer.

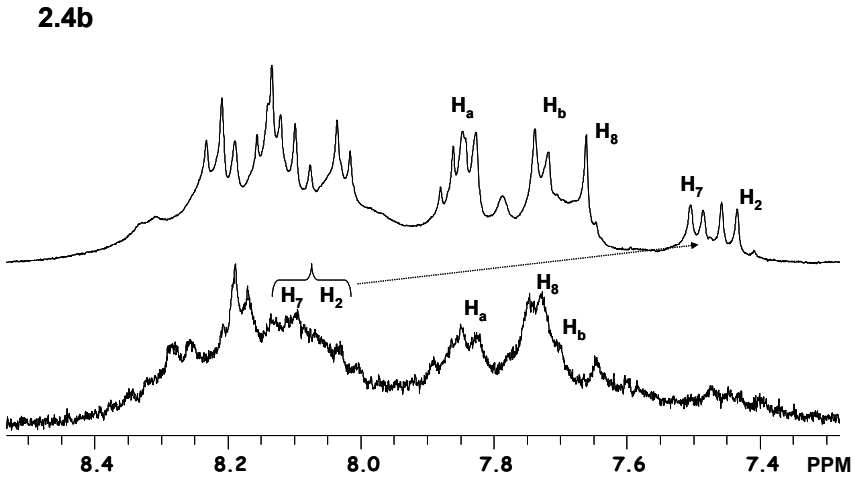

Figure 3.17 Partial ^{1}H NMR spectra of **2.4b** monomer (bottom) and $[\mathbf{G}]_8$ (top) ($CDCl_3$).

Such an arrangement of the phenyl ring relative to the guanine plane was also predicted by quantum chemical calculations at the B3LYP/6-311G** level for the ground state optimized structure of **2.4b**. Consequently, there is very little π - π stacking between the two phenyl rings in the **2.4b** octamer. This is entirely consistent with the signals for H_a and H_b showing little variations between **2.4b** monomers and octamers. Another piece of evidence suggesting π - π stacking between the pyrenyl rings in the **2.4b** octamer comes from the NOESY data. In the NOESY spectrum shown in Figure 3.19, the weak cross peaks are observed between H_7 and H_2 of the pyrenyl group. The distance between H_2 and H_7 within the same pyrenyl ring is approximately 8.027 Å. This distance is generally too long to generate any NOE effect. On the other hand, the **2.4b** octamer model suggests that the distance between H_2 and H_7 from two different G-quartets (inter-quartet) is about 3.475 Å. This is a reasonable short contact for producing the observed NOE cross peaks.

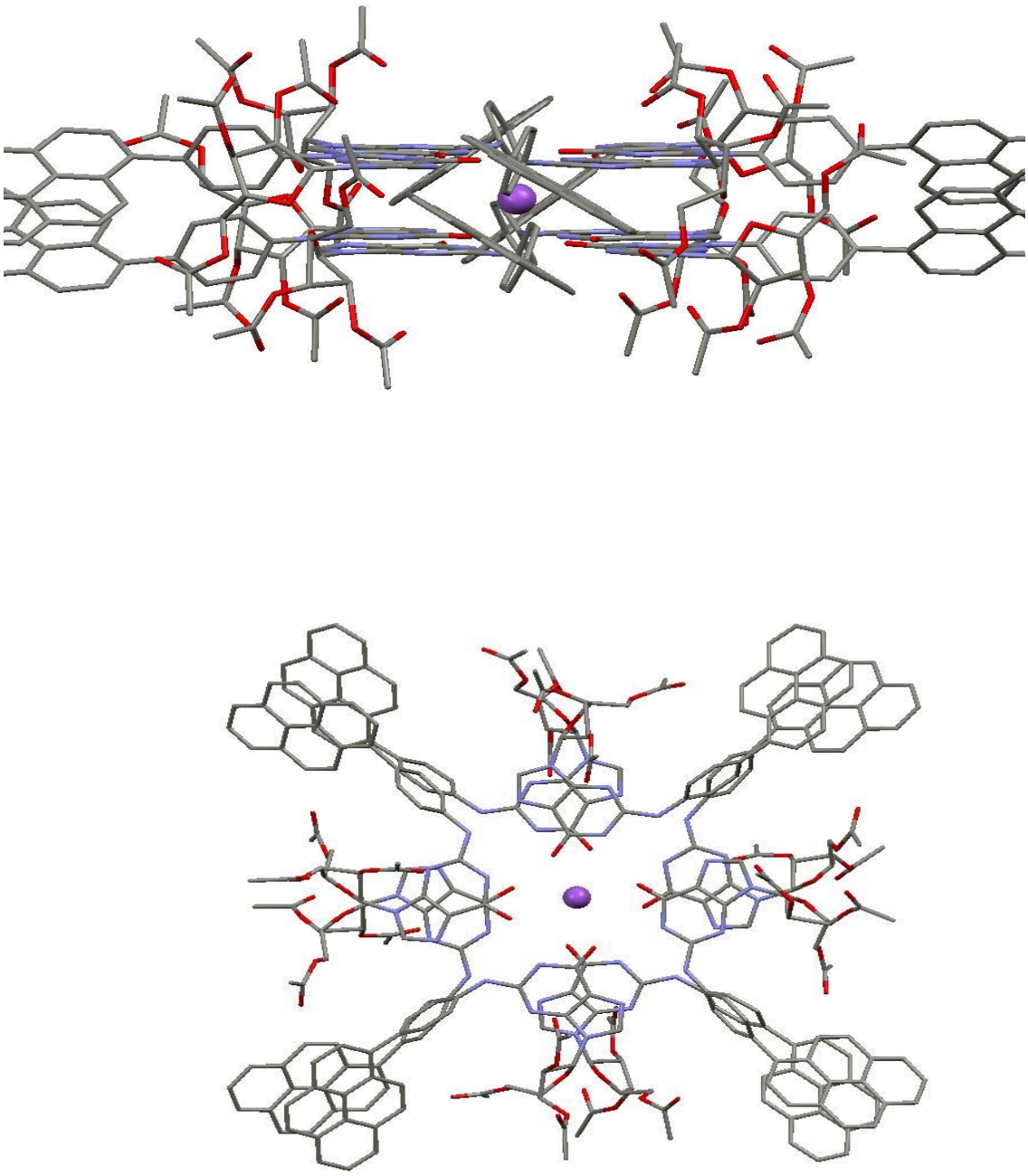

Figure 3.18 Molecular model of [**2.4b-G**]$_8$•M$^+$ octamer side view and top view.

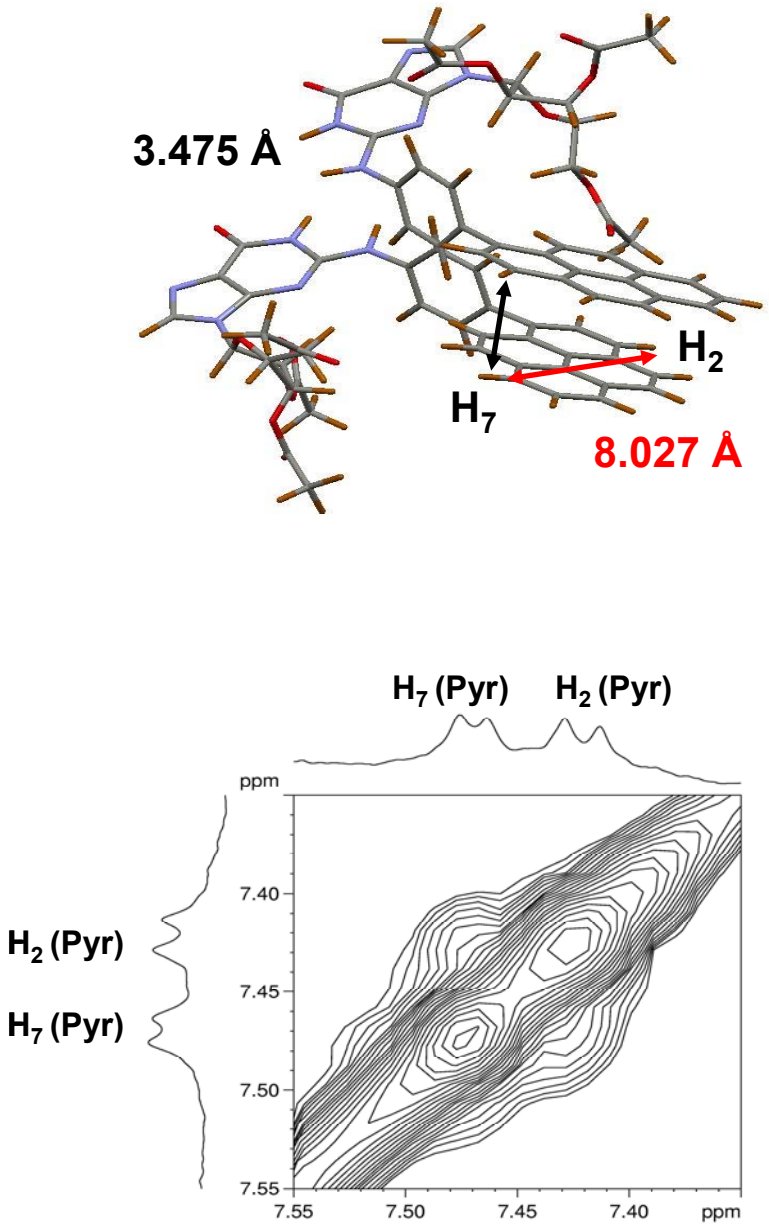

Figure 3.19 Molecular model of the **2.4b** octamer (two **N^{2}Gs** are shown only) showing distances for the pyrenyl groups and the NOE interaction between H_2 and H_7 protons.

All **N^{2}Gs** form discrete G-octamers with all *syn* molecules. The stacking between the two G-quartets is most likely in a *tt* fashion. In [**G**]$_8$, the main forces holding the two G-quartets together are the ion-carbonyl interactions and the π - π stacking between the guanine bases. The NMR results strongly suggest the presence of hydrophobic interactions between the phenyl or pyrenyl groups in the [**G**]$_8$, respectively. This interesting octamer stability of **N^{2}Gs**, seen from the NMR evidence, can be attributed to the interquartet π – π stacking between N^2-aryl groups as shown in Figure 3.20.

It is plausible that the additional π - π stacking between the N^2 side arms in the [**G**]$_8$ further stabilizes the final structures. It would be interesting to design new N^2-modified guanosine derivatives where the π - π stacking between N^2 groups can be optimized. It might also be possible that such a π - π stacking between N^2 groups would provide strong enough attraction to hold the two G-quartets so that the central cation becomes unnecessary, giving rise to an "empty" G-octamer. We will explore such structures in the next chapter.

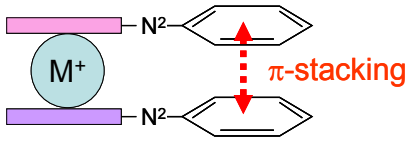

Figure 3.20 Stabilizing interquartet π - π stacking interactions.

3.3.4 Self-assembly of hydrophilic N^{2}Gs

This section focuses on the similarities and differences between self-assembly of lipophilic and hydrophilic **N^{2}Gs**. To our knowledge, the self-assembly of the hydrophilic **N^{2}Gs** has not been studied due to their poor solubility. To examine the self-assembly of

hydrophilic G-nucleosides we have investigated compounds **2.1a** – **2.3a**. Due to the limited solubility of these compounds, the studies were performed in CD_3CN/THF-d_8 (5:1 %vv) in the presence of $KClO_4$. Addition of K^+ to the solutions of **2.1a** or **2.3a** did not result in any changes in their ^{1}H NMR spectra.

Under identical experimental conditions, in the presence of $KClO_4$, compound **2.2a** undergoes self-assembly as suggested by the complex ^{1}H NMR spectrum in Figure 3.21. The ^{1}H NMR spectrum reveals the presence of the sharp peaks above 11 ppm which is direct evidence of H-bonding. Three types of signals, in a 1:1:1 ratio, were distinguished using 2D COSY, NOESY and DOSY experiments. We assigned one set of the ^{1}H NMR signals, the most deshielded ones, to monomeric [**G**], while the other two sets of ^{1}H NMR signals, always present in a 1:1 ratio, were identified as aggregates $[\mathbf{G}]_n$. Furthermore, the monomer/aggregate ratio does not vary with temperature even after cooling to 253 K, which indicates that the two species are not undergoing exchange.

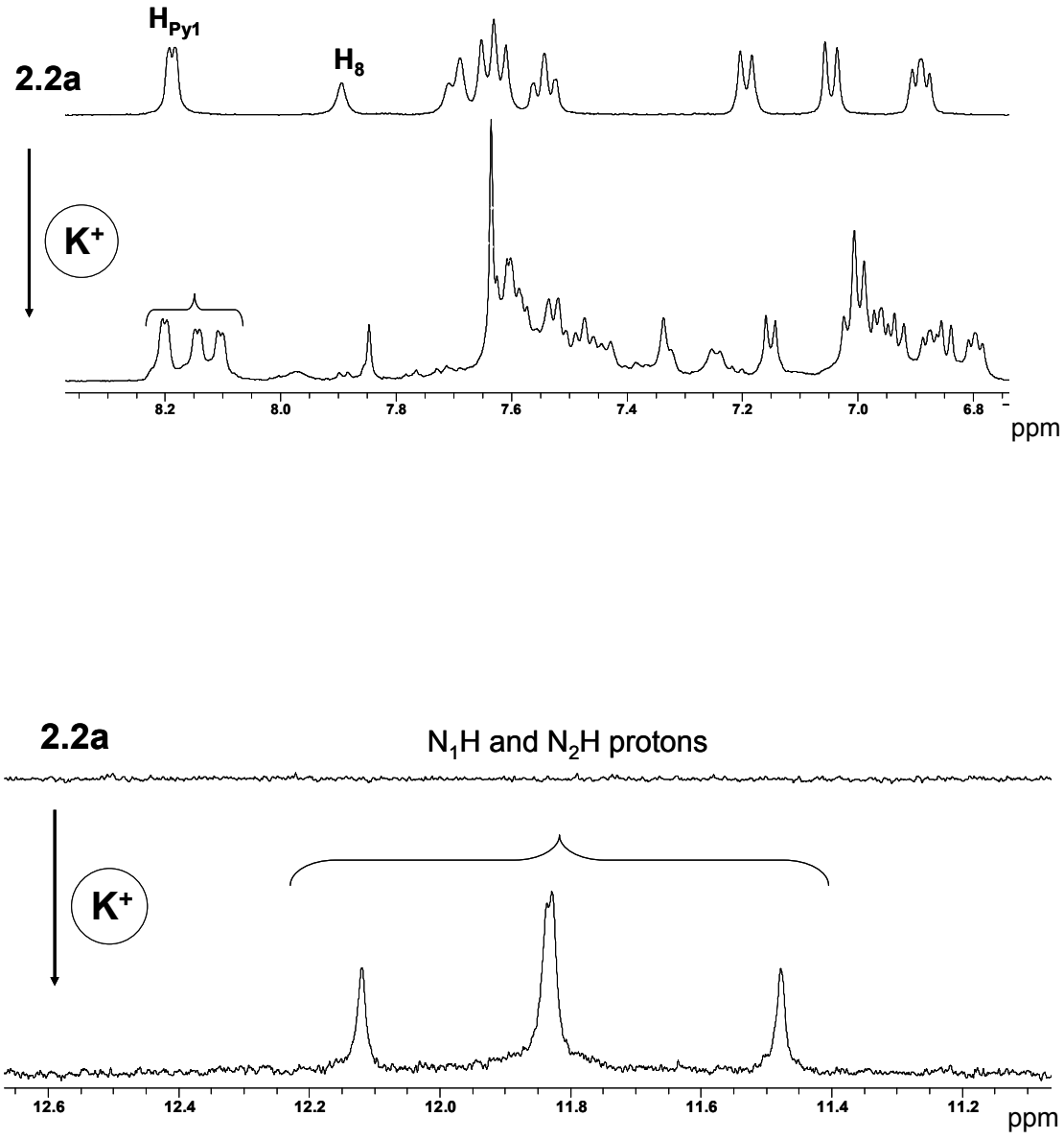

Figure 3.21 Partial ^{1}H NMR spectra of compound **2.2a** in the presence of $KClO_4$ (CD_3CN/THF-d_8 (5:1 %vv)).

Due to the complexity of the ^{1}H NMR spectra in the ribose region, we have decided to use D_2O in order to identify the hydroxyl groups in the aggregates. As shown in Figure 3.22, addition of D_2O to the complex leads to the exchange with the hydroxyl groups (at 2' and 3' positions), which in turn disappear, while the deuteration of other hydroxyl groups further simplifies the spectrum, many of the 4', 5' and 5'' protons could not be distinguished due to the overlap with the THF peak at 3.58 ppm. Notably, an excess of D_2O disrupts the H-bonding in the aggregates as would be expected in the presence of a highly polar solvent capable of competitive H-bonding.

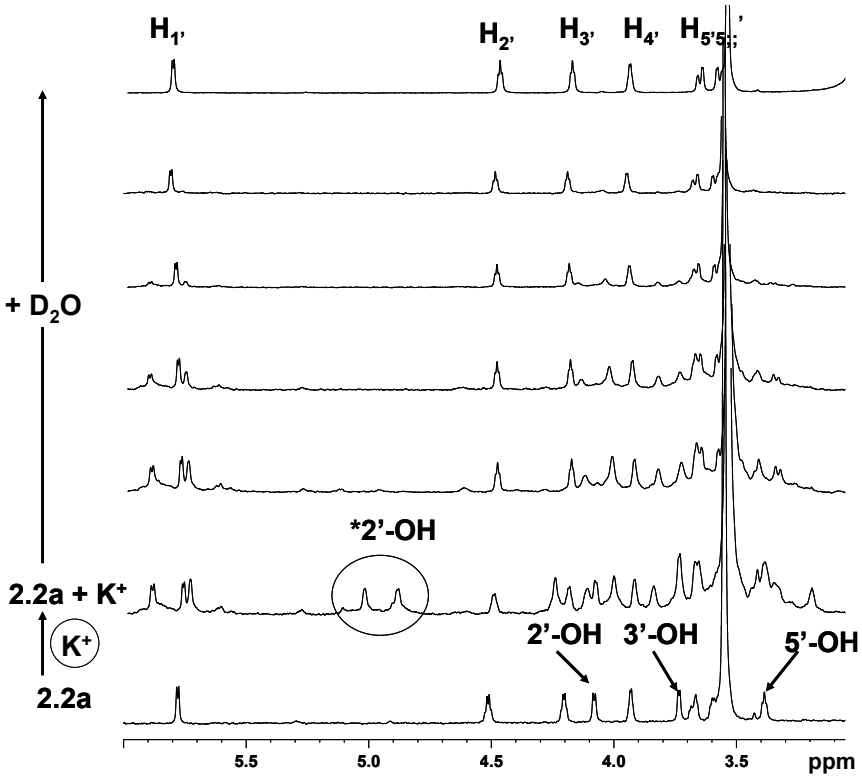

Figure 3.22 Partial ^{1}H NMR spectra of free **2.2a** (bottom, CD_3CN/THF-d_8 (5:1 %vv)), in the presence of $KClO_4$ and upon addition of aliquots of D_2O to the aggregates (298 K).

The structural elucidation of the two aggregates was done in the series of steps. Firstly, imino and amino protons associated with the specific aggregates were identified and were further linked to their respective H_a (*ortho* protons) and H_8 protons as depicted in Figure 3.23. In G-quartet I (solid circle) the ribose conformation could not be determined due to the strong NOE interactions between H_8/H_a proton signals with $H_{1'}$, $H_{2'}$ and $H_{3'}$. The small value of ^3J ($H_{1'}$,$H_{2'}$) (small $H_{1'}$ splitting) indicates C3'-*endo* puckering in G-quartet I.

In G-quartet II (star) in Figure 3.24, the ^3J ($H_{1'}$,$H_{2'}$) value is much larger (~ 6.2 Hz from DQF-COSY) suggesting C2'-*endo* puckering and an all *anti* glycosidic conformation due to the strong NOE between H_8 and $H_{5'}$. The puckering assignment is similar to that reported by Wu et al. for two identical aggregates with different ribose puckering.[44] Two aggregates have been identified as the G-quartet-based structures. However, it is still unclear if they belong to the same structure. Most informative are the two hydroxyl groups found in the 5.5 – 6.5 ppm region, which exhibit strong NOE with each other but which do not belong to the same G-quartets. The overall chemical shift position of these two hydroxyl groups suggests that they are involved in H-bonding.

In order to discriminate between true NOE and chemical exchange, for the exchangeable protons, ROESY NMR was attempted. However, we could not observe any cross peaks between ribose units due to the low sample concentration and short experiment time. Despite this drawback, additional NOE cross peaks between non-exchangeable ribose protons were observed which eliminates the possibility of chemical exchange between two different G-quartets.

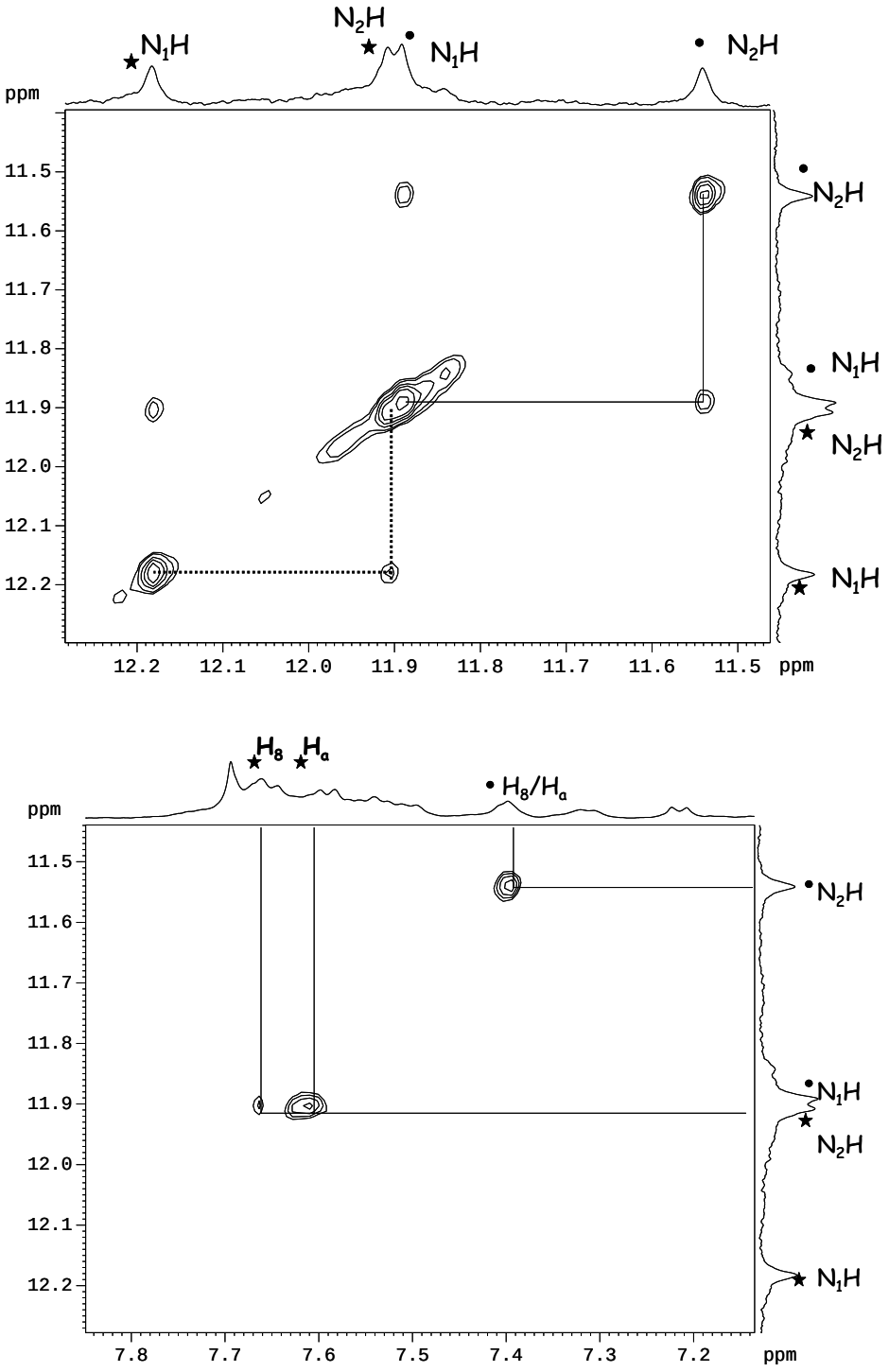

Figure 3.23 Partial NOESY NMR spectra of **2.2a** in the presence of $KClO_4$ (G-quartet I (circle) and G-quartet II (star), 298 K).

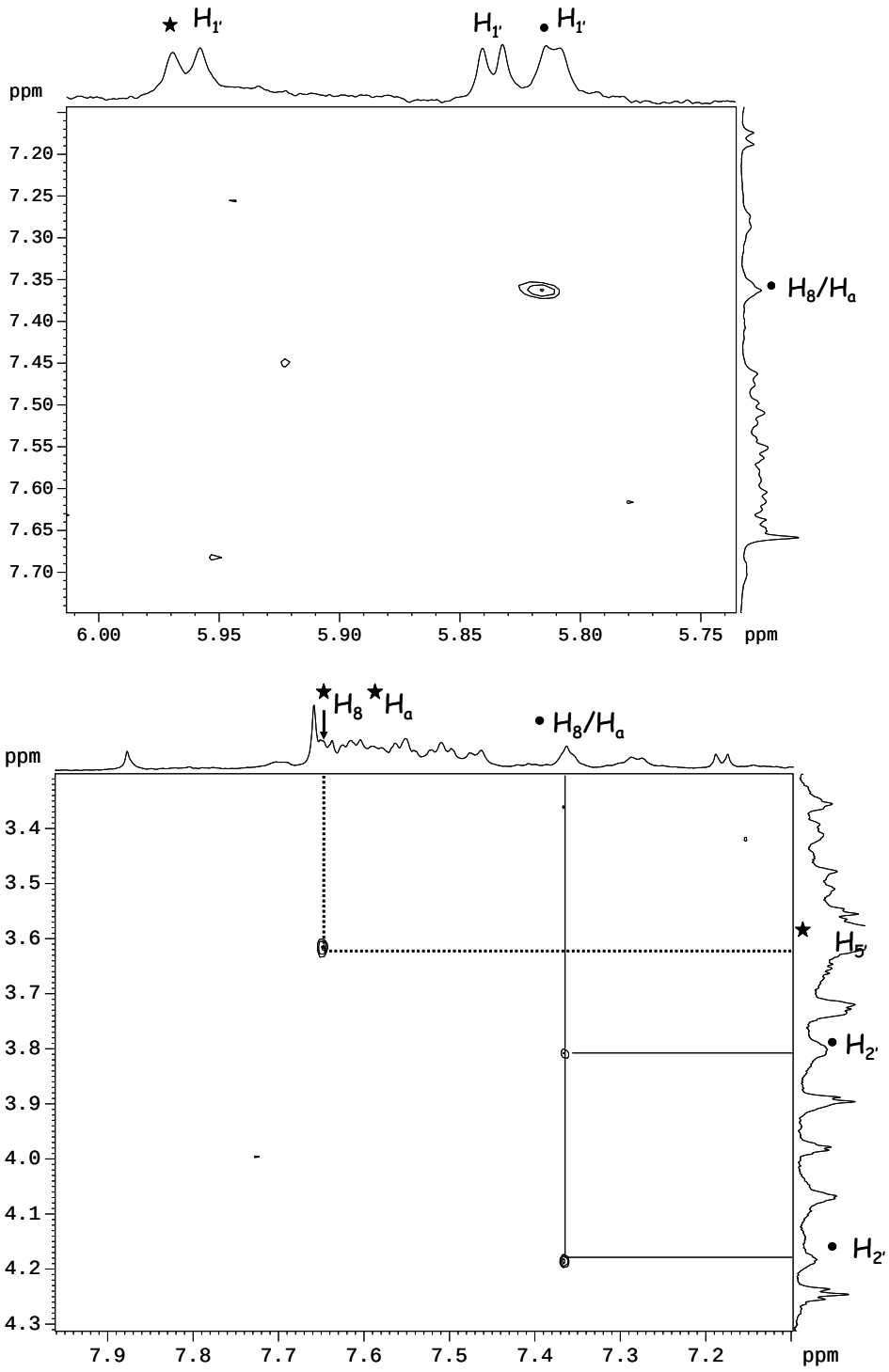

Figure 3.24 Partial NOESY NMR spectra of **2.2a** in the presence of $KClO_4$ (G-quartet I (circle) and G-quartet II (star), 298 K).

DOSY NMR was used to discriminate between the monomer and different complexes. Analysis of the non-exchangeable protons provided diffusion coefficients of D_m = 9.3 x 10^{-10} m^2s^{-1} for the monomer and D_c = 3.8 x 10^{-10} m^2s^{-1} for the complexes (Figure 3.25). The experimental ratio of D_c/D_m was found to be ~ 0.41. The theoretical ratios for D_8/D_m and D_{16}/D_m were previously determined to be 0.50 and 0.36. From the comparison between the theoretical and experimental data it is unclear whether $[\mathbf{G}]_{16}$ or $[\mathbf{G}]_8$ exists. We have yet to identify the exact structures. DOSY NMR spectra alone could not distinguish between two potential scenarios: a) non-equivalent G-quartets within a $[\mathbf{G}]_8$ or b) two separate $[\mathbf{G}]_8$ within $[\mathbf{G}]_{16}$. In order to solve this puzzle, we turn to a NOESY NMR study.

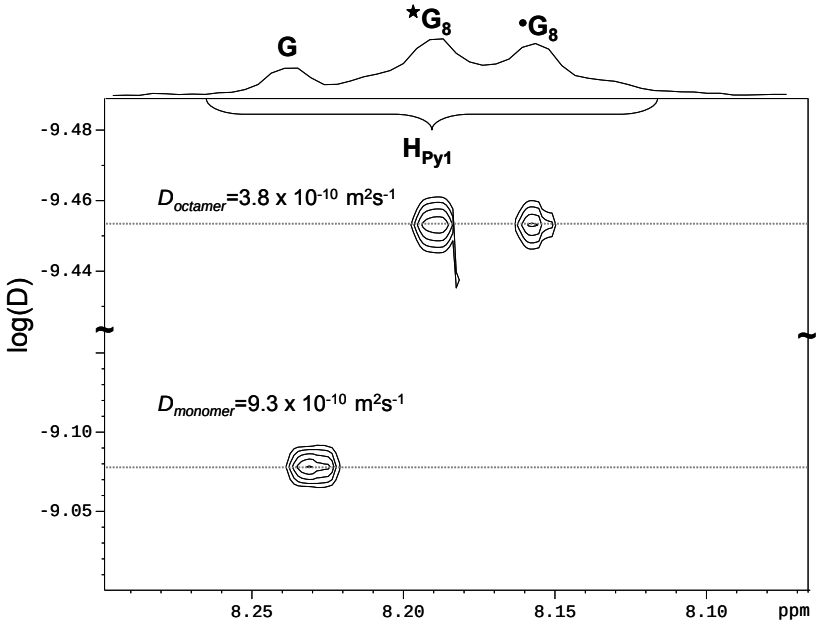

Figure 3.25 Partial 2D DOSY NMR spectra of **2.2a** in the presence of $KClO_4$ (298 K).

Several interquartet NOESY cross peaks were observed which suggest that the two complexes are not equivalent. First, an interquartet NOE cross peak between the hydroxyl $C_{2'}$-OH and $C_{3'}$-OH groups suggests that the two G-quartets are in close proximity. In addition, interquartet $H_{1'}$ and $C_{3'}$-OH exhibit NOE interactions as well. Secondly, NOEs between H_8/H_a of one G-quartet and N_2H of the other suggest a similar conclusion, i.e., the presence of interquartet interactions. Lastly, the stacking of G-quartets was confirmed by CD spectroscopy, as there were ~ 20 – 30 % signal amplifications observed at 250 and 350 nm after addition of $KClO_4$.

From NMR data it can be proposed that the final spectrum consists of monomer and G-quartet motifs in a high-order structure which could not be fully identified. However, we postulate that either $[\mathbf{G}]_{16}$ exists with non-equivalent octamers or $[\mathbf{G}]_8$ with two non-equivalent G-quartets. The latter possibility can be explained as follows. The octamer is composed of G-quartet I containing the C3'-*endo* puckering of an undetermined glycosidic conformation on top of the G-quartet II, with all *anti* conformers and C2'-*endo* puckering in a *hh* fashion as presented in Figure 3.26. However, the possibility of $[\mathbf{G}]_{16}$ made from two non-equivalent octamers cannot be excluded. The $[\mathbf{G}]_{16}$ structure also matches the interquartet NOE interactions between two inner G-quartets, but the final structure might entail two *tt* octamers analogous to **2.2b**. The outer 2'-OH and 3-OH sites of one octamer could be used to H-bond with another octamer producing the $[\mathbf{G}]_{16}$ structure shown in Figure 3.26.

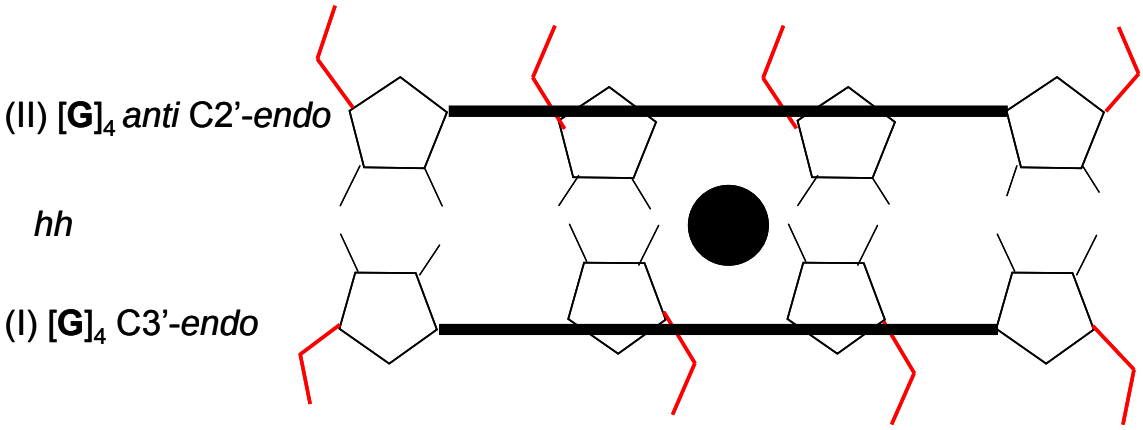

Octamer $[\mathbf{G}]_8$

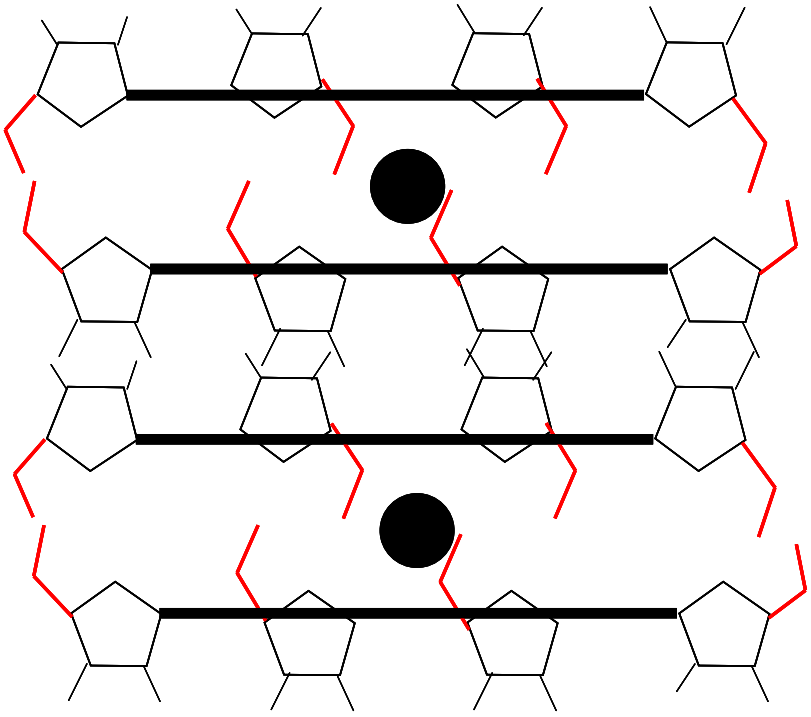

Hexadecamer $[\mathbf{G}]_{16}$

Figure 3.26 Structural representation of proposed $[\mathbf{G}]_8$ (top) and $[\mathbf{G}]_{16}$ (bottom) for the **2.2a** aggregates.

Two other aspects regarding the self-assembly of the hydrophilic **N^2G** are worth mentioning. First, the self-association of **2.2a** appears to be selective for the metal cation. Addition of K^+[picrate]$^-$ to a solution of **2.2a** promotes self-association, similar to $KClO_4$, however, only in a 2:1 ([**G**]:[**G**]$_n$) ratio as determined from the ^{1}H NMR integrations. Interestingly, $NaClO_4$ did not result in any self-assembly, nor did the addition of $Ba(ClO_4)_2$, Ba^{2+}[picrate]$^-_2$, or Sr^{2+}[picrate]$^-_2$ salts. The selectivity can be explained by considering the "optimal fit" model,[10] where K^+ ion has a higher affinity for the channel site than does Na^+, a notion which has been previously demonstrated for the 5'-GMP case.[11] The preference for K^+ (1.3 Å) over Na^+ (0.9 Å) can be explained due to its optimal ionic radius; however, the same reasoning fails when Ba^{2+} (1.4 Å) and Sr^{2+} (1.3 Å) are considered. Indeed, divalent metal ions were shown to promote octamer formation rather than hexadecamer, which suggests that the final structure formed by **2.2a** might be [**G**]$_{16}$ rather than [**G**]$_8$. Secondly, the self-assembly of hydrophilic **N^2Gs** is dependent on the nature of the substituent at the N^2-site. Our observations can be explained in terms of the relative solubility of each compound stemming from the N^2-moiety, while keeping in mind that the critical total concentration might be necessary for the self-assembly to take place.

3.3.5 Study of the self-assembly by fluorescence spectroscopy

Due to the inherent luminescence of the new **N^2Gs**, the fluorescence spectroscopy was used to monitor the G-quartet formation. Liquid-liquid or solid-liquid extractions using salts, such as $NaClO_4$, $KClO_4$, KI, KCl, $NaBPh_4$ (tetraphenylborate = BPh_4) and $KBPh_4$, did not promote self-assembly. Only the picrate salts were successfully used in the ligand-metal ion complexation. While the exact role of the picrate anion is not very

well understood, DOSY NMR results suggest that picrate is not bound to the $[\mathbf{G}]_8$, rather it is free in solution. Since the picrate anion is a quencher on its own, at high concentrations, the fluorescence could not be quantitatively used for the study of G-quartet formation by lipophilic **N^{2}Gs**, to our disappointment. However, the comparison of monomer fluorescence with that of $[\mathbf{G}]_8$ indicates that fluorescent intensity is retained upon self-assembly. Hence, the $[\mathbf{G}]_8$ are fluorescent as well.

We have established by NMR that the hydrophilic compound **2.2a**, forms aggregates in solution in the presence of $KClO_4$. The self-assembly was monitored by fluorescence spectroscopy and it was found that only ~ 5 % increase in the fluorescence intensity was observed after the addition of the salt. This finding can be explained in several ways: a) G-quartet and $[\mathbf{G}]_n$ formation does not affect the fluorescent property of the monomer and b) the emission of the residual monomers in the mixture (monomer and aggregate) counteracts the potential fluorescent intensity change correlated with the $[\mathbf{G}]_n$ formation.

3.3.6 Thermodynamic and kinetic study of the monomer-to-octamer exchange

While the **N^{2}G**-octamers are preferably formed in chlorinated solvents, the monomers and octamers co-exists in CD_3CN. Understanding the dynamics of the non-covalent self-assemblies will provide an insight into the self-association mechanism. In the study of monomer-to-hexadecamer exchange, based on *5'-O*-TBDMS-*2',3'-O*-isopropylideneguanosine, Davis et al.[5] concluded that the nucleation-elongation mechanism and positive cooperativity are the operating mechanisms in the process. **N^{2}Gs** form $[\mathbf{G}]_8$ in CD_2Cl_2 and $CDCl_3$, however, in CD_3CN a [**G**] and $[\mathbf{G}]_8$ coexist for compounds **2.1b** – **2.2b** and **nBuGTAG**, since the CD_3CN is of suitable polarity to allow

for the monomer and aggregates to exist (ε_r = 39). For the complete study of the monomer/octamer system **nBuGTAG** was chosen due its simpler structure.

The ^{1}H NMR spectrum of **nBuGTAG** in CD_3CN, prepared in the presence of Na^+ ions, generally exhibits two sets of NMR signals. These separate signals, in slow exchange on the NMR chemical shift time-scale, were distinguished using 2D COSY, NOESY and DOSY experiments. The NOESY NMR at 218 K presented in Figure 3.27 was used to establish the G-quartet structure and to assign one of the species as an $[\mathbf{G}]_8$ based on the NOE between H_8 and N_2H protons

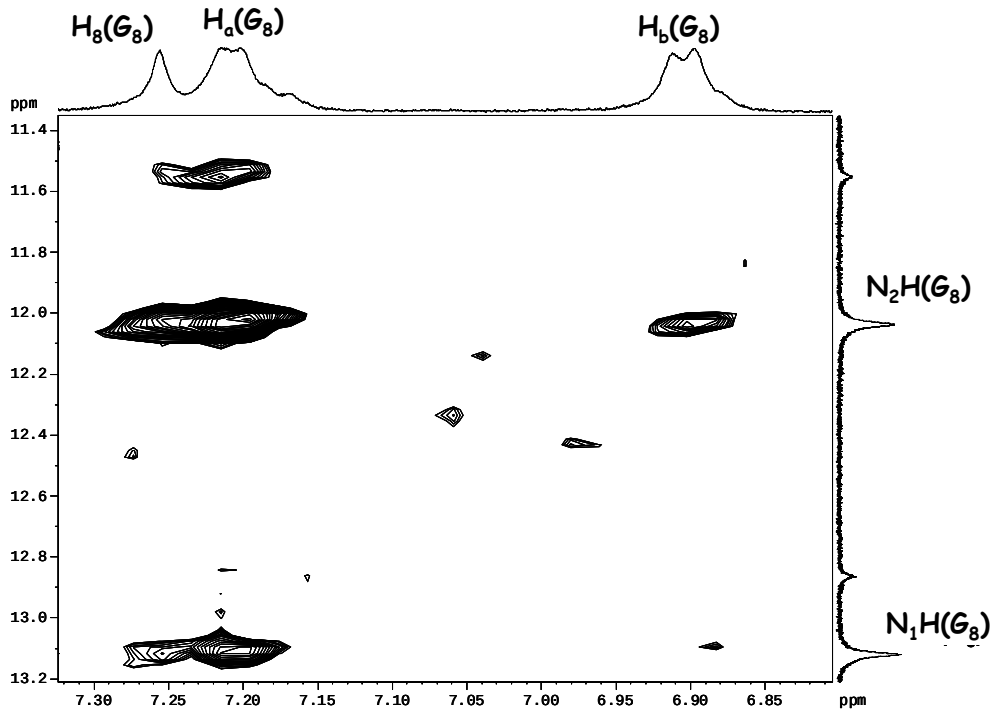

Figure 3.27 Partial NOESY spectra of $[\mathbf{G}]_8 \bullet Na^+$ (CD_3CN, 218 K).

The other component was identified by comparing the experimental diffusion data for the two species at 298 K. Actually, the two sets of signals exhibit quite different D_t values: 4.76 and 9.28 × 10^{-10} m^2s^{-1}. The calculated $D_{octamer}/D_{monomer}$ ratio was ~ 0.51 which immediately suggests that **nBuGTAG** exists as a mixture of [**G**] and $[\mathbf{G}]_8$ in CD_3CN. This situation is best illustrated in the 2D representation of the DOSY data shown in Figure 3.28.

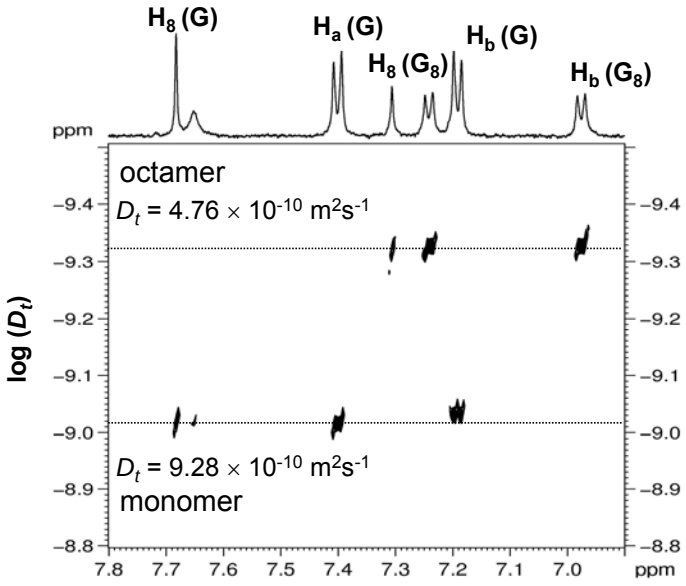

Figure 3.28 2D DOSY NMR spectrum for **nBuGTAG** (CD_3CN, 298 K).

Another interesting observation is that the NOE cross peaks due to monomers and octamers have opposite signs. This can be understood on the basis of the fact that monomers and octamers have very different rotational correlation times (τ_C). It is well known that for small molecules where τ_C is short relative to $1/\omega_0$ (ω_0 is the angular Larmor frequency of the nucleus under observation), the NOE cross peaks exhibit an opposite sign as the diagonal peaks. On the other hand, for large molecules or molecular

aggregates with a long τ_C value relative to $1/\omega_0$, NOE cross peaks have the same sign as the diagonal peaks. In the present case, because **nBuGTAG** octamers (ca. 4300 Da) are much larger than monomers (540 Da), they have quite different values of τ_C, thus giving rise to NOE cross peaks with opposite signs. This observation, in turn, is in agreement with the NOESY NMR results depicted in Figure 3.29.

The monomer-to-octamer ratio is temperature dependent, indicating that the octamer formation is an exothermic process. At 324 K, only NMR signals for monomer are observed in Figure 3.30 but as the temperature is decreased, more octamer is formed. Similarly, variable temperature CD data suggest that the amplitude of the G-quartet signature curve, a biphasic CD couplet, decreases with the increase in temperature, the finding which parallels our dynamic NMR data (Figure 3.31). NMR dilution experiments in CD_3CN also suggest that the octamer formation is favoured at higher concentrations at 298 K, while a concentration effect is negligible at 283 K (Figure 3.32). At high dilution, the percentage of $[\mathbf{G}]_8$ decreases to the extent that only monomers are present in solution. Hence, it can be concluded that the self-assembly takes place only above a critical total concentration and that aggregates always coexist in equilibrium with a significant amount of monomer in solution. Increasing the total concentration beyond the limiting value only increases the total population of the octamer. Hence a step-wise self-assembly can be ruled out, where an octamer is built one monomer at the time. The absence of discrete NMR signals for the G-quartet, or other intermediate aggregates, indicates a highly cooperative formation of the octamer.

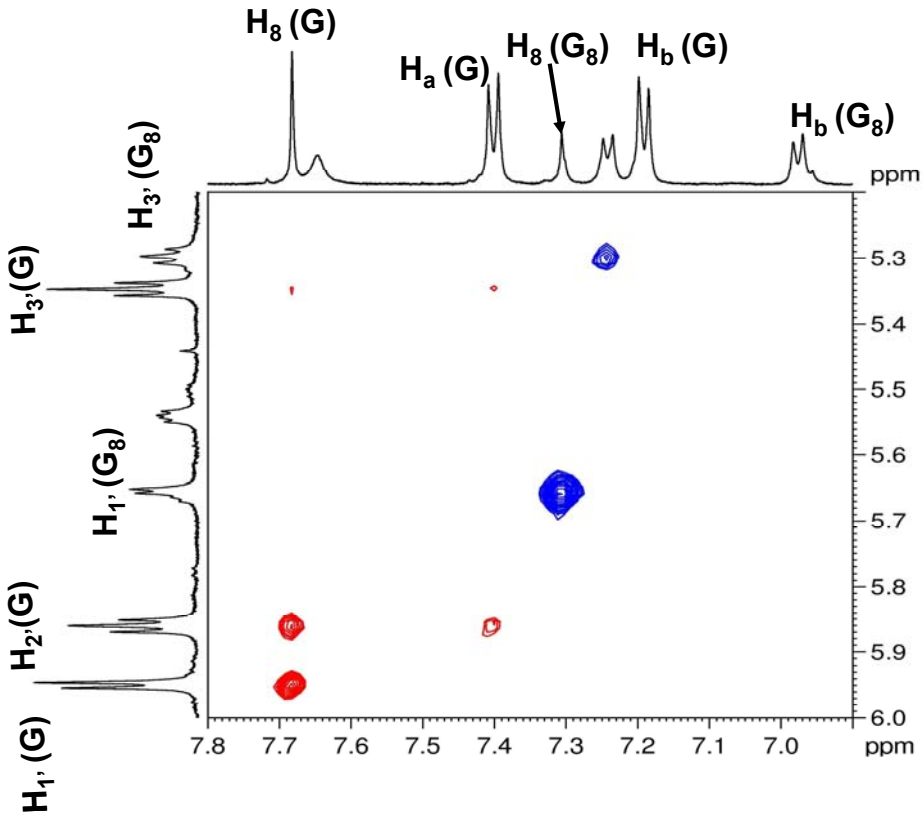

Figure 3.29 A spectral region of the NOESY spectrum of **nBuGTAG** (CD_3CN, 298 K, NOE cross peaks in blue and red have the same and opposite signs as the diagonal peaks, respectively).

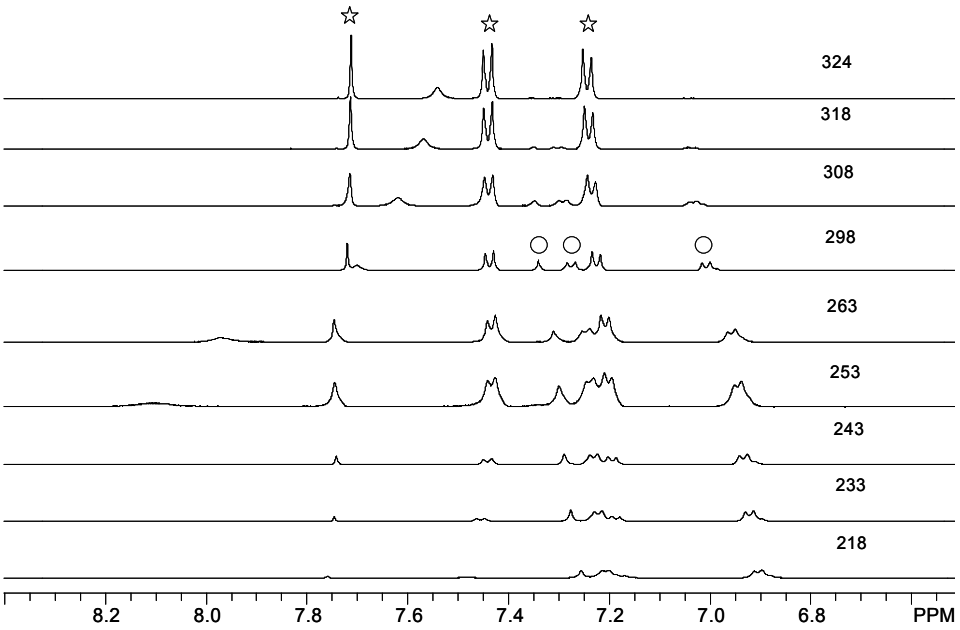

Figure 3.30 Variable temperature ^{1}H NMR spectra of **nBuGTAG** (CD_3CN, star - monomer, circle – octamer, temperature is given in K).

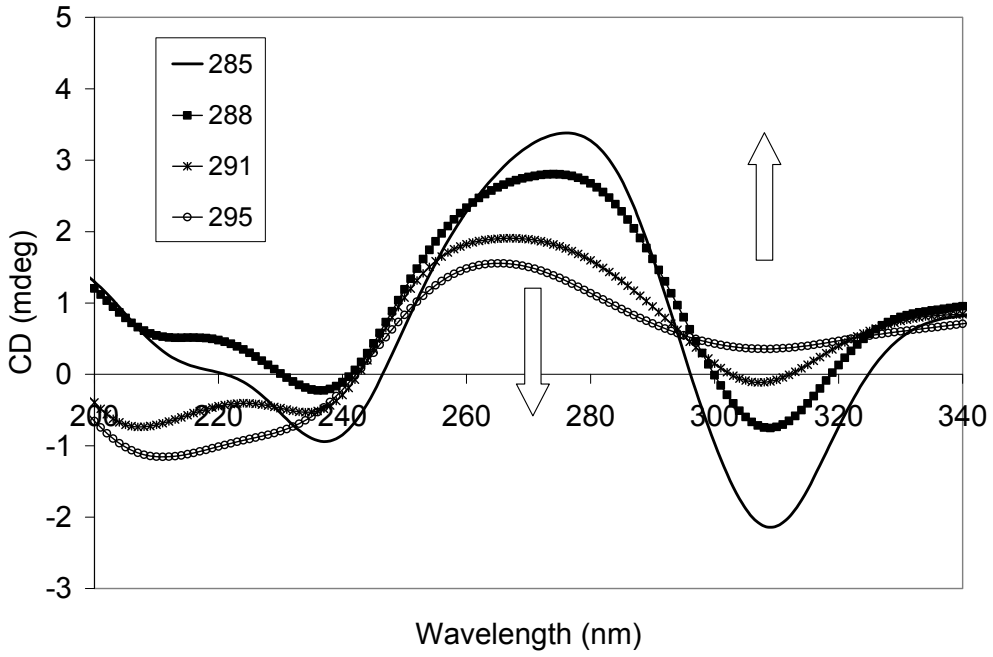

Figure 3.31 CD spectra of **nBuGTAG** (CD_3CN, 0.25 mM, temperatures shown in K).

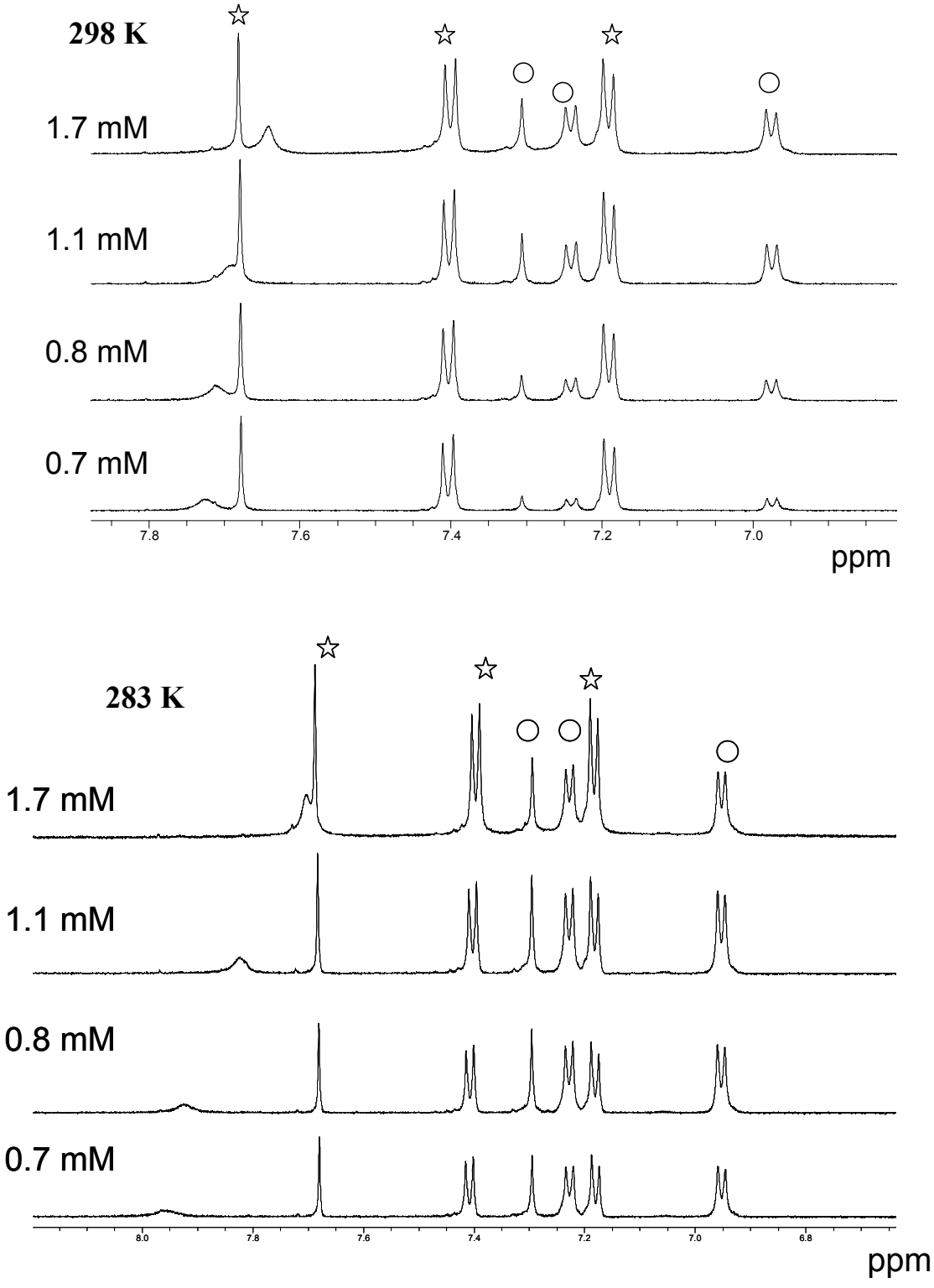

Figure 3.32 NMR dilution experiments of **nBuGTAG** at 298 K and 283 K (star - monomer, circle – octamer, CD_3CN)**.**

The proof of exchange comes from the phase of the cross peaks in the NOESY spectra in Figure 3.33. Wherein, the chemical exchange cross peaks between the monomer and the octamer have the same phase as the diagonal, those that are true NOE within the monomer have the opposite phase. Hence, we observed chemical exchange between H_8(G) and H_8(G_8) and NOE between H_a(G) and H_b(G), as shown below.

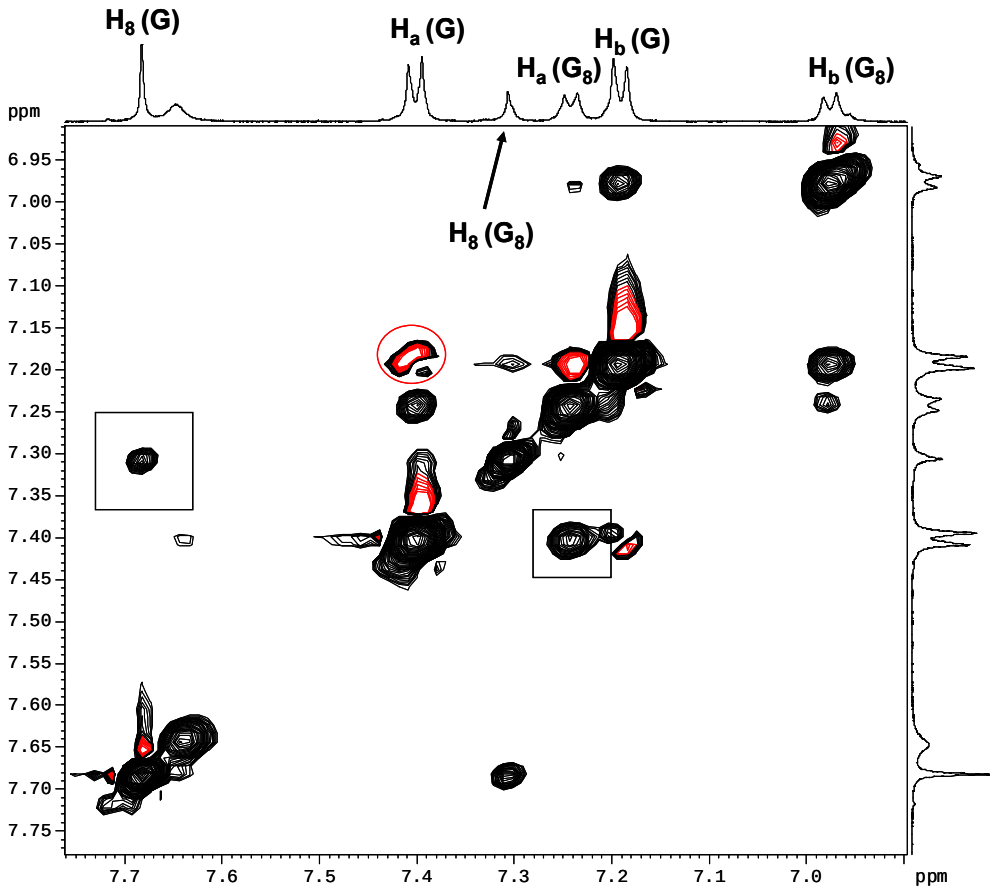

Figure 3.33 Partial NOESY spectrum of **nBuGTAG** (298 K, CD_3CN, box=chemical exchange between monomer and octamer, circle=NOE within monomer).

We extended the scope of our investigation to the study of macroscopic parameters of the system, such as the standard enthalpy, entropy and free energy changes. So far, only a few studies exist on the thermodynamics of the self-assembly of guanosine-related molecules. Previously, the monomer-to-pentamer chemical exchange of isoG in the small temperature range (277 - 298 K) produced the linear van't Hoff plot from which the free enthalpy, free entropy and free energy were determined to be -4.5 $kJmol^{-1}$, -80 $Jmol^{-1}K^{-1}$ and -3 $kJmol^{-1}$, respectively. In the monomer-to-tetramer exchange, the isoG tetramer was determined to be thermodynamically stable with the stability constant K_s and $\Delta G°$ of G-quartet formation ~ 10^9 M^{-3} and -53 $kJmol^{-1}$, respectively, at 298 K.

The exchange between the guanosine monomer and octamer has not been previously studied. The NMR intensities of the two species are typically used for the determination of the equilibrium constant. Since the NMR data above suggest that the exchange between monomer and octamer is slow on the NMR time scale, we determined the binding constant for the process by integrating the NMR signals of the involved species. At equilibrium, both aggregation and de-aggregation are taking place at the same rate, and therefore the structures of these species are dynamic and constantly fluctuating. However, in order to gain further understanding of the thermodynamics of the monomer-to-octamer exchange we considered the expression given in Figure 3.34. Because we are looking at the thermodynamic equilibrium state, the equations do not have to express the most kinetically favoured process but they do have to correctly correlate the concentrations with thermodynamic constant.

Figure 3.34 Schematic representation of monomer-to-octamer exchange and the equilibrium constant expression.

Since the dilution NMR study suggests that the equilibrium constant varies with the total concentration, we have decided to use the above expression for the thermodynamic studies. The binding constant is related to the free energy of the association process for octamer formation as shown in eq 3.1. At 298 K, the stability constant K_s and $\Delta G°$ of octamer formation were found to be 1.5×10^8 M^{-7} and -47 $kJmol^{-1}$. The high stability constant of the octamer and a large negative value of free energy of formation suggest that the octamer is a thermodynamically stable complex.

$$\Delta G = -RT \ln K \qquad (3.1)$$

The van't Hoff equation relates the change in equilibrium constant to the change in temperature the given the standard enthalpy change for the process. The plot of the natural logarithm of the equilibrium constant versus the reciprocal temperature should gives a straight line the slope of which is equal to negative of the standard enthalpy change divided by the gas constant and the intercept is equal to the standard entropy change divided by the gas constant (eq 3.2).

$$\ln K = -\frac{\Delta H}{RT} + \frac{\Delta S}{R} \qquad (3.2)$$

A plot of ln K_{eq} against 1000/T for the monomer-to-octamer exchange is presented in Figure 3.35. The identical van't Hoff plots were observed in both directions (either by cooling or heating) suggesting that the unusual behaviour is reproducible. The deviation from the straight line was dependent on the total concentration which is unusual since the van't Hoff plot should be concentration independent. The curvature in van't Hoff plots is independent of the equilibrium expression used. Notably, the more dilute solutions produced less deviations. Apparent deviations observed in Figure 3.35 could be avoided by performing the experiments at much lower concentrations. The curvature in the van't Hoff plots can be attributed to the large temperature range used. In the literature, the van't Hoff plots of protein unfolding transitions are found to be non-linear provided the transition covers a wide temperature range. This is an indication that enthalpy is temperature dependent which is seen only when the heat capacities of products and reactants differ.[5] Despite the curvature of our van't Hoff plot we have extrapolated enthalpy and entropy values, from the linear part of the most dilute curve in Figure 3.36, to be - 502 $kJmol^{-1}$ and -1500 $Jmol^{-1}K^{-1}$, respectively. The small negative enthalpy suggests that the octamer formation is a slightly exothermic reaction, so that K_{eq} decreases with increasing temperature, while the large negative value of entropy indicates the decrease in rotational freedom, as is expected for self-assembly. The break in linearity in the van't Hoff plot could suggest that the thermodynamic driving force for the reaction above a certain temperature becomes more dependent on entropy changes. Such behaviour has been previously reported for 5'-GMP binding to guanosine kinase.[12] Moreover, the changes in the slopes suggest potentially the presence of two different competing processes. Consequently, the equilibrium expression considered above is only a simplistic approach.

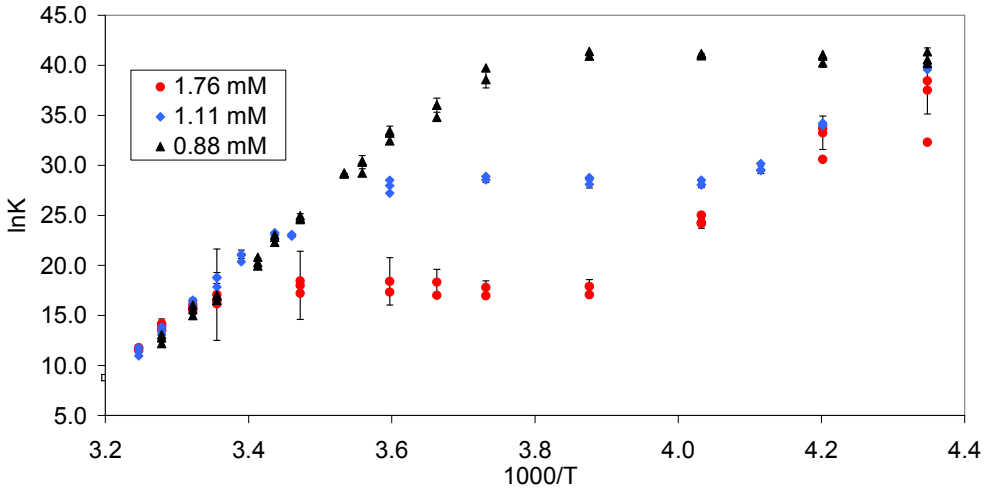

Figure 3.35 The van't Hoff plots for the monomer-to-octamer exchange process at different concentrations.

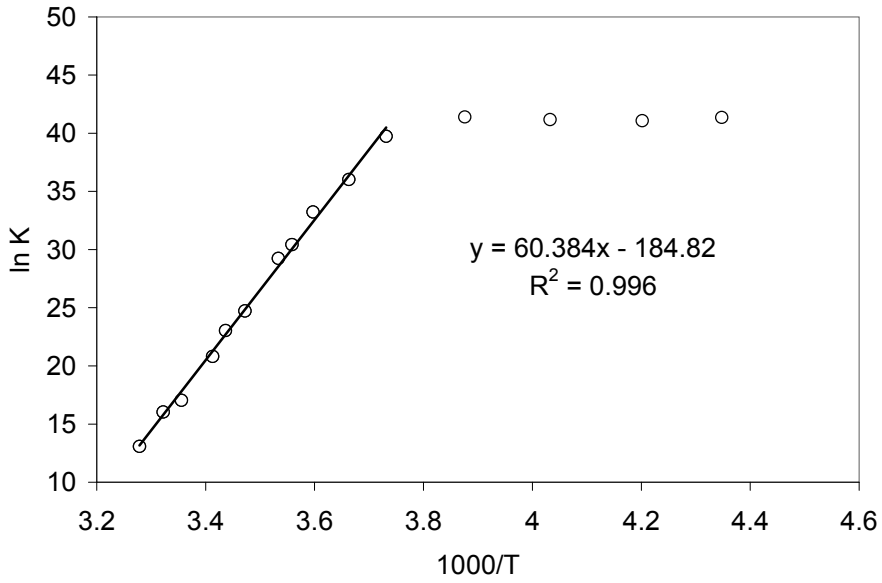

Figure 3.36 The van't Hoff plot at 0.88 mM and extrapolation of the thermodynamic parameters.

There are several contributing factors to the thermodynamic stability of G-octamer: a) interquartet hydrophobic interactions, b) intraquartet H-bonding and c) ion-dipole interactions. The monomer-to-octamer exchange can be explained as all-or-nothing event that exhibits nucleation-elongation mechanism shown in Figure 3.37 (Model II), rather than linear polymerization (Model I). Since octamer shows heat-induced de-aggregation, this is an indication that the octamer formation is an enthalpically driven process. Two types of $\pi - \pi$ stacking contribute to the stability of the octamer, interguanine and inter N^2-aryl interactions. However, the extent of the stability depends on the enthalpic strength of the latter stacking interaction and the entropic loss necessary for adopting required geometry upon octamer formation. Rigidity produced by introducing the substituent at the N^2-site promotes an even higher degree of stereoselectivity.

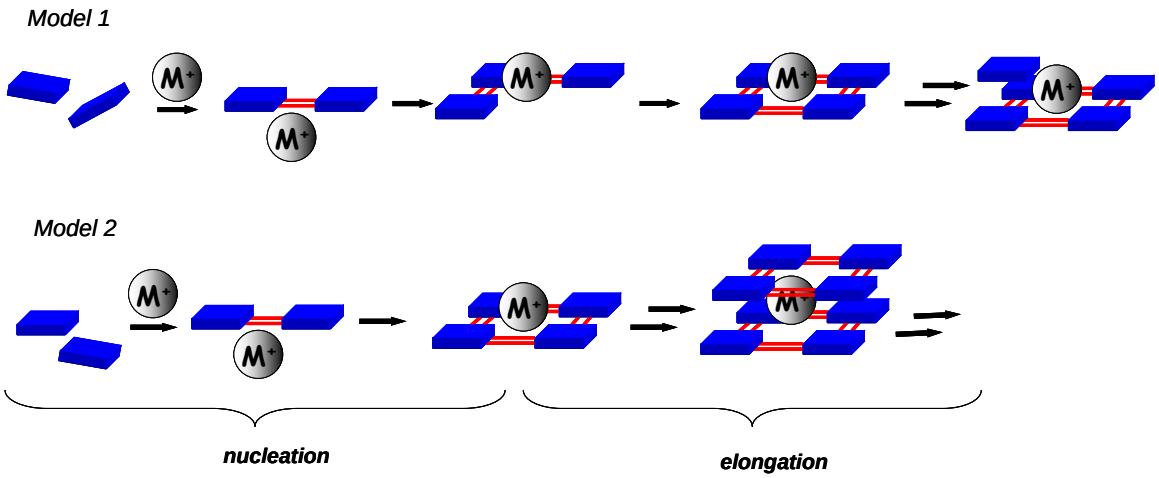

Figure 3.37 Representative models of linear elongation (Model 1) and nucleation-elongation mechanisms (Model 2).

In addition to the thermodynamic study, the temperature dependence of the exchange rates was used to obtain information about the energetics of the activation process, such as enthalpy, entropy and free energy of activation. Despite the fact that intermolecular exchange involves two or more species, typically pseudo-first-order kinetics is used in NMR spectroscopy.[13] Intermolecular reactions are pseudo-first-order since all of the effects of the process studied on the NMR spectrum are effectively first-order. Hence, only proton signals at the two sites: monomer and octamer were monitored. This provides an excellent opportunity to examine ligand exchange between the free (monomers) and bound (octamers) states. However, the variable temperature ^{1}H NMR spectra presented above do not exhibit any significant line broadening, indicating that the ligand exchange rate is much slower than the NMR chemical shift time scale. Since the rate is comparable to spin-relaxation times we can use Overhauser effects to study the exchange. The process involves the two spins or two states, hence the relaxation of one affects the other. For this reason, a saturation transfer NMR technique[14] was employed to measure ligand exchange rates. More precisely, 1D selective inversion experiments were chosen for the study of the exchange. After the selective inversion of one site the system is then allowed to relax by using a range of relaxation delays. Typically, the saturation transfer NMR experiments are performed by selectively saturating one NMR signal (signal A) from the monomer (or the octamer) and then monitoring the time evolution of the signal (signal B) from the octamer (or the monomer). As suggested by Bainet et al., the saturation of one site can cause the change in the intensity of the other site, in both exchange and dipolar relaxation.[13] According to Forsen and Hoffman,[14] the time evolution of signal A under the condition of complete saturation of signal B can be

written as in eq 3.3. where T_{1A} is the spin-lattice relaxation time constant of signal A and τ_A is the life-time of molecules in state A.

$$\frac{M_z^A(t)}{M_0^A} = \frac{T_{1A}}{T_{1A} + \tau_A} e^{-\left(\frac{1}{\tau_A} + \frac{1}{T_{1A}}\right)t} + \frac{\tau_A}{T_{1A} + \tau_A} \qquad (3.3)$$

Because it is possible to find ^{1}H NMR spectral regions where signals for both monomers and octamers are well resolved, the saturation transfer experiments were performed by saturating signals from monomers and octamers separately. In principle these 1D NOE experiments can give us the exchange rates. The respective signal intensities of the monomer and the octamer, as a function of the mixing time (t_{mix}) at different temperatures, are presented in Figure 3.38.

The saturation transfer experiments were fit using the eq 3.3 and the resulting life-times (τ) and average exchange rates (k) were extrapolated. The life-times τ reported below are in agreement with those reported for K^+-based decamer of isoG. Davis et al. also found that the type of bound cation influences the ligand exchange as well, however we have not investigated this aspect of the exchange. Table 3.2 summarizes the saturation transfer NMR experimental results for **nBuGTAG** in CD_3CN at different temperatures. The ligand exchange rates are on the order of a few s^{-1}. These values are comparable to those reported by Davis et al. for isoG. We also performed saturation transfer experiments at 298 K at different concentrations and the results suggest that ligand exchange rates decrease upon dilution (0.8 mM (0.36 s^{-1}); 1.1 mM (0.55 s^{-1}); 1.9 mM (0.59 s^{-1})), indicating that exchange does not follow zero order kinetics. An Arrhenius analysis of the data shown in Table 3.2 yields an activation energy (E_a) of 26 ± 5 kJ mol^{-1} for the kinetic ligand exchange process.

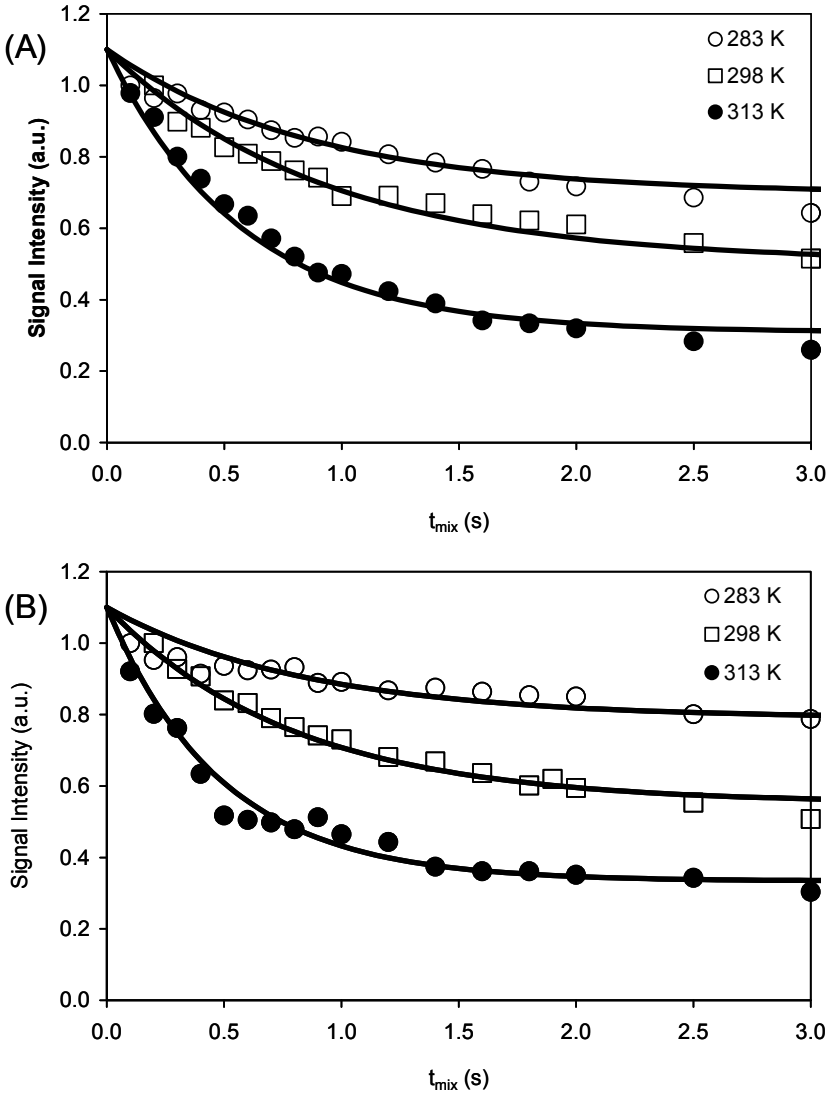

Figure 3.38 Saturation transfer NMR experiments for **nBuGTAG** ligand exchange in CD_3CN. (A) Saturation of the NMR signal from octamer and (B) saturation of the NMR signal from monomer.

Table 3.2 Saturation transfer NMR experimental results for **nBuGTAG** kinetic ligand exchange in CD_3CN (1.1 mM).

	Saturation of ***octamer*** *signals*			*Saturation of* ***monomer*** *signals*		
Temperature (K)	T_{1A} (s)	τ_A (s)	$k = 1/\tau_A$ (s^{-1})	T_{1A} (s)	τ_A (s)	$k = 1/\tau_A$ (s^{-1})
283	1.39 (H_8)	2.4 ± 0.4	0.4	1.18 (H_8)	3.0 ± 0.5	0.3
298	2.01 ($H_{1'}$)	1.7 ± 0.2	0.6	1.59 ($H_{1'}$)	1.6 ± 0.2	0.6
313	2.05 (H_8)	0.8 ± 0.1	1.3	1.61 (H_8)	0.7± 0.1	1.4

To obtain the activation parameters for the reaction, the monomer-to-octamer exchange was examined at several temperatures using the Eyring equation shown in eq 3.4, where k_{obs} is the rate constant, k_B is the Boltzmann constant, h is Planck constant, T is the temperature, and R is the gas constant.

$$\ln\left(\frac{k_{obs}}{T}\right) = -\frac{\Delta H^{\neq}}{R}\left(\frac{1}{T}\right) + \ln\left(\frac{k_B}{h}\right) + \frac{\Delta S^{\neq}}{R} \qquad (3.4)$$

We have also applied an Eyring analysis for the saturation transfer data in Figure 3.39 and obtained the enthalpy of activation and the entropy of activation for the transition state: $\Delta H^{\neq} = 24 \pm 5$ kJmol^{-1} and $\Delta S^{\neq} = -166 \pm 10$ Jmol^{-1} K^{-1}. Again, a large and negative value of $\Delta S^{\neq}$ is in agreement with the associative mechanism for ligand exchange. It should be kept in mind that the Eyring equation is based on the transition state theory and so the parameters extracted relate only to the TS. The kinetic ligand exchange between monomers and octamers is generally slow on the order of a few s^{-1} between 283 and 313 K.

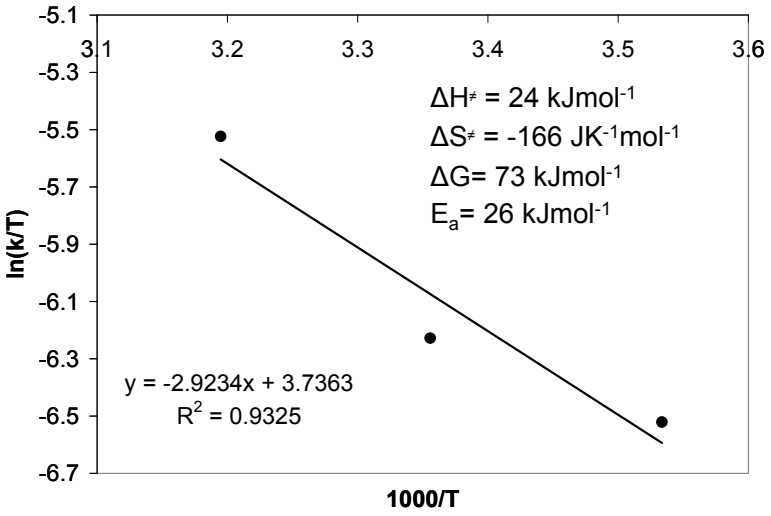

Figure 3.39 Eyring plot for monomer-to-octamer transformation.

The monomer-to-octamer exchange rate was found to be concentration dependent indicating that exchange proceeds *via* a bimolecular mechanism.[15] An associative mechanism implies formation of a transition-state such $[\mathbf{G}]_8\mathbf{G}^*$. The reasonable ligand exchange mechanism parallels that reported by Davis et al. in that a bimolecular process takes place between $[\mathbf{G}]_8$ and **G*** to give a short lived intermediate $[\mathbf{G}]_8\mathbf{G}^*$ which quickly dissociates into products as shown in Figure 3.40. Moreover, the formation of the octamer was found to be highly cooperative judging by the presence of only monomer and octamer species. No NMR evidence for any kinetically stable intermediates was observed in CD_3CN. This study provides new insights into the self-assembly of $\mathbf{N^2Gs}$ in organic solvents.

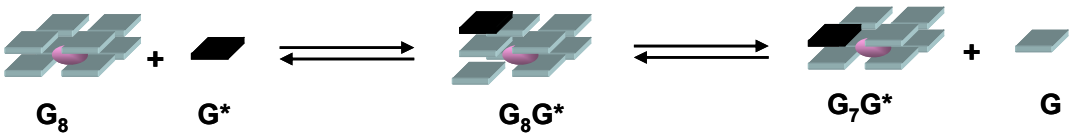

Figure 3.40 Proposed ligand exchange mechanism scheme.

3.4 Conclusions

The experimental results presented in this chapter strongly suggest that N^2-modification of guanine is a promising route to developing fluorescent supramolecular building blocks. The fluorescent **N^2Gs** reported in this chapter are remarkable examples of selective $[\mathbf{G}]_8$ formation with high fidelity. Substitution at the N^2-site governs the formation of diastereoisomers due to the larger surface area and hydrophobicity. The complexation induced upfield shifts in the aromatic proton resonances of N^2-aryl groups suggests extensive π - π stacking between them which provides a secondary stabilizing force in addition to interquartet guanine interactions. This interaction between the N^2-aromatic arms is significant since it can potentially be used to promote octamer formation in the absence of any metal cations, giving rise to "empty" octamers. All lipophilic **N^2Gs** self-assemble, in the presence of metal cations, into discrete all *syn tt* octamers $[\mathbf{G}]_8$ in CD_2Cl_2 or $CDCl_3$. Unlike lipophilic **N^2Gs**, the hydrophilic **2.2a** self-associates into larger aggregates whose stereoselectivity is driven by H-bonding between the hydroxyl groups of the ribose units. Protection of ribose units does not lead to the isostructural self-assembly of **N^2Gs** in organic media. Self-assembly of hydrophilic **N^2Gs** depends on two factors: 1) the nature of N^2-subtituent and 2) the type of metal cation. For the first time, detailed studies have been made towards the understanding of electronic and steric impacts on the kinetics and thermodynamics of **N^2G** self-assembly.[16] The thermodynamically driven monomer-to-octamer chemical exchange is slow with the life-times for octamer on the order of seconds. More precisely, the octamer formation is favoured due to an enthalpic gain stored in H-bonding and extensive π - π interactions.

3.5 References

[1] (a) Davis, J. T. *Angew. Chem. Int. Ed.* **2004**, *43*, 668. (b) Gottarelli, G.; Spada, G. P. *Chem. Rec.* **2004**, *4*, 39.

[2] (a) Sessler, J. L.; Sathiosatham, M.; Doerr, K.; Lynch, V.; Abboud, K. A. *Angew. Chem. Int. Ed.* **2000**, *39*, 1300. (b) Gubala, V.; Betancourt, J. E.; Rivera, J. M. *Org. Lett.* **2004**, *6*, 4735. (c) Arriaga, M. G.; Hobley, G.; Rivera, J. M. *J. Am. Chem. Soc.* **2008**, *130*, 10492.

[3] Liu, X.; Kwan, I. C. M.; Wang, S.; Wu, G. *Org. Lett.* **2006**, *8*, 3685.

[4] (a) Sket, P.; Crnugelj, M.; Kozminski, W.; Plavec, J. *Org. Biomol. Chem.* **2004**, *2*, 1970. (b) Sacca, B.; Lacroix, L.; Mergny, J. L. *Nucleic Acids Res.* **2005**, *33*, 1182.

[5] Cai, M.; Sidorov, V.; Lam, Y. F.; Flowers, R. A.; Davis, J. T. *Org. Lett.* **2000**, *2*, 1665.

[6] Davis, J. T.; Tirumala, S.; Jenssen, J. R.; Radler, E.; Fabris, D. *J. Org. Chem.* **1995**, *60*, 4167.

[7] Jurga-Novak, H.; Banachowicz, E.; Dobek, A.; Patkowski, A. *J. Phys. Chem. B* **2004**, *108*, 2744.

[8] Kaucher, M. S.; Lam, Y. F.; Pierracini, S.; Gottarelli, G.; Davis, J. T. *Chem. Eur. J.* **2005**, *11*, 164.

[9] Graziano, C.; Masiero, S.; Pieraccini, S.; Lucarini, M.; Spada, G. P. *Org. Lett.* **2008**, *10*, 1739.

[10] Pinnavaia, T. J.; Marshall, C. L.; Mettler, C. M.; Fisk, C. L.; Miles, H. T.; Becker, E. D. *J. Am. Chem. Soc.* **1978**, *100*, 3625.

[11] Wong, A.; Wu, G. *J. Am. Chem. Soc.* **2003**, *125*, 13895.

[12] McCune, R. W.; Gill, G. N. *J. Biol. Chem.* **1979**, *254*, 5083.

[13] Bain, A. *Modern Mag. Res.* **2008**, 421.

[14] (a) Forsen, S.; Hoffman, R. A. *J. Phys. Chem.* **1963**, *39*, 2892. (b) Forsen, S.; Hoffman, R. A. *J. Phys. Chem.* **1964**, *40*, 1189.

[15] Briere, K. M.; Detellier, C. *J. Phys. Chem.* **1992**, *96*, 2185.

[16] Martic, S.; Liu, X. Y.; Wang, S.; Wu, G. *Chem. Eur. J.* **2008**, *14*, 1196.

Chapter 4
Formation of "Empty" Octamer From N^2-Modified Guanosines in the Gas Phase

4.1 Introduction

Self-assembly of **N^2Gs** in solution was shown in the previous chapter to lead to **[G]$_8$** formation. While G-quartet formation is typically driven by the presence of metal cations, several exceptions exist where G-quartets are formed without cations, ie., "empty" G-quartets. The first case was reported by Sessler et al. who found "empty" G-quartets from a C^8-modified G-nucleoside.[1] The "empty" G-quartets were identified by NMR and X-ray crystallography. "Empty" G-quartets have also been observed for guanine on the gold surface.[2] In addition, a ^{15}N-labeled dG derivative was found to form G-quartets in the solid state without metal cations.[3] Despite the strong experimental evidence for the formation of "empty" G-quartets in solution and solid state, it is unclear whether two "empty" G-quartets may stack on top of one another forming an "empty" [**G**]$_8$.

Since the formation and identification of **N^2G**-aggregates in solution was established (see Chapter 3), we decided to investigate the stability of these complexes in the gas phase. Given the success of using ESI MS for the study of G-nucleoside[4] self-assembly, we have used similar methods to investigate the self-assembly of **N^2Gs**. In this chapter the formation of aggregates in the gas phase was studied in the presence and absence of metal cations.

4.2 Experimental Procedure

4.2.1 General considerations

All reagents were purchased from the Aldrich Chemical Co. and used without further purification unless stated otherwise. CH_3NO_2 (puriss > 98.5% GC grade) was purchased from Fluka and CH_3CN (HPLC grade, 0.2 micron filtered) from Fisher Scientific.

4.2.2 ESI MS experiments

ESI MS experiments were performed using the positive ionization mode on QSTAR XL MS/MS Systems using Analyst QS Method. The samples were dissolved in CH_3NO_2 or CH_3CN and were injected using nanospray tips. CH_3CN was the cleaner solvent with a minimal concentration of the metal ions. Spectra were acquired over *m/z* range of 100 - 10000. Theoretical MS peaks were generated using Data Explorer v. 4.0.0.0. (1997 - 2000) by Applied Biosystems. The tandem ESI-MS experiments were performed using nitrogen as collision gas. The declustering potential (DP) was set to 20V or 80V during the tandem ESI-MS experiments. Collision induced dissociation (CID) energy of 35 eV was applied and the fragmentation was monitored. Calibration was done prior to each set of measurements.

4.3 Results and Discussion

4.3.1 Methodology and the sample preparation

Since it has been established that under negative ion electrospray conditions there is little tendency to form large guanosine clusters,[5] the positive ion mode was used for all ESI MS studies. Using regular positive mode ESI MS, it was discovered that the overall

m/z intensities of aggregates were much lower than those seen for monomers in the given spectrum. For that purpose we extended the utility of ESI MS to the nanospray ESI MS method allowing the use of only a few μL of highly concentrated sample solution. Under the higher loading concentrations much higher overall aggregate intensities were obtained for all **N^{2}Gs**. Due to the incompatibility of chlorinated solvents in MS analysis, more polar solvents such as CH_3CN or CH_3NO_2 had to be employed, which potentially disrupt the H-bonding in the complex producing significant amount of monomer adducts.

ESI MS experiments were performed on three different samples: a) ligand after liquid - liquid extraction, b) free ligand and c) cleaned ligand. Since **nBuGTAG** has not been investigated in terms of its self-assembly in the gas phase we have included this compound in our study as well, along with compounds **2.1b** – **2.2b**.

4.3.2 ESI MS study of filled octamers

*4.3.2.1 Self-assembly of **2.1b** in the gas-phase*

Figure 4.1 shows ESI spectra of **2.1b** aggregates in the presence of K^+ ion. The full mass spectrum, in the presence of K^+[picrate]$^-$, shows the formation of singly charged monomers and dimers at *m/z* 767.21 and 1495.48, respectively. The highly charged complexes, such as $[6M+2H]^{3+}$ and $[8M+2K]^{2+}$ at *m/z* 1982.95 and 2954.02, respectively, are very stable structures given their relatively high overall intensities. In order to learn more about the nature and stability of these filled octamers collision induced dissociation (CID) MS was performed. Tandem ESI MS employs CID to fragment a parent ion in order to elucidate the molecule size, composition and stability. In the tandem ESI-MS

spectrum for *m/z* 2952.90 $[8M+2K]^{2+}$ parent ion (Figure 4.1) the stable divalent $[8M+2K]^{2+}$ and $[7M+2K]^{2+}$ were observed along with typical monovalent monomer, dimer and trimer.

In the presence of $Ba^{2+}[picrate]^{-}_2$, **2.1b** forms a number of different clusters, such as monovalent monomers, divalent and trivalent octamers at *m/z* 728.25, 1989.07 and 2983.53, respectively as presented in Figure 4.2. The filled octamers at *m/z* 2983.53 is associated with $[8M+Ba]^{2+}$ complex. Tandem ESI MS spectrum clearly shows minimal fragmentation of the parent ion, $[8M+Ba]^{2+}$ (Figure 4.2).

For both complexes of **2.1b**, the experimental and theoretical isotopic patterns of $[8M+2K]^{2+}$ and $[8M+Ba]^{2+}$ are a good match as evidenced by Figure 4.3 confirming the presence of discrete filled octamers. The distance of ~ 0.5 Da between two vicinal isotope peaks confirms the doubly charged states of the octamer adducts.

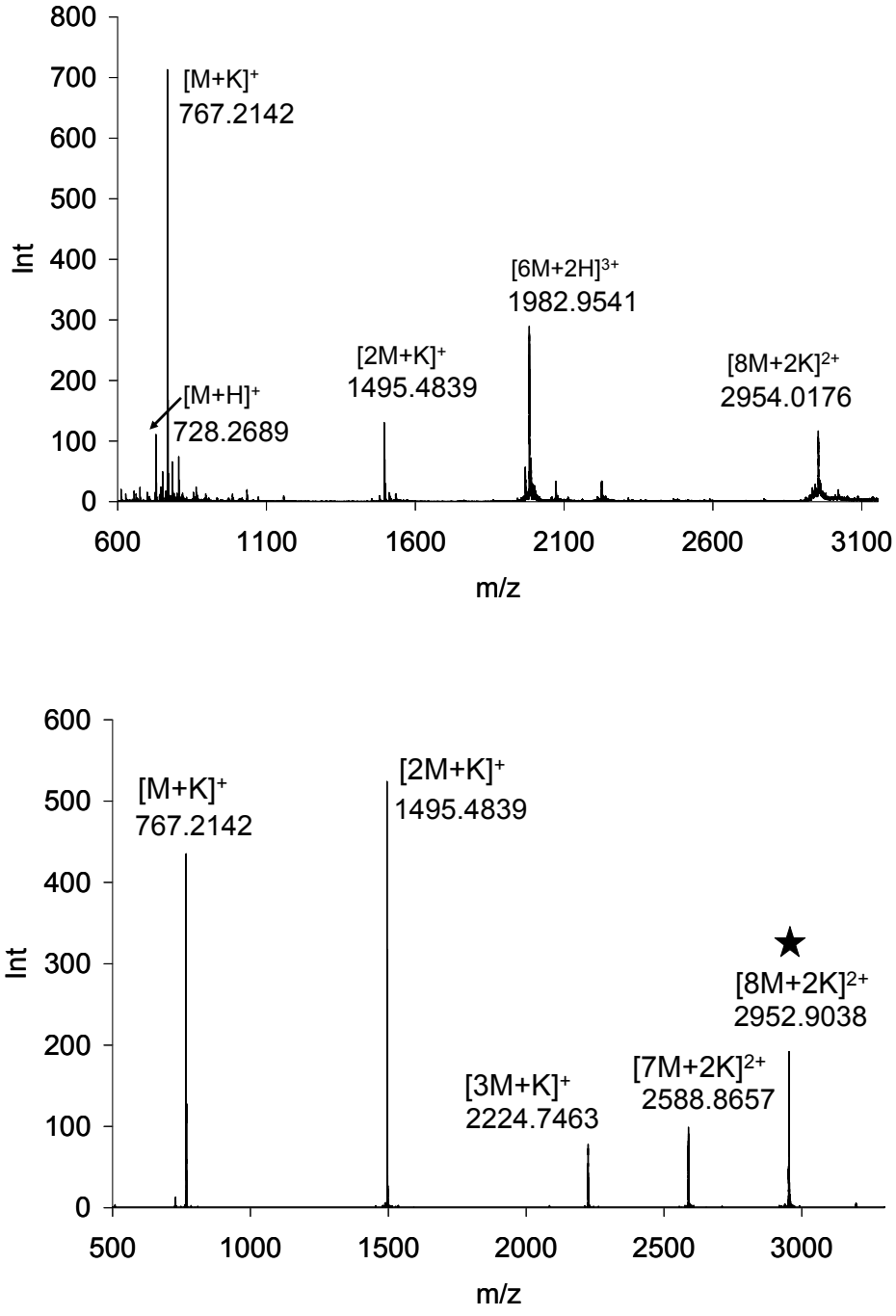

Figure 4.1 ESI MS spectrum (top) of **2.1b** with K^+[picrate]$^-$ and tandem ESI MS spectrum of *m/z* 2952.9083 $[8M+2K]^{2+}$ parent ion.

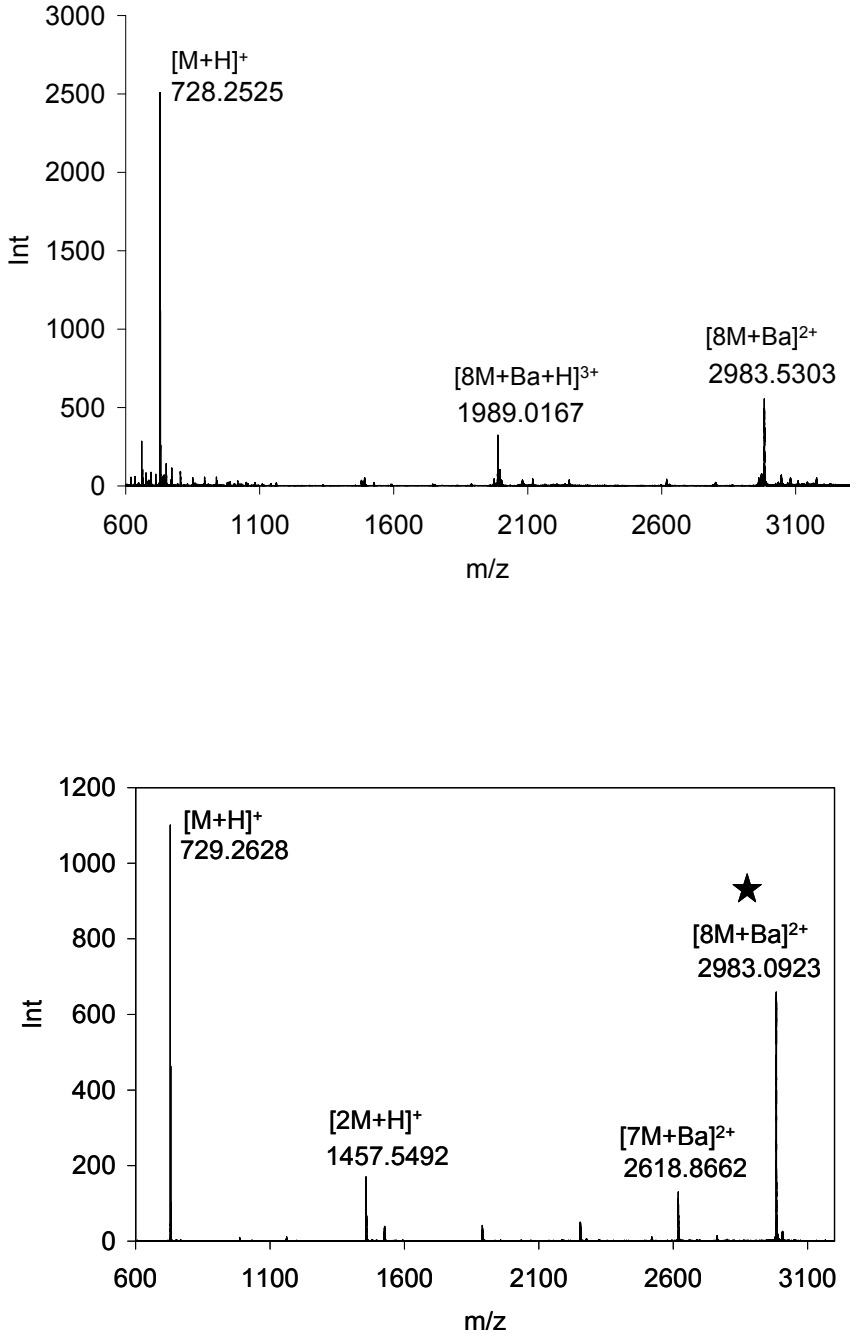

Figure 4.2 ESI MS spectrum (top) of **2.1b** with $Ba^{2+}[picrate]^-_2$ and tandem ESI MS spectrum of *m/z* 2983.0923 $[8M+Ba]^{2+}$ parent ion.

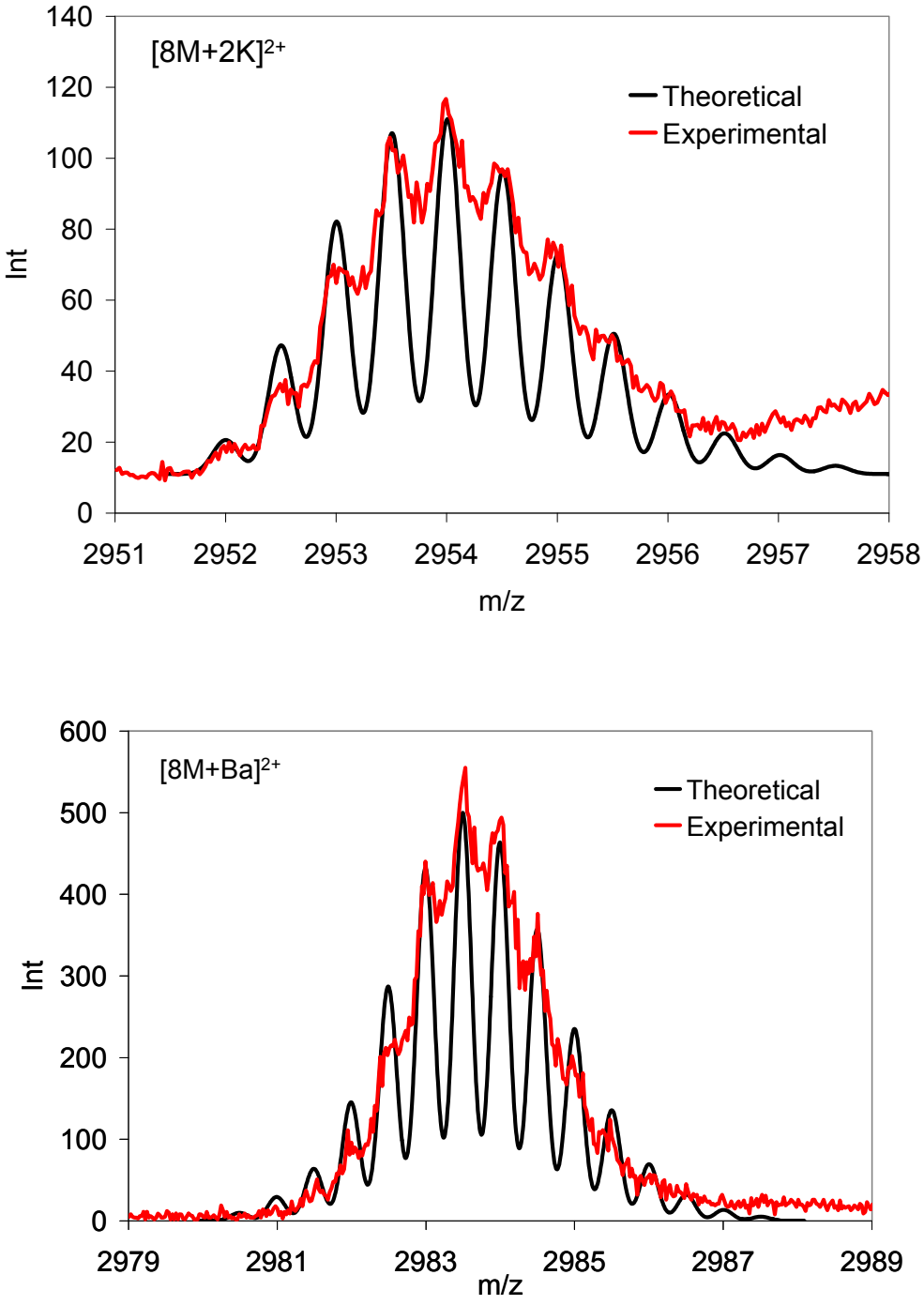

Figure 4.3 Experimental and theoretical ESI MS spectrum of $[8M+2K]^{2+}$ and $[8M+Ba]^{2+}$ complexes of **2.1b**.

*4.3.2.2 Self-assembly of **2.2b** in the gas-phase*

The ESI MS spectra of **2.2b** show the stable monovalent monomers and mixed divalent octamers in the presence of $K^+[picrate]^-$ (Figure 4.4). The $[\mathbf{G}]_8$ complex at *m/z* 2942.43 corresponds to $[8M+K+H]^{2+}$ adduct. CID experiments show that significant fragmentation of parent ion at *m/z* 2942.43 $[8M+K+H]^{2+}$ results in the formation of divalent heptamers, hexamers and pentamers at *m/z* 2577.34, 2211.76 and 1846.61, respectively.

In the presence of $Ba^{2+}[picrate]^-_2$, the gas phase behaviour is quite similar to that seen for **2.1b**. The octamer complex at *m/z* 2990.96 corresponds to $[8M+Ba]^{2+}$ adducts which are shown in Figure 4.5. Moreover, tandem ESI MS spectrum clearly indicates that filled Ba^{2+} octamer is more stable than the mixed octamer, $[8M+K+H]^{2+}$ adduct, because minimal fragmentation is observed with the former. The isotopic distribution and fittings were used in order to identify the aggregates with greater certainty. The theoretical isotope patterns depicted in Figure 4.6 for doubly charged octamers $[8M+K+H]^{2+}$ and $[8M+Ba]^{2+}$ match reasonably well with the experimental ones.

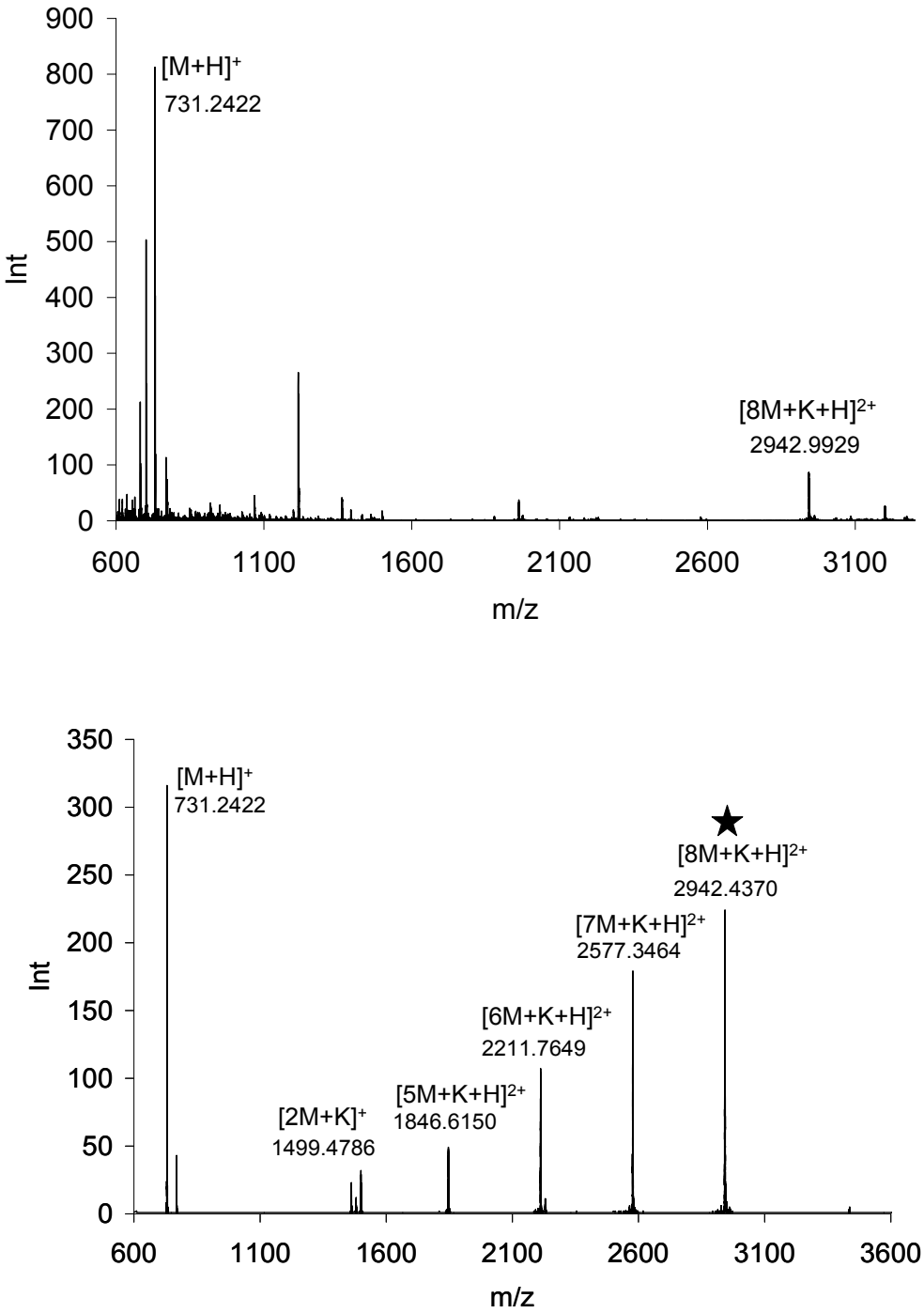

Figure 4.4 ESI MS spectrum (top) of **2.2b** with K^+[picrate]$^-$ and tandem ESI MS spectrum of *m/z* 2942.43 $[8M+K+H]^{2+}$ parent ion.

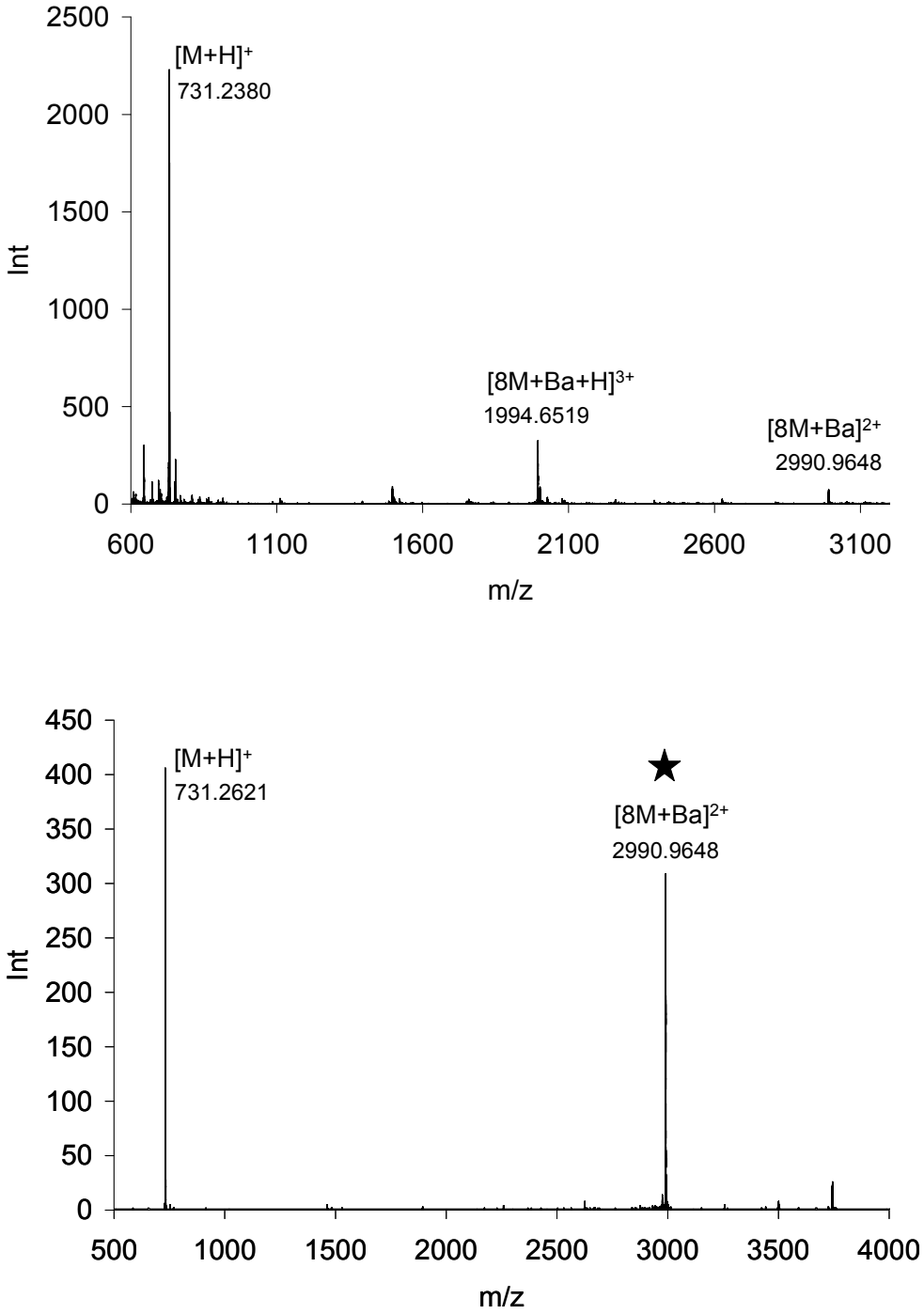

Figure 4.5 ESI MS spectrum (top) of **2.2b** with $Ba^{2+}[picrate]^-_2$ and tandem ESI MS spectrum of *m/z* 2990.9648 $[8M+Ba]^{2+}$ parent ion.

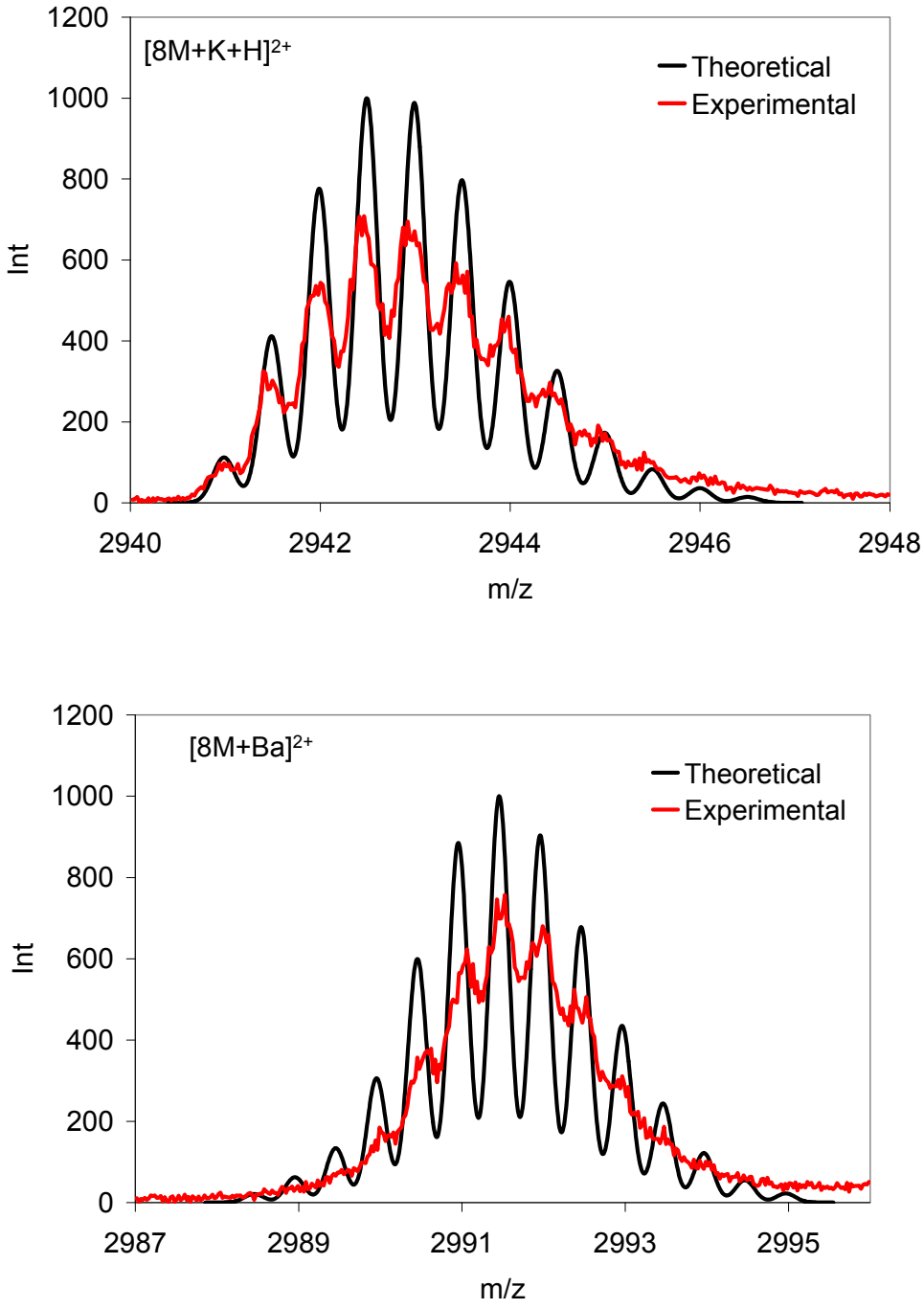

Figure 4.6 Experimental and theoretical ESI MS spectrum of $[8M+K+H]^{2+}$ and $[8M+Ba]^{2+}$ complexes of **2.2b**.

*4.3.2.3 Self-assembly of **nBuGTAG** in the gas-phase*

Similar to **2.1b** and **2.2b**, **nBuGTAG** forms divalent mixed and filled octamers at *m/z* 2186.37 and 2204.35, respectively, in the presence of K^+ (Figure 4.7). The greater abundance of mixed octamer, $[8M+K+H]^{2+}$, over other complexes suggests that this is a discrete and highly stable structure. A careful analysis of tandem ESI MS spectrum indicates that $[8M+2K]^{2+}$ does not have a parent ion, further signifying the octamer stability. The $[8M+K+H]^{2+}$ adduct is isotopically well resolved and it is an excellent match with the calculated one on the basis of natural isotope abundance as shown in Figure 4.8.

In conclusion, in the presence of excess metal cations, preferentially filled or mixed $[\mathbf{G}]_8$ are formed. Notably, the monovalent G-quartet or $[\mathbf{G}]_8$ were not observed in our study. The preference for $[\mathbf{G}]_8$ formation over other high-order structures is in agreement with the results of NMR studies. A minimal fragmentation and the absence of higher mass ions in tandem ESI MS spectra also suggest that octamer is a unique entity of high stability.

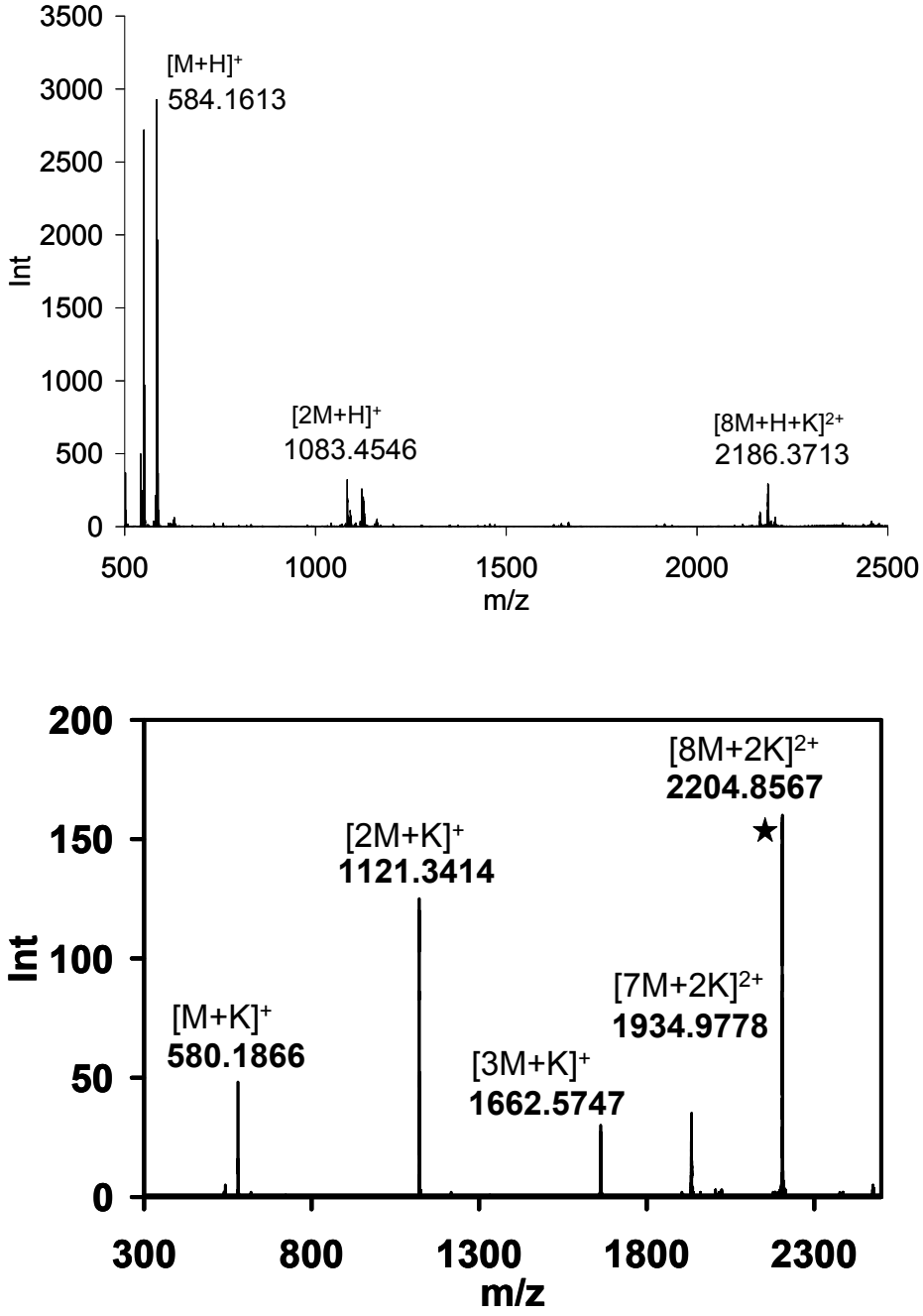

Figure 4.7 ESI MS spectrum (top) of **nBuGTAG** with $K^+[picrate]^-$ and tandem ESI MS spectrum of *m/z* 2204.8531 $[8M+2K]^{2+}$ parent ion.

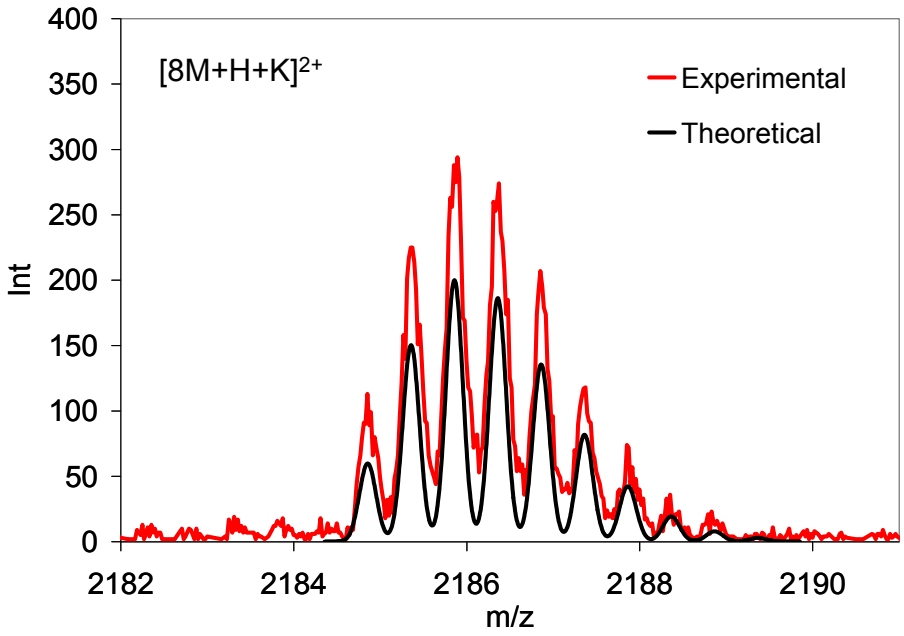

Figure 4.8 Experimental and theoretical ESI MS spectrum of $[8M+H+K]^{2+}$ complex of **nBuGTAG**.

4.3.3 ESI-MS study of mixed octamers

As suggested in Chapter 3, extensive π – π stacking between N^2-aryl arms provides enhanced stabilization of $[\mathbf{G}]_8$. To investigate the possibility of forming "empty" octamers, free of metal cations, further ESI MS experiments were performed. Since the "empty" $[\mathbf{G}]_8$ were not observed in solution, we turned to the gas phase studies in order to probe this hypothesis. Following experiments were performed on pure ligands without the addition of metal ions other than those already present in the sample introduced during the synthesis or from the solvent used in this study.

The most abundant ion observed for all three compounds was $[M+H]^+$ at *m/z* 729.31, 731.22 and 542.19 for **2.1b** (Figure 4.9)**, 2.2b** (Figure 4.10) and **nBuGTAG**

(Figure 4.11), respectively. In the mass spectral region of interest, it is clear that **2.1b** forms mixed and filled $[\mathbf{G}]_8$, such as $[8M+Na+H]^{2+}$, $[8M+2Na]^{2+}$ and $[8M+Na+K]^{2+}$ as shown in Figure 4.9. Similarly, **2.2b** forms mixed or filled $[\mathbf{G}]_8$ as well, such as $[8M+H+Na]^{2+}$, $[8M+H+K]^{2+}$, $[8M+Na+K]^{2+}$ and $[8M+2K]^{2+}$ adducts (Figure 4.10). **nBuGTAG** aggregates into divalent mixed $[\mathbf{G}]_8$, which are a combination of potassium and sodium adducts as well (Figure 4.11). In dramatic contrast to the experiments in the presence of excess metal cations, the intensities of aggregates are compromised. Hence, the octamer formation is more likely in the presence of excess metal cations.

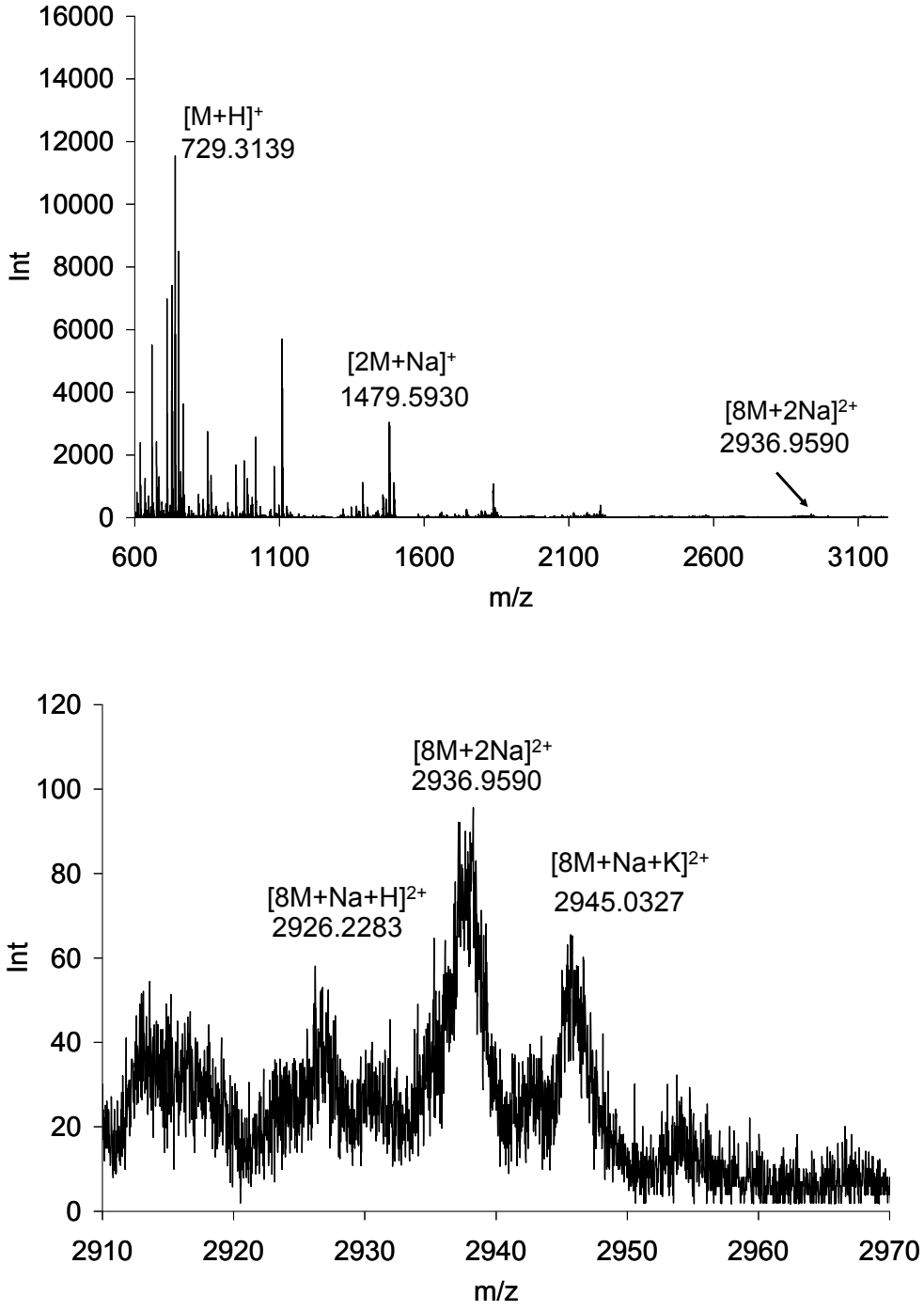

Figure 4.9 ESI MS spectrum (top) of **2.1b** and the partial ESI MS spectrum (bottom) of divalent octamers.

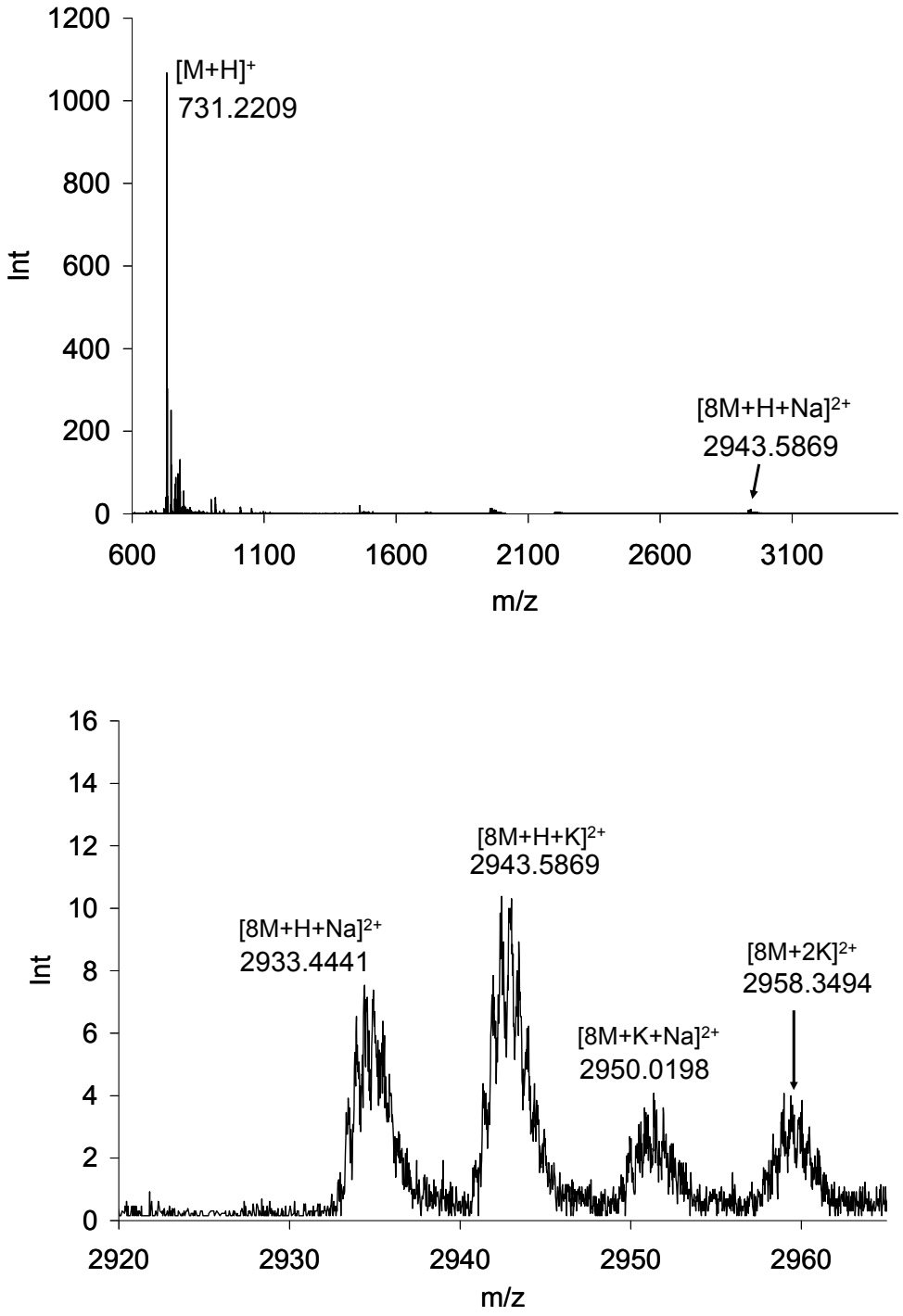

Figure 4.10 ESI MS spectrum (top) of **2.2b** and the partial ESI MS spectrum (bottom) of divalent octamers.

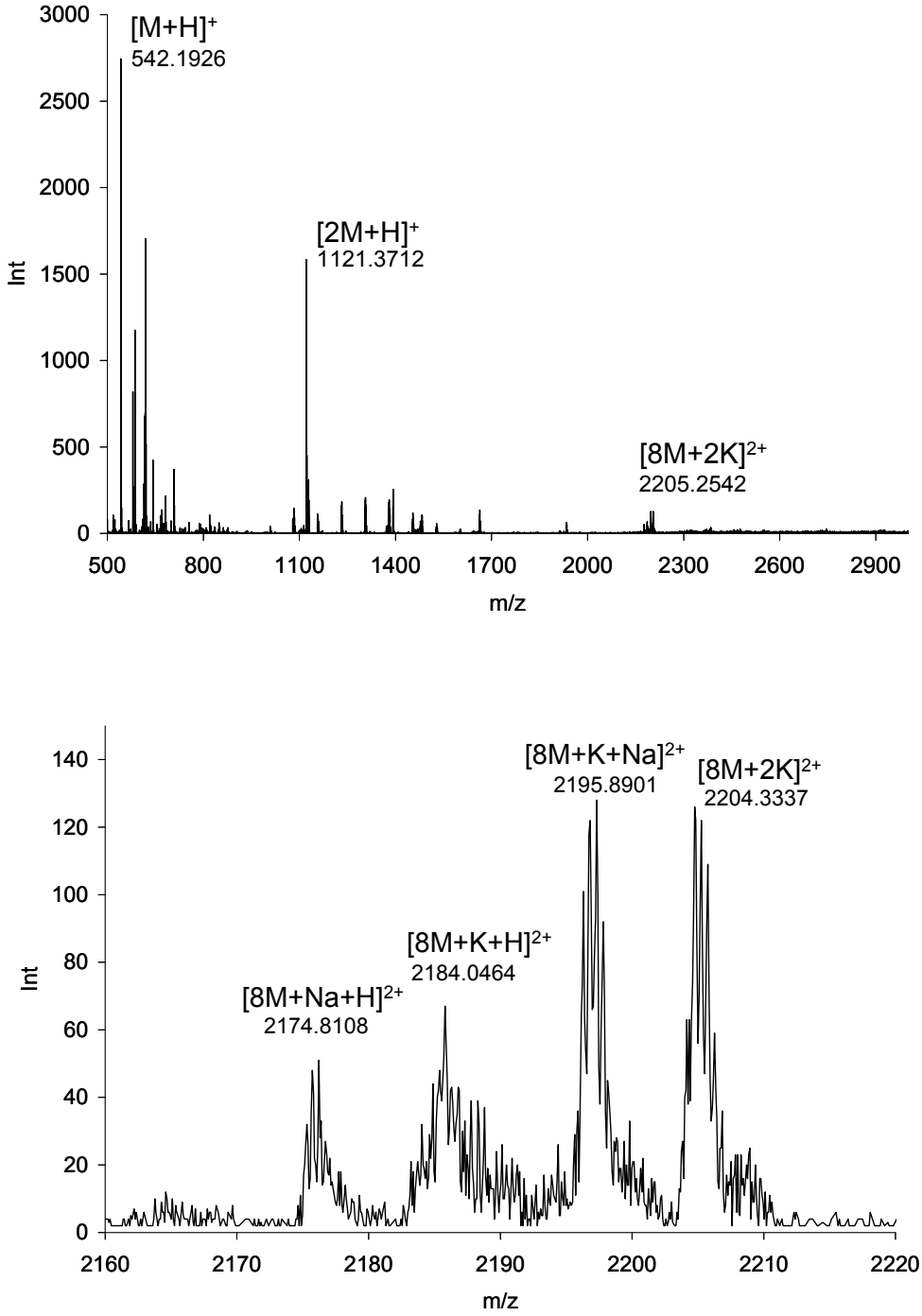

Figure 4.11 ESI MS spectrum (top) of **nBuGTAG** and the partial ESI MS spectrum (bottom) of divalent octamers.

4.3.4 ESI MS study of "empty" octamers

In order to promote the formation of "empty" $[\mathbf{G}]_8$ it is critical to have a metal-free environment. The general idea was to successfully remove metal cations in order to promote the formation of "empty" $[\mathbf{G}]_8$ which have not been previously observed in the gas phase. To this end we introduced in the sample preparation a new extensive solid-liquid extraction process with ammonium bicarbonate ($aqNH_4HCO_3$) solution as shown in Figure 4.12. Exchange of alkali metal cations with NH_4^+ ions against ammonium bicarbonate solution has been successfully used in order to improve sensitivity of MS methods by reducing the spectral distribution over the large range.[6] Only compounds **2.1b** and **nBuGTAG** were treated with this method due to their insolubility in aqueous solution. Cleaned and dried samples were dissolved in CH_3CN or CH_3NO_2 for further ESI MS analysis. Both solvents were used without further purification. It was found that CH_3CN was much cleaner than CH_3NO_2 in terms of the metal ions composition.

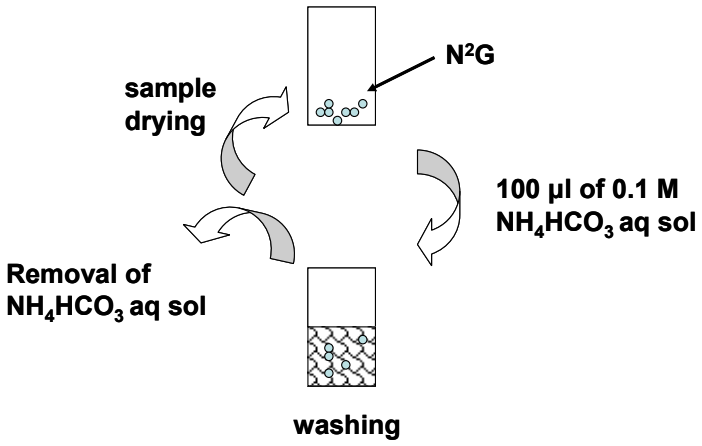

Figure 4.12 Structural representation of sample clean-up for removal of residual salts.

Examination of the partial ESI MS spectra, in Figure 4.13, of cleaned compound **2.1b** allows for the identification of monovalent $[4M+H]^+$ and divalent $[8M+2H]^{2+}$ aggregates. In order to further identify the structures and ascertain the stability of the "empty" octamers, tandem ESI MS experiment was performed on the parent peak at *m/z* 2914.07 $[8M+2H]^{2+}$ (Figure 4.13). From the fragmentation pattern in the tandem ESI MS spectrum we conclude that the composition of this complex is comparable to that of the filled or mixed $[\mathbf{G}]_8$. Experimental and theoretical isotope patterns presented in Figure 4.14 are a good match, further supporting the presence of "empty" octamer $[8M+2H]^{2+}$ and G-quartet $[4M+2H]^+$.

In the absence of metal ions, **nBuGTAG** self-assembles into the stable G-quartet and "empty" $[\mathbf{G}]_8$ which are shown in Figure 4.15 and have been identified by isotope pattern fitting (Figure 4.16). The aggregates were identified as $[8M+2H]^{2+}$ and $[4M+H]^+$. Tandem ESI MS results show that the "empty" $[\mathbf{G}]_8$ is of similar composition as the filled octamers reported previously, further supporting its identity.

The cleaning procedure shown above proved to be an efficient method for removal of the residual metal ion present in the solid $\mathbf{N^2G}$ samples. These finding suggests that the "empty" octamer $[8M+2H]^{2+}$ is a stable structure and not a product of the gas phase reactions. The population of $[8M+2H]^{2+}$ is higher at low metal ions concentrations, indicating that the filled $[\mathbf{G}]_8$ containing a metal ion is much more stable than an "empty" octamer.

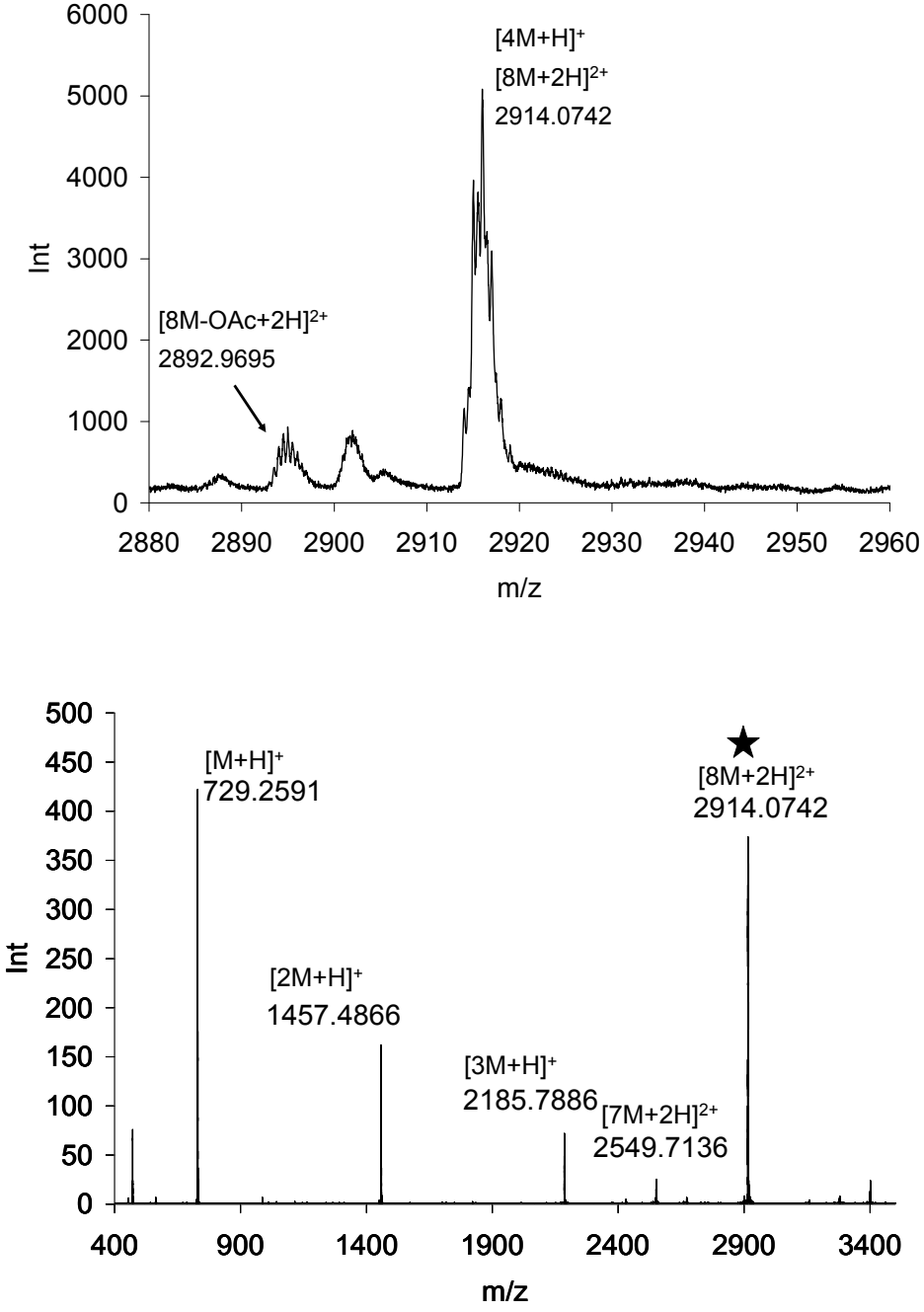

Figure 4.13 ESI MS spectrum (top) of cleaned **2.1b** and tandem ESI MS spectrum of *m/z* 2914.0742 $[8M+2H]^{2+}$ parent ion.

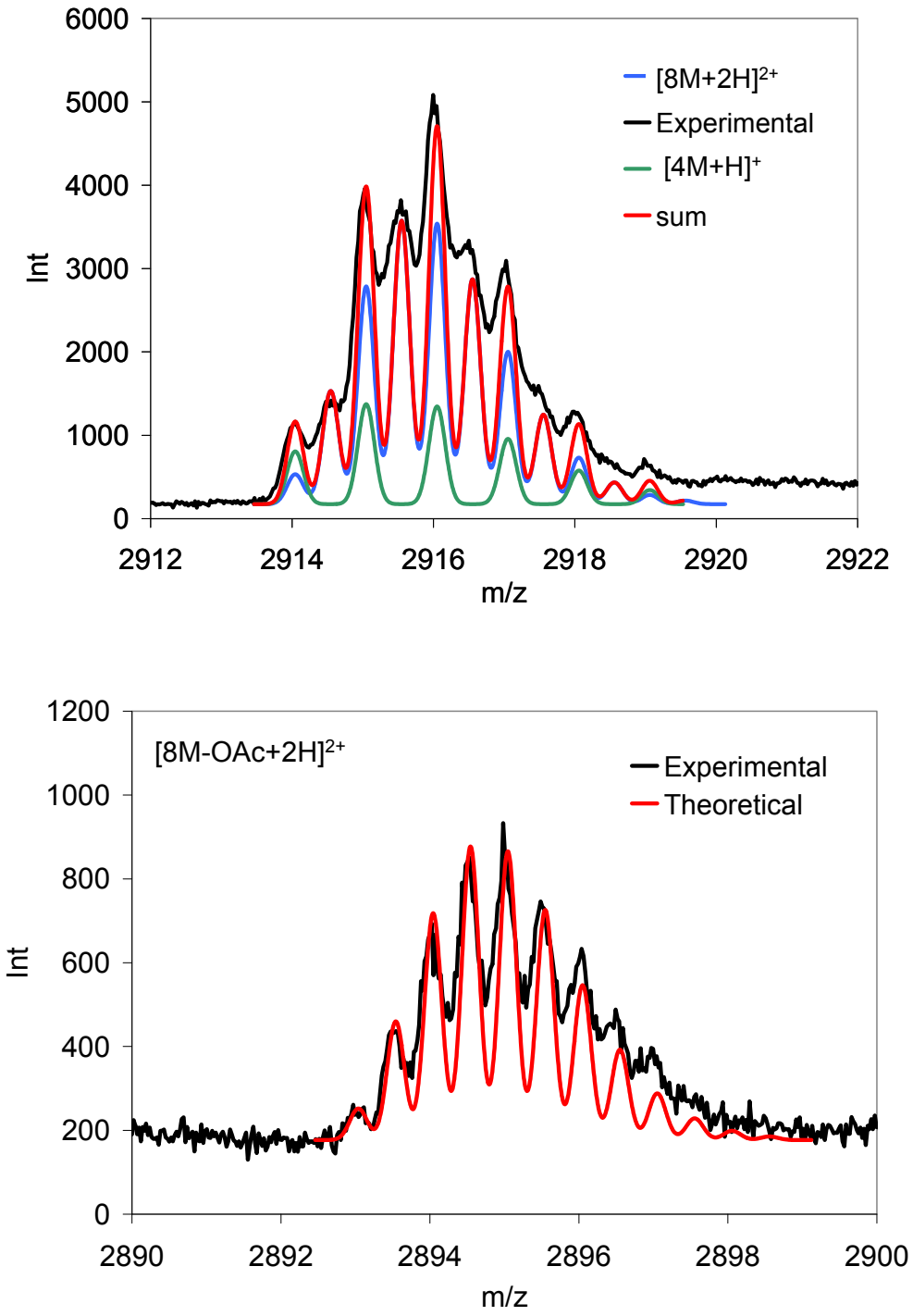

Figure 4.14 Experimental and theoretical ESI MS spectrum of $[8M+2H]^{2+}$, $[4M+H]^{2+}$ and $[8M\text{-}OAc+2H]^{2+}$ complexes of **2.1b**.

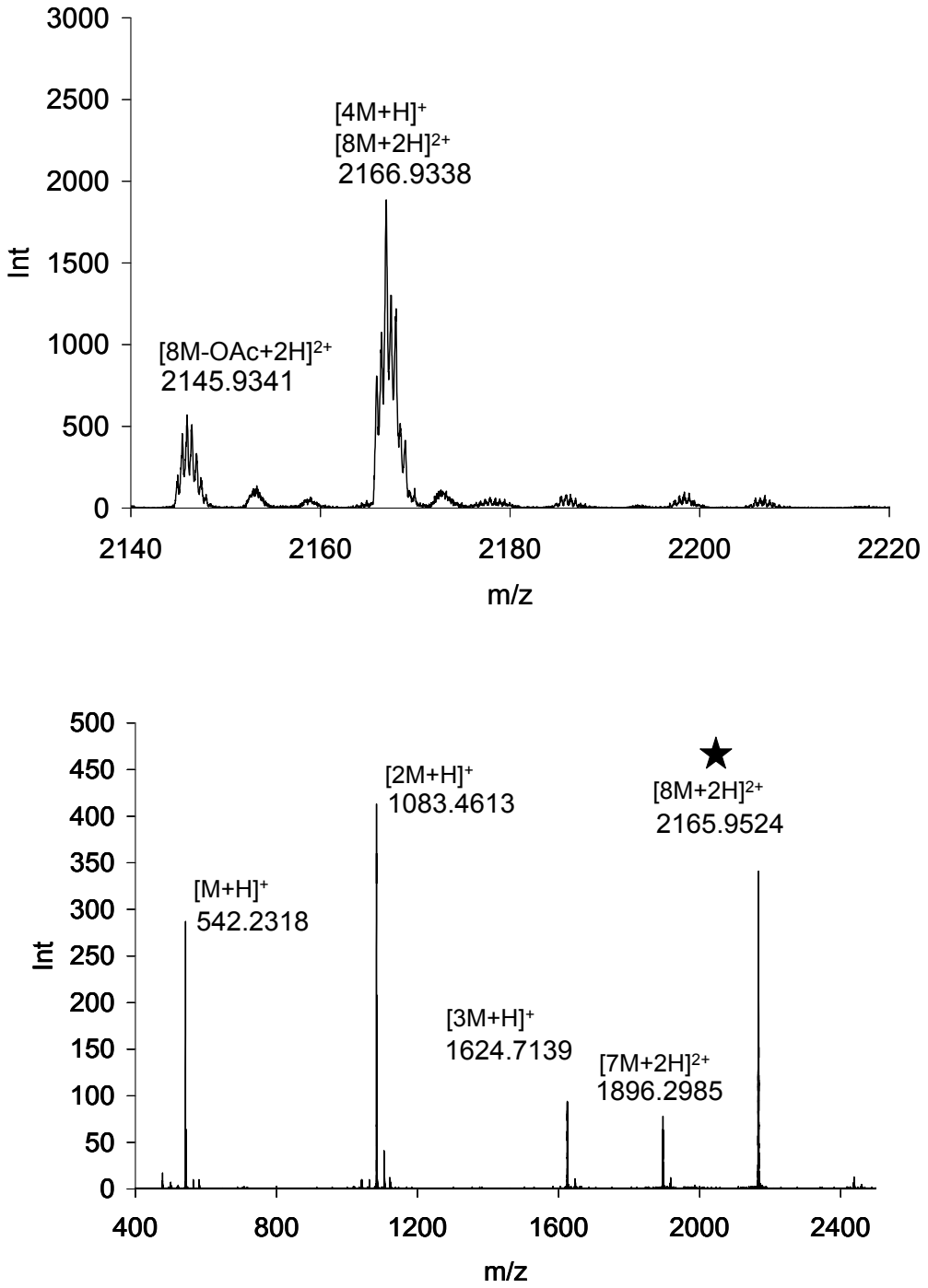

Figure 4.15 ESI MS spectrum (top) of cleaned **nBuGTAG** and tandem ESI MS spectrum of *m/z* 2165.9524 $[8M+2H]^{2+}$ parent ion.

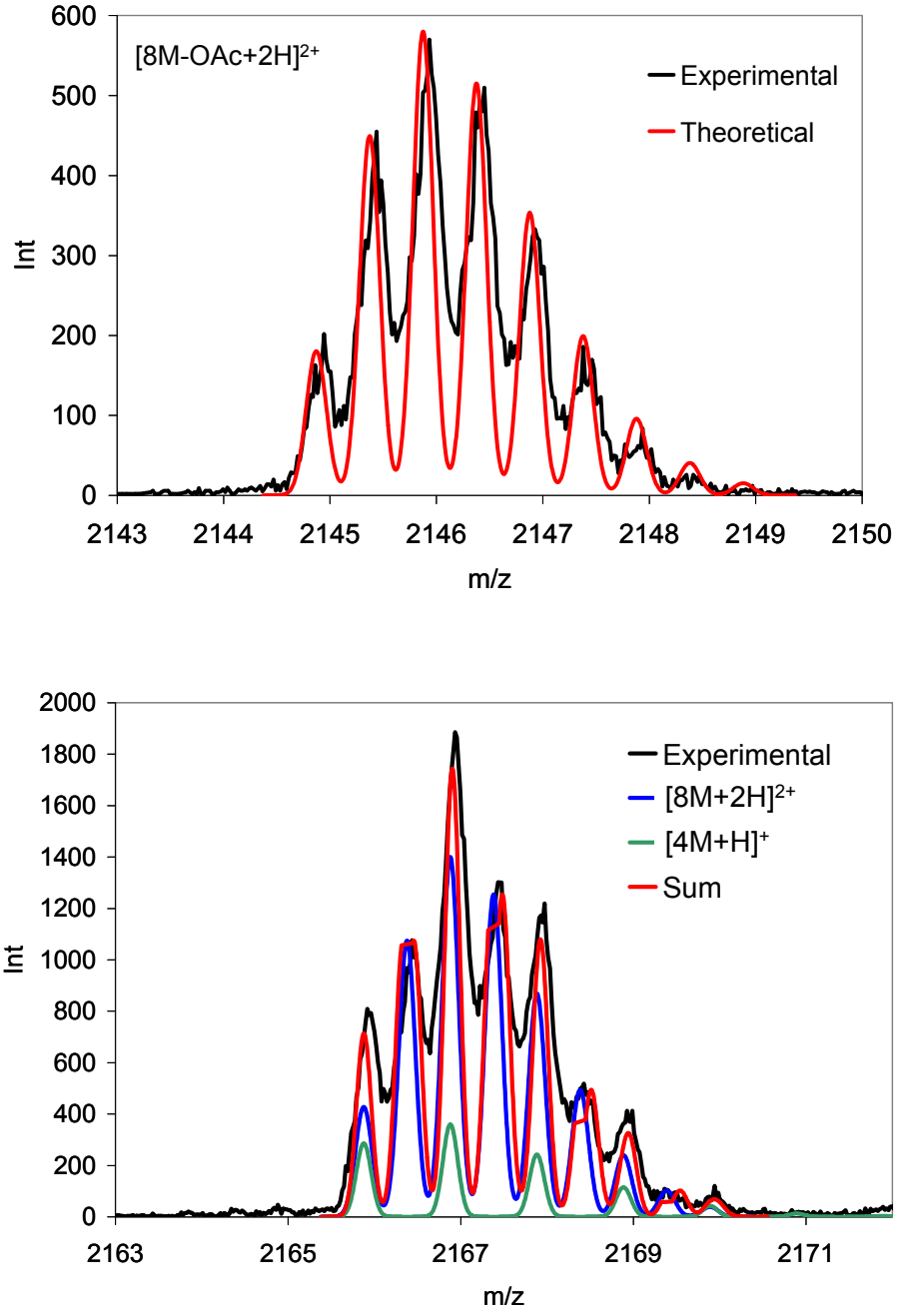

Figure 4.16 Experimental and theoretical ESI MS spectrum of $[8M+2H]^{2+}$, $[4M+H]^{2+}$ and $[8M\text{-}OAc+2H]^{2+}$ complexes of **nBuGTAG**.

It is likely that $[8M+2H]^{2+}$ ion peak corresponds to the "empty" octamer which is a hollow structure and that protons are used only to form ionizable adducts in the gas phase. "Empty" $[\mathbf{G}]_8$ are easily filled with metal ions whenever the latter are available. Moreover, in the presence of metal ions, the competition favours significantly the filled $[\mathbf{G}]_8$ formation. It is noteworthy to mention that **TAG** does not form "empty" $[\mathbf{G}]_8$ in the solution or gas phase, indicating that N^2-substituent is critical for the stabilization of these "empty" structures.

4.4 Conclusions

In this chapter we provide ESI MS evidence for the mixed and filled $[\mathbf{G}]_8$ of compounds **2.1b** – **2.2b** and **nBuGTAG**. Two experimental findings attest to their composition and stability, the absence of additional higher-order structures in the ESI MS spectra and a minimal fragmentation in the tandem ESI MS spectra. These results are in parallel with those seen in NMR. In this ESI MS study, stable "empty" $[\mathbf{G}]_8$ was indeed observed, for the first time, with high fidelity for **2.1b** and **nBuGTAG**. The additional stability provided by the interquartet stacking of N^2-aryl groups is believed to promote the formation of "empty" $[\mathbf{G}]_8$ in the gas phase. Direct comparison of ESI MS spectra of $\mathbf{N^2Gs}$, prepared with and without the metal ions, provides an indirect analytical way for monitoring the self-association and its dependence on metal cations.

4.5 References

[1] Sessler, J. L.; Sathiosatham, M.; Doerr, K.; Lynch, V.; Abboud, K. A. *Angew. Chem. Int. Ed.* **2000**, *39*, 1300.

[2] Otero, R.; Schock, M.; Molina, L. M.; Leagsgaard, E.; Stensgaard, I.; Hammer, B.; Besenbacher, F. *Angew, Chem. Int. Ed.* **2005**, *44*, 2270.

[3] Pham, T. N.; Masiero, S.; Gottarelli, G.; Brown, S. P. *J. Am. Chem. Soc.* **2005**, *127*, 16018.

[4] (a) Sakamoto, S.; Nakatani, K.; Saito, I.; Yamaguchi, K. *Chem. Commun.* **2003**, 788. (b) Aggerholm, T.; Nanita, S. C.; Koch, K. J.; Cooks, R. G. *J. Am. Chem. Soc.* **2003**, *38*, 87. (c) Mezzache, S.; Alves, S.; Paumard, J. P.; Pepe, C.; Tabet, J. C. *Rapid Commun. Mass Spectrom.* **2007**, *21*, 1075. (d) Fukushima, K.; Iwahashi, H. *J. Chem. Soc., Chem. Commun.* **2000**, 895.

[5] (a) Koch, K. J.; Aggerholm, T.; Nanita, S. C.; Cooks, R.G. *J. Mass Spectrom.* **2002**, *37*, 676. (b) de Hoffmann, E.; Stroobant, V. *Mass Spectrometry: Principles and Applications*; John Wiley & Sons: Chichester, 2007.

[6] Cavanagh, J.; Benson, L. M.; Thompson, R.; Naylor, S. *Anal. Chem.* **2003**, *75*, 3281.

Chapter 5
Watson-Crick H-Bonding by N^2-Arylguanosines

5.1 Introduction

GC base pair is of great research interest due to its biological relevance and large association constant. Several NMR studies exist on the topic of H-bonding between cytosine and guanine.[1] Watson-Crick H-bonding has also been monitored by using functionalized base pairs, such as fluorescently labeled guanine-cytosine ensembles containing the donor/acceptor combinations.[2] The fluorophores were typically attached at the C^8-, N^7- or N^9- sites of G-nucleosides and were used with the fluorescently-labeled cytosine or cytidine for study of electron transfer *via* H-bonding. Less work has been done on using fluorescent guanosines with unmodified cytidine.[3] For the study of nucleobase interactions, inherently fluorescent **N^2Gs** could render themselves useful. In addition to the self-assembly into G-quartets, as shown in Chapter 3 and 4, the lipophilic **N^2Gs** are theoretically capable of Watson-Crick H-bonding as well. To our knowledge, several **N^2Gs** carrying fluorescent groups have been synthesized, however none of them have been investigated in terms of H-bonding.[4] As a result, the goal of the investigation is to examine the GC base pair by using the fluorescent **N^2Gs**.

In addition, the fluorescent $[\mathbf{G}]_8$ formed by **N^2Gs** can be potentially used to probe the G-octamer-to-GC base pair structural changes. This is a biologically relevant process and it has been extensively studied through G-quadruplex-to-duplex systems by means of FRET between the terminally attached donor and acceptor dyes on oligonucleotides. The

fluorescent $[\mathbf{G}]_8$ formed by $\mathbf{N^2Gs}$ can potentially be used as the model system towards greater understanding of such interactions.

This chapter describes the use of NMR, fluorescence, CD, and ESI-MS methods to study the interactions of luminescent $\mathbf{N^2G}$ derivatives (described in Chapter 2 - 3), **2.1b** and **2.2b**, with the complementary base, N^4-acetyl-*2',3',*5'-*O*-triacetylcytidine (**4-C**) shown in Figure 5.1. In addition, a G-octamer-to-GC base pair transformation was investigated using fluorescent $[\mathbf{G}]_8$.

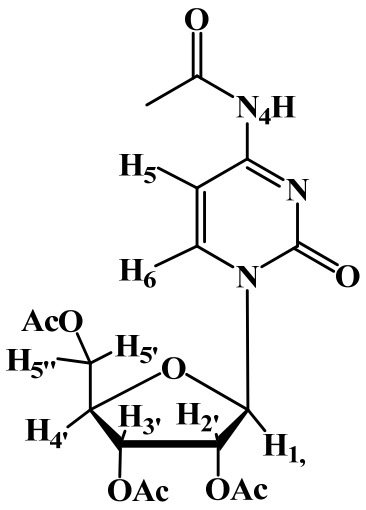

Figure 5.1 Structure of nucleoside **4-C**.

5.2 Experimental Procedure

5.2.1 General considerations

All reagents were purchased from the Aldrich Chemical Co. and used without further purification unless stated otherwise. For the study of G-octamer-to-GC base pair transformation, previously synthesized $[\mathbf{2.1b\text{-}G}]_8 \bullet K^+$ octamer described in Chapter 3 was used. All 1D NMR experiments were recorded on Bruker Avance 600 MHz

spectrometers at 298 K, unless otherwise specified, with the solvent peaks used as the reference. Low resolution and high-resolution mass spectrometry experiments were performed using the electrospray ionization mode on QSTAR XL MS/MS Systems using Analyst QS Method. Excitation and emission spectra were recorded on a Photon Technologies International QuantaMaster Model C-60 spectrometer. Standard CD spectra were recorded on Jasco 715 circular dichroism spectrometer in a 1 cm path length cell. The wavelength was varied from 190 - 600 nm at 200 nm a minute with 5 overall scans.

5.2.2 Fluorescence titration experiments

To the prepared solutions of **2.1b** (2.5×10^{-5} M), **2.2b** (2.5×10^{-5} M) and [**2.1b-G**]$_8$•K^+ (1.0×10^{-5} M) in CH_2Cl_2, the solution of **4-C** (6.0×10^{-3} M) in CH_2Cl_2 was added in 5 μL aliquots.

5.2.3 NMR titration experiments

To the solutions of **2.1b** (6.8×10^{-4} M), **2.2b** (1.6×10^{-2} M) and [**2.1b-G**]$_8$•K^+·picrate (1.0×10^{-3} M) in CD_2Cl_2, the solution of **4-C** in CD_2Cl_2 was added in 10 μL aliquots.

Diffusion experiments were carried out with Bruker Avance-600 MHz spectrometer using the pulse sequence of longitudinal–eddy-current delay (LED) with bipolar-gradient pulses. The ^{1}H 90^o and 180^o pulse widths were 10 and 20 μs, respectively. The pulse field gradient duration was varied from 4-15 ms, and the variable gradient (G) was changed from 6 to 350 mT/m. The diffusion period was varied from 50 to 90 ms. A total of 16 transients were collected for each of the 32 increment steps with a 12 s recyling delay. The eddy-current delay was set to 5 μs. Diffusion coefficients were

obtained by integration of the desired peaks to a single exponential decay curve using "Simfit Bruker XWINNMR" software. Calibration of the field gradient strength was achieved by measuring the value of translational diffusion coefficient (D) for the residual ^{1}H signal in D_2O (99.99%, ^{2}H atom), $D = 1.91 \times 10^{-9}$ m^2/s.

NOESY NMR spectra were recorded on a 400 MHz spectrometer. All NOESY spectra at 298 K were acquired using a mixing time of 0.3 or 0.4 s and the total of 64 transients with the 10 s recycling delay. NOESY experiment at 195 K was acquired using a mixing time of 0.1 s and the 2 s recycling delay and the total of 64 transients.

ROESY NMR spectra were recorded on 400 MHz spectrometer at 195 K using a variable mixing times of 0.08, 0.1 and 0.3 s, the relaxation delay of 3 s and the total of 64 transients.

5.3 Results and Discussion

5.3.1 Formation of the GC base pair

5.3.1.1 NMR study

The structure of the GC base pair is provided in Figure 5.2 along with the labeled protons for reference. In the absence of **4-C**, N^2-arylguanosines, **2.1b** and **2.2b**, exist predominantly as monomers in CD_2Cl_2 at 298 K. The sequential addition of **4-C** to the solutions of **2.1b** or **2.2b** in CD_2Cl_2 causes a dramatic change of the H_6 and H_5 resonances of **4-C** which shift ~ 0.1 – 0.4 ppm downfield upon GC base pair formation as shown in Figure 5.3 and Figure 5.4. The small changes occur with non-exchangeable **N^{2}G** protons.

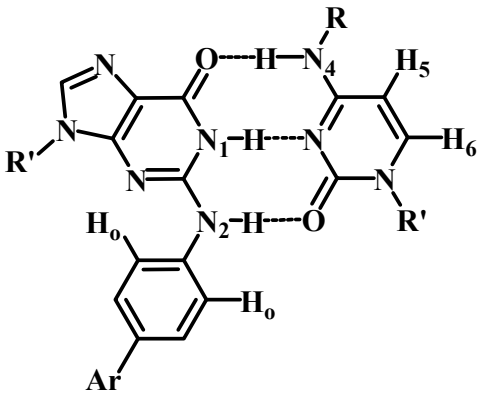

Figure 5.2 Structure of GC base pair formed by **N^{2}Gs**.

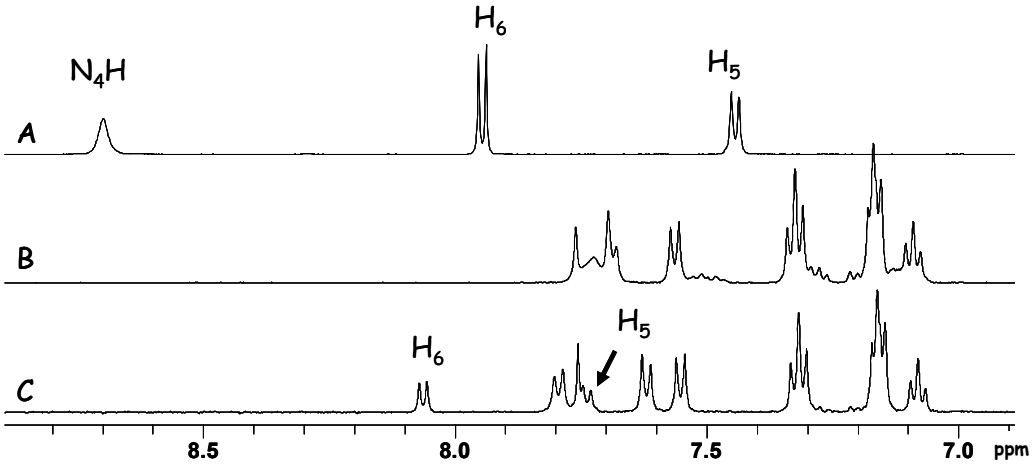

Figure 5.3 Partial ^{1}H NMR spectra of A) **4-C**, B) **2.1b** and C) [**2.1b-G**]:[**4-C**] (CD_2Cl_2, 298 K).

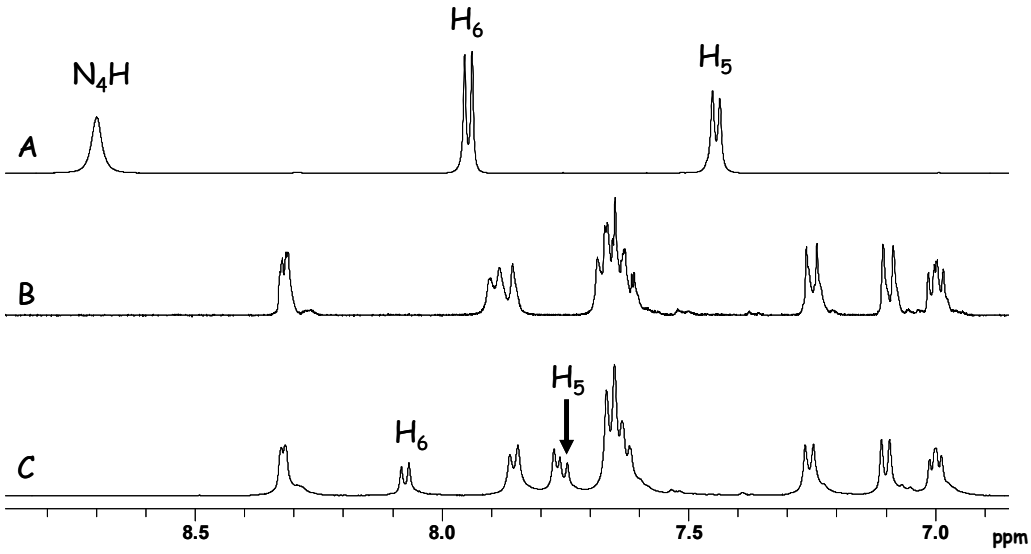

Figure 5.4 Partial ^{1}H NMR spectra of A) **4-C**, B) **2.2b** and C) [**2.2b-G**]:[**4-C**] (CD_2Cl_2, 298 K).

Notably only one type of guanine and cytosine protons are observed after 1 eq of **4-C** was added, which indicates that exchange between free and bound molecules is fast on the NMR time scale.

In order to establish the GC dimer formation, the NOESY NMR spectra in Figure 5.5 and Figure 5.6 were recorded to establish the correlation between the N_1H (G) with the N_4H (C) at 228 K for both **2.1b** and **2.2b**. Upon cooling to 228 K, the [**2.1b-G**]:[**4-C**] and [**2.2b-G**]:[**4-C**] base pairs can be clearly identified through the sharp peaks at ~ 13.1, 12.2, 10.7 ppm that can be assigned to the N_1H (G), N_4H (C) and N_2H (G) protons, respectively. The NOESY NMR was used to correlate the N_1H (G)/N_4H (C) protons which is a key NOE interaction for the GC base pair.

To further demonstrate the role of N^2-arylguanosine in GC pair formation, we examined the interaction of the N^2-acetyl-N^2-arylguanosine, **2.2c**, with **4-C**. In **2.2c** H-donor site of the amino group is blocked by an acetyl group. The ^{1}H NMR spectrum of **2.2c** with 1 equivalent **4-C**, shown in Figure 5.7, clearly indicates that blocking the H-donor site prevents Watson-Crick H-bonding. Not surprisingly, **2.2c** fails to form a GC dimer.

An association constant could not be determined by NMR for either of GC pairs due to several reasons. **N^2G** derivatives are sparingly soluble in CD_2Cl_2 in the absence of **4-C**, which makes binding studies challenging. The chemical shifts of exchangeable protons of **N^2Gs** exhibit substantial broadening while those of the non-exchangeable protons of interest overlap, hence these protons could not be used for the determination of binding constants. An NMR dilution method was ineffective due to the strong GC association which is also insensitive to an increase in temperature.

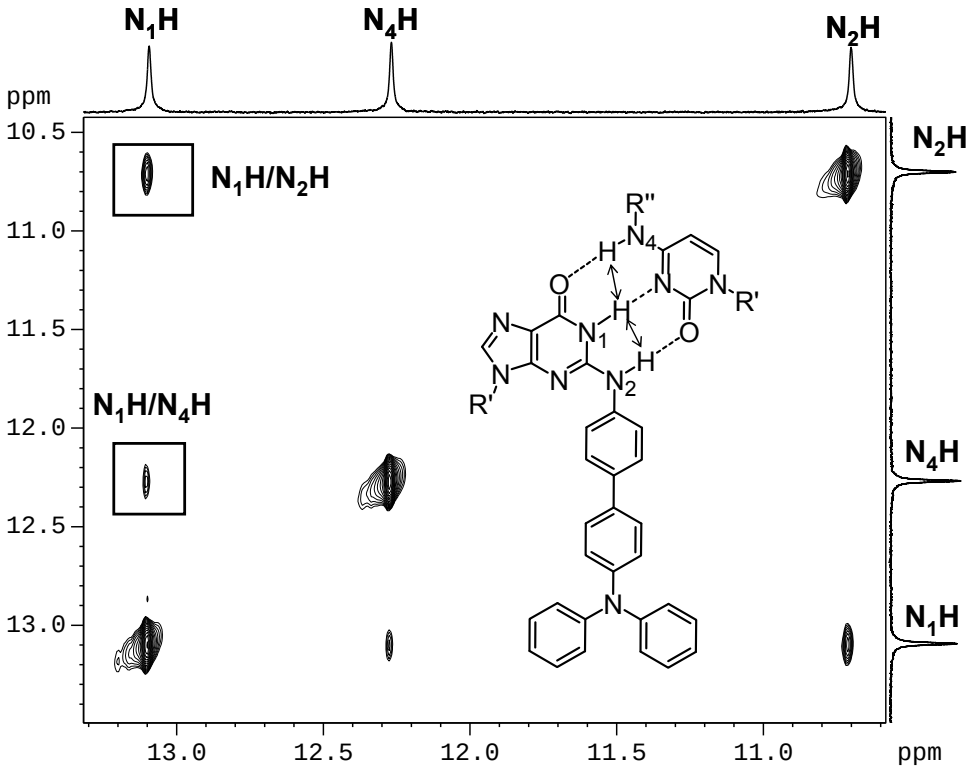

Figure 5.5 Partial NOESY spectrum of **[2.1b-G]:[4-C]** ([**2.1b**] = 6.8 x 10^{-4} M, CD_2Cl_2, 228 K).

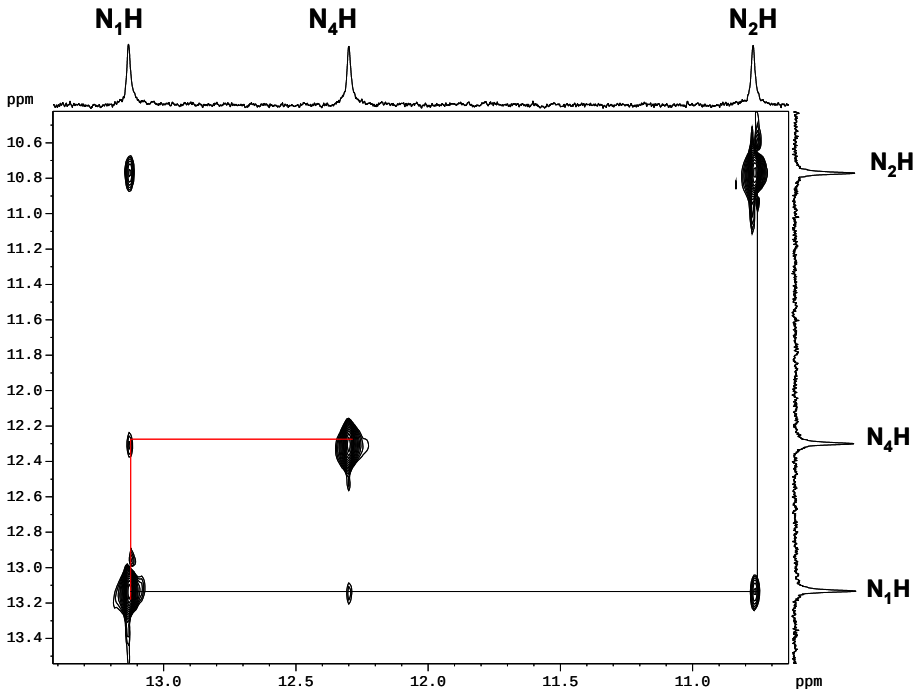

Figure 5.6 Partial NOESY spectrum of **[2.2b-G]:[4-C]** ([**2.2b**] = 1.6 x 10^{-2} M, CD_2Cl_2, 228 K).

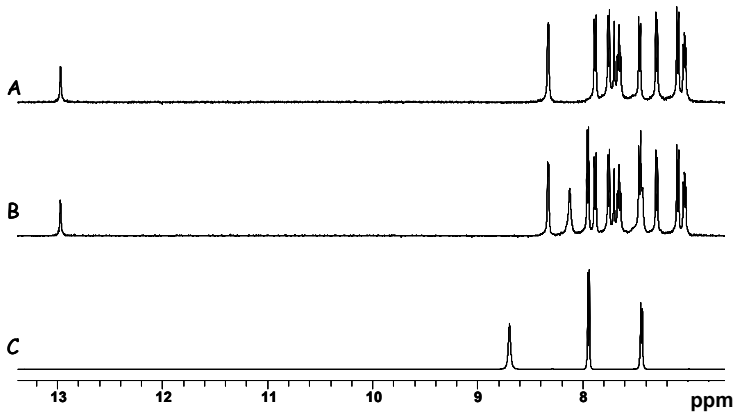

Figure 5.7 Partial ^{1}H NMR spectra of A) **2.2c**, B) **[2.2c-G]:[4-C]** and C) **4-C** (298 K, CD_2Cl_2).

5.3.1.2 ESI-MS study

The identification of GC dimer was also achieved by ESI-MS using the 1:1 mixture of [**2.1b-G]:[4-C]** in CH_3NO_2. Figure 5.8 shows a full mass spectrum of the mixture with significant population of monomer [**2.1b**+H]$^+$ and [**4-C**+H]$^+$ ions. The molecular ion at *m/z* 1140.39 was assigned to the GC base pair, [[**2.1b-G]:[4-C]**+H]$^+$. It should be noted that the GC dimer is less stable than its respective monomers in the gas phase. The ESI-MS spectrum of **2.2b** presented in Figure 5.9 is dominated by the [**2.2b**+H]$^+$ and [**4-C**+H]$^+$ adducts along with the poorly resolved [[**2.2b-G]:[4-C]**+H]$^+$ dimer at *m/z* 1142.38.

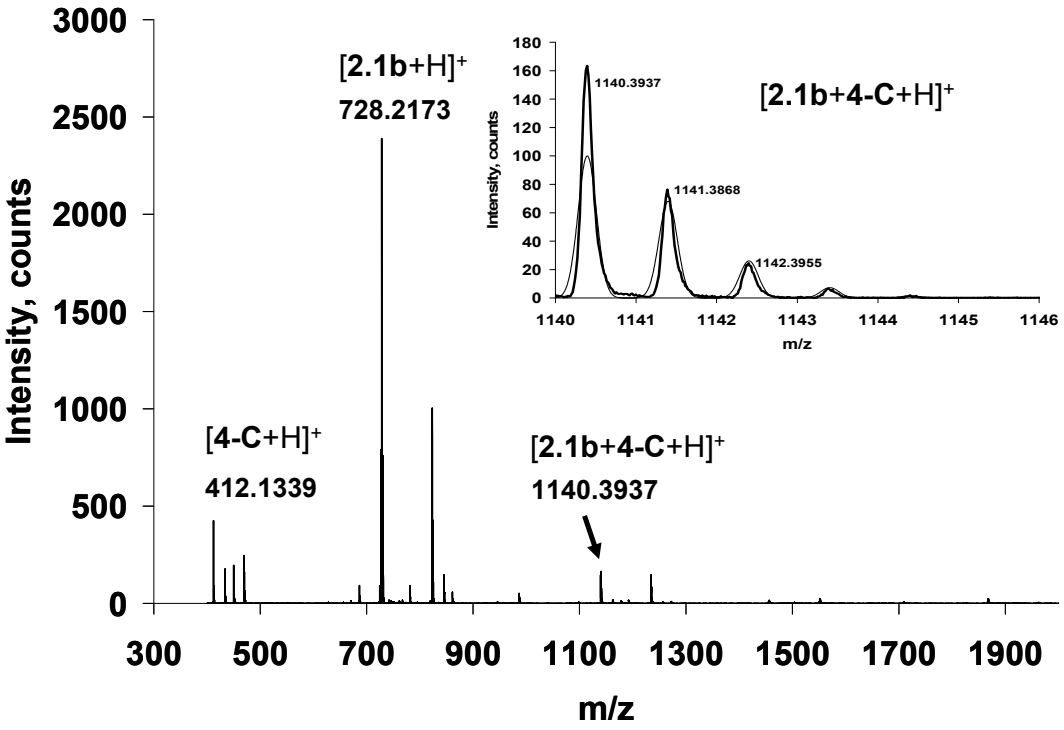

Figure 5.8 Full ESI-MS spectrum of [**2.1b-G**]:[**4-C**] (inset: experimental and predicted isotope pattern of [[**2.1b-G**]:[**4-C**]+H]$^+$ ion, CH_3NO_2).

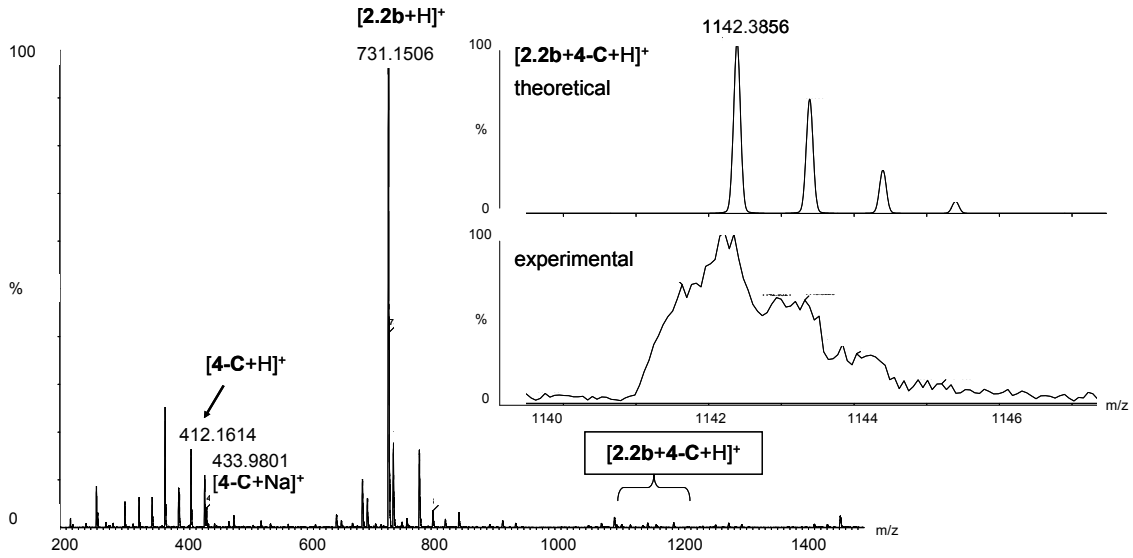

Figure 5.9 Full ESI-MS spectrum of [**2.2b-G**]:[**4-C**] (Inset: experimental (bottom) and predicted (top) isotope pattern of [[**2.2b-G**]:[**4-C**]+H]$^+$ ion, CH_3NO_2).

5.3.1.3 Fluorescence study

Having identified the GC base pair formation by NMR, for both **N^{2}G** compounds, fluorescence spectroscopy was used to monitor the impact of GC pair formation on fluorescence of **2.1b** and **2.2b**. Addition of **4-C** solution to **2.1b** or **2.2b** solutions in CH_2Cl_2 results in the quenching of fluorescent emission of N^2-guanosines as shown in Figure 5.10. From the Stern-Volmer plots, it is evident that the extent of quenching starts to level off after the addition of approximately 1 equivalent of **4-C** (Inset). The binding constants for GC complexes were determined by using the non-linear least-square fitting procedure for a 1:1 [**G**]:[**4-C**] binding model[5] presented in Figure 5.11 to be 5 x 10^5 M^{-1} and 2 x 10^6 M^{-1} for **[2.1b-G]:[4-C]** and [**2.2b-G]:[4-C]**, respectively. These binding constants are in agreement with those reported in the literature for other GC ensembles formed between guanosine and cytidine derivatives.[6] Addition of organic solvent such as ethanol, which is a well known competitive H-bonding solvent, to the GC base pair

solution results in the partial restoration of the fluorescent intensity, further supporting that the observed quenching is due to the formation of H-bonds between guanine and cytosine. In comparison, the fluorescent intensity of the **2.2c**, which contains a blocked N_2H group, does not change in the presence of **4-C**, as expected. Appreciable fluorescent quenching in **2.1b** and **2.2b** can only be explained by the intramolecular charge transfer in the H-bonded GC conjugate. The dramatic fluorescent quenching by cytidine in forming the GC pair is most likely caused by the G-to-C photo-induced proton-transfer mechanism through the H-bonds, as established for a simple GC pair in gas phase.[7] This demonstrates that the fluorescent **N^2G** can be used effectively in monitoring the GC base pair formation. UV and CD titration data of **2.1b** and **2.2b** with **4-C** did not produce any meaningful information due to the strong absorption of **4-C** in the UV region.

In order to ascertain the selectivity of **2.1b** and **2.2b** as sensing probes for cytidine, the competition experiments of *2',3',5'-O*-triacetyladenosine (A) and *3',5'-O*-diacetylthymidine (T) with **4-C** were carried out. Figure 5.12 and Figure 5.13 show that both acetylated adenosine and acetylated thymidine have no impact at all on the fluorescent spectra of **2.1b** and **2.2b**. Furthermore, the addition of **4-C** to these solutions causes quenching of **2.1b** and **2.2b** fluorescent emissions, further supporting the idea that fluorescent quenching takes place exclusively *via* Watson-Crick H-bonding. The high selectivity observed with **N^2Gs** for **4-C** supports that these nucleosides can potentially be used as sensors/probes for GC pair formation through specific recognition.

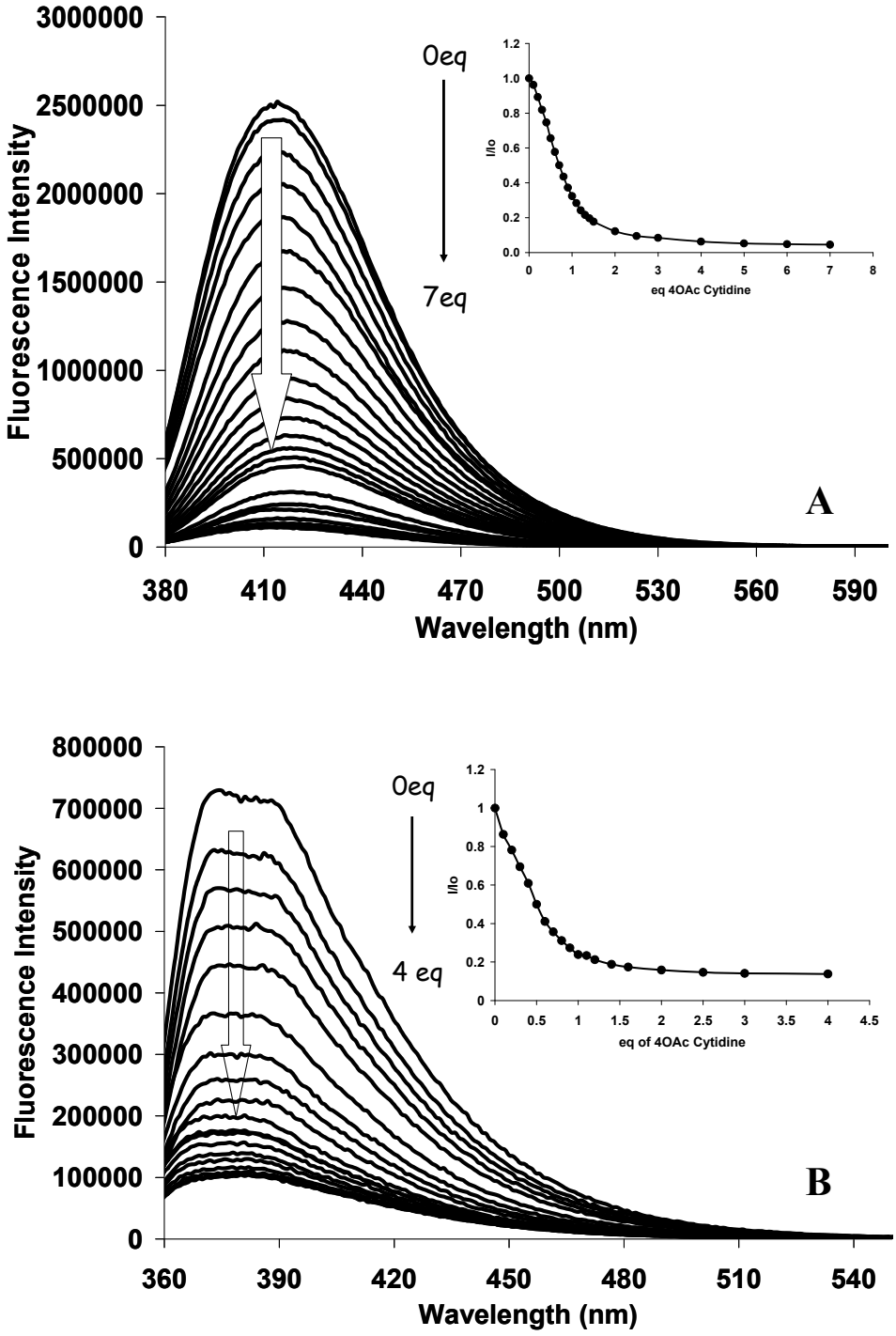

Figure 5.10 Fluorescence titrations of A) **2.1b** and B) **2.2b** with **4-C** in CH_2Cl_2 ([**2.1b**] = 2.5 x 10^{-5} M, [**2.2b**] = 2.5 x 10^{-5} M, inset: Stern-Volmer plots).

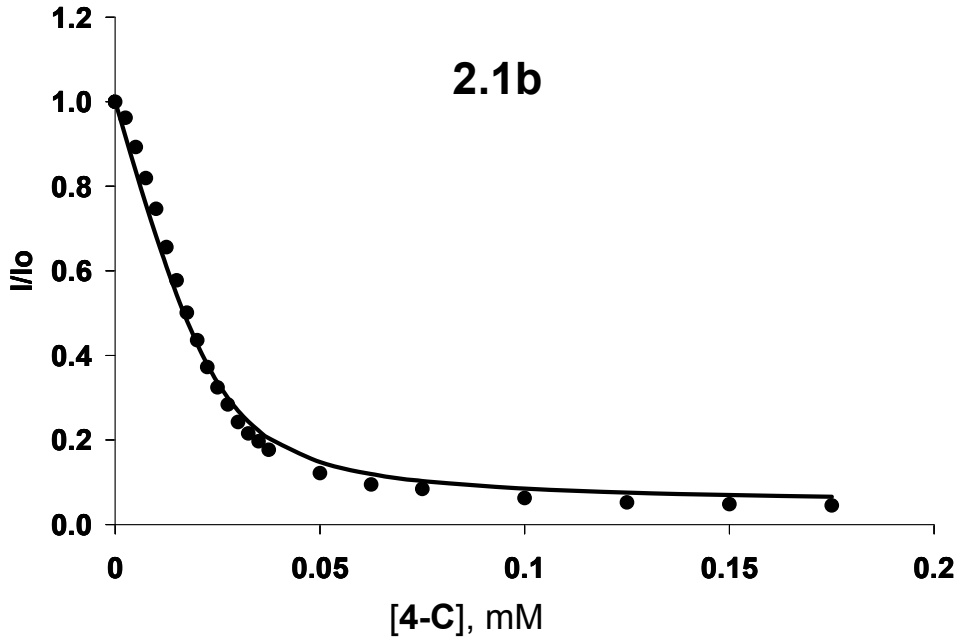

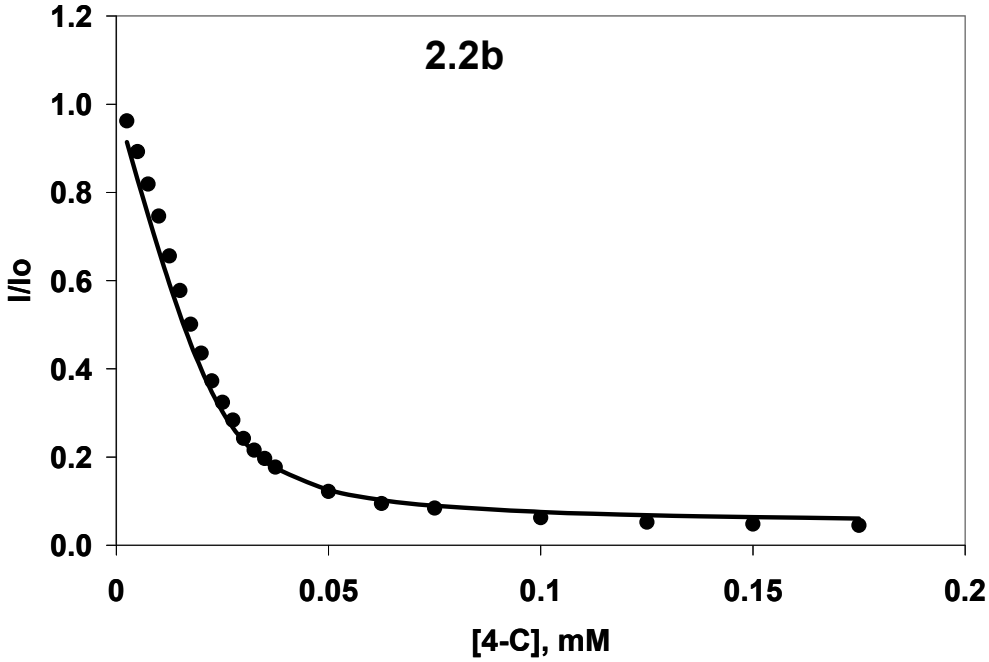

Figure 5.11 Binding constant determination of GC base pair association.

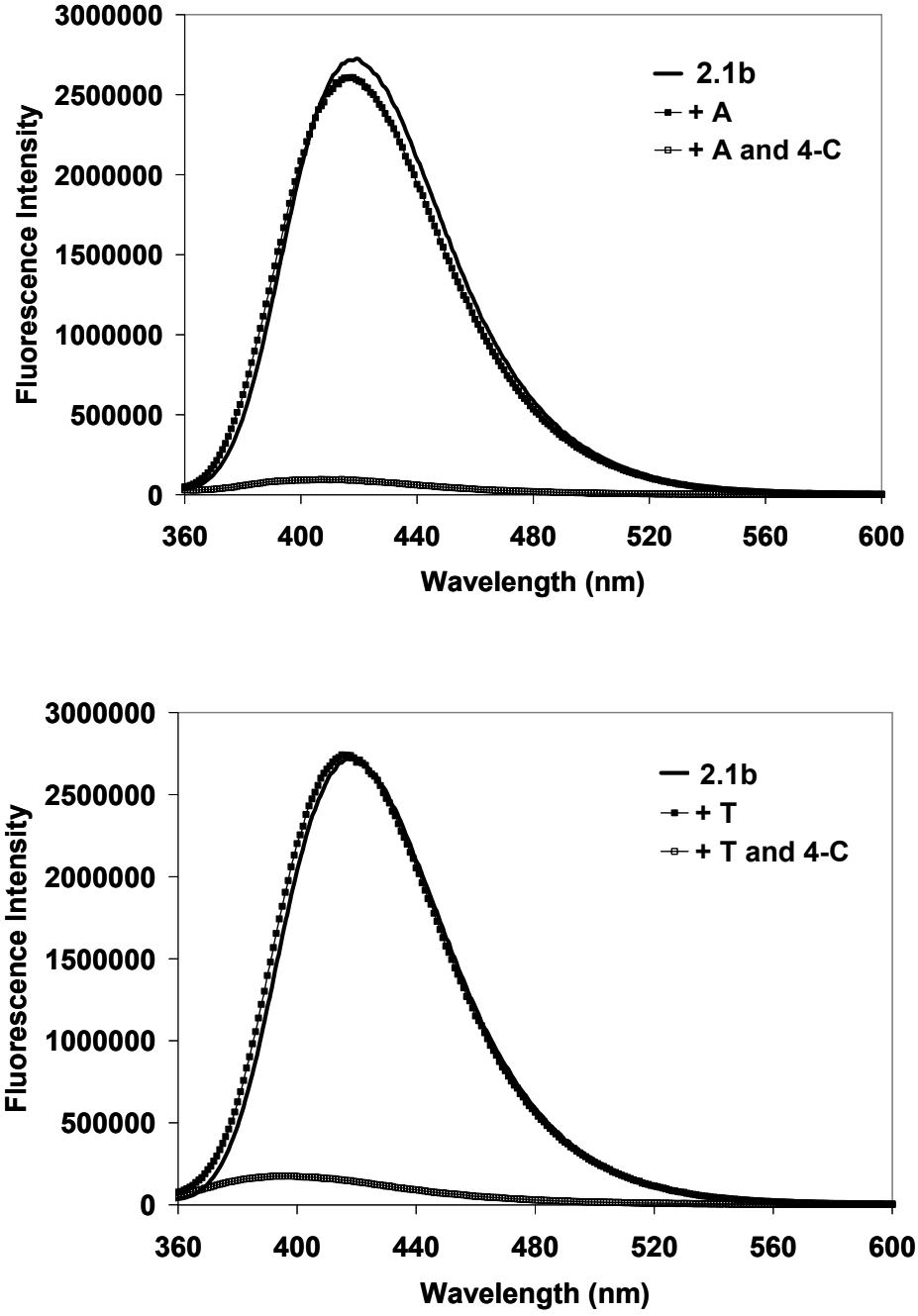

Figure 5.12 Fluorescence spectra of **2.1b** in the presence of different nucleosides: adenosine (A), thymidine (T) and **4-C** (CH_2Cl_2).

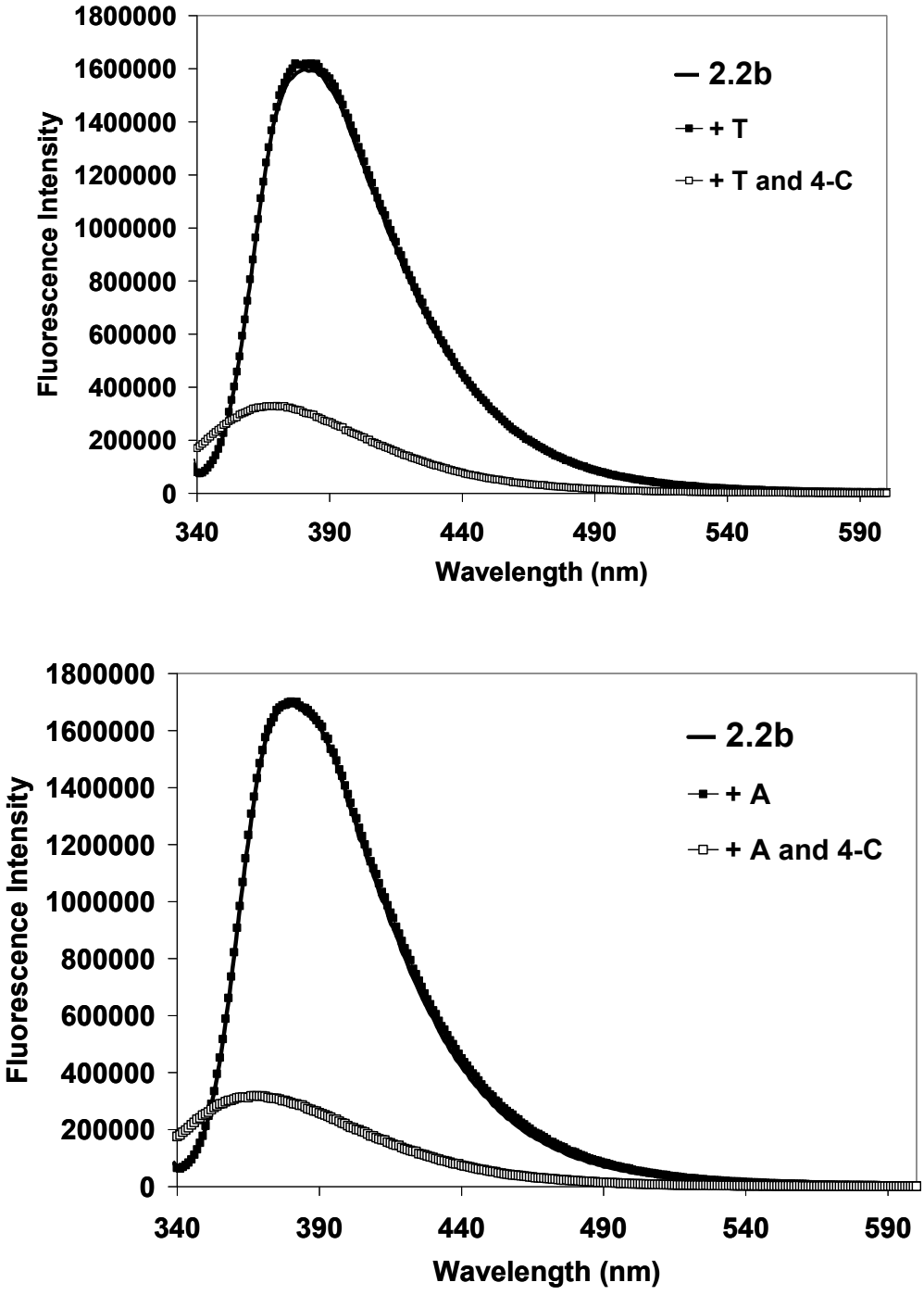

Figure 5.13 Fluorescence spectra of **2.2b** in the presence of different nucleosides: adenosine (A), thymidine (T) and **4-C** (CH_2Cl_2).

5.3.1.4 Molecular orbital calculations of GC base pair

The fluorescent emission of **2.1b** or **2.2b** is ascribed to the singlet state emission from the photo-excited guanine-biphenyl-diaryl chromophore as discussed in Chapter 2. The HOMO and LUMO orbital diagrams for monomer **2.1b** and **2.2b** are localized over the whole molecule. Hence the lowest electronic transitions for these compounds may be assigned to $\pi - \pi^*$ transitions centered on guanine and the biphenyl-NAr_2 group. The MO calculation results indicate that there is little difference between **2.1b** and **2.2b** in terms of HOMO and LUMO locations, which is consistent with their similar luminescent properties. Due to the fact that the emission stems from the guanine-N^2aryl chromophore, the fluorescent quenching observed upon addition of **4-C** suggests that the quenching process is related to the H-bond formation.

In order to gain insight into the nature of electronic transitions upon GC base pair formation DFT calculations were performed. The ground-state structure of the [**2.1b-G**]:[**4-C**] dimer was fully geometry optimized by density-functional theory (DFT) at a B3-LYP/6-311G** level of theory and is presented in Figure 5.14 along with the diagrams of its HOMO and LUMO levels. The HOMO level of [**2.1b-G**]:[**4-C**] consists of π orbitals of N^2-biaryldiphenylamino group while the LUMO level is made of entirely the π^* orbitals of the cytosine ring. Hence, in contrast to **2.1b**, where the lowest electronic transition is from a $\pi - \pi^*$ transition localized on the same part of the molecule, the lowest electronic transition of [**2.1b-G**]:[**4-C**] is a charge transfer from the N^2-substituent to the cytosine. The low lying LUMO of the cytosine in the GC pair is therefore clearly responsible for quenching the emission of **2.1b**. The guanine ring has no contributions to either the HOMO or the LUMO level of the GC pair and it probably acts as a bridge to

facilitate H-bonds and electronic transitions between the N^2-substituent and the cytidine ring. Previous reports have showed that the charge transfer in the GC base pair takes place from G to C that can be exclusively accessed only through Watson-Crick type H-bonding.[8] Our finding is in line with the previous study except that upon substitution by the electron donating diarylamino-biphenyl group at the N^2 site, the HOMO shifts from the guanine ring to the N^2-substituent. From the steady-state fluorescence study and the molecular orbital calculations it can be concluded that a three point H-bonding, as seen in Watson-Crick motif, leads to the fluorescent quenching *via* charge transfer mechanism.

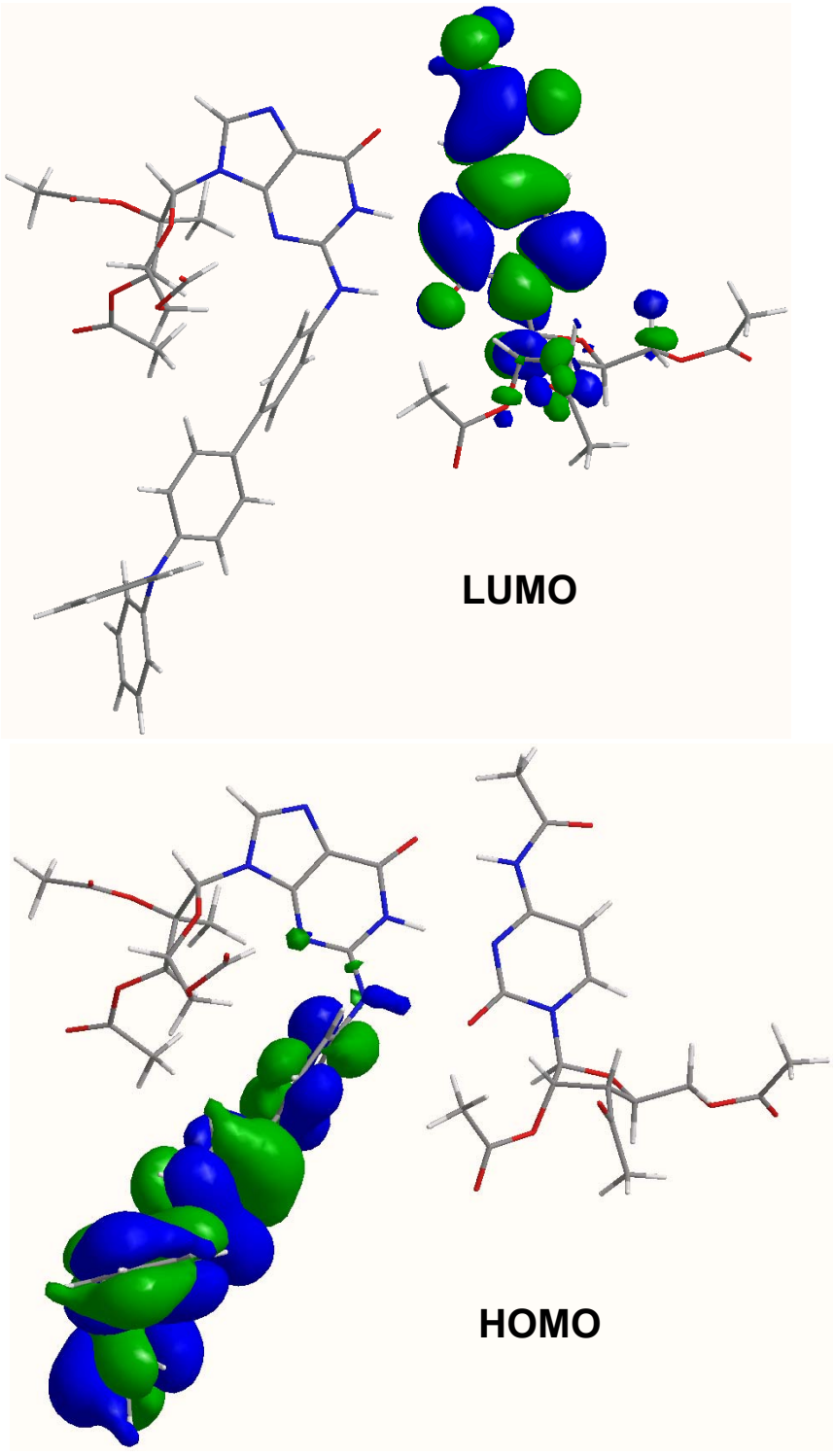

Figure 5.14 HOMO and LUMO orbitals of **[2.1b-G]**:[**4-C**] base pair.

5.3.2 Interaction of GC pair with excess 4-C

5.3.2.1 NMR study

While GC base pair formation has been investigated in great detail by us and others, little is known about the interactions of a GC dimer with other nucleobases. For example, in the NMR study of a GC pair with excess guanosine, a GCG trimer was identified.[9] The exact nature of the interactions of the GC dimer with the excess cytidine still remains unclear.

The GC base pairs formed by **2.1b** and **2.2b** with **4-C** provided us an opportunity to study the interaction of GC dimer with additional **4-C** by NMR spectroscopic methods. As shown in Figure 5.15, the ^{1}H NMR spectra of the [**G**]:[**C**]$_n$ with n > 1 are very different from that of the [**2.1b-G]:[4-C]** and [**2.2b-G]:[4-C]** base pairs. The common trend for both compounds is the dramatic upfield shifts associated with the H_5 (C) and H_6 (C) protons upon the addition of **4-C**.

A more detailed examination of the ^{1}H NMR titration data of the [**2.1b-G]:[4-C]** is presented in Figure 5.16. The addition of more than 1 equivalent of **4-C** to the solution of **2.1b** causes sharpening of the N_1H (G) and N_2H (G) resonances along with the slight downfield shift. Surprisingly, the N_4H (C) proton is upfield shifted (~ 3 ppm) and broadened, along with the upfield shifts of H_5 (C) and H_6 (C) resonances. The final ^{1}H NMR spectrum of the [**2.1b-G**]:[**4-C**]$_4$ is characterized by one type of **2.1b** and one type of **4-C** peaks.

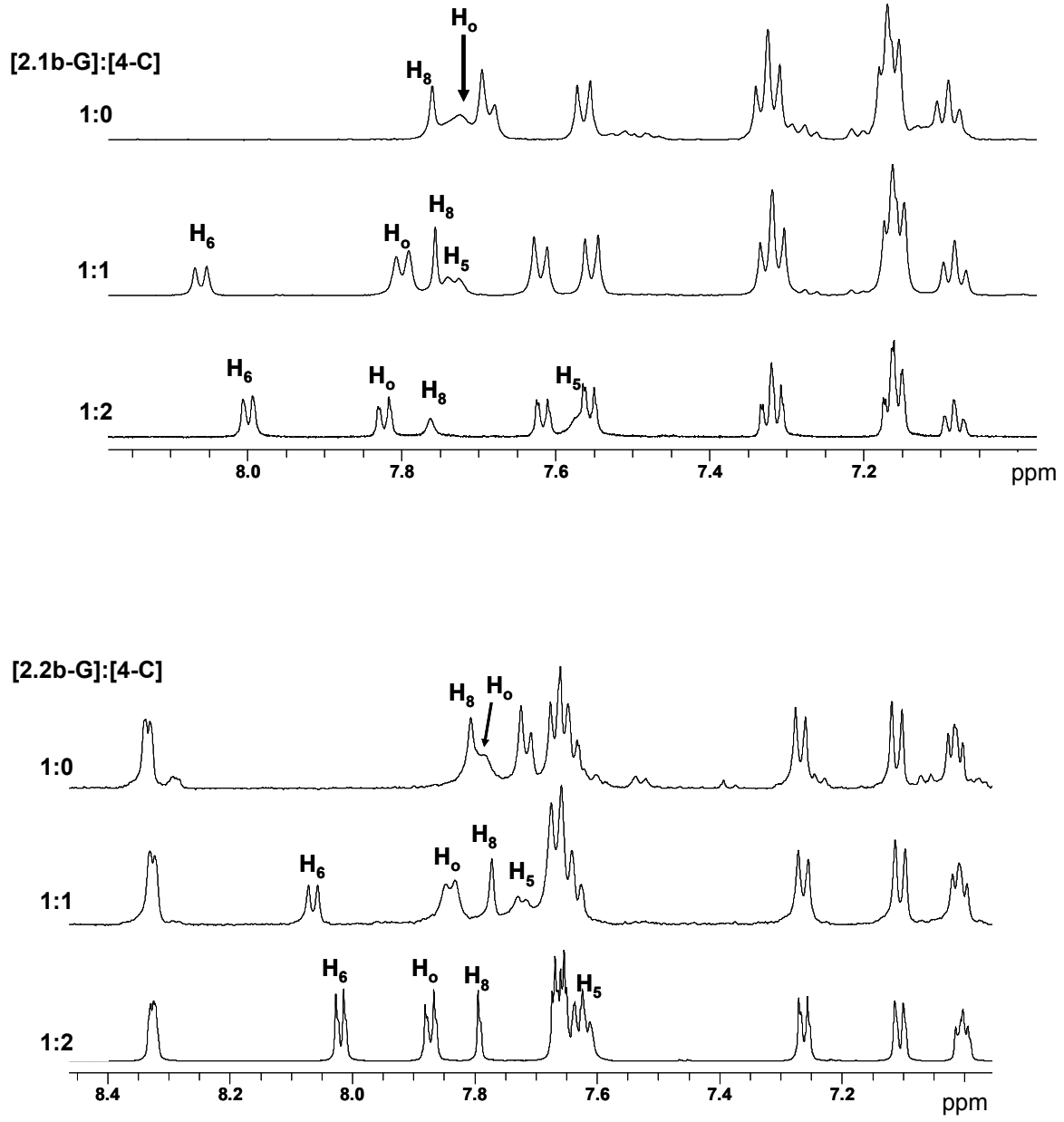

Figure 5.15 Partial ^{1}H NMR spectra of **2.1b** and **2.2b** with different amounts of **4-C** (298 K, CD_2Cl_2).

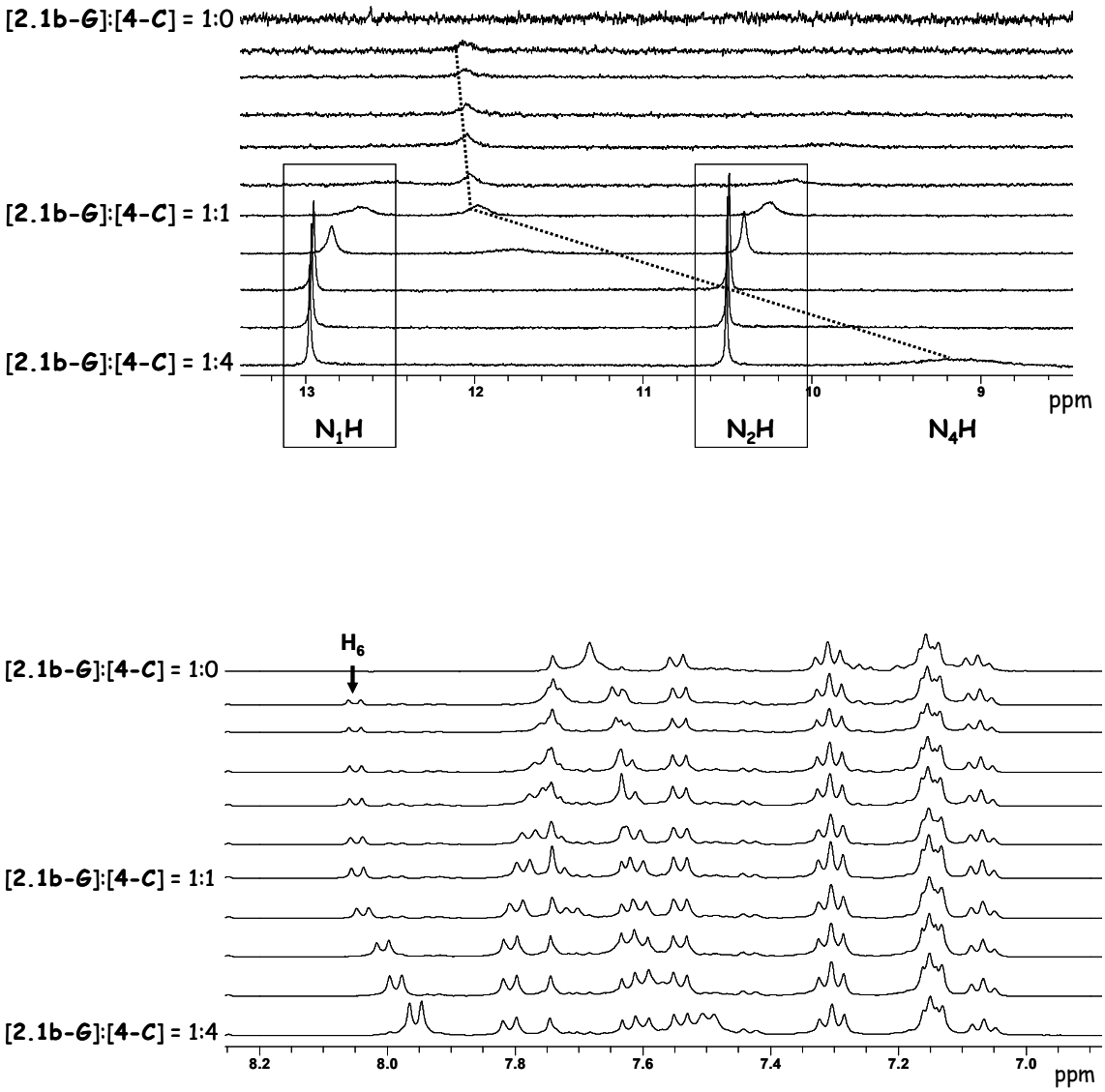

Figure 5.16 Partial ^{1}H NMR spectra showing different spectral regions during the titration of **2.1b** with **4-C** (CD_2Cl_2, 298 K, [**2.1b**] = 6.8 x 10^{-4} M).

The overall chemical shift positions and the sharpness of the exchangeable guanine protons suggest the complex formation by H-bonds. In the final ^{1}H NMR spectrum of [**2.1b-G**]:[**4-C**]$_4$ the chemical shifts of **2.1b** protons remain similar to those seen for the [**2.1b-G**]:[**4-C**] base pair, while the chemical shifts of **4-C** exhibit major changes. These findings suggest that **2.1b** remains involved in the H-bonding in the [**2.1b-G]:[4-C]** pair even in the presence of excess **4-C**, while **4-C** experiences some dynamic behaviour.

The NOESY NMR was used to gain more structural information at 298 K. NOESY spectra of GC base pairs of **2.1b** and **2.2b** were recorded and they share similar NOE interactions. However, the broad signal associated with N_4H (C) was more easily located in the presence of **2.2b**. For the purpose of structural elucidation, the study is focused on the [**2.2b-G]:[4-C]**$_2$ complex. The chemical exchange cross peaks are observed between N_4H (C) and N_1H (G) as can be seen from Figure 5.17. A true NOE cross peak was observed between N_2H (G) and H_o (G) which helped in identifying the guanine component. The N_1H (G) and N_2H (G) protons also exhibit NOE, as expected since they belong to the same guanine molecule. In addition, the true NOE observed between N_4H (C) proton and N^4Ac (C) group clearly suggests that the average conformation of N^4-acetyl group is similar to the one observed for **4-C** monomer (Figure 5.17). Hence, a rotation around C-N bond of **4-C** cannot be used to explain the dynamic behaviour observed in [**G**]:[**C**]$_n$ system when n > 1.

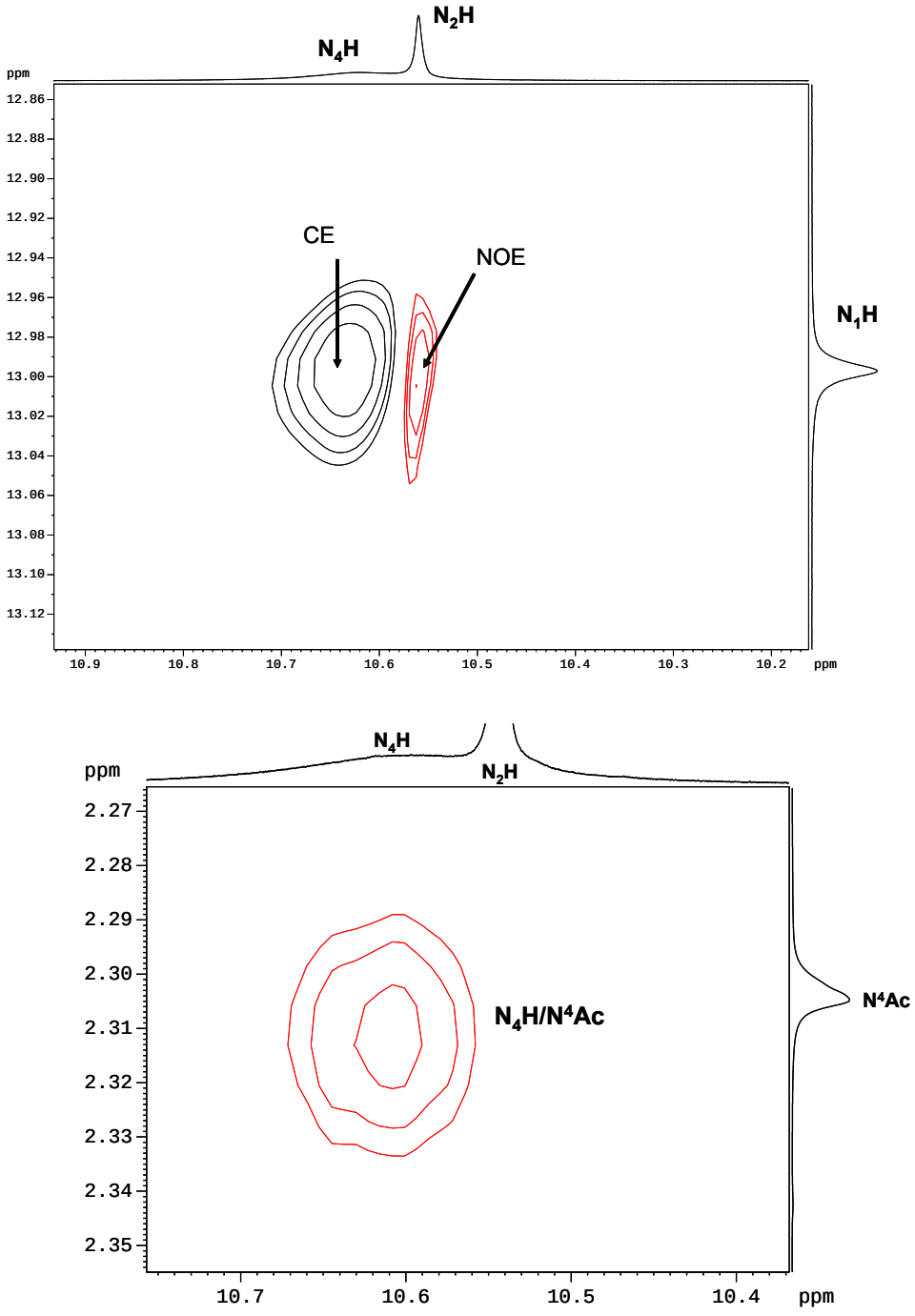

Figure 5.17 Partial NOESY spectra of **[2.2b-G]:[4-C]**$_2$ (black-chemical exchange (CE); red-NOE; [**G**]:[**C**] = 1:2, 298 K, CD_2Cl_2).

To establish the size of the aggregates, DOSY NMR was performed at different [**G**]:[**C**]$_n$ (n = 0, 1, 2) ratios. Figure 5.18 shows that a monomer of **4-C** has the largest D_t value, followed by the **N^{2}G** monomers (either **2.1b** or **2.2b**). Upon formation of the GC dimer (n = 1), D_t values associated with the guanine and cytosine groups are 4.99 x 10^{-10} m^2/s and 5.64 x 10^{-10} m^2/s, respectively. The ratios of D_t(GC) / D_t(monomer) are 0.77 and 0.65 for guanine and cytosine, respectively. Similar D_t ratios for guanine and cytosine components at n = 1 indicates that they belong to the same aggregate, which is the GC base pair.

With an increase in the **4-C** concentration and the formation of [**G**]:[**C**]$_2$ complex, D_t value of **N^{2}G** increases to 5.34 x 10^{-10} m^2/s (~ 7%) while D_t value of **4-C** increases up to 6.52 x 10^{-10} m^2/s (~ 13%). The diffusion coefficient of the complex was found to be similar to that obtained for [**G**]:[**C**]$_n$ (n = 1), indicating that the final structure cannot be a GCC trimer but it may be related to a dynamic process. Hence a more detailed NMR experiments are required in order to identify the nature of the species present.

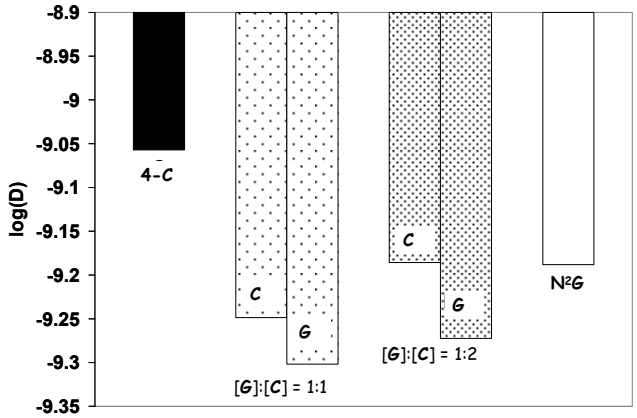

Figure 5.18 Extrapolated diffusion coefficients (D_t) for **4-C**, **N^{2}G** and [**G**]:[**C**]$_n$ for n = 1, 2 (CD_2Cl_2, 298 K).

Variable temperature ^{1}H NMR experiments were performed for both **N^{2}G** derivatives, **2.1b** and **2.2b**, in the presence of excess **4-C**. However, only VT NMR data for **2.1b** will be discussed in more detail. In Figure 5.19 at temperatures below 228 K one type of **2.1b** and two types of **4-C** peaks (denoted as **4-C** (bound cytidine) and **4-C*** (free cytidine) were observed. The sharp peaks between 10.5 and 13.4 ppm fit perfectly well with the N_2H (G), N_1H (G) and N_4H (C) of the standard GC base pair. A broad resonance at 10.6 ppm can be assigned to a N_4H* of the free **4-C*** species. Since the N_4H* proton remains broad and below 12 ppm we can conclude that it does not belong to a typical [**4-C**]$_2$ dimer. Further lowering of the temperature to < 188 K results in the splitting of non-exchangeable protons of **4-C** as well, such as H_6, $H_{1'}$ and N^4Ac as presented in Figure 5.20.

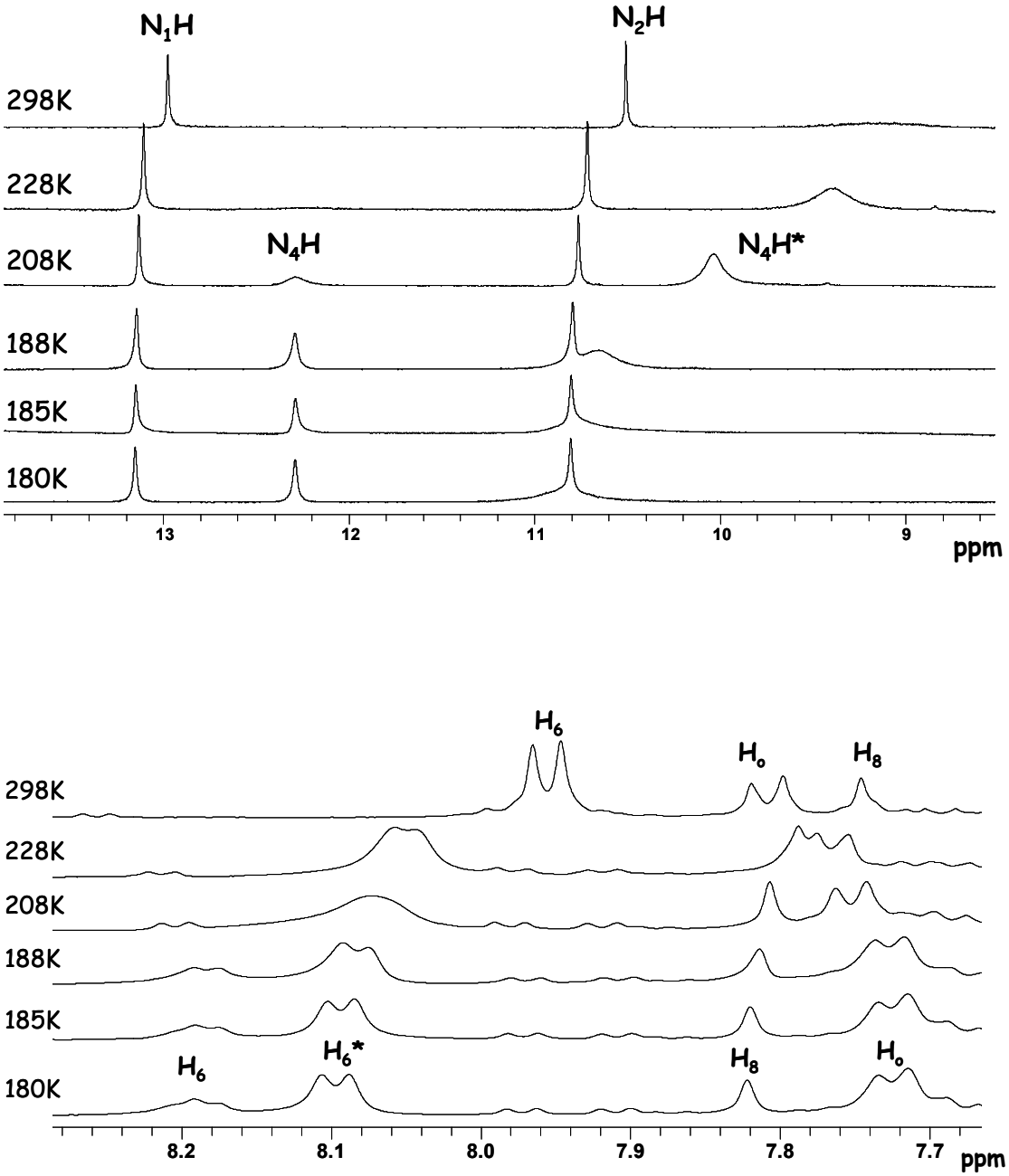

Figure 5.19 Partial variable temperature ^{1}H NMR spectra of [**2.1b-G]:[4-C**]$_4$ (CD_2Cl_2).

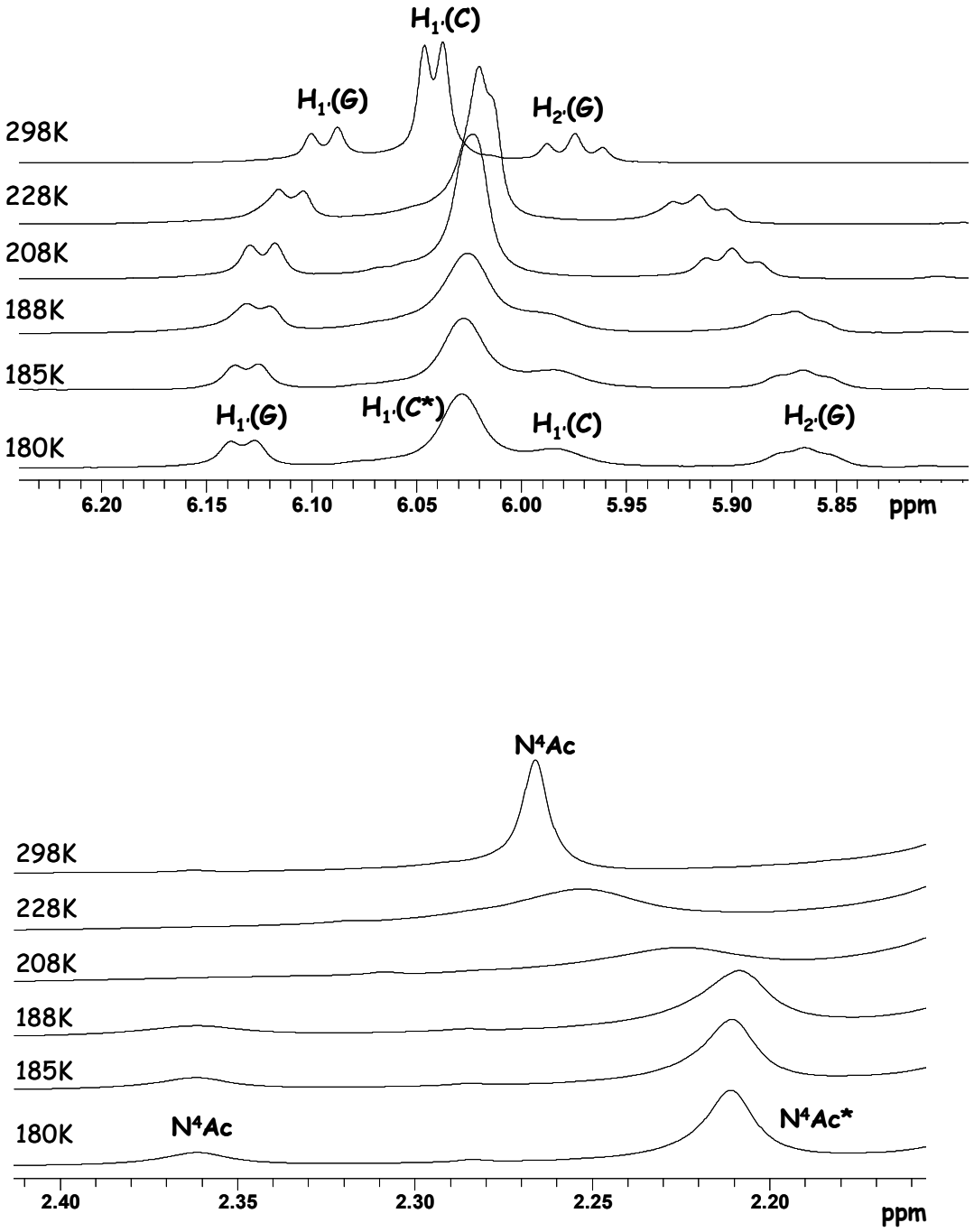

Figure 5.20 Partial variable temperature ^{1}H NMR spectra of [**2.1b-G]:[4-C**]$_4$ (CD_2Cl_2).

To gain structural information about the dynamics of this system and to establish the connectivity between GC pair and the free **4-C***, the NOESY and ROESY NMR were performed. The NOESY NMR was performed for **2.1b** and **2.2b** in the presence of excess **4-C.** The optimal NOESY NMR spectrum at 195 K was obtained with [**2.2b-G**]:[**4-C**]$_2$ and hence it will be used here for investigation of closely related protons. Figure 5.21 shows the strong signature cross peak between the N_2H (G) and N_1H (G) resonances which helps in identification of guanine related protons. Since the location of the chemical shifts of these exchangeable protons of guanine resembles those of the [**2.2b-G**]:[**4-C**] base pair it can be concluded that at 195 K, **2.2b** exists as a part of dimer. The strong NOE correlation between the N_1H (G) and N_4H (C) protons indicative of Watson-Crick H-bonding were also observed thus locking in the [**2.2b-G**]:[**4-C**] base pair structure. It is also worth noting that the NOE interaction between N_1H (G), N_4H (C) and N_4H* (C) with N^4Ac (C) and N^4Ac* (C*) indicate that these protons are in close proximity to each other. To confirm these NOE correlations and to distinguish them from chemical exchange interactions, the ROESY NMR was recorded on the [**2.2b-G**]:[**4-C**]$_2$ at 195 K.

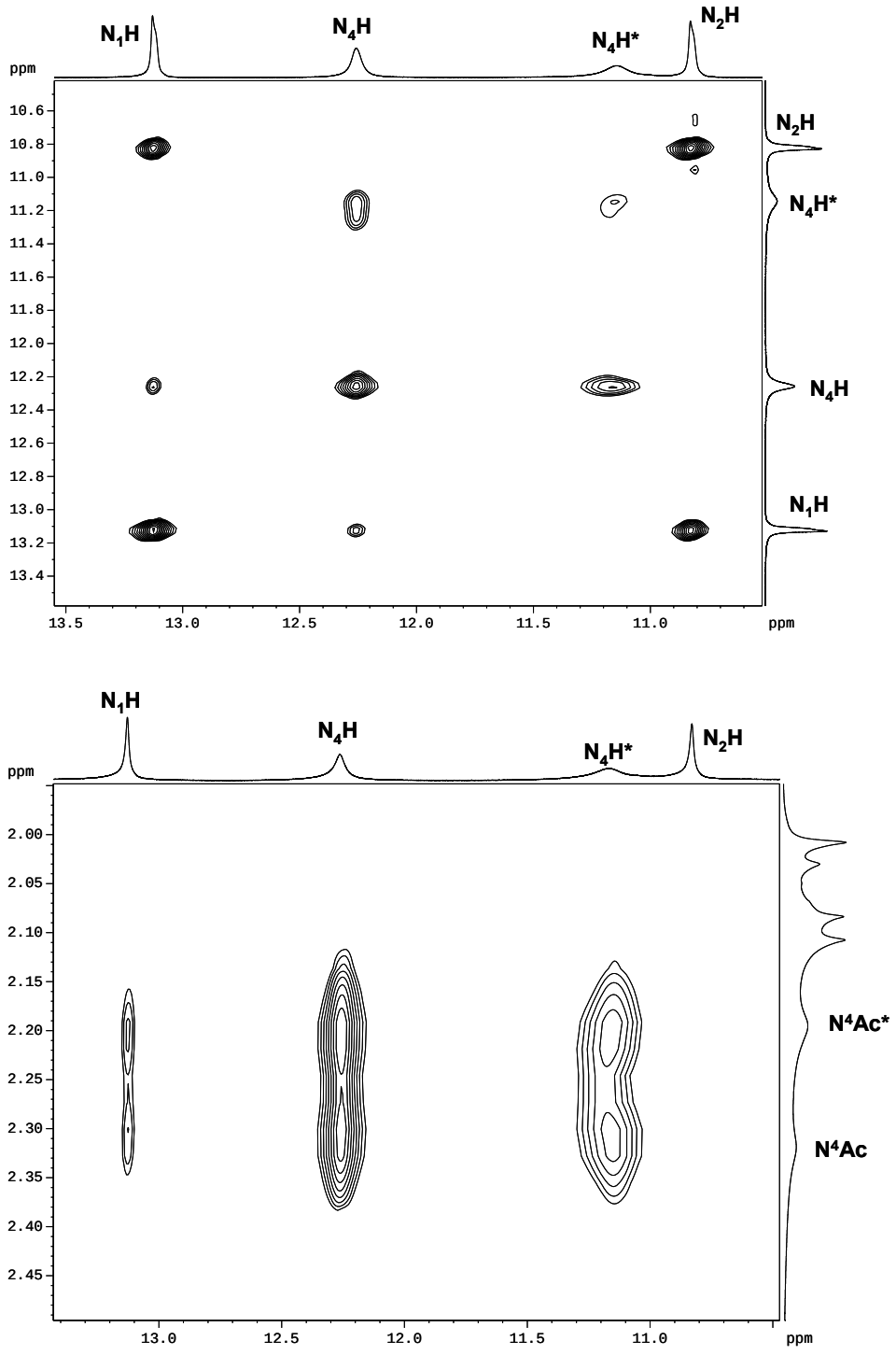

Figure 5.21 Partial NOESY NMR spectra of [**2.2b-G**]:[**4-C**]$_2$ (195 K, CD_2Cl_2).

In the ROESY NMR spectrum of the [**2.2b-G**]:[**4-C**]$_2$ shown in Figure 5.22, clear NOE cross peaks between the bound **4-C** and free **4-C*** were observed, such as N_4H (C)/N^4Ac* (C*) and N_4H* (C*)/N^4Ac (C). Most informative is the chemical exchange interaction presented in Figure 5.23 between following proton pairs: H_6 (C)/H_6^* (C*), H_5 (C)/H_5^* (C*) and $H_{2'}$ (C)/$H_{2'}^*$ (C*). Hence, it can be concluded that there are two types of cytidine, free **4-C*** and bound **4-C**, that undergo chemical exchange with each other, thus explaining the averaging of the **4-C** signals above 208 K. Further, the H_6 (C) proton has NOE cross peaks with H_5 (C) (as expected) but also with H_5^* (C*) protons (Figure 5.24). In addition, the ribose protons associated with **4-C** in the [**2.2b-G**]:[**4-C**] base pair are in close proximity to H_6^* (**4-C***) and vice versa.

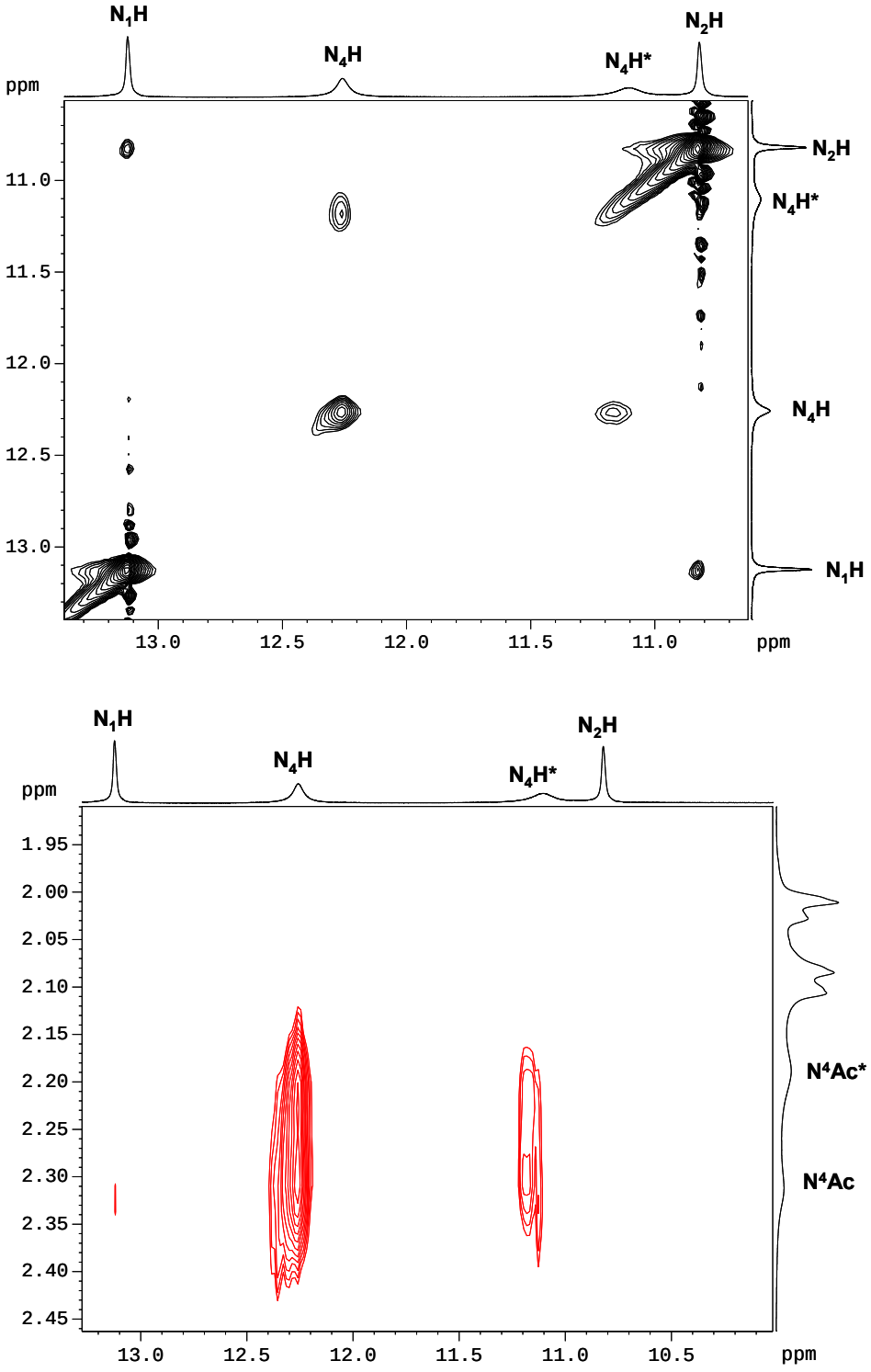

Figure 5.22 Partial ROESY NMR spectra of [**2.2b-G**]:[**4-C**]$_2$ (black-chemical exchange; red-NOE, 195 K, CD_2Cl_2).

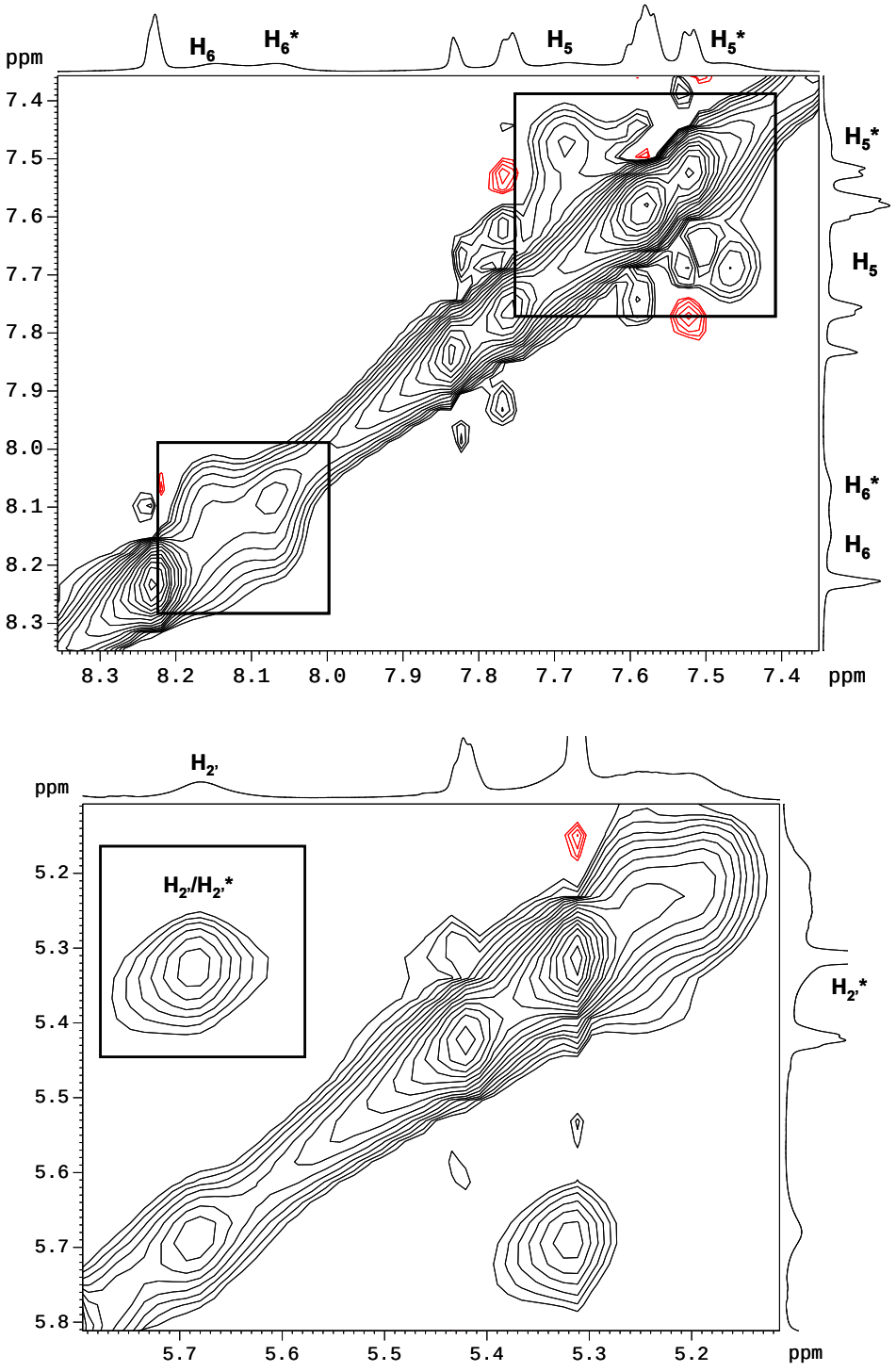

Figure 5.23 Partial ROESY NMR spectra of [**2.2b-G**]:[**4-C**]$_2$ (black-chemical exchange, 195 K, CD_2Cl_2).

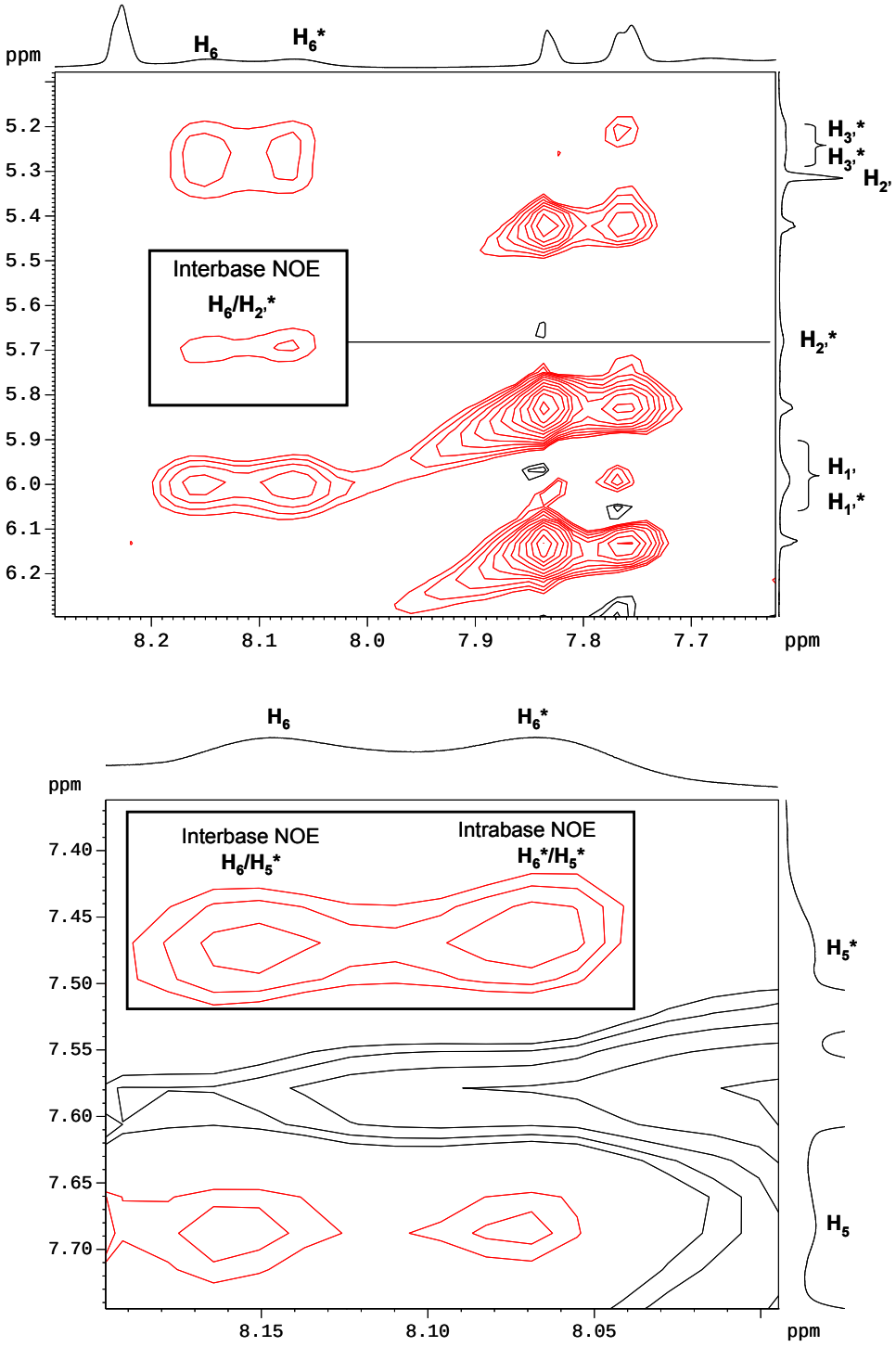

Figure 5.24 Partial ROESY NMR spectra of [**2.2b-G**]:[**4-C**]$_2$ (black-chemical exchange, red-NOE, 195 K, CD_2Cl_2).

5.3.2.2 Proposed exchange pathway of GC base pair with ***4-C****

These NMR findings rule out the possibility of the planar trimeric structure where a **4-C*** would bind at the Hoogsteen edge of GC base pair. Since $\mathbf{N^2G}$ does not exhibit NOE with the H_6* (C*) and H_5^* (C*) protons, the possibilities of π - π interactions between the $\mathbf{N^2G}$ in GC pair and **4-C*** are unlikely. Rather, π - π stacking interactions between **4-C** in GC pair and free **4-C*** are more likely. The proposed intermediate, based on NMR data, is formed by the interactions between GC pair and free **4-C*** as depicted in Figure 5.25.

From the above NMR results, it can be concluded that the exchange between GC base pair and free **4-C*** is fast, resulting in the averaging of all cytidine chemical shifts, above 208 K. These conclusions are further supported by the NOESY and ROESY NMR data at 195 K, which show evidence of GC base pair and of chemical exchange between free **4-C*** and **4-C** molecule within GC base pair. The overall proposed exchange pathway is presented in Figure 5.25. Since the peak broadening occurs at ~ 208 K, the coalescence method was used to determine the values for the exchange rate k_c and the activation free energy $\Delta G^{\ddagger}$ for the processes to be 88 s^{-1} and 43 $kJmol^{-1}$, respectively. The exchange is fast enough so that the ^1H resonances of exchangeable protons of guanine do not experience a large change but rather remain sharp.

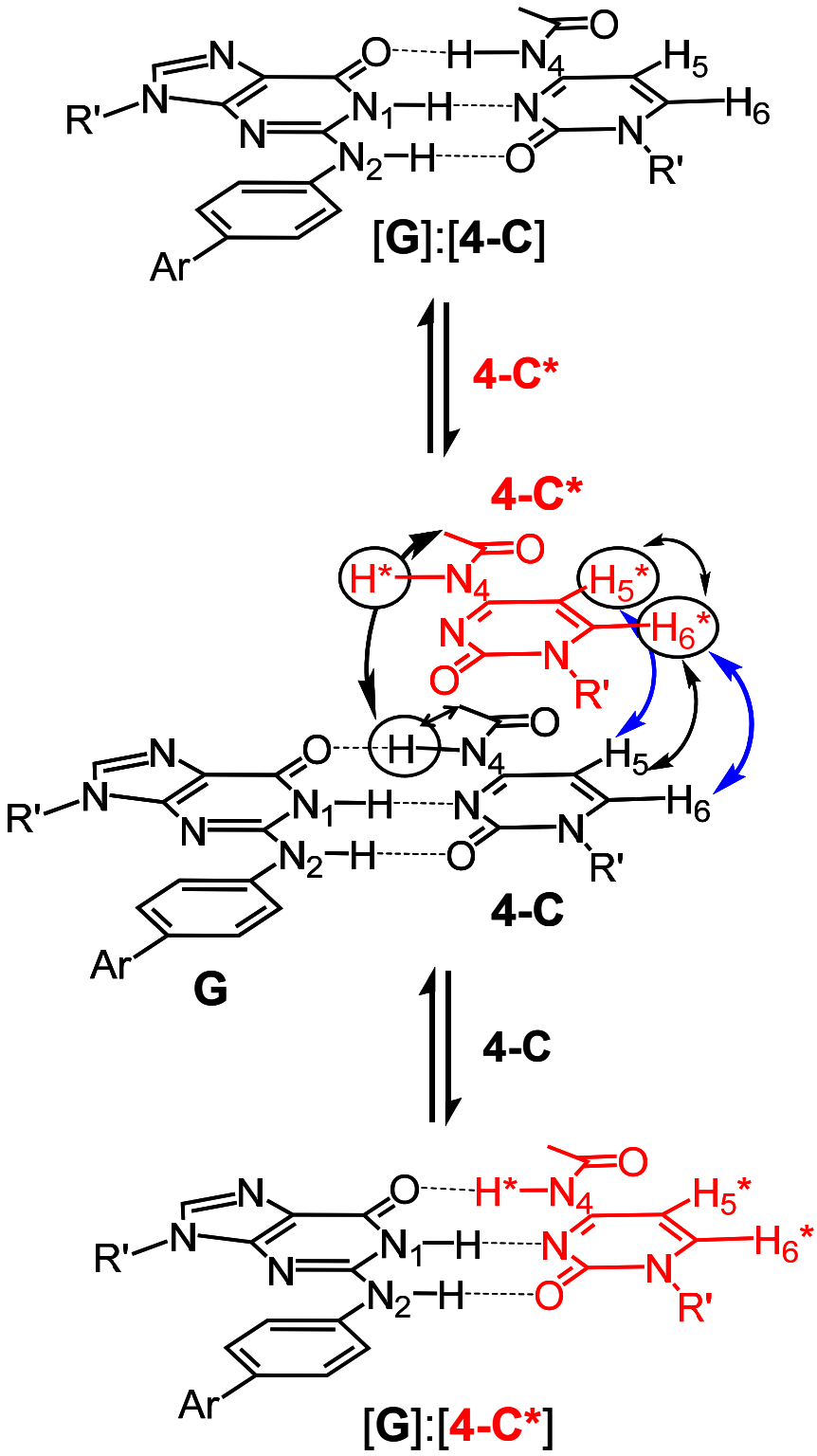

Figure 5.25 Proposed exchange pathway in [**G**]:[**4-C**]$_n$ (n > 1) and intermediate (intra- and internucleobase NOE interactions (blue = chemical exchange, black = NOE)).

It should be pointed out that the behaviour observed for **2.1b** and **2.2b**, is not limited to **N^{2}Gs**, because unmodified guanosine such as **TAG** behaves similarly. ^{1}H NMR titration of **TAG** solution with **4-C** results in the broadening of exchangeable N_1H (G) and N_4H (C) which move downfield while N_2H_2 (G) remains broadened due to the free rotation about C-N bond. In the presence of excess **4-C**, N_1H (G) sharpens up, N_4H (C) remains broadened and moves upfield while N_2H_2 (G) remains unchanged, further supporting that the dynamic behavior of [**G**]:[**C**]$_n$ when n > 1 is not limited to **N^{2}G**.

5.3.3 G-Octamer-to-GC base pair structural transition

The fluorescent *tt* octamer, [**G**]$_8$•K$^+$, formed by the lipophilic **N^{2}Gs** as described in Chapter 3 is shown in Figure 5.26 (simplified structure). To investigate the competition between G-quartet and GC base pair, [**2.1b-G**]$_8$•K$^+$[picrate]$^-$ was examined. Its stability toward **4-C** was probed using NMR, fluorescence and CD spectroscopy.

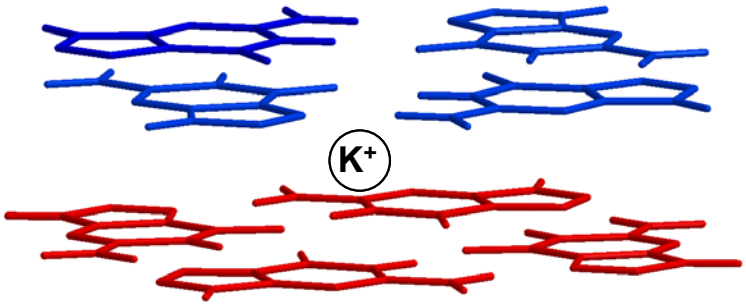

Figure 5.26 Structural representation of [**G**]$_8$•K$^+$.

5.3.3.1 NMR study

In Figure 5.27, the addition of **4-C** solution to the [**2.1b-G**]$_8$•K^+ solution causes a gradual decrease in the intensity of the N_1H (G) and N_2H (G) protons which are involved in the G-quartet formation. The decrease in the [**2.1b-G**]$_8$•K^+ population is followed by the appearance of the new set of peaks related to the [**2.1b-G**]:[**4-C**] base pair. The distinct chemical shifts associated with the [**2.1b-G**]$_8$•K^+ and [**2.1b-G**]:[**4-C**] base pair suggest that a very slow chemical exchange exists, if any, between the two species. The addition of ~ 1 equivalent of **4-C** leads to a complete conversion to the [**2.1b-G**]:[**4-C**] dimer. In the presence of excess **4-C** the chemical exchange phenomenon occurs that is similar to that observed for the monomer **2.1b** in the presence of excess **4-C**, which was also confirmed by the NOESY NMR data. The detailed mechanism of the G-octamer-to-GC base pair transformation is not known yet. It is noteworthy that [**2.1b-G**]$_8$•K^+ dimerizes rather weakly with **4-C** compared to monomer **2.1b**. This may be attributed to the stability of [**2.1b-G**]$_8$•K^+ exerted by H-bonds, ion-dipole interactions between K^+ and guanine units, and π - π stacking interactions between two G-quartets when **N^2G** is used as the building unit. Unlike **N^2Gs**, unmodified lipophilic guanosine, **TAG**, self-assembles into the poorly defined aggregates in the presence of K^+ ions. As a result, the G-quartet-to-GC base pair structural transformation cannot be easily studied using **TAG**. Indeed, N^2-modification of guanosine simplifies the study of G-quartet-to-GC base pair transformation.

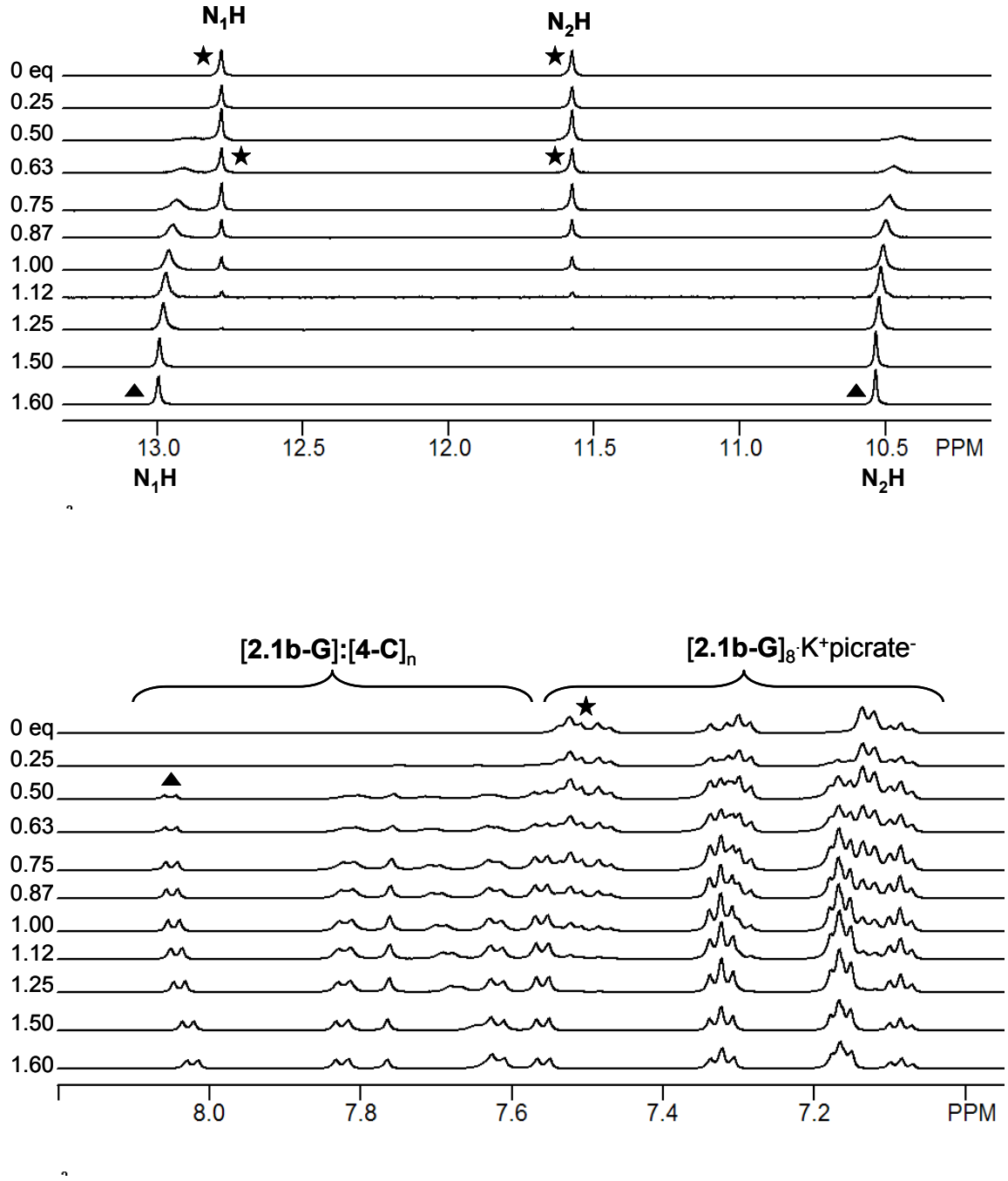

Figure 5.27 ^{1}H NMR titration of [**2.1b-G**]$_8$•K$^+$[picrate]$^-$ with **4-C** ([**2.1b**] = 1 x 10^{-3} M, CD_2Cl_2, star is [**2.1b-G**]$_8$•K$^+$[picrate]$^-$, triangle is [**2.1b-G**]:[**4-C**]$_n$).

5.3.3.2 CD study

The G-octamer-to-GC dimer transformation was also monitored by CD spectroscopy. While CD was not very useful in the titration of monomer N^2-guanosines, **2.1b** or **2.2b**, it proved to be an important tool for the study of competition between GC and G-quartet in general. Unlike monomer **2.1b** which has a very weak CD signature, the CD spectrum of the $[\mathbf{2.1b\text{-}G}]_8 \bullet K^+[picrate]^-$ displays the characteristic stacked G-quartet signature peaks including the negative exciton couplet at 292 nm, the negative bands at 310 and 350 nm and the positive bands at 266 and 285 nm. Not surprisingly, the addition of **4-C** causes the decrease of the negative exciton couplet and the CD signature peak is dominated by that of **4-C**, as shown in Figure 5.28. The CD spectrum after addition of 1.8 eq of **4-C** resembles that of non-bound **4-C*** and cannot be used to extract any data in terms of exchange between the two species. However, such a dramatic change in CD signature is not common for the other G-quadruplex-to-duplex systems which suggests that N^2-modified guanosine model systems can be used as the effective sensing tools for the study of $[\mathbf{G}]_8$-to-GC transformation.

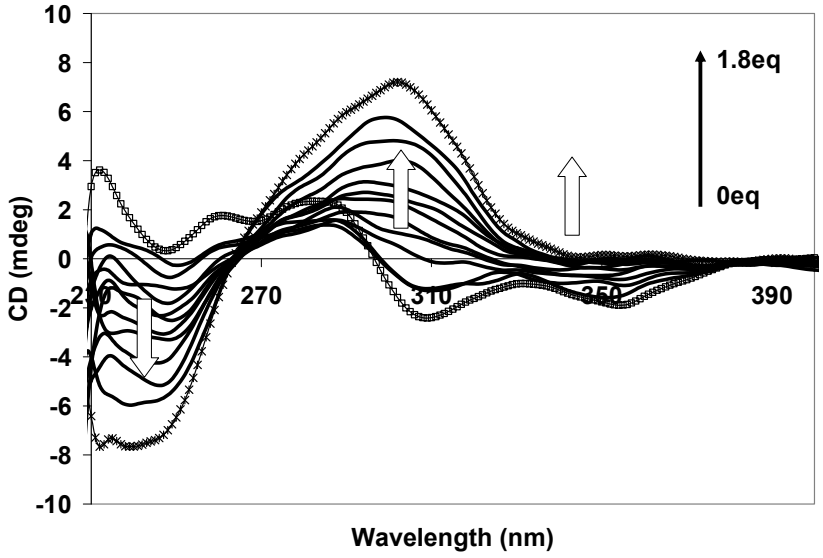

Figure 5.28 CD titration spectra of [**2.1b-G**]$_8$•K^+[picrate]$^-$ with **4-C** (CH_2Cl_2, [**2.1b**] = 1 x 10^{-5} M).

5.3.3.3 Fluorescence study

In Chapter 3 it was established that [**2.1b-G**]$_8$ and **2.1b** have similar fluorescent emissions. Fluorescence spectroscopy was therefore used to monitor the interactions of fluorescent [**2.1b-G**]$_8$ with **4-C**. As seen in Figure 5.29, the addition of **4-C** to the solution of octamer results in the overall quenching of fluorescence, similar to that observed for the intearctions of **2.1b** with **4-C,** supporting the formation of GC base pair. The fluorescence spectroscopy could only be qualitatively used to probe G-quartet-to-GC change, due to the fact that a complex equilibrium exists, which further complicates the study.

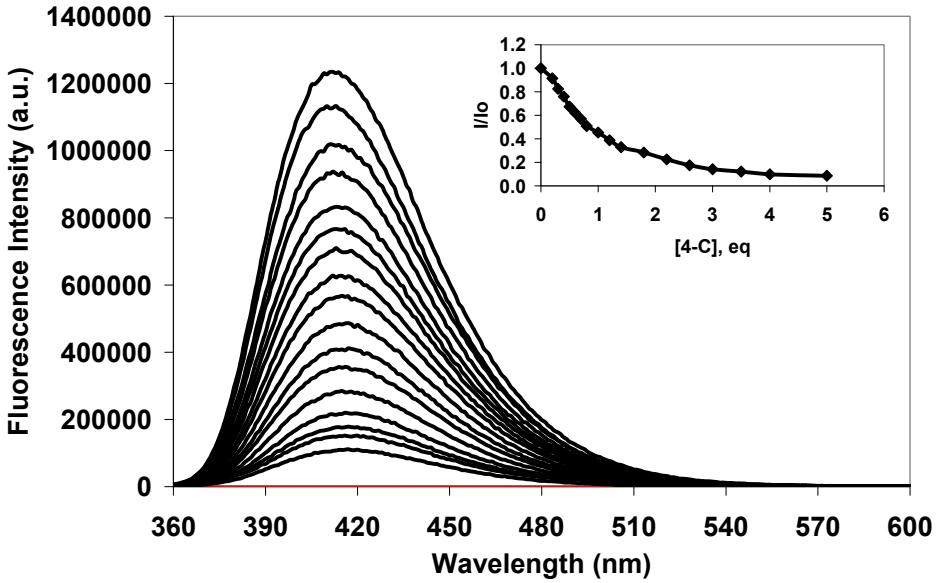

Figure 5.29 Fluorescence titration data of [**2.1b-G**]$_8$•K^+[picrate]$^-$ with **4-C** (CH_2Cl_2, [**2.1b**] = 1 x 10^{-5} M).

5.4 Conclusions

We have investigated the GC base pair formation between acetylated **N^{2}Gs** and **4-C**, by using NMR, fluorescence, and CD spectroscopy. From the steady-state fluorescence study, it can be concluded that exclusively a three point H-bonding, as seen in the Watson-Crick motif, leads to the "turn-off" fluorescent response *via* charge transfer mechanism.

In the presence of excess **4-C**, the chemical exchange takes place between free and bound **4-C**. The π - π stacking between free and bound cytidine molecules has been proposed as the driving force for the intermediate formation in the classical exchange process involving GC pair and the free cytidine **4-C***.

Fluorescent [**G**]$_8$ has also been successfully used to study the G-octamer-to-GC base pair structural transformation.

5.5 References

[1] (a) Williams, N. G.; Williams, L. D.; Shaw, B. R. *J. Am. Chem. Soc.* **1989**, *111*, 7205. (b) Williams, L. D.; Williams, N. G.; Shaw, B. R. *J. Am. Chem. Soc.* **1990**, *112*, 829. (c) Kyogoku, Y.; Lord, R. C.; Rich, A. *Science* **1966**, *154*, 518.

[2] (a) Harriman, A.; Magda, D. J.; Sessler, J. L. *J. Phys. Chem.* **1991**, *95*, 1530. (b) Harriman, A.; Magda, D. J.; Sessler, J. L. *J. Chem. Soc., Chem. Commun.* **1991**, 345. (c) Sessler, J. L.; Jayawickramarajah, J.; Gouloumis, A.; Pantos, G. D.; Torres, T.; Guldi, D. M. *Tetrahedron* **2006**, *62*, 2123. (d) Sessler, J. L.; Lawrence, C. M.; Jayawickramarajah, *J. Chem. Soc. Rev.* **2007**, *36*, 314.

[3] Kawai, T.; Ikegami, M.; Kawai, K.; Majima, T.; Nishimura, Y.; Arai, T. *Chem. Phys. Lett.* **2005**, *407*, 58.

[4] (a) Champeil, E.; Pradhan, P.; Lakshman, M. K. *J. Org. Chem.* **2007**, *72*, 5035. (b) Kim, H. Y. H.; Cooper, M.; Nechev, L. V.; Harris, C. M.; Harris, T. M. *Chem. Res. Toxicol.* **2001**, *14*, 1306.

[5] (a) Munoz de la Pena, A.; Slinas, F.; Gomez, M. J.; Acedo, M. I.; Pena, S. M. *Incl. Phenom. Mol. Recogn. Chem.* **1993**, *15*, 131. (b) Connors, K. A. *Binding Constants. The Measurement of Molecular Complex Stability;* John Wiley & Sons: New York, 1987.

[6] (a) Encinas, S.; Simpson, N. R.; Andrews, M. D.; Ward, C. M.; White, C. M.; Armaroli, N.; Barigelletti, F.; Houlton, A. *New J. Chem.* **2000**, *24*, 987. (b) Harriman, A.; Kubo, Y.; Sessler, J. L. *J. Am. Chem. Soc.* **1992**, *114*, 388. (c) Sessler, J. L.; Jayawickramarajah, J.;

Goulomis, A.; Torres, T.; Guldi, D. M.; Maldonado, S.; Stevenson, K. J. *Chem. Commun.* **2005**, 1892.

[7] Schwalb, N. K.; Temps, F. *J. Am. Chem. Soc.* **2007**, *129*, 9272.

[8] Mallajosyula, S. S.; Datta, A.; Pati, S. K. *Synthetic Metals* **2005**, *115*, 398.

[9] Williams, L. D.; Chawla, B.; Shaw, B. R. *Biopolymers* **1987**, *26*, 591.

Chapter 6
Interactions of N^2-Arylguanosines with Group 12 Metal ions

6.1 Introduction

Despite the extensive interest in metallo-G-nucleosides,[1] little is known about the potential of fluorescent G-nucleoside sensors/probes for detecting metal ions. The fluorescent **N^2Gs**, described in Chapter 2, can act as the potential sensing probes for metal ions, due to their chelating ability. To demonstrate the potential use of **N^2G** in metal ion sensing, Group 12 metal ions were investigated with the emphasis on Zn^{2+}, because of its biological importance.[2] First, numerous enzymes[3] require Zn^{2+} in their active sites for structural, chemical, and regulatory function. Many nucleic acid polymerases[4] require Zn^{2+} to catalyze the template-directed synthesis of oligonucleotides as well as take part in RNA/DNA hydrolysis.[5] Second, zinc centers in the protein, such as "zinc-fingers",[6] are involved in the control of gene expression. Third, Zn^{2+} stabilizes the structures of nucleic acids as in pyrimidine-purine-purine triplex.[7] These are some of the valid reasons for studying the Zn^{2+}-nucleobase interactions. Despite this interest, sensing and monitoring Zn^{2+} levels is challenging due the spectroscopically silent nature of Zn^{2+}.

For this purpose, compounds **2.1a – 2.3a** were investigated (Figure 6.1) by using fluorescence, CD, UV-Vis, and NMR spectroscopies and ESI MS spectrometry. The non-chelate guanosine **2.1a** was a control molecule used to elucidate the impact of the guanine unit and the chelate groups in **2.2a** and **2.3a** on the metal ion binding. The investigation of the metal ion-nucleobase interactions was extended to Cd^{2+} and Hg^{2+} ions, due to their

hazardous impact on the environment and human health. In addition, the effects of anions on the fluorescence, UV-Vis and CD absorption were also investigated. The results are provided and discussed in the chapter herein.

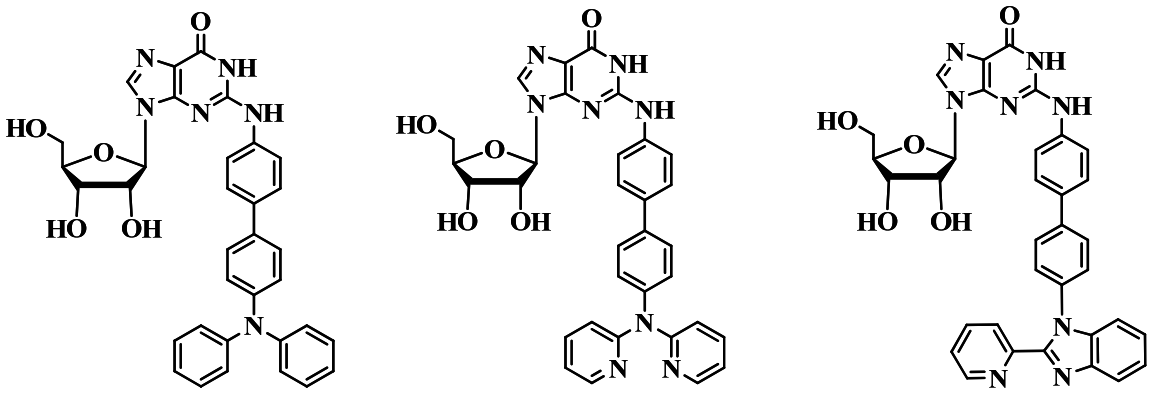

2.1a **2.2a** **2.3a**

Figure 6.1 Structures of N^2-modified guanosines **2.1a** – **2.3a** investigated.

6.2 Experimental Procedure

6.2.1 General considerations

All reagents were purchased from the Aldrich Chemical Co. and used without further purification unless stated otherwise. All 1D and 2D NMR experiments (COSY) were recorded on Bruker Avance 400 MHz or 500 MHz spectrometers at 298 K, unless otherwise specified, with the solvent peaks used as the reference. Low resolution and high-resolution mass spectrometry experiments were performed using the electrospray ionization mode on QSTAR XL MS/MS Systems using Analyst QS Method. Excitation and emission spectra were recorded on a Photon Technologies International QuantaMaster Model C-60 spectrometer. All UV-Vis spectra were collected by using

Ocean Optics Inc. spectrometer and Spectra Suite software. Circular dichroism (CD) spectra were recorded on a Jasco 715 spectrometer with a 1 cm path length cell at 298 K.

6.2.2 Synthesis of chiral Zn^{2+} salts

The following complexes $Zn[(S)\text{-}O_2CCH(Br)CH(CH_3)CH_3]_2$, $Zn[(R)\text{-}O_2CCH(Br)CH(CH_3)CH_3]_2$, and $Zn[(S)\text{-}O_2CCH(CH_3)CH(CH_3)CH_3]_2$ have been previously prepared in our laboratory by Theresa McCormick and they were used with permission. Typical synthesis involves the use of ZnO (1 mmol) and *(R)* or *(S)*-2-bromo-3-methylbutyric acid or *(S)*-2-methyl-3-methylbutyric acid (2 mmol) in degassed toluene under an inert atmosphere at ambient temperature.

6.2.3 Fluorescence, UV-Vis and CD titrations

Aliquots of 1 μL or 2 μL stock solutions of $Zn(tfa)_2$ ($tfa^- = CF_3CO_2^-$), $Zn(ClO_4)_2$, $Zn(OAc)_2$ ($OAc^- = CH_3CO_2^-$), $Cd(ClO_4)_2$, $Zn[(S)\text{-}O_2CCH(Br)CH(CH_3)CH_3]_2$, $Zn[(R)\text{-}O_2CCH(Br)CH(CH_3)CH_3]_2$, $Zn[(S)\text{-}O_2CCH(CH_3)CH(CH_3)CH_3]_2$, and $Hg(ClO_4)_2$ in dry THF were added to the solutions of **2.1a** - **2.3a** in dry THF (1.7×10^{-5} M, 3×10^{-5} M or 7×10^{-5} M). Due to a minimal dilution upon titration, the binding constants were determined without the volume correction.

6.2.4 NMR titrations

NMR titration experiments were carried out using the following ligand solutions, 1.9×10^{-4} M and 1.3×10^{-4} M, 1.4×10^{-4} M, 1.5×10^{-4} M for **2.1a**, **2.2a** and **2.3a**, respectively in THF-d_8 at room temperature. The solution of $Zn(ClO_4)_2$ or $Zn(tfa)_2$ in THF-d_8 was added incrementally by using a micro-pipette.

6.2.5 Binding constant determination

The binding constants were determined in two ways, using fluorescence and NMR titration data. The fluorescence data for $Zn(tfa)_2$ or $Zn(OAc)_2$ titrations were fitted using the 1:1 (ligand:metal ion (L:M)) model and the expression given in eq 6.1 for the weak binding:[8]

$$\frac{F}{F_o} = 1 + \left(\frac{F_\infty}{F_o} - 1\right)\frac{[M]K}{(1+[M]K)} \qquad (6.1)$$

For the NMR titrations, 1:1 (L:M) binding model was assumed using the expression given in eq 6.2:[8b]

$$\mathbf{L} + \mathrm{M} \rightarrow \mathbf{L}\mathrm{M}$$

$$\delta = \frac{[L]\delta_L + K[L][M]\delta_{\lim} - [M]}{C_L}$$

$$[M] = \frac{(KC_M - KC_L - 1 + \sqrt{[(KC_M - KC_L - 1)^2 + 4KC_M]}}{2K} \qquad (6.2)$$

$$[L] = \frac{(KC_L - KC_M - 1 + \sqrt{[(KC_L - KC_M - 1)^2 + 4KC_L]}}{2K}$$

6.3 Results and Discussion

The crystal growth of Zn^{2+} complexes was unsuccessful; hence, an NMR method was used in order to obtain information about the nature of binding sites. To determine the binding site of the metal ions, the Zn^{2+} complexes of **2.1a – 2.3a** were studied by ^1H NMR in the presence of $Zn(tfa)_2$ and $Zn(ClO_4)_2$ in THF-d_8.

6.3.1 Spectral study of 2.1a with Group 12 metal ions

6.3.1.1 Fluorescence and UV-Vis Study

The non-chelating **2.1a** exhibits overall fluorescent quenching with all Zn^{2+} salts used; however, the overall magnitude of the fluorescent response was highly dependent on the nature of anions. UV and fluorescence titration profiles of **2.1a** in the presence of $Zn(ClO_4)_2$ (Figure 6.2), $Zn(tfa)_2$ (Figure 6.3) and $Zn(OAc)_2$ (Figure 6.4) as shown below. The addition of $Zn(ClO_4)_2$ causes a significant fluorescent quenching (~ 80%), while $Zn(tfa)_2$ or $Zn(OAc)_2$ result in only ~ 40% decrease in the fluorescent intensity. Stern-Volmer plots show that ~ 0.5 equivalent of Zn^{2+} is needed to reach the saturation point when $Zn(ClO_4)_2$ is used, but that ~ 1 equivalent of $Zn(tfa)_2$ or $Zn(OAc)_2$ are required to reach the same point (Figure 6.5). In terms of UV absorbance, the greatest enhancement was observed in the presence of $Zn(ClO_4)_2$. The binding constants were determined for $Zn(tfa)_2$ and $Zn(OAc)_2$ by using 1:1 (ligand (L):metal ion(M)) binding model, and were found to be 2.5 x 10^4 M^{-1} and 8.0 x 10^4 M^{-1}, respectively (Figure 6.6). The experimental results obtained with $Zn(ClO_4)_2$ could not be fit to 1:1 or 1:2 (L:M) binding models. Since the guanine is involved in the lowest electronic transition that gives rise to a blue emission, any interaction between metal ion and guanine should affect the ligand luminescence. Due to the absence of a chelate site in **2.1a**, the fluorescent quenching observed in this ligand must be a direct result of Zn^{2+} interactions with the guanine core *via* most likely the N^7 atom. The N^7-site of guanine represents the major binding site for metal ions.[9] In fact, binding of Zn^{2+} ion at the N^7-site of guanine has been reported previously.[10] In addition, the possibility of H-bonding between O^6 atom of guanine and auxiliary ligands on the metal ion cannot be excluded.

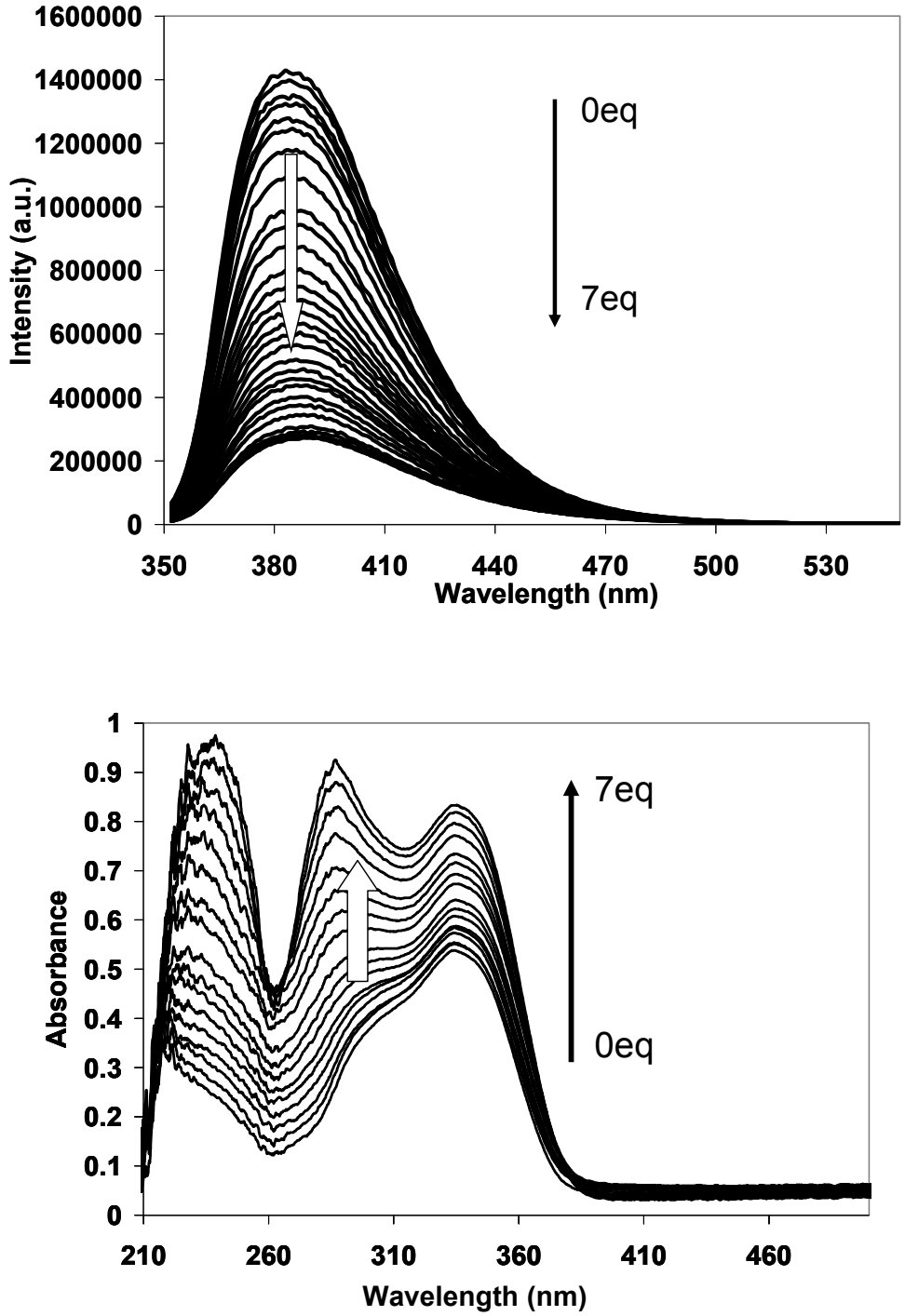

Figure 6.2 Fluorescence (top) and UV-Vis (bottom) titrations of **2.1a** using $Zn(ClO_4)_2$ ([**2.1a**] = 1.7 x 10^{-5} M, THF, λ_{ex} = 358 nm).

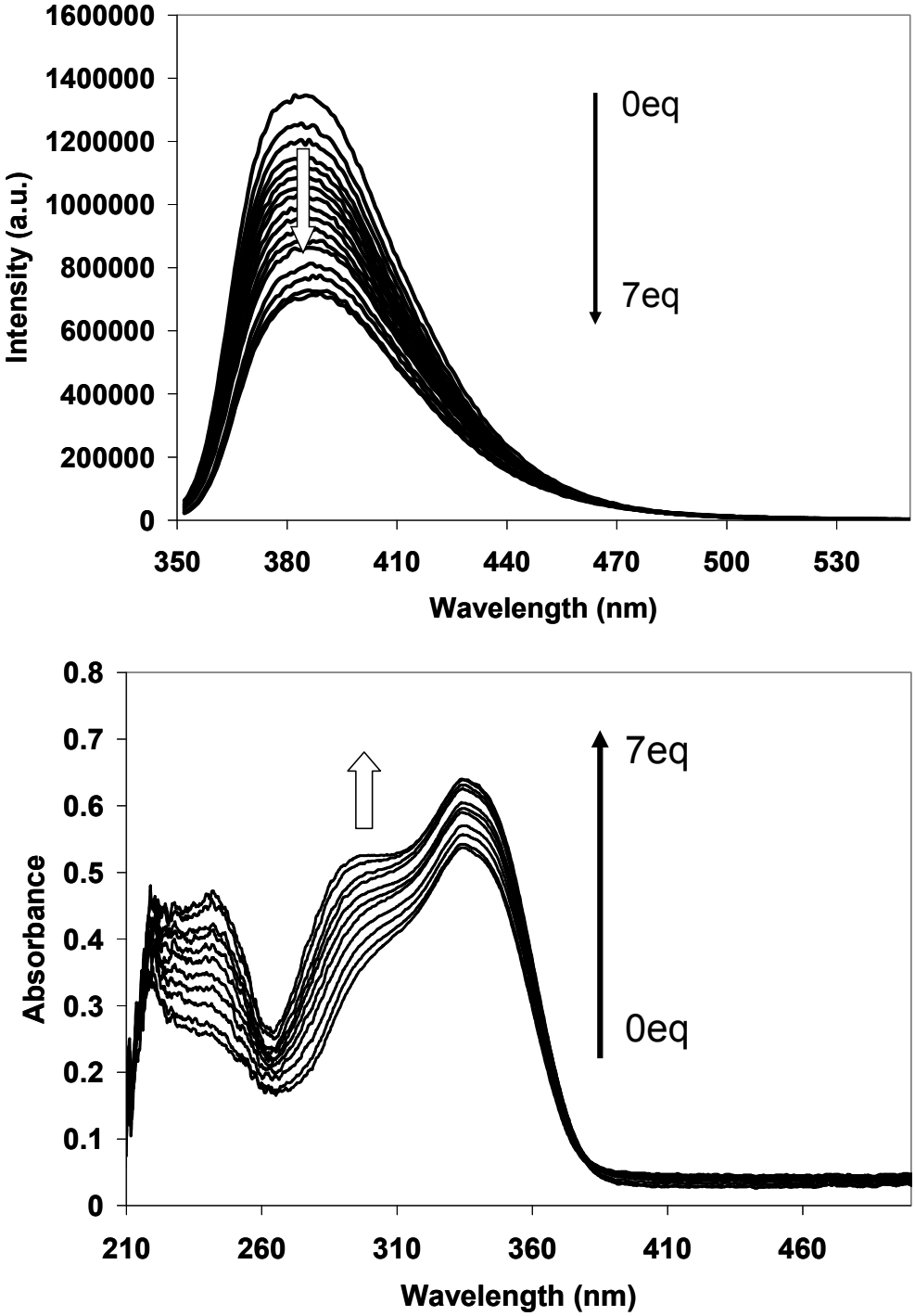

Figure 6.3 Fluorescence (top) and UV-Vis (bottom) titrations of **2.1a** using $Zn(tfa)_2$ [**2.1a**] = 1.7 x 10^{-5} M, THF, λ_{ex} = 358 nm).

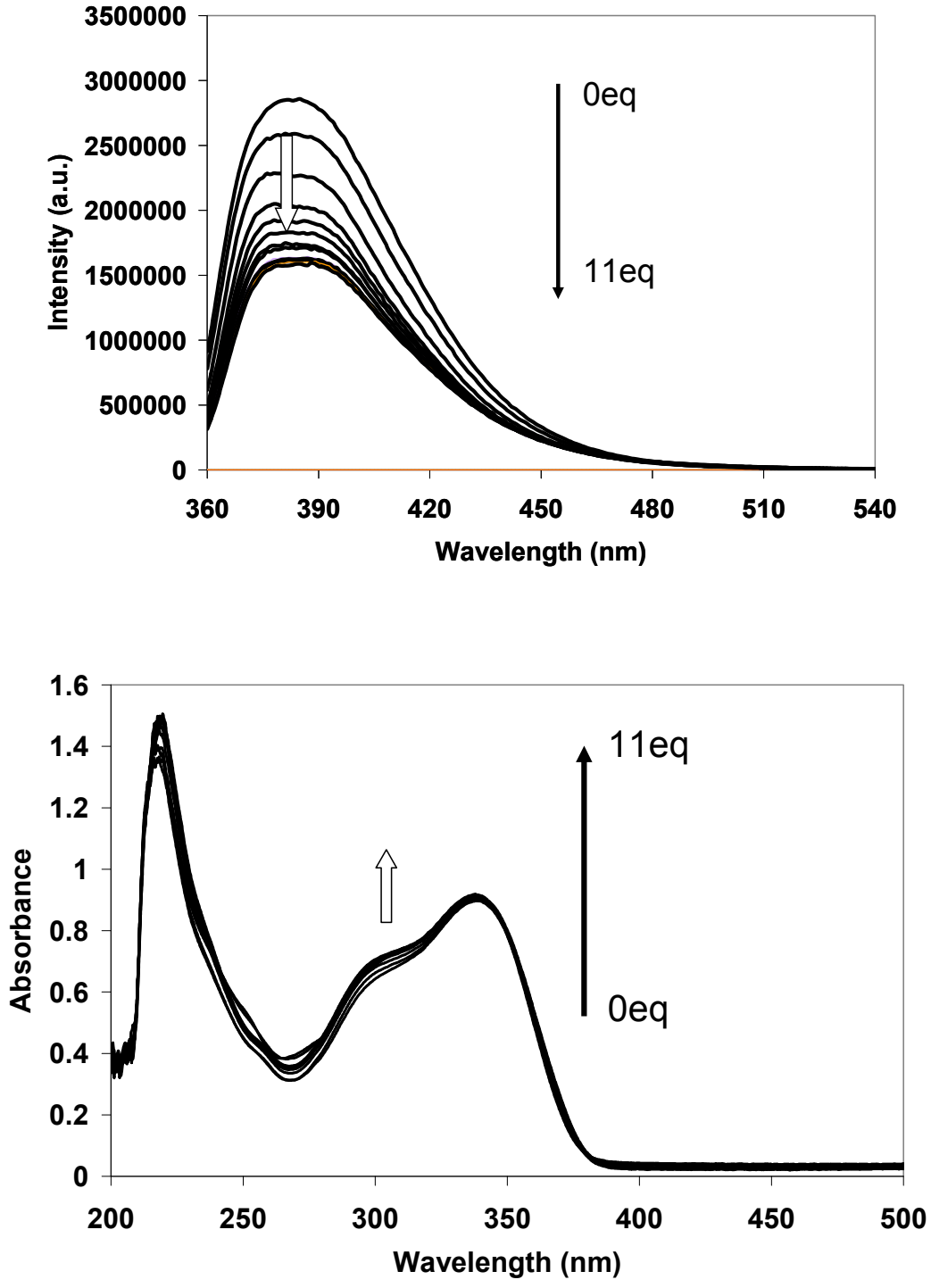

Figure 6.4 Fluorescence and UV-Vis titrations of **2.1a** using $Zn(OAc)_2$ ([**2.1a**] = 1.7 x 10^{-5} M, THF, λ_{ex} = 358 nm).

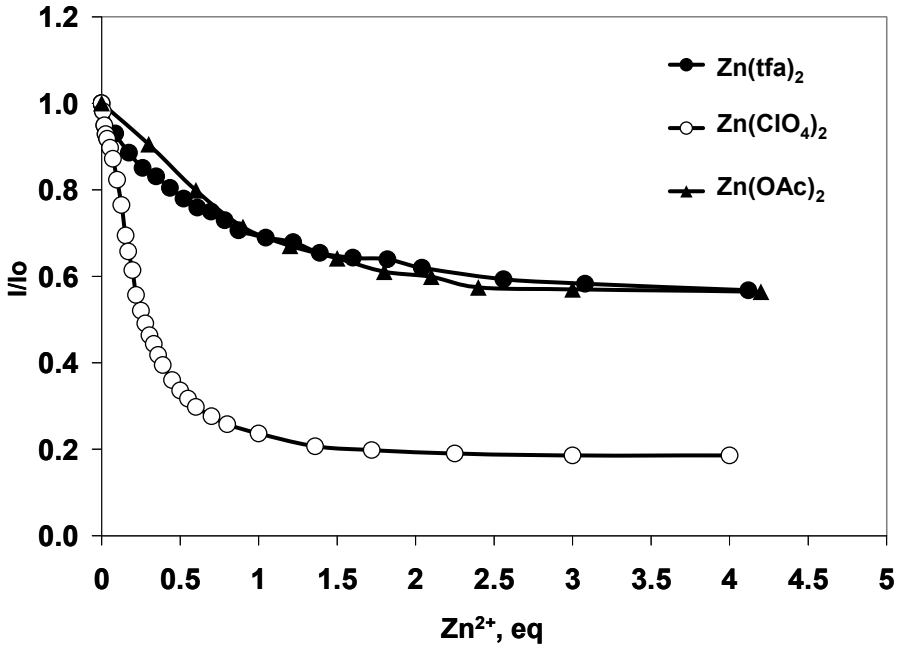

Figure 6.5 Stern-Volmer plots of **2.1a** with various Zn^{2+} salts (THF, λ_{em} = 395 nm).

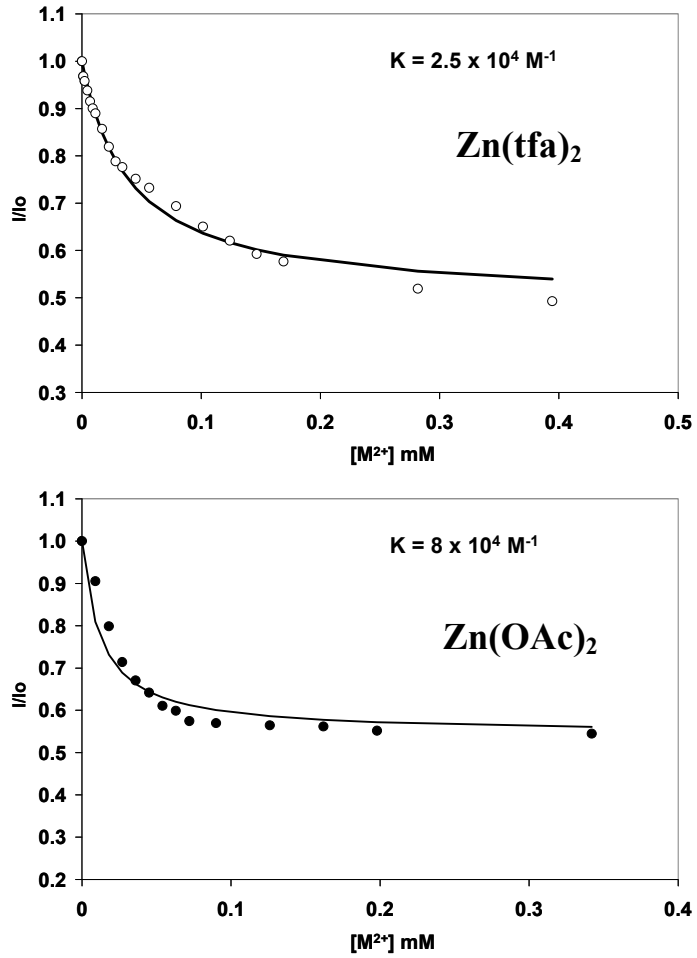

Figure 6.6 Binding constant determination from the fluorescence titrations data of **2.1a** in the presence of $Zn(tfa)_2$ or $Zn(OAc)_2$ in THF.

In order to obtain a complete picture of the interactions between Group 12 metal ions and **2.1a**, zinc congeners, perchlorate salts of Cd^{2+} and Hg^{2+} ions were investigated as well in terms of the fluorescent response. Addition of these metal ions leads to the fluorescent quenching as shown in Figure 6.7. The fluorescent response of **2.1a** is very dependent on the type of metal ion. The extent of the quenching of the emission intensity follows the order: $Cd^{2+} < Zn^{2+} < Hg^{2+}$ as can be seen from Stern-Volmer plots (Figure 6.8).

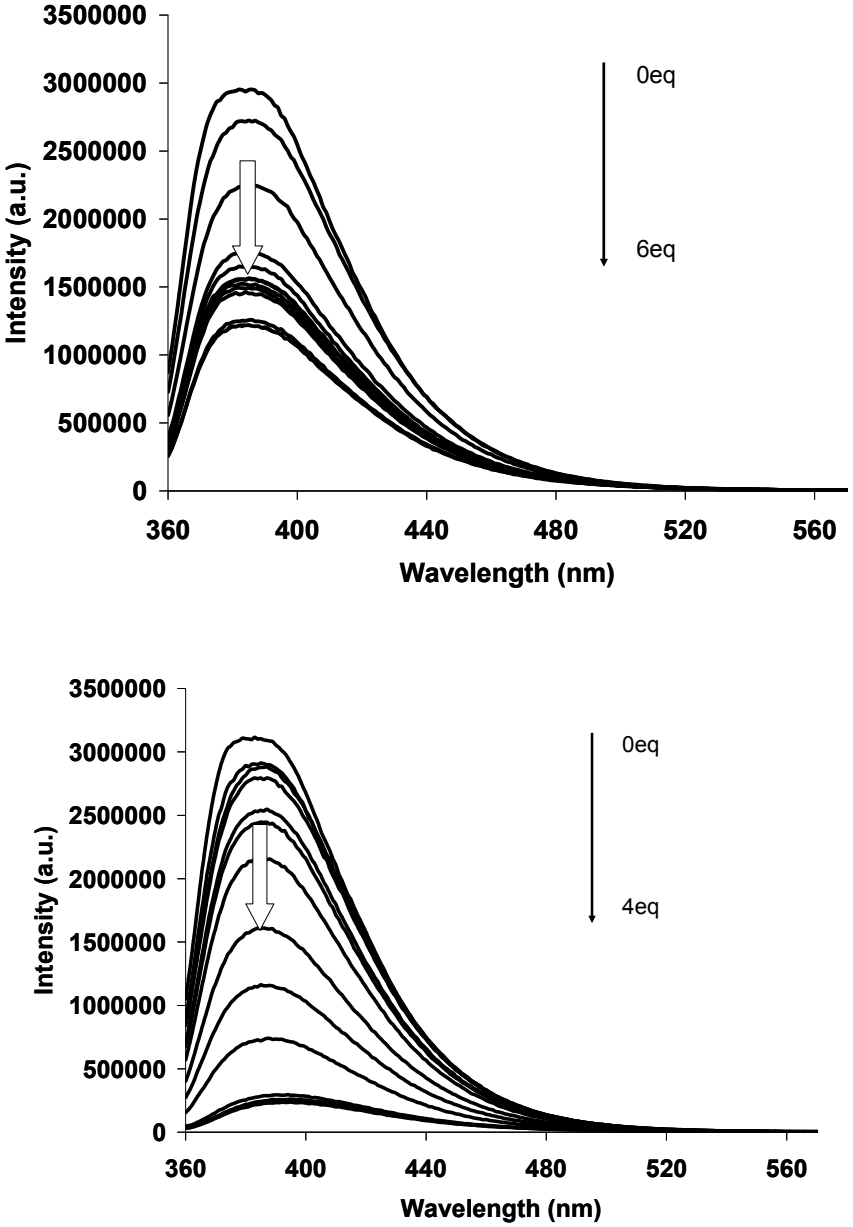

Figure 6.7 Fluorescence titration of **2.1a** with $Cd(ClO_4)_2$ (top) and $Hg(ClO_4)_2$ (bottom) (THF, [**2.1a**] = 7 x 10^{-5} M, λ_{ex} = 358 nm).

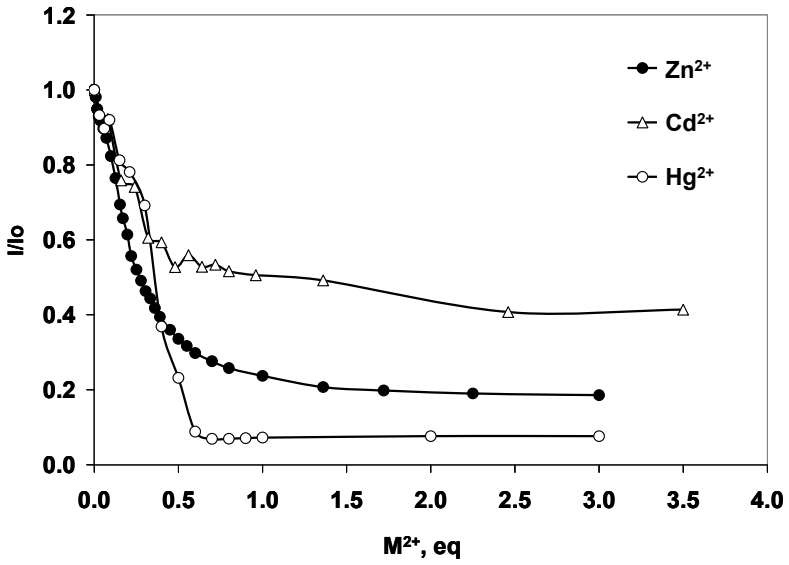

Figure 6.8 Comparison of **2.1a** response towards Group 12 metal ions ($M(ClO_4)_2$, λ_{em} = 395 nm).

*6.3.1.2 NMR Study of **2.1a** with Zn^{2+} ions*

In order to learn more about the nature of interactions between metal ions and **2.1a** we have performed ^1H NMR titration studies using the two representative examples in terms of binding strength, $Zn(ClO_4)_2$ and $Zn(tfa)_2$. The partial ^1H NMR spectra of titration with $Zn(ClO_4)_2$ are shown in Figure 6.9. The addition of Zn^{2+} to the solution of **2.1a**, causes a dramatic downfield chemical shift of the H_8 resonance (~ 1.0 ppm), supporting the idea that Zn^{2+} ion interacts with the N^7-site of the guanine base. A similar downfield shift and broadening of the proton resonances upon Zn^{2+} ion coordination has been reported by Shipman et al.[11] for the complex of $Zn(NO_3)_2$ with a guanine analogue which exhibited a tetrahedral coordination geometry with one guanine bound *via* N^7 site, without participation of the N^3- or O^6-sites. A dramatic downfield shift experienced by exocyclic amine of guanine can also be explained by the formation of the new Zn^{2+} complex, which electronically changes the environment around that amine. A maximum

downfield NMR chemical shift was observed only after 0.5 equivalent of Zn^{2+}, which matches well the fluorescence studies and further suggest the possibility of 2:1 (L:M) complex, with two guanine molecules bound to a single Zn^{2+} center.

^{1}H NMR titration data using $Zn(tfa)_2$ presented in Figure 6.10 clearly show only gradual downfield shift of guanine H_8 proton resonance by ~ 0.3 ppm after over 2 eq of Zn^{2+}. The broadening of all proton signals in the presence of excess Zn^{2+} is due to a medium to fast exchange between the bound and free ligand. The trend is attributable to the relatively strong donor ability of the tfa^- which competes with **2.1a** for the binding to Zn^{2+}. The binding constant was extrapolated from the ^{1}H NMR titration by following the chemical shift change observed for H_8 proton and was found to be ~ 1.8 x 10^5 M^{-1} assuming the 1:1 (L:M) binding fit model.

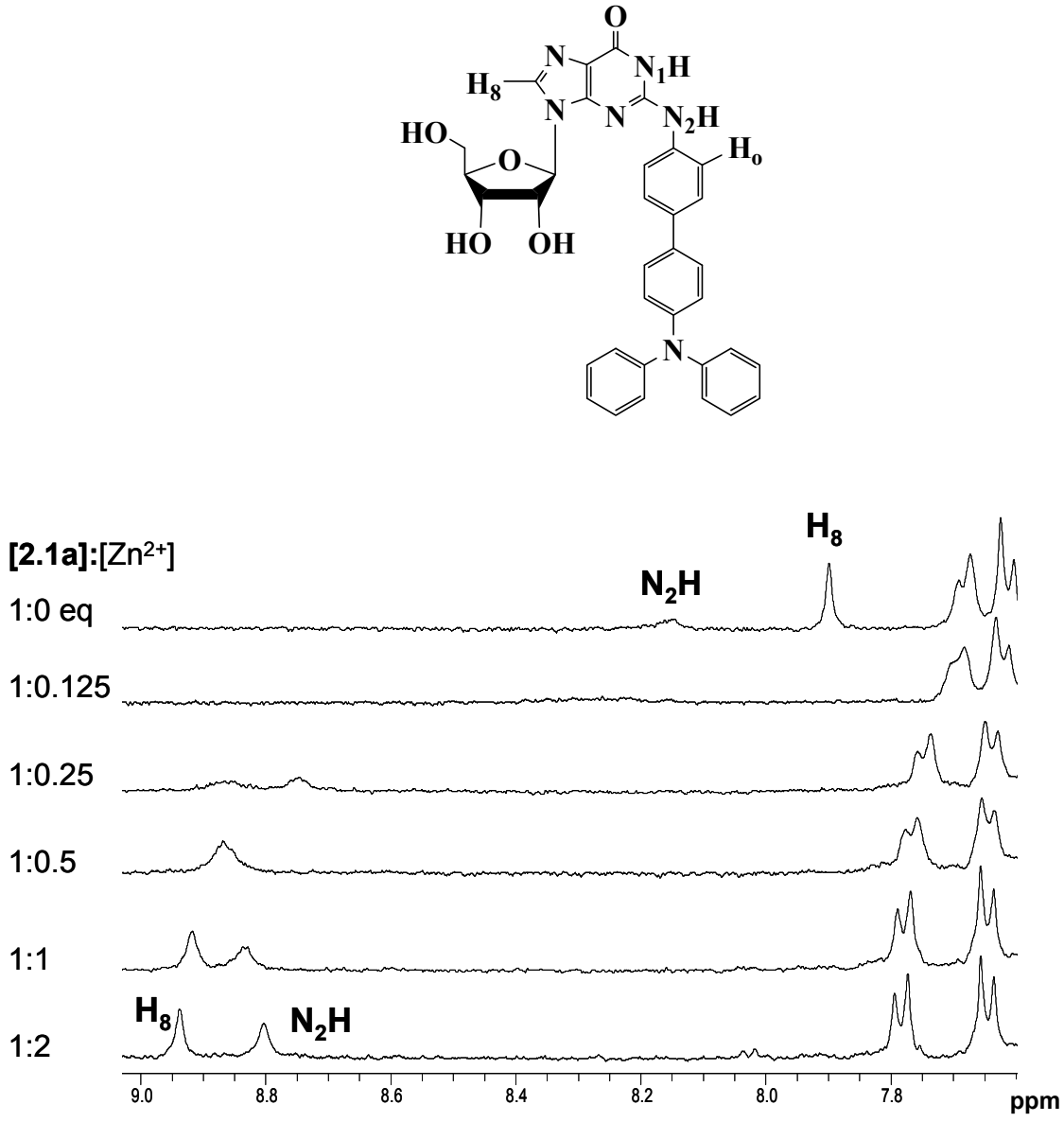

Figure 6.9 Structure of **2.1a** and ^{1}H NMR titration of **2.1a** using $Zn(ClO_4)_2$ (298 K, [**2.1a**] = 1.9 x 10^{-4} M, THF-d_8).

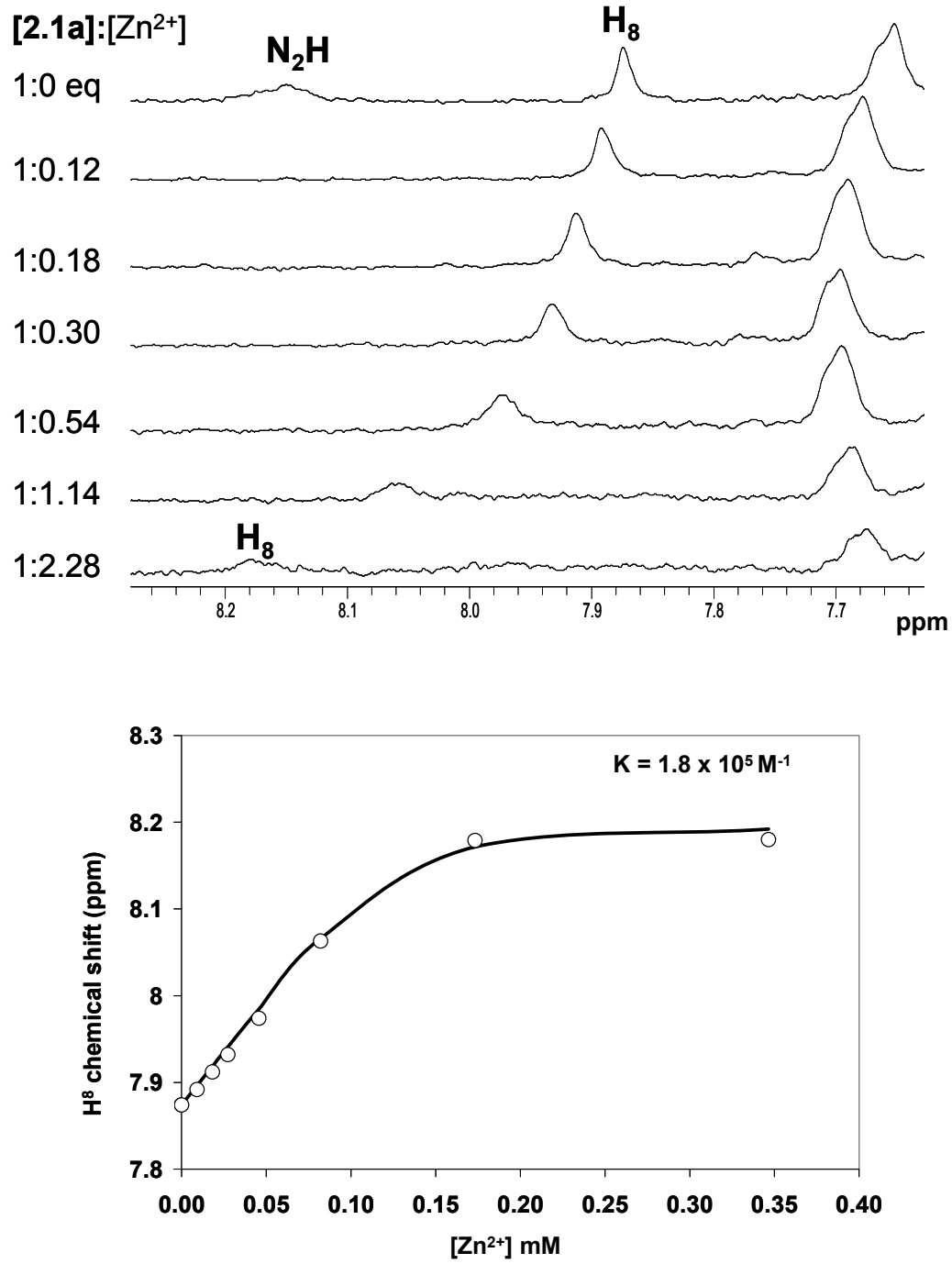

Figure 6.10 ^{1}H NMR titration of **2.1a** using $Zn(tfa)_2$ (298 K, [**2.1a**] = 1.3 x 10^{-4} M, THF-d_8) (top) and binding constant determination (bottom).

6.3.1.3 ESI MS study of ***2.1a*** *with* Zn^{2+} *ions*

In order to gain more information about the stoichiometry of the complexes of **2.1a,** ESI MS study was performed by using 1:1 mixture of **2.1a** and $Zn(ClO_4)_2$. Since ESI MS is incompatible with THF, DMSO was used as the solvent. The full spectrum of 1:1 mixture is not very well defined and contains multiple adducts. Several Zn^{2+} complexes of **2.1a** were identified and are presented in Figure 6.11. It is evident that **2.1a** forms singly charged complexes only. Moreover, a Zn^{2+} dimer, $[2M+K+Zn+2Cl]^+$, is present in the great abundance suggesting that 2:1 (L:M) complexes are highly stable. The characterization of the Zn^{2+} complexes formed by **2.2a – 2.3a** by ESI MS was attempted but unsuccessful.

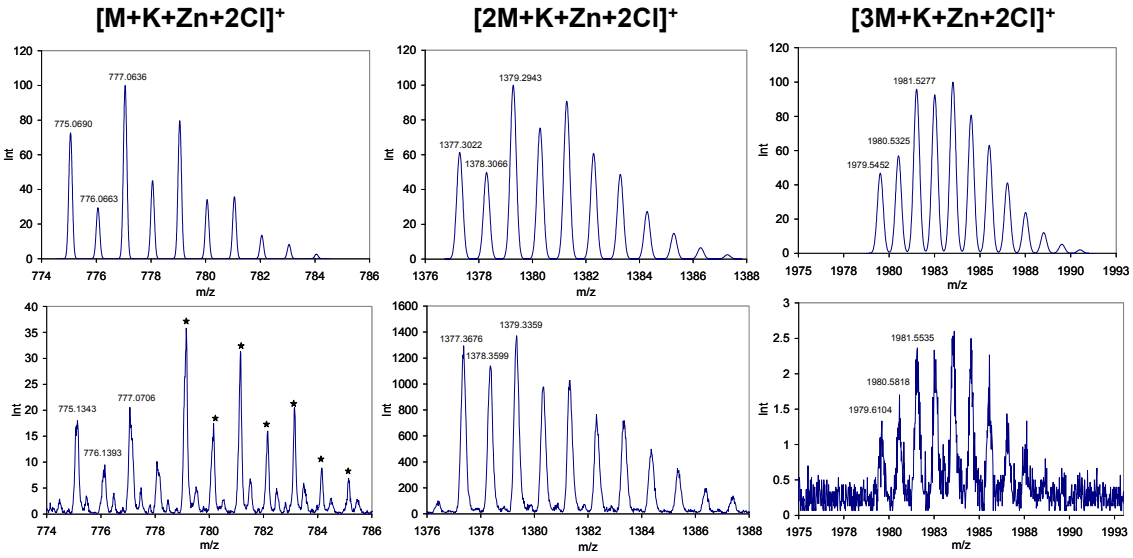

Figure 6.11 Partial ESI MS spectra of various **2.1a** complexes in the presence of $Zn(ClO_4)_2$ in DMSO (top-theoretical and bottom-experimental; stars-unidentified species).

6.3.2 Interaction of 2.2a with Group 12 metal ions

6.3.2.1 Fluorescence and UV-Vis study

Upon addition of any Zn^{2+} salt, the emission of **2.2a** is steadily quenched as demonstrated in Figure 6.12, Figure 6.13 and Figure 6.14. The addition of $Zn(ClO_4)_2$ results in the greatest fluorescent quenching and appearance of an isoemissive point in the spectra at ~ 470 nm (Figure 6.12). As a matter of fact, a weak and broad emission band appears in the 450 – 550 nm region.

Most informative is the UV-Vis titration. The absorption band decreases in intensity and a weak absorption band appears in the 350 - 450 nm region, an indication that $Zn(ClO_4)_2$ may be interacting with both guanine and the 2,2'-dipyridylamino groups in **2.2a**, which is consistent with the appearance of a broad but weak emission band in the fluorescence titration spectra. The isosbestic point, at ~ 350 nm, suggests that two major species coexist, the free and bound ligand. $Zn(ClO_4)_2$ is a more effective quencher than $Zn(tfa)_2$, as seen in the Stern-Volmer plots in Figure 6.15, which can be attributed to the fact that the tfa^- anion is a much stronger donor than the ClO_4^- anion, hence it can compete more effectively with **2.2a** for binding to Zn^{2+} ions than the ClO_4^- anion can.

The binding constant was determined for $Zn(tfa)_2$ binding using 1:1 (L:M) model and was found to be $5.4 \times 10^4\ M^{-1}$ (Figure 6.16). The appearance of a red shifted emission must be related to the coordination to 2,2'-dipyridylamino group rather than guanine in **2.2a**, since the exclusive binding via guanine in **2.1a** did not cause a similar trend. Due to the weak binding of 2,2'-dipyridylamino group, the competition for the Zn^{2+} by guanine cannot be excluded. It has been shown previously in our group that the binding of a Zn^{2+} ion to a 2,2'-dipyridylamino ligand causes fluorescent quenching and a spectral red

shift.[12] We confirmed this by titrating the model compound *p*-2,2'-dipyridylaminoiodobiphenyl (**2.2**) with $Zn(ClO_4)_2$ which showed the appearance of a red-shifted weak emission band with the addition of excess Zn^{2+} ions as can be seen in Figure 6.17.

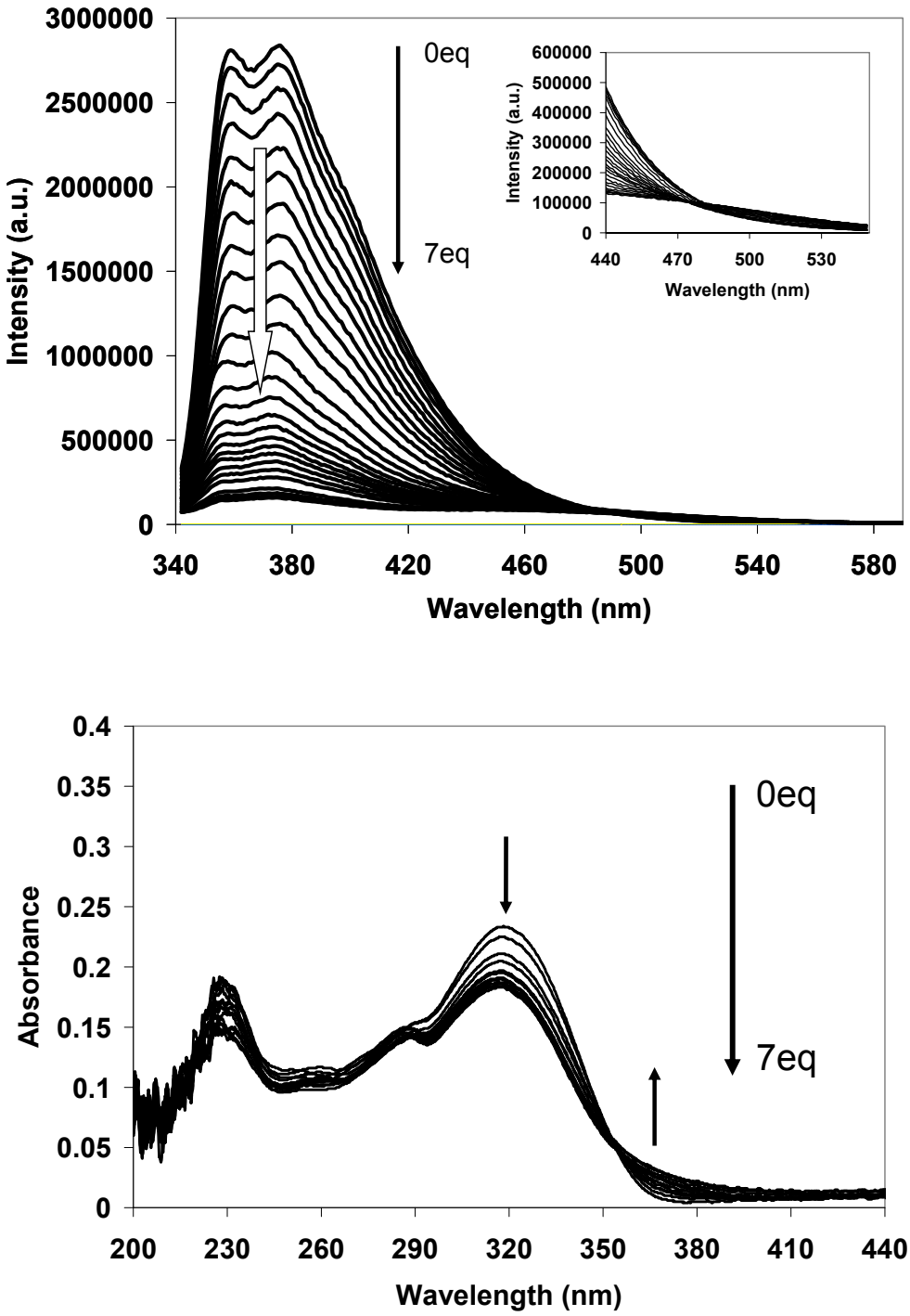

Figure 6.12 Fluorescence and UV-Vis titrations of **2.2a** using $Zn(ClO_4)_2$ ([**2.2a**]=1.7 x 10^{-5} M, THF, λ_{ex} = 346 nm).

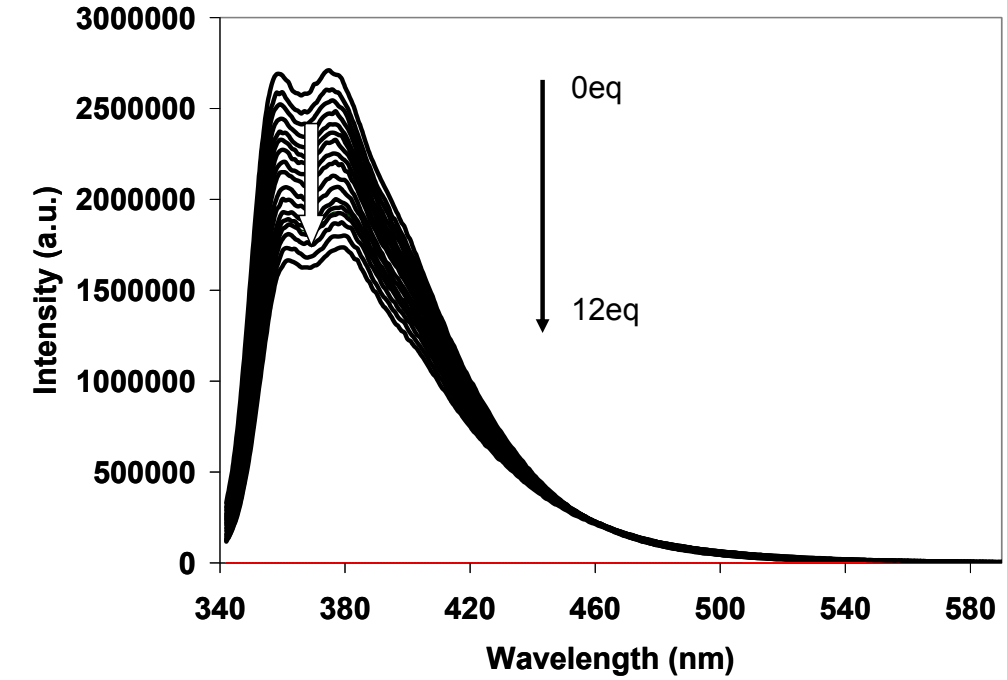

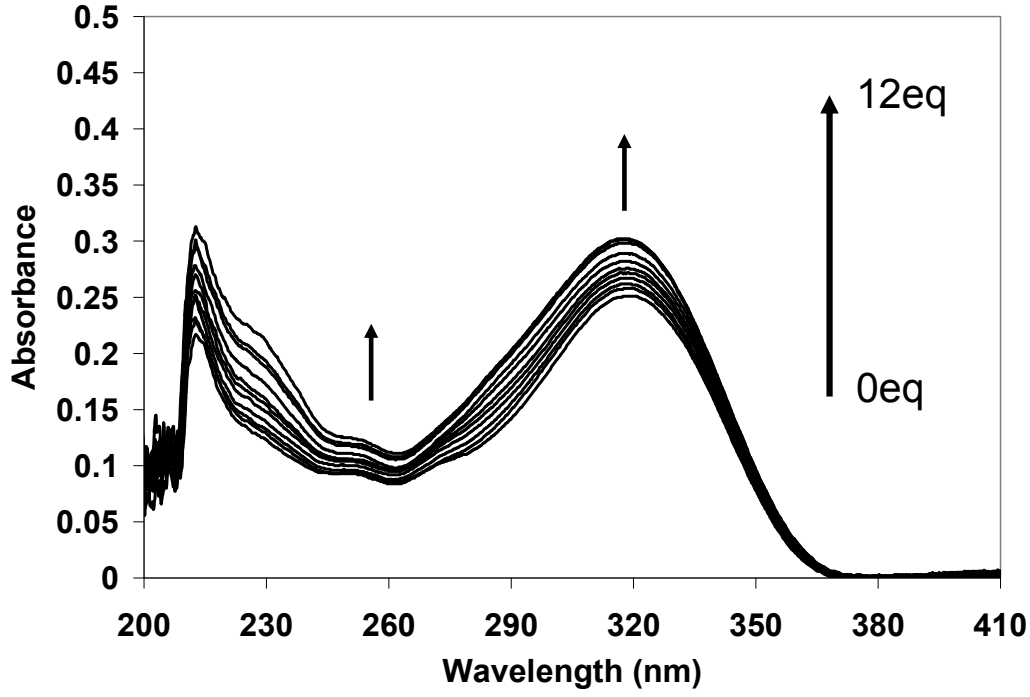

Figure 6.13 Fluorescence and UV-Vis titrations of **2.2a** using $Zn(tfa)_2$ ([**2.2a**]=1.7 x 10^{-5} M, THF, λ_{ex} = 346 nm).

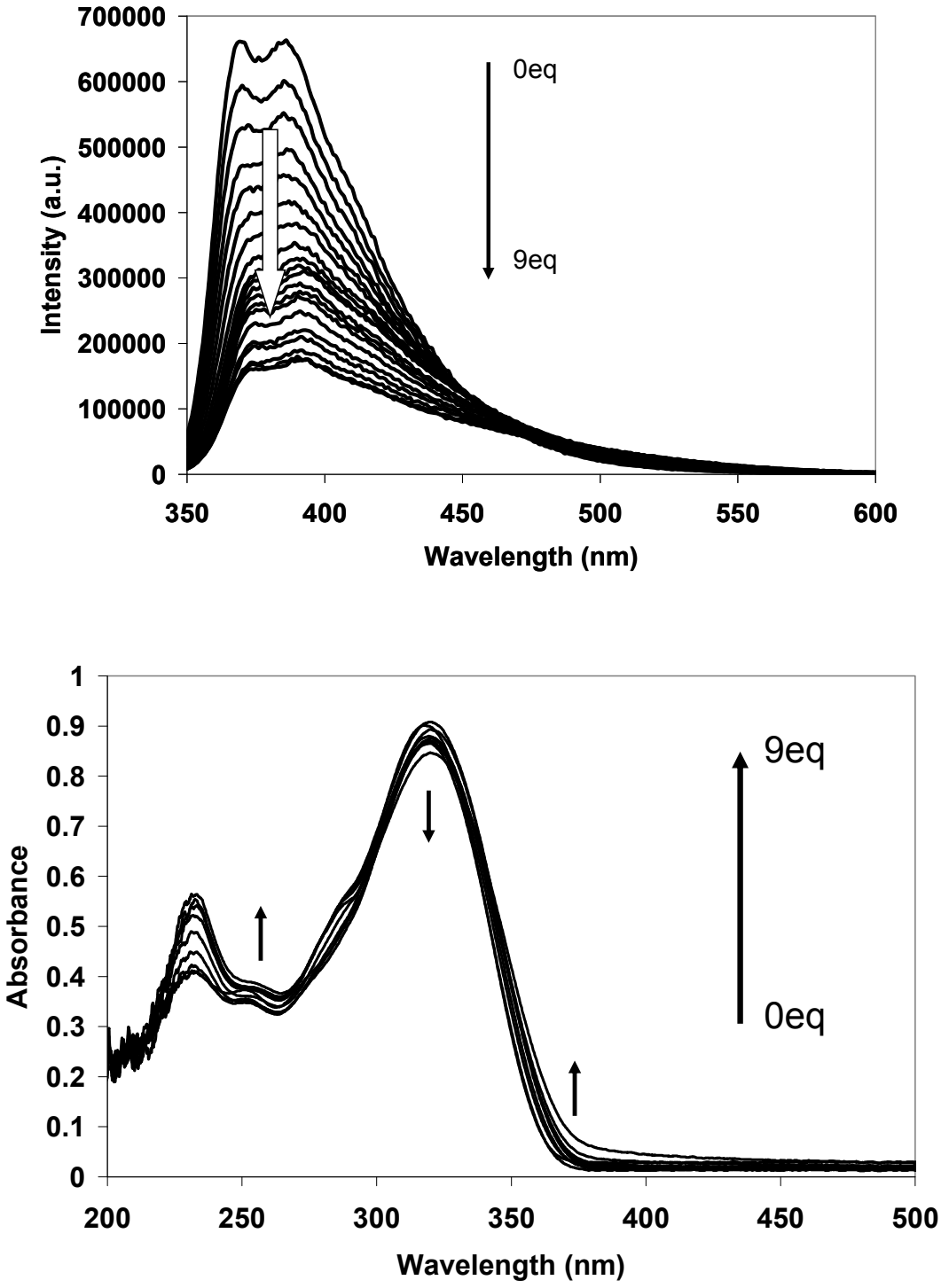

Figure 6.14 Fluorescence and UV-Vis titrations of **2.2a** using $Zn(OAc)_2$ ([**2.2a**]= 3 x 10^{-5} M, THF, λ_{ex} = 346 nm).

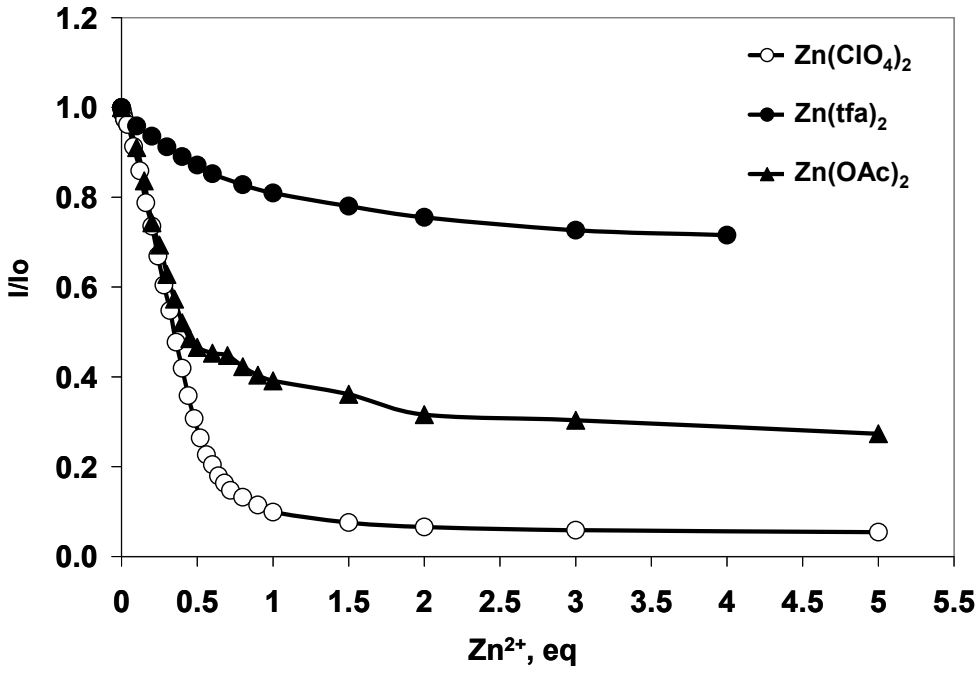

Figure 6.15 Stern-Volmer plots of **2.2a** with various Zn^{2+} salts (THF, λ_{em} = 370 nm).

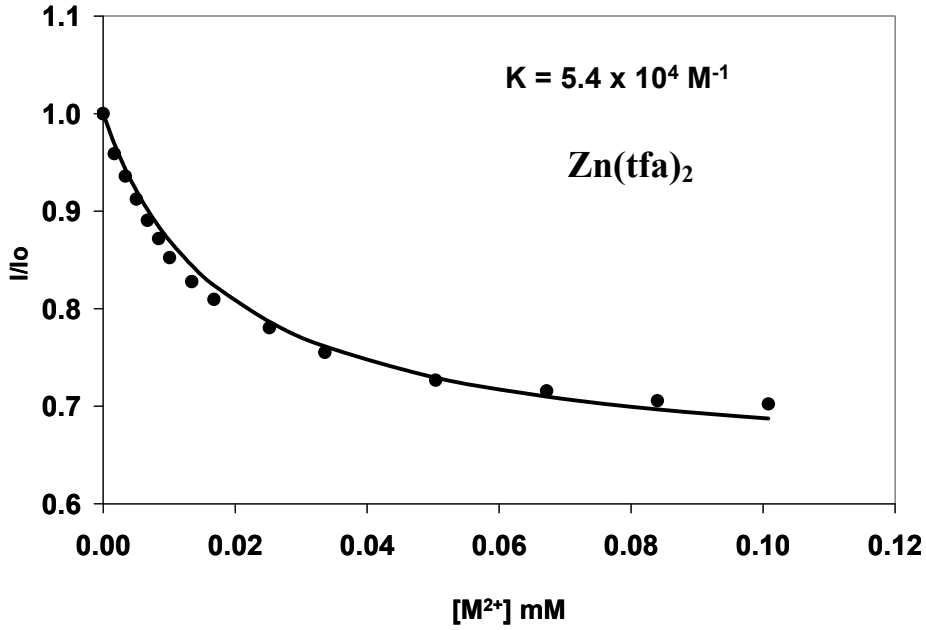

Figure 6.16 Binding constant determination from the fluorescence titration of **2.2a** in the presence of $Zn(tfa)_2$ in THF.

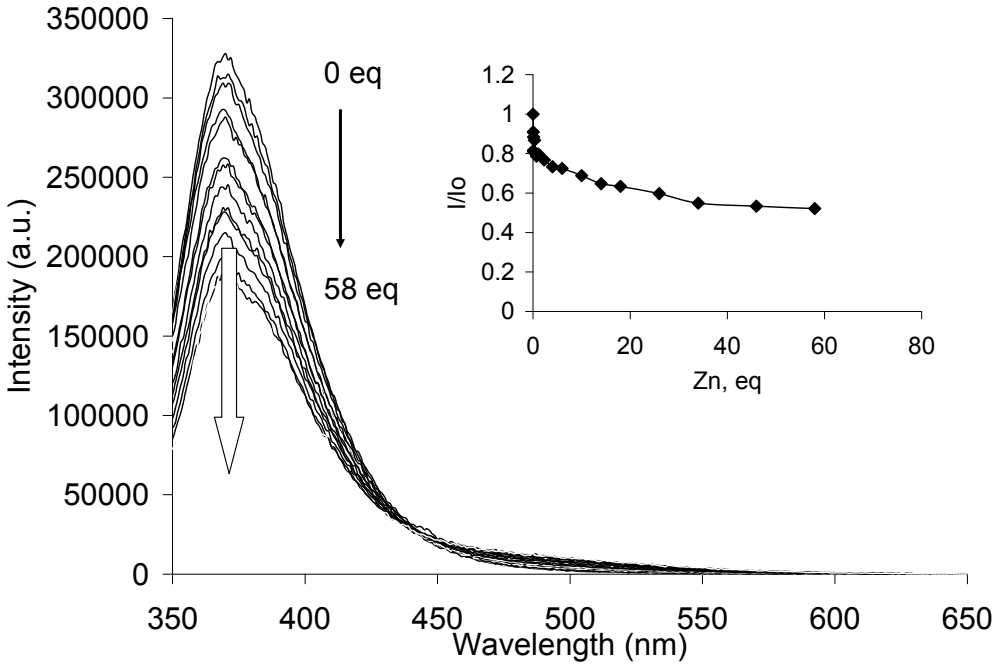

Figure 6.17 Fluorescence titrations of **2.2** using $Zn(ClO_4)_2$ ([**2.2**]= 7 x 10^{-5} M, THF).

Compound **2.2a** exhibits a similar response towards Cd^{2+} and Hg^{2+} ions, as Zn^{2+}, with overall quenching of fluorescent emission observed in Figure 6.18. A strong binding was observed for all three metal ions. The heavy-atom effect can be used to explain the overall emission quenching, especially for Hg^{2+}. The stoichiometry of all three complexes of **2.2a** might exhibit 2:1 (L:M) ratios, as suggested by Stern-Volmer plots (Figure 6.19).

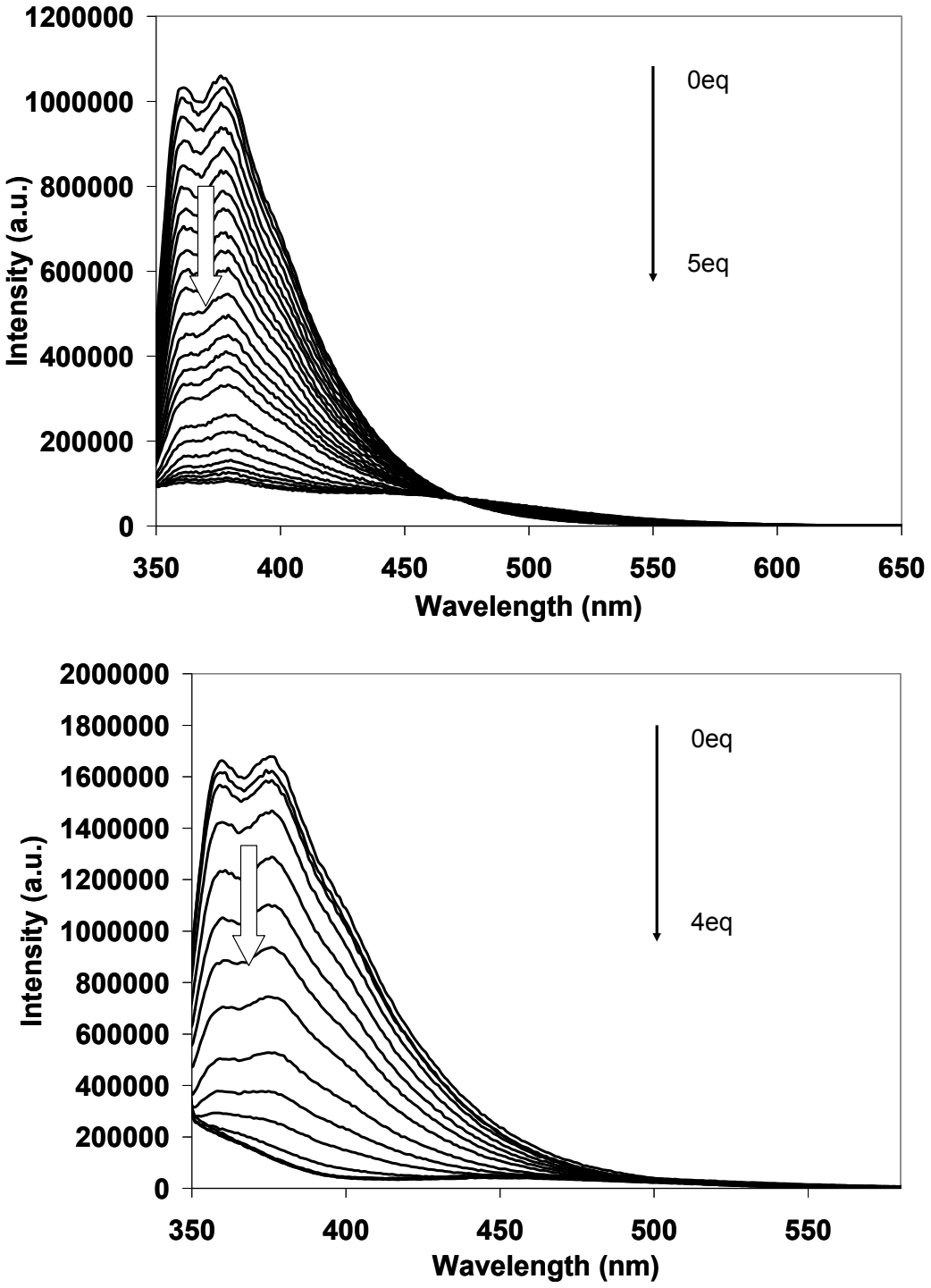

Figure 6.18 Fluorescence titration of **2.2a** with $Cd(ClO_4)_2$ (top) and $Hg(ClO_4)_2$ (bottom) (THF, [**2.2a**] = 7 x 10^{-5} M, λ_{ex} = 346 nm).

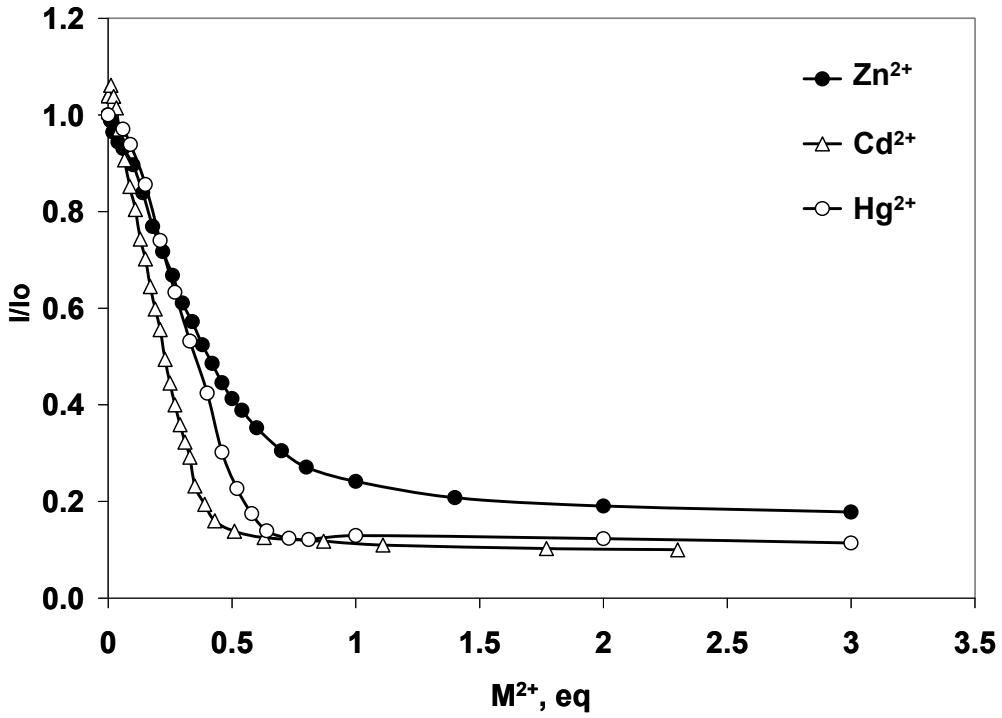

Figure 6.19 Comparison of **2.2a** response towards Group 12 metal ions ($M(ClO_4)_2$, λ_{em} = 370 nm).

6.3.2.2 NMR study

^{1}H NMR titration experiments were used in order to learn more about binding of **2.2a** to metal ions. Similarly to **2.1a**, the addition of $Zn(ClO_4)_2$ to the solution of **2.2a** results in a downfield chemical shift of the H_8 resonance by ~ 0.1 ppm as seen from Figure 6.20. Moreover, the pyridyl H_{Py1} resonance at 8.2 ppm in **2.2a** broadens and experiences a small downfield chemical shift upon the addition of Zn^{2+}. The trends are consistent with the binding of metal ions at the 2,2'-dipyridylamino and the guanine N^7 sites. Actually, a further addition of Zn^{2+} results in the precipitate formation, indicating that the final Zn^{2+}-guanosine complex is insoluble.

Upon addition of $Zn(tfa)_2$, we observe a gradual downfield shift in H_8 proton resonance suggesting that the initial binding occurs at the N^7-site of guanine (Figure

6.21). The broadening of the H_{Py1} proton resonance of the N^2-substituent suggests that the binding also occurs at the 2,2'-dipyridylamino group. NMR titration data were fitted with the assumption that 1:1 (L:M) binding takes place and the binding constant was estimated to be ~ 7.6 x 10^3 M^{-1}. The extracted binding constant is only a poor estimate since a number of different binding events could be taking place due to the presence of two competing binding sites.

The broad ^{1}H NMR signals at 298 K are attributed to the dynamic equilibrium between the bound and free ligand, and between guanine and 2,2'-dipyridylamino group, which was confirmed by the variable temperature ^{1}H NMR spectra in 190 – 308 K range. At 190 K the extra peaks in Figure 6.22 are indicative of the presence of multiple species. Moreover, the broad peaks at δ > 10 ppm are likely due to the imino and amino protons of **2.2a** involved in H-bonding. Overall, the complex low temperature ^{1}H NMR spectrum of **2.2a** in the presence of $Zn(tfa)_2$ likely has contributions from both the variable Zn^{2+} complexes and oligomeric species formed by H-bonding between guanine units.

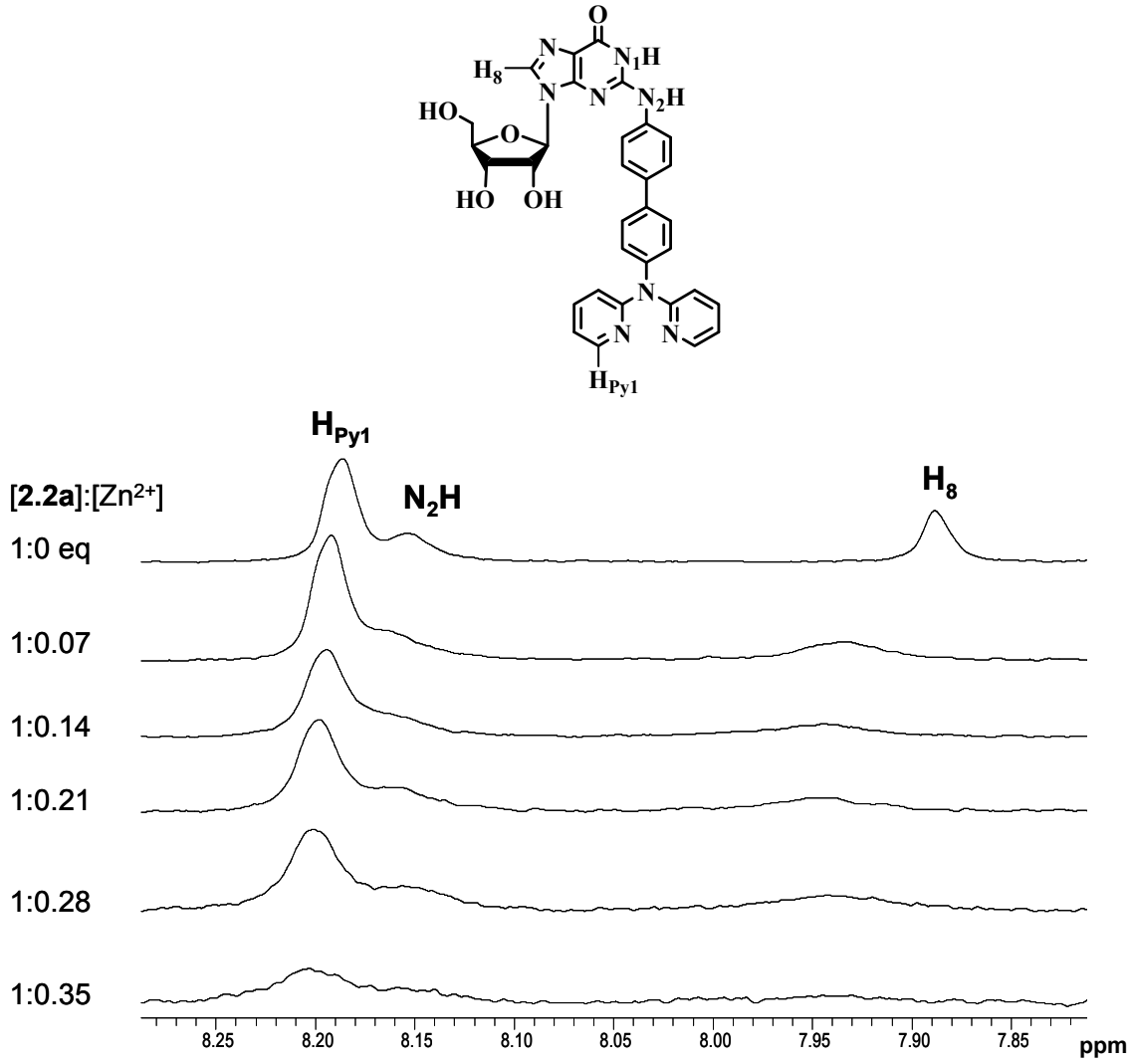

Figure 6.20 ^{1}H NMR titration of **2.2a** using $Zn(ClO_4)_2$ (298 K, [**2.2a**] = 1.4 x 10^{-4} M, THF-d_8).

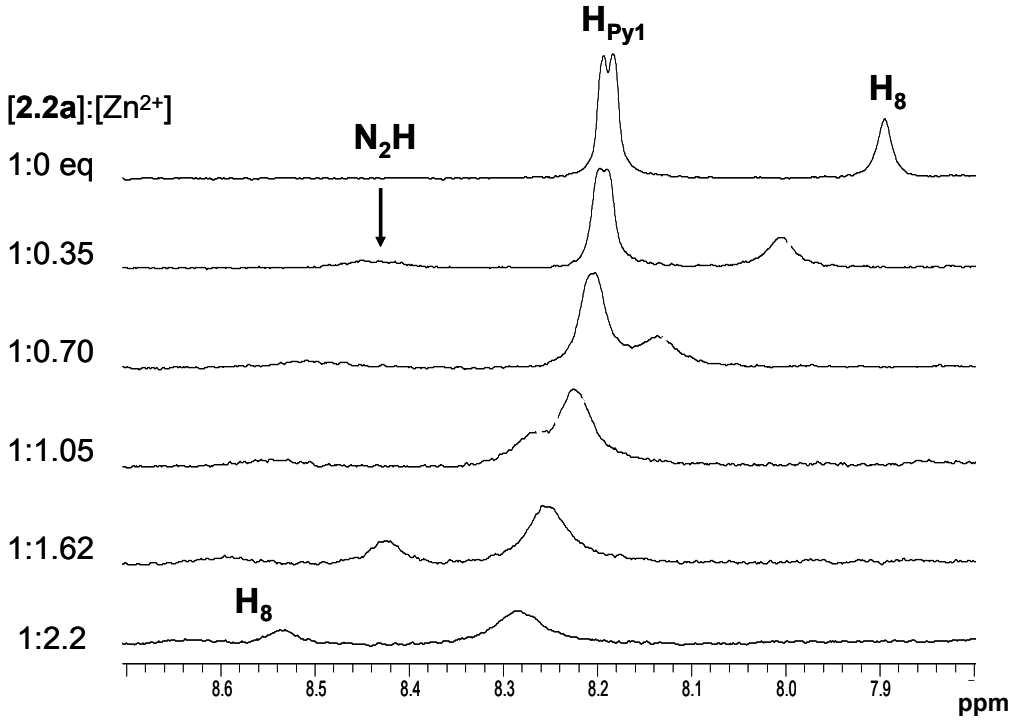

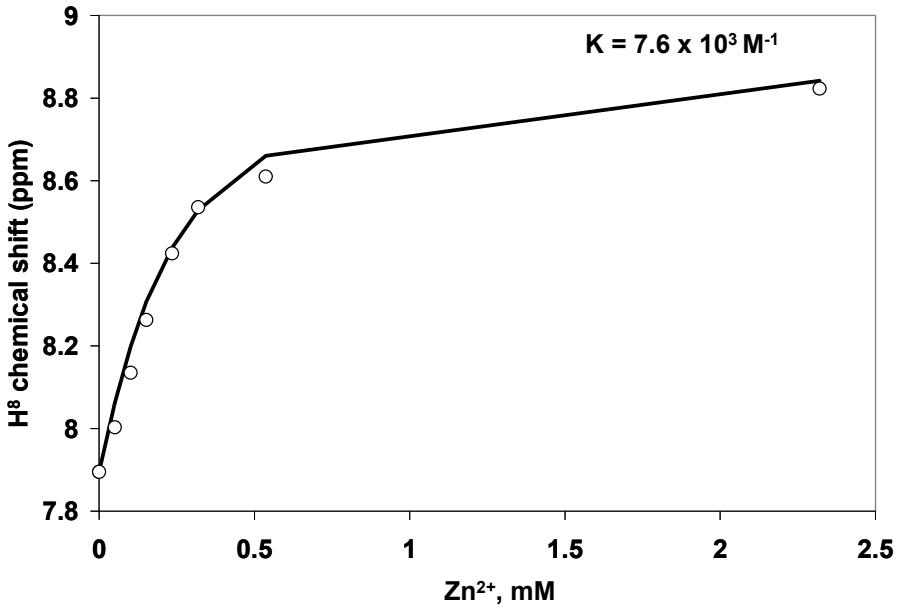

Figure 6.21 ^{1}H NMR titration of **2.2a** using $Zn(tfa)_2$ (298 K, [**2.2a**] = 1.4 x 10^{-4} M, THF-d_8) and binding constant fitting.

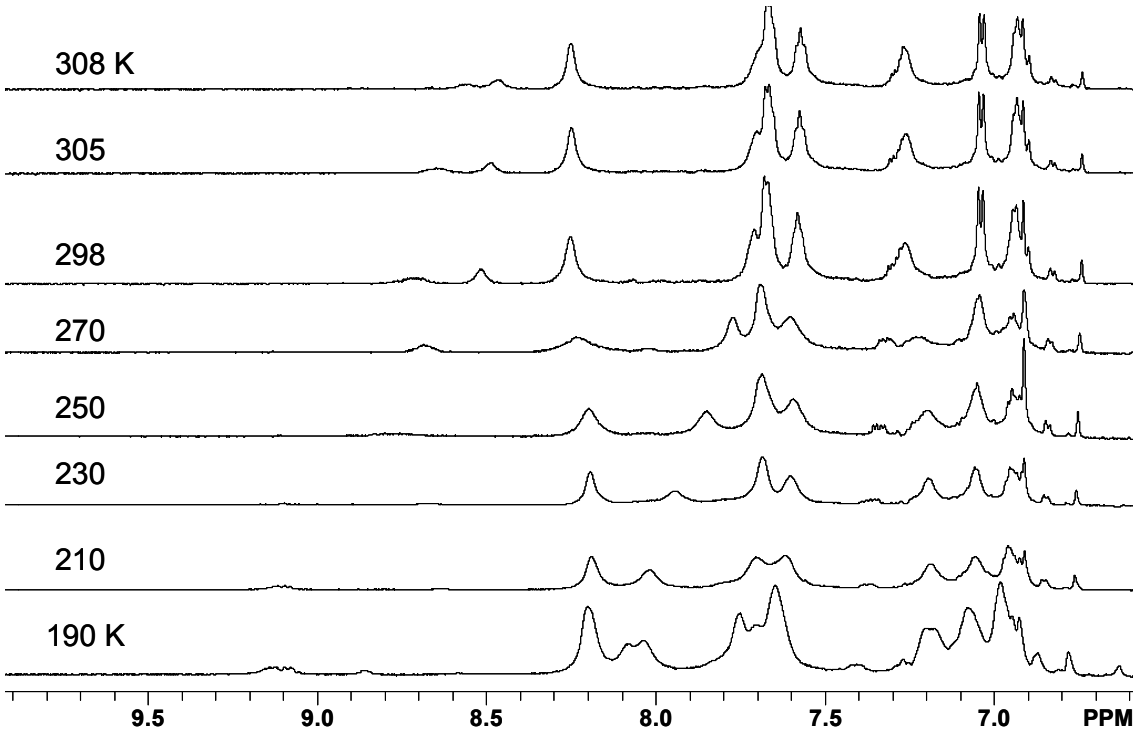

Figure 6.22 Variable temperature ^{1}H NMR spectra of **2.2a** with $Zn(tfa)_2$ (1:2 (L:M) molar ratio, THF-d_8).

6.3.3 Interactions of 2.3a with Group 12 metal ions

6.3.3.1 Fluorescence and UV-Vis study

The response of **2.3a** toward Zn^{2+} ions is unique among the three molecules. As shown in Figure 6.23, the addition of $Zn(ClO_4)_2$ to **2.3a** in THF results in the quenching of the emission peak at ~ 410 nm but "turns-on" a new broad emission band at λ_{max} ~ 490 nm which increases in intensity with the addition of Zn^{2+} ions. The absorption band at λ_{max} = 315 nm of **2.3a** also experiences a distinct red shift with the addition of Zn^{2+} ions. Titration experiments with $Zn(tfa)_2$ (Figure 6.24) also show initial fluorescent emission quenching followed by a slight enhancement at ~ 490 nm. A distinct isosbestic point at ~ 335 nm in UV-Vis spectra of **2.3a,** which is most evident in the presence of $Zn(OAc)_2$

in Figure 6.25, is suggestive of the two types of species coexisting in solution, mainly free and bound ligand. Such a response is unique to the chelating N^2-guanosines and has not been observed for non-chelating compound **2.1a**. Notably, the absence of isosbestic point in the $Zn(ClO_4)_2$ is consistent with the presence of multiple species, such as free ligand, 1:1 (L:M) and 2:1 complexes. To understand the origin of the emission color change of **2.3a** with the addition of Zn^{2+} ions, we carried out the $Zn(ClO_4)_2$ titration experiment with the model compound *p*-2-(2'-pyridyl)benzimidazolyliodobiphenyl (**2.3**), as shown in Figure 6.26. The binding of Zn^{2+} to this ligand causes a red shift (~ 40 nm) and a "turn-on" fluorescent response. This trend is consistent with the previous reports in the literature.[13] Based on this observation and the molecular orbital calculation results (reported in Chapter 2), the fluorescent response of **2.3a** toward Zn^{2+} can be attributed to the binding of the metal ions to the 2-(2'-pyridyl)benzimidazolyl chelate site that quenches the $\pi \rightarrow \pi^*$ emission involving the biphenyl-guanine and the charge transfer emission between the 2-(2'-pyridyl)benzimidazolyl and the biphenyl-guanine groups but turns on the $\pi \rightarrow \pi^*$ emission of the 2-(2'-pyridyl)benzimidazolyl group. The red shift can be attributed to an increasing planarity of the ligand, while the increase in fluorescence can be ascribed to the increased ligand rigidity which reduces an energy loss *via* thermal decay. The "turn-on" fluorescent response of **2.3a** toward Zn^{2+} ions is interesting since it makes ratiometric fluorescent sensing of Zn^{2+} ions possible, a feature that is highly desired in fluorescent sensing technologies due to the elimination of background interference.

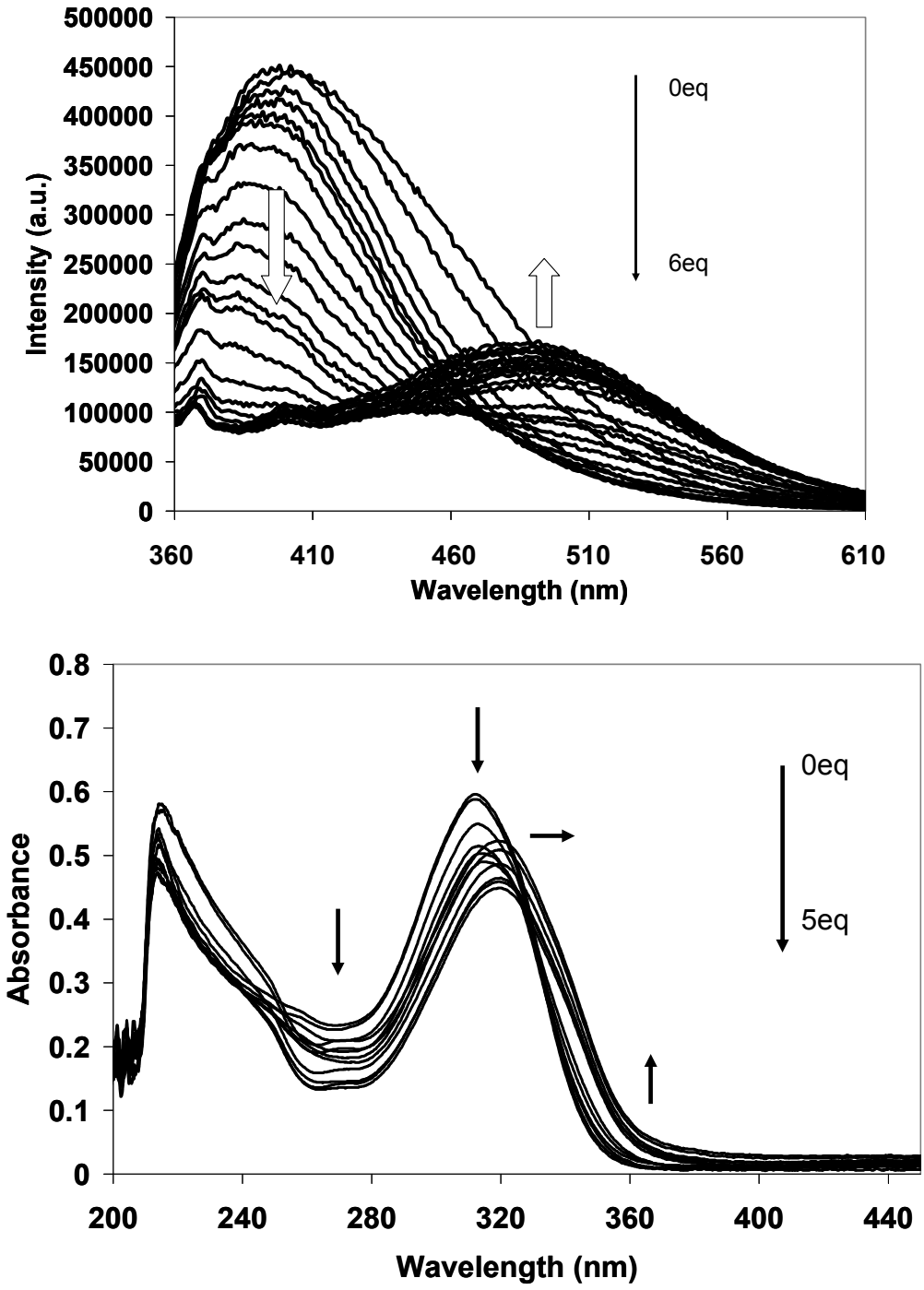

Figure 6.23 Fluorescence and UV-Vis titrations of **2.3a** using $Zn(ClO_4)_2$ ([**2.3a**] = 1.7 x 10^{-5} M, THF, λ_{ex} = 343 nm).

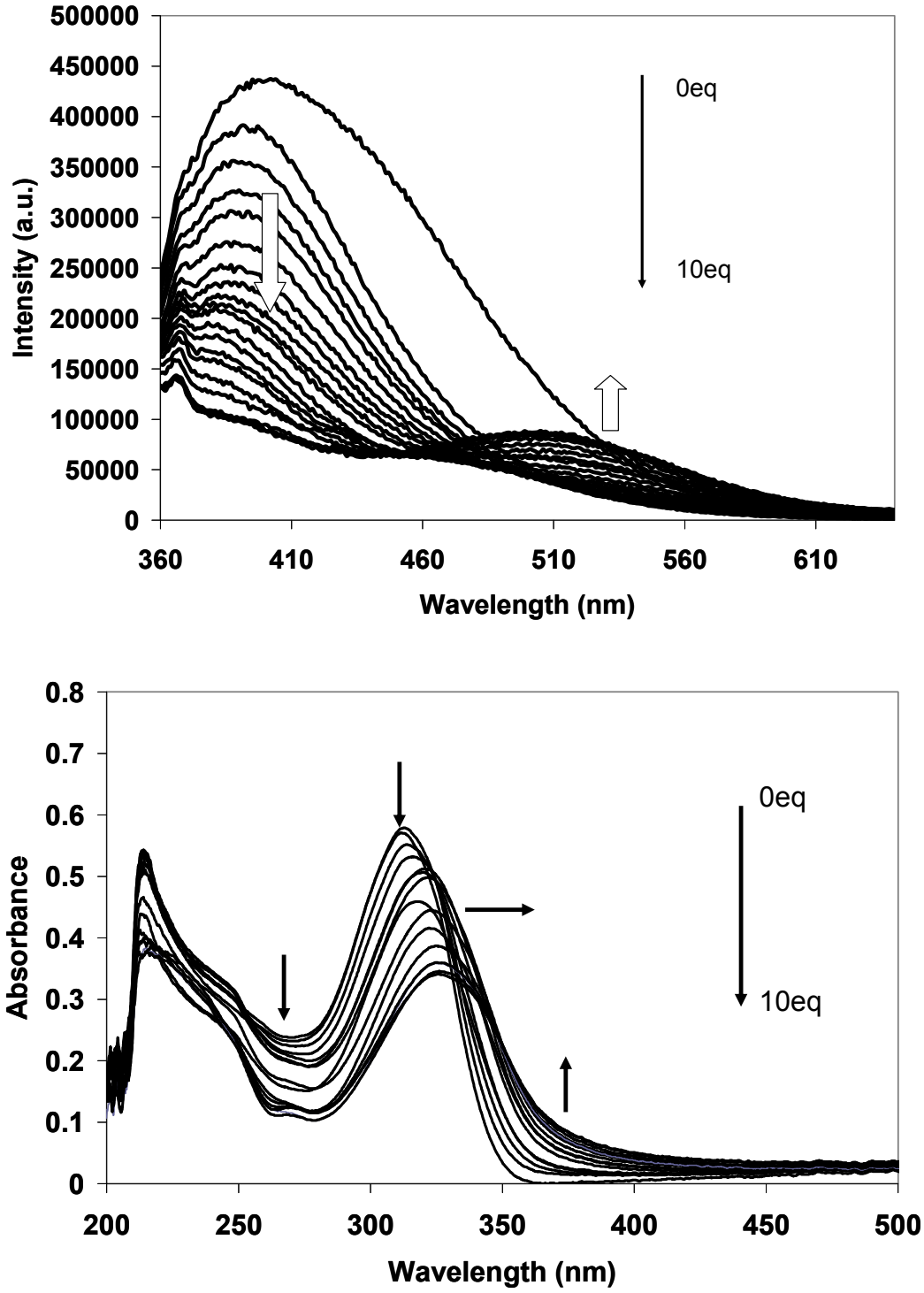

Figure 6.24 Fluorescence and UV-Vis titrations of **2.3a** using $Zn(tfa)_2$ ([**2.3a**] = 1.7 x 10^{-5} M, THF, λ_{ex} = 343 nm).

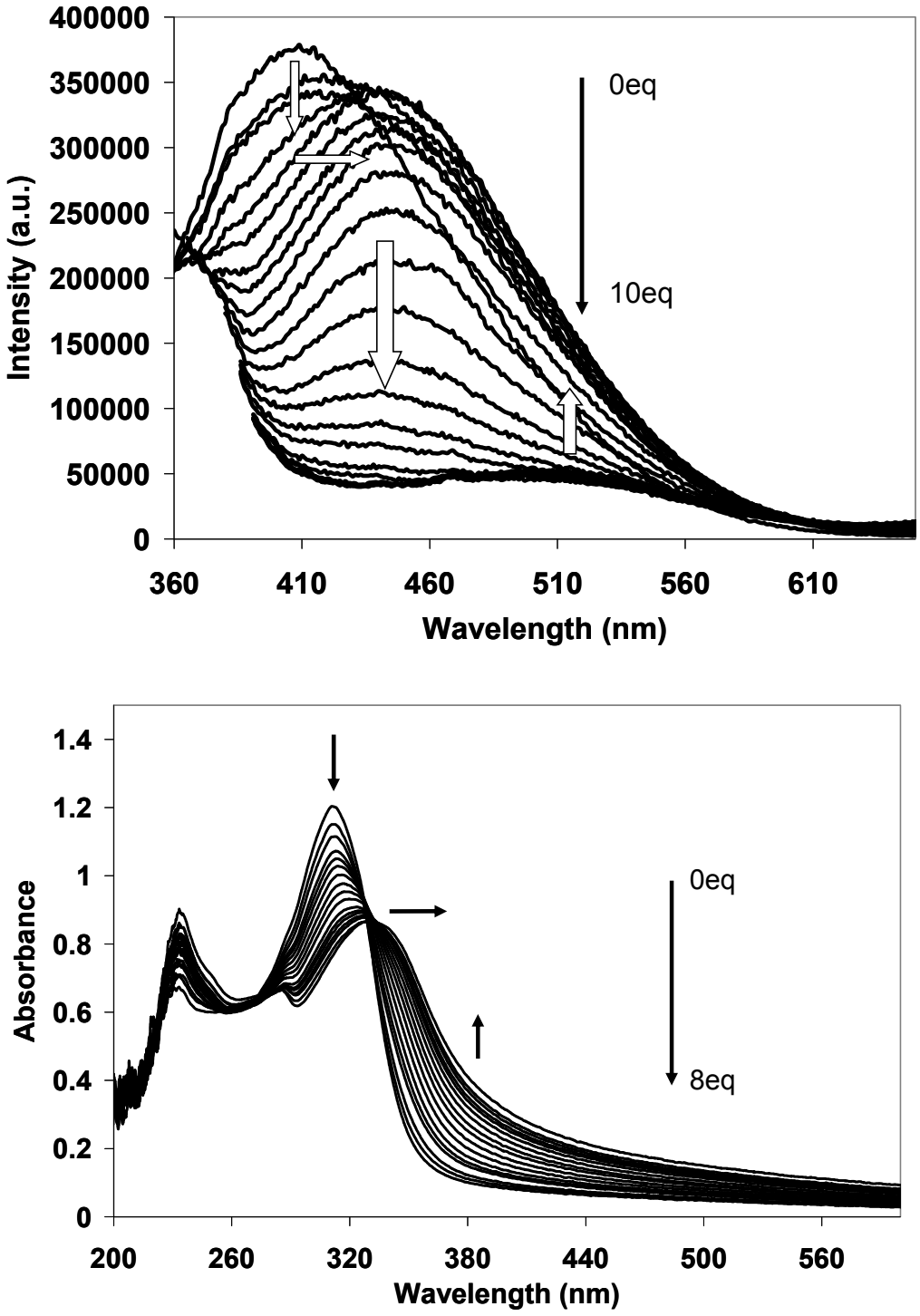

Figure 6.25 Fluorescence and UV-Vis titrations of **2.3a** using $Zn(OAc)_2$ ([**2.3a**] = 3 x 10^{-5} M, THF, λ_{ex} = 343 nm).

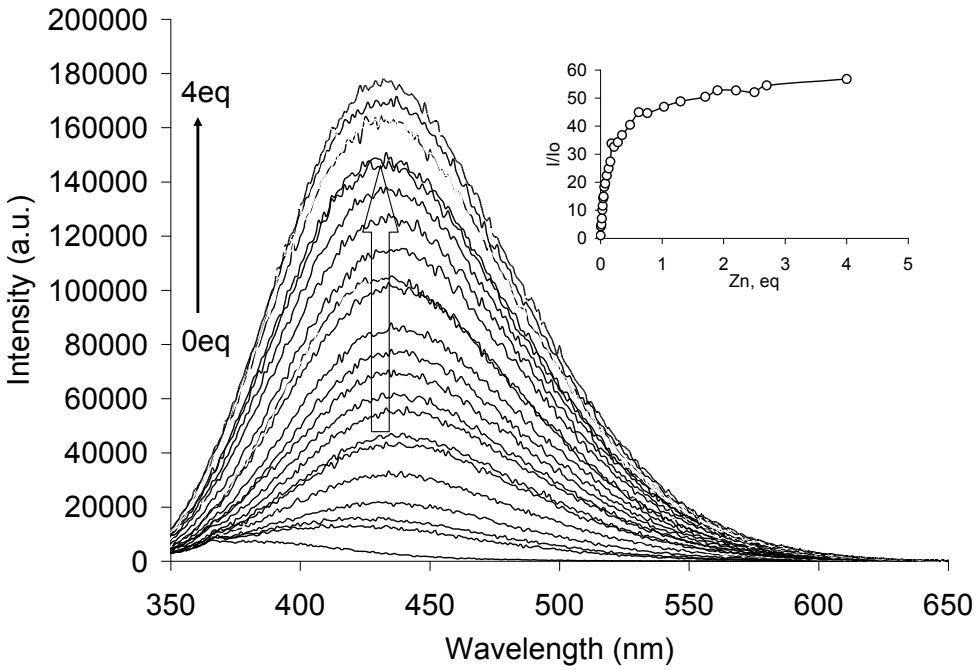

Figure 6.26 Fluorescence titrations of **2.3** using $Zn(ClO_4)_2$ ([**2.3**] = 5 x 10^{-5} M, THF).

Stern-Volmer plots presented in Figure 6.27 show that all Zn^{2+} salts have a dramatic effect on the fluorescent emission of **2.3a**, with 2:1 or 1:1 (L:M) stoichiometries depending on the counterion. Indeed, previously reported crystal structure of 2-(2'-pyridyl)benzimidazolyl- Zn^{2+} complex, by our group, exhibits 2:1 (L:M) ratio with Zn^{2+} in the trigonal bipyramidal geometry[14] with one molecule of water coordinated to the metal center (Figure 6.28).[13,15] The formation of a 1:1 complex was not observed and this phenomenon was attributed to the poor coordinating ability of the ClO_4^- anion compared to *N,N*-chelate ligand. Analogous to Zn^{2+}, the red shift in the fluorescent emission (~ 100 nm) and the enhancement in fluorescent intensity were observed for **2.3a** with Cd^{2+} and Hg^{2+} ions in Figure 6.29. The binding strength of N^2-chelate ligand is similar for all of the Group 12 metal ions with possible 2:1 (L:M) stoichiometry, as can be seen from Stern-Volmer plots (Figure 6.30).

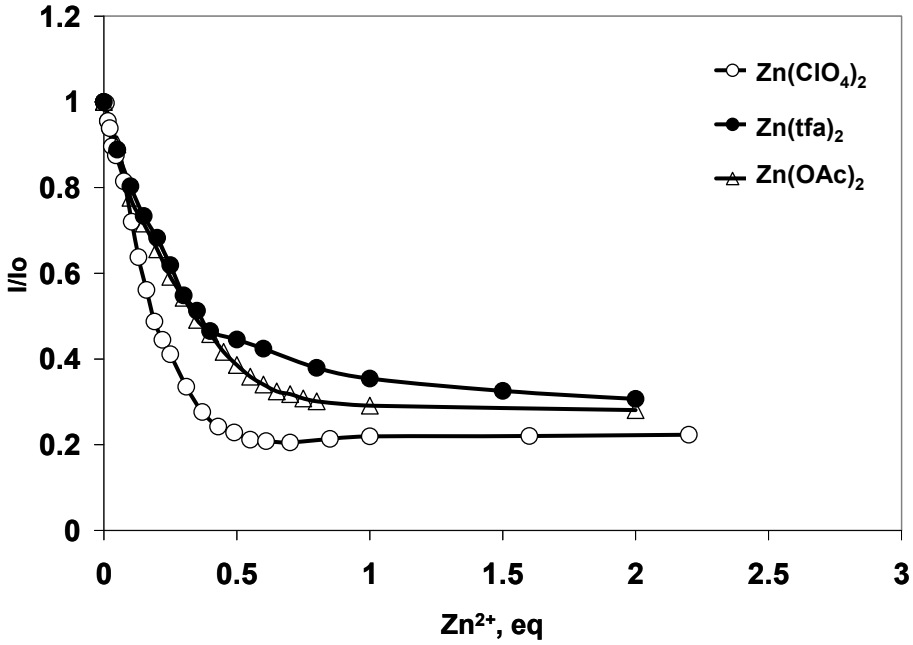

Figure 6.27 Stern-Volmer plots of **2.3a** with various Zn^{2+} salts (THF, λ_{em} = 410 nm).

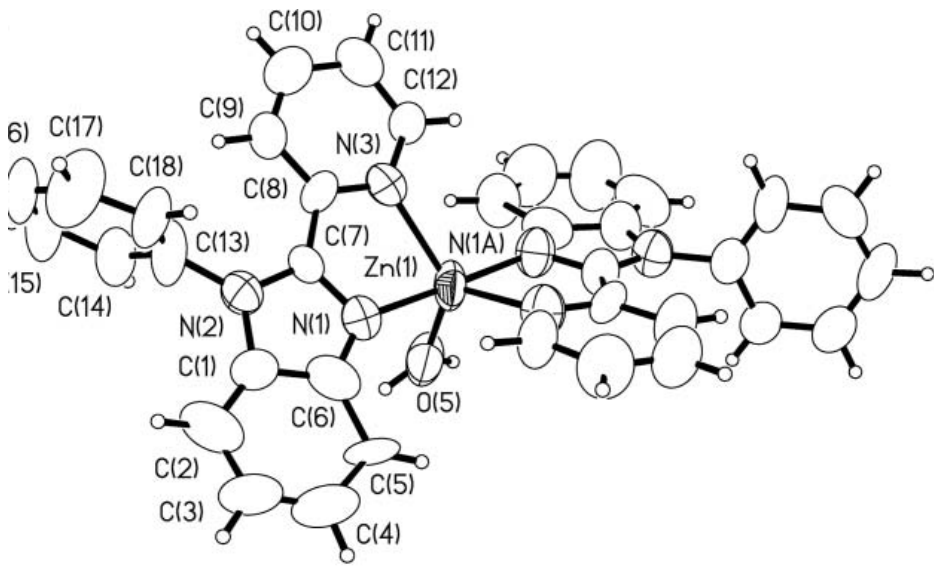

Figure 6.28 The molecular structure of the Zn^{2+} complex of 2-(2'-pyridyl)benzimidazolyl ligands)-type ligands.[15]

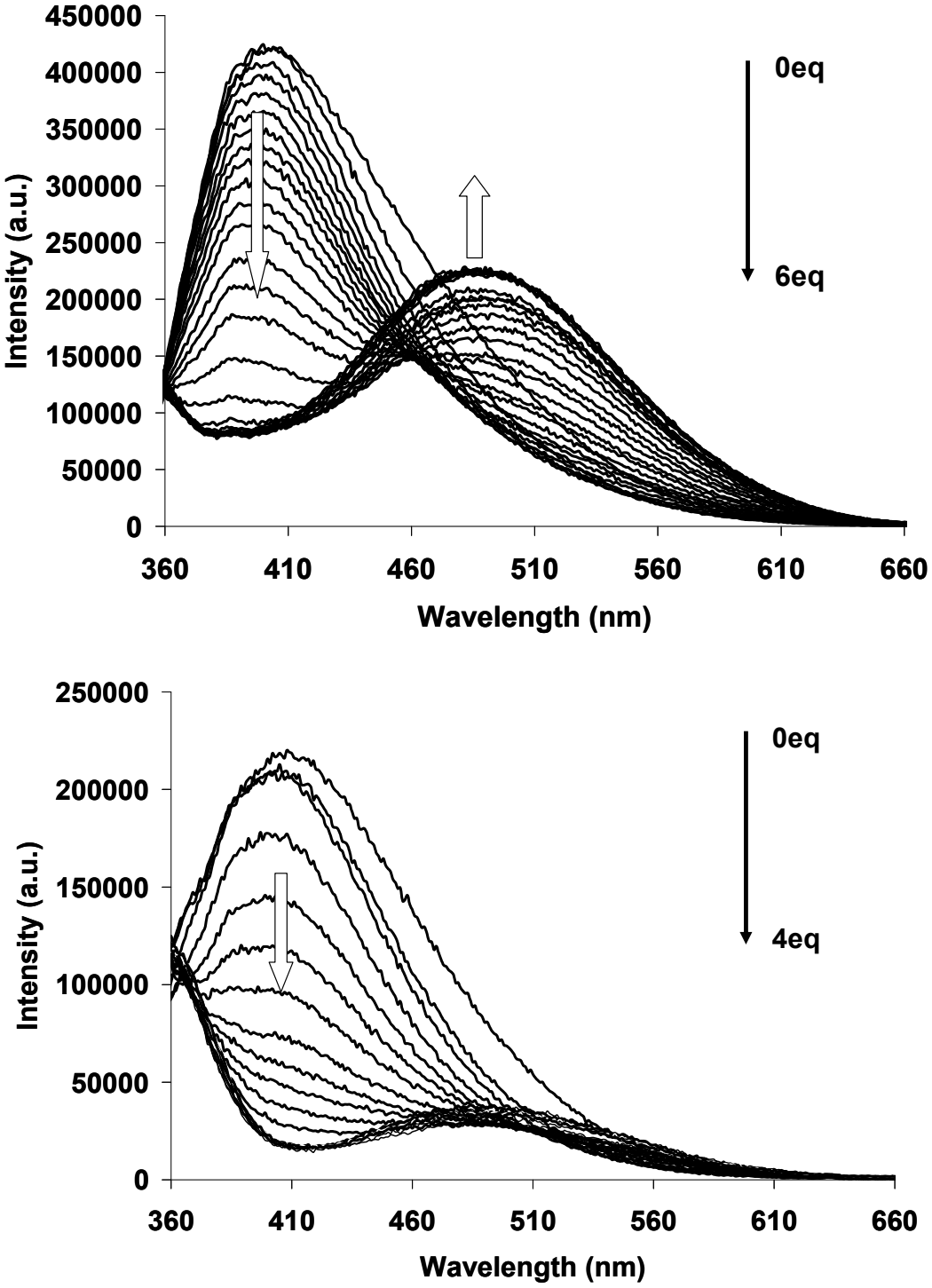

Figure 6.29 Fluorescence titration of **2.3a** with $Cd(ClO_4)_2$ (top) and $Hg(ClO_4)_2$ (bottom) (THF, [**2.3a**] = 7 x 10^{-5} M, λ_{ex} = 343 nm).

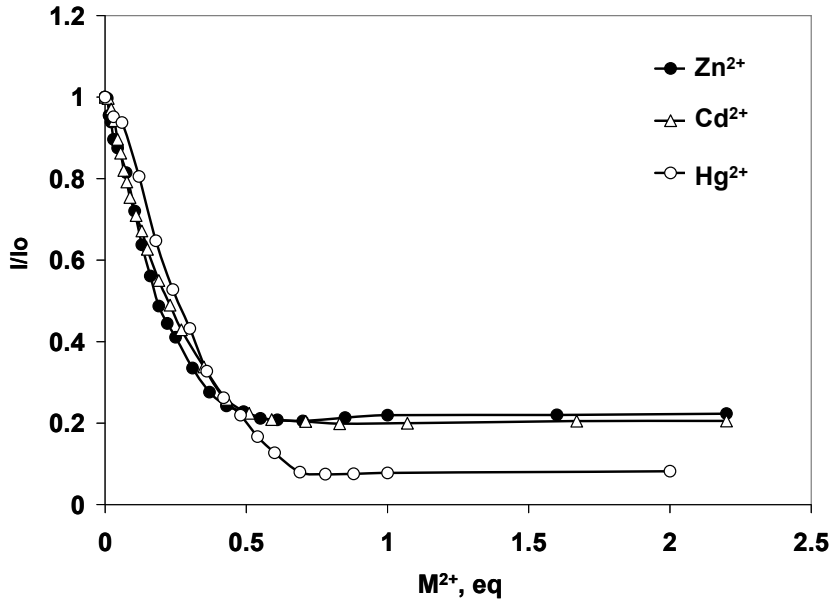

Figure 6.30 Stern-Volmer plots of response of **2.3a** towards Group 12 metal ions ($M(ClO_4)_2$, λ_{em} = 410 nm).

6.3.3.2 NMR study

The study of the metal ion binding mode in **2.3a** was performed by ^{1}H NMR. The addition of up to 0.2 equivalent of $Zn(ClO_4)_2$ to the THF-d_8 solution of **2.3a** (this is the maximum amount that can be added before precipitation occurs due to the poor solubility of the complex) results in the immediate broadening of the H_{Py1} peak of the pyridyl ring and the H_{Bn1} peak of the benzimidazolyl group, while the H_8 resonance of the guanine remains unaffected (Figure 6.31). The addition of $Zn(tfa)_2$, causes the broadening of 2-(2'-pyridyl)benzimidazolyl peaks, while the H_8 resonance of guanine remains unchanged as shown in Figure 6.32. Similarly to **2.2a**, the ^{1}H NMR spectrum of **2.3a** with $Zn(tfa)_2$ is dominated by the broad signals over a large temperature range (220 - 298 K), which can be attributed to dynamic exchange between the bound and free lignd and possible H-bonding among guanine units. Moreover, the broadness of the proton signals can also be

ascribed to the polymeric structures, since $Zn(tfa)_2$ is known to form bridging extended oligomers.

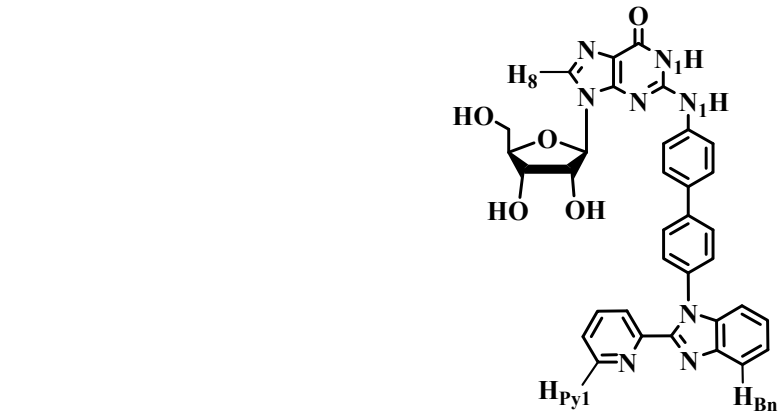

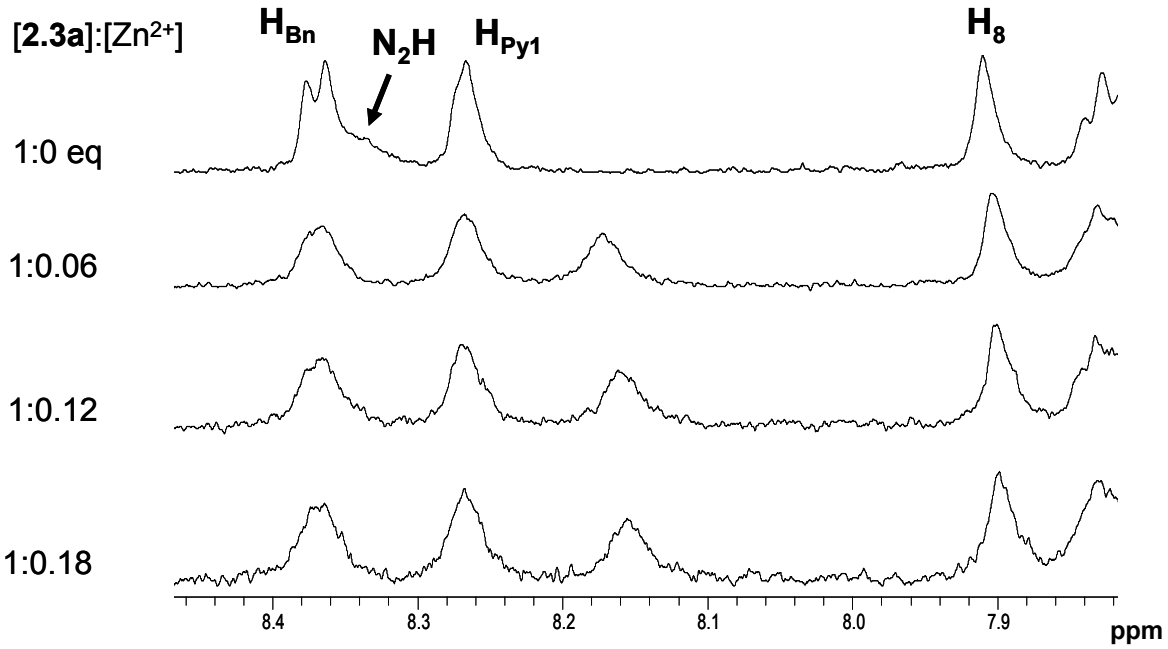

Figure 6.31 ^{1}H NMR titration of **2.3a** using $Zn(ClO_4)_2$ (298 K, [**2.3a**] = 1.5 x 10^{-4} M, THF-d_8).

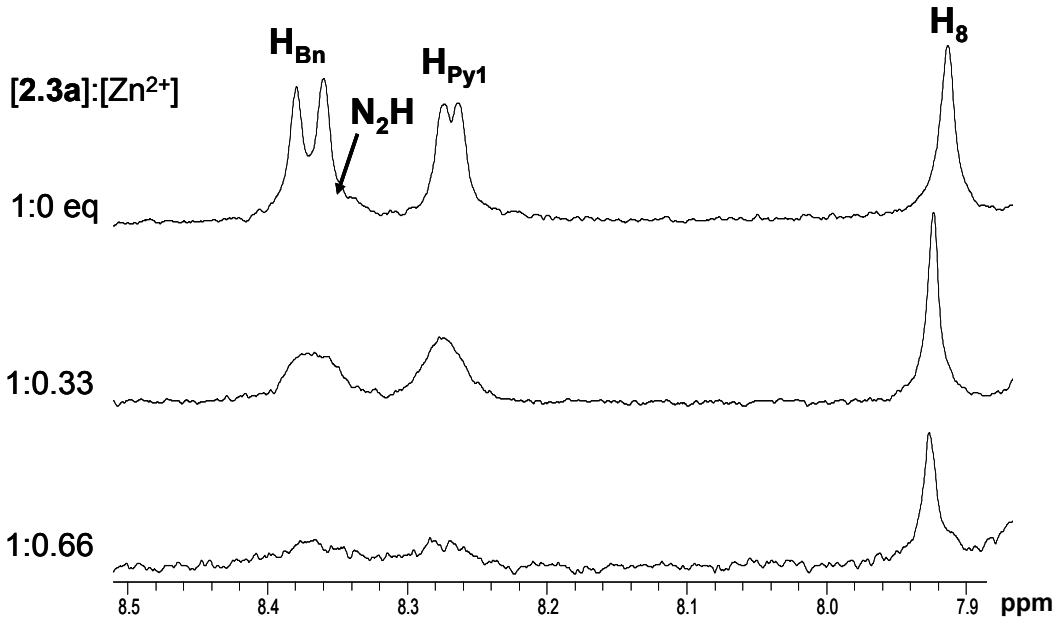

Figure 6.32 ^{1}H NMR titration of **2.3a** using $Zn(tfa)_2$ (298 K, [**2.3a**] = 1.5 x 10^{-4} M, THF-d_8).

6.3.4 Comparison study of 2.1a – 2.3a with Group 12 metal ions

For comparison, the fluorescent response of the **2.1a – 2.3a** toward Group 12 metal ion and different anions was investigated. Our studies show that all three compounds exhibit some affinity toward Group 12 metal ions. As shown in Figure 6.33, in the presence of $Zn(tfa)_2$, compound **2.3a** clearly shows a much stronger binding than **2.1a** and **2.2a**, while for $Zn(ClO_4)_2$, all three compounds appear to have a similar binding strength.

The Stern-Volmer plots for the fluorescence titration data of $Zn(tfa)_2$ suggest a formation of 1:1 (L:M) complex for compounds **2.1a** and **2.2a**, and 2:1 (L:M) complex for **2.3a**. The complexes of $Zn(ClO_4)_2$ exhibit initial 2:1 binding stoichiometry for all

three compounds. It is very likely that at a relatively high concentration of $Zn(ClO_4)_2$, a complex equilibrium between 2:1, 1:1 (and 1:2 in case of **2.2a** due to the extra chelate site) coexist in solution, making the extraction of the binding constant challenging. The poor solubility of some of the Zn^{2+}-complexes complicates the investigation as well.

Importantly, compound **2.3a** binds very strongly to Zn^{2+} ions independent of anion used, which suggests that 2-(2-pyridyl)benzimidazolyl site is the preferred site and indicates that secondary interactions between counterions and the ligand do not affect the overall fluorescent response. Unlike **2.3a**, the response of compound **2.1a** is highly dependent on the counterion, in that $Zn(ClO_4)_2$ causes the most dramatic fluorescent response. Since in **2.1a** the only binding site is guanine, the observed trend in fluorescent response must be due to the coordination ability of N^7-site of guanine and to the secondary interactions between counterions and guanosine. The response of **2.2a** falls somewhere in between the other two ligands, which indicates that 2,2'-dipyridylamino group has similar binding affinity with guanine, which may significantly affect its fluorescent response.

For a head-to-head comparison of the effects of Group 12 metal ions on the luminescence of all three compounds, the normalized emissions were compared at the end of each titration and are presented in Figure 6.34. For **2.1a**, the addition of the metal ions causes a slight red shift by ~ 10 nm, while **2.2a** exhibits a dramatic red shift ~ 100 nm that is most evident for Cd^{2+} and Hg^{2+} complexes. In case of **2.3a**, the fluorescent emission in the presence of all three metal ions is essentially identical and red shifted by ~ 100 nm with respect to the free ligand.

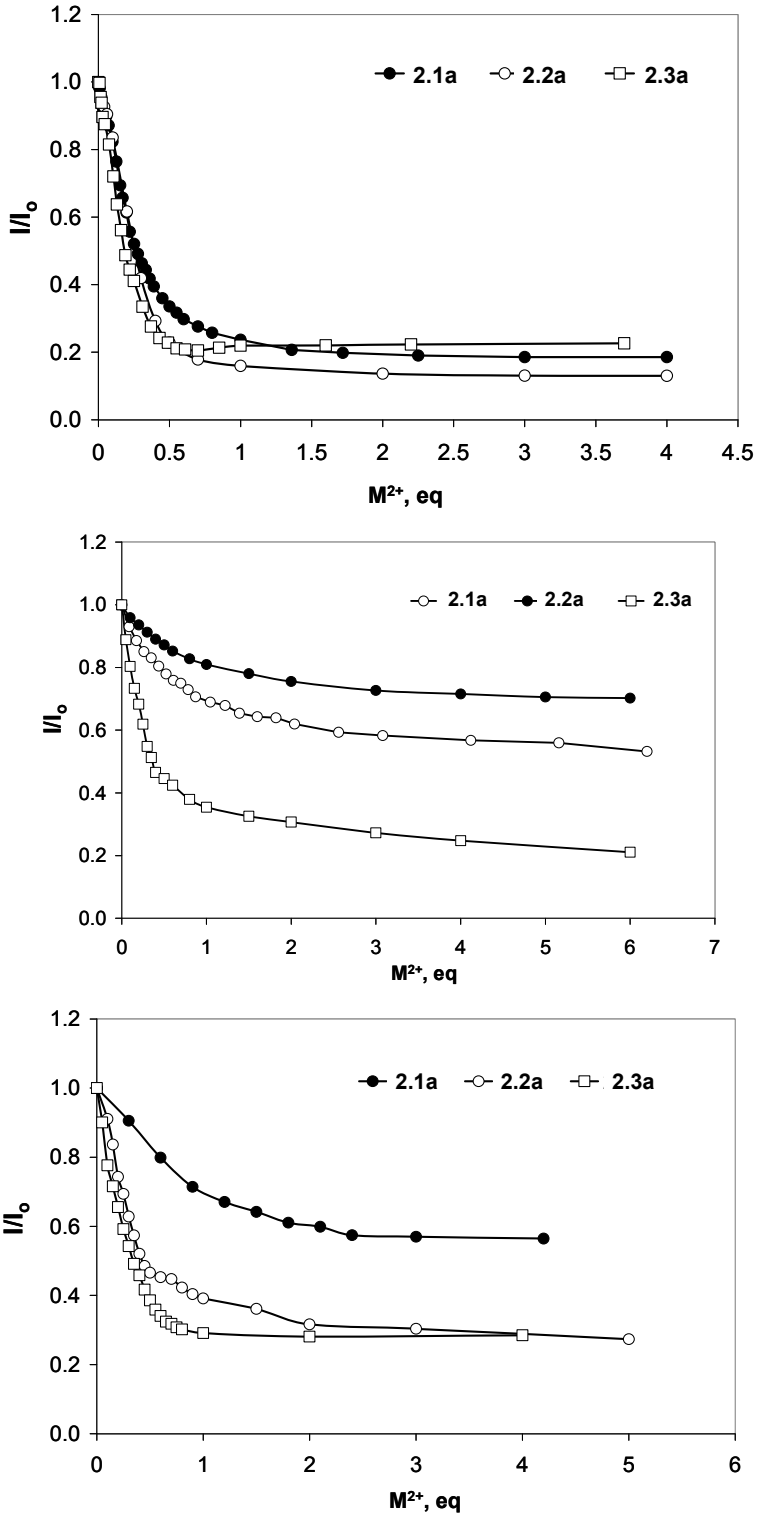

Figure 6.33 Comparison of **2.1a – 2.3a** fluorescent response towards $Zn(ClO_4)_2$ (top), $Zn(tfa)_2$ (middle) and $Zn(OAc)_2$ (bottom). The emission peak of the free ligands was monitored.

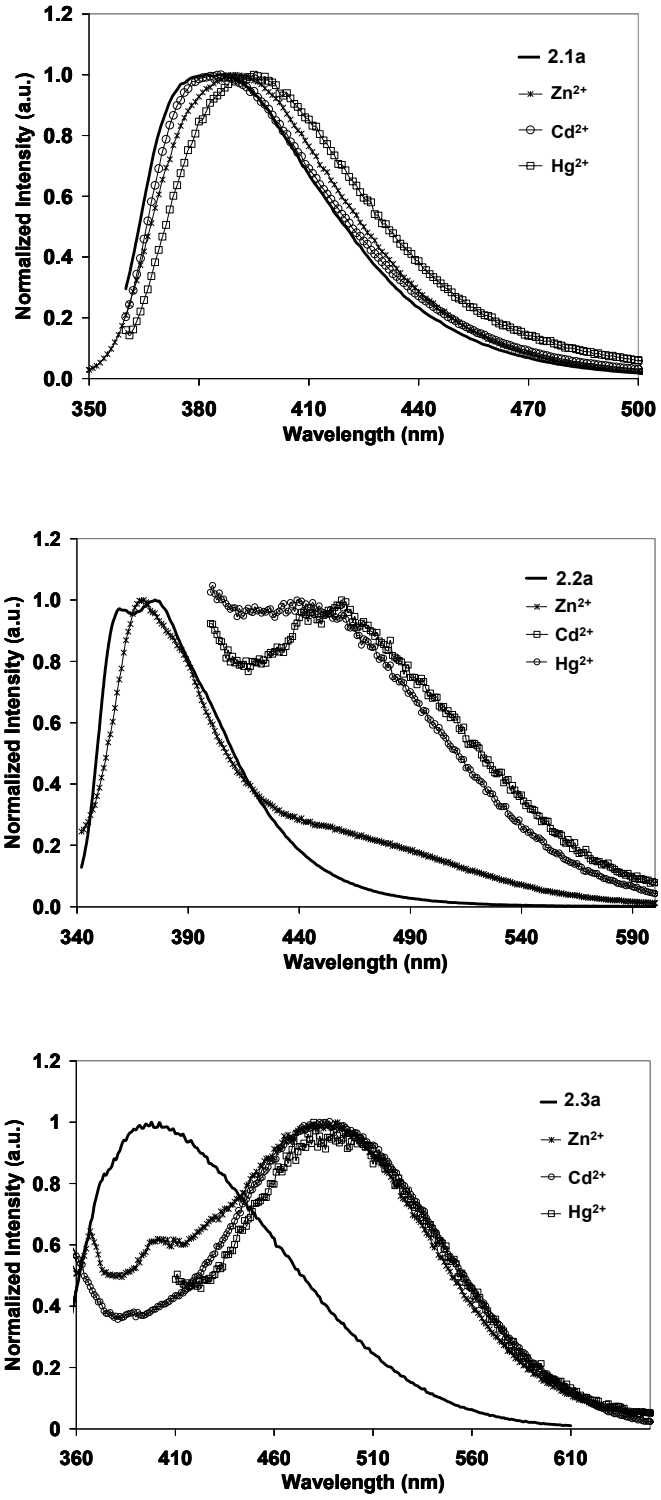

Figure 6.34 Normalized emission spectra of **2.1a** – **2.3a** in the presence of Group 12 metal ions ($M(ClO_4)_2$, THF, λ_{ex} = 358, 346 and 343 nm for **2.1a** – **2.3a**, respectively).

The dramatic red shift in the fluorescence of the metal ion-complexes of **2.2a** and **2.3a** can be ascribed to the increase in the planarity of the chelator upon binding, which was not observed for **2.1a** since guanine ring does not undergo such changes upon metal ion coordination. Overall, the red shift in the fluorescent emission is due to the presence of N^2-chelate ligand in some of the **N^2Gs**.

6.3.5 Proposed binding modes of N^2Gs with Zn^{2+} ions

*6.3.5.1 Binding modes of **2.1a***

A combination of fluorescence, UV-Vis and NMR data were used to establish the binding modes of Group 12 metal ions for all three compounds. Since compound **2.1a** lacks a chelating group at N^2-site, the only possible mode for metal ion binding is at the guanine ring. Zn^{2+} complexes of guanine, reported previously, were characterized by the tetrahedral geometry and one guanine unit coordinated *via* N^7-atom. It can be proposed that the complexes of **2.1a** with $Zn(OAc)_2$ and $Zn(tfa)_2$, also take on a tetrahedral geometry with one guanine unit, one terminally bound anion and one coordinating anion to complete the coordination shell as depicted in Figure 6.35.

Changing the counter-ion from acetates to ClO_4^- causes a change in the final stoichiometry of the complex, as suggested by Stern-Volmer plots. This behaviour is expected since ClO_4^- is not a coordinating ligand, hence the lack of chelation of this counter-ion leaves enough room around the metal center for the second guanine which leads to the formation of possible bis(guanosine) 2:1 complex (L:M). To complete the tetrahedral geometry, two water molecules, from the atmosphere or due to use of the $Zn(ClO_4)_2 \bullet 2H_2O$ salt during titration, are bound to the metal center, as well. The bis(guan(os)ine) complexes are commonly seen in platinum chemistry, however, they are

rarely seen in relations to the Group 12 metal ions.[16] An example of bis(guanine) Cd^{2+} complex has been prepared by Buncel et al.[17] from 2:1 mixture of guanine to $Cd(OAc)•2H_2O$. In the octahedral cadmium complex, the axial sites are occupied by N^7-atoms of guanines while equatorial positions are taken up by water molecules. Hence, the proposal for the tetrahedral or octahedral bis(guanine) complexes of **2.1a** is reasonable.

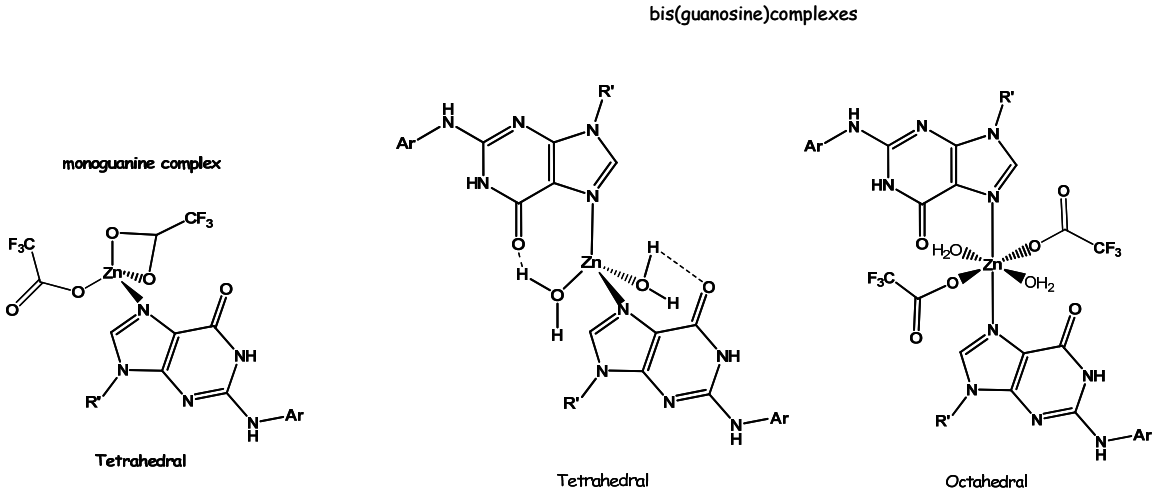

Figure 6.35 Proposed mono- and bis(guanosine) complexes of **2.1a**.

*6.3.5.2 Binding modes of **2.2a***

Previous work in our group on 2,2'-dipyridylamino-Zn^{2+} complexes indicates that the Zn^{2+} coordination is extremely anion and solvent dependent. By varying the water content during the reaction and recrystallization process, a number of different coordination geometries around Zn^{2+} center could be obtained as shown in Figure 6.36.[18] Analogous to these findings, we propose that compound **2.2a** exhibits a tetrahedral geometry with two terminally coordinated tfa^- counter-ions, in 1:1 (L:M) complex. Octahedral Zn^{2+} complexes containing two 2,2'-dipyridylamino moiety is also not unusual and has been observed previously, with two terminal tfa^- anions completing the coordination shell.

The observation of 2:1 stoichiometry for **2.2a** can be explained in two ways: 1) coordination around single Zn^{2+} ion between 2,2'-dipyridylamino and guanine groups of two independent **N^2Gs** or 2) coordination of two 2,2'-dipyridylamino groups as in bis(2,2-dipyridylamino) complex. These binding modes can lead to the formation of polymeric structures, which could be used to explain the broadness of the ^{1}H NMR signals. Unlike the OAc^- anion, ClO_4^- is a non coordinating anion and typically leads to the formation of bis(ligand) Zn^{2+} complexes in tetrahedral or octahedral geometries. Because of the poor donor capability of the ClO_4^- anion, it is proposed that $Zn(ClO_4)_2$ may form a 2:1 complex (L:M) with **2.2a** producing a similar bis(2,2'-dipyridylamino) complexes.

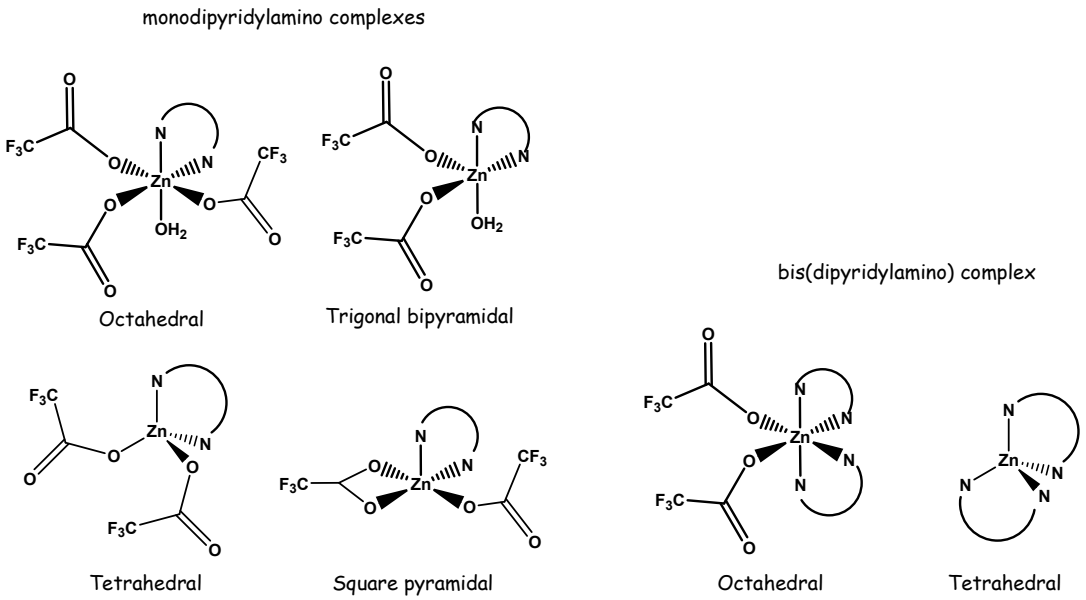

Figure 6.36 Proposed mono- and bis(2,2'-dipyridylamino) complexes of **2.2a**.

*6.3.5.3 Binding modes of **2.3a***

In terms of the binding modes of **2.3a** it is clear that N^2-chelate ligand is preferably involved in metal ion coordination due to its stronger binding affinity over the guanine ring. The lack of the metal ion binding *via* N^7-site of guanine is further supported

by the small changes associated with H_8 proton during ^{1}H NMR titrations. All of the **2.3a** complexes potentially adopt 2:1 (L:M) stoichiometry regardless of the type of anion or metal ions used. The Zn^{2+} complexes containing various acetates are believed to adopt Oh geometry shown below. Previous reports on the 2-(2'-pyridyl)benzimidazolyl group[15] reveal the formation of the tetrahedral bis-complexes with $Zn(ClO_4)_2$, hence, similar conclusions can be made concerning the coordination of **2.3a** (Figure 6.37).

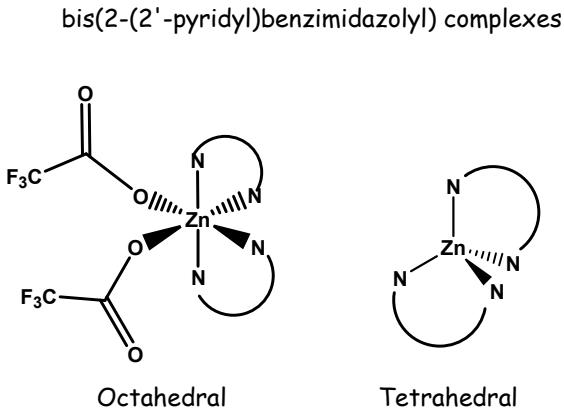

Figure 6.37 Proposed bis(2-(2'-pyridyl)benzimidazolyl) complexes of **2.3a**.

6.3.6 CD spectroscopic study of 2.1a -2.3a response towards Zn^{2+} ions

*6.3.6.1 Interactions of **2.1a** with achiral Zn^{2+} salts*

To simplify the study, **2.1a** was investigated first due to its single binding site. Interestingly, we have found that the degree and the pattern of the induced CD change in the presence of Zn^{2+} ions is highly dependent on the type of anion. The most surprising finding is that the weakest anion, ClO_4^- ion, which results in the strongest Zn^{2+} binding in fluorescence, did not affect much the CD profile of **2.1a**, as shown in Figure 6.38A. Addition of $Zn(ClO_4)_2$ to **2.1a** causes little change in 250 - 400 nm region, while the addition of $Zn(tfa)_2$ induces a CD couplet with a positive peak at 320 nm and the negative

peaks at ~ 255, 290 and 350 nm (Figure 6.38B). The second surprising thing is that two different carboxylate anions produce relatively different CD responses. For example, $Zn(OAc)_2$ induces a CD couplet with a positive peak at 360 nm and two negative peaks in the 250 - 290 nm region, respectively, that resemble the peaks induced by tfa^- ion in the same region (Figure 6.38C). The reason for such a trend is not very well understood but it could potentially be due to the orientation of the carboxylates and their interactions with the ribose unit.

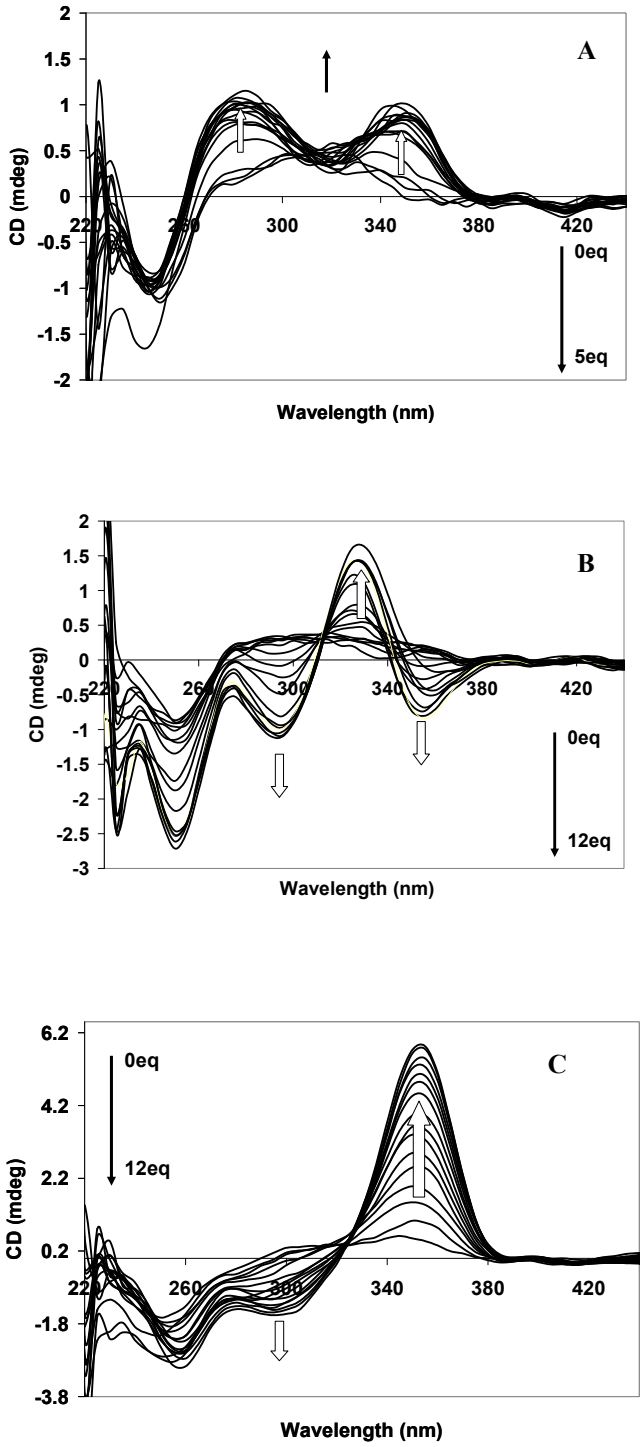

Figure 6.38 CD titrations of **2.1a** using A) $Zn(ClO_4)_2$, B) $Zn(tfa)_2$ and C) $Zn(OAc)_2$ (THF, [**2.1a**] = 3 x 10^{-5} M).

*6.3.6.2 Interactions of **2.2a** with achiral Zn^{2+} salts*

A comparison CD study with a chelating analogue **2.2a** reveals new information. Similarly to compound **2.1a**, the addition of excess $Zn(ClO_4)_2$ does not result in the dramatic change in the CD spectra of **N^2Gs**, so it was not further studied. By contrast, the addition of $Zn(tfa)_2$ and $Zn(OAc)_2$ gives rise to CD amplification judging by the positive couplet centered at 310 nm. In Figure 6.39, the negative band in 230 – 310 region is coupled with the positive band in the 310 – 370 nm range which belong to the guanine and N^2-aryl group, respectively. The CD response of **2.2a** toward Zn^{2+} ions is similar to that of **2.1a**, suggesting that the binding environments are similar for both guanosines, involving most likely the guanine N^7-site. The competitive binding to the chelate ligand at N^2-site, in **2.2a**, cannot be excluded. Both carboxylates result in the similar CD pattern of **2.2a**, unlike the trend that was observed for **2.1a**.

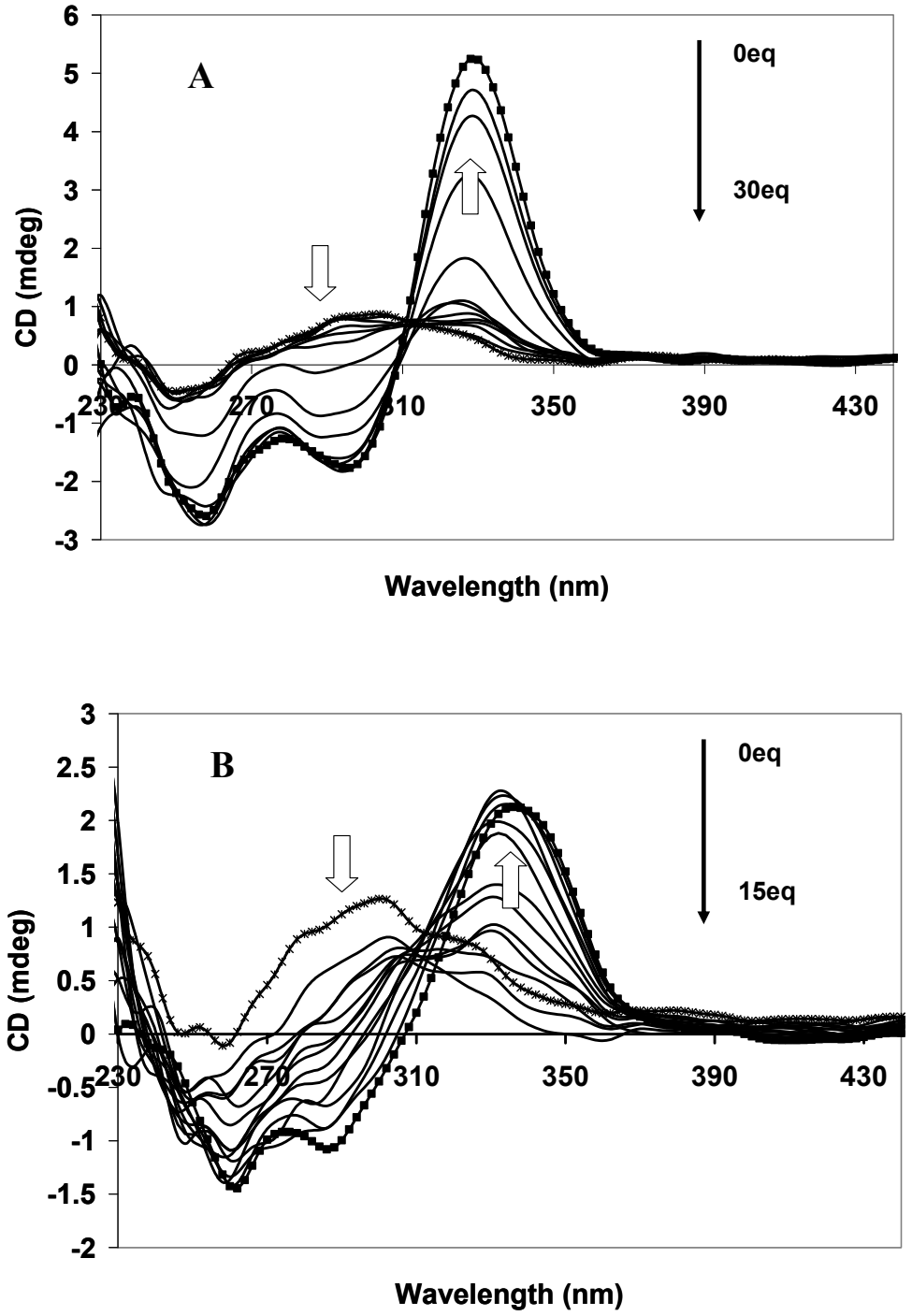

Figure 6.39 CD titrations of **2.2a** using A) $Zn(tfa)_2$ and B) $Zn(OAc)_2$ (THF, [**2.2a**] = 3 x 10^{-5} M, cross (0 eq Zn^{2+}) and solid square (end point)).

*6.3.6.3 Interactions of **2.3a** with achiral Zn^{2+} salts*

Compound **2.3a** has the strongest chelating site, as demonstrated in the previous section, and preferentially binds to the Group 12 metal ions. From the CD titration experiments in Figure 6.40, a minimal change is associated with compound **2.3a** in the presence of $Zn(tfa)_2$ or $Zn(OAc)_2$. The CD response of **2.3a** is weak and lacks a positive CD enhancement in the 250 - 400 nm region, which is consistent with the binding of Zn^{2+} ions at the 2-(2'-pyridyl)benzimidazolyl site rather than guanine. Since the binding event is far away from the chiral ribose group and guanine, little impact is seen on the CD spectra. A control study was performed using the parent ligand, **2.3**, in order to demonstrate that the metal ion coordination at the 2-(2'-pyridyl)benzimidazolyl site does not induce CD signal. As expected, no CD signal change was observed. These findings suggest that the coordination at the N^2-site of **2.3** results in the CD signal loss.

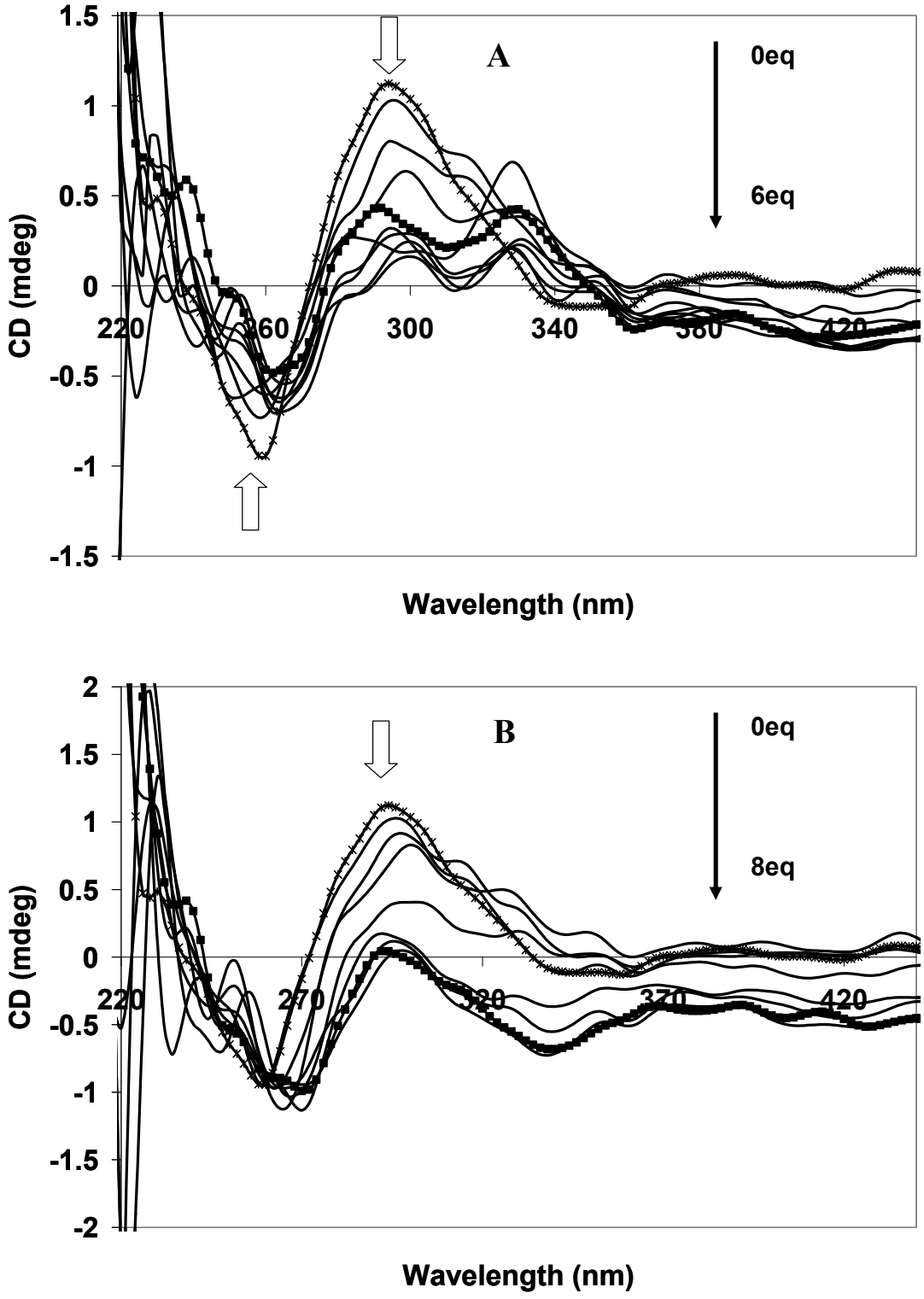

Figure 6.40 CD titration of **2.3a** using A) $Zn(tfa)_2$ and B) $Zn(OAc)_2$ (THF, [**2.3a**] = 3 x 10^{-5} M, cross (0 eq Zn^{2+}) and solid square (end point)).

6.3.6.4 Interactions of ***2.1a – 2.3a*** *with chiral* Zn^{2+} *carboxylates*

Since the chirality induction is stemming from the coordination to the guanine site of the chiral **N²Gs** using achiral Zn^{2+} salts, it would be interesting to investigate the response towards chiral Zn^{2+} salts. For that reason, CD response of chiral **N²G** towards chiral Zn^{2+} carboxylates was investigated. The chiral carboxylates Zn[(*S*)-$O_2CCH(Br)CH(CH_3)CH_3]_2$ (Zn(S)Br), Zn[(*R*)-$O_2CCH(Br)CH(CH_3)CH_3]_2$ (Zn(R)Br) and Zn[(*S*)-$O_2CCH(Br)CH(CH_3)CH_3]_2$ (Zn(S)Me) were synthesized in-house using ZnO and the corresponding butyric acid derivatives in toluene under inert atmosphere.

For **2.1a** the CD spectral change induced by the two chiral carboxylates is similar in pattern to achiral $Zn(OAc)_2$, given the positive CD band at ~ 350 nm and a negative band in 240 – 320 nm region as shown in Figure 6.41 and Figure 6.42. Slightly greater CD amplification was observed with Zn(S)Br over Zn(R)Br. Compound **2.2a** exhibits similar response in terms of CD amplification, but its positive CD band is blue shifted to 335 nm with the greater CD enhancement induced by Zn(S)Br carboxylate. The results indicate that the chirality of the carboxylate bound to Zn^{2+} has little impact on the CD band of the N^2-aryl substituent. For **2.3a**, the addition of the chiral Zn^{2+} carboxylates does not lead to a CD couplet formation analogous to the results observed for the achiral Zn^{2+} salts.

To establish the role of the N^2-substituent on the CD amplification with **N²Gs**, a control CD experiments were performed using the unmodified guanosine, **TAG**. From Figure 6.43 it can be seen that **TAG** has a very weak CD signature peak in the absence of Zn^{2+} ions. Addition of Zn(R)Br results in the initial increase in 260 nm and 295 nm bands, however, the CD response becomes unstable in the presence of excess Zn^{2+}. The

addition of Zn(S)Br to **TAG** solution causes only increase in 260 nm peak; however, the stability of the CD signal is compromised at high concentrations of Zn^{2+}. These different CD trends in **TAG** are not very well understood and have not been further explored. However, a general observation can be made in that compounds **2.1a** and **2.2a** are much more sensitive towards chiral Zn^{2+} carboxylates in the CD mode than **TAG**.

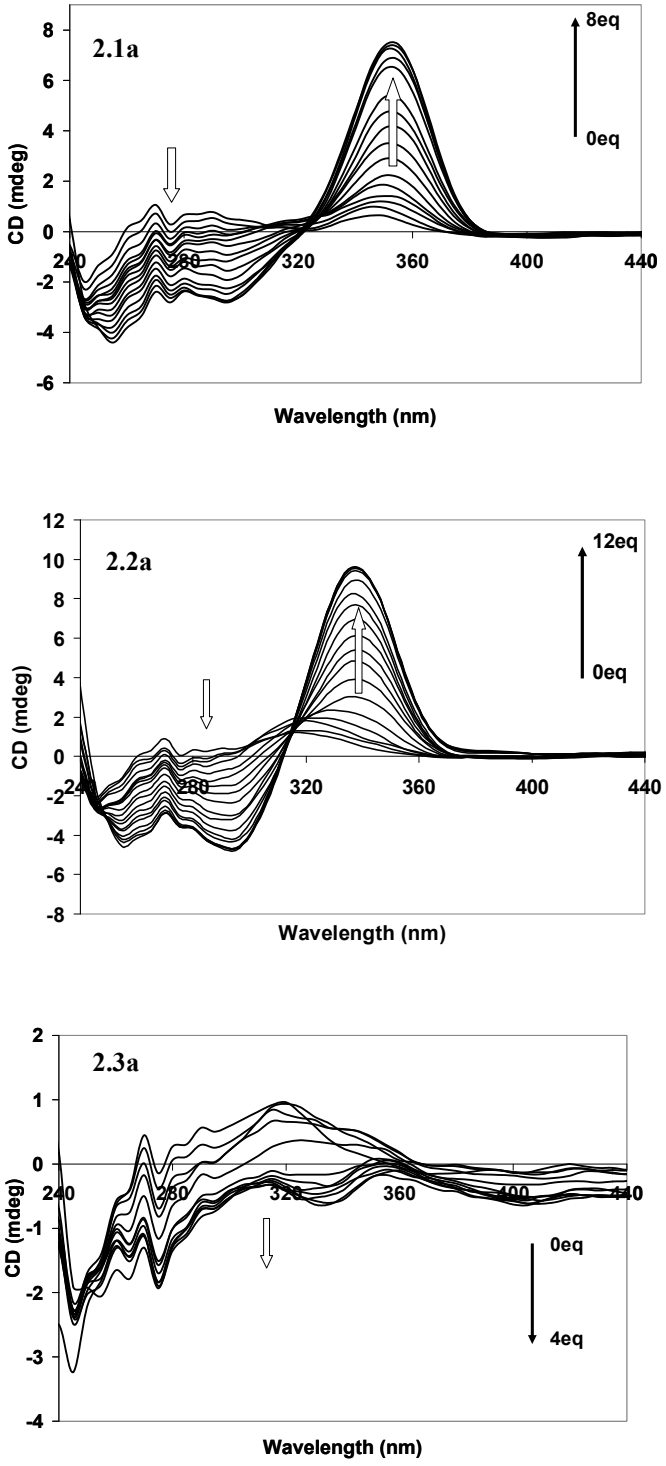

Figure 6.41 CD titrations of **2.1a** - **2.3a** using Zn[(*S*)-O_2CCH(Br)CH(CH_3)CH_3]$_2$ (THF, 3 x 10^{-5} M).

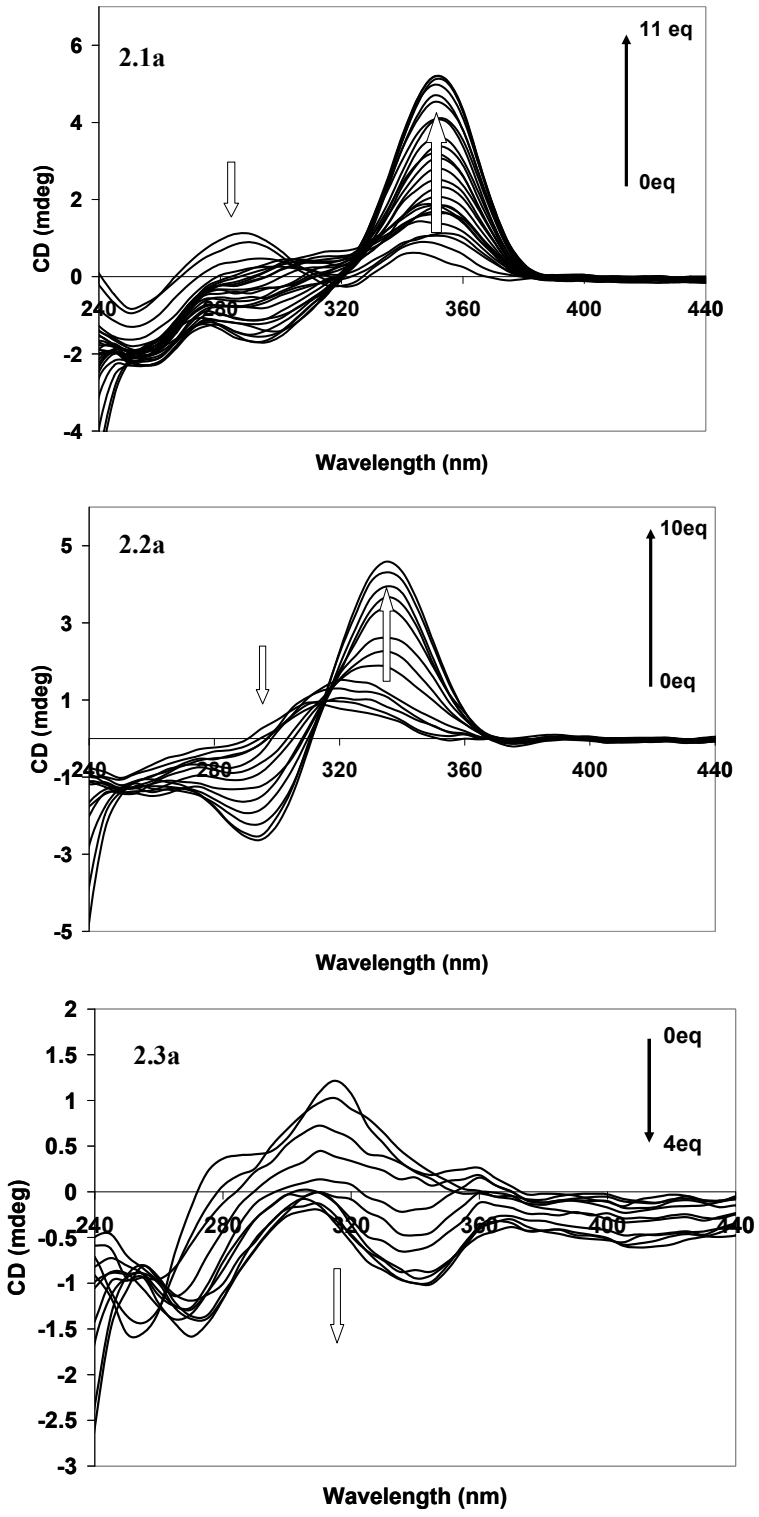

Figure 6.42 CD titrations of **2.1a** - **2.3a** using Zn[(*R*)-O_2CCH(Br)CH(CH_3)CH_3]$_2$ (THF, 3 x 10^{-5} M).

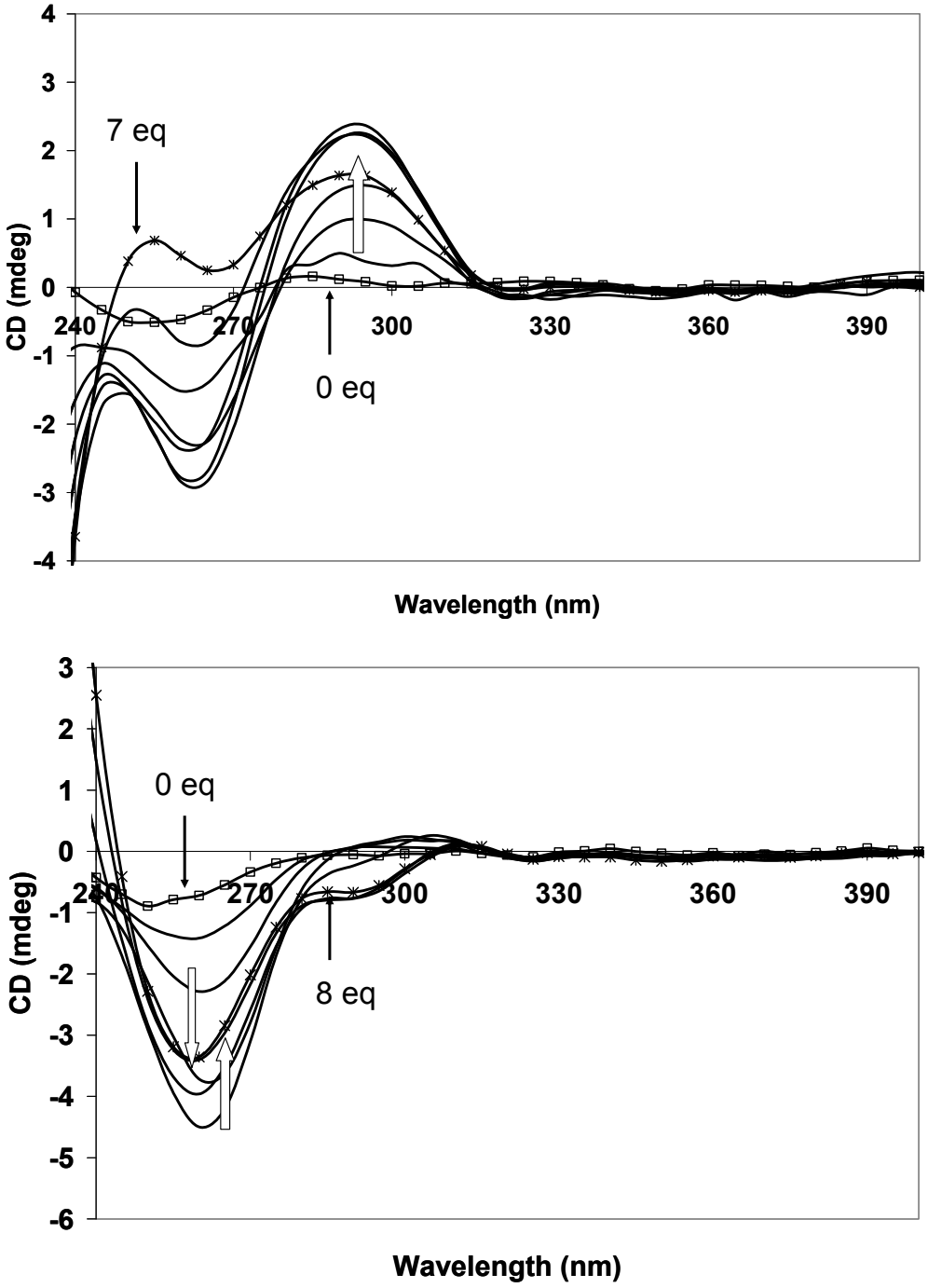

Figure 6.43 CD titrations of **TAG** using Zn[(*R*)-O_2CCH(Br)CH(CH_3)CH_3]$_2$ (top) and Zn[(*S*)-O_2CCH(Br)CH(CH_3)CH_3]$_2$ (bottom) (THF, 3 x 10^{-5} M).

*6.3.6.5 Fluorescence study of **2.1a – 2.2a** with chiral Zn^{2+} carboxylates*

Since the fluorescent change can also be monitored during the CD studies, the comparison of the two methods is possible. Stern-Volmer plots presented in Figure 6.44 show that compound **2.1a** exhibits stronger emission quenching over **2.2a** for most of the carboxylates except for $Zn(OAc)_2$. Both **N^2Gs** exhibit a slightly greater fluorescent quenching with the Zn(S)Br over Zn(R)Br carboxylates, analogous to CD response, which indicates that the potential chiral recognition by fluorescence is possible when using **N^2G**.

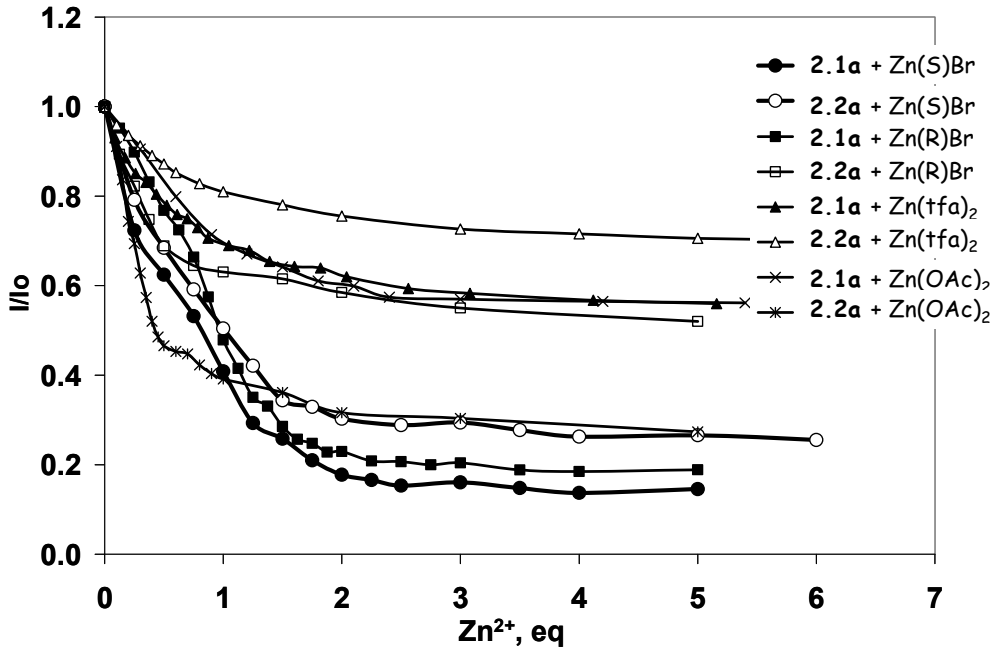

Figure 6.44 Stern-Volmer plots of fluorescent response of **2.1a** (solid) and **2.2a** (hollow) with various Zn^{2+} carboxylates.

6.3.6.6 Rationalization of the CD response

Since the preferred binding modes have been established from the fluorescence, UV-Vis and NMR, the focus is on the secondary interactions. Hence, a distinct CD spectral response observed for **2.1a – 2.3a** in the presence of Zn^{2+} can be attributed to several factors: a) interactions between ribose and carboxylates, b) the ribose conformation and c) the guanine orientation around the Zn^{2+} center.

A coordination geometry and coordination number around the Zn^{2+} center may play an important role in our system. It is well known that, in square-planar platinated bis(guanosine) complexes, the CD signal in the 200 - 350 nm range is due to the chiral coupling between the *cis*-guanine electronic transitions.[16] The observation was attributed to the guanine bases being canted on the coordination plane and the change in the canting direction was related to the Cotton effect, with certain orientations producing negligible CD signal. Hence, the amplification of the CD signal can be related to the exciton chiral coupling via π - π^* transitions between guanines. CD amplification is not limited only to the square planar platinum complexes. Zimmer et al.[19] have observed CD amplification for tetrahedral Zn^{2+}-dinucleotide guanosine complex. Here, the conformational change from preferential *anti* to *syn* orientation of the ribose unit allows for the greater intramolecular stacking between two guanines and in turn produces an observed CD signature band. On account of this, the bis(guanosine) complexes formed by **2.1a** or **2.2a** with $Zn(ClO_4)_2$ must result in the orientation of guanine units that amount to zero Cotton effect, since no CD amplification was observed.

The CD response can also be explained by the electronic structure and steric hindrance of anions. Since the Lewis basicity of the anions follows the order of OAc^- >

$tfa^- > ClO_4^-$, it is conceivable that the observed CD spectral difference may be influenced by the extent of H-bonding between the anions and ribose. For OAc^-, an internal H-bond between the oxygen atom of the acetate ligand bound with Zn^{2+} and the OH group on the $C_{5'}$ of the ribose in **2.1a** is possible, as supported by molecular modeling in Figure 6.45, which will certainly provide a greater conformational rigidity to the ribose, thus causing a greater positive enhancement of the 360 nm CD band. This is also one of the binding modes for **2.2a**. The 2nd binding mode for **2.2a** involves the coordination of $Zn(OAc)_2$ at the 2,2'-dipyridylamino site. For the tfa^- anion, a similar internal H-bonding is possible, but due to the reduced Lewis basicity, the H-bond is likely much weaker, thus resulting in less rigid conformation of the ribose, compared to OAc^-. The ClO_4^- anion is a poor donor and unlikely bound to the Zn^{2+} ion and, as a result, it is unlikely to form an internal H-bonds with the ribose. Hence, no CD amplification is observed in the presence of $Zn(ClO_4)_2$. Dalabar et al.[20] ascribed enhancement in CD amplitude due to the changes around the glycosidic angle. Any small changes associated with the ribose or its atoms can have a profound impact on the sign of the Cotton effect.

In order to probe the effects of the electronic structure of counterions on the chiral amplification, a methylated $Zn[(S)\text{-}O_2CCH(\mathbf{CH_3})CH(CH_3)CH_3]_2$ (Zn(S)Me) analogue was used with **2.1a**. Interestingly, similar CD spectra were obtained as with Zn(S)Br, with ~ 10 % lower CD amplification.

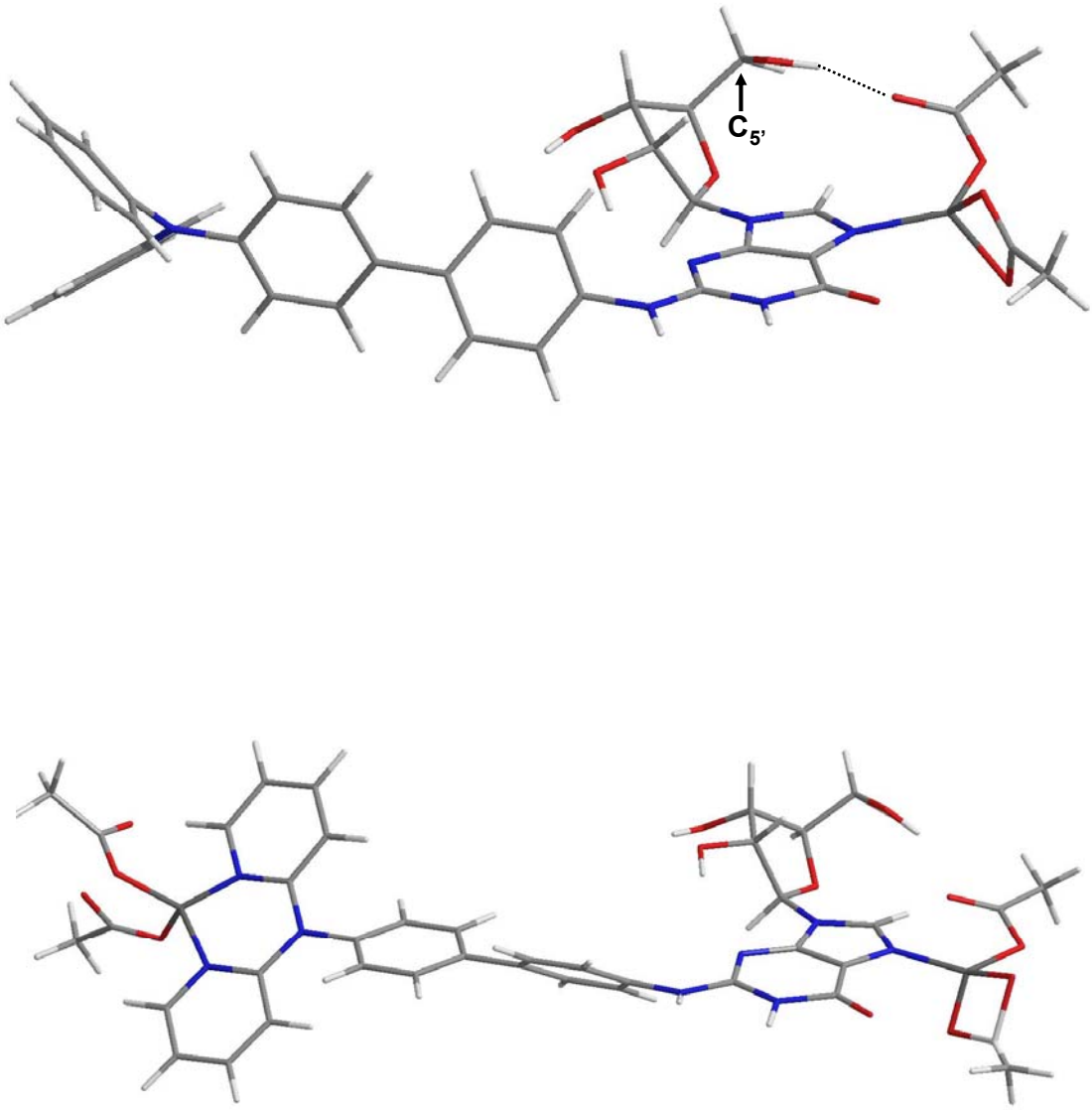

Figure 6.45 Molecular modeling of Zn^{2+} carboxylate complexes of **2.1a** (top) and **2.2a** (bottom).

The study of the effects of the steric hindrance on the chiral induction has been reported previously for a number of organic hosts and guests molecules.[21] Steric hindrance is an important factor in CD sensing, along with solvent and overall structure. A comparison study shows that the addition of $Zn(OAc)_2$ to **2.1a** leads to a most dramatic amplification of CD signal which could be explained in terms of steric hindrance of counterions depicted in Figure 6.46. Large anions, such as butyrate analogues, provide more steric constraints and in turn reduce the favourable interactions of Zn^{2+} with **N²Gs**, which translates into the lower CD enhancement. The proposed binding sites of Group 12 metal ions with **2.1a – 2.3a** considering all the spectroscopic data are depicted in Figure 6.47.

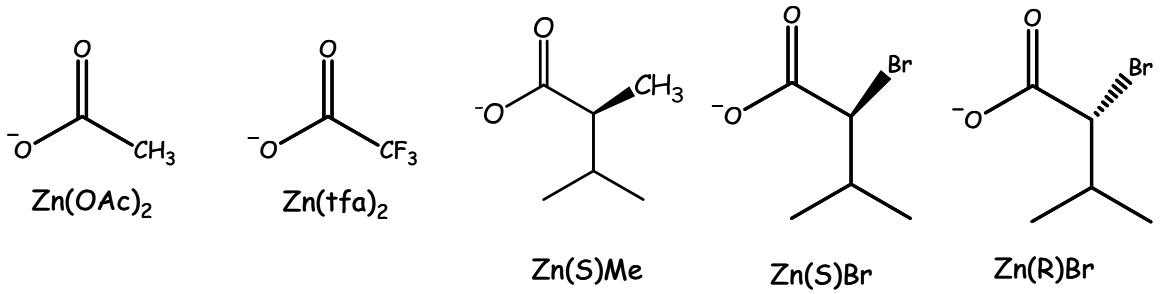

Figure 6.46 Structural representation of various carboxylates.

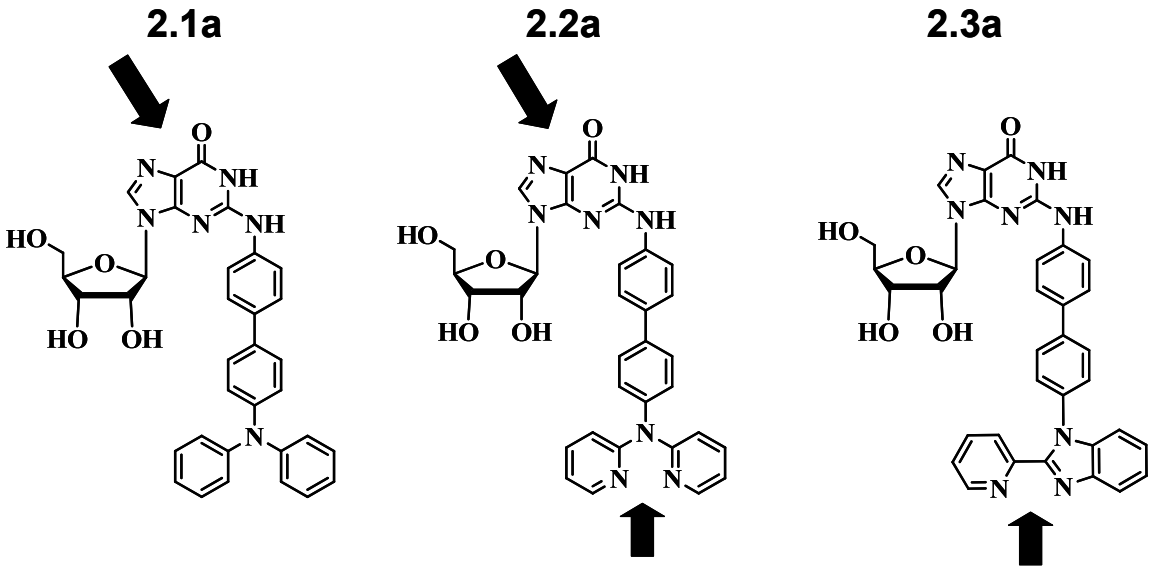

Figure 6.47 Proposed binding modes of **2.1a – 2.3a** in the presence of Group 12 metal ions.

6.4 Conclusions

In this chapter, we demonstrated that the hydrophilic luminescent **N^{2}Gs** are useful probes for the study of metal ion-guanosine interactions *via* fluorescence and CD modes. All three **N^{2}Gs** are sensitive fluorescent probes towards Group 12 metal ions, but their response is dependent of the nature of N^2-substituent and the counterion. In the fluorescence mode, the compound **2.1a** exhibits a "turn-off" fluorescent response while compounds **2.1a** - **2.3a** have a unique "turn-on" fluorescent response toward Group 12 metal ions. The spectroscopic data suggest that the preferred binding site for the metal ions in **2.1a** and **2.2a** is at the guanine N^7-site. For **2.2a**, the 2,2'-dipyridylamino group, albeit a weaker binding site than the guanine, is likely competing for the metal ion. In compound **2.3a**, the preferred binding site is the 2-(2'-pyridyl)benzimidazolyl chelate due to its higher binding affinity. This difference in coordination site is believed to be a

reason for the distinct fluorescent response observed for the non-chelating versus chelating **N^2Gs**.

In the CD mode, both **2.1a** and **2.2a** are highly responsive to Zn^{2+} carboxylates, due to the coordination *via* guanine as well as due to the secondary interactions between the ribose and these anions. Exclusive coordination by the N^2-chelate ligand in **2.3a** results in a negligible CD signal. While these luminescent **N^2Gs** are incapable of effective chiral discrimination by fluorescence or CD, they have a potential as anion sensors due to their ability to differentiate counterions associated with the Zn^{2+} center.

The covalent attachment of the chromophores to the chiral guanosine is clearly important for achieving the distinct fluorescent and CD response upon binding to metal ions. Selectivity and sensitivity observed with the chiral luminescent **N^2Gs** make these biomolecules valuable probes for the study of metal ion-nucleobase interactions. A subsequent incorporation of N^2-arylguanosines into oligonucleotides will allow for determination of their usefulness as the sensing probes.

6.5 References

[1] (a) Zelenak, V.; Gyoryova, K.; Ceckova, M. *Thermochim. Acta* **2001**, *371*, 103. (b) Sigel, H. *J. Am. Chem. Soc.* **1975**, *97*, 3209.

[2] Bozym, R. A.; Thompson, R. B.; Stoddard, A. K.; Fierke, C. A. *Chem. Biol.* **2006**, *1*, 103.

[3] (a) Kimura, E.; Koike, T. *Adv. Inorg. Chem.* **1997**, *44*, 229. (b) Vallee, B. L.; Falchuk, K. H. *Physiol. Rev.* **1993**, *73*, 79.

[4] Wu, F. Y. H.; Wu, C. W. *Metal Ions Biol. Syst.* **1983**, *15*, 157.

[5] Butzow, J. J.; Eichhorn, G. L. *Biopolymers* **1965**, *3*, 95.

[6] (a) Junker, M.; Rodgers, K. K.; Coleman, J. *Inorg. Chim. Acta* **1998**, *275/276*, 481. (b) O'Halloran, T. V. *Science* **1993**, *261*, 715.

[7] Martinez, B. A.; Azorin, F. *Nucleic Acids Res.* **1993**, *11*, 2557.

[8] (a) Munoz de la Pena, A.; Salinas, F.; Gomez, M. J.; Acedo, M. I.; Pena, M. S. *J. Incl. Phenom. Mol. Recogn. Chem.* **1993**, *15*, 131. (b) Connors, K. A. *Binding Constants. The Measurement of Molecular Complex Stability*; John Wiley & Sons: New York, 1987.

[9] (a) Marzotto, A.; Ciccarese, A.; Clemente, D. A.; Valle, G. *J. Chem. Soc., Dalton Trans.* **1995**, 1461. (b) Bolos, C. A.; Christidis, P. C.; Triantafyllou, S. T. *Polyhedron* **1998**, *17*, 2119.

[10] Li, J.; Zheng, W.; Kwon, A. H.; Lu, Y. *Nucleic Acids Res.* **2000**, *28*, 481.

[11] Tanaka, Y.; Toyozawa, A.; Kondo, Y. *Nucleic Acids Res.* **2002**, *2*, 187.

[12] Seward, C.; Pang, J.; Wang, S. *Eur. J. Inorg. Chem.* **2002**, *6*, 1390.

[13] Durantaye, L. D. L.; McCormick, T.; Liu, X. Y.; Wang, S. *Dalton Trans.* **2006**, 5675.

[14] (a) Smith, H. W. *Acta Crystallogr. Sect. B,* **1975**, *31*, 2701. (b) Kerr, M. C.; Preston, H. S.; Ammon, H. L.; Huheey, J. E.; Stewart, J. M. *J. Coord. Chem.* **1981**, *11*, 111.

[15] Liu, S. F.; Wu, Q.; Schmider, H. L.; Aziz, H.; Hu, N. X.; Popovic, Z.; Wang, S. N. *J. Am. Chem. Soc.* **2000**, *122*, 3671.

[16] Benedetti, M.; Tamasi, G.; Cini, R.; Natile, G. *Chem. Eur. J.* **2003**, *9*, 6122.

[17] Buncel, E.; Kumar, R.; Norris, A. R.; Beauchamp, A. L. *Can. J. Chem.* **1985**, *63*, 2575.

[18] (a) Yang, W.; Schmider, H.; Wu, Q.; Zhang, Y.; Wang, S. *Inorg. Chim. Acta* **2000**, *39*, 2397. (b) Seward, C.; Pang, J.; Wang, S. *Eur. J. Inorg. Chem.* **2002**, *6*, 1390. (c) McCormick, T. M.; Wang, S. *Inorg. Chem.* **2008**, *47*, 10017.

[19] Zimmer, C.; Luck, G.; Holy, A. *Nucleic Acids Res.* **1976**, *3*, 2757.

[20] Dalabar, J. M.; Guschlbauer, W. *J. Am. Chem. Soc.* **1973**, *95*, 5729.

[21] Furusho, Y.; Kimura, T.; Mizuno, Y.; Aida, T. *J. Am. Chem. Soc.* **1997**, *119*, 5267.

Chapter 7
Interactions of N^2-Arylguanosines with Phosphorescent Metal Ions

7.1 Introduction

In addition to fluorescent G-nucleosides, development of phosphorescent nucleosides is also of current interest motivated by the high fidelity recognition and self-assembly properties of the substrates. A metallo-nucleoside with a combination of phosphorescence and H-bonding sites can provide the basis for powerful biomolecular sensor, due to its recognition component and photophysical properties. However, designing and developing phosphorescent G-nucleosides[1] bioconjugates is challenging, especially if the synthetic approach mandates the use of the guanine ring. Amongst the target metallo-nucleosides, complexes based on luminescent Ln^{3+} or Ru^{2+} are ideal because some of these metal complexes usually have large Stokes shifts, sharp emissions, low energy emission band, redox stability which make for a desirable biosensor. In previous chapters it was shown that coordination of fluorescent **N^2Gs** to Group 1 and 2 metal cations occurs exclusively at the O^6 atom of guanine, leading to formation of stable fluorescent chiral octamers. By contrast, binding of Group 12 metal ions to fluorescent **N^2Gs** is highly dependent on the type of chelating sites, which in turn governs the fluorescence and CD response of these nucleosides. In this chapter the focus is on the interactions between phosphorescent metal ions and **N^2Gs**.

Several Ln^{3+} complexes, which lack a nucleoside moiety, have been investigated as probes for RNA tertiary structure and folding, as well as for detecting metal binding

sites in RNA.[2] Nonetheless, studies on interactions of Ln^{3+} with nucleosides[3] are limited due to the lack of useful model systems. The luminescent **N^2Gs** developed in previous chapters may be useful for the study of phosphorescent metal ion binding. The chelate site in some of these **N^2Gs** may be used to form coordination compounds with Ln^{3+} ions. Therefore, the first part of this chapter focuses on the fluorescence study of N^2-guanosines, **2.1a – 2.3a**, with Ln^{3+} ions including La^{3+}, Eu^{3+} and Tb^{3+} ions. Tb^{3+} and Eu^{3+} ions were chosen since they are most easily sensitized and produce the bright green and red emissions, respectively.

The other attractive target molecule is a red emissive nucleoside based on the Ru^{2+} complexes. Several phosphorescent Ru^{2+} complexes have been previously synthesized using nucleosides, such as uridine[4], cytosine[5], thymine[6], aden(os)ine[7] and guan(os)ine[1a] by directly attaching the Ru^{2+} moiety *via* conjugated tethers. Ru^{2+} complexes of G-nucleosides are most desirable because they may lead to the formation of phosphorescent supramolecular architectures with interesting photophysical and electrochemical properties. Phosphorescent Ru^{2+}-guanosines can potentially be used to study H-bonding by electrochemistry, since these complexes would exhibit characteristic reduction and oxidation potentials. Hence, the second part of this chapter is devoted to development of Ru^{2+} complexes of **N^2G**. The synthesis and full characterization of a new Ru^{2+} complex **7.1a** (Figure 7.1) is presented, along with its potential application as a sensing probe toward metal ions, anions, nucleosides and polynucleotides.

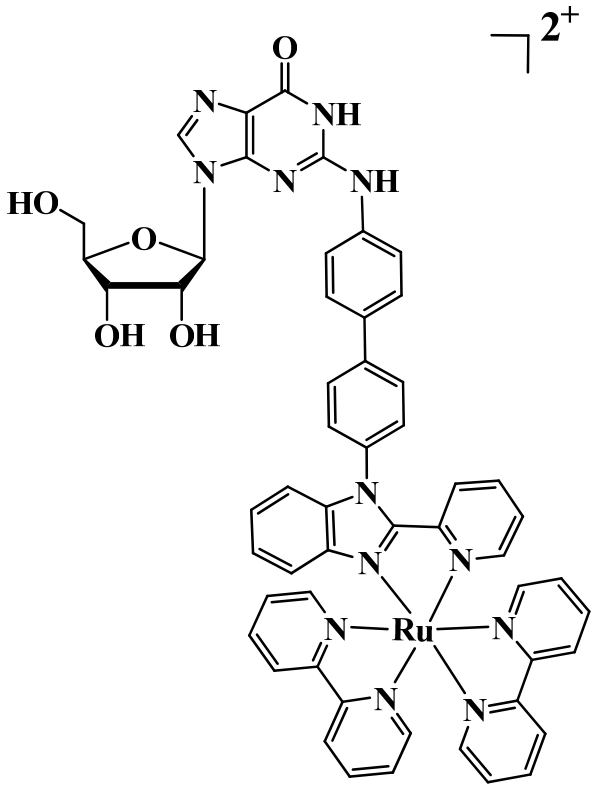

7.1a

Figure 7.1 Structure of **7.1a** complex.

7.2 Experimental Procedure

7.2.1 General considerations

All reagents were purchased from the Aldrich Chemical Co. and used without further purification unless stated otherwise. Typical coupling reactions were carried under nitrogen atmosphere while the coupling reaction involving guanosine was performed in a sealed tube. Thin-layer chromatography was carried out by using silica gel 60 plates, and the column chromatography was performed by using silica gel of particle size 60 – 200 μm and C-18 silica gel for reversed-phase chromatography, all of which were purchased from Silicycle. All 1D and 2D NMR experiments (COSY, NOESY and HMQC) were

recorded on Bruker Avance 400 MHz or 500 MHz spectrometers at 298 K, unless otherwise specified, with the solvent peaks used as the reference. Low resolution and high-resolution mass spectrometry experiments were performed using the electrospray ionization mode on QSTAR XL MS/MS Systems using Analyst QS Method. Excitation and emission spectra were recorded on a Photon Technologies International QuantaMaster Model C-60 spectrometer. All UV-Vis spectra were collected by using Ocean Optics Inc. spectrometer and Spectra Suite software. Circular dichroism (CD) spectra were recorded on a Jasco 715 spectrometer with a 1 cm path length cell at 298 K. Cyclic voltammetry was performed in DMF using BAS CV-50W analyzer with a scan rate of 500 mV s^{-1} and by using the conventional Pt working electrode, Pt auxiliary electrode, Ag/AgCl reference electrode and 0.1 M tetrabutylammonium hexafluorophosphate (TBAP) as the supporting electrolyte.

7.2.2 Synthesis of *p*-2-(2'-pyridyl)benzimidazolyliodobiphenyl-bis(2,2'-bipyridine)ruthenium (II) (7.1)

A mixture of *cis*-dichlorobis(2,2'-bipyridine)ruthenium(II) dihydrate (1.10 g, 2.11 mmol), *p*-2-(2'-pyridyl)benzimidazolyliodobiphenyl (**2.3**) (1.02 g, 2.14 mmol) and ethylene glycol (40 mL) was heated to reflux at 140 ^{o}C for 6 h, then cooled to room temperature. Water (100 mL) was added to the mixture, followed by addition of an aqueous solution (40 mL) of NH_4PF_6 (5.58 g). The resulting precipitate was filtered off and rinsed with water (2 x 20 mL). Rescrystallization from CH_3CN-Et_2O afforded compound **7.1** as a red solid (1.78 g, 82% yield). mp. 207-211 ^{o}C. ^{1}H NMR (500 MHz, $(CD_3)_2CO$, 298 K) δ 8.83 (td, *J* = 8.1, 9.0 Hz, 4H), 8.33 (d, *J* = 4.4 Hz, 1H, Py), 8.32 (m, 2H), 8.23-8.15 (m, 6H), 8.12 (d, *J* = 5.4 Hz, 1H), 8.06 (d, *J* = 5.3 Hz, 1H), 8.00 (dd, *J* = 1.9, 8.2 Hz, 1H), 7.95 (m, 2H), 7.86 (dd, *J* = 2.0, 8.1 Hz, 1H), 7.71-7.68 (m, 3H), 7.62-

7.52 (m, 7H), 7.35 (d, J = 8.3 Hz, 1H), 7.2 (t, J = 7.3, 8.7 Hz, 1H), 6.09 (d, J = 6.8 Hz, 1H) ppm. ^{13}C NMR (500 MHz, $(CD_3)_2CO$, 298 K) δ 158.7, 158.3, 157.7, 157.6, 153.6, 153.0, 152.8, 152.6, 152.3, 151.1, 149.3, 143.1, 141.2, 139.1, 138.7 (2C), 138.6, 138.5, 138.4, 138.3, 138.1, 134.0, 131.4, 129.7 (2C), 129.6, 129.2, 129.1, 128.5, 128.4, 128.3, 128.1, 127.9, 127.3, 126.1, 125.7, 124.9, 124.8, 124.7, 124.5, 119.5, 116.3, 113.1, 94.4 (C-I) ppm. HRMS EI$^+$ *m/z* calcd for $C_{44}H_{32}N_7IRu^{2+}$ 443.5398, found 443.5405.

7.2.3 Synthesis of N^2-(*p*-4,4'-biphenyl-2-(2'-pyridyl)benzimidazolyl)-bis(2,2'-bipyridine)ruthenium(II)guanosine (7.1a)

To a mixture of *p*-2-(2'-pyridyl)benzimidazolyliodobiphenyl-bis(2,2'-bipyridine)ruthenium(II) (**7.1**) (1.72 g, 1.46 mmol), guanosine (0.41 g, 1.45 mmol), cesium carbonate (0.56 g, 1.7 mmol) and copper iodide (0.04 g, 0.22 mmol, 15%), DMSO was added (2 mL). The solution was degassed with nitrogen for 10 minutes. Preheated oil bath was used and the reaction was carried out at 140 ^{o}C for 20 h. To the reaction mixture water (10 mL) was added, and the solution was neutralized to pH ~ 7 using aqueous HCl (0.1 M). Further addition of water (30 mL) led to precipitation of the product as red solid. The solid was washed further with water to remove unreacted guanosine. The crude solid was further purified using the silica gel column with CH_2Cl_2, followed by CH_3CN:H_2O (4:1), and CH_3CN:H_2O:KNO_3 (4:1:1) as the eluents to provide compound **7.1a** as an aqueous red solution. Addition of NH_4PF_6 (0.13 g) resulted in the red precipitate formation, which was isolated and washed with water (10 mL). The product was recrystallized from CH_3CN:Et_2O solvent mixture to give **7.1a** as the red solid (0.07 g, 4 % yield). m.p. 233-240 ^{o}C. ^{1}H NMR (600 MHz, $(CD_3)_2CO$, 298 K) δ 8.12 (dt, J = 7.2, 8.0 Hz, 4H), 8.41-8.28 (m, 3H), 8.25-8.18 (m, 7H), 8.08 (d, J = 5.4 Hz, 1H), 8.02 (s, 1H, H8), 7.98 (t, J = 8.2, 9.3 Hz, 1H), 7.91 (d, J = 7.2 Hz, 2H), 7.87 (d, J = 8.4 Hz, 2H), 7.79 (d, J

= 6.9 Hz, 1H), 7.67 (t, *J* = 6.6, 8.2 Hz, 1H), 7.61 (m, 4H), 7.55-7.51 (m, 2H), 7.47 (t, *J* = 7.9, 8.7 Hz, 1H), 7.36 (d, *J* = 8.3 Hz, 1H), 7.19 (t, *J* = 7.8, 9.1 Hz, 1H), 6.06 (d, *J* = 8.4 Hz, 1H), 6.00 (d, *J* = 4.1 Hz, 1H, $H_{1'}$), 4.71 (m, 2H, C_2-OH, C_3-OH), 4.43 (t, *J* = 4.3, 5.1 Hz, 1H, $H_{2'}$), 4.36 (d, *J* = 4.0 Hz, 1H, C_5-OH), 4.21 (t, *J* = 3.9, 5.3 Hz, 1H, $H_{3'}$), 4.08 (d, *J* = 3.3 Hz, 1H, $H_{4'}$), 3.38 (m, *J* = 7.4, 11.4 Hz 1H, $H_{5'}$), 3.74 (m, *J* = 7.6, 11.2 Hz, 1H, $H_{5''}$) ppm. ^{13}C NMR (400 MHz, DMSO-d_6, 298 K) δ 158.4, 158.0, 157.4, 157.3, 157.1, 153.5, 153.1, 152.7, 152.6, 152.2, 152.0, 150.9, 149.7, 148.9, 141.8, 140.1, 139.5, 139.2, 138.9 (2C), 138.8 (2C), 133.6, 129.5, 129.2, 129.1, 128.9 (2C), 128.8, 128.7 (2C), 128.5 (2C), 128.4 (2C), 128.3, 127.4, 127.3, 126.0, 125.5, 125.4, 125.2 (2C), 125.0 (2C), 124.8, 120.1, 115.7, 97.3, 86.2 (C_1), 78.9 (C_4), 74.2 (C_2), 71.9 (C_3), 62.5 (C_5) ppm. ESI-MS$^+$ *m/z* 521.6068 [$C_{54}H_{44}N_{12}O_5Ru^{2+}$], 1187.1965 [$C_{54}H_{44}N_{12}O_5Ru{\cdot}PF_6^+$]. HRMS ESI$^+$ *m/z* calcd for $C_{54}H_{44}N_{12}O_5Ru^{2+}$ 521.1295, found 521.1293.

7.2.4 Fluorescence titration experiments

To the solutions of **2.1a**, **2.2a** and **2.3a** (3 mL, 7 x 10^{-5} M, THF) various Ln^{3+} acetylacetonato (acac) salts ($La(acac)_3$, $Eu(acac)_3$ and $Tb(acac)_3$) in THF were added in 2 μL aliquots.

7.3 Results and Discussion

7.3.1 Interactions of 2.1a - 2.3a with lanthanides

Acetylacetonato complexes ($La(acac)_3$, $Eu(acac)_3$ and $Tb(acac)_3$) were chosen because of their solubility in organic solvents. Notably, UV-Vis and CD spectroscopies

are not useful for studying lanthanides, due to the strong absorption of $Ln(acac)_3$ in UV-Vis spectra. CD spectra of the ligands remain unaffected in the presence of Ln^{3+} ions. The investigation therefore relies on fluorescence and NMR spectroscopies.

*7.3.1.1 Interactions of **2.1a** with Ln^{3+} ions*

The fluorescent titration data of **2.1a** are presented in Figure 7.2 and it can be seen that fluorescent quenching of the ligand emission (~ 386 nm) occurs with the addition of $La(acac)_3$, $Eu(acac)_3$ and $Tb(acac)_3$. More importantly, the absence of the characteristic Eu^{3+} and Tb^{3+} emission peaks above 500 nm suggests that activation of Ln^{3+} emission is inefficient. The Stern-Volmer plots shown in Figure 7.3 indicate that the efficiency of the ligand fluorescent quenching follows the order: $La^{3+} < Tb^{3+} \approx Eu^{3+}$ ions.

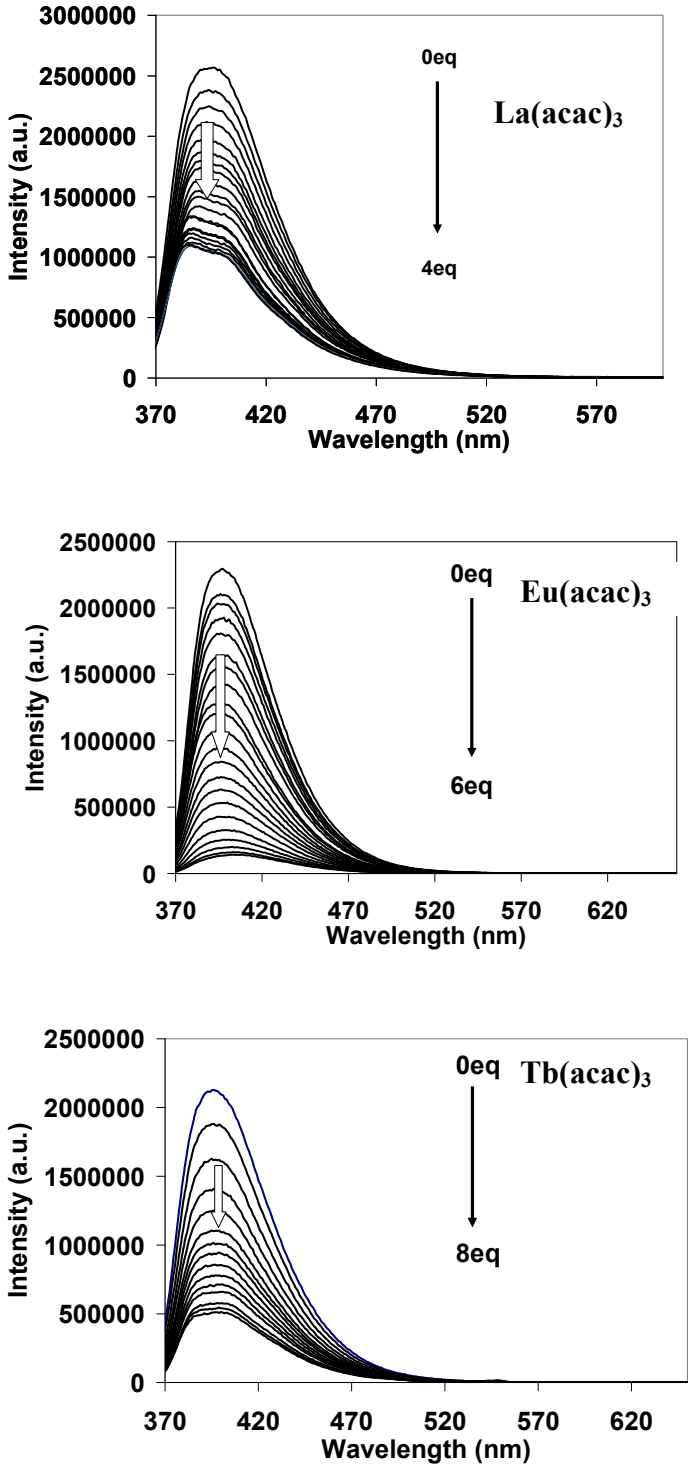

Figure 7.2 Fluorescence titrations of **2.1a** in the presence of different $Ln(acac)_3$ (THF, 7 x 10^{-5} M, λ_{ex} = 358 nm).

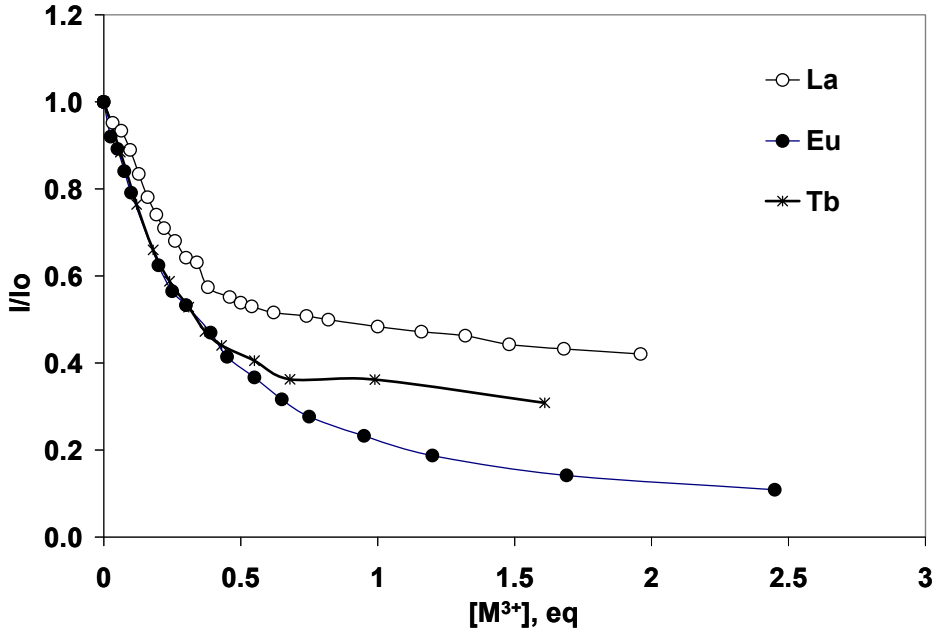

Figure 7.3 Stern-Volmer plots of fluorescence titrations of **2.1a** in the presence of different $Ln(acac)_3$ (THF, 7 x 10^{-5} M, λ_{em} = 386 nm).

Excitation dependent emission was investigated using the spectra of **2.1a** at the end point of the titration experiments. When ligand excitation at ~ 358 nm is used the emission spectrum of compound **2.1a**, in the presence of $Tb(acac)_3$, is characterized by the ligand emission in 350 – 470 range which stems from the $\pi - \pi^*$ transition centered on the guanine-N^2-aryl group (Figure 7.4). A negligible Tb^{3+} emission at 548 nm, associated with $^5D_4 \rightarrow {}^7F_5$ transition, is observed. The excitation at 324 nm results in the sharp emission peaks above 470 nm. The weaker emission bands at 493 nm and 588 nm are due to $^5D_4 \rightarrow {}^7F_6$ and $^5D_4 \rightarrow {}^7F_4$ transitions of Tb^{3+}, respectively. A control study was performed with the solution of $Tb(acac)_3$ and it was found that the excitation at ~ 330 nm also leads to a maximum Tb^{3+} emission, indicating that the excitation band ~ 330 nm is related to acac absorption. Hence, acac ligands are capable of activating Tb^{3+} emissions

much more efficiently than **2.1a** can. There is very little contribution in the 320 – 400 nm range of the excitation band from **2.1a**, indicating that an energy transfer between **2.1a** and Tb^{3+} center is inefficient.

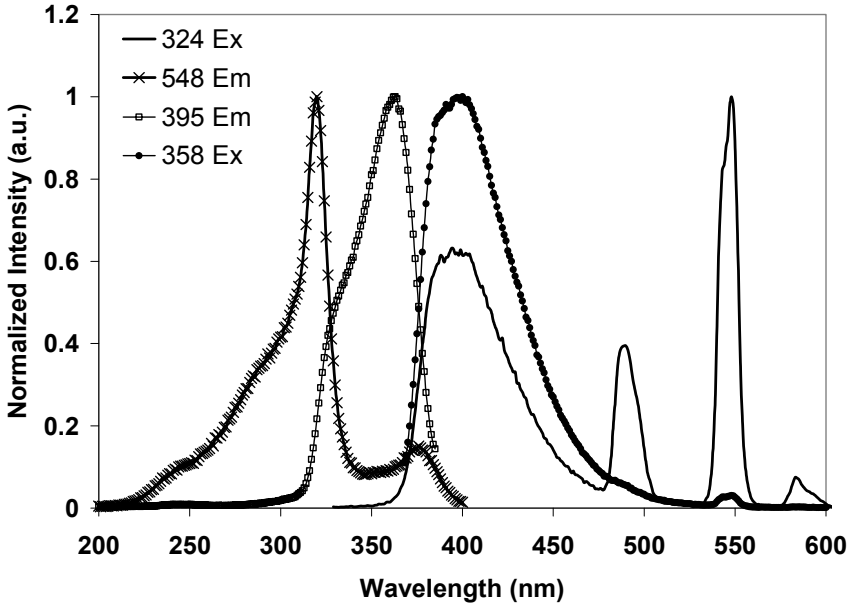

Figure 7.4 Spectra showing excitation and excitation-dependent emissions of **2.1a** with $Tb(acac)_3$ (THF, 7 x 10^{-5} M).

From the normalized emission intensity plot for compound **2.1a**, in the presence of $Eu(acac)_3$, a weak Eu^{3+} emission is observed. The excitation band in 300 – 450 nm range matches well with the absorption of the ligand (Figure 7.5). In addition to ligand absorption, a sharp excitation peak was observed at 465 nm, which can be attributed to the $^5D_2 \rightarrow {}^7F_{0,1}$ transitions and is related to the Eu^{3+} center. Notably, very little contribution from acac ligands is observed in the excitation spectrum indicating that acac is not an efficient sensitizer of Eu^{3+}. The excitation at the 465 nm also leads to the

emission at 613 nm; however, the emission is weaker than when ligand excitation is used. Hence, the activation of Eu^{3+} can be achieved by a direct- and indirect excitation.

The interaction between **2.1a** and $La(acac)_3$ was studied by ^1H NMR in DMSO-d_6 and THF-d_8. In both cases, addition of La^{3+} causes the broadening of H_8 and H_o protons which suggests that the primary binding could be at the guanine ring (Figure 7.6). The exact location, however, could not be determined by NMR.

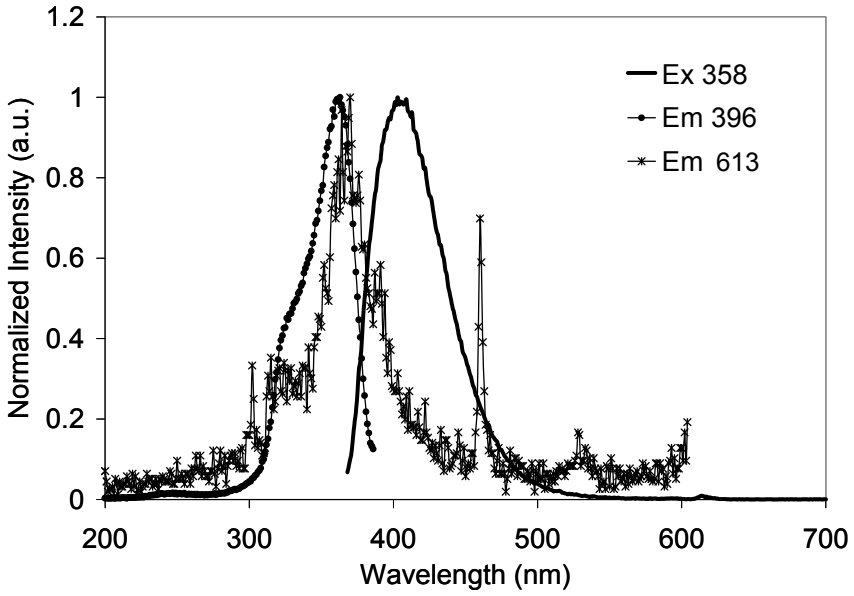

Figure 7.5 Spectra showing excitation and excitation-dependent emissions of **2.1a** with $Eu(acac)_3$ (THF, 7 x 10^{-5} M).

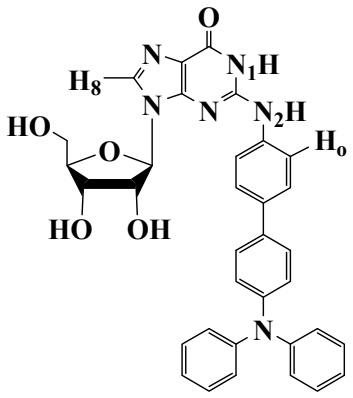

2.1a

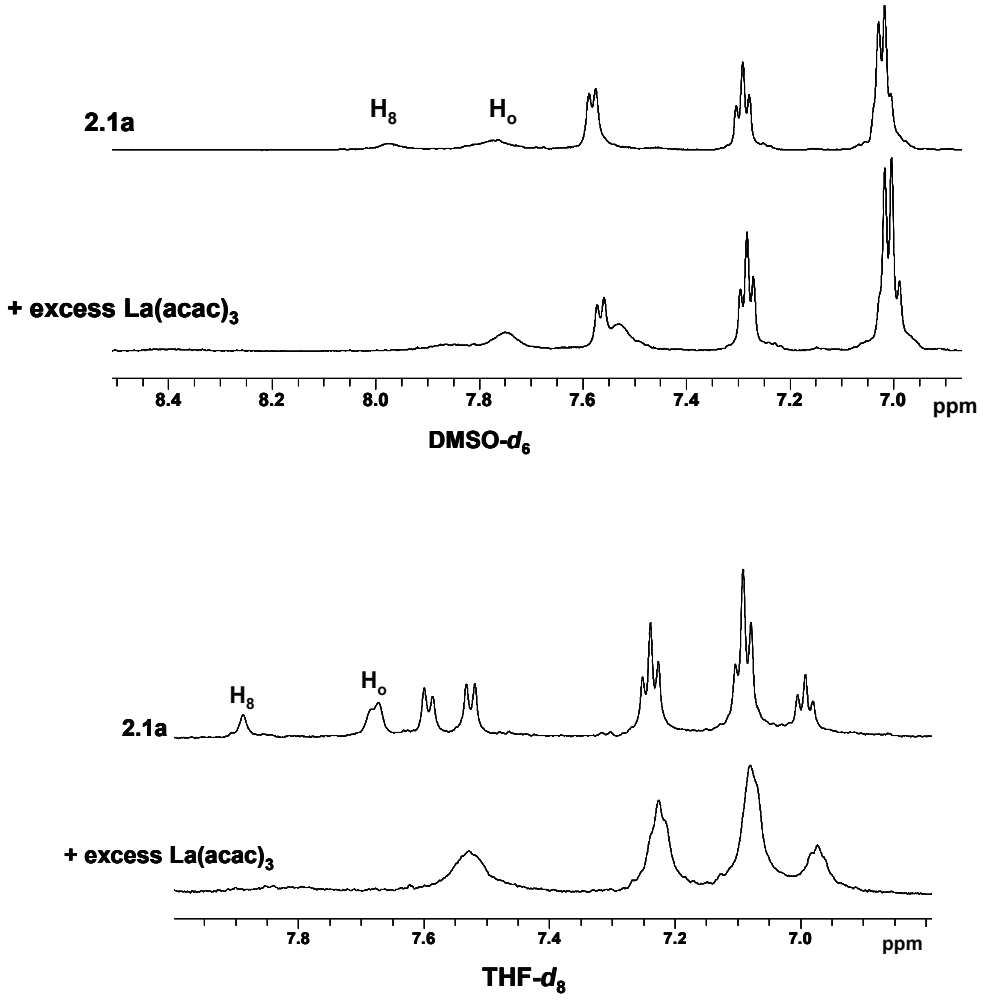

Figure 7.6 ^{1}H NMR spectra of **2.1a** with excess La(acac)$_3$ (DMSO-d_6 (top), THF-d_8 (bottom), 298 K).

The fluorescence and NMR data for **2.1a** in the presence of Ln^{3+} ions indicate that some interaction takes place between metal ions and guanine group, however, the exact location of the binding site could not be determined. Earlier studies on the interactions between Ln^{3+} and G-nucleosides[1d] show that the Ln^{3+} binding takes place at N^7- and/or O^6-sites of guanine. More recently, Wu group[8] has shown that Ln^{3+} interacts with **TAG**, presumably through the O^6 site of guanine, and results in the formation of G-quartet aggregates. Hence, the interactions between Ln^{3+} ions and **2.1a** could potentially involve coordination *via* N^7 or O^6 atoms, or combination thereof, as shown in Figure 7.7.

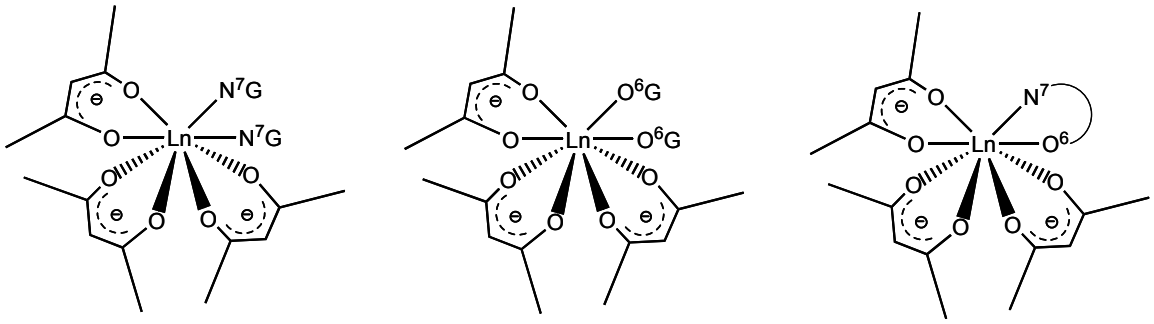

Figure 7.7 Proposed binding modes of **2.1a** with Ln^{3+}.

*7.3.1.2 Interactions of **2.2a** with Ln^{3+} ions*

Unlike **2.1a**, compound **2.2a** contains a chelate 2,2'-dipyridylamino group at the N^2-site, and hence, a different response towards Ln^{3+} ions is therefore expected. Unlike **2.1a**, compound **2.2a** is capable of activating Tb^{3+} emission which is evident by the peak at 546 nm shown in Figure 7.8. **2.2a** is not an effective Eu^{3+} activator and appears to be unstable with $La(acac)_3$. The cause for such anomalous behaviour with La^{3+} is not very well understood but the experimental conditions might be the reason. From the Stern-Volmer plots presented in Figure 7.9 it is unclear which stoichiometric ratio, 1:1 or 2:1

(L:M), is most likely for Ln^{3+}-complexes of **2.2a**. Overall, a fluorescent quenching of ligand emission was observed with the following order of quenching efficiency: $La^{3+} < Tb^{3+} < Eu^{3+}$.

In order to learn more about the source of Tb^{3+} and Eu^{3+} activation, the final fluorescent excitation and emission spectra were analyzed. The excitation at ~ 346 nm, which corresponds to **2.2a** absorption, results in the significant ligand emission band at ~ 370 nm. Furthermore, the presence of very small sharp emission peaks associated with Tb^{3+} indicate that the energy transfer from ligand to Tb^{3+} is not very efficient (Figure 7.10). It should be pointed out, however, that the main difference between **2.1a** and **2.2a** can be found in the 340 - 400 nm region of the excitation spectrum. A larger band in this range is observed for **2.2a** suggesting a greater contribution of the N^2-guanosine in Tb^{3+} activation process. Excitation at the shorter wavelength causes the greatest Tb^{3+} emission, however this process is ascribed to the activation by the supporting acac ligands. The overall Tb^{3+} emission process is induced mostly by the activation from acac with some contributions from the **2.2a**.

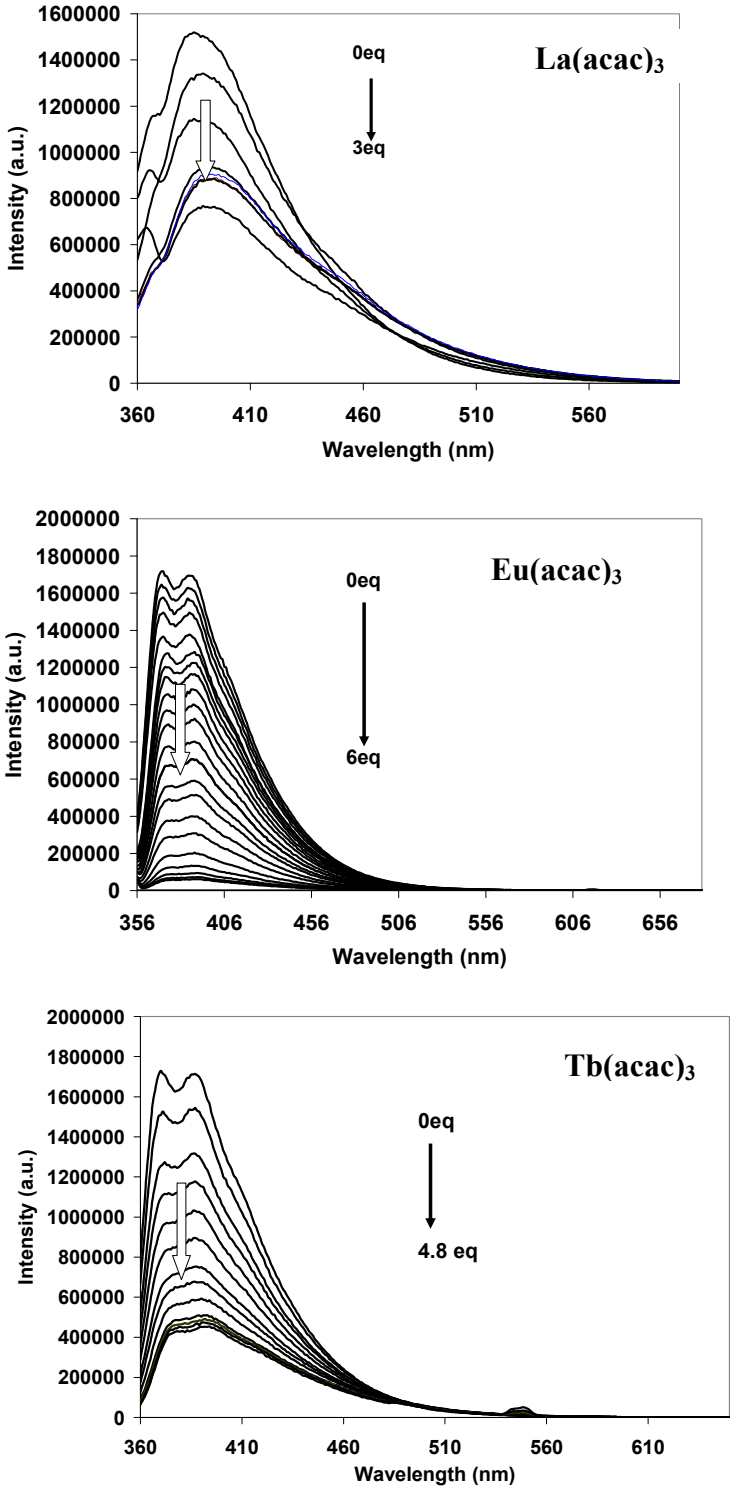

Figure 7.8 Fluorescence titrations of **2.2a** in the presence of different $Ln(acac)_3$ (THF, 7 x 10^{-5} M, λ_{ex} = 346 nm).

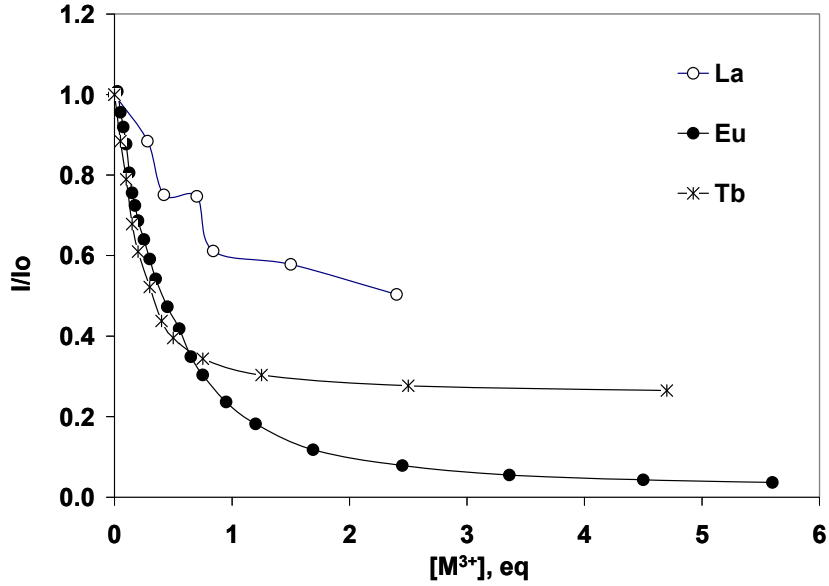

Figure 7.9 Stern-Volmer plots of fluorescence titrations of **2.2a** in the presence of different $Ln(acac)_3$ (THF, 7 x 10^{-5} M, λ_{em} = 370 nm).

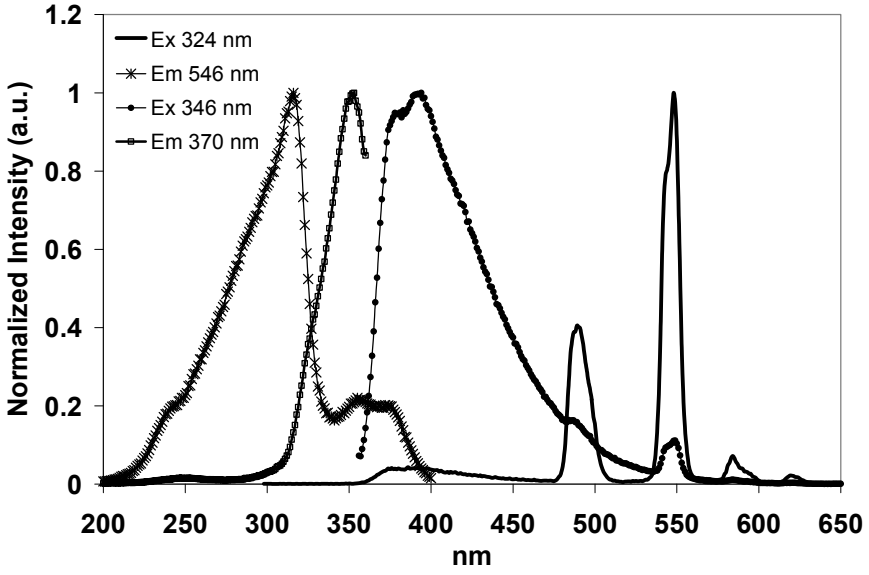

Figure 7.10 Spectra showing excitation and excitation-dependent emissions of **2.2a** with $Tb(acac)_3$ (THF, 7 x 10^{-5} M).

In Figure 7.11, the normalized emission spectra of **2.2a** in the presence of excess Eu^{3+} is characterized by the ligand emission in 350 – 500 nm range with little contribution from the Eu^{3+} emission at 613 nm. Similarly to **2.1a**, the excitation spectrum of **2.2a** is dominated by the ligand absorption in addition to the sharp peak at 465 nm which is related to Eu^{3+} center. The excitation at this longer wavelength also leads to Eu^{3+} emission. The overall process of Eu^{3+} activation can be described as a combination of indirect- and direct excitations.

In order to gain information about the binding site of Ln^{3+}, a ^1H NMR titration of **2.2a** was performed using $La(acac)_3$ in two different solvents. In DMSO-d_6, addition of La^{3+} results in several changes in the ^1H NMR spectra as shown in Figure 7.12: a disappearance of exchangeable protons, N_1H and N_2H, a significant upfield shift of H_8 proton and downfield shift of H_o proton. More importantly, the pyridyl rings remain unaffected. The hydroxyl groups of ribose ring undergo slight changes suggesting that some secondary binding might be taking place with La^{3+} ions. These findings support the idea that the primary binding site is at the guanine ring, however, the exact location could not be determined by NMR. In THF-d_8, the addition of La^{3+} results in the broadening of all peaks in addition to the shifting of the H_8 and H_o resonances, however, the final assignments could not be made due to the extensive overlap and broadness of the peaks.

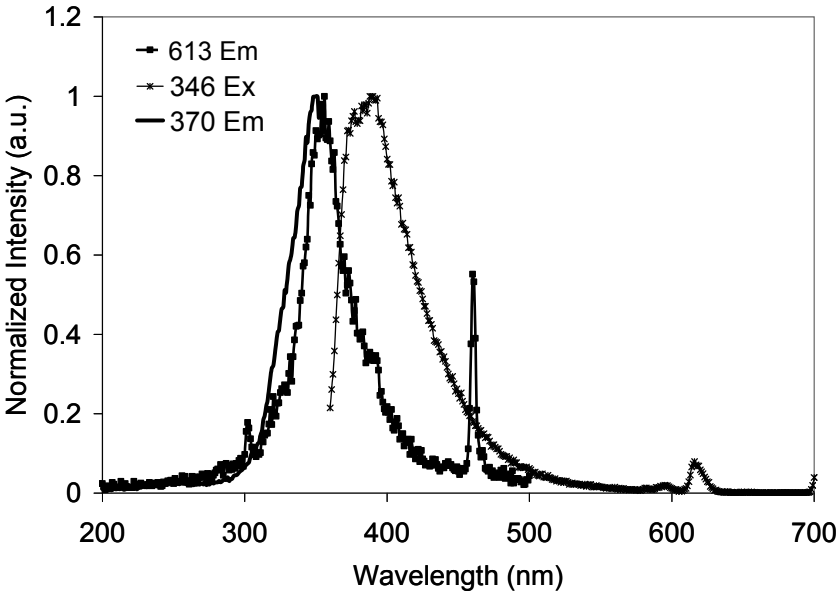

Figure 7.11 Spectra showing excitation and excitation-dependent emissions of **2.2a** with $Eu(acac)_3$ (THF, 7 x 10^{-5} M).

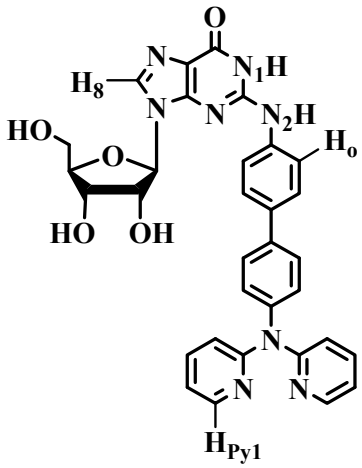

2.2a

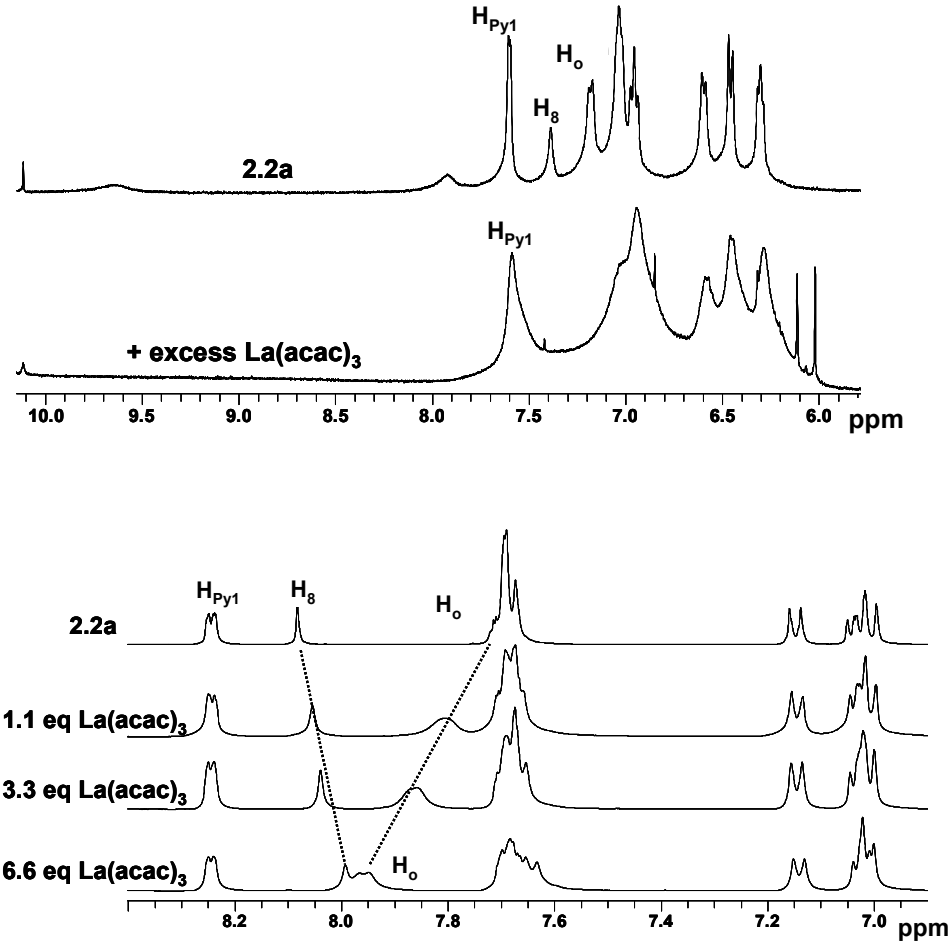

Figure 7.12 ^{1}H NMR titration of **2.2a** with La(acac)$_3$ in THF-d_8 (top) and DMSO-d_6 (bottom) ([**2.2a**] = 1.1 x 10^{-2} M, 298 K).

Taking the fluorescence and NMR data in consideration, several conclusions can be made about Ln^{3+} complexes of **2.2a**. NMR data point towards the coordination of guanine in DMSO-d_6, with minimal involvement by N^2-chelate, but, the situation in THF-d_8 is a little different. Due to the extensive broadening of all ^1H NMR signals it can be proposed that the competition exists between guanine and 2-(2'-dipyridyl)amino groups for La^{3+} ions. For that reason, the Ln^{3+} coordination to the chelate ligand cannot be excluded. Some Ln^{3+} complexes of 2,2'-dipyridyl[9] with La^{3+} and Lu^{3+} were previously identified to have distorted square antiprism geometry with the coordination number eight. In these complexes, 2,2'-dipyridyl acts as a bidentate ligand, along with three acac ligands, completing the coordination sphere. Similar coordination was demonstrated for Pr^{3+} and Eu^{3+} complexes of 2,2'-dipyridylamino ligands.[10] Hence, the proposed binding modes of **2.2a** with Ln^{3+} involve the interactions with N^2-chelate, as reported in literature, or interactions with N^7- and/or O^6-site of guanine, analogous to **2.1a** (Figure 7.13).

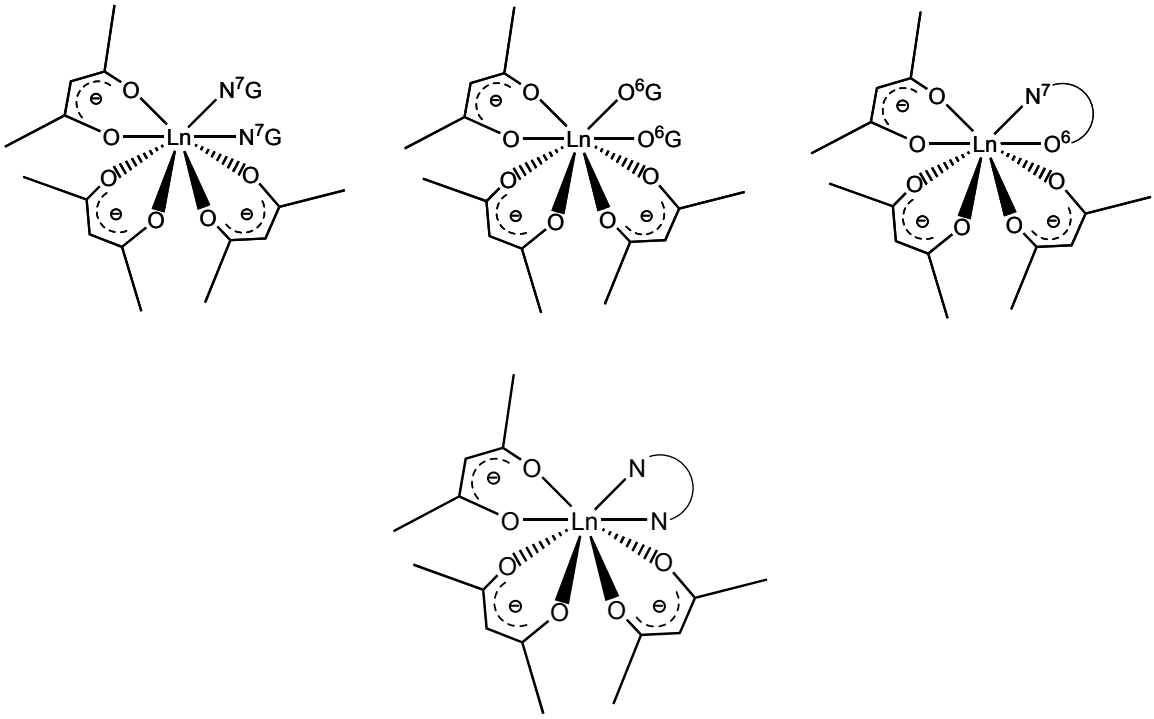

Figure 7.13 Proposed binding modes of **2.2a** with Ln^{3+}.

*7.3.1.3 Interactions of **2.3a** with Ln^{3+} ions*

In the presence of La^{3+}, a negligible fluorescent quenching of **2.3a** at ~ 412 nm is followed by the red shift (~ 50 nm) and the recovery of fluorescence intensity as shown in Figure 7.14. The addition of Eu^{3+}, on the other hand, results in the dramatic fluorescence quenching followed by a similar red shift. The response towards Tb^{3+} lies somewhere in between La^{3+} and Eu^{3+} in that it starts with a red shift (~ 50 nm) followed by ~ 40 % quenching of fluorescent intensity. Unlike **2.2a**, **2.3a** is more efficient in activating Eu^{3+} and Tb^{3+} emissions, as can be seen by the sharp peaks at 613 nm and 546 nm, respectively. The quenching efficiency follows the same trend as that seen for the two other ligands (Figure 7.15).

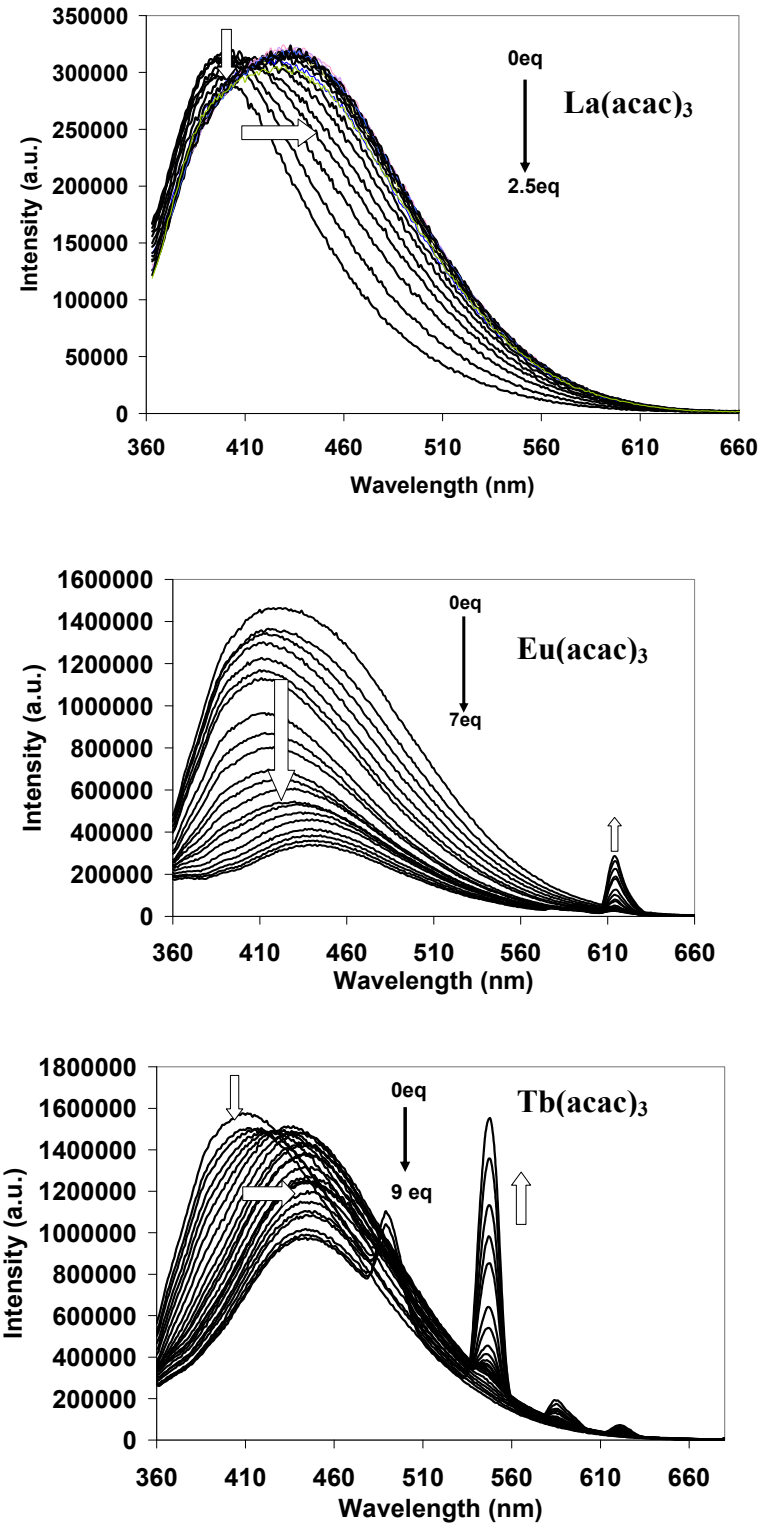

Figure 7.14 Fluorescence titrations of **2.3a** in the presence of different Ln(acac)$_3$ (THF, 7 x 10^{-5} M, λ_{ex} = 343 nm).

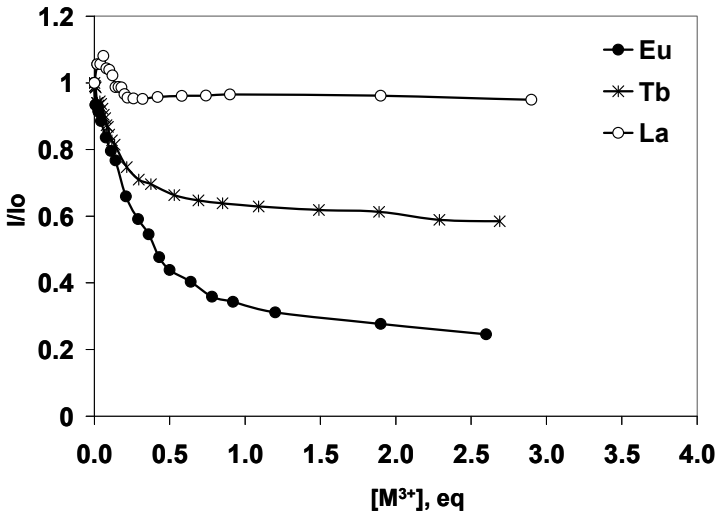

Figure 7.15 Stern-Volmer plots of fluorescence titrations of **2.3a** in the presence of different $Ln(acac)_3$ (THF, 7 x 10^{-5} M, λ_{em} = 412 nm).

The investigation of the final emission spectrum in the presence of Tb^{3+} clearly indicates that the efficient sensitization is taking place. The emission spectrum in Figure 7.16 is dominated by the **2.3a** contribution. The source of Tb^{3+} emission at 546 nm comes from the direct energy transfer from acac ligands but it also contains a broad excitation band in 320 – 410 nm range, indicative of the large contribution from the N^2-ligand.

From the final emission spectra, in the presence of $Eu(acac)_3$, it can be seen that the excitation at the absorption of **2.3a** causes large activation of Eu^{3+} emission. The narrow emission band at 613 nm is due to $^5D_0 \rightarrow {}^7F_2$ transition while the weak emission bands are associated with the $^5D_0 \rightarrow {}^7F_1$ and $^5D_0 \rightarrow {}^7F_0$ transitions (Figure 7.17). Notably, the fluorescence intensity of **2.3a** in 370 – 570 nm range is comparable to the emission intensity related to Eu^{3+} (~ 613 nm). A very small contribution from the excitation peak at 465 nm, compared to the ligand excitation at 344 nm, indicates that the sensitization

process is mostly *via* energy transfer induced by an indirect excitation of Eu^{3+}. This suggests that the Eu^{3+} activation is mostly due to energy-transfer from the **2.3a** to the metal center rather than through a direct excitation.

A dramatic red shift in the fluorescent emission of **2.3a**, upon addition of Ln^{3+}, indicates that the major binding site in **2.3a** is at the 2-(2'-pyridyl)benzimidazolyl group, analogues to the trends observed with Group 12 metal ions reported in Chapter 6. In the presence of Ln^{3+}, the emission energy of **2.3a** is red-shifted from 410 nm to 444 nm. Indeed, a number of Ln^{3+} complexes based on the same chelate site exist.[11] For example, the Eu^{3+} ion can bind one 2-(2'-pyridyl)benzimidazolyl ligand in a bidentate fashion along with three acac ligands to complete a coordination sphere. Based on the previous findings, we can propose that **2.3a** potentially forms similar Ln^{3+} complexes which contain one N^2-chelate ligand analogous to **2.2a** (Figure 7.18).

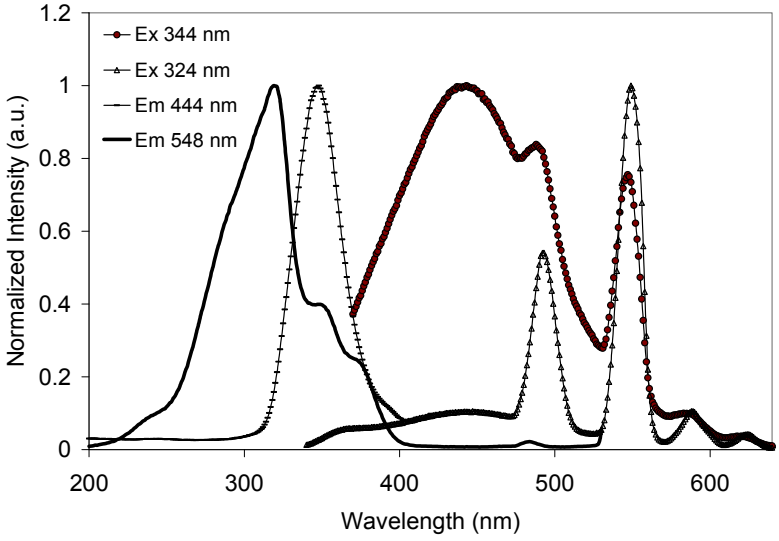

Figure 7.16 Spectra showing excitation and excitation-dependent emissions of **2.3a** with $Tb(acac)_3$ (THF, 7 x 10^{-5} M).

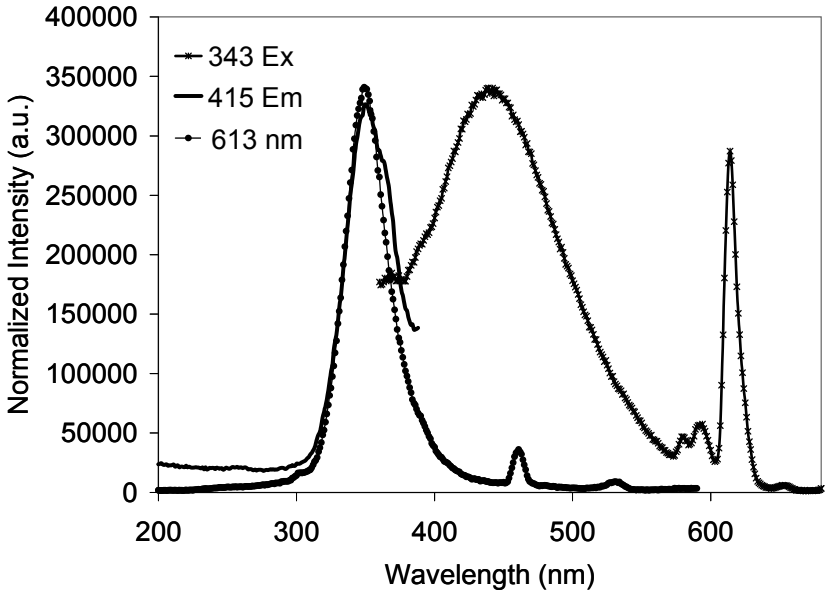

Figure 7.17 Spectra showing excitation and excitation-dependent emissions of **2.3a** with $Eu(acac)_3$ (THF, 7 x 10^{-5} M).

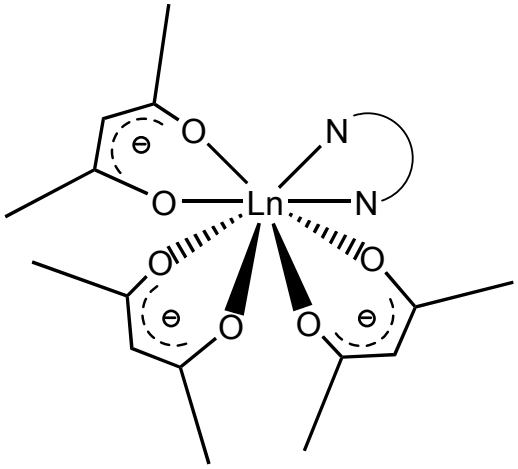

Figure 7.18 Proposed binding site of **2.3a** with Ln^{3+} ion.

*7.3.1.4 Comparison study of fluorescent response of **2.1a – 2.3a** towards $Ln(acac)_3$*

As demonstrated above, the activation of Tb^{3+} emission in all three ligands is two-fold, stemming from the indirect energy transfer from the supporting acac ligands or from

N^2Gs, depending on the N^2-substituent. However, the greater the ligand contribution in the final excitation spectrum, judging by the broad absorption in the 310 – 400 range, the more efficient Tb^{3+} sensitization by that ligand.

For the purpose of comparing the extent of fluorescent quenching of ligand emissions with the Ln^{3+} emission (either Tb^{3+} or Eu^{3+}), two Stern-Volmer plots are presented. From the Stern-Volmer plots with $Tb(acac)_3$ in Figure 7.19 it can be seen that excitation at the ligand absorption in **2.1a** leads to Tb^{3+} emission only after addition of over 1 eq of metal ions. By contrast, the excitation at the absorption of **2.2a** and **2.3a** causes immediate activation of Tb^{3+} emission, indicating that these two compounds are better sensitizers. The extent of ligand quenching is not related to the efficiency of Ln^{3+} activation, which is evident by comparing **2.1a** and **2.2a**, both of which undergo similar fluorescent quenching but behave differently in activating Tb^{3+} emission.

Similar trends are observed for the fluorescence data in the presence of Eu^{3+} ions. The Stern-Volmer plots presented in Figure 7.20 indicate that **2.1a** is a poor activator of Eu^{3+} emission at 613 nm, unlike compounds **2.2a** and **2.3a**. The overall quenching of ligand emission is not directly related to the activation of Eu^{3+}. For example, while the emissions of **2.1a** and **2.2a** are equally quenched, the latter is much more effective in the activation of Eu^{3+} emission.

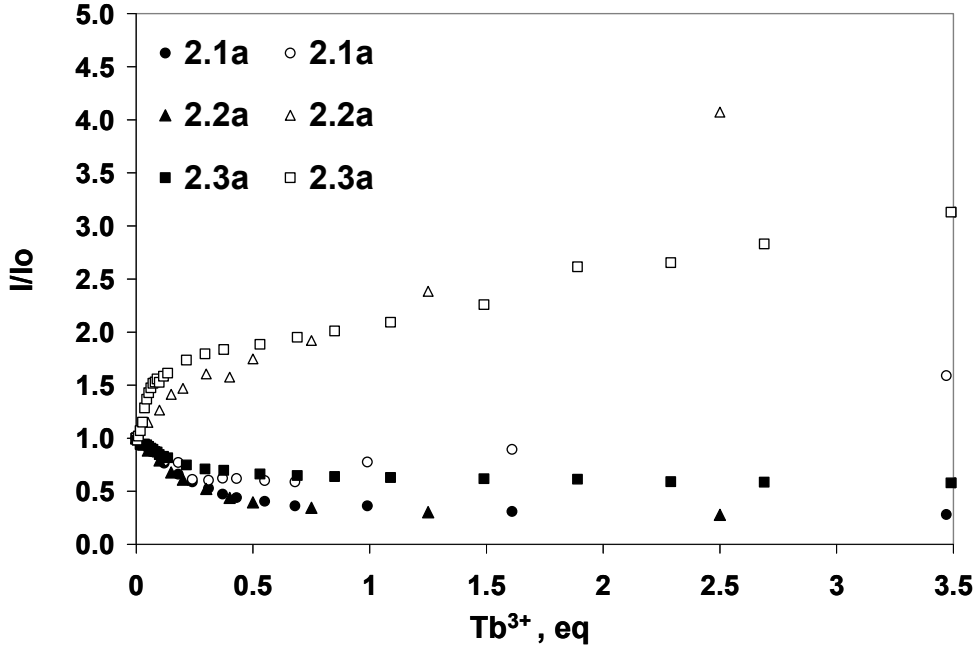

Figure 7.19 Stern-Volmer plots of compounds **2.1a** – **2.3a** in the presence of $Tb(acac)_3$ (THF, 7 x 10^{-5} M, solid = ligand emission, empty = emission at 548 nm).

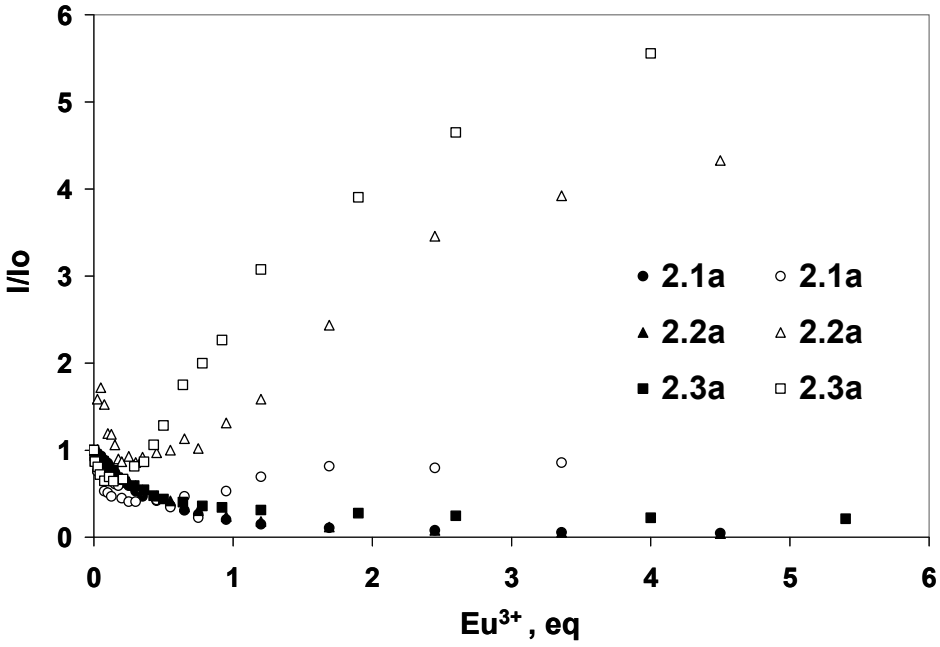

Figure 7.20 Stern-Volmer plots of compounds **2.1a** – **2.3a** in the presence of $Eu(acac)_3$ (THF, 7 x 10^{-5} M, solid = ligand emission, empty = emission at 613 nm).

The difference in the efficacy of Ln^{3+} sensitization can be explained by the matching of energies between excited states of ligands with that for the excited state of Ln^{3+}. For the sensitization process to be thermodynamically favourable the energy of T_1 of the chromophore should be above the excited state (f^*) of Ln^{3+} to prevent the back energy transfer from the lanthanide excited state (f^*) to T_1 of the ligand.[12] The energies of T_1 of the **2.1a, 2.2a** and **2.3a** have not been determined. In all three compounds, the emission band from the ligand is significant in intensity indicating that the energy transfer is not very efficient. A poor performance of these G-nucleosides may be due to the poor match between the energies of T_1 of ligands with the absorption of $Ln(acac)_3$. We were unable to quantify the efficiency of **N^2Gs** in terms of energy transfer with Ln^{3+}. It is possible that **N^2Gs** may be effective activators for other Ln^{3+} complexes due to the supporting ligand influence on the absorption spectra of the complex. Due to the solubility issues associated with **N^2Gs**, which in turn limits the choice of Ln^{3+} complex, other complexes were not studied. In conclusion, compound **2.1a** is a poor activator of Ln^{3+} emissions, while **2.2a** and **2.3a** are promising sensitizers of the Ln^{3+} *via* indirect excitation pathway.

7.3.2 Phosphorescent Ru^{2+} complexes of N^2Gs

7.3.2.1 Syntheses

The choice of using 2-(2'-pyridyl)benzimidazolyl ligand in our study is based on several considerations. First, it has been demonstrated that this ligand is an excellent chelate ligand for binding to Ru^{2+} metal center.[13] Second, we have shown in Chapter 2 that N^2-modified guanosine, **2.3a**, is a bright blue emitter, hence it would be interesting to

develop its Ru^{2+} analogue for comparison study. All Ru^{2+}-complexes were fully characterized by 1D and 2D NMR and high-resolution mass spectrometry.

*7.3.2.1.1 Synthesis of **7.1***

The first step towards the synthesis of Ru^{2+}-complexes involves the complexation of chelating iodoaryl, **2.3**, with $Ru(bpy)_2Cl_2$ by using the procedure previously reported by Wang group.[13] The complex **7.1** was obtained in high yield by performing the reaction in ethylene glycol at 140 ^{0}C, as shown in Figure 7.21. The final complex was isolated by precipitation with NH_4PF_6 and further recrystallized with CH_3CN:Et_2O.

Since the complexation involves the use of racemic $Ru(bpy)_2Cl_2$, the final unsymmetrical complex, **7.1**, is not optically pure, rather it is a mixture of stereoisomers. All stereoisomers of **7.1** appear to be equivalent in the ^{1}H NMR spectrum at 298 K and could not be resolved even at low temperatures. The ^{1}H NMR data suggest that **7.1** is a mixture of isomers due to the steric hindrance associated with H_{Py1} proton of 2-(2'-pyridyl)benzimidazolyl and H_{bpy1} protons of the bpy ligands.

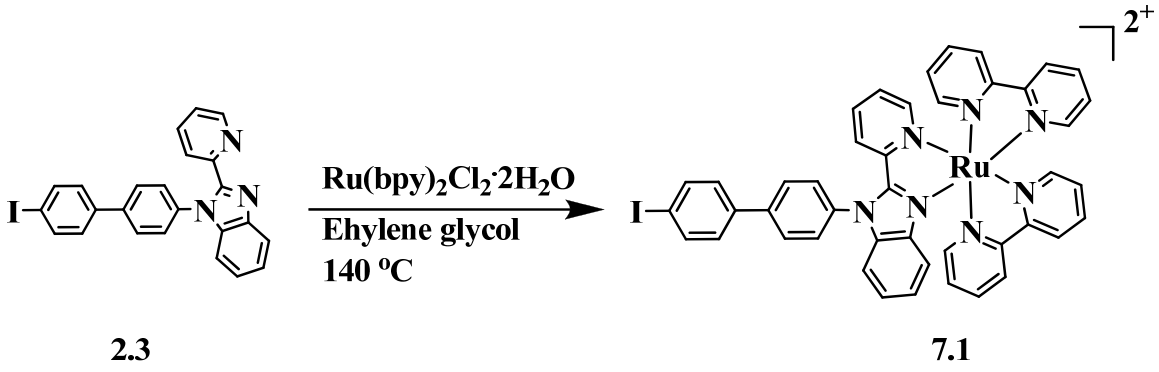

2.3 **7.1**

Figure 7.21 Reaction scheme for the synthesis of complex **7.1**.

*7.3.2.1.2 Attempted synthesis using direct coordination of **2.2.a** with Ru^{2+}*

Due to the chelating ability of several **N^2Gs**, described in Chapter 2, direct coordination chemistry was attempted for the synthesis of Ru^{2+} complex. Compound **2.2a** was chosen as the staring material since it has been isolated in the greater yield over other chelating **N^2G**. The initial synthesis involved the use of $Ru(bpy)_2Cl_2$ with chelating **2.2a**, as shown in Figure 7.22; however, no products were identified by ^{1}H NMR. This methodology was abandoned and the Ullmann condensation reaction was chosen for the synthesis of Ru^{2+}-guanosine complex, since it was shown to be an efficient way for making **N^2Gs** in general.

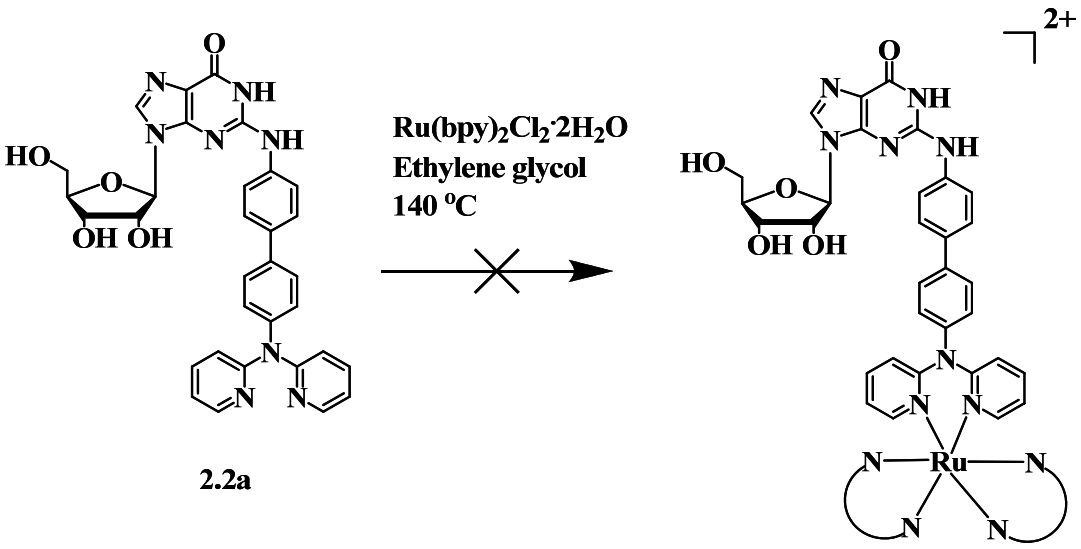

Figure 7.22 Proposed synthesis *via* direct coordination at N^2-chelate site.

*7.3.2.1.3 Synthesis of **7.1a**.*

For the synthesis of **7.1a,** Ullmann condensation reaction was used, as shown in Figure 7.23, analogous to the procedure reported in Chapter 2. Despite the low yield (~ 4 %), the methodology is promising since it involves a direct C-N cross-coupling by using unprotected guanosines in a single-step reaction. In addition, the isolated amount of the

product allowed for the full characterization and some preliminary sensing studies. Complex **7.1a** was isolated by silica gel column chromatography using a mixture of H_2O-CH_3CN-sat. KNO_3 (1:10:0.1) as eluents. The aqueous solution of the final product was treated with a saturated solution of NH_4PF_6 which resulted in the precipitate formation, [**7.1a**]•$2PF_6$. By anion exchange reaction, a chloride derivative, [**7.1a**]•Cl_2, was also obtained in order to extend the solubility of the final complex.

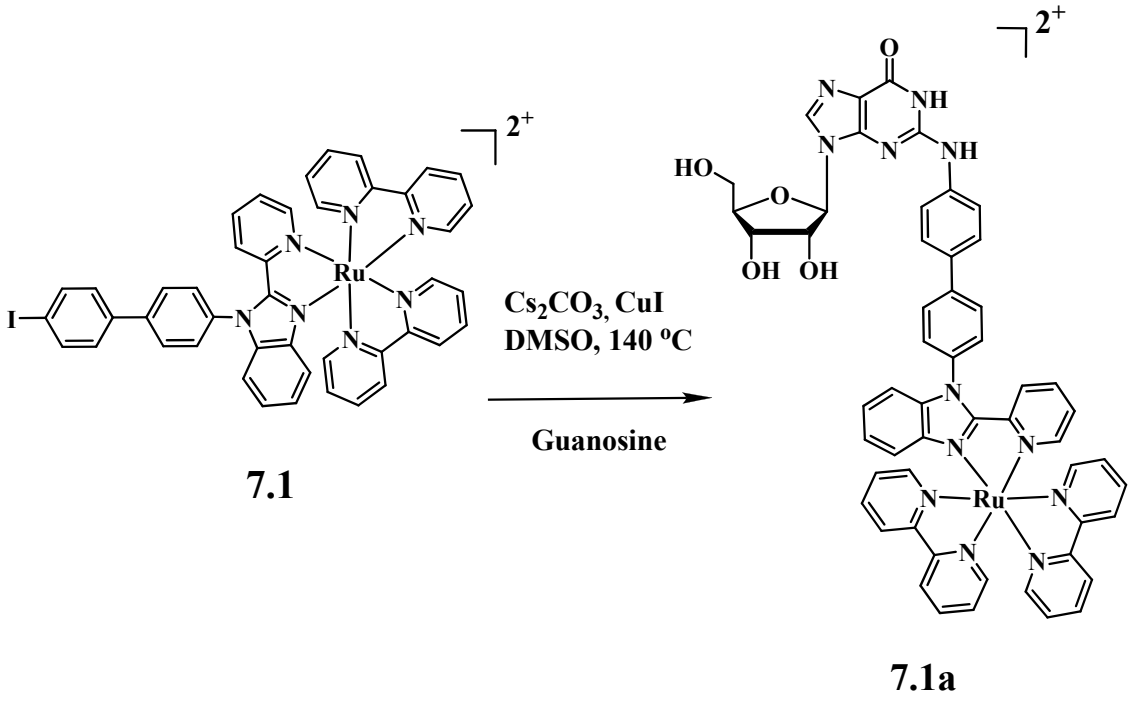

Figure 7.23 Reaction scheme for the synthesis of the complex **7.1a**.

The final Ru^{2+}-complex, **7.1a**, is a mixture of stereoisomers, due to the coupling of homochiral D-guanosine with isomers of **7.1**. The stereoisomers of **7.1a** are non-separable using column chromatography and appear to be equivalent in the ^1H NMR spectra in D_2O, acetone-d_6 and DMSO-d_6 given in Figure 7.24.

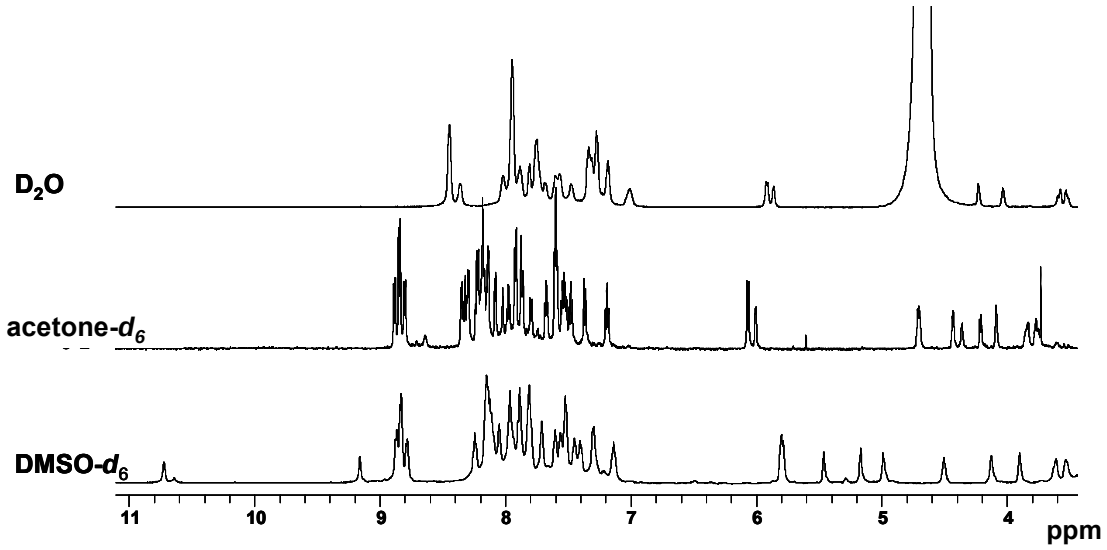

Figure 7.24 Partial ^{1}H NMR spectra of **7.1a** in different solvents (298 K).

7.3.2.1.4 Attempted synthesis of optically pure Ru^{2+} complex

A pure chiral Ru^{2+}-polypyridyl complex is a desirable biological probe for chiral recognition and discrimination.[14] Hence, synthesizing the optically pure metal complexes is of interest. Since the starting material used in the previous section was not optically pure, we decided to prepare an optically pure Δ-$[Ru(bpy)_2(py)_2]^{2+}$-*O*,*O*-dibenzoyl (*S*,*S*)-tartrate salt as a starting material by using the literature method.[15] For the synthesis of optically pure Ru^{2+}-guanosine complex the working assumption is that the substitution of the pyridyl groups in the chiral complex can be achieved with the retention of configuration under certain reaction conditions.

Unlike ligand **2.3a,** the chelating ligand **2.2a** is symmetric thus reduces the number of possible stereoisomers when bound to $[Ru(bpy)_2]^{2+}$. In addition, due to the greater availability of **2.2a** over **2.3a**, the former ligand was used in the synthesis. The

proposed reaction pathway shown in Figure 7.25 involves the use of **2.2a** and Δ-$[Ru(bpy)_2(py)_2]^{2+}$-*O*,*O*-dibenzoyl (*S*,*S*)-tartrate salt at high temperatures.

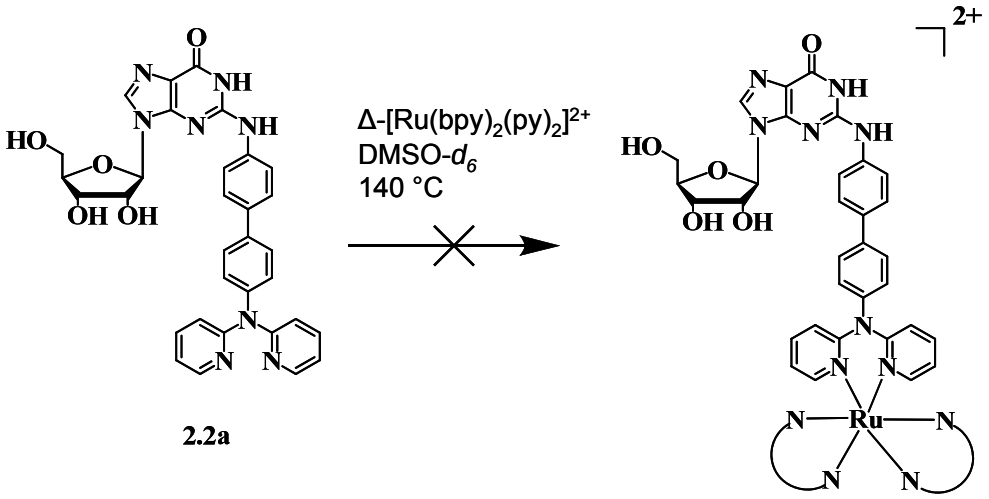

Figure 7.25 Reaction scheme for synthesis of Δ-$[Ru(bpy)_2(\mathbf{N^2G})]^{2+}$.

Due to the limited amount of the starting material, pure Δ-Ru complex, the reaction was monitored and performed in a sealed NMR tube in DMSO-d_6. ^{1}H NMR spectra of the pure ligand **2.2a** and the Δ-$[Ru(bpy)_2(py)_2]^{2+}$-*O*,*O*-dibenzoyl (*S*,*S*)-tartrate salt are shown in Figure 7.26, along with the reaction mixture (1:1) at t = 0 h and t = 5 h. The most informative proton resonance indicative of the successful ligand substitution reaction is associated with the H_{Py1} protons of 2,2'-dipyridylamino group in **2.2a**. Clearly no changes are observed for these protons suggesting that coordination of **2.2a** to Ru^{2+} did not take place. The dramatic change associated with Δ-$[Ru(bpy)_2(py)_2]^{2+}$ complex at t = 5 h can be explained as follows. The substitution reaction involving DMSO-d_6 and pyridyl groups could result in a number of different Ru^{2+} complexes along with Ru^{2+} precursor, and hence in appearance of multiple signals in NMR spectrum.

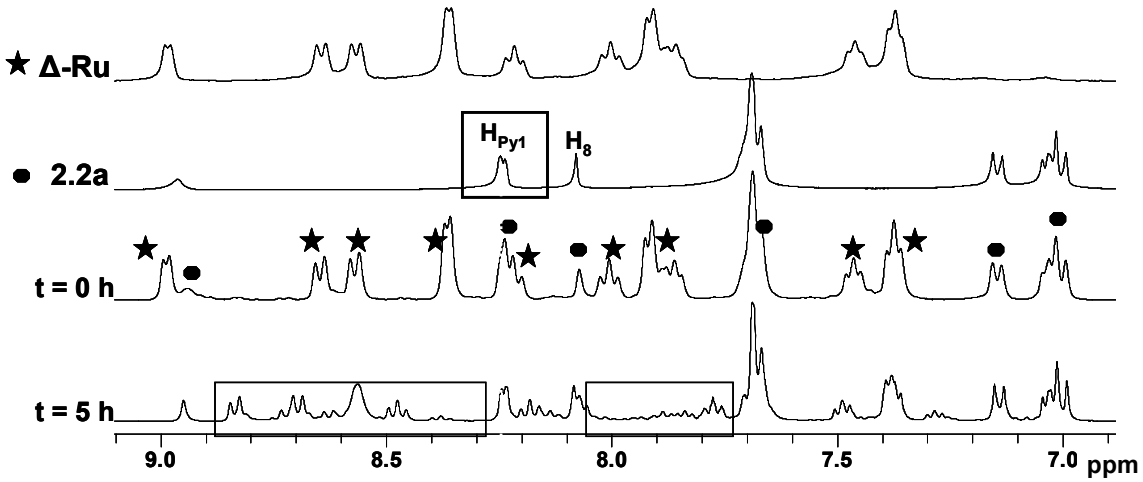

Figure 7.26 Partial ^{1}H NMR spectra of pure Δ-$[Ru(bpy)_2(py)_2]^{2+}$, **2.2a** and reaction mixture (1:1) at t = 0 h and t = 5 h (298 K, DMSO-d_6).

*7.3.2.2 Photophysical properties of **7.1** and **7.1a**.*

UV-Vis absorption and emission data are presented in Table 7.1. Compared to the corresponding ligand (**7.1**), the final guanosine complex, **7.1a**, has a similar UV-Vis absorption bands at 202, 240, 291 and 463 nm in CH_3CN as shown in Figure 7.27. The absorption bands at ~ 290 and ~ 460 nm are typically associated with π – π* transition within bpy moieties and d – π* transition within Ru^{2+} complex, respectively. The weak and broad absorption band in 390 – 540 nm region gives the compounds **7.1** and **7.1a** the red colour which is typically attributed to MLCT. The optical energy gaps of **7.1** and **7.1a** were determined from the absorption edge of their respective UV-Vis spectra.

When excited by light at the wavelength that corresponds to the MLCT absorption band, both Ru^{2+} complexes, **7.1** and **7.1a**, emit a bright red colour in solution with the nearly identical phosphorescent emission bands at ~ 615 nm (Figure 7.27). The

phosphorescence decay lifetime of **7.1a** was determined to be ~ 6 μs, which is comparable to other Ru^{2+} complexes. From the relative emission spectra it is evident that **7.1a** has a weaker emission, possibly due to the quenching effect by guanine unit. The similarity in the optical properties of the guanosines-containing and guanosine-free Ru^{2+} complex suggests that a very weak electronic communication exists between guanine chromophore and Ru^{2+} center.

Table 7.1 Photophysical properties of **7.1** and **7.1a**.[a]

Compound	**Absorption**	**Emission**	**τ**	**Optical bandgap**
	λ_{max} (ε_{max}) [nm ($M^{-1}cm^{-1}$)]	λ_{ex} / λ_{em} (nm)	(μs)	(eV)
7.1a	202 (53000) 240 (15900) 291 (29500) 463 (5900)	466 / 615	6.1	2.19
7.1	206 (48533) 244 (24633) 289 (49360) 462 (10232)	466 / 615	7.6	2.19

[a] 1 x 10^{-5} M, CH_3CN.

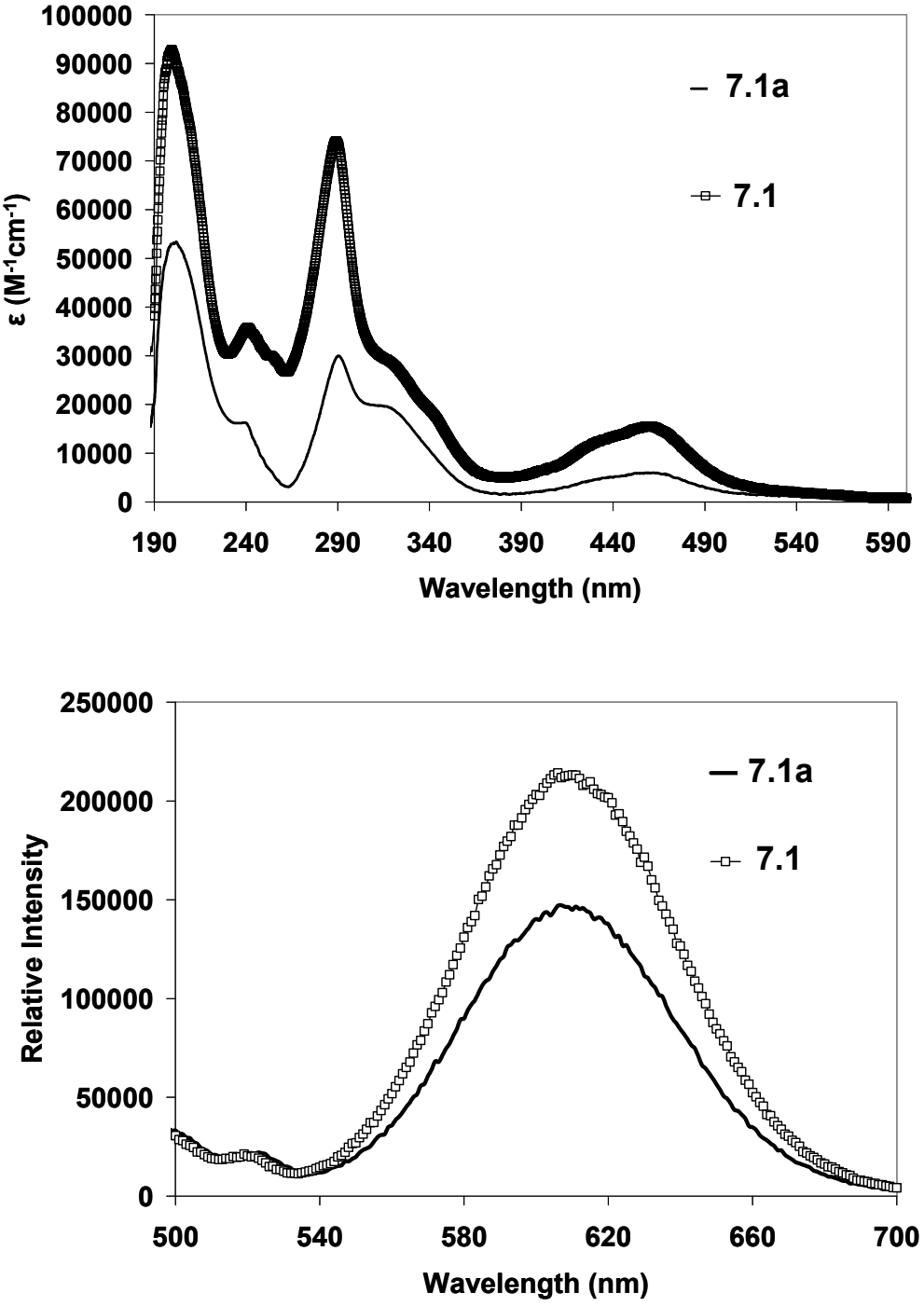

Figure 7.27 UV-Vis (top) and emission spectra (bottom) of compounds **7.1** and **7.1a** (1 x 10^{-5} M, CH_3CN, λ_{ex} = 468 nm and λ_{em} = 615 nm).

*7.3.2.3 Electrochemical properties of **7.1** and **7.1a**.*

The electrochemical data for **7.1a** and for the parent compound **7.1** are presented in Table 7.2. Complexes of **7.1** and **7.1a** have nearly identical one electron reversible oxidation peak in the cyclic voltammogram at ~ 1.31 V. In Figure 7.28, the compound **7.1** displays reversible reduction characterized by three peaks at -1.18, -1.38, and -1.67 V which can be attributed to the reduction of the ligands, 2-(2'-pyridyl)benzimidazolyl and bpy. The reduction peaks of **7.1a** compared to those in **7.1** are not as well resolved and are shifted to a more positive potentials, -1.16, -1.35 and -1.63 V. A more positive reduction potential observed for **7.1a** is possibly due to lower LUMO level caused by the conjugation with the electron withdrawing guanine. Similar effect on the redox potential was observed for Ru^{2+} complexes of adenine derivatives substituted at C^8-site *via* phenylene linker.[7]

Table 7.2 Electrochemical properties of **7.1** and **7.1a**.

Compound	**E_{Ox}**	**E_{Red}[a]**	**Electrochemical bandgap**
	(V)	(V)	(eV)
7.1a	1.31	-1.16	2.47
7.1	1.31	-1.18	2.49

[a] The first reduction peak, DMF vs Ag/AgCl.

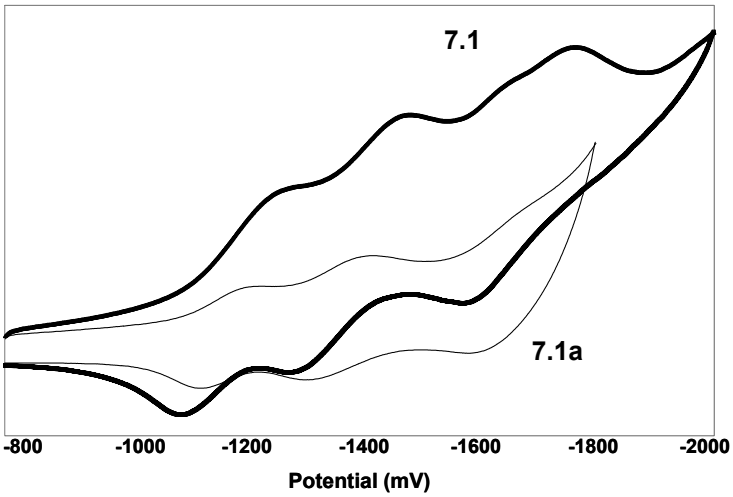

Figure 7.28 Cyclic voltammogram of **7.1** and **7.1a** (DMF, $E^{1/2}(FeCp_2^{0/+})$ = 0.55 V).

*7.3.2.4 Investigation of **7.1a** as a potential sensing probe*

A phosphorescent and redox active G-nucleoside probe could render themselves useful in terms of sensing applications, with number of target molecules, such as anions, cations, nucleosides and oligonucleotides. For that purpose, compound **7.1a** was investigated and the preliminary results are presented.

*7.3.2.4.1 Self-assembly of **7.1a***

N^2Gs are capable of self-assembly into $[\mathbf{G}]_8$ as demonstrated in Chapter 3. To examine the impact of the Ru^{2+} unit on the self assembly of **N^2G**, the H-bonding ability of **7.1a** was investigated in solution. The self-assembly was studied in different solvents, such as D_2O/H_2O or CD_3CN, and in the presence of different metal salts, such as KI, $KClO_4$, K(picrate) and NH_4PF_6. All efforts to induce G-quartet formation by **7.1a** were unsuccessful. The reasons for this behaviour may be attributed to several factors. Most likely the cationic bulky Ru^{2+} groups on the extended N^2-substituents prevent the H-bonding. The solvents used might also compete for H-bonds.

*7.3.2.4.2 Interactions of **7.1a** with fluoride ions*

The interest in monitoring fluoride ion concentration stems from its biological and environmental impact. Hence, the H-bond donor sites, imino and amino protons, in **7.1a** can potentially be used to bind F^- ion. The addition of ~ 30 equivalents of tetrabutylammonium fluoride (TBAF) to a solution of **7.1a** causes a ~ 20 % decrease in the emission as presented in Figure 7.29 which indicates that a relatively weak interaction exist between F^- ions and **7.1a**.

In terms of CV response, the addition of excess F^- anion to the solution of **7.1a** causes a dramatic change in the CV profile which is characterized by the elimination of the first redox potential (Figure 7.30). The first reversible reduction couple at ~ -1.2 V can be ascribed to the reduction of the ligand, possibly 2-(2'-pyridyl)benzimidazolyl, which might have some contribution from guanine. Notably, no such anion effects were observed for **7.1**, due to the lack of guanine group. Hence, the major contributing factor towards the CV change is the interaction between guanine unit in **7.1a** and F^- ion.

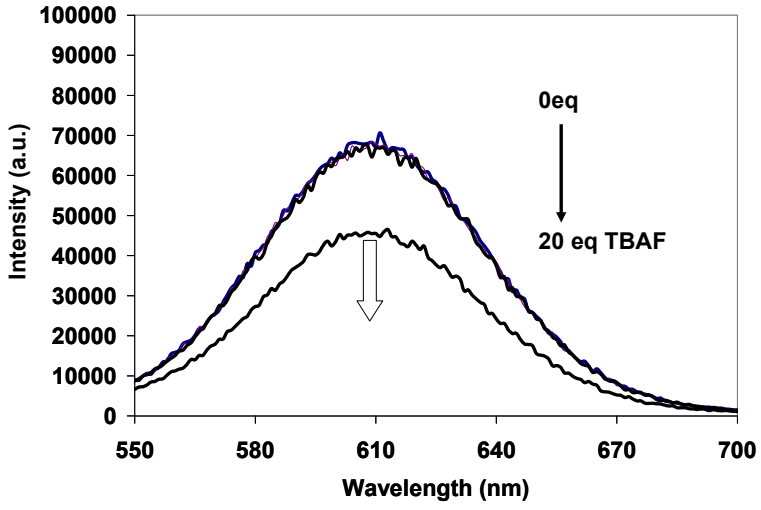

Figure 7.29 The titration spectra of **7.1a** with TBAF (CH_3CN, [**7.1a**] = 1 x 10^{-5} M).

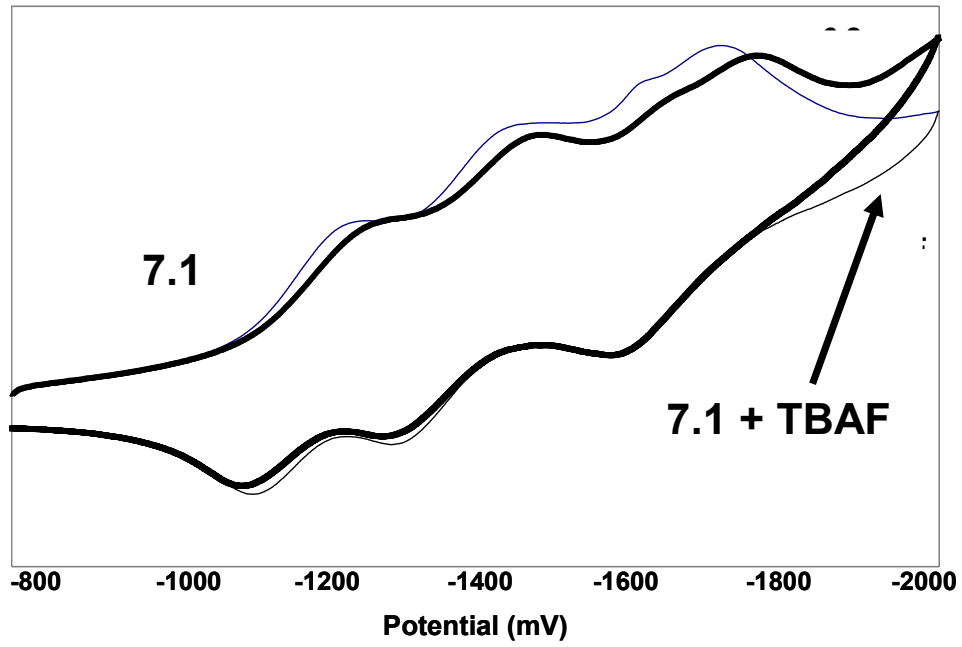

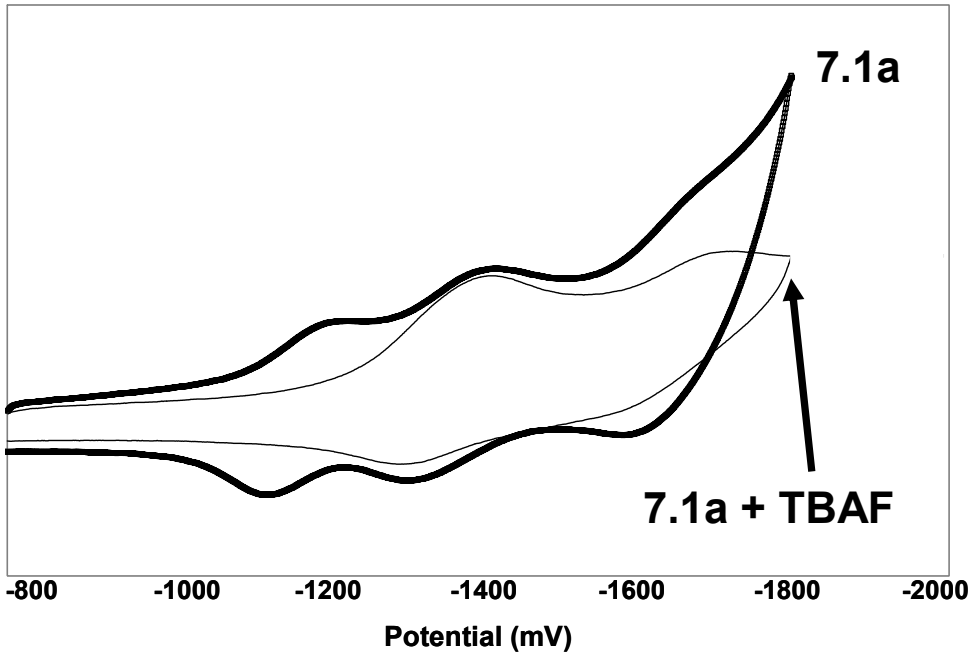

Figure 7.30 Cyclic voltammograms of **7.1** (top) and **7.1a** (bottom) with excess TBAF (DMF).

*7.3.2.4.3 Interactions of **7.1a** with **4-C***

Another potential application of **7.1a** is in the recognition of the complementary base, cytidine. **N^2Gs** strongly bind **4-C** over other nucleosides as shown in Chapter 5, causing the dramatic change in the fluorescent emission. In contrast, the addition of excess **4-C** to the solution of **7.1a** in CH_3CN does not result in any change in UV-Vis absorption, CD absorption or phosphorescent emission. These preliminary studies should be followed by a complete investigation using electrochemistry.

*7.3.2.4.4 Interactions of **7.1a** with a polynucleotide*

In order to take advantage of the cationic nature of **7.1a** and its guanine unit, the poly(cytidylic) acid (poly-rC) was investigated. The titration studies were performed in two different aqueous solutions, under neutral (0.2 M $NaHPO_4$, 0.2 M Na_2PO_4, pH 7.5) and acidic (0.1 M NaCl, 0.2 M $NaOAc_{aq}$, 0.2 M glacial acetic acid, pH 4.4) conditions due to the fact that the conformation of poly-rC is highly pH dependent. At alkaline and neutral pH poly(rC) exists as a single-stranded helical structure, while at acidic pH a double-stranded helix is formed.[16]

At neutral pH, no changes in the CD spectra of poly-rC were observed, while a slight increase in the emission and UV-Vis absorption can be correlated to a simple increase in **7.1a** concentration upon titration. A reversed titration was also performed using a neutral aqueous solution of **7.1a** to which a solution of poly-rC was added, however, no changes in UV-Vis absorption or phosphorescence were observed. A small increase in the CD absorption band, upon titration, is simply due to the increase in poly-rC concentration. The poor sensitivity of **7.1a** in aqueous solution was attributed to the disruption of H-bonding between guanine and cytosine; hence, to avoid the undesirable

H-bonding competition by solvent, the experiments were performed in organic solvents. However, the titrations in the mixed solvents such as CH_3CN:DMSO (2%) or CH_2Cl_2:DMSO (2%) were not fruitful either.

Under acidic pH (~ 4.4), poly-rC is well known to exist as a dimer due to the H-bonding between protonated and unprotonated C-residues. We propose that the formation of GC base pairs will break the CC^+ dimer and will induce changes in the CD profile. However, the addition of **7.1a** to the solution of poly-rC did not result in any changes in CD, UV-Vis or phosphorescent spectra.

7.4 Conclusions

In summary, **N^2Gs** can be used as the model systems for the study of phosphorescent metal ions. The interaction with Ln^{3+} causes fluorescent quenching of ligand emission for **2.1a** and **2.2a**. In case of **2.3a**, the fluorescent response is a combination of a fluorescent quenching and a red shift, depending on the nature of Ln^{3+} ions. The quenching of ligand emission is most dramatic in the presence of Eu^{3+} and least in the presence of La^{3+} ions. The efficiency of ligands in terms of Ln^{3+} activation follows the order: **2.3a** > **2.2a** > **2.1a**, and the sensitization process is overall greater for Tb^{3+} over Eu^{3+}. For **2.3a** the emission of Eu^{3+} is driven by the energy-transfer process from the ligand to the metal center rather than through direct-excitation. Sources of Tb^{3+} activation vary anywhere from the energy-transfer from the supporting acac ligands to N^2-guanosines, depending on the N^2-substituent. Overall, the chelating ligands, such as **2.2a** or **2.3a**, are potential activators of Tb^{3+} emission.

The Ru^{2+} complex based on N^2-modified guanosine, **7.1a**, has been synthesized and characterized, and it was found to displays a red emission in the solution and the solid

state. For the sensing purpose, the interactions of **7.1a** with anions, cations, nucleosides and polynucleotides were investigated using a number of spectroscopic and electrochemical methods. The preliminary results on **7.1a** indicate that further optimizations of the molecule or experimental conditions are needed to achieve the optimal performance with this G-nucleoside.

7.5 References

[1] (a) Vrabel, M.; Horakova, P.; Pivonkova, H.; Kalachora, L.; Cernocaka, H.; Cahova, H.; Pohl, R.; Sebest, P.; Havran, L.; Hocek, M.; Fojta, M. *Chem. Eur. J.* **2009**, *15*, 1144. (b) Chatterjee, D.; Ward, M. S.; Shepherd, R. E. *Inorg. Chim. Acta* **1999**, *285*, 170. (c) Ringer, D. P.; Burchett, S.; Kizer, D. E. *Biochemistry* **1978**, *17*, 4118.

[2] (a) Sigel, R. K.; Pyle, A. M. *Met. Ions Biol. Syst.* **2003**, *40*, 477. (b) Matsmura, K.; Komiyama, M. *J. Biochem.* **1997**, *122*, 387. (c) Hargittai, M. R.; Musier, F. K. *RNA* **2000**, *6*, 1672.

[3] Formoso, C. *Biochem. Biophys. Res. Commun.* **1973**, *53*, 1084.

[4] (a) Hurley, D. J.; Seaman, S. E.; Mazura, J. C.; Tor, Y. *Org. Lett.* **2002**, *4*, 2305. (b) Hurley, D. J.; Tor, Y. *J. Am. Chem. Soc.* **2002**, *124*, 13231. (c) Hurley, D. J.; Tor, Y. *J. Am. Chem. Soc.* **1998**, *120*, 2194. (d) Hurley, D. J.; Tor, Y. *J. Am. Chem. Soc.* **2002**, *124*, 3749.

[5] (a) Ward, M. D.; White, C. M.; Barigelletti, F.; Armaroli, N.; Calogero, G.; Flamigni, L. *Coord. Chem. Rev.* **1998**, *171*, 481. (b) Armaroli, N.; Barigelletti, F.; Calogero, G.; Flamigni, L.; White, C. M.; Ward, M. D. *Chem. Commun.* **1997**, 2181.

[6] (a) White, C. M.; Gonzales, M. F.; Bardwell, D. A.; Rees, L. H.; Jeffery, J. C.; Ward, M. C.; Armaroli, N.; Calogero, G.; Barigelletti, F. *J. Chem. Soc., Dalton Trans.,* **1997**, 727. (b) Wang, P.; Miller, J. E.; Henling, L. M.; Stern, C. L.; Frank, N. L.; Eckermann, A. L.; Maede, T. J. *Inorg. Chem.* **2007**, *46*, 9853.

[7] (a) Vrabel, M.; Pohl, R.; Klepetarova, B.; Votruba, I.; Hocek, M. *Org. Biomol. Chem.* **2007**, *5*, 2849. (c) Vrabel, M.; Pohl, R.; Votruba, I.; Sajdi, M.; Kovalenko, S. A.; Ernsting, N. P.; Hocek, M. *Org. Biomol. Chem.* **2008**, *6*, 2852.

[8] Kwan, I. C. M.; She, Y. M.; Wu, G. *Chem. Commun.* **2007**, 4286.

[9] Rogachev, A. Y.; Mironov, A. V.; Broyanov, S. I.; Kuzmina, N. P.; Nemukhin, A. V. *J. Mol. Struct.* **2006**, *789*, 187-194.

[10] Yang, W. Y.; Chen, L.; Wang, S. *Inorg. Chem.* **2001**, *40*, 507.

[11] (a) Huang, L.; Wang, K. Z.; Huang, C. H.; Gao, D. G.; Jin, L. P. *Synthetic Metals* **2002**, *128*, 241. (b) Elhabiri, M.; Hamacek, J.; Bunzli, J. G. C.; Gary, A. M. A. *Eur. J. Inorg. Chem.* **2004**, 51.

[12] Gunnlaugsson, T.; Leonard, J. P. *Chem. Commun.* **2005**, 3114.

[13] Jia, W. L.; Hu, Y. F.; Gao, J.; Wang, S. *Dalton Trans.* **2006**, 1721.

[14] (a) Yamagishi, A. *J. Phys. Chem.* **1984**, *88*, 5709. (b) Kumar, C. V.; Barton, J. K.; Turro, N. J. *J. Am. Chem. Soc.* **1985**, *107*, 5518.

[15] (a) Morgan, O.; Wang, S.; Bae, S. A.; Morgan, R. J.; Baker, A. D.; Strekas, T. C.; Engel, R. *J. Chem. Soc., Dalton Trans.* **1997**, 3773. (b) Kolp, B.; Viebrock, H.; von Zelewsky, A.; Abeln, D. *Inorg. Chem.* **2001**, *40*, 1196. (c) Hua, X.; von Zelewsky, A. *Inorg. Chem.* **1995**, *34*, 5791.

[16] Zarudnaya, M. I.; Samijlenko, S. P.; Potyahaylo, A. L.; Hovorun, D. M. *Nucleos. Nucleot. Nucleic Acids* **2002,** *21*, 125.

Chapter 8
Summary and Perspectives

8.1 Summary

The work presented in this thesis is aimed at developing new functional guanosines for potential use as sensing probes. Hence the work started with the synthesis of new **N^2G** compounds containing fluorescent, phosphorescent or chelate ligands. To obtain target molecules, an Ullmann condensation reaction was used for the first time in direct N^2-guanosine functionalization. It was found that this method is very effective for synthesis of all **N^2G** ligands with high regioselectivity and moderate yields. The functionalities such as diphenylamino, 2,2'-dipyridylamino, 2-(2'-pyridyl)benzimidazolyl and *p*-phenylpyrenyl were introduced at the N^2-site of guanine. Chemical modification at the N^2-site influences the electronic structure of guanine, by extending the π conjugation and causing fluorescent blue emission. DFT calculations were used to gain more insights into the photophysical properties of these new **N^2G** ligands. The guanine ring was found to be extensively involved in the lowest electronic transitions in all ligands. This electronic feature makes **N^2G** desirable since the guanine group can be used as a receptor in the sensing studies.

To further explore the effects of chemical modification on the self-assembly of **N^2G**, solution and gas-phase studies were performed. Compared to unmodified guanosines, **N^2Gs** display a greater diastereoselectivity which leads to exclusive octamer formation in the presence of metal ions, a characteristic that was attributed to extensive π - π stacking interactions between N^2-substituents of the **N^2G** ligands. This secondary

hydrophobic interaction was later discovered to be a driving force in the formation of "empty" octamers in the gas phase. This was the first observation of "empty" octamers. While the original intention was to introduce fluorescent N^2-groups to monitor G-quartet formation, it was discovered that self-assembly into G-quartets does not affect the luminescent properties of **N^2G** ligands.

Although the G-quartet formation could not be monitored by fluorescence, we have successfully used luminescent **N^2G** ligands and luminescent **N^2G** octamer for the study of Watson-Crick H-bonding with its complementary base cytidine. The investigation was focused on probing the base pair formation and G-octamer-to-GC base pair structural transformation. Using fluorescence spectroscopy, all **N^2G** ligands investigated in this thesis form GC base pairs with high association constants. **N^2G** compounds were found to be highly selective fluorescent probes for cytidine over other nucleosides. The fluorescent **N^2G** octamers were successfully used for the study of G-octamer-to-GC transformation for the first time by fluorescence and CD spectroscopies.

In order to probe the function of **N^2G** ligands, a significant part of this work was focused on the interactions between metal ions and new **N^2Gs**. The investigation was focused on the Group 12 metal ions, with the emphasis on Zn^{2+}, and it was discovered that **N^2G** ligands exhibit two distinct responses towards Zn^{2+} ions. A "turn-off" fluorescent response was observed with non-chelating **N^2G** while chelating **N^2G** ligands were characterized by a "turn-on" response. The contrasting fluorescent responses were ascribed to the nature of the N^2-chelate sites, and it was demonstrated that the chemical modification at N^2-site of guanine can be used to design switchable metal ion probes.

The last part of this thesis concerned the development of new phosphorescent **N^2G** complexes using Ln^{3+} and Ru^{2+} metal ions. It was found that several **N^2G** ligands can potentially act as activator of Eu^{3+} and Tb^{3+} emissions, however, these Ln^{3+} complexes were not isolated. To further explore the chemistry of Ru^{2+} complexes, a ligand based on 2-(2'-pyridyl)benzimidazolyl was used and a phosphorescent ruthenium complex of N^2-arylguanosine was synthesized, isolated and fully characterized. The preliminary sensing studies involving the use of this phosphorescent **N^2G** complex indicate that it is a potentially useful probe.

This research has established that careful selection of N^2-substituents can influence the photophysical and structural properties of the final target molecule. Several new **N^2G** ligands have been shown to undergo self-assembly, with high fidelity, into octamers and can potentially act as the sensing probes for the complementary base pairing and for the metal ions interactions.

8.2 Future Directions

On the basis of this work, future directions could encompass several aspects. First, it is worth incorporating triflate salts of Group 1 and 2 metal ions to drive self-assembly since they might behave similarly to picrate salts. However, unlike picrate, a triflate anion is unlikely to act as a fluorescence quencher and hence might make study of H-bonding by fluorescence more feasible. Changing the ribose protecting groups might increase the solubility of lipophilic N^2-arylguanosines and induce easier crystallization of ligands and their self-assembled structures. Second it would be interesting to revisit the synthesis of boron-containing guanosines (**N^2GB**) depicted in

Figure 8.1 *via* N^2-modification of guanosine. This compound is an attractive target molecule due to the possibility of intermolecular charge transfer involving the three-coordinate boron site. It can be proposed that the charge transfer may take place between all nitrogen-quartet of **N^2G** and all-boron quartet of **N^2GB** as shown in

Figure 8.1. Another interesting approach would involve the generation of intramolecular CT by using C^8,N^2-substituted guanosine, **G-BN**, presented in Figure 8.2. A disubstituted G-nucleoside may potentially be useful in the study of G-quartet formation, wherein H-bonding between guanine units would "turn-off" the charge transfer between N- and B-substituents, and in turn change the nature of the lowest electronic transition which could be monitored by fluorescence spectroscopy.

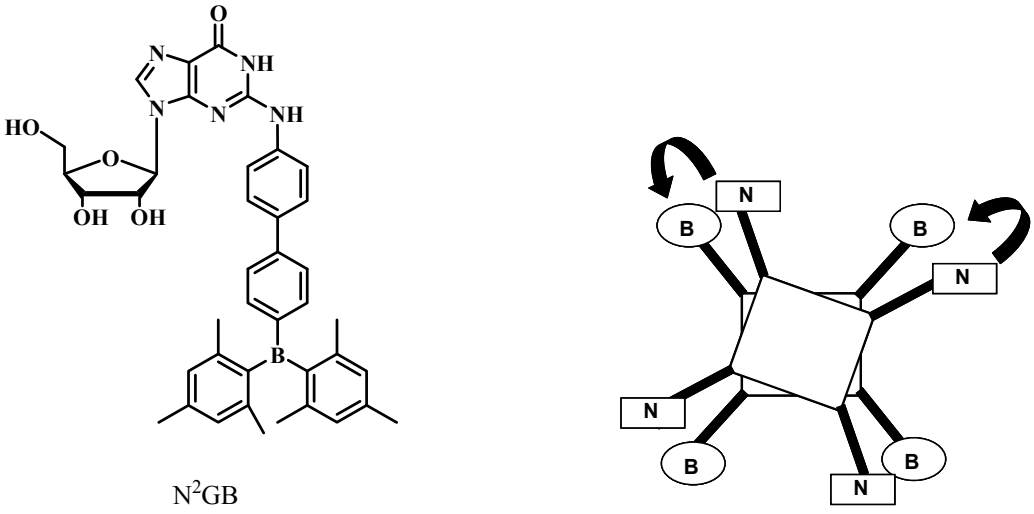

Figure 8.1 Proposed structure of boron-containing guanosine compound, **N^2GB,** and the proposed CT between all donor and all acceptor G-quartets.

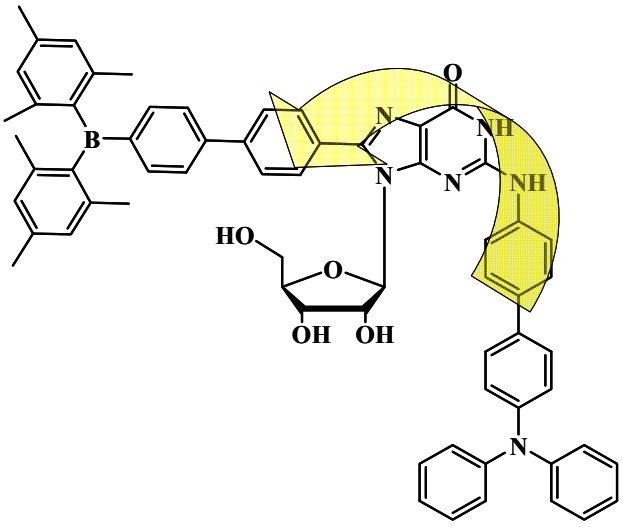

G-BN

Figure 8.2 Proposed structure of B- and N-containing guanosine compound, **G-BN** and the proposed intramolecular CT.

Another direction of future research may be the development of N^2G-phosphoramidite intermediates for the subsequent incorporation into oligonucleotides. One of my latest efforts during the thesis work was to attempt the synthesis of such precursors by using standard literature procedures. To simplify the synthesis, a deoxy analogue was prepared, **N^2dG,** in good yield. The preliminary synthetic results are illustrated in Figure 8.3. The initial reaction yields for the synthesis of **N^2dG-5'-DMT** and **N^2dG-5'-DMT-3'-phosphoramidite** were very low, with the final isolated yield of ~ 5 % for **N^2dG-5'-DMT-3'-phosphoramidite.** Since the subsequent incorporation into oligonucleotide requires large quantities of the compound (> 20 mg), the synthesis has to be repeated by using optimized procedure. Future research efforts on the topic of oligonucleotide chemistry are recommended.

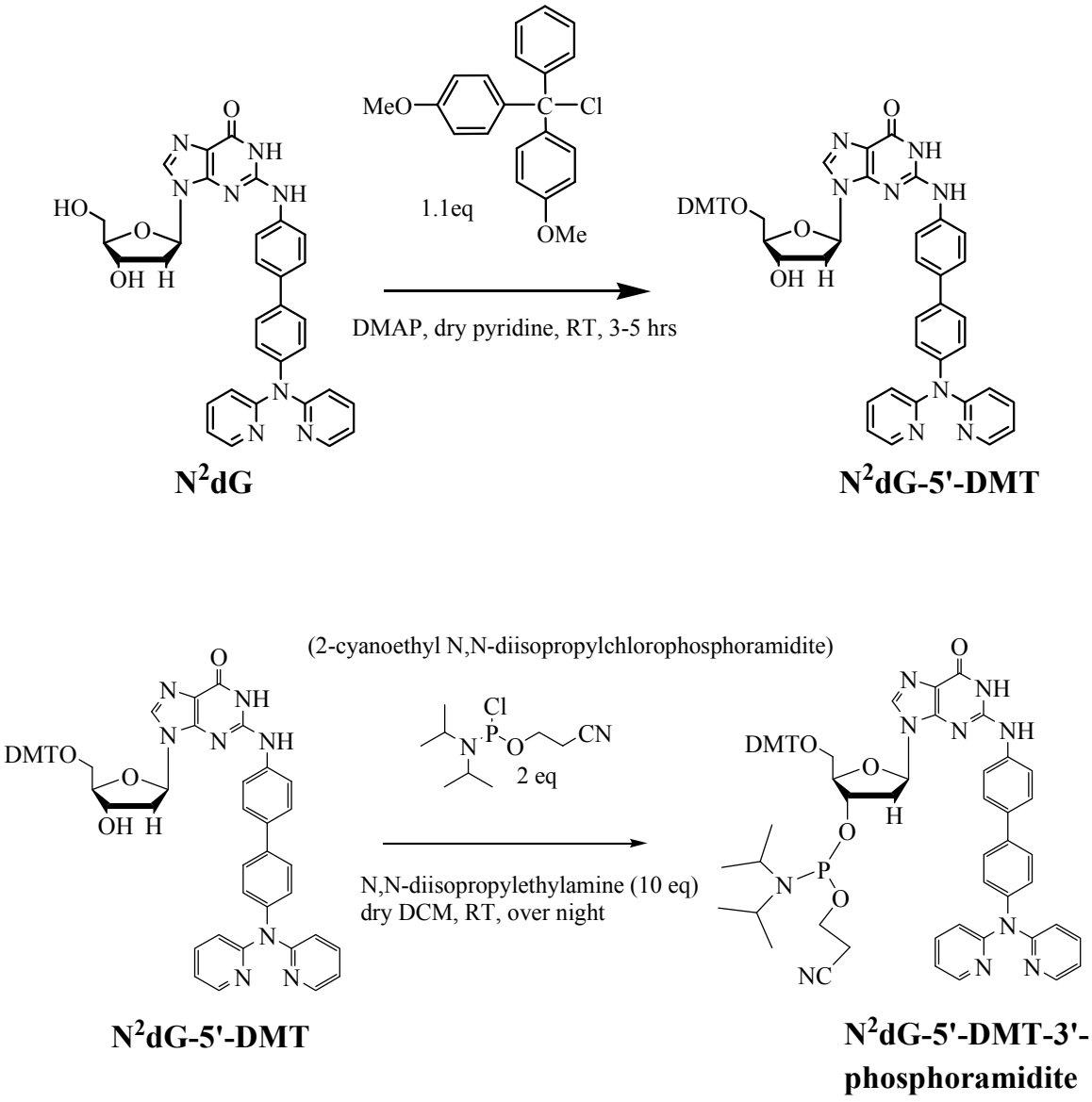

Figure 8.3 Proposed reaction schemes for the synthesis of N^2dG-phosphoramidite.